CORA Cork Open Research Archive
Cartlann Taighde Oscailte Chorcaí

Title	Impurity profiling and synthesis of a series of analogues and isomers of Bromo-DragonFLY
Authors	Jones, Roisin Anne
Publication date	2019-10-01
Original Citation	Jones, R. A. 2019. Impurity profiling and synthesis of a series of analogues and isomers of Bromo-DragonFLY. PhD Thesis, University College Cork.
Type of publication	Doctoral thesis
Rights	© 2019, Roisin Anne Jones. - https://creativecommons.org/licenses/by-nc-nd/4.0/
Download date	2026-11-04 02:36:26
Item downloaded from	https://hdl.handle.net/10468/9972

UCC
University College Cork, Ireland
Coláiste na hOllscoile Corcaigh

Impurity Profiling and Synthesis of a Series of Analogues and Isomers of Bromo-DragonFLY

by Róisín Anne Jones, BSc



ucc

Coláiste na hOllscoile Corcaigh, Éire
University College Cork, Ireland

A thesis presented for the degree of

DOCTOR OF PHILOSOPHY

to

National University of Ireland, Cork

School of Chemistry,
University College Cork

October 2019

Head of School: Dr. Humphrey Moynihan

Research Supervisor: Dr. J.J. Keating

Abstract

BromoDragon-FLY (BDF) is a highly hallucinogenic amphetamine that fits into a category known as New Psychoactive Substances (NPS), a group of illicit drugs which has risen to prominence in the last two decades. The most common route to making amphetamine-type stimulants (ATS) in clandestine laboratories is the Leuckart reaction, which converts a precursor ketone to the desired amine. The Leuckart reaction produces characteristic route-specific impurities that can facilitate the identification of the synthetic pathway employed. The Leuckart impurities typically present in the highest yield are isomeric benzyl and phenyl pyrimidines.

The aim of this thesis work was first to independently synthesise, isolate and characterise a series of pyrimidines related specifically to the Leuckart synthesis of BDF, and then to use those pyrimidines as analytical standards in HPLC analysis of the corresponding Leuckart reactions. In addition to the pyrimidines, an isomeric impurity in the synthesis of a BDF precursor was also targeted as a potential impurity in BDF (though not related to the Leuckart reaction specifically): the independent synthesis, isolation and characterisation of this isomeric impurity was also a key aim of this thesis work in order to contribute to the overall understanding of the potential impurity profile of BDF.

There are three synthetic steps from a 2,3,6,7-tetrahydrobenzo[1,2-*b*:4,5-*b'*]difuran (THBD) ketone precursor to BDF: bromination, aromatisation and the Leuckart reaction. Depending on the order that these steps are performed in, there are eight potential pyrimidine impurities arising from the formation of BDF. In this work, seven of these eight pyrimidines are independently synthesised and fully characterised (by $^{1}H/^{13}C$ nuclear magnetic resonance (NMR) spectroscopy, infrared (IR) spectroscopy and mass spectrometry (MS)) as analytical standards, using palladium-catalysed coupling reactions. Several alternate synthetic pathways to the pyrimidines are also explored, and although none of these alternate routes were

successful, a number of novel compounds were successfully isolated and characterised.

As mentioned, there are three steps to BDF from THBD which can be carried out in any order: four Leuckart reactions were completed to simulate each of the possible synthetic routes from THBD to BDF. Impurity profiling was carried out by high-performance liquid chromatography (HPLC) analysis, using the previously synthesised analytical standards and the crude reaction mixtures generated during the Leuckart reactions. This work determined that the pyrimidine impurities generated during the Leuckart reaction are detectable and distinguishable by HPLC, making them useful route-specific markers for the Leuckart reaction.

Previous work in our group discovered that during the bromination of the phenyl core *en route* to THBD, a small percentage of the 2,3-dibromo isomer was formed in conjunction with the desired 2,5-dibromo isomer. When carried through the Grignard ring-closing step, an isomer of THBD was formed in < 1 % overall yield: 1,2,7,8-tetrahydrobenzo[1,2-*b*:4,3-*b'*]difuran (iTHBD).

This isomer of THBD is not known in the literature, and was immediately identified as a compound of interest due to its status as a potential pharmacophore of unknown properties, and also as a potential impurity in illicitly sold BDF. To this end, a synthetic pathway was designed to produce iTHBD specifically, which was sucessfully carried out in ~ 5 % overall yield over four steps from *p*-benzoquinone starting material. This yield was significantly impacted by the formation of inseparable regioisomers in the second step of the synthetic pathway, but nonetheless represents an improvement over the yield seen when iTHBD is produced as a side-product in the synthesis of THBD.

Declaration

I hereby declare that the submitted work for the thesis entitled “Impurity Profiling and Synthesis of a Series of Analogues and Isomers of Bromo-DragonFLY” is entirely my own. Any reference made to the works of others is clearly cited, the details of which can be found in the bibliography at the end of each chapter. The work contained within this thesis has not been presented at this, or any other university, as part of another degree.

Signature: _____

Roisin Anne Jones

Date: _____

Acknowledgements

The list of people I need to thank is almost inexhaustible; there is no way I could have done this on my own, and I have many, many people to whom I owe massive thanks.

First and foremost, I'd like to thank IRCSET for giving me funding, without which this project would never have happened. A huge thank you also to my supervisor, JJ, who was always easy to approach with any concerns I had during the many years of my PhD, and who invariably went out of his way to help with those concerns. His support and insight have been particularly invaluable during the writing of my thesis in this past year.

My personal PhD support network definitely started with the other members of the JJK research group. Thanks and affection in equal measure must go to Richard, for introducing me to the lab and always having time to talk me through whatever problem of the day I was having; to Jonathan, for constantly keeping me entertained and for not killing me when I spilled half of his final product as an undergrad student; and to Ryan, for keeping me going over the last leg of this marathon effort, always there to help me out and cheer me up.

A big shout of appreciation also to the many other people that I shared a lab and an office with over the years, who laughed with me on the good days and commiserated on the bad ones: Kate, Mike, Chloe, Claire, Rose, Tricia, Laura, Valerie, Patrick, Hiren, Pavan and Therese and also the innumerable other people within the Chemistry department who I relied on for support and friendship over the years. Special mentions must go to Davey, for all the impromptu mechanism brainstorming sessions, and more importantly the banter; and to Fiona, the best fumehood neighbour and partner in crime I could have asked for.

Thanks as well to all the technical people around UCC who have helped me out in so many ways over the years: to Dr. Denis Lynch, Dr. Lorraine Bateman and Dr. Dan McCarthy for all their help with NMR analysis, to Mr.

Michael O'Shea for mass spectroscopy, and to Dr. Nuala Maguire for her invaluable help with HPLC analysis.

Moving on to the people who supported me outside of college, they were just as important in keeping me sane and healthy over the years. To my colleagues in GSK Cork (or Thermofisher Scientific as it is soon to be), especially those that I share/shared an office with – Sarah, Aoife, Eddie, Donncha, Denis, Suri, Sean, Damien, Daves (both of them!) and Tricia – a huge thanks for the moral support, most of you have been down the exact same road and were always generous with your sympathy and advice.

To all my friends, to Louise, Shelly, Aoibhin and Trisha: thank you for all the good times and the support, and most importantly, the understanding when I had to change plans last minute! To Cressi, who supported me in so many ways, from formatting this very document to keeping me company on long nights in the lab, and perking my spirits up with her indomitable optimism when I was down, I want to say a huge thank you.

Finally, to my family, who have been constant pillars of support without whom I would never have gotten to this point. To Kerry, who's been here for the whole journey and miraculously hasn't either murdered me or emigrated to Mexico, and has provided me with endless and invaluable support, I can't even begin to express the level of thanks due. To my siblings, my eternal partners in mischief and joy, to Mairead, Fiachra, Ruadhan and Seanan, thank you, thank you, thank you; I know my thesis has been a series of ups and downs to which you've all been subjected, but you were always there for me whether it was for a cry or a triumph, and I love you all to bits. Last but most certainly not least, to my Mam and Dad, who are always interested in what I am up to and who always have time to listen to me complain or enthuse (depending on the day) and who I know are only too thrilled for me and proud of me for finally finishing this particular journey: thank you a million times over, I love you both.

Abbreviations

^{13}C-NMR	carbon-13 nuclear magnetic resonance
2C-B	2,5-dimethoxy-4-bromophenethylamine
2C-B-FLY	2-(8-bromo-2,3,6,7-tetrahydrobenzo[1,2-*b*:4,5-*b'*]difuran-4-yl)ethan-1-amine
2D-NMR	two-dimensional nuclear magnetic resonance
^{1}H-NMR	proton nuclear magnetic resonance
5-HT	5-hydroxytryptamine
ACN	acetonitrile
aq.	aqueous
ATS	Amphetamine-type stimulant(s)
BDF	Bromo-DragonFLY
calc.	calculated
cAMP	cyclic adenosine monophosphate
CE	capillary electrophoresis
cm	centimetre(s)
CNS	central nervous system
conc.	concentrated
COSY	correlated spectroscopy
d	doublet
DAD	diode array detector
dba	dibenzylideneacetone
DCM	dichloromethane
DDP	4,5-dichloro-3,6-dihydroxyphtalonitrile
DDQ	2,3-dichloro-5,6-dicyano-1,4-benzoquinone
DG	Dawn Griffin
DIW	deionised water
dmdba	3,5,3′,5′-dimethoxydibenzylideneacetone
DMF	*N,N'*-dimethylformamide
DMSO	dimethylsulfoxide
DOB	2,5-dimethoxy-4-bromoamphetamine
DOI	2,5-dimethoxy-4-iodoamphetamine
DOM	2,5-dimethoxy-4-methylamphetamine

EC_{50}	median effective concentration
ED_{50}	median effective dose
eq.	equivalents
ERG	ergoline
ESI	electrospray ionisation
EtOAc	ethyl acetate
FTIR	Fourier-transform infrared
g	gram(s)
GC	gas chromatography
GPCR	G-protein coupled receptor
GDP	guanosine-5′-diphosphate
GTP	guanosine-5′-triphosphate
h	hour(s)
hex	hexane
HMBC	heteronuclear multiple bond correlation
HPLC	high performance liquid chromatography
HPPD	hallucinogen persisting perception disorder
HRMS	high resolution mass spectrometry
HSQC	heteronuclear single quantum correlation
Hz	Hertz
IR	infrared
iTHBD	1,2,7,8-tetrahydrobenzo[1,2-*b*:4,3-*b′*]difuran
IUPAC	International Union of Pure and Applied Chemistry
IV	intravenous
JQ	Jonathan Quille
K_d	off rate (enzyme binding)
K_i	binding affinity
LC-MS	liquid chromatography-mass spectrometry
lit.	literature
LRMS	low resolution mass spectrometry
LSD	lysergic acid diethylamide
m	multiplet
m.p.	melting point

m/z	mass to charge ratio
MAO	monoamine oxidase
mAU	milli-absorbance units
MDA	3,4-methylenedioxyamphetamine
MDMA	3,4-methylenedioxymethamphetamine
mg	milligram(s)
min	minute(s)
mL	millilitre(s)
mmol	millimole(s)
MS	mass spectrometry
MU	mescaline units
N/A	not available
NBS	*N*-bromosuccinimide
n-BuLi	*n*-butyllithium
NMR	nuclear magnetic resonance
NPS	new psychoactive substance
NT	neurotransmitter
OCD	obsessive compulsive disorder
ODS	octadecylsilyl
P2P	phenyl-2-propanone
PAC	pharmaceutically active compound
PLC	phospholipase C
PMI	parent molecular ion
ppm	parts per million
*p*TSA	*para*-toluene sulfonic acid
q	quartet
RBF	round-bottomed flask
recryst.	recrystallisation
R_f	retardation factor
RGS	regulator of G-protein signalling
ROC	Richard O'Connor
RT	room temperature
s	singlet

SAR	structure-activity relationship
sat.	saturated
SERT	serotonin transporter
SM	starting material
SSRI	selective serotonin reuptake inhibitor
temp.	temperature
TFAA	trifluoroacetic anhydride
THBD	2,3,6,7-tetrahydrobenzo[1,2-*b*:4,5-*b'*]difuran
THF	tetrahydrofuran
TLC	thin layer chromatography
TM	transmembranal helix/helices
TMS	tetramethylsilane
t_R	retention time
UK	United Kingdom
UNDCP	United Nations International Drug Control Program
UNODC	United Nations Office on Drugs and Crime
USA	United States of America
UV	ultraviolet
ν_{max}	peak maximum
VT-NMR	variable temperature NMR
δ	chemical shift (ppm)

Table of Contents

Abstract ..... **ii**

Declaration ..... **iv**

Acknowledgements ..... **v**

Abbreviations ..... **vii**

Table of Contents ..... **xi**

Chapter One - Introduction **1**

Chapter Two - Synthesis and Impurity Profiling of Benzyl and Phenyl Pyrimidines Associated with the Leuckart Synthesis of Bromo-DragonFLY **76**

Chapter Three - Development of a Direct Synthetic Route to the Novel Pharmacophore 1,2,7,8-Tetrahydrobenzo[1,2-*b*:4,3-*b'*]difuran **247**

Chapter Four - Experimental **316**

Overall Summary and Future Work **359**

Appendix - Pyrimidine Markers HPLC Data **364**

Chapter One: Introduction

Table of Contents

Table of Contents **2**

List of Figures **3**

List of Tables **5**

1 Introduction **6**

1.1 The Amphetamine Family 6

1.2 Pharmacology of Amphetamines 9

1.2.1 Amphetamine Pharmacology 11

1.2.2 Mechanism of Action 12

1.3 Hallucinogens 14

1.3.1 Neuropharmacology of Psychotropic Amphetamines 16

1.3.2 Mechanism of Action of NTs and Sympathomimetic Amines at 5-HT_2 Receptors 19

1.3.3 Mapping the Active Site of 5-HT_2 Receptors 21

1.4 Structure-Activity Relationships of Hallucinogenic ATS 40

1.5 Synthesis of ATS from P2P **(62)** Intermediates 47

1.6 Clandestine Laboratories 57

1.7 Impurity Profiling of Illicit Materials 60

1.8 Bromo-DragonFLY 62

1.9 Research Outline 65

References (Chapter One) **68**

List of Figures

Fig. 1-1: Amphetamine **(1)** and DOB **(2)** 7
Fig. 1-2: Examples of ATS 7
Fig. 1-3: Exogenous and Endogenous Neurotransmitters 9
Fig. 1-4: Diagram of a neuron[14] 10
Fig. 1-5: Communication between neurons 11
Fig. 1-6: Dopamine **(10)**, Noradrenaline **(11)** and Serotonin **(12)** 12
Fig. 1-7: Use of peyote in Native American religious services[23] 15
Fig. 1-8: LSD **(13)**, DOI **(5)** and DOM **(14)** 17
Fig. 1-9: 5-HT GPCR type transmembrane receptors[7] 19
Fig. 1-10: GDP **(16)**, GTP **(17)** and cAMP **(18)** 20
Fig. 1-11: Action of GPCRs[37] 21
Fig. 1-12: Basic map of 5-HT_2 agonist binding (Adapted from Monte *et al.*[42]) 23
Fig. 1-13: Tethered Analogues of 2,5-Dimethoxyamphetamines 24
Fig. 1-14: THBD-type ATS 24
Fig. 1-15: Substrates used by Parker *et al.*[47] in Binding Affinity Studies 27
Fig. 1-16: 5-HT_{2A} binding affinity (y-axis) correlated to lipophilicity of ligands (x-axis)[47] 28
Fig. 1-17: Substrates used by Schultz *et al.*[48] in Binding Affinity and Functional Potency Studies 30
Fig. 1-18: Substrates used by McLean *et al.*[49] in Binding Affinity and Drug Discrimination Studies 32
Fig. 1-19: Substrates used by Chambers *et al.*[50] in Binding Affinity Studies 33
Fig. 1-20: Two molecules of *(S)*-Citalopram (light blue) bound to SERT in central and allosteric sites[51] 35
Fig. 1-21: BDF **(15)**, *(S)*-Citalopram **(40)** and Paroxetine **(41)** 35
Fig. 1-22: LSD in the Orthosteric Cleft of 5-HT_{2B}[53] 36
Fig. 1-23: THBD **(42)** and Benzodifuran **(43)** 37
Fig. 1-24: 'Lid' formed by EL2 and the binding pocket[52] 38
Fig. 1-27: Substrates used by Ho *et al.*[58] in Functional Potency Studies 42

Fig. 1-33: Phenyl-2-propanone **(62)** analogue to Amphetamine **(1)** analogue 48
Fig. 1-34: Synthetic routes to Phenyl-2-propanone **(62)** 48
Fig. 1-35: Preparation of α-Phenylacetoacetonitrile **(67)** 49
Fig. 1-36: Preparation P2P **(62)** from α-Phenylacetoacetonitrile **(67)** 50
Fig. 1-37: Preparation of β-Nitrostyrene **(69)** 50
Fig. 1-37: Two Routes to P2P **(62)** from β-Nitrostyrene **(69)** 51
Fig. 1-39: Common synthetic routes from P2P **(62)** to Amphetamine **(1)** 52
Fig. 1-40: Leuckart Reaction and Hydrolysis to convert P2P **(62)** to Amphetamine **(1)** 53
Fig. 1-41: Pyrimidine formation in the Leuckart synthesis of Amphetamine **(1)** 54
Fig. 1-42: Pyridine and dihydropyridone impurities **79 - 84** arising from the Leuckart formation of amphetamine **(1)** from P2P **(62)**[85-87] 55
Fig. 1-43: Reductive Amination of P2P **(62)** to form Amphetamine **(1)** 55
Fig. 1-44: Iminium Cation **(85)** in the Reductive Amination of P2P **(62)** to form Amphetamine **(1)** 56
Fig. 1-45: Oxime Route to Form Amphetamine **(1)** 56
Fig. 1-46: Synthesis of Amphetamine **(1)** from β-Nitrostyrene **(69)** 56
Fig. 1-43: Potential Impurities in the Synthesis of Amphetamine **(1)** from β-Nitrostyrene **(69)** 57
Fig. 1-48: Small-scale clandestine laboratory[95] 58
Fig. 1-49: Large-scale “industrial” clandestine laboratory in Mexico[97] 59
Fig. 1-51: BDF **(1)**, 2C-B-FLY **(89)** and iTHBD **(90)** 65

List of Tables

Table 1-1: Binding activity and functional potency of **(29 - 32)**[48] 30
Table 1-2: Functional potency of **(14, 49 - 52)**[58] 42
Table 1-3: Functional potency of **(14, 56 - 58)**[58] 45
Table 1-4: Comparative *in vivo* activity of *p*-halogenated 2,5-dimethoxyamphetamines[10] 46

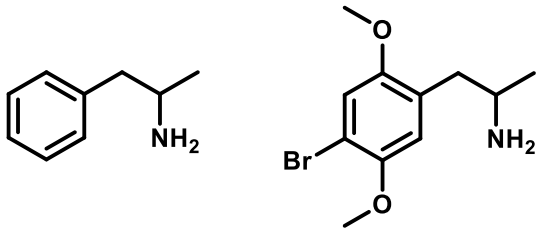
1 Introduction

1.1 The Amphetamine Family

Amphetamine **(1)** is a structurally simple molecule with the molecular formula $C_9H_{13}N$ and was first synthesised in 1887 by Lazar Edeleanu.[1] It was subsequently marketed in 1932 by Smith, French and Kline within an inhaler formulation to relieve nasal congestion.[2] However, in addition to its bronchodilator properties which led to its pharmaceutical development, amphetamine **(1)** also had other properties; most notably it is a powerful stimulant, which was used in a variety of situations, for example in World War II, where it was used to keep soldiers alert for longer. It was also used (legally) by laypeople for its stimulant properties, but unfortunately amphetamine **(1)** is also highly addictive and this stimulant use quickly led to stimulant abuse, which ultimately led to amphetamine **(1)** being declared a controlled substance in most jurisdictions.[2]

Amphetamine **(1)** itself is relatively easy to alter structurally due to its simplicity and as a result, there are many 'designer amphetamines'; amphetamine-type stimulants (ATS) that are designed to be structurally similar to amphetamine, but not identical, for example, the designer hallucinogen 2,5-dimethoxy-4-bromoamphetamine (DOB) **(2)** (see Figure 1-1).

There are often efforts to circumvent the controlled status of amphetamine **(1)** in many countries, and to confer desirable pharmacological effects. Consequently, designer amphetamines frequently have structures that are specifically designed to enhance certain effects of the drug, e.g. to confer a longer duration of action or greater hallucinogenic/entactogenic activity than amphetamine **(1)**. Note that although in some cases the stimulant effect of the structurally altered amphetamine substrate may be less than that of amphetamine **(1)** or may be overshadowed by a more dominant pharmacological effect (i.e. hallucinogenic or entactogenic properties), as a class, all 'designer amphetamines' are referred to as ATS.

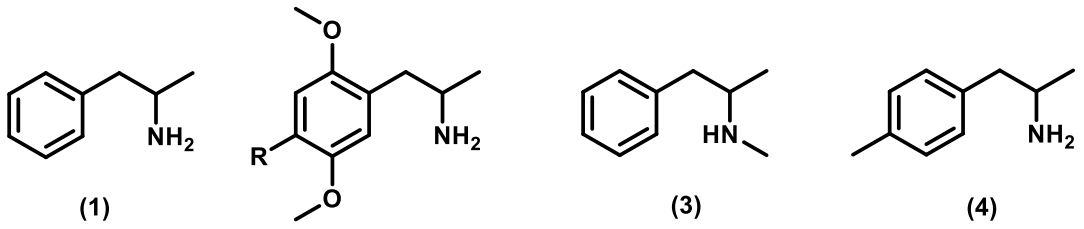


(1) (2)

*Fig. 1-1: Amphetamine **(1)** and DOB **(2)***

DOB **(2)** and other ATS pose a serious problem to law enforcement as it is difficult from a legislative perspective to keep up with the constant appearance of new compounds on the market: by the time the legislation has been designed to deal with known compounds, new ATS have already been released. This problem emphasises the need for researchers in the field of impurity profiling to keep up with new methods of synthesis and analysis to combat the speed with which designer amphetamines are developed. One potential method of circumventing this difficulty is to introduce legislation that forbids specific combinations of structural modifications to a specific core compound.[3]

ATS are compounds with amphetamine-type structures: they can have substituents on the phenyl ring, the isopropylamine side-chain and/or the nitrogen atom.[4] Amphetamine **(1)**, DOB **(2)**, methamphetamine **(3)**, *p*-methylamphetamine **(4)** and 2,5-dimethoxy-4-iodoamphetamine (DOI) **(5)** shown in Figure 1-2 represent a small number of the many known ATS.



(1) (3) (4)

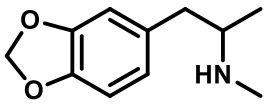
(2): R = Br
(5): R = I

Fig. 1-2: Examples of ATS

Illicit drugs can be classified in a number of different ways, including origin, pharmacological effect, and use (i.e. as an anaesthetic, to experience hallucinogenic effects, as a depressant, as a stimulant *etc*), with classification according to physiological response being a common method among researchers and law enforcement.[5] In keeping with this method of classification, there are five main categories into which illicit drugs can be classified: anabolic steroids, depressants, hallucinogens, narcotics and stimulants.[6]

Depending on the structure of the specific amphetamine and the dose taken, most ATS can be classed as stimulants and/or hallucinogens, though there are some exceptions. Stimulants are described as compounds that stimulate the central nervous system (CNS) causing alertness and interruptions to sleep.[7] Hallucinogens are described as drugs that alter perception of time and reality, affecting multiple senses (auditory, visual and kinesthetic in particular).[8]

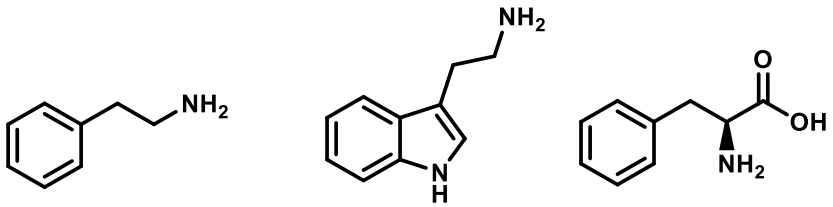
Some ATS, for example 3,4-methylenedioxymethamphetamine (MDMA, Ecstasy) **(6)**, are also considered to be entactogens (psychoactive drugs that induce distinguishing social and/or emotional effects).[9] As mentioned previously, it is possible for ATS to fit into classes apart from stimulants/hallucinogens as a result of their pharmacological versatility. The many pharmacological effects of amphetamines will be discussed in greater detail in Section 1.2.



(6)

Many hallucinogens have structures related to phenethylamine **(7)** or tryptamine **(8)** (see Figure 1-3).[10] Phenethylamines are based on a phenylalanine **(9)** backbone (i.e. their core structure mimics that of phenylalanine **(9)**), and act as neurotransmitters in the human CNS, leading to hallucinogenic effects.[11] The structure of amphetamine is very similar to

that of phenethylamine **(7)**, with the addition of a single methyl group to the α-carbon of the amino alkyl sidechain in amphetamine **(1)** when compared to phenethylamine **(7)**.



(7) **(8)** **(9)**

Fig. 1-3: Exogenous and Endogenous Neurotransmitters

The amphetamine family is wide-ranging, encompassing a seemingly infinite number of compounds, each with a slightly different structure and with slightly different pharmacological effects on the user. Different aspects of the amphetamine family (e.g. pharmacology, structure-activity relationships, synthetic routes, etc.) will be discussed at greater length in subsequent sections.

1.2 Pharmacology of Amphetamines

Pharmacology is the branch of medical science that concerns the uses, preparation and modes of action of pharmaceutically active compounds (PACs).[12] Neuropharmacology is a subset of this discipline, and is particularly concerned with the action of PACs in and on the nervous system.[13]

Neurons in the CNS interact by releasing signalling chemicals called neurotransmitters (NTs) at their points of interconnection, called synapses. All psychoactive drugs mimic or modify the release of NTs to realise their effect(s) on the CNS.

There are three discrete structures within neurons, as shown in Figure 1-4:

1. Cell body: this contains the nucleus and is responsible for protein and NT synthesis.
2. Axon: this is a filamental process which extends from the cell body and conducts signals from the cell to more distant neurons.
3. Dendrites: these are also filamental processes – multiple smaller out-branchings which receive signals from the axons of other neurons.

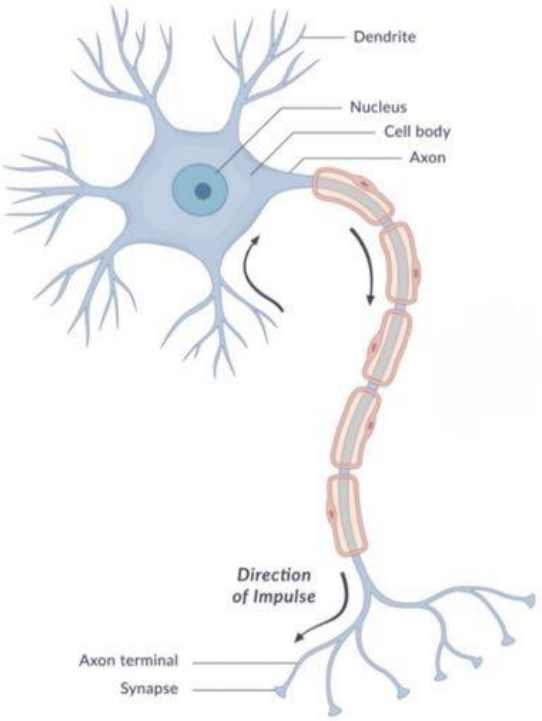


Fig. 1-4: Diagram of a neuron[14]

Neurotransmission occurs *via* release of NTs at the terminus of the axon, but the signal inside the neuron to release NTs is actually an electrochemical action potential radiating down the axon; this happens once an overall stimulus occurs that exceeds a certain threshold strength. The action potential is maintained *via* a sodium/potassium ion pump/gradient system; therefore the neuron acts like a biological capacitor, with the release of the action potential comparable to a depolarisation pulse.[15]

Once the action potential reaches the end of the axon and the NT is released into the space between neurons – known as the synapse or synaptic cleft – the NT is free to cross the narrow synaptic cleft and interact with a receptor on

another neuron. In general, the neuron from which the NT is released is known as the 'presynaptic neuron' and the neuron to which the NT then binds is known as the 'postsynaptic neuron'. However, the NT released from the presynaptic neuron can also bind to regulatory binding sites on the same neuron and upregulate or downregulate NT production.[15] In the following discussion, we will focus on the response of the postsynaptic neuron only.

Depending on the NT released, the postsynaptic neuron responds in one of two ways:[15]

- A receptor corresponding to a transmitter or ligand-gated ion channel is activated, resulting in an excitatory or inhibitory response (dependant on the NT and the channel).
- The NT binds to a G-Protein Coupled Receptor (GPCR), which in turn releases signalling molecules: these can produce widely varied results depending on the postsynaptic neuron activated.

This process is summarised graphically in Figure 1-5.

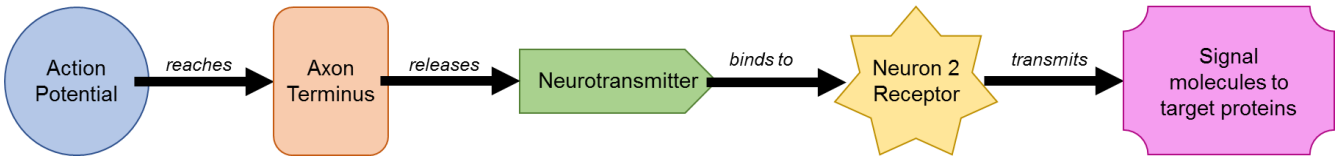


Fig. 1-5: Communication between neurons

1.2.1 Amphetamine Pharmacology

ATS can cause a variety of physiological responses, depending on the structure of the compound, the dose administered, and the method of administration. Most amphetamines are ingested orally, although many can also be administered intravenously or insufflated.[16]

Amphetamine **(1)** and ATS often generate a psychotropic response. They can alter perception, mood and behaviour and lead to extended periods of wakefulness and arousal. Even short-term use of small doses of ATS can cause serious cardiovascular problems, and long term use can lead to violent

behaviours as well as causing serious structural and functional changes to the brain.

Long-term amphetamine **(1)** use can also lead to a state of paranoid psychosis known as 'amphetamine psychosis' (this can also be more broadly referred to as 'stimulant psychosis' and is associated with long-term use of a broad variety of psychostimulants, a group which includes amphetamine **(1)**).[17] Symptoms include delusions of persecution and omnipotence, and visual and auditory hallucinations are also common. Amphetamine psychosis is often indistinguishable from normal psychosis, even for medical professionals; however, amphetamine psychosis tends to fade in a matter of days to weeks once the individual goes through withdrawal.[15]

1.2.2 Mechanism of Action

The pharmacological effect of ATS is mostly due to their similarities to endogenous neurotransmitters such as dopamine **(10)**, noradrenaline **(11)** and serotonin **(12)** (as seen in Figure 1-6).

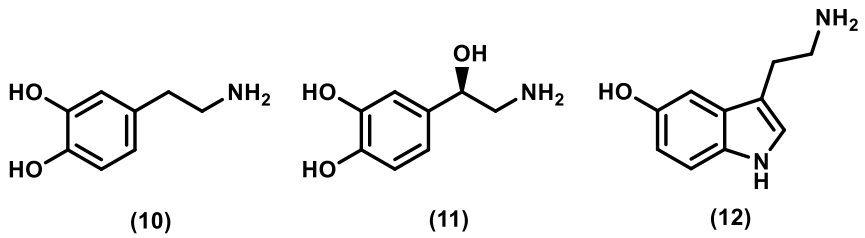


*Fig. 1-6: Dopamine **(10)**, Noradrenaline **(11)** and serotonin **(12)***

Due to these structural similarities, amphetamines can have a number of effects on brain chemistry:[15]

- Enhancement of catecholamine release.
- Inhibition of catecholamine re-uptake.
- Inhibition or enhancement of serotonin **(12)** uptake.
- Stimulation of α-adrenergic receptors.
- Stimulation of serotonin receptors (5-HT_{2A}, 5-HT_{2C})

Biologically active ATS are what are known as 'sympathomimetic amines', meaning that they mimic the effects of certain NTs in the sympathetic nervous system. The stimulant effects of ATS are caused by the forced release of catecholamines from neurons in the CNS.

Biologically active ATS have two catecholamine-related mechanisms of action. The first is release of dopamine **(10)**: as the amphetamine core is so structurally similar to dopamine **(10)** and other catecholamines in structure, ATS can bind to the catecholamine transporters at receptor sites and be transported into the neurons, where they are released. The transporters then bind to dopamine **(10)** and other catecholamine molecules, which they transport into the synaptic cleft when they leave the cell. This reduces levels of catecholamine NTs in the cytosol and causes the catecholamine concentration in the synaptic cleft to increase.[18]

The second catecholamine-related mechanism of action of ATS involves inhibition of reuptake of endogenous NTs. This is the main cause of ATS' stimulant effects. In normal circumstances, the effects of catecholamine NTs are stopped by reuptake of the NT into the presynaptic terminal. ATS with strong stimulant effects (as opposed to hallucinogenic or entactogenic) are highly effective inhibitors of this reuptake mechanism. This action is also responsible for high levels of catecholamine NTs in the cytoplasm of cells, generally in the brain and CNS.[19] In the short term, this high level of neurotransmitter leads to increased arousal and a decreased ability to sleep.[18] In the long term, catecholamine depletion can play a role in amphetamine psychosis and can lead to Parkinson's-type symptoms.[20]

The mechanism of action of psychotropic ATS, more commonly known as hallucinogens, differs from that of ATS with a stimulatory effect (and also from those with an entactogenic effect, though those are not discussed in this work) and primarily involves the agonism of serotonin receptors. This neuropharmacology will be covered in depth in Section 1.3.

As discussed later in Section 1.4, there are numerous substitution sites on both hallucinogenic and stimulatory ATS, leading to a huge number of possible permutations and variations in structure. As each structural change will cause a slightly different physiological effect, it is very difficult to make a general statement about the pharmacology of ATS (their effects, duration of effect, onset of actions, etc).

1.3 Hallucinogens

Hallucinogens, also known as psychedelics or psychotropic drugs, are a broad class of compounds encompassing many structural variations. Typically, they can be split into three main sub-categories based on their core structure: tryptamines, amphetamines and ergolines.[21]

There is a long history of psychedelic use, some of it predating written records, particularly in religious or spiritual contexts; for example, the use of *peyote* in Native American religious services (as seen in Figure 1-7) or the use of *teonanacatl* (psilocybins) in Aztec rituals.[22]



Fig. 1-7: Use of peyote in Native American religious services[23]

The physiological effects of hallucinogens on humans can be broadly divided into three categories based on the symptoms usually expected at low doses:[24]

- Somatic symptoms: dizziness, drowsiness, blurred vision, weakness, tremors, nausea
- Perceptual symptoms: altered shapes/colours, difficulty focusing, synaesthesias (rare)
- Psychic symptoms: alteration in mood, dreamlike feelings, depersonalisation, visual hallucinations

Many drugs are infamous for their addictive properties, however, this is not the case for most hallucinogens. This is hypothesised to be because they have little to no effect on dopamine neurotransmission, which appears to be a prerequisite for dependency.[25] Hallucinogens do have other dangers however: they can be responsible for injury and/or death due to depersonalisation and altered perceptions of reality (e.g. believing one can fly), they can lead to death by overdose, and can trigger psychosis and/or

depression, though usually only in persons who are predisposed towards these conditions.[22]

One commonly referenced side-effect of hallucinogen use is the occurrence of so-called 'flashbacks', more correctly known as Hallucinogenic Persisting Perception Disorder (HPPD), in which users re-experience the symptoms of hallucinogen use long after the effects of the actual dose have faded. While HPPD was widely discussed in the press particularly in the 1970s and 1980s, it is difficult to quantify these cases. However, the low numbers of substantiated reports combined with the high number of reported users leads to the conclusion that the actual incidence of HPPD is quite low.[26]

Another striking difference between hallucinogens and most other pharmaceutically active compounds which act in the CNS is the environmental influence on physiological effects: the expectations of the user (or 'set') and the environment in which the drug is taken or administered (the 'setting') can have a strong effect on the experience of the user, which gives an unpredictability which does not exist for other classes of compound. This lack of predictability extends to the varying effects of dosage: a high dose of a hallucinogen does not necessarily equal the same symptoms as a lower dose with greater intensity, but can lead to symptoms that are unique to the compound at that dose.[22]

1.3.1 Neuropharmacology of Psychotropic Amphetamines

Since the discovery of lysergic acid diethylamide (LSD) **(13)** in 1943,[22] a key goal in neuropharmacology has been to understand its mechanism of action, along with that of the other psychotropic drugs which have been discovered in the intervening seventy years. This task has proved challenging owing to the great complexity and number of receptor sub-types which have been proven to be involved, the most important of which will be discussed here.

Arguably the most important of these receptors with regards to the activity of psychotropic compounds is the serotonin or 5-hydroxytryptamine receptor, abbreviated as the 5-HT class. There are seven general types of 5-HT

receptors and fourteen subtypes, mostly G-Protein Coupled Receptors, with the exception of 5-HT_3, which is a ligand-gated ion receptor.[27]

While a number of human studies have been carried out using hallucinogens, these are limited in number, and were mostly carried out as psychological studies in the 1950s and 1960s: most of the mechanistic studies into hallucinogens have been carried out as drug discrimination studies in rats. This involves training rats to discriminate between saline and a training drug (usually LSD **(13)**, DOI **(5)** or 2,5-dimethoxy-4-methylamphetamine (DOM) **(14)** as shown in Figure 1-8).

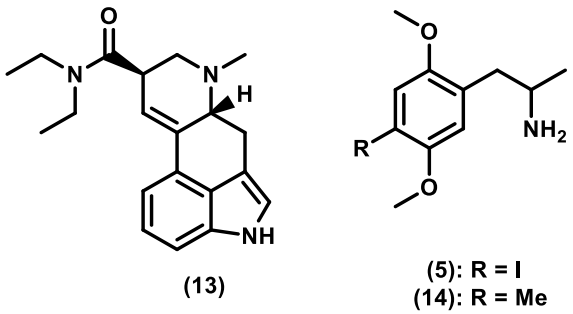


*Fig. 1-8: LSD **(13)**, DOI **(5)** and DOM **(14)***

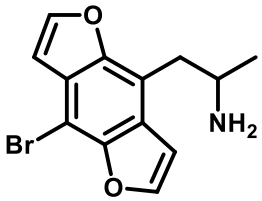
The rats then provide an indication of whether or not the test drugs have similar effects to the training drugs, and can also be used as a measure of potency. This has proven to be a robust method of determining hallucinogenic activity in the absence of human testing.[22]

Serotonin **(12)** was isolated and identified as a NT around the time that LSD **(13)** was discovered. The structural similarities (both have an indole incorporated into the core of the molecule with an amine moiety connected to the indole by an ethylene bridge: in LSD **(13)** this bridge is part of a cyclised system) and the possibility that LSD **(13)** could therefore act at serotonin receptors were soon realised.

A number of studies in the 1950s reported the interaction of LSD **(13)** with 5-HT receptors,[28] and many subsequent studies elaborated on the potential mode of action of hallucinogens at 5-HT receptors. At first, it was suspected

that hallucinogens acted to blockade 5-HT receptors in the CNS,[29] however, this theory was soon discarded in light of discoveries which suggested that hallucinogens actually act as agonists of 5-HT receptors.[30] Despite the extensive study dedicated to the topic, the first proof that hallucinogens work primarily at 5-HT_2 receptors was not reported until 1983 by Glennon *et al.* during drug discrimination studies using rats dosed with 5-HT_2 antagonists, which blocked the stimulus effects of phenethylamine and tryptophan hallucinogens.[31]

Similar studies were conducted to demonstrate that the 5-HT_{2A} receptor subtype is most integral to hallucinogenic action: for example, Bromo-DragonFLY (BDF) **(15)** is a potent agonist of the 5-HT_{2A} receptor (though it cannot be considered completely selective as it also interacts with the 5-HT_{2C} receptor).[27] Activity at both the 5-HT_{2A} and 5-HT_{2C} receptors is a common feature of hallucinogens, as these receptor subtypes have about 80 % genetic homology in their amino acid sequence, making selectivity difficult,[32] but the 5-HT_{2A} interactions play a bigger role in the actions of hallucinogens,[33] with the correlation between 5-HT_{2A} receptor affinity and human hallucinogenic potency being very strong indeed ($r^2 = 0.94$).[34]



(15)

The gene for the 5-HT_{2A} receptor is located on chromosome 13 and the receptor plays a role in regulating sleep, appetite, and body temperature, as well as affecting muscle contraction and cardiovascular function. The receptor also plays an important role in neuropsychiatric disorders and thus stimulating it can have more pharmacological effects than triggering hallucinations.[27,35]

1.3.2 Mechanism of Action of NTs and Sympathomimetic Amines at 5-HT$_2$ Receptors

As mentioned previously, the majority of 5-HT receptors are G-protein coupled receptors. These consist of seven connected, trans-membrane *α*-helices (Figure 1-9), which extend through the cell membrane into the cytoplasm to connect with G-proteins.

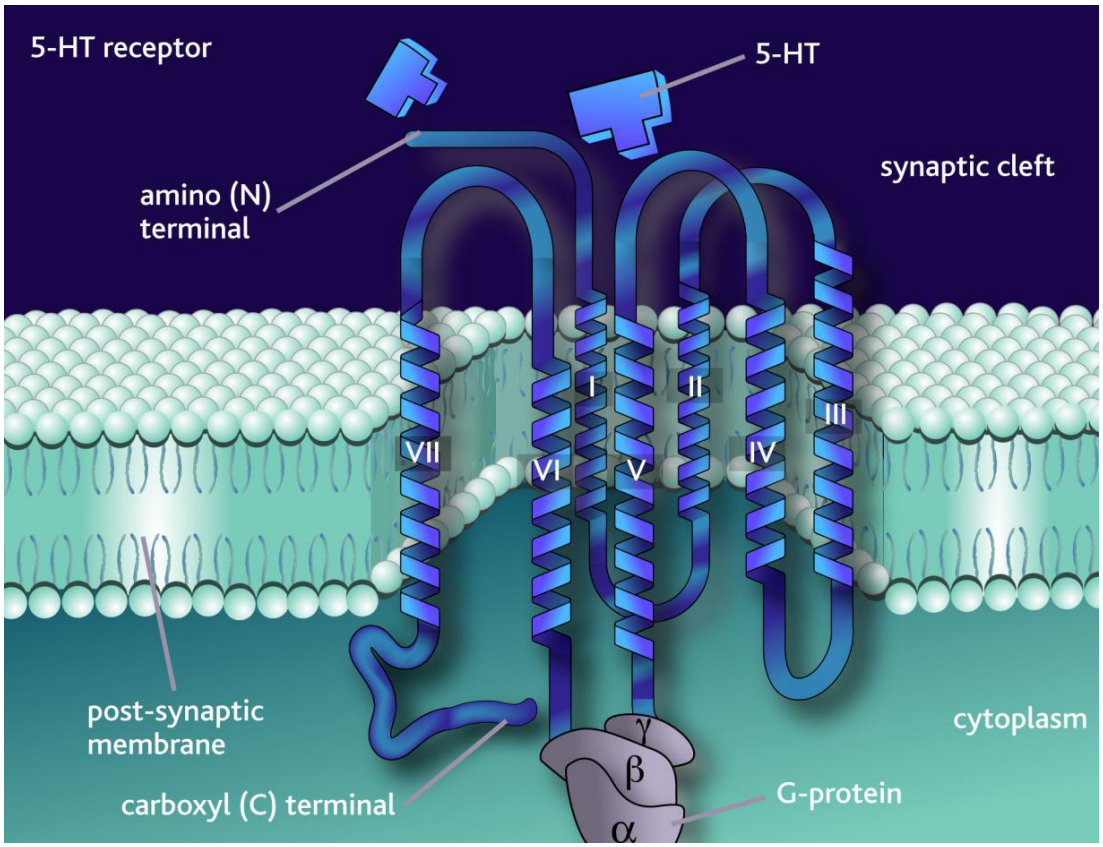


Fig. 1-9: 5-HT GPCR type transmembrane receptors[7]

When serotonin or a structurally similar molecule binds to the extracellular binding site of the receptor, these helical extensions alter, revealing a binding site for the G-protein. Once the G-protein binds, it releases a molecule of guanosine diphosphate (GDP) **(16)** (see Figure 1-10).

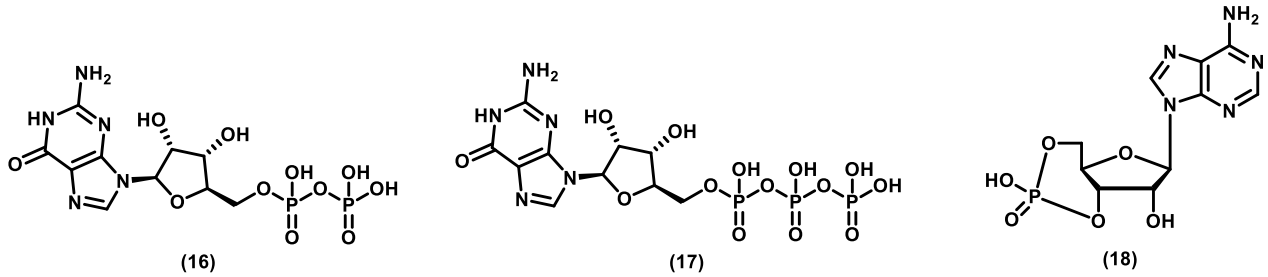


*Fig. 1-10: GDP **(16)**, GTP **(17)** and cAMP **(18)***

The empty binding site left behind is topographically altered so that a molecule of guanosine triphosphate (GTP) **(17)** can bind to it. When the GTP binds to a G-protein, the G-protein dissociates from the receptor, and binds to and activates an enzyme (the enzyme activated depends on the G-protein α-subunit) that produces cyclic adenosine monophosphate (cAMP) **(18)**, which is a major intercellular messaging molecule that produces a response in the target cell (this is illustrated in Figure 1-11). cAMP **(18)** can produce a widely varied response depending on the postsynaptic cell.

This allows for a diverse response from different postsynaptic neurons to the same initial neurotransmitter, and also amplifies the message as one neurotransmitter produces many cAMP **(18)** molecules.[15] A protein that regulates G-protein signalling (RGS protein) then mediates the hydrolysis of GTP **(17)** back to GDP **(16)** (i.e. loss of one phosphate group, labelled P_i in Figure 1-11), thereby deactivating the G-protein and returning it to a dormant state awaiting the next NT signal.[36]

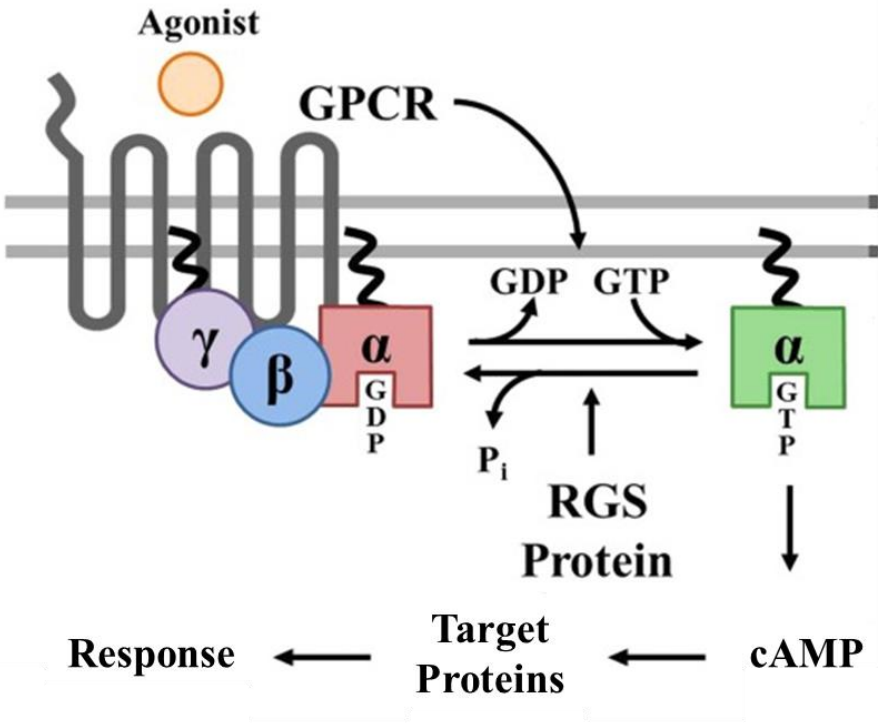


Fig. 1-11: Action of GPCRs[37]

The binding affinity of neurotransmitters for G-protein coupled receptors is generally higher than for ligand ion transmission receptors because the binding site is deeper in the receptor, therefore neurotransmission at G-protein coupled receptors tends to be prolonged, leading to the extended duration of action associated with ATS which interact primarily at 5-HT_2 receptors (e.g. the duration of action of BDF **(15)** in humans can be up to 48 hours, depending on the dose taken).[15,38]

1.3.3 Mapping the Active Site of 5-HT_2 Receptors

Since the confirmation of 5-HT_{2A} as the primary site at which hallucinogens act, molecular determinants for agonist binding at this site have become of particular interest so as to understand the physiological role of endogenous serotonin at this site. This goal is complicated because a wide variety of compound types appear to mediate their effects *via* 5-HT_{2A} activation (i.e. tryptamines, ATS, ergolines). Studies show that serotonergic hallucinogens exhibit symmetrical cross-tolerance (meaning that developing a tolerance to one compound of this type also confers tolerance to other compounds of this

type). Combined with their similar physiological effects this suggests a common mechanism of action.[34] This – along with the near-certainty that while 5-HT_{2A} may be the most crucial receptor subtype in hallucinogenic activity, other receptors are also likely to be involved[34] – makes it difficult to visualise what the functional topography of 5-HT_{2A} might be.[21]

The issue is further complicated by the fact that 5-HT_{2A} receptors are coupled to several different signalling pathways and there is some evidence that the 5-HT_{2A} response which mediates serotonergic hallucinogen response may also involve multiple signalling pathways (based on *in vivo* studies in mice).[34] This pleiotropism is known as 'functional selectivity', and in practice it means that as it is very difficult to tell which G-proteins are activated after a ligand binds: different agonists produce wildly different physiological effects by apparently binding at the same binding site on the same receptor.[22] Pleiotropism as a feature of 5-HT_2 receptors leads to difficulties both in mapping the binding site of the receptor, and in establishing a mechanism of action for hallucinogens, most of which are still not fully understood.

The most common approach adopted in the quest to solve these conundrums is the synthesis of highly selective ligands to act as potent 5-HT_{2A} agonists: by investigating the structure-binding affinity relationship for these ligands with the 5-HT_{2A} and 5-HT_{2C} receptors, it is possible to draw conclusions about potential topography for the active binding sites of these receptors.

From studies discussed in more detail in Section 1.4, it was discovered by Shulgin in the 1960s (and refined by Nichols in the 1980s) that the optimal substitution patterns for hallucinogenic amphetamines is to have a 2,4,5-trisubstitution pattern on the aromatic ring, with methoxy groups in the 2- and 5-positions and a lipophilic substituent in the 4-position (commonly a halogen or methyl group).[39-41] This facilitated the development of a basic map for 5-HT_2 agonist binding, which starts to build a picture of the general topography of the binding sites in these receptors. An adapted version of this basic map using a BDF-type phenethylamine as a prototypical example is shown in Figure 1-12.

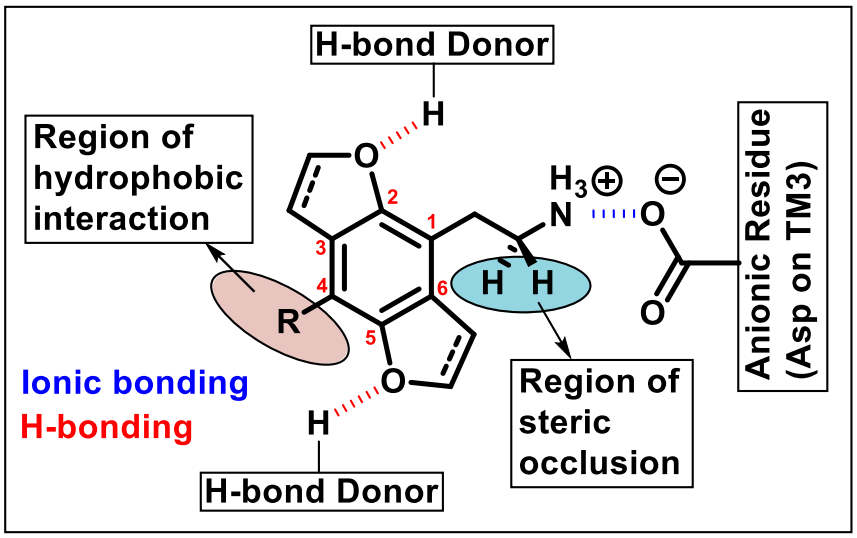


Fig. 1-12: Basic map of 5-HT_2 agonist binding (Adapted from Monte et al.[42])

In 1996, Monte *et al.* investigated this topography further by synthesising a series of tethered analogues of 2,5-dimethoxyamephetamines, with variants including a substrate with the 5-ether incorporated into a ring connected at C-4 on the aromatic ring **(19)**, a substrate with the 5-ether in a ring connected at C-6 **(20)** and the final analogues with the 2-ether in a ring which incorporates the aminoalkyl sidechain **(21 - 23)** (shown in Figure 1-13).

The conformational restriction conferred by the introduction of ring systems ensures that the oxygen lone pair of electrons in **19** are oriented *syn* to (or pointing towards) the aminoalkyl sidechain, while the lone pairs in **20** and **21 - 23** are *anti* to (or pointing away from) the sidechain (note: this refers only to the lone pairs on oxygen atoms incorporated into the ring systems. The oxygen

atoms of the methoxy groups are not conformationally restricted by ring systems and thus have no static orientation of lone pairs).[42]

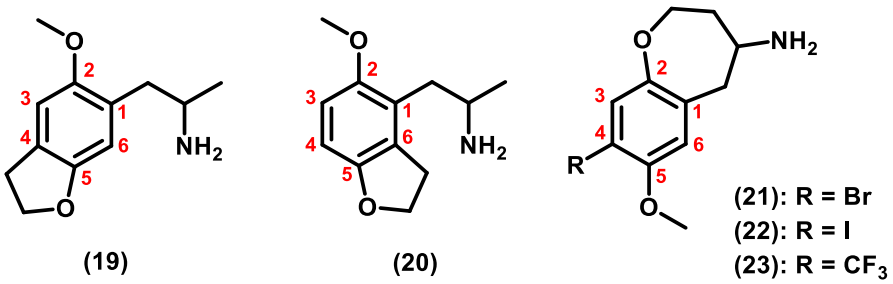


Fig. 1-13: Tethered Analogues of 2,5-Dimethoxyamphetamines

Binding affinity studies showed that **19** has greatly attenuated activity at 5-HT receptors compared to the untethered analogue (ED_{50} = 6.99 *µ*mol/kg *versus* 0.60 *µ*mol/kg for DOM **(14)**, a 12-fold decrease),[43] while **20** also has attenuated activity although to a lesser extent (ED_{50} = 5.23 *µ*mol/kg *versus* 0.60 *µ*mol/kg for DOM **(14)**, a 9-fold decrease),[43] which leads to the conclusion that the *anti* orientation of the oxygen lone pair in the 5-position is more favourable for intrinsic activity. The compounds **21 - 23** all had greatly attenuated binding activity, suggesting that the *anti* orientation of the oxygen lone pair in the 2-position is unfavourable, and that *syn* orientation would yield better results.[42]

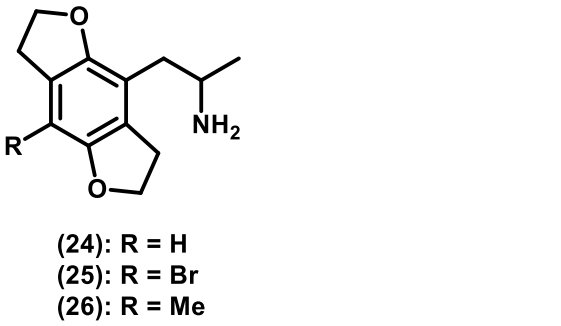


Fig. 1-14: THBD-type ATS

The same study reported the synthesis of a number of extremely potent analogues (**24 - 26)** of DOB **(2)** (shown in Figure 1-14),[42] in which the 2,5-ether substituents were incorporated in dihydrofuran rings in an attempt to

confirm hypotheses put forward in previous studies by Westkaemper and Glennon[44] that identified a number of serine residues in transmembranal helices (TM) 3 and 5 of the 5-HT_{2A} receptor which were determined as the most likely points of interaction for the 2,5-dimethoxy moieties, and to confirm their own findings regarding the *syn/anti* conformational requirements.

All of the analogues **24 - 26** were found to be extremely potent 5-HT_{2A} agonists in *in vivo* drug discrimination studies (using rats), with **25** found to be only slightly less potent than LSD **(13)** (ED_{50} = 0.061 mmol/kg *versus* 0.040 mmol/kg for LSD **(13)**) and in keeping with previously understood structure-activity relationships (SAR) requirements with respect to the need for a lipophilic substituent in the 4-position, **25** was more potent than **24** (ED_{50} = 0.061 mmol/kg *versus* 4.00 mmol/kg for **24**).

Not only did this result confirm the conformational requirements to have the 2 and 5-oxygen substituents (and thus their lone pairs of electrons) in *syn* and *anti* orientations respectively, but, assuming that the protonated amine interacts with an aspartate residue on TM3 as suggested by molecular modelling studies of GPCRs,[45] it also confirmed the conformation in which the putative H-bond donors to the 2,5-oxygen substituents must approach, strengthening the hypotheses previously put forward by Westkaemper and Glennon.[44]

Following on from the work of Monte *et al.*,[42] Parker *et al.* published a paper detailing the synthesis and *in vivo* activity of 1-(8-bromobenzo[1,2-*b*:4,5-*b'*]difuran-4-yl)propan-2-amine **(15)**, a highly potent 5-HT_{2A} agonist that would later become known as Bromo-DragonFLY.[46]

The extreme potency of **25** was discovered in a drug discrimination study in rats (ED_{50} = 61 nmol/kg versus 40 nmol/kg for LSD **(13)**), which was consistent with a binding site model previously proposed by Westkaemper and Glennon, in which there were two hydrogen-bond-donor residues lying at either side of the receptor which engage in hydrogen bonding with suitable substituents in the 2- and 5-positions of the aromatic ring. It was hypothesised that the

increased activity of **25** compared to its untethered analogue DOB **(2)** was due to the fixing of the oxygen atom lone pairs in the 2- and 5-positions into favourable conformations for hydrogen bonding. Based on this work, it was thought that conversion of **25** to its fully aromatised benzodifuran analogue **(15)** would provide valuable information about the effect of differing electronic systems on the agonist activity at 5-HT_{2A} receptors once hydrogen-bonding capacity had already been maximised.[46]

To this end, BDF **(15)** was synthesised and tested for its binding affinity to 5-HT_{2A} using rat cortical homogenates, where it was found to have 60-fold higher binding activity than its non-aromatised analogue **25** (K_i = 0.23 nM *versus* 14.8 nM for **25**). In a drug discrimination study using rats trained to discriminate LSD **(13)** from saline, it was found to have an ED_{50} of 22 nmol/kg, making it almost three times more potent than **25** (ED_{50} = 61 nmol/kg) and almost twice as potent as LSD **(13)** (ED_{50} = 40 nmol/kg), which is correlated to full efficacy at the 5-HT_{2A} receptor.[46] This makes it the first 5-HT_{2A} agonist to out-perform LSD **(13)** in a drug discrimination test, and the most potent 5-HT_{2A} agonist currently published in the literature (as of October 2019).

BDF **(15)** was also found to have double the affinity for the 5-HT_{2C} receptor compared to the 5-HT_{2A} receptor when tested using cloned human 5-HT receptors (K_i = 0.02 nM at 5-HT_{2C} versus 0.04 nM at 5-HT_{2A}), making it the most potent known agonist of the 5-HT_{2C} receptor subtype as well. While the binding affinity for 5-HT_{2C} was greater, it was not selective enough (between 5-HT_{2A} and 5-HT_{2C}) to selectively bind to one over the other, despite the original hopes of the authors. This strong binding affinity for both subtypes reinforced that the agonist binding sites on these receptor isoforms must be largely homologous.[46]

Parker *et al.* further investigated the extreme potency of BDF in a follow-up study looking at the differences in binding affinity and *in vivo* potency between BDF **(15)**, **25**, **27** and **28** (shown in Figure 1-15).[47]

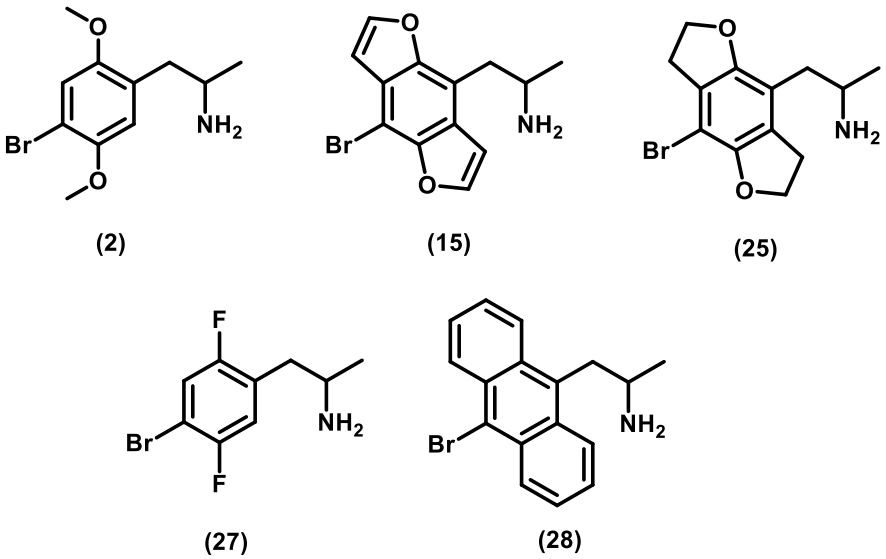


Fig. 1-15: Substrates used by Parker et al.[47] in Binding Affinity Studies

In their paper from 1998, Parker *et al.* determined that BDF **(15)** has greater potency and binding affinity than **25**;[46] in their follow-on work in 2008, they investigated two main hypotheses to explain this increased activity. These hypotheses were:[47]

1. Reduced hydrogen bond acceptor strength
2. Extended aromatic system

To test these hypotheses, **27** and **28** were synthesised and tested, using rat cortical homogenates to test binding affinity to 5-HT_{2A} and a drug discrimination study using rats trained to discriminate LSD **(13)** from saline to test the *in vivo* activity. Both **27** and **28** showed reasonable binding affinity of K_i = 2505 nM **(27)** and 313 nM **(28)**, however they lacked agonist activity (both acting as antagonists), with neither **27** nor **28** displacing LSD **(13)** in the drug discrimination study. This data implies that the 2,5-ether substituents are vital for agonist activity *in vivo*, as neither decreased hydrogen bond acceptor ability (in the case of **27** and **28**) nor extended aromaticity (in the case of **28**) were

enough to compensate for their removal (it is important to note that other studies have shown that expansion from a dihydrofuran to a dihydropyran moiety leads to decreased activity in **25**,[48] which may contribute to the attenuation of agonist activity in the case of **28**).

It was also noted that **27** (an antagonist) had significantly lower binding affinity for the 5-HT$_{2A}$ receptor subtype than DOB **(2)**, a powerful agonist (Ki = 2505 nM for **27** in comparison to 22 nM for DOB **(2)**).[47] This is interesting as it could be argued that DOB **(2)** is a better comparative substrate for **27** than BDF **(15)** or **25**, as it has no conformational restriction around the 2- and 5-ether positions. This offers further proof that having decreased hydrogen bond acceptor ability in the 2- and 5-positions has no beneficial effects on the binding affinity or agonist properties of a substrate.

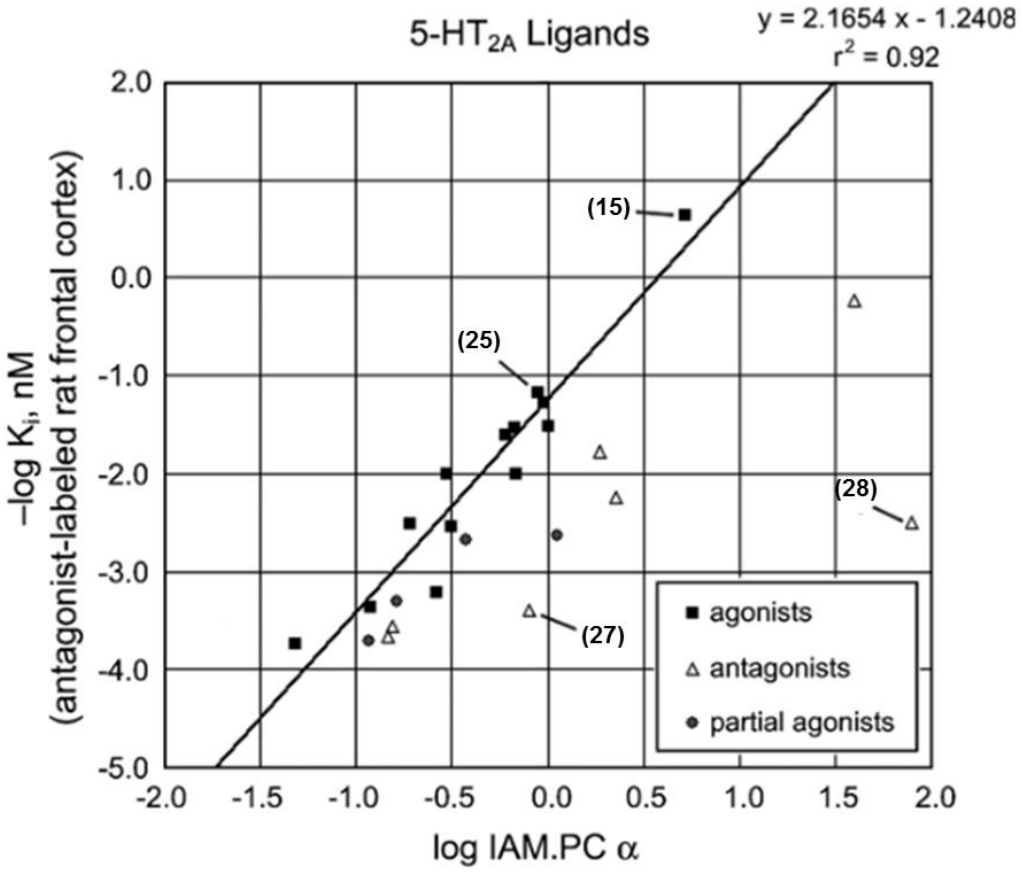


Fig. 1-16: 5-HT$_{2A}$ binding affinity (y-axis) correlated to lipophilicity of ligands (x-axis)[47]

Looking for another way to explain the increase in both binding activity and agonist potency from **25** to BDF **(15)**, Parker *et al.* tested the lipophilicity of a series of known 5-HT_{2A} agonists (including **25**, **27** and **28**) using a high performance liquid chromatography (HPLC) technique that employed an immobilised-artificial-membrane column with phosphatidylcholine head groups and then correlated their results with receptor binding affinity as seen in Figure 1-16.[47]

They found a strong correlation ($r^2 = 0.92$) between increased lipophilicity and binding affinity of those compounds classed as 5-HT_{2A} agonists and concluded that the relationship between these properties is linear for those compounds,[47] which is likely a function of the increased lipophilicity allowing deeper ingress into the hydrophobic binding site for agonists on the 5-HT_{2A} receptor.[21]

With regards to the activity of BDF **(15)** compared to **25**, Parker *et al.* concluded that the full aromatisation of the THBD system reduced the hydrogen bond acceptor ability, thereby rendering the ligand more lipophilic. However, BDF **(15)** is still capable of hydrogen bonding to the relevant serine residues (Ser-159 on TM3 and Ser-239 on TM5)[32] *via* the furan oxygen atoms, making BDF **(15)** an extremely potent agonist ligand.[47] This conclusion was echoed by Schultz *et al.*, who also noted that serotonin **(12)** possesses a bicyclic aromatic system, and so the extended aromatic system of the benzodifuran moiety in BDF **(15)** better mimics the indole system, and provides a greater area for π-π stacking interactions with aromatic residues in the binding site of the receptor.[48]

The same study by Schultz *et al.* further investigated the topography of the 5-HT_{2A} active site by synthesising a series of analogues **(29 - 32)** of **25** and BDF **(15)** with dihydropyran rings instead of dihydrofuran or furan rings (shown in Figure 1-17).[48]

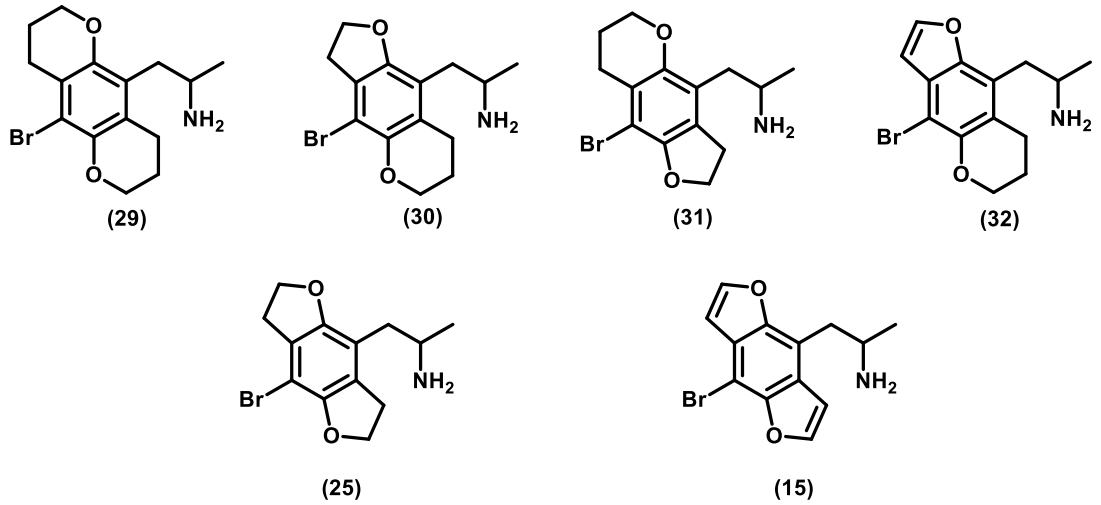


Fig. 1-17: Substrates used by Schultz et al.[48] in Binding Affinity and Functional Potency Studies

They then tested **(29 - 32)** to determine their binding affinity (K_i) to 5-HT_{2A} receptors in rat cortical homogenates, as well as functional potency (EC_{50}) using an inositol phosphate accumulation assay. These results are summarised in Table 1-1.

Compound	**25**	**29**	**30**	**31**	**32**
K_i (nM)	1.0	3.1	3.6	5.3	1.0
EC_{50} (nM)	13	258	19	78	13

*Table 1-1: Binding activity and functional potency of **(29 - 32)**[48]*

Replacing the two dihydrofuran rings of **25** with dihydropyran rings in compound **29** caused a 3-fold decrease in binding affinity to 5-HT_{2A}, implying that the receptor space around one or both oxygen lone pairs is sterically restricted. Virtual docking experiments suggest that the 5-HT_{2A} receptor binding site has greater steric tolerance around the oxygen moiety that is projected up towards the extracellular face of the receptor than it does around the oxygen moiety that points down into the receptor binding site. This, combined with the functional potency data for **30** and **31**, suggests that the

oxygen atom of the 2-ether is oriented downwards in the binding cavity while the oxygen atom of the 5-ether is projected upwards towards the extracellular face of the receptor.[48]

Compounds **30** and **31** both had 4 - 5 fold lower affinity than dihydrofuran analogue **25**, suggesting that the smaller rings of **25** are more compatible with the receptor binding site in both positions, while **32** had receptor affinity approximately 4-fold higher than the analogue **30** and on par with **25**, which is consistent with previous findings that extended aromaticity increases affinity.

While there was no significant difference in binding affinity noted for **30** versus **31**, the functional potency of **30** is around 4-fold greater than **31** and approximately equal to that of **32**, supporting the theory that the environment around the 2-ether in the receptor binding space is more sterically sensitive than its 5-ether counterpart, as affinity is a measure of how tightly the ligand binds to the receptor, while potency is a measure of the general complementarity between ligand and receptor. Thus these findings demonstrate that the agonist binding site of 5-HT_{2A} receptors is narrow and ill-equipped to deal with increased steric bulk, while also offering vital insights in the orientation of phenylalkylamines within the binding pocket, with the 2-ether placed deeper in the binding site than the 5-ether.[48]

A great deal of other work has been done to investigate the potential topography and structural tolerance of the 5-HT_{2A} binding pocket; this includes work by Chambers *et al.*,[21] who concluded that some of the increased affinity/potency of the fused ring systems in dihydrofuran analogues of DOB **(2)** is due to the orientation of the alkylamine side-chain, which in the rigid molecules (those with the ethers incorporated into a ring) is fixed in an periplanar position perpendicular to the aromatic core. If the out-of-plane rotamer is the biologically active species, the rigid analogues would have the advantage of spending the majority of their time in this conformation, thereby increasing their binding site compatibility compared to the 2,5-dimethoxy

analogues which have free rotation and would cycle rapidly through energy states.[21]

This hypothesis was later supported by experimental work conducted by McLean *et al.*, who synthesised a series of analogues of 2,5-dimethoxy-4-bromophenethylamine (2C-B) **(33)** with conformationally constrained alkylamine sidechains **(34 - 36)** (shown in Figure 1-18).[49]

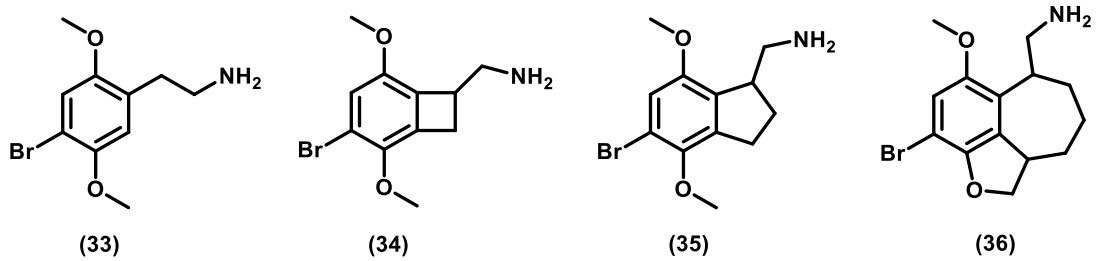


Fig. 1-18: Substrates used by McLean et al.[49] in Binding Affinity and Drug Discrimination Studies

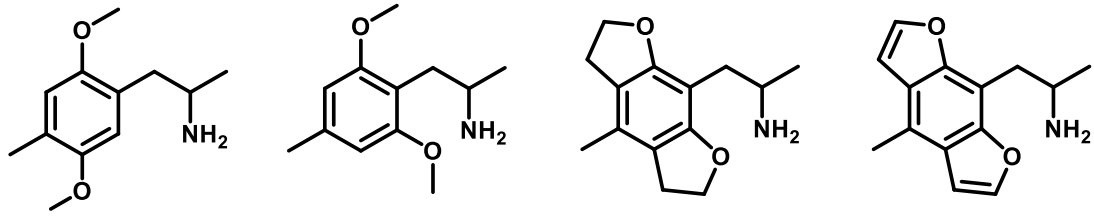
The *(R)*-enantiomer of cyclobutane analogue **34** was shown to be an extremely active 5-HT_{2A} agonist, proving 11-fold more potent than DOI **(5)** (ED_{50} = 24 nmol/kg for *(R)*-**34** compared to ED_{50} = 270 nmol/kg for **5**) and equipotent to LSD **(13)** (ED_{50} = 38 nmol/kg) in drug discrimination studies in rats. The *(S)*-enantiomer of **34** proved practically inactive, with no response recorded at a dose of 250 nmol/kg.[49]

McLean *et al.* did not carry out drug discrimination studies using **35** and **36** (both racemates), but both were shown to have attenuated binding affinity (K_i = 47 and 74 nM respectively) compared to 2C-B **(33)** (K_i = 0.88 nM) and *(R)*-**34** (Ki = 0.26 nM). Docking studies confirmed that the conformation of the alkylamine sidechain in *(R)*-**34** is perpendicular to the plane of the aromatic ring as previously hypothesised by Chambers *et al.*[21,49]

Another interesting point to note in McLean's work was that cyclobutane analogue *(R)*-**34** was found to be moderately functionally selective, with a 65-fold preference for activation of phosopholipase C (PLC) signalling pathways

over other responses in the 5-HT$_{2A}$ receptor, a hint that maybe the key to unlocking the holy grail of functional selectivity may lie at least partially in understanding the alkylamine sidechain conformation and interactions within the binding pocket of the receptor.[49]

More work by Chambers *et al.* in a different study tested the tolerance of the 5-HT$_{2A}$ receptor for changing the 2,5-ether substitution pattern to a 2,6-ether pattern, using both conformationally free and rigid phenylalkylamines **(37 - 39)** (shown in Figure 1-19).[50]



(14) **(37)** **(38)** **(39)**

Fig. 1-19: Substrates used by Chambers et al.[50] in Binding Affinity Studies

They found that changing from a 2,5-ether to 2,6-ether substitution pattern decreases binding affinity but does not eliminate it in a radioligand competition binding study at cloned rat 5-HT$_{2A}$ receptors. As predicted by previous studies, fully aromatised **39** has greater binding affinity than THBD-type **38** (K_i **39** = 1.8 nM *versus* K_i **38** = 6.3 nM) and both have much greater binding affinity than **37** (K_i = 49 nM). Compounds **38** and **39** are both still very potent 5-HT$_{2A}$ agonists (comparatively, DOM **(14)** has a K_i = 19 nM), so it seems likely that there is an amino acid residue within the active site which can hydrogen-bond with the 6-ether, although it is not clear whether it is the same Ser-239 in TM5 as is believed to be the binding site for the 5-ether.[32,50]

Work by Blaazer *et al.* summarised the topography of the 5-HT$_{2A}$ agonist binding site as deciphered by numerous SAR studies and docking studies using hallucinogenic isopropylalkylamines:[32]

- Hydrogen bonding between 2-ether (in the *syn* conformation) and Ser-159 and Thr-160 in TM3.
- Hydrogen bonding between 5-ether (in the *anti* conformation) and Ser-239 in TM5.
- Ionic bonding between the protonated amine and carboxylate group of Asp-155 in TM3 anchors the isopropylalkylamine in the binding pocket.
- *Para*-substituent on the phenyl ring projects into a lipophilic pocket created by Ile-206, Leu-215 and Gly-238: there are both lipophilic and steric interactions between the substituents and the amino acid residues.
- Phe-340 is involved in agonist recognition/binding *via* stabilisation of aromatic systems in ligands.
- If the isopropylalkylamine has an *N*-benzyl substituent, it interacts with Phe-339 *via* π-π stacking.

Recent work in 2016 by Coleman *et al.* and 2017 by Wacker *et al.* has investigated the action of non-endogenous neurotransmitters at the serotonin transporter (SERT) and the 5-HT_{2B} receptor subtype respectively: these sets of results give a new insight into possible binding modes of hallucinogenic isopropylalkylamines at 5-HT_2 receptor subtypes.[51,52]

Coleman *et al.* investigated the binding of two SSRIs ((*S*)-citalopram **(40)** and paroxetine **(41)** (see Figure 1-21)) to SERT: by measuring X-ray crystallographic data they discovered that when these drugs bind to SERT, the transporter adopts an outward-open conformation with the drug bound to the central site, halfway across the membrane, in a cavity made up of TMs 1, 3, 6, 8 and 10, as shown in Figure 1-20.

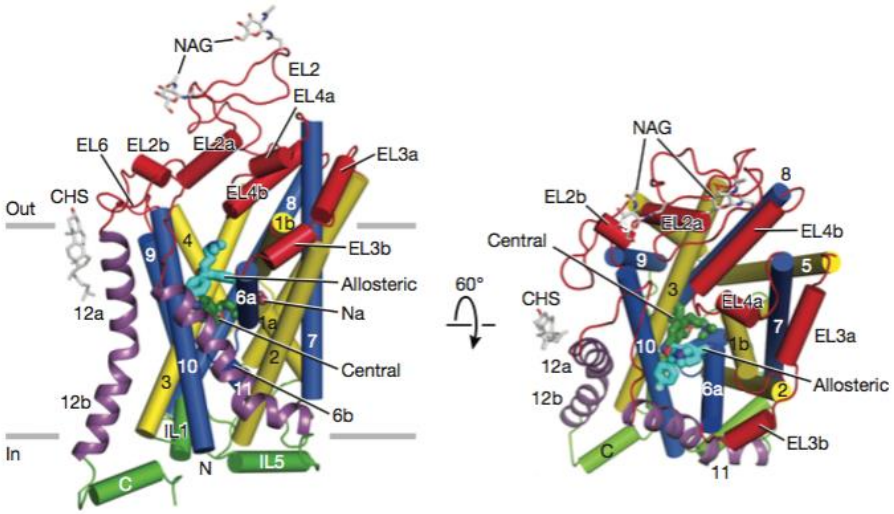
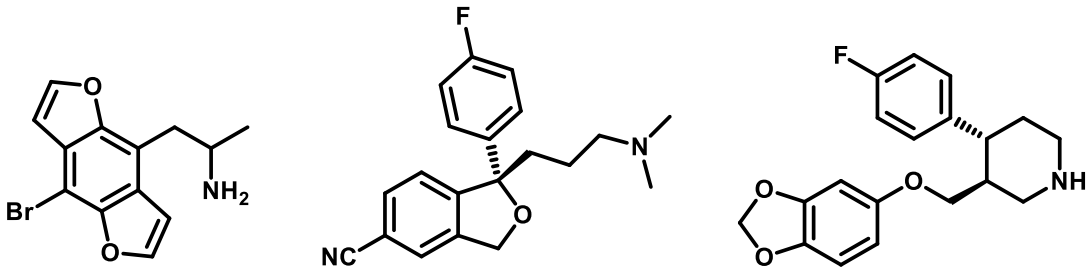


Fig. 1-20: Two molecules of (S)-Citalopram (light blue) bound to SERT in central and allosteric sites[51]

(*S*)-Citalopram **(40)** also binds allosterically, which increases its duration of action. This finding has interesting implications for very long-acting isopropylalkylamine hallucinogens such as BDF **(15)**, as greater affinity for an allosteric site or greater binding affinity when an allosteric site is occupied could explain the long-lasting effects of such compounds.[51]



(15) **(40)** **(41)**

*Fig. 1-21: BDF **(15)**, (S)-Citalopram **(40)** and Paroxetine **(41)***

While SERT is not one of the 5-HT$_2$ class of receptors, certain modes of binding are likely to be similar:[51]

- Ionic bonding between protonated amines and the carboxylate of an amino acid residue (Asp-98 in SERT).

- Interactions between the amine cation and the π bonding systems in the amino acid residues localised beneath amine-carboxylate bonding.
- Hydrophobic cavities lined by residues such as Ile, Phe, Ser, Ala and Leu which interact with small hydrophobic groups, e.g. Br, Me, I, F.
- Stacking and edge-to-face aromatic interactions between aromatic systems on the substrate and residues such as Phe.
- Allosteric interactions that affect K_d (the rate at which the ligand detaches from the binding site, also known as the 'off rate').

Subsequent work by Wacker *et al.* looked at the crystal structure of LSD **(13)** complexed with the 5-HT_{2B} receptor, a receptor that shares significant sequential homology with 5-HT_{2A}, and examined its binding, modes of action, and dissociation from the agonist binding site.[52] While LSD **(13)** is from a different structural family of hallucinogens, the effects it produces in humans are analogous to those produced by isopropylamine hallucinogens so it reasonable to assume that some of the modes of action are common to both families.

LSD **(13)** was found to bind to the primary or 'orthosteric' site on 5-HT_{2B} (as seen in Figure 1-22) while also engaging an extended binding site previously reported by Wang *et al.* which seems common to the 5-HT receptor subtypes (with the exception of 5-HT_3, which is not a GPCR).[53]

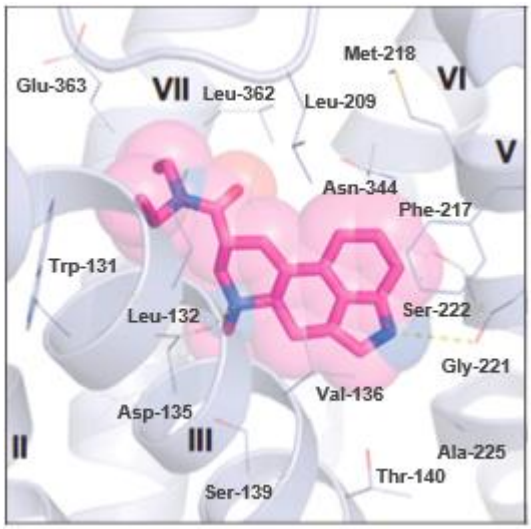
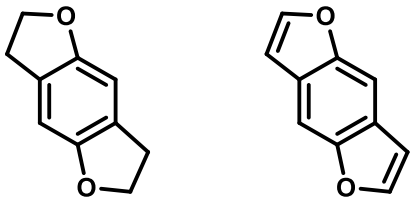


Fig. 1-22: LSD in the Orthosteric Cleft of 5-HT_{2B}[53]

The orthosteric pocket forms a narrow cleft, lined with mostly hydrophobic amino acid sidechains (e.g. leucine, glycine, tryptophan, phenylalanine, as seen in Figure 1-22) from TMs 3, 5, 6 and 7, again, a common feature of aminergic receptors, and also a possible explanation of why increasing the aromaticity from THBD **(42)** (as in **25**) to benzodifuran **(43)** (as in **15**) (see Figure 1-23) increases activity: the increased lipophilicity would lead to more favourable interactions, as posited earlier by Parker *et al.*[47,52]



(42) **(43)**

*Fig. 1-23: THBD **(42)** and Benzodifuran **(43)***

The LSD **(13)** molecule was anchored to the 5-HT_{2B} receptor by a conserved salt bridge between Asp-135 in TM3 and the basic amine, another interaction that appears common between all aminergic receptors. LSD's **(13)** ring system forms edge to face aromatic contacts with phenylalanines in TM6, an interaction thought to occur also in 5-HT_{2A} binding. The indole nitrogen was found to hydrogen-bond with the backbone oxygen of Gly-221 in TM5, which may be analogous to the role played by the 2,5-ethers in the BDF **(15)** system (see Figure 1-22).[52]

It was also found by Wacker *et al.* that LSD **(13)** has very slow binding kinetics: it dissociates very slowly from 5-HT_{2A} and 5-HT_{2B}, which may go some way to explaining its lengthy duration of action, similar to BDF **(15)**. It was hypothesised that this slow dissociation may be caused to some extent by a 'lid', formed by an extracellular loop EL2 (in 5-HT_{2B}) and the entrance to the binding pocket, as demonstrated in Figure 1-24.[52]

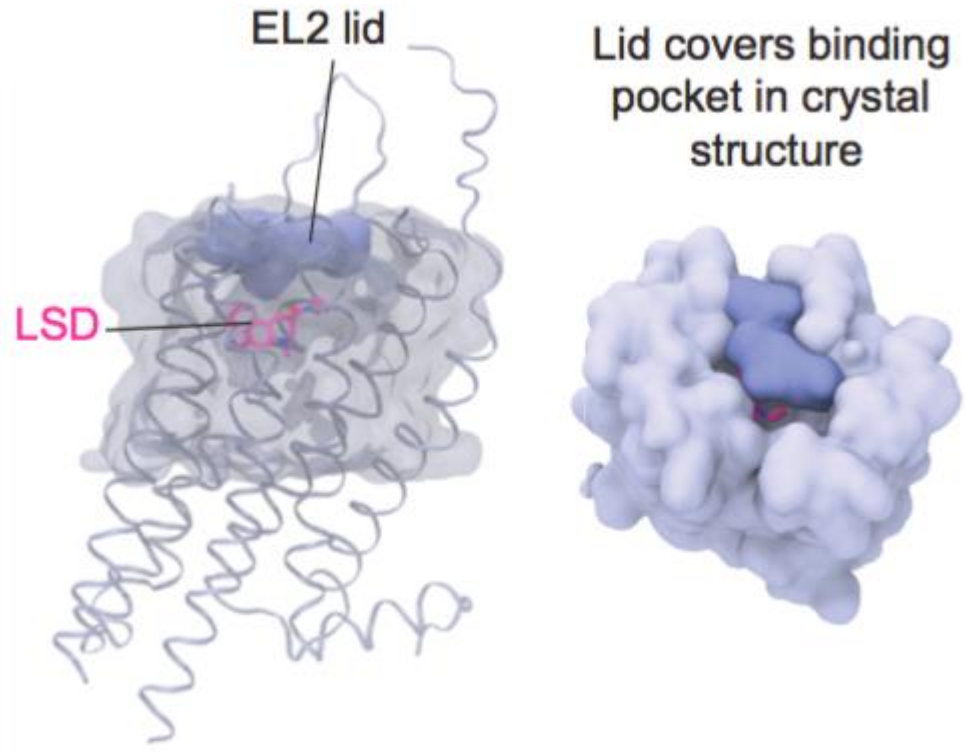
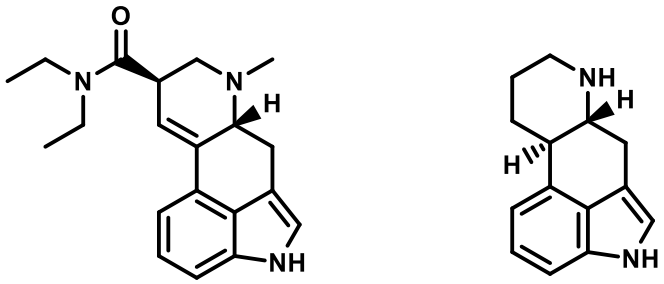


Fig. 1-24: 'Lid' formed by EL2 and the binding pocket[52]

When a ligand binds to a receptor, the shape of the binding site, or the ligand-binding surface, is altered by the interaction.[54] Comparisons between LSD-5-HT_{2B} and (ERG = ergoline **(44)**, see Figure 1-25) ERG-5-HT_{2B} complexes revealed that despite structural similarities between the ligands, they differentially shape the ligand-binding surface of the GPCR to give different physiological effects, i.e. functional selectivity. Therefore, it is reasonable to assume that BDF **(15)** also shapes the receptor pocket differently to achieve some of its physiological effects. Given the similarity to LSD **(13)** with regards to physiological effects, it is likely they have similar effects on the ligand-binding surface.

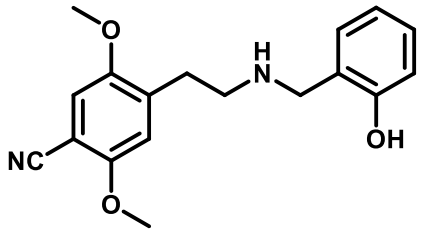


(13) (44)

*Fig. 1-25: LSD **(13)** and Ergoline **(44)***

This study by Wacker *et al.* is the closest look published thus far at a model system for a hallucinogen bound to the agonist site of a 5-HT_2 receptor, and the information it provides is invaluable in the absence of subtype-selective agonists, as it gives an insight into the likely binding modes of agonists at these aminergic receptors, and their potential physiological effects based on the differences in those binding modes.

Work remains on-going in the search to find a truly 5-HT_{2A} selective agonist which does not also act strongly at the 5-HT_{2C} subtype, as this will not only give valuable information about the topography of the agonist binding site, but also offer vital clues as to potential therapeutic targets for serotonergic drugs. Some success was reported by Hansen *et al.*, who found that *N*-(2-hydroxy)benzylation of the amine nitrogen gives a general increase in 5-HT_{2A} selectivity over other 5-HT_2 subtypes, with the dimethoxy nitrile **45** showing the greatest 5-HT_{2A} versus 5-HT_{2C} agonism at over 100-fold more selective for 5-HT_{2A}. The combination of the *N*-(hydroxybenzyl) substitution and the presence of a nitrile group in the crucial 4-position on the aromatic core provides a potential starting point for further SAR investigations into finding a truly selective 5-HT_{2A} agonist.[55]



(45)

BDF **(15)** and its ilk of super-potent agonists are valuable from a research perspective because they provide a basis for selective functional activity at the 5-HT_2 receptor subtypes, something which is important for the determination of the physiological effects of agonising these subtypes. While BDF and its analogues have proven less effective than originally hoped in terms of providing a truly selective 5-HT_{2A} agonist, with only mild selectivity observed thus far [49,55] – likely due to the sequential homology at receptor subtypes – they continue to present positive potential for true understanding of the agonist activity at these receptors, and the best models for investigation as therapeutic agents for those conditions where 5-HT_2 involvement is known to be key, such as depression, obsessive-compulsive disorder (OCD) and schizophrenia, although negative public perception and strict legal controls would have to be navigated to undertake any such investigations.[22,56]

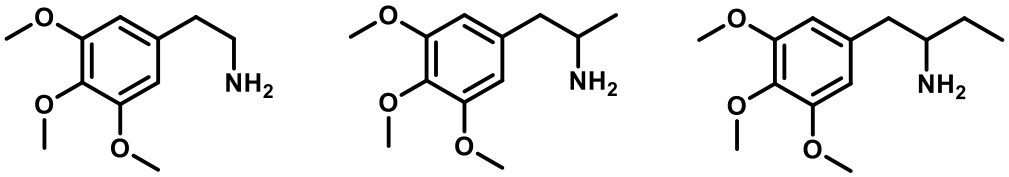
1.4 Structure-Activity Relationships of Hallucinogenic ATS

Structure-activity relationships (SAR) refer to the relationship between the structure of a molecule and its pharmacological effect. For example, in ATS, varying the substitution patterns both on the ethylamine sidechain or on the phenyl ring can amplify or reduce certain pharmacological outcomes, such as stimulant or hallucinogenic effects.

There are a number of factors to be taken into account when considering SAR. For example, many SAR studies have been carried out in animal models (due to the legal issues with carrying out testing in humans) and these do not always

accurately translate to a human model.[40] Furthermore, structure-activity relationships mostly focus on how a molecule behaves at the receptor at which it acts. This is measured by observing the activity of the drug *in vivo*, however, the activity represented *in vivo* is affected by how efficiently the compound is distributed to the part of the body where it acts. For example, a molecule with psychoactive potential may have high binding activity at the relevant receptor; however, it may be too large or too polar to traverse the blood-brain barrier. For this reason, when looking at SAR, one must consider the physical properties of the molecule as well as the activity at the receptor.[40]

Alexander Shulgin was a prominent researcher in the field of designer ATS. He synthesised many novel ATS and compared their action *in vivo* to that of a standard compound:[10] mescaline **(46)**, a naturally occuring psychoactive phenethylamine that is found in the peyote cactus.[57] There are two sites available for varying substitution patterns on mescaline **(46)**: the aromatic ring and the ethylamine sidechain. Considering the ethylamine sidechain first, research by Shulgin *et al.* has shown that addition of an α-methyl group to the sidechain, forming 3,4,5-trimethoxyamphetamine **(47)** (see Figure 1-26) increases the potency of the molecule two-fold when tested in humans.[41]



(46) **(47)** **(48)**

*Fig. 1-26: Mescaline **(46)**, 3,4,5-Trimethoxyamphetamine **(47)** and 1-(3,4,5-Trimethoxyphenyl)butan-2-amine **(48)***

Modification of the ethylamine sidechain by α-ethylation (or any other higher homologs) has been proven to eliminate the *in vivo* hallucinogenic activity of compound **48** completely when taken orally by humans in comparable doses to mescaline **(46)** or 3,4,5-trimethoxyamphetamine **(47)**.[39]

Another possible structural change in the ethylamine sidechain is *N*-methylation or dimethylation, modifications which generally attenuate the *in vivo* activity of substrates in conditional behaviour tests in rats, with tests carried out by Ho *et al.* on DOM **(14)** and its phenethylamine analogue **49**, along with *N*-methylated analogues **(50 - 52)** of both **14** and **49** (shown in Figure 1-27).[58]

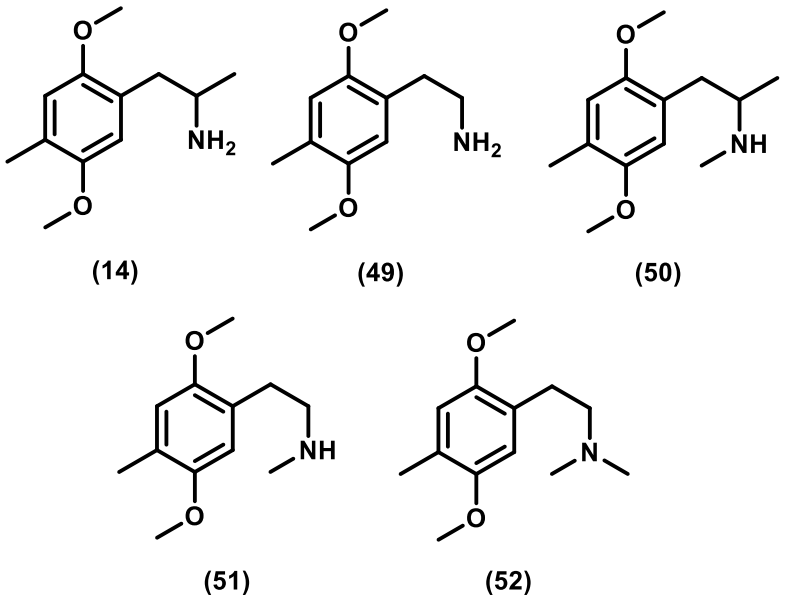


Fig. 1-27: Substrates used by Ho et al.[58] in Functional Potency Studies

The results of these behavioural tests are summarised in Table 1-2, where it can be seen that *N*-methylation results in a 4 - 7.5-fold loss in *in vivo* activity. It was noted that while *N,N*-dimethylation also results in a loss of *in vivo* activity, it is comparable to the loss that comes with *N*-methylation and does not further attenuate the *in vivo* activity.[58]

Compound	**14**	**49**	**50**	**51**	**52**
ED_{50} in rats (*μ*mol/kg)	5.4	7.2	22	54	46

*Table 1-2: Functional potency of **(14, 49 - 52)**[58]*

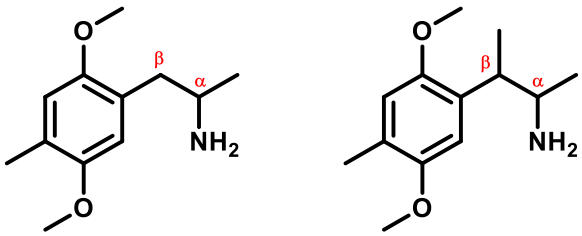
This trend in attenuated *in vivo* activity with *N*-methylation has some exceptions, the most famous of which is MDMA **(6)**, commonly known as Ecstasy. The *N*-methylation also affects the pharmacology of MDMA, as it is more entactogenic and less psychedelic than its amphetamine analogue 3,4-methylenedioxyamphetamine (MDA) **(53)** (shown in Figure 1-28).[59]



(6) **(53)**

*Fig. 1-28: MDMA **(6)** and MDA **(53)***

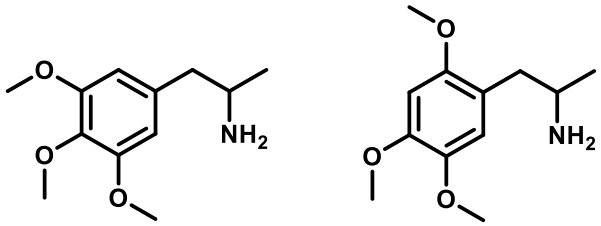
Another common variation in the ethylamine sidechain substitution pattern is the addition of substituents at the β-position. This has been found to severely attenuate the *in vivo* potency of hallucinogenic phenethylamines, e.g. introducing a methyl group at the β-position on the sidechain of DOM **(14)** results in the compound **54** becoming 13 times less potent (the dose of **54** required to induce a 1 °C temperature decrease in rabbit test subjects was 2.6 μmol/kg *versus* 0.2 μmol/kg for DOM **(14)**) (see Figure 1-29).[60]



(14) **(54)**

*Fig. 1-29: DOM **(14)** and 3-(2,5-dimethoxy-4-methylphenyl)butan-2-amine **(54)***

Substitutions on the aromatic ring can also affect the potency and *in vivo* mode of action of a compound. Studies by Shulgin *et al.* have shown that a 2,4,5-trisubstitution pattern on the aryl ring phenethylamines is optimal for *in vivo* activity in humans, with an 8-fold increase in activity from 3,4,5-trimethoxyamphetamine **(47)** (2.2 mescaline units) to 2,4,5-trimethoxyamphetamine **(55)** (17 mescaline units) (see Figure 1-30).[41]



(47) (55)

*Fig. 1-30: 3,4,5-trimethoxyamphetamine **(47)** and 2,4,5-trimethoxyamphetamine **(55)***

Note that mescaline units (M.U.) are a unit coined by Shulgin and refer to a comparison of the activity of each compound in relation to mescaline **(46)** as a standard. These comparisons are based on user-reported effects, with ED_{50} taken as the mean of the threshold dose (the minimum detectable dosage) and the dosage that was 'maximally effective' (this was taken to be the dose at which psychotomimetic effects were prolonged rather than intensified). Shulgin himself reports that as a result, the M.U. values should not be considered accurate to closer than 25 %.[41]

The most active of these 2,4,5-trisubstitued analogues have been found to have a methoxy group at the 2-position, and quite frequently at the 5-position as well.[40] Using higher homologs (e.g. ethoxy, propoxy, etc.), or halogens in the 2- and 5-positions has been found to create mostly inactive compounds. However, substituting a hydroxyl group for one of the methoxy groups in 2,5-dimethoxy compounds has been found to increase the *in vitro* affinity for the 5-HT receptor in a receptor affinity assay using rat fundus samples, although when tested in *in vivo* drug discrimination studies in rats, there is a slight attenuation in *in vivo* activity from the 2-methoxy **56** to the 2-hydroxyl **57** analogues, and a larger attenuation when going from the 5-methoxy **14** to the 5-hydroxyl **58** analogue.[61-63] This information is summarised in Figure 1-31 and Table 1-3.

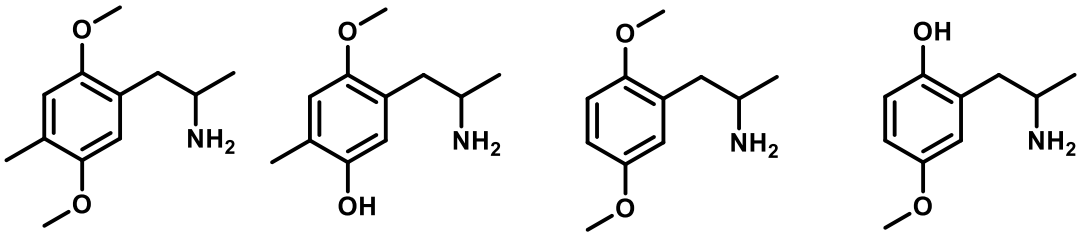


Fig. 1-31: SAR Studies on Substituents in the 2,5-Positions of ATS

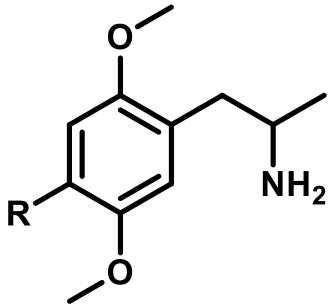
Compound	**14**	**58**	**56**	**57**
ED_{50} in rats (*μ*mol/kg)	22	126	30	39

*Table 1-3: Functional potency of **(14, 56 - 58)**[58]*

The 4-position on the aromatic ring of the phenethylamine is the most important in terms of substitution pattern and its effect on *in vivo* activity.[40] While the 4-substituent impacts the overall lipophilicity of the compound, thereby influencing the transversion of the blood-brain barrier, its unique influence is because the *para*-position corresponds to a hydrophobic position within the binding site of the 5-HT_{2A} and 5-HT_{2C} receptor subtypes, which gives it great influence over the *in vivo* activity of the compound.[64,65] This site can only accommodate substituents which are less than 5 - 6 Å in length, which explains why methylation at the 4-position increases the activity of a psychoactive compound, while using higher homologs (e.g. butyl, pentyl, etc.) renders a compound inactive.[66]

Many highly potent psychoactive phenethylamines have also been shown to have stable substituents in the 4-position, which most likely affords them a resistance to oxidative metabolism (for example, using a halogen instead of a methyl group which would be susceptible to aliphatic oxidation)[67], thereby increasing their duration of action.[40] Using halogens as alternatives to alkyl chains as *para*-substituents increases the *in vivo* activity of the

phenethylamines significantly in humans as summarised in Table 1-4, which deals with 2,5-dimethoxyamphetamines:[10]



(2): R = Br
(5): R = I
(14): R = Me
(59): R = Cl
(60): R = NO_2

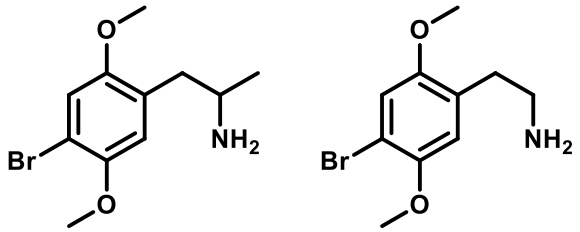
R =	Abbreviation	Potency	
		Dose (mg)	M.U.
CH_3	DOM **(14)**	3.0 - 10.0	50
Cl	DOC **(59)**	1.5 - 3.0	150
Br	DOB **(2)**	1.0 - 3.0	150
I	DOI **(5)**	1.5 - 3.0	150
NO_2	DON **(60)**	3.0 - 4.5	80

Table 1-4: Comparative in vivo activity of p-halogenated 2,5-dimethoxyamphetamines[10]

The conformation of the methoxy groups in 2,5-dimethoxyphenethylamines has proven to be extremely important with respect to their binding activity (to the 5-HT_{2A} and 5-HT_{2C} receptor subtypes) and their *in vivo* potency: by locking the methoxy groups into hydrofuran or furan rings, the affinity of the compound for the 5-HT_2 serotonin receptors is greatly increased.[42] This suggests that the receptor requires the methoxy groups to be in a coplanar conformation with the aromatic ring for it to bind correctly.[40] Independent methoxy groups have conformational freedom, thereby decreasing the activity at the serotonin receptors, but locking the methoxy groups into position ensures they are in the correct orientation for the oxygen lone pairs to hydrogen bond to residues in

the receptor binding sites, thereby enhancing the potency of the compound, as discussed extensively in Section 1.3.3.[42]

The α-methyl group protects isopropylalkylamines from metabolism by the enzyme monoamine oxidase (MAO), and also increases the hallucinogenic potency, which is evidenced by an increase in potency going from 2C-B **(33)** (EC_{50} of 689 nM) to DOB **(2)** (EC_{50} of 50 nM) when tested on cloned rat 5-HT_{2A} receptors (see Figure 1-32).[68]



(2) **(33)**

*Fig. 1-32: DOB **(2)** and 2C-B **(33)***

1.5 Synthesis of ATS from P2P (62) Intermediates

The synthesis of ATS is very versatile and can be done *via* many different routes and from many different starting materials, however, the choice of synthetic route depends primarily (though not solely) on the availability of precursors.[69] One such precursor is phenyl-2-propanone (P2P) **(62)**, an intermediate which is used very widely in ATS syntheses, including the Leuckart route which forms the basis for a large part of this thesis work.

When looking at the synthesis of ATS from P2P **(62)** and its analogues, there are two main steps in the pathway as highlighted in Figure 1-33:

1. Synthesis of the main ketone precursor, P2P **(62)** (or an analogue).
2. Synthesis of the ATS from the relevant P2P **(62)** analogue.

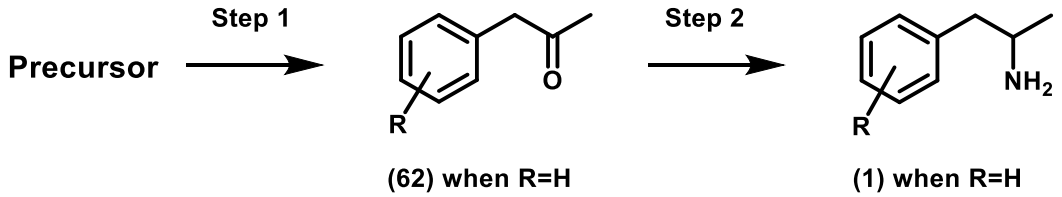


*Fig. 1-33: Phenyl-2-propanone **(62)** analogue to amphetamine **(1)** analogue*

Numerous routes have been developed for the synthesis of P2P **(62)**, as it is a molecule that has been in widespread use as a precursor to ATS for at least forty years.[70] The synthesis of P2P **(62)** became an issue for those manufacturing ATS illegally around 1980, when the compound was listed as a controlled precursor substance by the Department of Justice in the US due to its use as an ATS starting material.[71] Legislation has also been introduced in Ireland to control P2P **(62)**, under the European Communities (Control of Drug Precursors) Regulations 2009. Prior to 1980, P2P **(62)** was commercially available without restriction and therefore relatively easy to procure. A number of common P2P **(62)** synthetic routes are summarised in Figure 1-34.

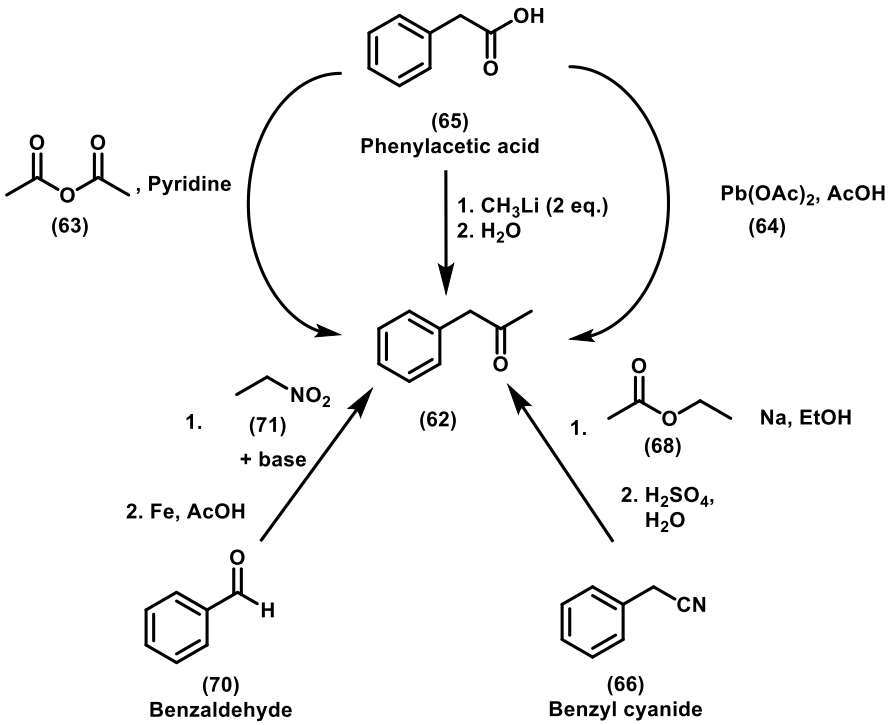


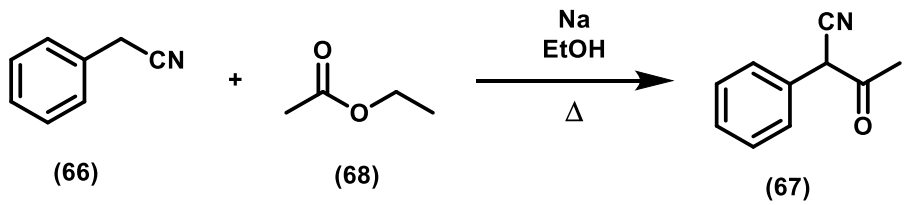
*Fig. 1-34: Synthetic routes to phenyl-2-propanone **(62)***

The most common synthetic route in illicit P2P **(62)** synthesis is the phenylacetic acid route (reported to be used in more than 75 % of recorded clandestine laboratories).[72] There are a number of variations on this route, the most common being reaction with acetic anhydride **(63)** (variation 1) or with lead acetate **(64)** (variation 2) as illustrated in Figure 1-34.

The procedure for the first variation on the phenylacetic route is to reflux phenylacetic acid **(65)** and acetic anhydride **(63)** in pyridine for approximately six hours at 150 °C and then quench the reaction mixture to isolate P2P **(62)** in 56 % yield.[70] The synthesis of the second variation using phenylacetic acid **(65)** and lead acetate **(64)** is slightly more complex. It involves heating the two compounds in acetic acid in a distillation apparatus, and two separate distillations with an intervening workup before pure P2P **(62)** is obtained in 50 % yield. Other synthetic routes that use phenylacetic acid **(65)** as a starting material include the use of sodium acetate instead of pyridine in conjunction with acetic anhydride **(63)** (not shown in Figure 1-34), and methyllithium addition to phenylacetic acid **(65)**.[70,73]

Another common synthetic route to P2P **(62)** involves the use of benzyl cynanide **(66)** as a starting material. This is estimated to be used in about 10 % of illicit syntheses of P2P **(62)**.[72]

The benzyl cyanide synthesis route takes place in two steps: step one is the synthesis of α-phenylacetoacetonitrile **(67)** with ethyl acetate (**68)**, which are heated to reflux with freshly prepared sodium ethoxide (average yield of 59 - 64 %,[74] see Figure 1-35).



(66) **(68)** **(67)**

*Fig. 1-35: Preparation of α-Phenylacetoacetonitrile **(67)***

Step two is the synthesis of P2P **(62)** from α-phenylacetoacetonitrile **(67)** by treatment with aqueous acid. The α-phenylacetoacetonitrile **(67)** is dissolved in sulfuric acid and added slowly and with vigorous stirring to water, after which the reaction mixture is heated to 150 °C for 4 h (average yield of 77 - 84 %[75] stated by Herbst *et al.* in 1938, though more recent work by Power *et al.* in 2013 reports the yield for this step is lower, at 74 %.[76] See Figure 1-36).

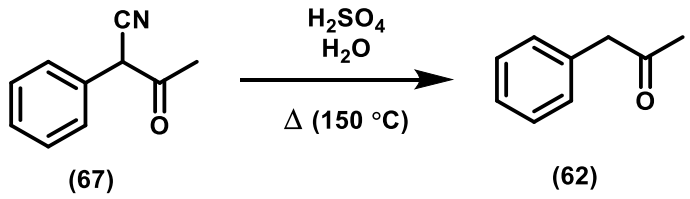


*Fig. 1-36: Preparation P2P **(62)** from α-Phenylacetoacetonitrile **(67)***

The clandestine synthesis of P2P **(62)** also occurs *via* the nitrostyrene route, which is estimated to be used in about 4 % of illicit syntheses.[72] This synthetic route also takes place in two steps. The first step is the synthesis of β-methyl-β-nitrostyrene **(69)** by condensation of benzaldehyde **(70)** with nitroethane **(71)** under basic conditions, a reaction known as the Henry-Knoevenagel condensation (see Figure 1-37). This involves refluxing equimolar amounts of benzaldehyde **(69)** and nitroethane **(71)** along with a catalytic quantity of *n*-butylamine (0.05 mol%) in absolute ethanol for 8 h and collecting the product *via* suction filtration after it precipitates out of solution on cooling (yield of 64 %).[77]

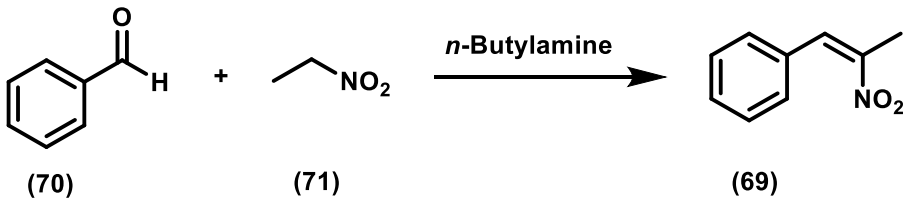


*Fig. 1-37: Preparation of β-Nitrostyrene **(69)***

Step two is the synthesis of P2P **(62)** from the nitrostyrene **69**. There are two viable synthetic routes for this step which are known to be used in clandestine settings.

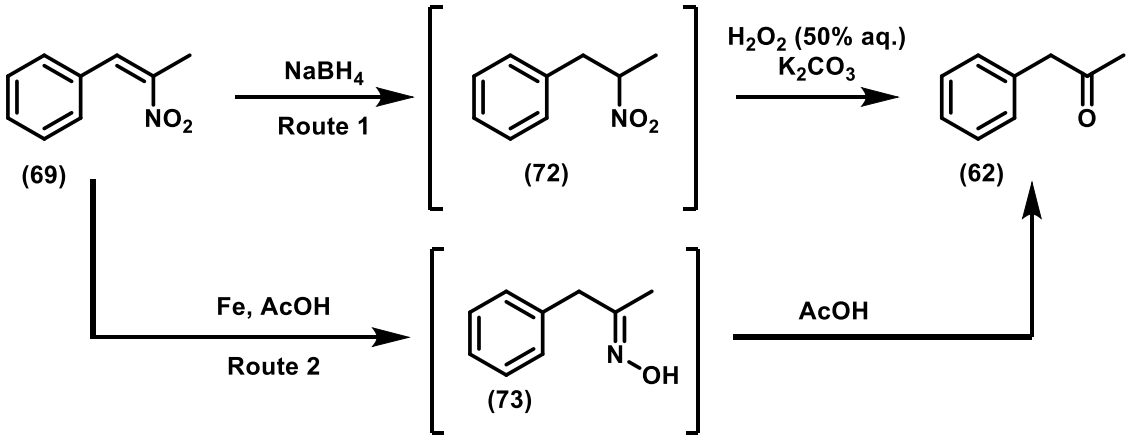


*Fig. 1-38: Two Routes to P2P **(62)** from β-Nitrostyrene **(69)***

Route 1 affords a yield of 60-70 % (depending on substituents on the aromatic ring), while route 2 affords a yield of 75 %.[78,79] Route 1 is a combination of an alkene reduction using sodium borohydride (gradual addition of sodium borohydride to nitrostyrene **69** in solution at 0 °C followed by 2 h stirring at ambient temperature) followed by hydrolysis of the nitroalkane **72** to P2P **(62)** (reaction mixture is cooled to 0 °C, hydrogen peroxide (50 % aqueous solution) and potassium carbonate are added and the mixture is stirred at ambient temperature for 18 h).[78]

Route 2 is a combination of an alkene reduction to an oxime intermediate **73**, followed immediately by acid hydrolysis *in situ* to P2P **(62)**.[79] The alkene reduction is performed by gradually adding the nitrostyrene **69** to a refluxing slurry of iron powder in acetic acid. Reflux is continued for 1.5 h before the reaction mixture is filtered (to remove iron) and quenched in water, and the P2P **(62)** is extracted in dichloromethane and recovered *in vacuo*.

These routes represent only some of the possible synthetic routes to P2P **(62)**, with many others recorded in the literature.[80-83] Once P2P **(62)** (or an

analogue) has been synthesised, it can be converted to amphetamine **(1)** (or analogous ATS) *via* a wide variety of synthetic pathways.

The second step in ATS synthesis is the synthesis of the target ATS from a P2P analogue. This usually takes place *via* one of three distinct synthetic routes: the Leuckart reaction, the reductive amination route and the oxime route, as illustrated in Figure 1-39. For simplicity, all routes here describe the synthesis of amphetamine **(1)** from P2P **(62)**, however, a wide variety of α-methylphenethylamine ATS can be synthesised using the same methods by introducing substituents onto the aromatic ring of the P2P **(62)** starting material.

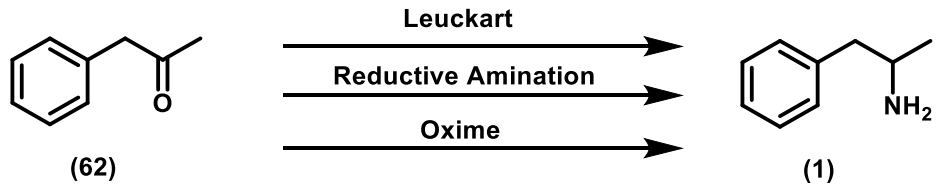


*Fig. 1-39: Common synthetic routes from P2P **(62)** to amphetamine **(1)***

The most common of these three pathways is the Leuckart route, which is used in more than 70 % of clandestine syntheses.[72] This route involves two steps: first, P2P **(62)** is refluxed with formamide and then the *N*-formyl intermediate **74** is hydrolysed to amphetamine **(1)** using HCl in MeOH.[9, 84]

The conversion of the ketone **62** to *N*-formyl intermediate **74** occurs *via* nucleophilic attack of a molecule of formamide at the carbonyl carbon atom of **62**, followed by elimination of water to form an imine. This water reacts with formamide to produce ammonia and formic acid. The formic acid then reduces the imine to the *N*-formyl intermediate **74**, a step which is shown in Figure 1-40 below.

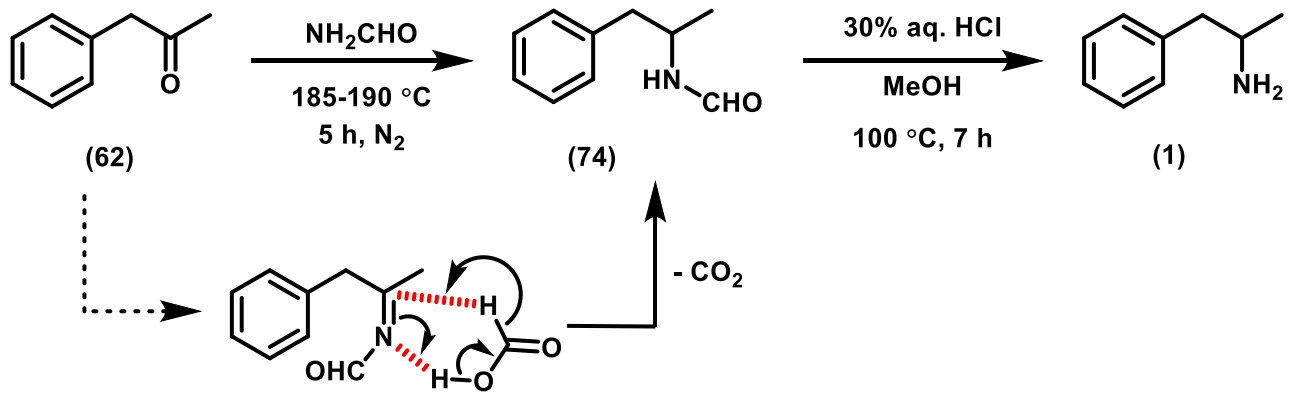


Fig. 1-40: Leuckart Reaction and Hydrolysis to convert P2P ***(62)*** *to Amphetamine* ***(1)***

Employment of the Leuckart route can be identified by impurity profiling, as it contains several route specific impurities that have been previously isolated and characterised. The most common impurities which arise during the Leuckart synthesis route are the intermediate *N*-formylamphetamine **(74)** and isomeric pyrimidines **75** and **76**, whose formation *via* intermediates **77** and **78** is summarised in Figure 1-41 (for a more detailed synthetic overview, see Section 2.1).[84] While previous work (both within our research group and in other literature sources) has isolated a number of pyrimidine impurities related to the Leuckart synthesis of ATS, the pyrimidine impurities characteristic of the Leuckart synthesis of BDF **(15)** have not yet been independently synthesised and characterterised in the literature, and this is the focus of Chapter 2 of this thesis.

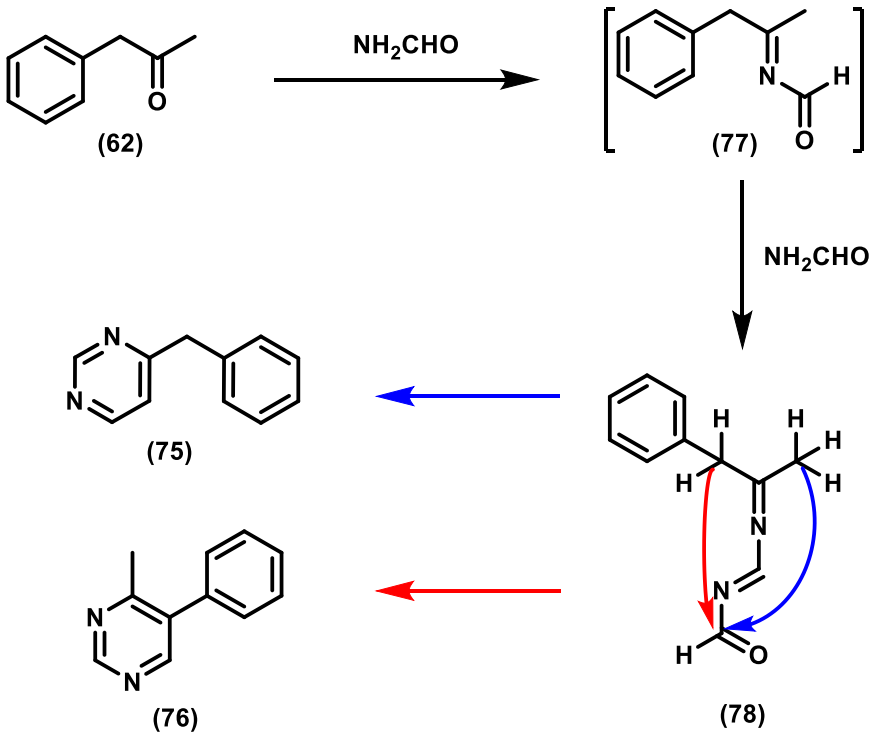


Fig. 1-41: Pyrimidine formation in the Leuckart synthesis of amphetamine ***(1)***

There are also other route specific impurities associated with the Leuckart synthesis of amphetamine **(1)**, including pyridines **79 - 83** and a dihydropyridone **84**, which were first reported by van der Ark *et al.* in a series of communications in 1977 and 1978, and which are summarised in Figure 1-42.[85-87] This abundance of route specific impurities make the Leuckart route comparatively easy to identify when considered alongside other routes such as reductive amination and oxime reduction, which have fewer characteristic impurities.

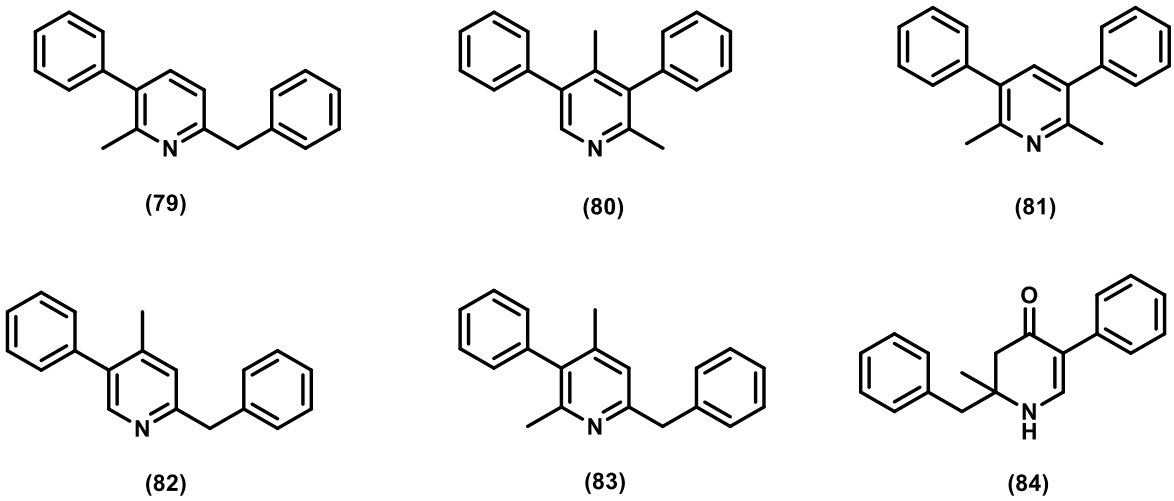


*Fig. 1-42: Pyridine and dihydropyridone impurities **79 - 84** arising from the Leuckart formation of amphetamine **(1)** from P2P **(62)**[85-87]*

The next most common synthetic route from P2P **(62)** to amphetamine **(1)** is the reductive amination route, which involves reduction in the presence of a nucleophilic amine (see Figure 1-43). Sodium cyanoborohydride is a common reagent choice in reductive amination as it can selectively reduce iminium intermediates in the presence of carbonyl groups.[88]

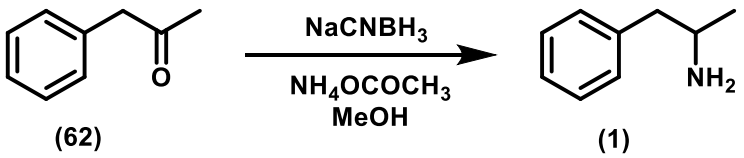


*Fig. 1-43: Reductive Amination of P2P **(62)** to Form Amphetamine **(1)***

This is a one pot synthesis, but there are actually two steps involved: nucleophilic addition of the nitrogen (in the form of ammonia from ammonium acetate) to the ketone to form an iminium ion **85**, followed by reduction of that intermediate to an amine (see Figure 1-44).[84]

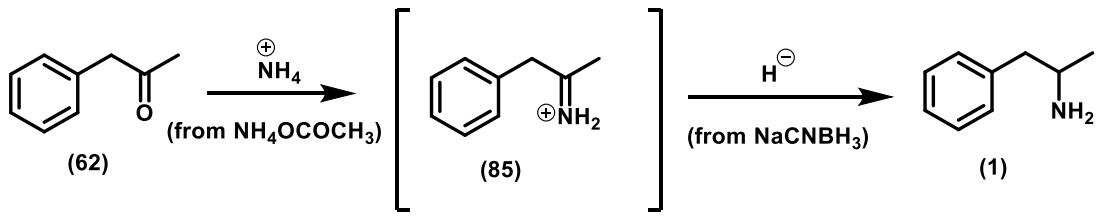


*Fig. 1-44: Iminium cation **(85)** in the Reductive Amination of P2P **(62)** to form Amphetamine **(1)***

The third synthetic route from P2P **(62)** to amphetamine **(1)** is known as the oxime route due to the formation of an oxime intermediate **73** (see Figure 1-45). It involves the reaction of P2P **(62)** with hydroxylamine and sodium hydroxide in water at 40 °C for one hour to form the oxime intermediate **73**, followed by reduction to amphetamine **(1)**.[89] Common reducing agents for the second step include H_2 on Pd/C or metal hydride reduction using $LiAlH_4$.[84]

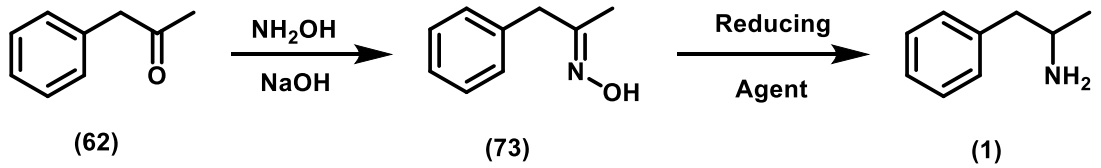


*Fig. 1-45: Oxime Route to form Amphetamine **(1)***

An alternative synthetic pathway for the formation of ATS is known as the nitrostyrene route, due to the formation of a nitrostyrene intermediate **69**. This route bypasses the formation of a P2P intermediate, and is a modification of the nitrostyrene synthesis sometimes used to form P2P **(62)**: after nitrostyrene **69** is formed, instead of treatment with iron in AcOH, reduction of **69** with a hydrogenating agent such as H_2, Pd/C affords amphetamine **(1)** in a yield of 64 % (see Figure 1-46).[90]

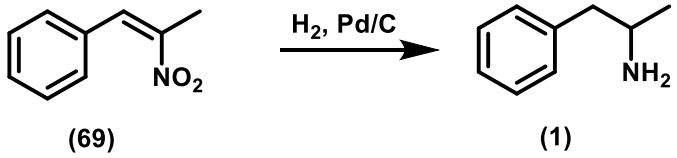
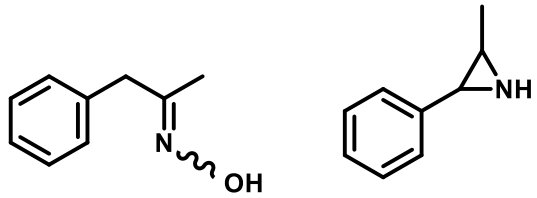


*Fig. 1-46: Synthesis of Amphetamine **(1)** from β-Nitrostyrene **(69)***

Possible impurities which can arise from the nitrostyrene synthetic route include the nitrostyrene **69** itself, benzylmethylketoxime **(73)** and 1-methyl-2-phenylaziridine **(86)**.[9]



(73) (86)

*Fig. 1-47: Potential Impurities in the Synthesis of Amphetamine **(1)** from β-Nitrostyrene **(69)***

1.6 Clandestine Laboratories

Clandestine drug manufacture can be described as the illicit synthesis or processing of narcotic, hallucinogenic, depressant or stimulant drugs.[91] With respect to size, clandestine laboratories can be split into three main categories, based both on the physical size of the laboratories and the scale of production:

1. Small scale ("kitchen") laboratories: these are found in small garages, apartments, barns or disused cars.[92] The operator skill level is low and only a small amount of product is recovered (probably intended for personal use).[93] An example of such an operation can be seen in Figure 1-48, which is a methamphetamine laboratory discovered in the bedroom of a property.[94]

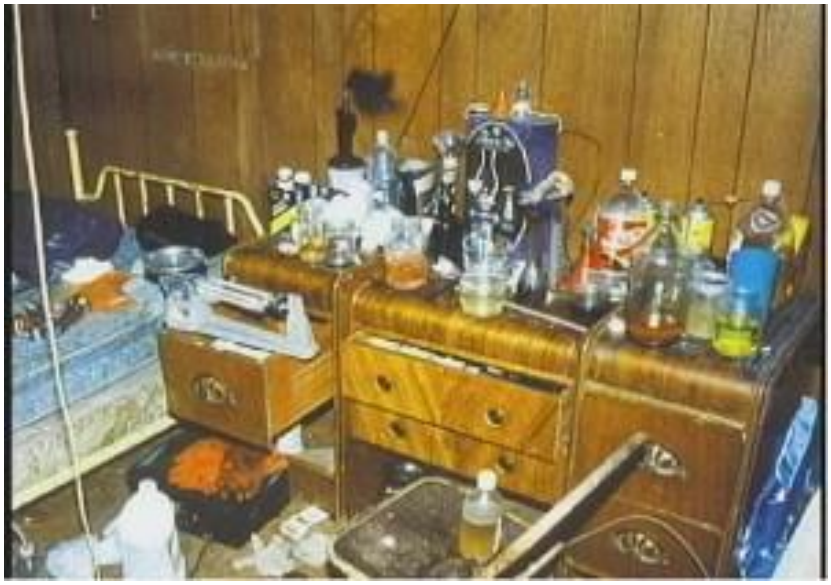


Fig. 1-48: Small-scale clandestine laboratory[95]

2. Medium scale laboratories: these occupy larger spaces than the small scale laboratories, often an entire room or garage, and also tend to involve more specialised glassware/equipment. Operators of these laboratories often have basic chemistry training. The output of these laboratories tends to be a few kilograms of material per batch, and they are often involved in small-scale supply of illicit drugs.
3. Large scale ("industrial") laboratories: also known as superlabs, these are very complex and can have a very large output, e.g. it is estimated that superlabs account for 80 % of methamphetamine **(3)** manufactured in North America.[93] The drums pictured in Figure 1-49 are from a recent raid of a methamphetamine laboratory in Mexico which recovered about 40 metric tonnes of methamphetamine **(3)** and other drug-making paraphernalia.[96]



Fig. 1-49: Large-scale "industrial" clandestine laboratory in Mexico[97]

Clandestine laboratories normally have some recognisable equipment (particularly those which produce illicit drugs on a large scale). Such equipment can include glass flasks, reaction vessels, hydrogen gas cylinders (particularly necessary for any laboratory producing ATS), a mechanical mixer and tableting machines and punches.[98]

According to the United Nations Office on Drugs and Crime (UNODC), 99 % of detected clandestine laboratories have been found to manufacture ATS. ATS are popular because they have good market potential, they are relatively low risk to synthesise and the syntheses themselves are low cost and simple to carry out. There are also a wide variety of synthetic routes and the synthesis is not geographically limited.[99] Within the window of ATS, new psychoactive substances (NPS) have experienced soaring popularity in clandestine circles, with overall reports of NPS synthesis increasing by over 250 % in the period from 2009-2014.[100]

The UNODC World Drug Report in 2018 also highlighted the prevalence of NPS in the world drug trade, with 803 discrete NPS reported in the period from 2009-2017. Although they state that since 2015 the rate of emerging NPS appears to have plateaued, there continue to be novel NPS reported each year, and the market for NPS remains substantial.[101]

1.7 Impurity Profiling of Illicit Materials

As illicitly manufactured drugs are frequently made in conditions which have minimal quality control, poor purification and poor chemical handling, the final 'product' can end up being a mixture of substances rather than one pure compound.[102] There may be a variety of impurities depending on the synthetic route. Impurity profiling normally focuses on organic impurities (though inorganic impurities are also possible), which are usually traces of starting material from incomplete reactions or by-products and decomposition products which are formed *in situ*.[84]

The types and frequencies of the impurities present in a 'final product' depend on a number of factors, including[84]

- The starting materials used and the purity of these materials,
- The skill level of the clandestine 'chemist',
- The degree and efficacy of purification carried out in each step,
- The synthetic route or routes employed,
- The processing, formulation and storage of the drug post-synthesis.

At least one of these parameters is changed for every batch of drug, and therefore no two batches of illicit drugs will have identical impurity profiles. This means that an impurity profile acts as a kind of 'fingerprint', allowing an analyst to propose a 'history' of the sample, information which can be used as a tool by law enforcement.[102]

As reported by the Scientific Section of the United Nations International Drug Control Program (UNDCP), impurity profiling can be very helpful to law enforcement agencies as it can provide a wealth of information, including establishing specific links between samples, which can link batches and therefore show the connections between suppliers, i.e. establish drug distribution patterns. Impurity profiles can help to identify the source of drug samples (some impurities can be geographically specific, for example,

biological contaminants such as spores or insects) and can also be used to monitor methods used for clandestine synthesis. This information can then be used to control the availability of key precursors.[102]

There are two main ways to approach impurity profiling. The first is to use chromatographic and spectroscopic techniques to directly analyse a street sample of an illicit drug. This involves carrying out presumptive tests to establish what type of illicit material is present. Typical presumptive tests include colour tests, anion tests and microcrystal tests: these can tell you the general class of drug with which you are dealing, e.g. ATS, cocaine, heroin. Presumptive testing is followed by thin layer chromatography (TLC) and more advanced spectroscopic techniques, e.g. HPLC, gas chromatography (GC), mass spectrometry (MS), Fourier-transform infrared spectroscopy (FTIR), nuclear magnetic resonance spectroscopy (NMR), etc.[84]

In the specific case of impurity profiling of amphetamines, information from the UNDCP recommends the use of hyphenated techniques such as gas chromatography-mass spectrometry (GC-MS) and liquid chromatography-mass spectrometry (LC-MS), along with any other analytical techniques deemed useful.[103] This is supported and elaborated upon by the UNODC, which details a large number of analytical techniques suitable for the impurity profiling, including GC-MS, HPLC, GC-FTIR, TLC, NMR, and capillary electrophoresis (CE).[84] In terms of BDF specifically, there have been a number of reported cases of ingestion and/or seizure, which have been confirmed using various analytical techniques, including GC-MS, LC-MS, LC-MS-MS, NMR and HPLC with diode array detection (HPLC-DAD).[104-106]

The second approach to impurity profiling involves controlled synthesis of illicit substances and subsequent identification of impurities. This involves a multistep synthesis of the illicit drug (e.g. amphetamine **(1)**) using novel and existing routes, isolation of the impurities from the crude reaction mixture and identifying the impurities using chromatographic and spectroscopic methods

as described in the previous paragraph. Having identified the impurities, they are then independently synthesised for use as analytical standards.

The two approaches described here are complementary, as there is a need to be able to both identify the impurities and determine how they arise. Furthermore, having isolated compounds and their spectroscopic data will simplify the determination of an impurity profile for other analysts.

1.8 Bromo-DragonFLY

1-(8-Bromobenzo[1,2-*b*:4,5-*b'*]difuran-4-yl)propan-2-amine **(15)**, more commonly known as Bromo-DragonFLY (BDF) and also by the pseudonyms 3C-Bromo-Dragonfly or DOB-Dragonfly,[107] was first reported by Matthew Parker in 1998, in the Nichols research group.[46] It was originally synthesised in search of a 5-HT_{2A} selective agonist, but was found to also be a potent agonist for the 5-HT_{2C} subtype. Biological testing revealed it to be an exceptionally potent hallucinogen (as discussed in Section 1.3.3), the first hallucinogen measured as more potent than LSD **(13)** in a drug discrimination study with rats, and the first compound to have LSD-like activity with an aromatic nucleus other than benzene or an indole.[46]

Following its synthesis and reporting in 1998, BDF **(15)** first surfaced on clandestine markets in Europe and the United States of America (USA) around mid-2005 according to the online drug-information forum Erowid.[108] BDF **(15)** has been generally available as a pink/white powder, but can also be marketed as a liquid formulation, in tablet form or as blotters/impregnated paper, and is mostly ingested orally, though it has been administered in intravenous (IV) form and insufflated.[109]

The dose range for BDF **(15)** has been reported to be anywhere from 100-2100 μg, with Erowid reporting that initially, two distinct batches appeared on the market: the European batch, with an active dose of 200-500 μg when ingested orally and the less potent American batch, with an active dose of 800-

2100 μg when ingested, however, given the clandestine nature of the drugs, it is difficult to be certain that the two 'batches' described by Erowid are both BDF **(15)**.[108,109]

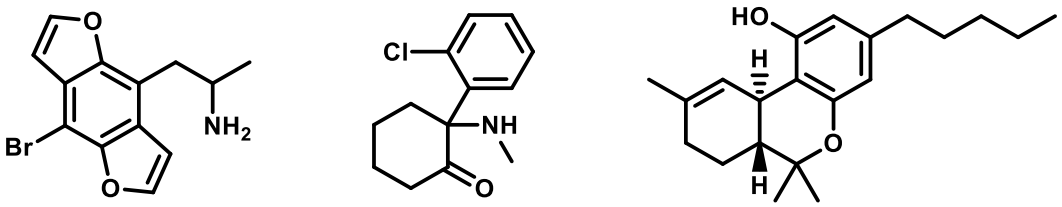
BDF **(15)** has a delayed onset of action, 30 - 60 minutes when insufflated (known colloquially as 'snorting') and 20 - 90 minutes when taken orally, though this can be up to 6 hours if ingested orally on a full stomach, potentially indicating that it may take time to cross membranal barriers, especially in the stomach and blood-brain barriers. Duration of action of BDF **(15)** can be prolonged compared to commercially available formulations of amphetamine **(1)**;[110] amphetamine **(1)** has a duration of action of 5 - 12 hours, while BDF **(15)** has a duration of action of at least 6 - 24 hours and sometimes up to 2 - 3 days if a larger than normal dose is taken (i.e. >2100 μg), although the physiological effects and duration of action do also vary by user.[109]

When taken recreationally, the desired effects of BDF **(15)** include kaleidoscopic hallucinations, altered space/time perception, increased energy, a feeling of well-being and mild euphoria, however, common and undesired side-effects include prolonged hallucinations/euphoria, flashbacks, anxiety, severe insomnia, headaches, nausea, diarrhoea, sweating, tightness, twitches, muscle tension, confusion, paranoia, delusions and memory alterations.[109]

By 2009, BDF **(15)** had been responsible for a number of deaths, such as one in Denmark that was reported by Andreasen *et al.*:[105] a young woman (deceased) and her boyfriend (survived) both orally ingested approximately 1 mL of a liquid solution later found to contain BDF **(15)**. An autopsy found oedema of the lungs, slight oedema of the brain, enlargement of the spleen, irritation of the mucous membrane in the stomach and ischaemic changes in the kidneys, along with residual BDF **(15)** in the blood, urine and vitreous humour, and it was concluded that the drug had led directly to her death. The deceased had apparently ingested approximately 700 μg of BDF **(15)**, which is within the usual reported dose range, however there are other factors which

may have affected the outcome: she may have been a poor metaboliser of the drug or may have actually ingested more than was reported by her boyfriend.[105]

A number of other fatalities attributed to BDF **(15)** have been reported in Sweden, Norway, Finland and the USA, and reports of hospitalisation after recreational use were also recorded.[109] One such case in the United Kingdom (UK) saw a male patient admitted to hospital after suffering seizures following insufflation of an unknown white powder later found to be BDF **(15)**. The patient was suffering from tachycardia and significant acidosis and was ventilated while being monitored for symptoms of serotonin **(12)** toxicity. Despite developing aspirate pneumonia, he was released four days after admission with no obvious ill effects, and subsequent toxicological analysis of urine and blood samples confirmed the presence of BDF **(15)** in combination with ketamine **(87)** and cannabinoids such as tetrahydrocannabinol **(88)** (see Figure 1-50).[111]



(15) **(87)** **(88)**

*Fig. 1-50: BDF **(15)**, Ketamine **(87)** and Tetrahydrocannabinol **(88)***

In many cases, particularly those leading to overdoses, BDF **(15)** is taken in a case of 'mistaken identity', with users thinking they are taking a drug with a quicker onset and a larger active dose. One such example is in cases where BDF **(15)** is mistaken for 2-(8-bromo-2,3,6,7-tetrahydrobenzo[1,2-*b*:4,5-*b'*]difuran-4-yl)ethan-1-amine (2C-B-FLY) **(89)** (see Figure 1-51) resulting in recreational users taking up to 20 times the active dose, resulting in severe unwanted side effects and in some cases, death.[112]

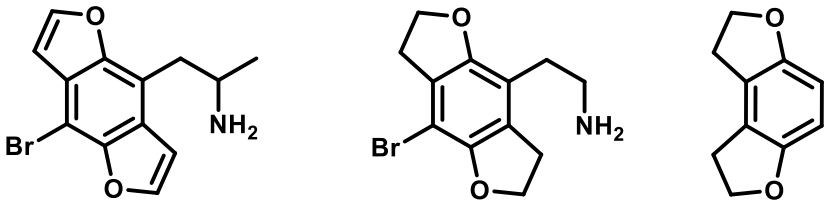


*Fig. 1-51: BDF **(1)**, 2C-B-FLY **(89)** and iTHBD **(90)***

While as a recreational drug BDF **(15)** can cause serious harm to unwitting users (as demonstrated here *via* case reports), in a therapeutic research setting, BDF **(15)** is an important compound which has advanced the understanding of agonist activity at 5-HT_2 receptors, and, as a result, both it and its structurally related byproducts (such as the isomeric 1,2,7,8-tetrahydrobenzo[1,2-*b*:4,3-*b'*]difuran (iTHBD) **(90)** investigated in Chapter 3 of this thesis) warrant further investigation to discover if they hold more answers to fundamental questions in neurochemistry.

1.9 Research Outline

In this thesis, I aim to expand the knowledge base on BDF **(15)** by independently synthesising structurally-related pyrimidines as analytical markers for the Leuckart route to BDF **(15)**, and using these markers as standards to perform impurity profiling on several BDF **(15)**-related Leuckart reactions.

Pyrimidine impurities which are structurally related to BDF **(15)** were targeted for several reasons:

- BDF **(15)** is in a category of illicit drugs known as NPS, a market which has been growing steadily since the early 2000s (see Section 1.6), and it is therefore important to generate data that may assist researchers/law enforcement bodies investigating the origin of impurities in BDF **(15)** and structurally related ATS.

- The pyrimidine impurities are the highest yielding impurities formed in the Leuckart route (generally ~4-5% of the yield) and are therefore good candidates for impurity profiling as there is a higher likelihood of detecting them in a crude reaction mixture by HPLC/^{1}H-NMR.
- In addition to their potential usefulness as analytical markers for identifying the Leuckart route to BDF **(15)**, these pyrimidines are novel compounds which have never been independently synthesised and characterised before.

This work is detailed in Chapter Two.

I also aim to lay the groundwork for the synthesis of a structurally-related isomer of BDF **(15)** by optimising a synthetic route to the iTHBD core **90**, a compound which was initially discovered as a by-product during the synthesis of THBD **(42)**. This novel compound **90** is also a pharmacophore of unknown and potentially useful biologically active properties. While its properties as a novel pharmacophore make it of interest to those involved in drug development, the synthesis of iTHBD **(90)** is also important to researchers investigating the origin of impurities in BDF **(15)** and structurally related compounds.

This is because all routes to BDF **(15)** involve the construction of a benzodifuran moiety at some point during the synthesis (to date, the synthesis of BDF **(15)** directly from benzodifuran **(43)** as a starting material has not been reported). Most routes seen in the literature involve the initial construction of THBD **(42)** followed by oxidation to a benzodifuran at some point during the synthetic pathway.

The presence of iTHBD **(90)** in a reaction mixture (either as a discrete molecule or as a core part of a compound which has undergone further functionalisation) is good evidence that dibromination was used during the synthesis of THBD **(42)** to direct a ring-closing reaction. This provides information about the synthetic route used to synthesise precursors when forming BDF **(15)**. In contrast to the work detailed in Chapter 2, impurity profile

information associated with the discovery of iTHBD **(90)** is independent of the Leuckart reaction, and can indicate synthetic procedures used much earlier in the synthetic route, giving valuable information about potential starting materials used by clandestine chemists.

The work to independently synthesise iTHBD **(90)** is detailed in Chapter Three.

References (Chapter One)

1. Edeleano, L., Ueber einige Derivate der Phenylmethacrylsäure und der Phenylisobuttersäure. *Berichte der deutschen chemischen Gesellschaft* **1887,** *20* (1), 616-622.
2. Amphetamines - History, http://science.jrank.org/pages/302/Amphetamines-History.html (Accessed 21/01/18).
3. The Challenge of New Psychoactive Substances. *Laboratory and Scientific Section, United Nations Office on Drugs and Crime, Vienna* **2013**.
4. Battaglia, G.; deSouza, E. B., Pharmacologic profile of amphetamine derivatives at various brain recognition sites: selective effects on serotonergic systems. *NIDA Research Monograph Series, U.S. Department of Health and Human Services, Washington, U.S.A.* **1989,** *94*, 240-258.
5. Houck, M. M.; Siegel, J. A.; Elsevier; Academic, P., *Fundamentals of forensic science*. Elsevier/Academic Press: Amsterdam, **2015**.
6. Drugs of Abuse - A DEA Resource Guide (2017 Edition) *Drug Enforcement Administration, U.S. Department of Justice* **2017**.
7. Drugs - Central Nervous System, http://chemistry.elmhurst.edu/vchembook/670drugcns.html (Accessed 21/01/2018).
8. DrugFacts - Hallucinogens, (Accessed 25/09/19) https://www.drugabuse.gov/publications/drugfacts/hallucinogens
9. Cole, M. D., *The Analysis of Controlled Substances*. John Wiley & Sons, Ltd., West Sussex, U.K.: **2003**.
10. Laing, R., *Hallucinogens: a forensic drug handbook*. Academic Press, London: **2003**.
11. Fantegrossi, W. E.; Murnane, K. S.; Reissig, C. J., The behavioral pharmacology of hallucinogens. *Biochemical Pharmacology* **2008,** *75* (1), 17-33.
12. Definition of Pharmacology in English (Accessed 21/01/18). https://en.oxforddictionaries.com/definition/pharmacology.
13. Definition of Neuropharmacology (Accessed 21/01/18). https://www.merriam-webster.com/dictionary/neuropharmacology.
14. What are the parts of the nervous system? (Accessed 17/11/18), https://www.nichd.nih.gov/health/topics/neuro/conditioninfo/parts
15. Perrine, D. M., *The Chemistry of Mind-altering Drugs: History, Pharmacology, and Cultural Context*. American Chemical Society: **1996**.
16. Maisto, S. A.; Galizio, M.; Connors, G. J., *Drug Use and Abuse*. 6th ed.; Wadsworth Cengage Learning, California, U.S.A: **2011**.
17. Shoptaw, S. J.; Kao, U.; Ling, W., Treatment for amphetamine psychosis. *Cochrane Database of Systematic Reviews* **2009,** (1), 1-17.
18. Ellinwood, E. H.; King, G.; Lee, T. H. Chronic Amphetamine Use and Abuse (Accessed 21/01/18). http://www.acnp.org/g4/gn401000166/ch162.htm.
19. Cooper, J. R.; Bloom, F. E.; Roth, R. H., *The Biochemical Basis of Neuropharmacology*. 8th ed.; Oxford University Press, New York: **2003**.

20. Iverson, S. D.; Iversen, L. L., *Behavioural Pharmacology*. 2nd ed.; Oxford University Press, New York: **1981**.
21. Chambers, J. J.; Kurrasch-Orbaugh, D. M.; Parker, M. A.; Nichols, D. E., Enantiospecific Synthesis and Pharmacological Evaluation of a Series of Super-Potent, Conformationally Restricted 5-$HT_{2A/2C}$ Receptor Agonists. *Journal of Medicinal Chemistry* **2001,** *44* (6), 1003-1010.
22. Nichols, D. E., Hallucinogens. *Pharmacology & Therapeutics* **2004,** *101* (2), 131-181.
23. The Peyote Ceremony and the Native American Church; https://www.firstpeople.us/native-american/photographs/the-peyote-ceremony-and-the-native-american-church.html (accessed 17/11/18).
24. Hollister, L. E., *Effects of Hallucinogens in Humans*. Raven Press: New York, **1984**.
25. O'Brien, C. P., *Drug Addiction and Drug Abuse*. McGraw-Hill: New York, **2001**.
26. Halpern, J. H.; Pope, H. G., Jr., Hallucinogen persisting perception disorder: what do we know after 50 years? *Drug & Alcohol Dependence* **2003***, 69* (2), 109-119.
27. Hannon, J.; Hoyer, D., Serotonin receptors and systems: endless diversity? *Acta Biologica Szegediensis* **2002,** *46* (1-2), 1-12.
28. Gaddum, J. H.; Hameed, K. A., Drugs Which Antagonize 5-Hydroxytryptamine. *British Journal of Pharmacology and Chemotherapy* **1954,** *9* (2), 240-248.
29. Woolley, D. W.; Shaw, E., A Biochemical and Pharmacological Suggestion About Certain Mental Disorders. *Proceedings of the National Academy of Sciences* **1954,** *40* (4), 228-231.
30. Andén, N. E.; Corrodi, H.; Fuxe, K.; Hökfelt, T., Evidence for a central 5-hydroxytryptamine receptor stimulation by lysergic acid diethylamide. *British Journal of Pharmacology* **1968,** *34* (1), 1-7.
31. Glennon, R. A.; Young, R.; Rosecrans, J. A., Antagonism of the effects of the hallucinogen dom and the purported 5-HT agonist quipazine by 5-HT2 antagonists. *European Journal of Pharmacology* **1983,** *91* (2), 189-196.
32. Blaazer, A. R.; Smid, P.; Kruse, C. G., Structure–Activity Relationships of Phenylalkylamines as Agonist Ligands for 5-HT_{2A} Receptors. *ChemMedChem* **2008,** *3* (9), 1299-1309.
33. van Wijngaarden, I.; Soudijn, W., 5-HT_{2A}, 5-HT_{2B} and 5-HT_{2C} receptor ligands. In *Pharmacochemistry Library*, Oliver B, v. W. I.; Soudijn, W., Eds. Elsevier: **1997**; Vol. Volume 27, pp 161-197.
34. Halberstadt, A. L., Recent advances in the neuropsychopharmacology of serotonergic hallucinogens. *Behavioural Brain Research* **2015,** *277*, 99-120.
35. Glennon, R. A.; Dukat, M.; Westkaemper, R. B. Serotonin Receptor Subtypes and Ligands (Accessed 22/01/18). http://www.acnp.org/g4/GN401000039/Ch039.html.
36. Roman, D. L.; Traynor, J. R., Regulators of G protein signaling (RGS) proteins as drug targets: modulating G-protein-coupled receptor (GPCR) signal transduction. *Journal of medicinal chemistry* **2011,** *54* (21), 7433-7440.
37. Stewart, A.; Fisher, R. A., Chapter One - Introduction: G Protein-coupled Receptors and RGS Proteins. In *Progress in Molecular Biology and*

Translational Science, Fisher, R. A., Ed. Academic Press: **2015**; Vol. 133, pp 1-11.
38. Corazza, O.; Schifano, F.; Farre, M.; Deluca, P.; Davey, Z.; Drummond, C.; Torrens, M.; Demetrovics, Z.; Di Furia, L.; Flesland, L.; Mervo, B.; Moskalewicz, J.; Pisarska, A.; Shapiro, H.; Siemann, H.; Skutle, A.; Pezzolesi, C.; Van Der Kreeft, P.; Scherbaum, N., Designer Drugs on the Internet: A Phenomenon Out-of-Control? The Emergence of Hallucinogenic Drug Bromo-Dragonfly. *Current Clinical Pharmacology* **2011,** *6* (2), 125-129.
39. Shulgin, A. T., Psychotomimetic agents related to mescaline. *Experientia* **1963,** *19* (3), 127-128.
40. Nichols, D. E., Structure-activity relationships of phenethylamine hallucinogens. *Journal of Pharmaceutical Sciences* **1981,** *70* (8), 839-849.
41. Shulgin, A. T.; Sargent, T.; Naranjo, C., Structure–Activity Relationships of One-Ring Psychotomimetics. *Nature* **1969,** *221*, 537.
42. Monte, A. P.; Marona-Lewicka, D.; Parker, M. A.; Wainscott, D. B.; Nelson, D. L.; Nichols, D. E., Dihydrobenzofuran Analogues of Hallucinogens. 3. Models of 4-Substituted (2,5-Dimethoxyphenyl)alkylamine Derivatives with Rigidified Methoxy Groups. *Journal of Medicinal Chemistry* **1996,** *39* (15), 2953-2961.
43. Nichols, D. E.; Snyder, S. E.; Oberlender, R.; Johnson, M. P.; Huang, X., 2,3-Dihydrobenzofuran analogs of hallucinogenic phenethylamines. *Journal of Medicinal Chemistry* **1991,** *34* (1), 276-281.
44. Westkaemper, R. B.; Glennon, R. A., *Molecular Modeling of the Interaction of LSD and Other Hallucinogens with 5-HT$_2$ Receptors*. NIDA: Rockville, **1994**.
45. Trumpp-Kallmeyer, S.; Hoflack, J.; Bruinvels, A.; Hibert, M., Modeling of G-protein-coupled receptors: application to dopamine, adrenaline, serotonin, acetylcholine, and mammalian opsin receptors. *Journal of Medicinal Chemistry* **1992,** *35* (19), 3448-3462.
46. Parker, M. A.; Marona-Lewicka, D.; Lucaites, V. L.; Nelson, D. L.; Nichols, D. E., A Novel (Benzodifuranyl)aminoalkane with Extremely Potent Activity at the 5-HT2A Receptor. *Journal of Medicinal Chemistry* **1998,** *41* (26), 5148-5149.
47. Parker, M. A.; Kurrasch, D. M.; Nichols, D. E., The role of lipophilicity in determining binding affinity and functional activity for 5-HT2A receptor ligands. *Bioorganic & Medicinal Chemistry* **2008,** *16* (8), 4661-4669.
48. Schultz, D. M.; Prescher, J. A.; Kidd, S.; Marona-Lewicka, D.; Nichols, D. E.; Monte, A., 'Hybrid' benzofuran–benzopyran congeners as rigid analogs of hallucinogenic phenethylamines. *Bioorganic & Medicinal Chemistry* **2008,** *16* (11), 6242-6251.
49. McLean, T. H.; Parrish, J. C.; Braden, M. R.; Marona-Lewicka, D.; Gallardo-Godoy, A.; Nichols, D. E., 1-Aminomethylbenzocycloalkanes: Conformationally Restricted Hallucinogenic Phenethylamine Analogues as Functionally Selective 5-HT2A Receptor Agonists. *Journal of Medicinal Chemistry* **2006,** *49* (19), 5794-5803.
50. Chambers, J. J.; Kurrasch-Orbaugh, D. M.; Nichols, D. E., Translocation of the 5-alkoxy substituent of 2,5-dialkoxyarylalkylamines to the

6-position: effects on 5-HT2A/2C receptor affinity. *Bioorganic & Medicinal Chemistry Letters* **2002,** *12* (15), 1997-1999.
51. Coleman, J. A.; Green, E. M.; Gouaux, E., X-ray structures and mechanism of the human serotonin transporter. *Nature* **2016,** *532* (7599), 334-339.
52. Wacker, D.; Wang, S.; McCorvy, J. D.; Betz, R. M.; Venkatakrishnan, A. J.; Levit, A.; Lansu, K.; Schools, Z. L.; Che, T.; Nichols, D. E.; Shoichet, B. K.; Dror, R. O.; Roth, B. L., Crystal Structure of an LSD-Bound Human Serotonin Receptor. *Cell* **2017,** *168* (3), 377-389.e12.
53. Wang, C.; Jiang, Y.; Ma, J.; Wu, H.; Wacker, D.; Katritch, V.; Han, G. W.; Liu, W.; Huang, X.-P.; Vardy, E.; McCorvy, J. D.; Gao, X.; Zhou, X. E.; Melcher, K.; Zhang, C.; Bai, F.; Yang, H.; Yang, L.; Jiang, H.; Roth, B. L.; Cherezov, V.; Stevens, R. C.; Xu, H. E., Structural Basis for Molecular Recognition at Serotonin Receptors. *Science* **2013,** *340* (6132), 610-614.
54. Ma, B.; Shatsky, M.; Wolfson, H. J.; Nussinov, R., Multiple diverse ligands binding at a single protein site: A matter of pre-existing populations. *Protein Science : A Publication of the Protein Society* **2002,** *11* (2), 184-197.
55. Hansen, M.; Phonekeo, K.; Paine, J. S.; Leth-Petersen, S.; Begtrup, M.; Bräuner-Osborne, H.; Kristensen, J. L., Synthesis and Structure–Activity Relationships of N-Benzyl Phenethylamines as 5-HT2A/2C Agonists. *ACS Chemical Neuroscience* **2014,** *5* (3), 243-249.
56. Trachsel, D.; Nichols, D. E.; Kidd, S.; Hadorn, M.; Baumberger, F., 4-Aryl-Substituted 2,5-Dimethoxyphenethylamines: Synthesis and Serotonin 5-HT2A Receptor Affinities. *Chemistry & Biodiversity* **2009,** *6* (5), 692-704.
57. Marnell, T., *Drug Identification Bible*. Amera-Chem Inc, Grand Junction, CO: **1995**.
58. Ho, B.-T.; Tansey, L. W.; Balster, R. L.; An, R.; McIsaac, W. M.; Harris, R. T., Amphetamine analogs. II. Methylated phenethylamines. *Journal of Medicinal Chemistry* **1970,** *13* (1), 134-135.
59. Erowid MDA Vault (Accessed 22/01/18). https://http://www.erowid.org/chemicals/mda/mda.shtml.
60. Aldous, F. A. B.; Barrass, B. C.; Brewster, K.; Buxton, D. A.; Green, D. M.; Pinder, R. M.; Rich, P.; Skeels, M.; Tutt, K. J., Structure-activity relations in psychotomimetic phenylalkylamines. *Journal of Medicinal Chemistry* **1974,** *17* (10), 1100-1111.
61. Anderson, G. M., 3rd; Castagnoli, N., Jr.; kollman, P. A., Quantitative structure-activity relationships in the 2,4,5-ring substituted phenylisopropylamines. *NIDA research monograph* **1978,** (22), 199-217.
62. Shulgin, A. T., Ethyl homologs of 2,4,5-trimethoxyphenylisopropylamine. *Journal of Medicinal Chemistry* **1968,** *11* (1), 186-187.
63. Glennon, R. A.; Liebowitz, S. M.; Leming-Doot, D.; Rosecrans, J. A., Demethyl analogs of psychoactive methoxyphenalkylamines: synthesis and serotonin receptor affinities. *Journal of Medicinal Chemistry* **1980,** *23* (9), 990-994.
64. Barfknecht, C. F.; Nichols, D. E.; Dunn, W. J., Correlation of psychotomimetic activity of phenethylamines and amphetamines with 1-

octanol-water partition coefficients. *Journal of Medicinal Chemistry* **1975,** *18* (2), 208-210.
65. Nichols, D. E.; Shulgin, A. T.; Dyer, D. C., Directional lipophilic character in a series of psychotomimetic phenethylamine derivatives. *Life Sciences* **1977,** *21* (4), 569-576.
66. Shulgin, A. T.; Dyer, D. C., Psychotomimetic phenylisopropylamines. 5. 4-Alkyl-2,5-dimethoxyphenylisopropylamines. *Journal of Medicinal Chemistry* **1975,** *18* (12), 1201-1204.
67. Nassar, A. E.; Kamel, A. M.; Clarimont, C., Improving the decision-making process in the structural modification of drug candidates: enhancing metabolic stability. *Drug discovery today* **2004,** *9* (23), 1020-8.
68. Acuña-Castillo, C.; Villalobos, C.; Moya, P. R.; Sáez, P.; Cassels, B. K.; Huidobro-Toro, J. P., Differences in potency and efficacy of a series of phenylisopropylamine/phenylethylamine pairs at 5-HT_{2A} and 5-HT_{2C} receptors. *British Journal of Pharmacology* **2002,** *136* (4), 510-519.
69. Freeman, S.; Alder, J. F., Arylethylamine psychotropic recreational drugs: a chemical perspective. *European Journal of Medicinal Chemistry* **2002,** *37* (7), 527-539.
70. Synthesis of Phenyl-2-Propanone (P2P) (Accessed 29/01/18). https://http://www.erowid.org/archive/rhodium/chemistry/phenylacetone.html.
71. U.S. Controlled Substances Act (Accessed 29/01/18). http://isomerdesign.com/Cdsa/scheduleUS.php?schedule=2&section=6&structure=U&structure=C.
72. Frank, R., The Clandestine Drug Laboratory Situation in the United States. *Journal of Forensic Sciences* **1983,** *28* (1), 18-31.
73. Inaba, S.-i.; Rieke, R. D., Metallic nickel: A coupling reagent of benzyl halides and acyl halides to yield benzyl ketones. *Tetrahedron Letters* **1983,** *24* (24), 2451-2452.
74. Julian, P. L.; Oliver, J. J.; Kimball, R. H.; Pike, A. B.; Jefferson, G. D., Alpha-Phenylacetoacetonitrile. *Organic Syntheses* **1938,** *18*, 66.
75. Herbst, R. M.; Manske, R. H.; Julian, P. L.; Oliver, J. J., Methyl Benzyl Ketone. *Organic Syntheses* **1938,** *18*, 54.
76. Power, J. D.; Clarke, K.; McDermott, S. D.; McGlynn, P.; Barry, M.; White, C.; O'Brien, J.; Kavanagh, P., The identification of 4-methylamphetamine and its synthesis by-products in forensic samples. *Forensic Science International* **2013,** *228* (1), 115-131.
77. Hass, H. B.; Susie, A. G.; Heider, R. L., Nitro Alkene Derivatives 1. *The Journal of Organic Chemistry* **1950,** *15* (1), 8-14.
78. Ballini, R.; Bosica, G., Chemoselective Conversion of Conjugated Nitroalkenes into Ketones by Sodium Borohydride-Hydrogen Peroxide: A New Synthesis of 4-Oxoalkanoic Acids, Dihydrojasmone and (±)-exo-Brevicomin. *Synthesis* **1994,** *1994* (07), 723-726.
79. Shulgin, A. T.; Shulgin, A., *PiHKAL: A Chemical Love Story*. Transform Press, Berkeley, California: **1991**.
80. Stoermer, R.; Stroh, H., Die Phenyl-benzyl-bernsteinsäuren. *Berichte der deutschen chemischen Gesellschaft (A and B Series)* **1935,** *68* (11), 2112-2116.

81. Mason, J. P.; Terry, L. I., Preparation of Phenylacetone. *Journal of the American Chemical Society* **1940,** *62* (6), 1622-1622.
82. Lee, K.; Oh, D. Y., Reaction of conjugated nitro olefins with aromatic compounds: a new acylmethylation of aromatic compounds. *Tetrahedron Letters* **1988,** *29* (24), 2977-2978.
83. Okabe, K.; Ohwada, T.; Ohta, T.; Shudo, K., Novel electrophilic species equivalent to .alpha.-keto cations. Reactions of 0,0-diprotonated nitro olefins with benzenes yield arylmethyl ketones. *The Journal of Organic Chemistry* **1989,** *54* (4), 733-734.
84. Laboratory and Scientific Section, U. N. O. D. C., Vienna, *Recommended Methods for the Identification and Analysis of Amphetamine, Methamphetamine and their Ring-Substituted Analogues in Seized Materials*. United Nations, New York: **2006**.
85. van der Ark, A. M.; Sinnema, A.; Theeuwen, A. B. E.; van der Toorn, J. M.; Verweij, A. M. A., Impurities in Illicit Amphetamine 3. Isolation and Identification of 2,4-dimethyl-3,5-diphenylpyridine, 2,6-dimethyl-3,5-diphenylpyridine and 4-methyl-5-phenyl-2-(phenylmethyl)pyridine. *Pharmaceutisch Weekblad* **1978,** *113*, 41-45.
86. van der Ark, A. M.; Sinnema, A.; van der Toorn, J. M.; Verweij, A. M. A., Impurities in Illicit Amphetamine 4. Isolation and Identification of 2-methyl-3-phenyl-6-(phenylmethyl)pyridine and 2,4-dimethyl-3-phenyl-6-(phenylmethyl)pyridine. *Pharmaceutisch Weekblad* **1978,** *113*, 341-343.
87. van der Ark, A. M.; Sinnema, A.; van der Toorn, J. M.; Verweij, A. M. A., Impurities in Illicit Amphetamine 2. Isolation and Identification of 2-benzyl-2-methyl-5-phenyl-2,3-dihydropyrid-4-one. *Pharmaceutisch Weekblad* **1977,** *112*, 980-982.
88. Hutchins, R. O.; Hutchins, M. K.; Crawley, M. L.; Mercado-Marin, E. V.; Sarpong, R., Sodium Cyanoborohydride. In *Encyclopedia of Reagents for Organic Synthesis*, **2016**.
89. Wilson, J. W., Synthesis of dl-amphetamine sulfate labeled with C14. *Journal of the American Pharmaceutical Association (Scientific ed.)* **1950,** *39* (12), 687-688.
90. Bryan, L. A. Hydrogenation of 1-phenyl-2-nitropropene to alpha-methylphenethylamines. US3458576A, **1969**.
91. Soine, W. H., Clandestine drug synthesis. *Medicinal Research Reviews* **1986,** *6* (1), 41-74.
92. Identifying and Differentiating among Clandestine Biological, Chemical, Explosives, and Methamphetamine Laboratories. DHS/I&A Chemical, Biological, Radiological, Nuclear Branch/Borders and CBRN Division and the Los Angeles Joint Regional Intelligence Centre: **2008**.
93. Scott, M. S., Clandestine Drug Labs. Office of Community Oriented Policing Services, U.S. Department of Justice: **2002**; Vol. 16.
94. Villano, M. Meth Labs' Long-Lasting Toxic Legacy (Accessed 01/02/18). http://luxecoliving.com/meth-labs-toxic/.
95. More About Meth Detection - Environmental Testing Company (Accessed 24/11/18). http://www.envtesting.com/more-about-meth

96. Grillo, I. Why Mexican crystal meth is America's problem (Accessed 01/02/18). https://www.minnpost.com/global-post/2009/07/why-mexican-crystal-meth-americas-problem.
97. 'El Chapo' Guzmán's home turf is becoming a hotbed for synthetic-drug production, https://www.businessinsider.sg/sythetic-drug-meth-production-el-chapo-guzman-home-turf-2016-10/ (Accessed 24/11/18).
98. Clandestine Labs (Accessed 01/02/18). http://www.apaic.org/index.php?option=com_content&view=article&id=363&Itemid=793.
99. Laboratory and Scientific Section, U. N. O. D. C., Vienna, *World Drug Report 2010*. United Nations, New York: **2010**.
100. Miliano, C.; Serpelloni, G.; Rimondo, C.; Mereu, M.; Marti, M.; De Luca, M. A., Neuropharmacology of New Psychoactive Substances (NPS): Focus on the Rewarding and Reinforcing Properties of Cannabimimetics and Amphetamine-Like Stimulants. *Frontiers in Neuroscience* **2016,** *10* (153).
101. Laboratory and Scientific Section, U. N. O. D. C., Vienna, *World Drug Report 2018*. United Nations, New York: **2018**.
102. Scientific Section of United Nations International Drug Control Program, V., *Drug Characterization/Impurity Profiling: Background and Concepts*. United Nations, New York: **2004**.
103. Remberg, B.; Stead, A. H., *Drug characterization/impurity profiling, with special focus on methamphetamine: Recent work of the United Nations International Drug Control Programme*. **1999**; Vol. 51, p 97-117.
104. Zaitsu, K.; Katagi, M.; Kamata, H.; Nakanishi, K.; Shima, N.; Kamata, T.; Nishioka, H.; Miki, A.; Tatsuno, M.; Tsuchihashi, H., Simultaneous analysis of six novel hallucinogenic (tetrahydrobenzodifuranyl)aminoalkanes (FLYs) and (benzodifuranyl)aminoalkanes (DragonFLYs) by GC-MS, LC-MS, and LC-MS-MS. *Forensic Toxicology* **2010,** *28* (1), 9-18.
105. Andreasen, M. F.; Telving, R.; Birkler, R. I. D.; Schumacher, B.; Johannsen, M., A fatal poisoning involving Bromo-Dragonfly. *Forensic Science International* **2009,** *183* (1–3), 91-96.
106. Duffau, B. E.; Laurie, R. C.; Rojas, S.; Rocha, R., Analysis of Bromo-DragonFLY by high-performance thin-layer chromatography. *JPC - Journal of Planar Chromatography - Modern TLC* **2016,** *29* (5), 394-396.
107. Erowid Bromo-Dragonfly Vault, https://www.erowid.org/chemicals/bromo_dragonfly/bromo_dragonfly.shtml (Accessed 21/01/18).
108. Erowid Bromo-Dragonfly Vault : Dosage, https://www.erowid.org/chemicals/bromo_dragonfly/bromo_dragonfly_dose.shtml (Accessed 09/04/18).
109. Coppola, M.; Mondola, R., Bromo-DragonFly: Chemistry, Pharmacology and Toxicology of a Benzodifuran Derivative Producing LSD-Like Effects *Journal of Addiction Research & Therapy* **2012,** *3* (4).
110. Millichap, J. G., Chapter 9: Medications for ADHD In *Attention Deficit Hyperactivity Disorder Handbook: A Physician's Guide to ADHD* 2nd ed.; Springer: New York, **2010**; p 112.
111. Wood, D. M.; Looker, J. J.; Shaikh, L.; Button, J.; Puchnarewicz, M.; Davies, S.; Lidder, S.; Ramsey, J.; Holt, D. W.; Dargan, P. I., Delayed onset

of seizures and toxicity associated with recreational use of Bromo-dragonFLY. *Journal of Medical Toxicology* **2009,** *5* (4), 226-229.
112. Erowid 2-CB-Fly Vault: Death Reports 2009, https://http://www.erowid.org/chemicals/2cb_fly/2cb_fly_death1.shtml (Accessed 16/04/18).

Chapter Two: Pyrimidine Impurities in the Leuckart Reaction

Table of Contents

Table of Contents **77**

List of Figures **81**

List of Tables **87**

2 Synthesis and Impurity Profiling of Benzyl and Phenyl Pyrimidines Associated with the Leuckart Synthesis of Bromo-DragonFLY **89**

2.1 Introduction 89

2.2 Synthesis of Phenyl Pyrimidines Associated with the Leuckart Synthesis of Bromo-DragonFLY 96

2.2.1 Synthesis of Boronic Acids 98

2.2.1.1 Boronic Acid Synthesis in the Literature 98

2.2.1.2 Synthesis of Aryl Bromide Starting Materials as Developed by ROC..... 99

2.2.1.3 Synthesis of (2,3,6,7-Tetrahydrobenzo[1,2-*b*:4,5-*b'*]difuran-4-yl)boronic Acid **(123)** 103

2.2.1.4 Synthesis of Benzo[1,2-*b*:4,5-*b'*]difuran-4-ylboronic Acid **(125)**..... 104

2.2.1.5 Synthesis of (8-Bromo-2,3,6,7-tetrahydrobenzo[1,2-*b*:4,5-*b'*]difuran -4-yl)boronic Acid **(126)** 105

2.2.1.6 Synthesis of (8-Bromobenzo[1,2-*b*:4,5-*b'*]difuran-4-yl)boronic Acid **(129)** 109

2.2.1.7 Characterisation of Boronic Acids 109

2.2.1.8 Attempted Synthesis of (4-Methylpyrimidin-5-yl)boronic Acid **(130)**..... 112

2.2.2 Synthesis of 5-Bromo-4-methylpyrimidine **(113)** 114

2.2.2.1 Synthesis of 4-Hydroxy-6-methylpyrimidine **(135)**..... 114

2.2.2.2 Synthesis of 5-Bromo-4-hydroxy-6-methylpyrimidine **(138)**..... 117

2.2.2.3 Synthesis of 5-Bromo-4-chloro-6-methylpyrimidine **(139)** 119

2.2.2.4 Synthesis of 5-Bromo-4-methylpyrimidine **(113)** 126

2.2.3 Suzuki-Miyaura Reactions to Form Phenyl Pyrimidines 129

2.2.4 Attempted Alternate Syntheses of 5-(8-bromo-2,3,6,7-tetrahydrobenzo[1,2-*b*:4,5-*b'*]difuran-4-yl)-4-methylpyrimidine **(104)** ... 139

2.2.4.1 Attempted Synthesis from the Nonbrominated Analogue **101** Using NBS 139

2.2.4.2 Attempted Synthesis of **104** from Nonbrominated Analogue **101** using Elemental Bromine 141

2.2.4.3 Attempted Synthesis of **104** using a Three-Component Coupling Reaction 146

2.2.5 Attempted Alternate Syntheses of 5-(Benzo[1,2-*b*:4,5-*b'*]difuran-4-yl)-4-methylpyrimidine **(106)** 170

2.2.5.1 Attempted Synthesis of **106** from Unaromatised Analogue **101** using NBS 170

2.2.5.2 Attempted Synthesis of **106** from Unaromatised Analogue **101** using DDQ 170

2.2.6 Isolation of 5-(8-Bromobenzo[1,2-*b*:4,5-*b'*]difuran-4-yl)-4-methylpyrimidine **(108)** 173

2.3 Synthesis of Benzyl Pyrimidines Associated with the Leuckart Synthesis of Bromo-DragonFLY 176

2.3.1 Optimisation of C-H Activation Coupling Reaction 178

2.3.2 Synthesis of Benzyl Pyrimidine Series using Optimised C-H Activation Coupling Reaction 183

2.3.3 Attempted Optimisation of the C-H Activation Coupling Reaction for Benzodifuran Substrates 186

2.3.3.1 Catalyst 186

2.3.3.2 Reaction Time 187

2.3.4 Attempted Alternate Syntheses of Benzodifuran Benzyl Pyrimidines **105** and **107** 188

2.3.4.1 DDQ 188

2.3.4.2 Chloranil 191

2.3.4.3 NBS 192

2.4 Leuckart Reactions to Produce Bromo-DragonFLY and Structrual Analogues 195

2.4.1 Preparation of Ketone Starting Materials for Leuckart Reactions…. 197

2.4.1.1 Synthesis of 1-(8-Bromo-2,3,6,7-tetrahydrobenzo[1,2-*b*:4,5-*b'*]difuran-4-yl)propan-2-one **(109)** 197

2.4.1.2 Synthesis of 1-(Benzo[1,2-*b*:4,5-*b'*]difuran-4-yl)propan-2-one **(110)** and 1-(8-Bromobenzo[1,2-*b*:4,5-*b'*]difuran-4-yl)propan-2-one **(111)**…… 201

2.4.1.3 Characterisation of Ketone Precursors 202

2.4.1.4 Impurity Profiling of DDQ oxidations of Benzylic Ketones 205

2.4.2 Preparation of *N*-Formyl Intermediates from Precursor Ketones *via* the Leuckart Reaction 210

2.4.2.1 Characterisation of *N*-Formyl Intermediates **102, 181 - 183** ……211

2.4.2.2 Impurity Profiling of *N*-Formyl Intermediates 215

2.4.3 Hydrolysis of *N*-Formyl Intermediates to Amphetamines **15, 24, 25** and **112** 223

2.5 Impurity Profiling of Amphetamine-Forming Reactions and Route-Specific Impurities by HPLC 225

2.5.1 HPLC Analysis of Individual Impurities 226

2.5.2 HPLC Analysis of Pyrimidine Isomer Mixtures 227

2.5.3 HPLC Analysis of Crude Leuckart Reaction Mixtures 228

2.5.4 HPLC Analysis of 'Clandestine' Amphetamine-Forming Hydrolysis Reactions 232

2.6 Summary of Results and Conclusions 235

References (Chapter Two)..... 242

List of Figures

Fig. 2-1: Mechanism of pyrimidine impurity formation during the Leuckart reaction to amphetamine **(1)**[1] 90
Fig. 2-2: Impurities arising from the Leuckart synthesis of 2,5-dimethoxyamphetamine **(56)**[1] 92
Fig. 2-3: Synthesis of BDF **(15)** from ketone precursor **99** 93
Fig. 2-4: Leuckart reactions of THBD-P2P **(99)** and structurally related analogues **(109 - 111)** to form amphetamines **(15, 24, 25, 112)** 96
Fig. 2-5: Suzuki-Miyaura coupling to form phenyl pyrimidines (R = H, F, OMe, CF_3, OEt, SMe)[7] 96
Fig. 2-6: Convergent synthesis of phenyl pyrimidine **101** 97
Fig. 2-7: Literature synthesis of aryl boronic acids[8,9] 98
Fig. 2-8: Synthesis of aryl bromides **116** - **119** from THBD **(42)** 99
Fig. 2-9: ^{1}H-NMR spectrum of reaction mixture at 90 h showing fully aromatised product **119** and partially aromatised intermediate **120** 100
Fig. 2-10: Attempted oxidation of **116** using chloranil 101
Fig. 2-11: Synthesis of boronic acid **123** 103
Fig. 2-12: General structure of benzodichalcogenophene systems 104
Fig. 2-13: Synthesis of benzodifuran boronic acid **125** 105
Fig. 2-14: Attempted bromination of **123** using NBS 106
Fig. 2-15: Synthesis of brominated boronic acid **126** 107
Fig. 2-16: Assignments of ^{1}H-NMR signals to boronic acid protons 108
Fig. 2-17: Assignments of ^{1}H- and ^{13}C-NMR signals to boronic acids **123**, **125** and **126** 111
Fig. 2-18: Different approaches to the Suzuki-Miyaura coupling to produce phenyl pyrimidines 112
Fig. 2-19: Attempted synthetic route to (4-methylpyrimidin-5-yl)boronic acid **(130)** 113
Fig. 2-20: Alternate attempted synthetic route to (4-methylpyrimidin-5-yl)boronic acid **(130)** 114
Fig. 2-21: Synthesis of 4-hydroxy-6-methylpyrimidine **(135)** 115
Fig. 2-22: ^{1}H- and ^{13}C-NMR signals of 4-hydroxy-6-methylpyrimidine **(135)** 116

Fig. 2-23: Synthesis of 5-bromo-4-hydroxy-6-methylpyrimidine **(138)** 117
Fig. 2-24: Differences in ^{1}H-NMR spectra between 4-hydroxy-6-methylpyrimidine **(135)** to 5-bromo-4-hydroxy-6-methylpyrimidine **(138)** 118
Fig. 2-25: Synthesis of 5-bromo-4-chloro-6-methylpyrimidine **(139)** 119
Fig. 2-26: Assignments of ^{1}H- and ^{13}C-NMR signals to proposed structure 5-bromo-4-ethoxy-6-methylpyrimidine **(140)** 120
Fig. 2-27: Acid Hydrolysis of Ethyl Acetate 121
Fig. 2-28: Proposed mechanism for the formation of **140** 122
Fig. 2-29: ^{1}H- and ^{13}C-NMR signals of proposed impurity 5-bromo-4-methoxy-6-methylpyrimidine **(141)** 123
Fig. 2-30: Hydrolysis of acetonitrile in the presence of strong acid 123
Fig. 2-31: Attempted synthesis of 5-bromo-4-chloro-6-methylpyrimidine **(139)** using oxalyl chloride and catalytic DMF 124
Fig. 2-32: Synthesis of 5-bromo-4-methylpyrimidine **(113)** 126
Fig. 2-33: Mechanism for the conversion of 5-bromo-4-chloro-6-methylpyrimidine **(139)** to 5-bromo-4-methylpyrimidine **(113)** 127
Fig. 2-34: Rotamers of azide intermediate **142** 129
Fig. 2-35: Synthesis of 5-bromo-4-methylpyrimidine **(113)** from 4-methylpyrimidine **(134)** 129
Fig. 2-36: Suzuki-Miyaura reactions to form novel phenyl pyrimidines **101**, **104** and **106** 130
Fig. 2-37: ^{1}H-NMR spectrum of **101** 132
Fig. 2-38: Potential rotational hindrance in phenyl pyrimidine **101** 133
Fig. 2-39: VT-NMR experiment with phenyl pyrimidine **101** 134
Fig. 2-40: ^{1}H- and ^{13}C-NMR shift values of the phenyl pyrimidine series **101**, **104** and **106** 135
Fig. 2-41: ^{1}H-^{1}H COSY-NMR spectrum of **101** 136
Fig. 2-42: ^{1}H-^{1}H COSY-NMR correlations in phenyl pyrimidines **104** and **106** 137
Fig. 2-43: ^{1}H-^{13}C HSQC-NMR correlations of the phenyl pyrimidine series 138
Fig. 2-44: Attempted bromination of phenyl pyrimidine **101** using NBS 139
Fig. 2-45: Synthesis of benzodifuran phenyl pyrimidine **106** using NBS 139

Fig. 2-46: Proposed mechanism for the conversion of **101** to **106** using NBS as a radical initiator 140
Fig. 2-47: Attempted bromination of THBD pyrimidine **101** using bromine in acetic acid 141
Fig. 2-48: ^{1}H-NMR spectrum of precipitate isolated from reaction of **101** with bromine in acetic acid 142
Fig. 2-49: Potential bromination products from reaction of **101** with bromine in acetic acid 143
Fig. 2-50: ^{13}C-NMR of precipitate isolated from reaction of **101** with bromine in acetic acid 144
Fig. 2-51: HSQC-NMR of precipitate isolated from reaction of **101** with bromine in acetic acid 145
Fig. 2-52: Formation of pyrimidines using a three-component coupling reaction 146
Fig. 2-53: Synthesis of pyrimidine **104** using a three-component coupling reaction 147
Fig. 2-54: Reaction pathway proposed by Sasada *et al.* for a three-component coupling reaction to form a pyrimidine[35] 148
Fig. 2-55: Preparation of ketone starting material **153** using a Friedel-Crafts acylation 149
Fig. 2-56: ^{1}H-NMR of Friedel-Crafts crude reaction mixture containing **153** 150
Fig. 2-57: Pseudo-symmetry in the THBD-ketone **153** 151
Fig. 2-58: HSQC-NMR spectrum of **153** 153
Fig. 2-59: HMBC-NMR analysis of **153** 154
Fig. 2-60: ^{13}C-NMR assignments of **153** as inferred from HMBC-NMR 155
Fig. 2-61: ^{1}H- and ^{13}C-NMR signals of THBD propiophenone **153** 156
Fig. 2-62: ^{1}H-NMR spectra of aliquots from the Friedel-Crafts formation of **153** 158
Fig. 2-63: Optimised conversion of **116** to **153** using a Friedel-Crafts reaction 159
Fig. 2-64: Attempted synthesis of brominated phenyl pyrimidine **104** using a three-component coupling reaction 160

Fig. 2-65: Modified synthesis of brominated phenyl pyrimidine **104** using a three-component coupling reaction 160
Fig. 2-66: Formation of enamine **154** using ammonium acetate **(148)** in ethanol 165
Fig. 2-67: Modified formation of enamine **154** using methanolic ammonia . 166
Fig. 2-68: ^{1}H-NMR spectra of ketone **153** and potential enamine **154** 167
Fig. 2-69: Conversion of aldehydes to imines using methanolic ammonia . 168
Fig. 2-70: ^{1}H-NMR spectra of imines **156** and **157** 168
Fig. 2-71: Synthesis of brominated phenyl pyrimidine **104** using extended reaction time 169
Fig. 2-72: Attempted synthesis of benzodifuran pyrimidine **106** using DDQ 171
Fig. 2-73: ^{1}H-NMR analysis of reaction product from attempted synthesis of **106** from unaromatised analogue **101** using DDQ 172
Fig. 2-74: Proposed reaction scheme for DDQ-mediated benzylic carbonylation on the aryl methyl group of **101**. 173
Fig. 2-75: Comparison of ^{1}H- and ^{13}C-NMR spectra of **106** and **108** 175
Fig. 2-76: Negishi palladium coupling reaction to produce a benzyl pyrimidine 176
Fig. 2-77: Proposed synthetic pathway from THBD **(42)** to the analogous benzyl zinc chloride **164** 177
Fig. 2-78: C-H activation coupling reaction to form benzyl pyrimidines 177
Fig. 2-79: Attempted synthesis of THBD benzyl pyrimidine **100** 178
Fig. 2-80: Attempted synthesis of 4-benzylpyrimidine **(168)** 179
Fig. 2-81: ^{1}H-NMR spectra of crude reaction mixture from C-H activation coupling reaction using Fairlamb's catalyst 180
Fig. 2-82: Modified synthesis of THBD benzyl pyrimidine **100** 181
Fig. 2-83: ^{1}H-NMR spectrum of **100** 182
Fig. 2-84: ^{1}H- and ^{13}C-NMR data for THBD benzyl pyrimidine **100** 183
Fig. 2-85: Synthesis of benzyl pyrimidines **103**, **105** and **107** via C-H activation coupling reaction 183
Fig. 2-86: ^{1}H-NMR data for benzyl pyrimidines **103**, **105** and **107** 185
Fig. 2-87: ^{13}C-NMR data for benzyl pyrimidines **103**, **105** and **107** 186

Fig. 2-88: Use of $Pd_2(dba)_3$ as a catalyst in the attempted C-H activation coupling reaction of **117** and **134**.....187
Fig. 2-89: Attempted synthesis of benzodifuran benzyl pyrimidines **105** and **107** using DDQ 188
Fig. 2-90: ^{1}H-NMR spectra of attempted DDQ oxidations of **100** (top) and **103** (bottom) 190
Fig. 2-91: Oxidation of benzyl pyrimidine **100** using chloranil.....192
Fig. 2-92: Attempted synthesis of benzodifuran benzyl pyrimidine **107** using NBS 193
Fig. 2-93: ^{1}H-NMR analysis of attempted oxidation of **103** using NBS.....194
Fig. 2-94: Leuckart route from P2P **(62)** to amphetamine **(1)** 196
Fig. 2-95: Leuckart reaction analysis strategy.....196
Fig. 2-96: Leuckart synthesis of amphetamines **15**, **24**, **25** and **112** 197
Fig. 2-97: Iron reduction reaction to convert nitrostyrene **174** to ketone **109** 198
Fig. 2-98: Optimised conversion of nitrostyrene **174** to ketone **109** 200
Fig. 2-99: DDQ oxidation of THBD ketones **99** and **109** 201
Fig. 2-100: ^{1}H-NMR signal assignments in ketones **99**, **109** - **111** 204
Fig. 2-101: ^{13}C-NMR signal assignments in ketones **99**, **109** - **111**.....205
Fig. 2-102: ^{1}H-NMR analysis of a potential aldehyde impurity **177** arising from DDQ oxidation of THBD ketone **99**.....206
Fig. 2-103: Decomposition of 2-propanone aryl ketone **179** to 2,5-dimethoxybenzaldehyde **(180)**.....207
Fig. 2-104: ^{13}C-NMR signal assignments for aldehyde **177**.....208
Fig. 2-105: ^{1}H-NMR analysis of potential aldehyde **178**.....209
Fig. 2-106: Preparation of *N*-formyl intermediates **102**, **181** - **183** via the Leuckart reaction 210
Fig. 2-107: Rotamers of N-formyl substrate **102** (R = THBD) 212
Fig. 2-108: ^{1}H-NMR spectrum of *N*-formyl substrate **102**.....214
Fig. 2-109: ^{1}H-NMR spectra of a mixture of benzyl and phenyl pyrimidines **100** and **101** and independently synthesised standards of **100** and **101** 216
Fig. 2-110: ^{1}H- NMR spectra of a mixture of benzyl and phenyl pyrimidines **103** and **104** and independently synthesised standards of **103** and **104** 217

Fig. 2-111: ^{1}H-NMR of a mixture of benzyl and phenyl pyrimidines **105** and **106** 218
Fig. 2-112: ^{1}H- and ^{13}C-NMR signal assignments for phenyl pyrimidine **108** 220
Fig. 2-113: ^{1}H- and ^{13}C-NMR signal assignments for **184** and **185** 223
Fig. 2-114: Hydrolysis reaction conditions for conversion of *N*-formyl substrates **102**, **181** - **183** to analogous amphetamines **15**, **24**, **25** and **112** 223
Fig. 2-115: HPLC chromatograms of isomeric pyrimidine mixtures 228
Fig. 2-116: HPLC analysis of Leuckart reaction to produce nonbrominated THBD *N*-formyl substrate **102** (top) and comparison to analytical standards **100** (middle) and **101** (bottom) 229
Fig. 2-117: HPLC analysis of Leuckart reaction to produce brominated THBD *N*-formyl substrate **181** (top) and comparison to analytical standards **104** (middle) and **103** (bottom) 230
Fig. 2-118: HPLC analysis of Leuckart reaction to produce nonbrominated benzodifuran *N*-formyl substrate **182** (top) and comparison to analytical standards **105** (middle) and **106** (bottom) 231
Fig. 2-119: HPLC analysis of Leuckart reaction to produce brominated benzodifuran *N*-formyl substrate **183** (top) and comparison to analytical standard for **107** (bottom) 232
Fig. 2-120: HPLC analysis of nonbrominated (a) and brominated (c) THBD hydrolysis reactions compared with relevant isomeric pyrimidine mixtures (b) and (d) respectively 233
Fig. 2-121: HPLC analysis of nonbrominated benzodifuran hydrolysis reaction (top) compared with benzyl pyrimidine **105** (middle) and phenyl pyrimidine **106** (bottom) standard markers 234
Fig. 2-122: HPLC analysis of brominated benzodifuran hydrolysis reaction (top) compared with the analytical standard marker for **107** (bottom) 235
Fig. 2-123: First strand of phenyl pyrimidine synthetic plan 237

List of Tables

Table 2-1: Eight potential pyrimidines formed in the Leuckart synthesis of BDF **(15)** 95
Table 2-2: Yield, m.p., R_f and HRMS data for aryl bromides **116** - **119** 102
Table 2-3: Yield, m.p., R_f, IR and ^{1}H-NMR data for boronic acids **123**, **125** and **126** 110
Table 2-4: Yield, m.p., R_f, IR and HRMS data for 4-hydroxy-6-methylpyrimidine **(135)** 116
Table 2-5: Yield, m.p., R_f, IR and HRMS data for 5-bromo-4-hydroxy-6-methylpyrimidine **(138)** 117
Table 2-6: Yield, m.p., R_f, and HRMS data for 5-bromo-4-chloro-6-methylpyrimidine **(139)** 125
Table 2-7: Yield, m.p., R_f, and HRMS data for 5-bromo-4-methylpyrimidine **(113)** and azide intermediate **142** 128
Table 2-8: Yield, m.p., R_f, and HRMS data for novel phenyl pyrimidines **101**, **104** and **106** 131
Table 2-9: ^{1}H-NMR signals of precipitate isolated from the reaction of **101** with bromine in acetic acid 143
Table 2-10: Yield, m.p., R_f, IR and HRMS data for THBD ketone **153** 150
Table 2-11: HMBC-NMR data measured for **153** 154
Table 2-12: Percentage conversion to pyrimidine **104** in three-component coupling reaction 162
Table 2-13: M.p., R_f, and HRMS data for brominated benzodifuran phenyl pyrimidine **108** 175
Table 2-14: Yield, m.p., R_f, and HRMS data for THBD benzyl pyrimidine **100** 181
Table 2-15: Yields of the benzyl pyrimidine series 184
Table 2-16: Yield, m.p., R_f, and HRMS data for benzyl pyrimidines **103**, **105** and **107** 184
Table 2-17: Yield, m.p., R_f, IR and HRMS data for benzyl pyrimidine **169** .. 191
Table 2-18: Yield, m.p., R_f, IR and HRMS data for ketones **99**, **109** - **111** .. 203
Table 2-19: Yield, m.p., R_f, IR and HRMS data for aldehyde **177** 208
Table 2-20: Yield, m.p., R_f, IR and HRMS data **102**, **181** - **183** 211

Table 2-21: Ratio of Benzyl:Phenyl Pyrimidines Isolated during Leuckart Reaction Impurity Profiling 219
Table 2-22: Yield, m.p., R_f, and HRMS data for **184** and **185** 220
Table 2-23: HMBC-NMR interactions recorded for phenyl pyrimidine **108** . 221
Table 2-24: Yield, m.p., R_f, IR and HRMS data for **15**, **24**, **25** and **112** 224
Table 2-25: Retention times of Leuckart route-specific impurities by HPLC 226

2 Synthesis and Impurity Profiling of Benzyl and Phenyl Pyrimidines Associated with the Leuckart Synthesis of Bromo-DragonFLY

As discussed in Section 1.5, the Leuckart reaction is a popular route for the synthesis of ATS and results in a number of route-specific impurities, including benzyl and phenyl pyrimidines, which account for approximately 5 % of the overall yield in a typical Leuckart reaction. In the case of BDF **(15)**, these pyrimidines have been observed, but have not been isolated, synthesised or characterised in the literature. These compounds are important from an impurity profiling perspective, as they are formed in the latter stages of product synthesis and are likely to be carried over into the finished product, meaning they are key to identifying the Leuckart route when it is used to synthesise BDF **(15)**. The work in this chapter describes the synthesis and/or isolation of eight isomeric pyrimidine impurities and their subsequent characterisation by ^{1}H-NMR, ^{13}C-NMR, IR and HRMS. HPLC profiles were also generated for the majority of the pyrimidines. Leuckart reactions were run using P2P **(62)** analogues as starting materials, and the resultant reaction mixtures were also profiled by HPLC, using the generated impurities as analytical standards to identify components within the mixtures. This data may be useful to researchers investigating the origin of impurities in BDF **(15)** and structurally related ATS.

2.1 Introduction

The pyrimidine impurities inherent to the Leuckart route to amphetamine **(1)** are formed during the condensation of the ketone starting material P2P **(62)** with formamide, as can be seen in Figure 2-1.

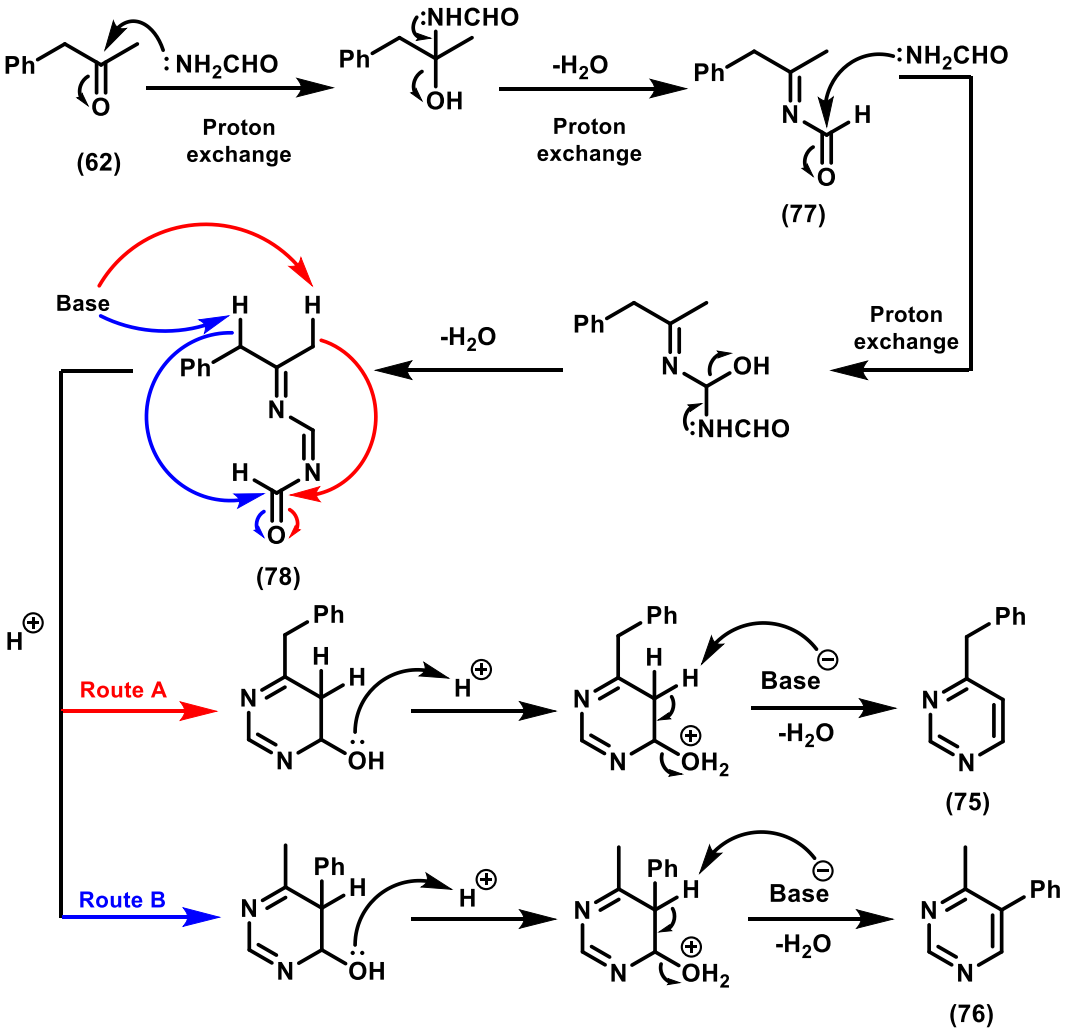
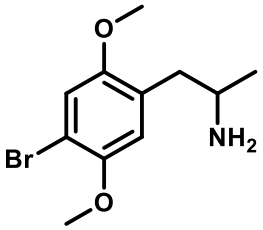


Fig. 2-1: Mechanism of pyrimidine impurity formation during the Leuckart reaction to amphetamine ***(1)***[1]

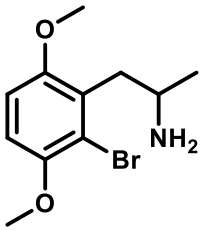
Pyrimidine impurities were first reported as characteristic impurities of the Leuckart synthetic route to amphetamine **(1)** by van der Ark *et al.* in 1978, in which they also proposed a mechanism as illustrated in Figure 2-1, where one molecule of P2P **(62)** is condensed with two molecules of formamide to form a pair of isomeric pyrimidines, **75** and **76**.[2] A subsequent review by Sinnema and Verweij in 1981 concluded that 4-methyl-5-benzylpyrimidine **(76)** was particularly important in determining the use of the Leuckart route as it was present in quantities that made it easily detectable in nearly all illicit amphetamine **(1)** tested.[3]

Further investigations into the Leuckart synthesis of amphetamine **(1)** and the impact of experimental conditions on attendant impurity profiles were carried out by Sanger *et al.* in 1985, which showed that 4-methyl-5-benzylpyrimidine **(76)** has been formed as early as 30 min into a 6 h reaction, suggesting that it forms concurrently with the *N*-formyl product **(74)**.[4] Related work by Lambrechts *et al.* in 1984 investigated differences in the impurity profile of Leuckart-synthesised amphetamine **(1)** depending on the method of purification, (i.e. steam distillation, diethyl ether extraction, recrystallisation) and found that 4-methyl-5-benzylpyrimidine **(76)** was present in all samples, though the proportion of it was less in the recrystallised sample.[5]

While investigating synthetic routes to 2,5-dimethoxyamphetamines, Dawn Griffin (DG), a previous member of our research group, isolated several route-specific impurities in the Leuckart synthesis of 2,5-dimethoxyamphetamine **(56)**, the structures of which are summarised in Figure 2-2. As expected, two isomeric pyrimidines **(91** and **92)** were isolated (which accounted for 4.9 % of the yield with respect to the *N*-formyl intermediate) along with an assortment of isomeric pyridines **(93 - 96)** (a combined 0.6 % of the yield) and a dimeric *N*-formyl impurity **(97)** (0.1 % of the yield). These trends, both in structural types of impurities and in their proportions, remained consistent across all the Leuckart reactions that Griffin performed on a variety of ketone starting materials, including those producing DOB **(2)** and 6-bromo-2,5-dimethoxyamphetamine **(98)**.[1]



(2)



(98)

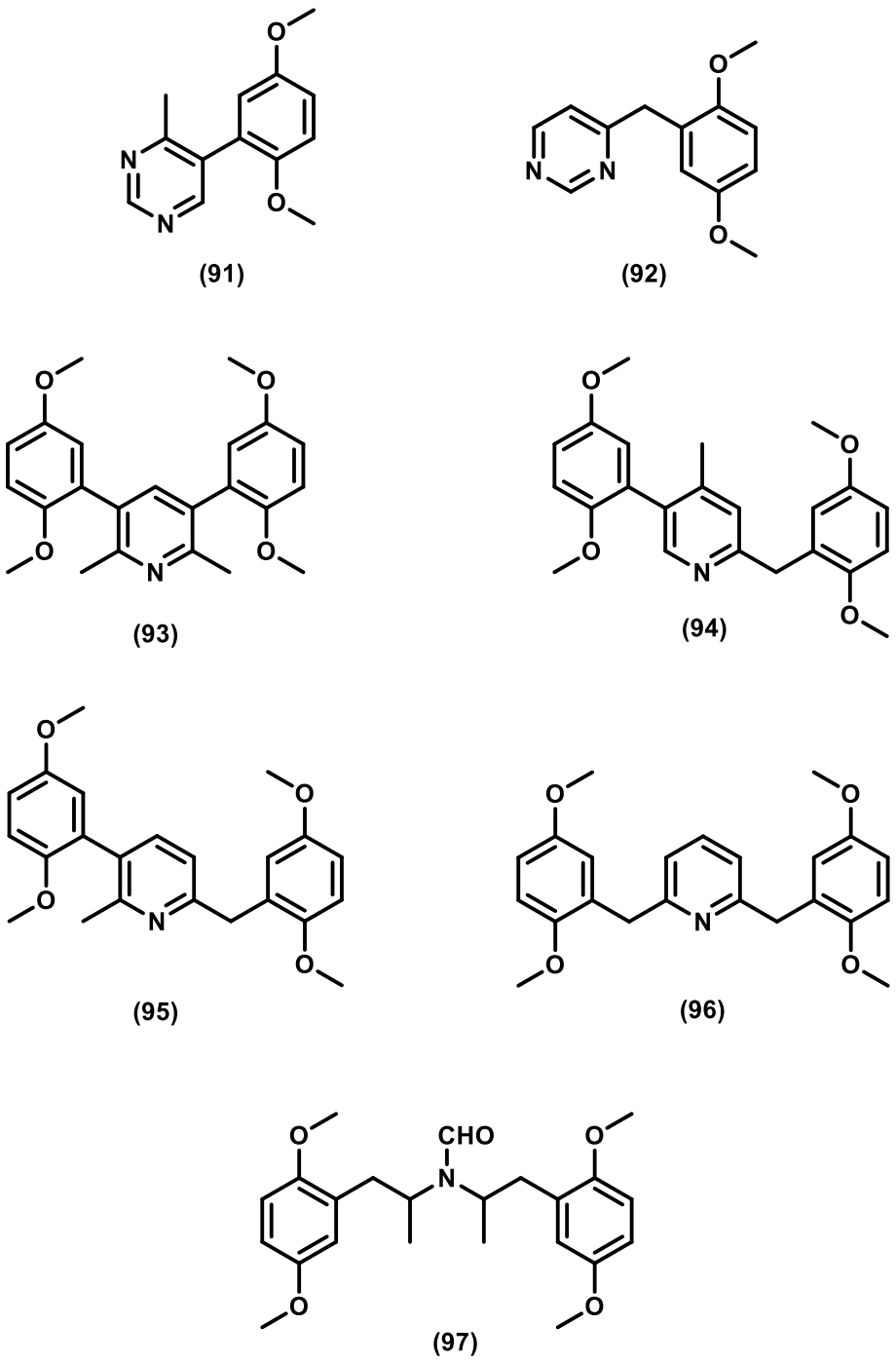
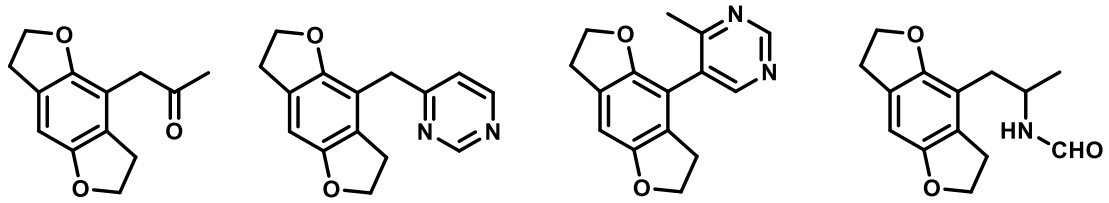


Fig. 2-2: Impurities arising from the Leuckart synthesis of 2,5-dimethoxyamphetamine ***(56)***[1]

While the pyrimidines can be separated from the *N*-formyl product by column chromatography, it has proven more difficult to separate the benzyl and phenyl isomers from each other, as they are often close in terms of their respective polarities. This was seen in work by Richard O'Connor (ROC), another former

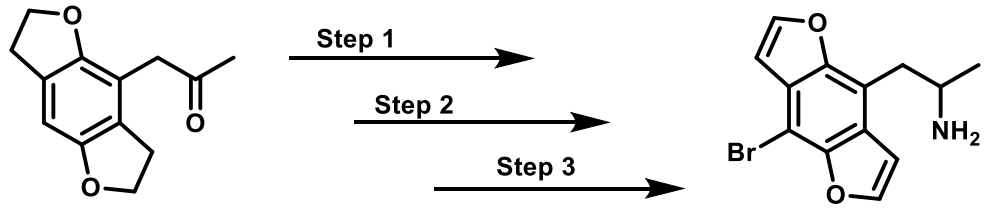
member of our research group, who described a Leuckart reaction between THBD-P2P **(99)** and formamide. He subsequently attempted to separate the isomeric pyrimidines (**100** and **101**) which were formed, but while they could be separated from the main *N*-formyl product **102**, it was not possible to completely separate **100** and **101** from each other even after extensive flash column chromatography.[6]



(99) (100) (101) (102)

To unambiguously characterise **100** and **101**, it is prudent therefore to independently synthesise both pyrimidine isomers. Those syntheses will be described later in this chapter. The targeted independent synthesis of the phenyl and benzyl pyrimidines is also necessary as proof of structure, as analytical standards need to be synthesised independently rather than isolated as by-products from reaction mixtures.

When synthesising BDF **(15)** from the nonbrominated THBD ketone precursor **(99)** as in Figure 2-3, there are three necessary chemical transformations:

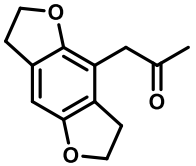
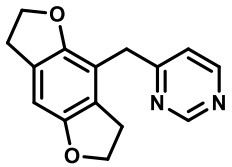
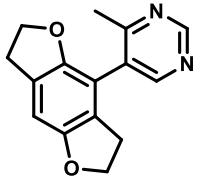
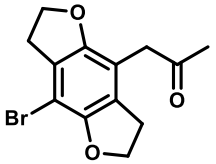
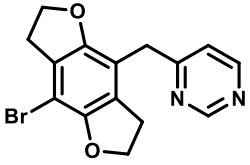
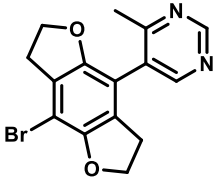
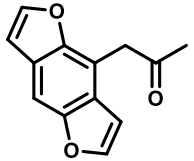
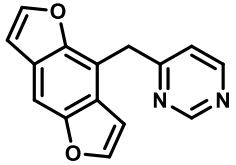
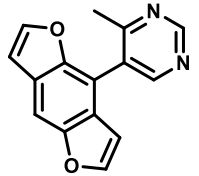
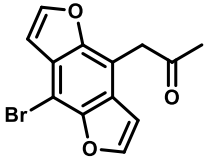
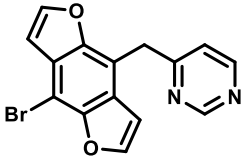
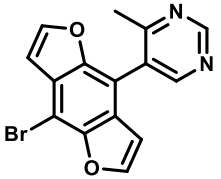


(99) (15)

*Fig. 2-3: Synthesis of BDF **(15)** from ketone precursor **99***

1. Bromination of the 4-position on the phenyl ring
2. Aromatisation of the tetrahydrobenzodifuran to a benzodifuran system
3. Leuckart reduction of the ketone to the corresponding amine

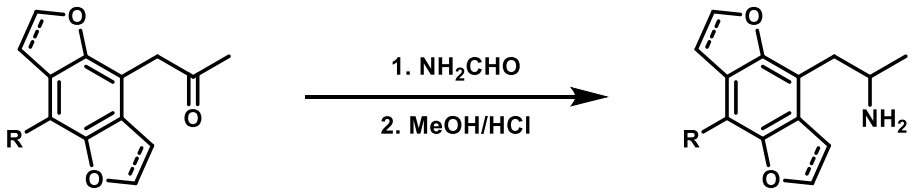
Theoretically, these three steps could be performed in any order, leading to eight potential pyrimidine impurities (four benzyl **(100, 103, 105, 107)** and four phenyl **(101, 104, 106, 108)**) depending on when in the sequence the Leuckart reaction is performed. These eight target pyrimidines **(100, 101, 103 - 108)** and the respective synthetic routes that would lead to their formation are summarised in Table 2-1 (note that the starting material for Step 1 in each case is THBD-P2P **(99)**).

Step 1	Step 2	Step 3	S.M. for Leuckart Reaction	Benzyl Pyrimidine	Phenyl Pyrimidine
Leuckart Reaction	Bromination*	Aromatisation*	 (99)	 (100)	 (101)
Bromination	Leuckart Reaction	Aromatisation	 (109)	 (103)	 (104)
Aromatisation	Leuckart Reaction	Bromination	 (110)	 (105)	 (106)
Bromination*	Aromatisation*	Leuckart Reaction	 (111)	 (107)	 (108)

**Bromination and aromatisaion can be performed in any order without impacting pyrimidine formation*

Table 2-1: Eight potential pyrimidines formed in the Leuckart synthesis of BDF ***(15)***

The purpose of this section of work is to independently synthesise and fully characterise all eight pyrimidine impurities described in Table 2-1, and to then use them as analytical standards to see if the same pyrimidines can be detected by HPLC in the reaction mixtures of the four associated Leuckart reactions described in Figure 2-4.



(99): R=H, THBD
(109): R=Br, THBD
(110): R=H, Benzodifuran
(111): R=Br, Benzodifuran

(24): R=H, THBD
(25): R=Br, THBD
(112): R=H, Benzodifuran
(15): R=Br, Benzodifuran

Fig. 2-4: Leuckart reactions of THBD-P2P ***(99)*** *and structurally related analogues* ***(109 - 111)*** *to form amphetamines* ***(15, 24, 25, 112)***

2.2 Synthesis of Phenyl Pyrimidines Associated with the Leuckart Synthesis of Bromo-DragonFLY

A review of the literature highlighted a paper by Blachut *et al.*, which used a Suzuki-Miyaura coupling between a pyrimidyl bromide and a phenyl boronic acid to synthesise a variety of phenyl pyrimidines as indicated in Figure 2-5.[7]

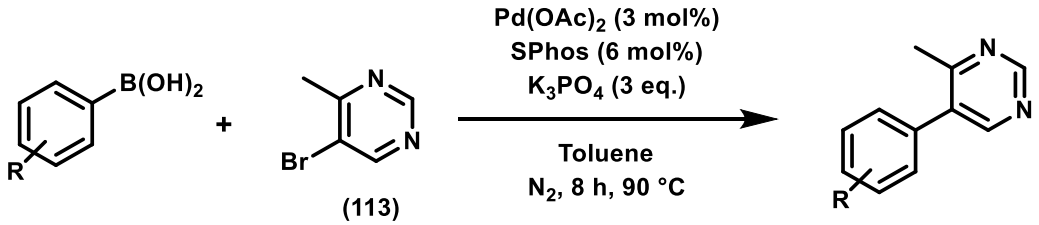


Fig. 2-5: Suzuki-Miyaura coupling to form phenyl pyrimidines (R = H, F, OMe, CF_3, OEt, SMe)[7]

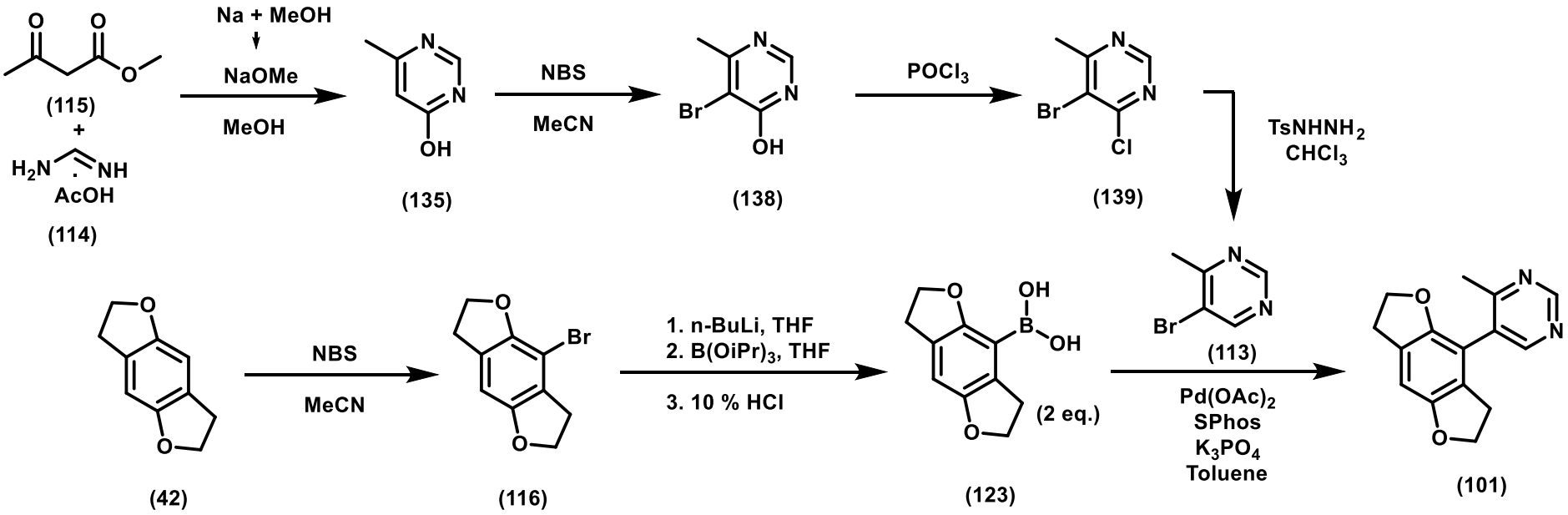


Fig. 2-6: Convergent synthesis of phenyl pyrimidine ***101***

Neither the 5-bromo-4-methylpyrimidine **(113)** nor the boronic acids required for this work were available commercially, therefore a convergent synthesis was devised in this work for the synthesis of **101**, as illustrated in Figure 2-6. This strategy employs the brominated pyrimidine **113** and boronic acid **123** in a Suzuki-Miyaura coupling final step, using THBD **(42)**, formamidine acetate **(114)** and methyl acetoacetate **(115)** as initial starting materials.

2.2.1 Synthesis of Boronic Acids

2.2.1.1 Boronic Acid Synthesis in the Literature

A review of the literature focused on synthesising boronic acids with a 2,5-alkoxy substitution pattern indicated that there are two main strategies for the synthesis of boronic acids of this type (see Figure 2-7):

1. Use of *n*-BuLi with an aryl bromide, followed by formation of a borate ester and subsequent hydrolysis using a mild acid.[8]
2. Formation of a Grignard intermediate using activated magnesium and an aryl bromide, followed by formation of a borate ester and subsequent hydrolysis using a mild acid.[9]

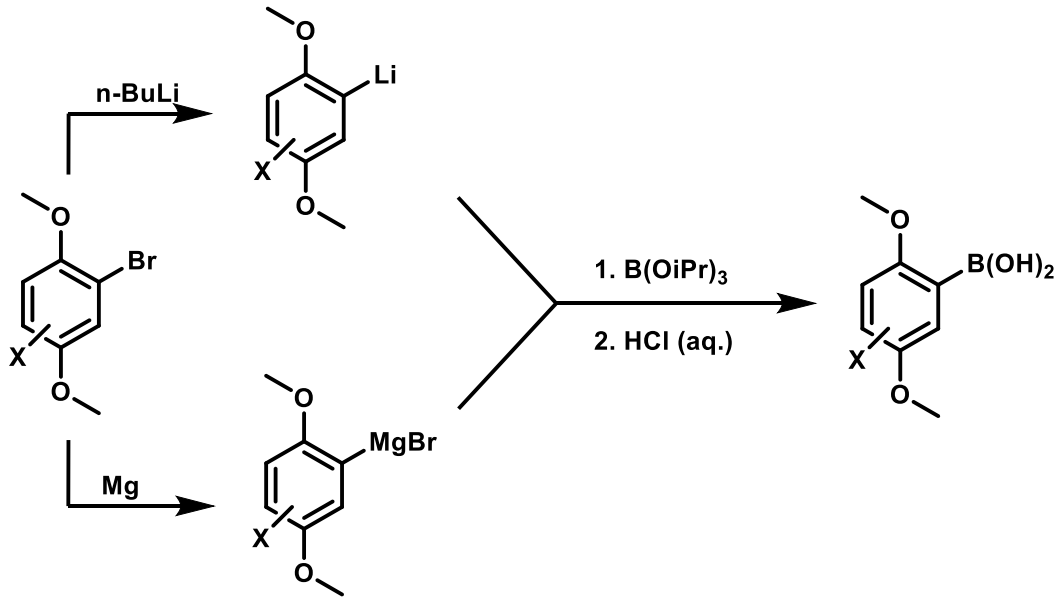


Fig. 2-7: Literature synthesis of aryl boronic acids[8,9]

2.2.1.2 Synthesis of Aryl Bromide Starting Materials as Developed by ROC

The first step in synthesising the BDF **(15)** related boronic acids **123**, **125**, **126** and **129** necessary for the Suzuki-Miyaura couplings in this work was the synthesis of the corresponding aryl bromides **116** - **119**: these were all synthesised using THBD **(42)** as a starting material, according to conditions established by ROC in his PhD thesis as illustrated in Figure 2-8:[10,11]

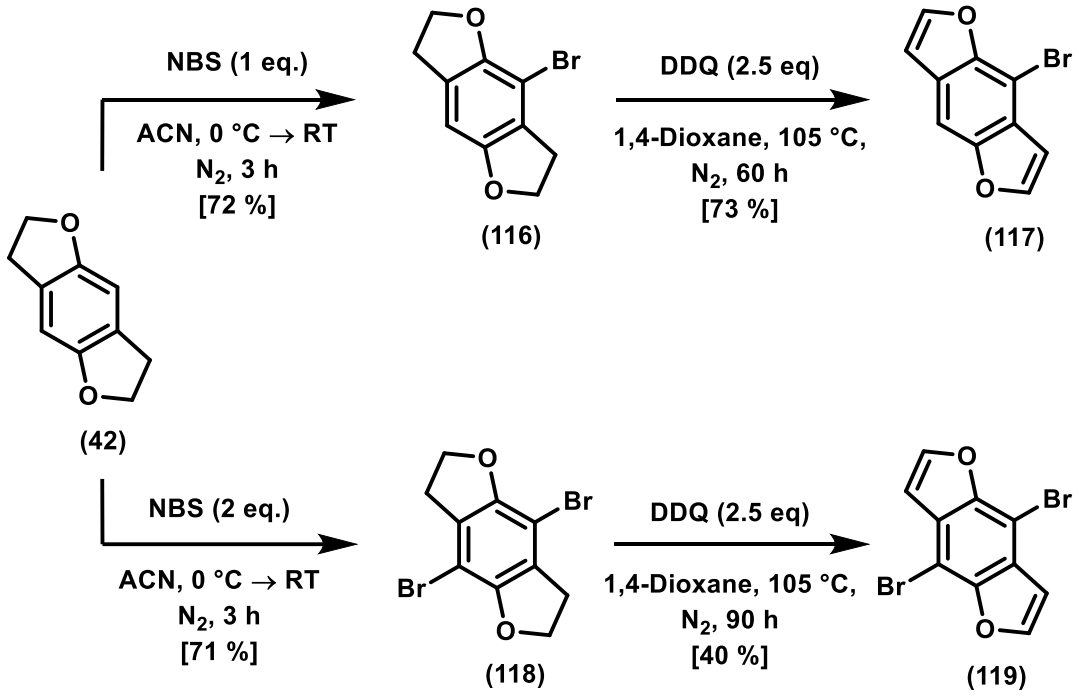


*Fig. 2-8: Synthesis of aryl bromides **116** - **119** from THBD **(42)***

The details of these procedures can be found in Chapter 4: Experimental (4.2.1); both brominations involved a transformation using *N*-bromosuccinimide (NBS) in acetonitrile (ACN), with two equivalents of NBS used to ensure dibromination in the case of **118**. For monobromination, the NBS is added portion-wise over 30 min with the reaction mixture cooled on an ice bath to prevent over-bromination. However, as this was not a concern for dibrominated compound **118**, neither cooling nor potion-wise addition was employed.

The oxidation of the tetrahydrobenzodifuran ring to a benzodifuran system using 2,3-dichloro-5,6-dicyano-1,4-benzoquinone (DDQ) was a more difficult

reaction to manage than the NBS bromination, as the use of DDQ had to be approached carefully: it releases cyanide gas in contact with water, and thus must always be carefully handled to ensure no contact with water.

Research by O'Connor *et al.* showed that it is more favourable to brominate THBD **(42)** before attempting oxidation using DDQ. However, the reaction still requires 2.5 - 3.0 equivalents of DDQ and extended reaction times of up to 90 hours to go to completion.[10] The monobrominated THBD **116** is more active towards aromatisation than its dibrominated analogue **118**: under the same reaction conditions, the aromatisation of **116** went to completion to form **117** in 60 hours, while the aromatisation of **118** was found to be only partially complete after 90 hours, with 63 % conversion to product **119** and 37 % conversion to a partially aromatised intermediate **120** observed by ^{1}H-NMR, as shown in Figure 2-9.

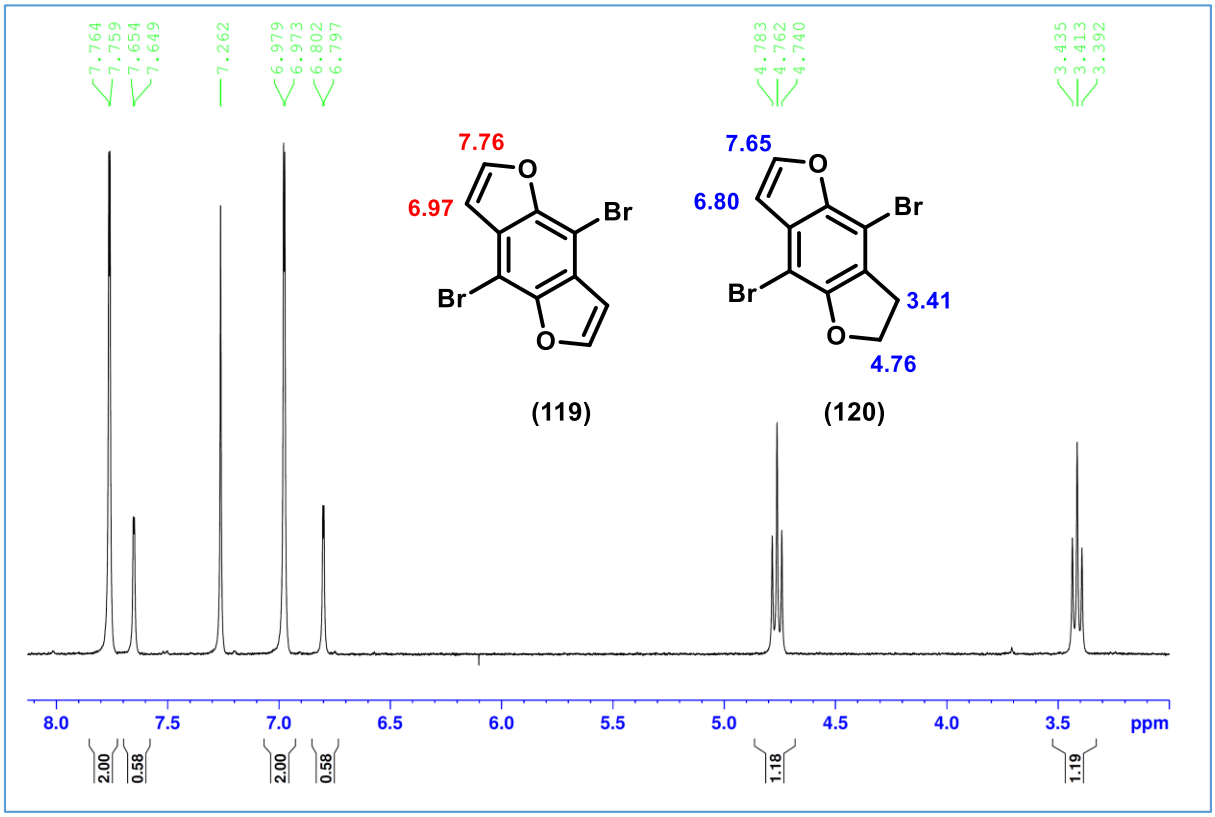


*Fig. 2-9: ^{1}H-NMR spectrum of reaction mixture at 90 h showing fully aromatised product **119** and partially aromatised intermediate **120***

After an attempt to separate **119** and **120** using column chromatography in this work was unsuccessful, a literature procedure was discovered describing the

separation of compounds based on the number of π-bonds in each compound.[12] This was done using column chromatography on silica gel impregnated with $AgNO_3$ (5 g of $AgNO_3$ on a 2.2 x 30 cm column of silica gel). A small-scale version of this column was attempted as a trial, however, it proved ineffective and no separation was seen between the product **119** and intermediate **120**. Subsequently the mixture of product and intermediate was reacted with excess DDQ (equivalents and conditions as described in Figure 2-8) and full conversion to **119** was seen by ^{1}H-NMR analysis.

An attempt was made at replacing DDQ as an oxidant with chloranil, a reagent without the toxic by-products that make DDQ so difficult to handle. This reaction was run with monobrominated THBD **116** using the same conditions as the DDQ variant, as shown in Figure 2-10. However, analysis of the crude reaction mixture by ^{1}H-NMR showed that while some product **117** was formed, most of the mixture was composed of the two partially aromatised intermediates **121** and **122** and some latent starting material **116**. These proved inseparable by column chromatography and it was concluded that chloranil was not a suitable oxidant for the desired transformation.

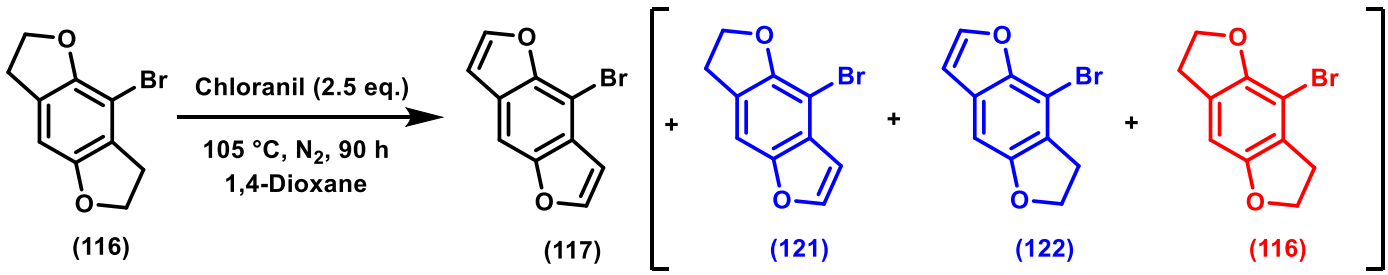


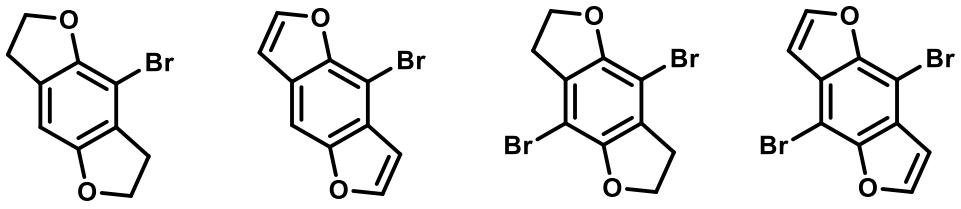
*Fig. 2-10: Attempted oxidation of **116** using chloranil*

In conclusion, the four aryl bromides required for boronic acid synthesis were synthesised in yields ranging from 40 - 73 % and characterised as summarised below in Table 2-2.

Compound Number	Yield (%)	m.p. (°C) *[Lit m.p.]*	R_f (Hex:EtOAc)	HRMS (*m/z*)	
				Calc.	Found
116	72	80 – 82 (MeOH), *[79 - 81[10] (MeOH)]*	0.60 (4:1)	240.9864	240.9864
117	73	107 - 109 (Hexane), *[107 – 109[10] (Hexane)]*	0.77 (4:1)	235.9473	Not Found
118	71	*207 - 209 (EtOH)* *[207 - 209[11] (EtOH)]*	0.69 (2:1)	318.8869	318.8873
119	40	233 - 235 (Hexane) *[235 - 237[11] (EtOH)]*	0.77 (9:1)	314.8656	314.8659

*Table 2-2: Yield, m.p., R_f and HRMS data for aryl bromides **116** - **119***

In addition to the data summarised in Table 2-2, ^{1}H- and ^{13}C-NMR spectra were also measured for each of the four aryl bromides: these were compared to the literature values published by O'Connor to confirm the structures.[10] The ^{1}H-NMR spectra were as expected: the signals for the THBD protons in **116** and **118** were seen at ~3.20 ppm (for -C**H$_2$**-CH$_2$-O-) and ~4.60 ppm (for -CH$_2$-C**H$_2$**-O-), with an aromatic 1H singlet also appearing in the spectrum of **116** at 6.56 ppm. For benzodifuran compounds **117** and **119**, there were no signals in the aliphatic region of the ^{1}H-NMR spectrum. Both substrates had signals in the aromatic region at ~6.90 ppm (for -C**H**=CH-O-) and ~7.70 ppm (for -CH=C**H**-O-), with an extra aromatic 1H singlet in the spectrum of monobrominated substrate **117** at 7.61 ppm.



The ^{13}C-NMR spectra of aryl bromides **116** - **119** were also as expected. For dibrominated substrates **118** and **119**, the ^{13}C-NMR spectra were relatively simple: these compounds are symmetrical and so only had five signals in each ^{13}C-NMR spectrum. In the THBD substrates **116** and **118**, the signals representing the aliphatic THBD carbon atoms appeared at ~31 ppm (for -**C**H$_2$-CH$_2$-O-) and ~72 ppm (for -CH$_2$-**C**H$_2$-O-). In all four substrates, signals for phenyl ring carbon atoms bound directly to bromine (**C**-Br) appeared at ~95 - 98 ppm, while those carbon atoms in the benzene ring bound to the ether oxygen atoms (**C**-O) had signals at ~149 - 154 ppm. The signals of the aryl **C**-H carbon atoms in **116** and **117** appeared at 104.9 ppm and 101.6 ppm respectively, while the remaining signals (those representing the quaternary carbon atoms in the benzene ring bound only to other carbon atoms) appeared at ~126 - 128 ppm in all four substrates.

*2.2.1.3 Synthesis of (2,3,6,7-Tetrahydrobenzo[1,2-b:4,5-b']difuran-4-yl)boronic Acid **(123)***

Based on the work of Redondo *et al.*, an initial attempt was made to synthesise THBD boronic acid **123** using *n*-BuLi and triisopropyl borate, followed by hydrolysis of the borate ester **124** to the boronic acid **123** using 10 % aq. HCl, as shown in Figure 2-11.[8]

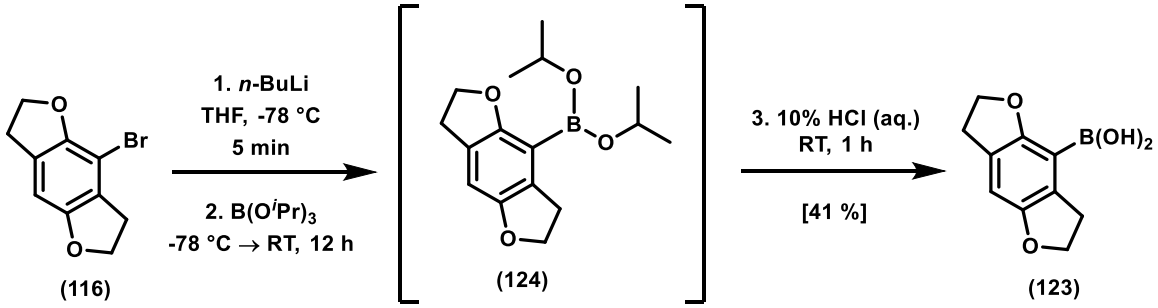


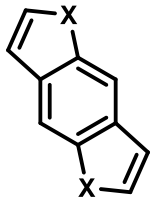
*Fig. 2-11: Synthesis of boronic acid **123***

A ^{1}H-NMR spectrum of the crude product **123** indicated *via* the characteristic signal for the boronic acid protons at δ = 5.6 ppm that **123** was formed, though the reaction had not gone to completion as starting material **116** was still evident in the reaction mixture. The crude mixture was purified by column chromatography and the isolated yield was calculated as 41 %. The yield was improved in later batches by extending the reaction time at room temperature from 12 to 20 hours, which achieved isolated yields of up to 66 % for these attempts; these are in line with the yields seen by Redondo *et al.* in their work.[8]

In some cases, column chromatography was not sufficient to completely purify the boronic acid; in these cases, acid/base extraction was used to great effect. This involved dissolving the boronic acid in chloroform, extracting with aqueous base (10 % aq. NaOH) and subsequently acidifying the aqueous layer to pH 2 with concentrated aq. HCl. At pH 2, a solid precipitated out of solution: this was filtered and was found to be pure product when analysed by ^{1}H-NMR.

*2.2.1.4 Synthesis of Benzo[1,2-b:4,5-b']difuran-4-ylboronic Acid **(125)***

While preparing to synthesise the benzodifuran boronic acid **125**, a study by Nakano *et al.* was found stating that benzodichalcogenophenes (see Figure 2-12) are not reactive towards borylation, requiring at least two days to react even with the addition of the powerful C-H activation catalyst (1,5-cyclooctadiene)(methoxy)iridium(I) dimer.[13] Nakano *et al.* surmised that the low reactivity was due to steric hindrance around the sites to be borylated, caused by the chalcogenophene rings.



X = Group 16 element,
e.g. O, S, Se

Fig. 2-12: General structure of benzodichalcogenophene systems

On this basis, it was decided to run the standard conditions developed for THBD boronic acid **123** to prepare the desired boronic acid **125**, but to extend the reaction time at room temperature from 20 hours to 140 hours as shown in Figure 2-13.

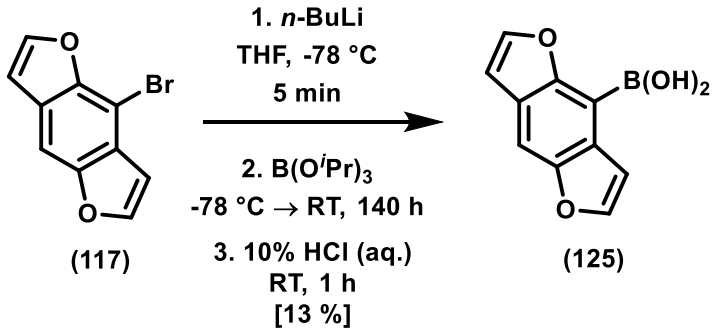


*Fig. 2-13: Synthesis of benzodifuran boronic acid **125***

The reaction was monitored by TLC (during the 140 h at room temperature in step two) and there appeared to be a decrease in starting material over time and appearance of a spot assumed to be product. However, when the reaction was worked up and the material purified by flash chromatography, the product **125** was isolated in a disappointing yield of only 13 %. This yield was over 50 % lower than for the THBD analogue **123**, under the same reaction conditions and with an extended reaction time. Given the literature precedent and the low yielding result, it was decided to investigate other more economical options for synthesising the benzodifuran phenyl pyrimidine outside of the Suzuki-Miyaura coupling.

*2.2.1.5 Synthesis of (8-Bromo-2,3,6,7-tetrahydrobenzo[1,2-b:4,5-b']difuran-4-yl)boronic Acid **(126)***

When synthesising boronic acids, whether using *n*-BuLi or a Grignard method, the starting material is invariably an alkyl or aryl halide: as the standard methods of producing a boronic acid involve cleavage of the carbon-halide bond, this presents an immediate problem when attempting to produce a brominated boronic acid as one of the carbon-bromine bonds in the dibrominated substrate is required to remain unreacted.

An initial attempt to circumvent this problem in this work was made by attempting to brominate **123** directly using NBS in a way that mimicked the process used to brominate THBD **(42)** without a boronic acid group (see Figure 2-14).

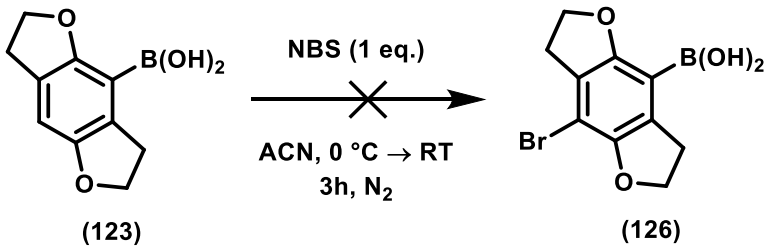
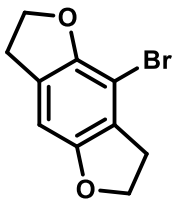


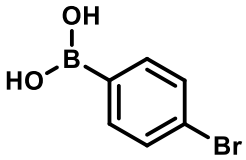
*Fig. 2-14: Attempted bromination of **123** using NBS*

^{1}H-NMR analysis of the crude reaction mixture revealed that the THBD benzene ring had been brominated, but the boronic acid group was cleaved (no boronic acid signal was observed in the 5 - 6 ppm region), giving brominated THBD **116** instead of the desired product **126**.



This is not an unexpected result as there are reports in the literature which detail borate esters and boronic acids being used as directing groups for aryl bromination.[13]

As direct bromination proved unviable, a careful review of the literature revealed that a number of studies reported the synthesis of brominated boronic acids, both by use of *n*-BuLi[14,15] and *via* a Grignard intermediate.[16,17] While the papers found reported only simple boronic acids without extensive aromatic substitution (such as (4-bromophenyl)boronic acid **(127)**), one factor was encouraging: the fact that all of the brominated boronic acids were synthesised from symmetrical dibrominated starting materials, a paradigm into which the dibrominated THBD **118** also fits.



(127)

It was decided based on previous success with the *n*-BuLi approach to the nonbrominated THBD boronic acid **123** that an initial attempt at a synthesis of **126** would be made based on a procedure put forward by Imrie *et al.*[15] This involved the use of 1.5 equivalents of *n*-BuLi followed by 6 equivalents of triisopropyl borate and subsequent hydrolysis of the borate ester **128** to the boronic acid using 10 % aq. HCl, as shown in Figure 2-15.

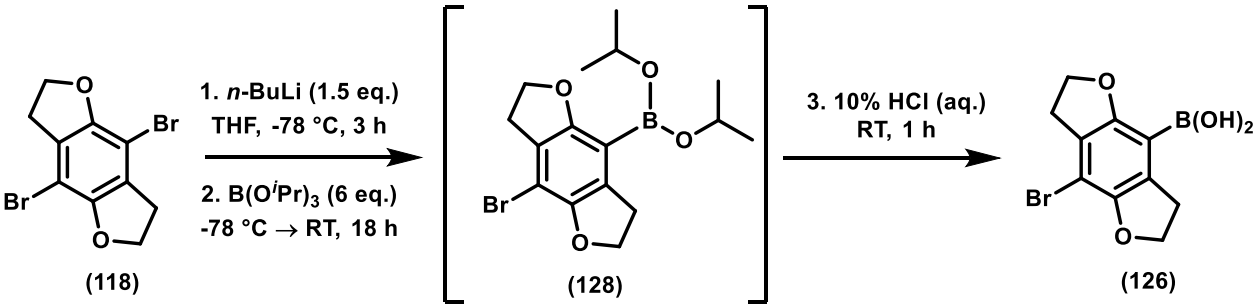


*Fig. 2-15: Synthesis of brominated boronic acid **126***

After work up, ^{1}H-NMR analysis revealed a mixture of boronic acids, with signals at δ = 5.62 and δ = 5.46 ppm, which were postulated to be the hydroxyl protons of two boronic acids. Based on past analysis, it was confirmed that the signal at δ = 5.62 ppm corresponded to the nonbrominated THBD boronic acid **123**, while the signal at δ = 5.46 ppm was tentatively assigned as the signal for the boronic acid protons of the desired product **126** as seen in Figure 2-16. This was supported by the absence of an additional signal in the aromatic region, as would be expected for the brominated boronic acid **126** (the signal for the aromatic proton in **123** was seen at δ = 6.64 ppm).

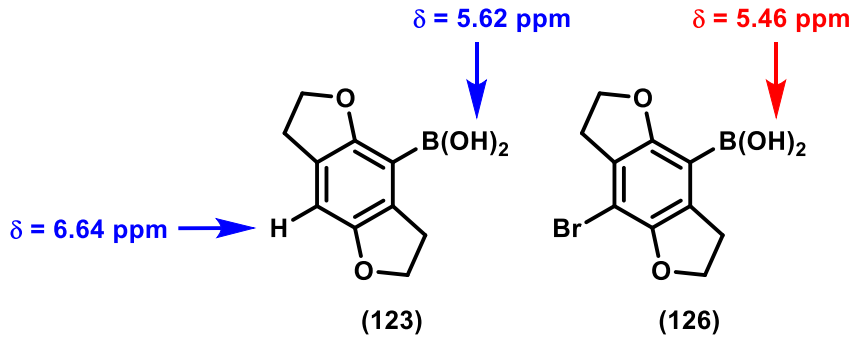


Fig. 2-16: Assignments of ^{1}H-NMR signals to boronic acid protons

Flash column chromatography proved ineffective at separating the two boronic acids with all fractions containing both **123** and **126** in varying ratios.

In an attempt to reduce the amount of **123** being formed, it was decided to reduce the equivalents of *n*-BuLi used from 1.5 to 1.0 to prevent cleavage of the second carbon-bromine bond. This was partially successful: it reduced the ratio of nonbrominated **123** to brominated **126** boronic acid from ~1:1 (50 % **123**) to ~1:20 (5 % **123**, estimated by ^{1}H-NMR integration), however column chromatography continued to be unsuccessful, with streaking noted on all attempts using a hexane:ethyl acetate solvent system on silica gel.

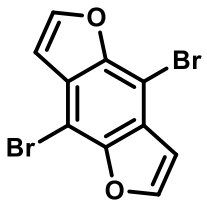
Another attempt at this reaction with the new conditions (equivalents of *n*-BuLi reduced from 1.5 to 1.0) was mostly successful: the formation of **123** was suppressed to < 5 %, as had been seen previously, however separation of the desired product **126** from other impurities (including THBD **(42)**, brominated THBD **(116)** and dibrominated THBD **(118)**) continued to be problematic.

Trituration of the crude product mixture from 9:1 hexane:diethyl ether partially purified the product **126**, however, multiple triturations were required to increase the purity of **126** to > 98 % (purity determined by ^{1}H-NMR analysis). ^{1}H-NMR analysis of the residues left when each triturate was dried *in vacuo* showed some product **126** was being lost to the triturate each time. The isolated yield of **126** from this reaction was 44 %, much lower than the 66 % seen for the THBD analogue **123** under similar reaction conditions.

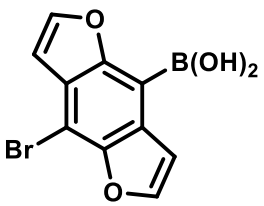
A breakthrough was made when running the reaction with 1.0 equivalent of *n*-BuLi for a third time: the reaction proceeded as normal but after the addition of the 10 % aq. HCl in step three, a white precipitate was noticed in the batch. This precipitate was collected by vacuum filtration and ^{1}H-NMR analysis confirmed it to be almost completely pure product **126**. The compound was recrystallised from absolute ethanol to remove an impurity with a broad signal at δ = 6.5 ppm in the ^{1}H-NMR (likely boric acid), leaving pure product in a good yield of 78 %.

*2.2.1.6 Synthesis of (8-Bromobenzo[1,2-b:4,5-b']difuran-4-yl)boronic Acid **(129)***

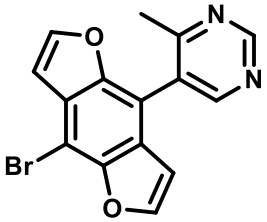
Based on the extremely poor yield of benzodifuran boronic acid **125** and the difficulty in synthesising the dibrominated benzodifuran starting material **119** in large quantities, it was decided not to attempt the synthesis of the brominated benzodifuran boronic acid **129** and to attempt to synthesise the brominated benzodifuran phenyl pyrimidine **108** by other means, which are discussed in Section 2.2.4.3.



(119)



(129)



(108)

2.2.1.7 Characterisation of Boronic Acids

Once synthesised and purified, all boronic acids were fully characterised as summarised in Table 2-3 (note: all these boronic acids are novel compounds, and do not have literature melting point values for comparison):

Compound Number	Yield (%)	m.p. (°C)	R_f (Hex:EtOAc)	IR ν_{max} O-H (cm^{-1})	^{1}H-NMR δ (ppm) of $B(OH)_2$ signals
123	66	160 - 162 (MeOH)	0.06 (6:1)	3375	5.62
125	13	174 - 175 (MeOH)	0.12 (6:1)	3401	5.59
126	78	232 - 235 (EtOH)	0.09 (6:1)	3374	5.46

*Table 2-3: Yield, m.p., R_f, IR and ^{1}H-NMR data for boronic acids **123**, **125** and **126***

The boronic acids proved to be incompatible with electrospray ionisation mass spectrometry (ESI-MS), with no molecular ions detected either in LRMS or HRMS modes: this was unexpected as there are reports of aryl boronic acids being analysed by ESI-MS in the literature.[18] Wang *el al*. described a number of potential molecular ions that could be identified after boronic acids reacted with water or methanol, including $[M+17]^-$ (after the addition of water), $[M-1]^-$ (dehydration from $[M+17]^-$) and $[M+59]^-$ (formation of $-B(OMe)_3$ in place of $-B(OH)_2$).[18] However, none of these alternate molecular ions were detected in our multiple unsuccessful attempts to measure the mass spectra of this series of boronic acids by ESI-MS before they were deemed incompatible.

The compounds were easily differentiated based on their ^{1}H-NMR spectra, with different δ values for each of the boronic acid proton signals as highlighted in Table 2-3, along with all signals for **125** in the aromatic region, and a complete lack of aromatic signals in the spectrum of **126**.

Along with ^{1}H-NMR spectra, ^{13}C-NMR spectra were also measured (full assignments can be seen in Figure 2-17). These were each characteristic of the compounds analysed, however all the ^{13}C-NMR spectra shared one common feature: the signal for the carbon atom bound to the boron atom of the boronic acid was absent in their respective spectra.

This lack of a **C**-$B(OH)_2$ signal is well documented in the literature. A paper by Bruns *et al.* explained that the lack of an *ipso* carbon signal in the ^{13}C-NMR spectra of areneboronic acids is due to quadropolar relaxtion of the ^{11}B nucleus (which has a spin of $^3/_2$): this leads to a short relaxation time and line broadening in the ^{13}C-NMR spectrum, effectively making the **C**-$B(OH)_2$ signal invisible.[19]

In Figure 2-17, there are several of the ^{13}C-NMR signal assignments marked with an asterisk (*****): these signals appear very close together in their respective ^{13}C-NMR spectra. A tentative assignment has been made based on the expected inductively electron withdrawing effect of the boronic acid moiety on the carbon atom substituent in the *ortho* position on the benzene ring (*ortho* with respect to the boronic acid), however, these signals cannot be unambiguously assigned without further 2D-NMR analysis being conducted, due to their proximity in their respective ^{13}C-NMR spectra.

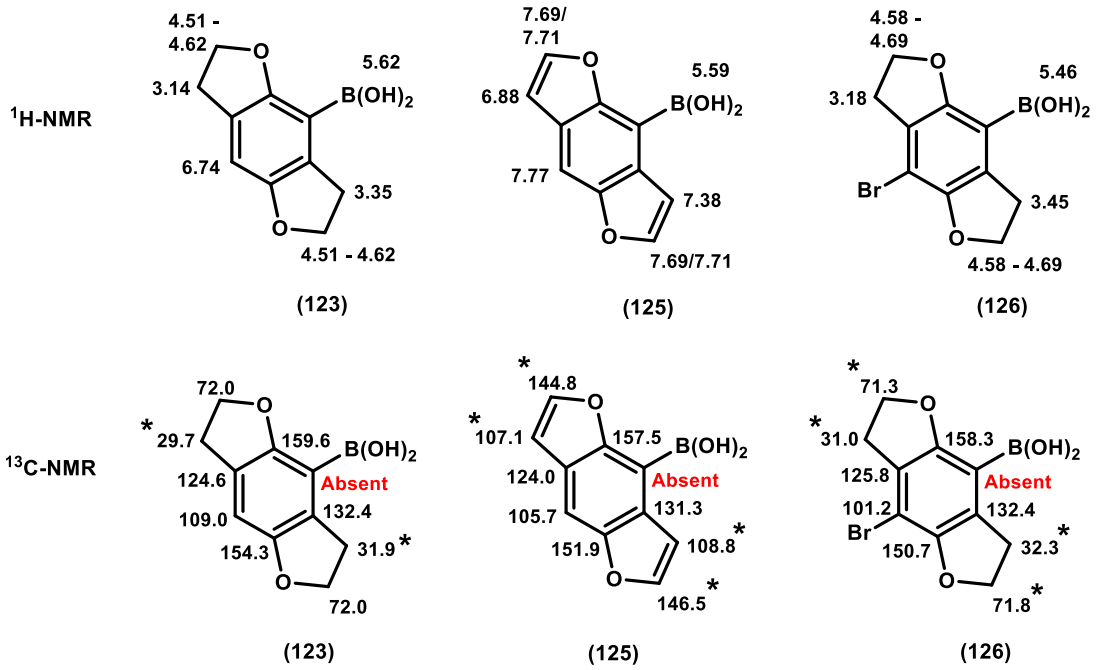


*Fig. 2-17: Assignments of ^{1}H- and ^{13}C-NMR signals to boronic acids **123**, **125** and **126***

*2.2.1.8 Attempted Synthesis of (4-Methylpyrimidin-5-yl)boronic Acid **(130)***

After the difficulties encountered synthesising benzodifuran boronic acid **125** (very low yielding, see Section 2.2.1.4), an alternate synthetic route was briefly explored involving the potential to synthesise a pyrimidinyl boronic acid **130** and employing it in a Suzuki-Miyaura coupling with the aryl bromide starting materials **117** and **119** that had already been synthesised (see Section 2.2.1.2). The purpose of this alternative strategy was primarily the hope that it would be possible to synthesise the pyrimidinyl boronic acid **130** in yields significantly higher than the 13 % which was seen when synthesising benzodifuran boronic acid **125**. This would eliminate the need to synthesise the benzodifuran boronic acids **125** and **129**, the former of which had already proven to be prohibitively low-yielding.

The differences between this proposed alternate Suzuki-Miyaura route and the Suzuki-Miyaura route that was originally planned (in Figure 2-6) are laid out in Figure 2-18.

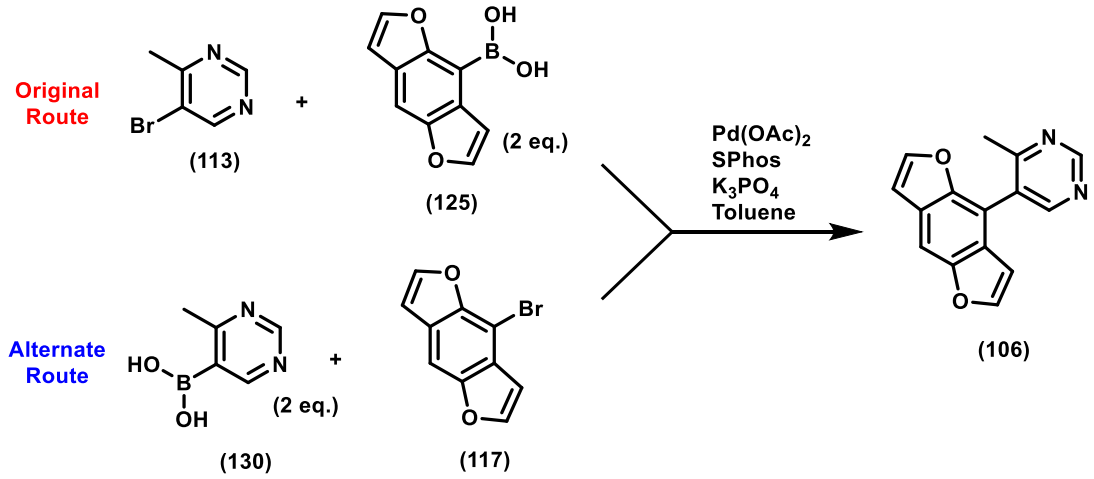
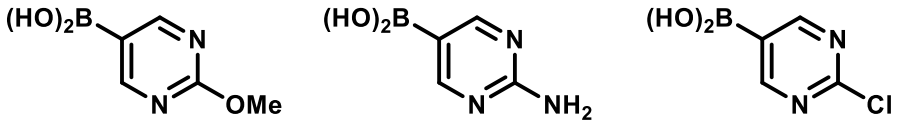


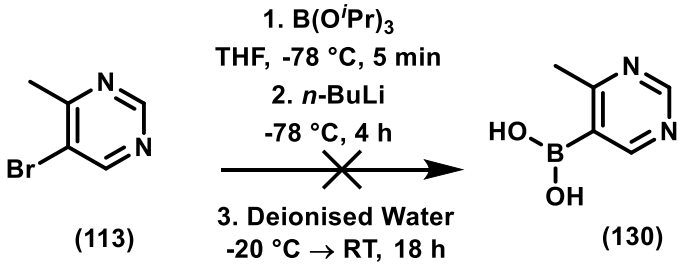
Fig. 2-18: Different approaches to the Suzuki-Miyaura coupling to produce phenyl pyrimidines

Synthesis of pyrimidinyl boronic acids has been reported in the literature by a number of different groups, including Saygili *et al.*, Naseer *et al.* and Clapham *et al.*,[20-22] all of which involve the use of *n*-BuLi, followed by triisopropyl borate and aqueous acid to hydrolyse the borate esters to the corresponding boronic acids **131 - 133**.



(131) (132) (133)

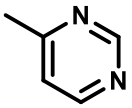
One cautionary factor which was noted was that in all of the literature examples, the boronic acid moiety was installed in a position which did not have any substituents in the *ortho* position, and frequently had a resonance electron donating substituent in the *para* position, which was not the case for the starting material of choice in this work, 5-bromo-4-methylpyrimidine **(113)** (the synthesis of which is detailed in Section 2.2.2.4). Nonetheless, an attempt was made to synthesise the corresponding boronic acid **130** using a procedure adapted from Clapham *et al.* as detailed in Figure 2-19.[22]



(113) (130)

*Fig. 2-19: Attempted synthetic route to (4-methylpyrimidin-5-yl)boronic acid **(130)***

However, the compound did not precipitate out of solution as described in the literature procedure (according to Clapham *et al.*, the work up contained an acidification step during which the product was described as precipitating from solution)[22] and when worked up using a liquid-liquid extraction, ^{1}H-NMR analysis showed that the reaction mixture contained a majority of starting material **113**, along with 4-methylpyrimidine **(134)** where the bromide had been cleaved and a small amount of what could be the desired product **130**, a mixture which proved inseparable by column chromatography.



(134)

A second attempt at the synthesis of **130** was made, this time using the procedure previously adapted from Redondo *et al.* and used to synthesise boronic acids **123, 125** and **126**, as shown in Figure 2-20.[8]

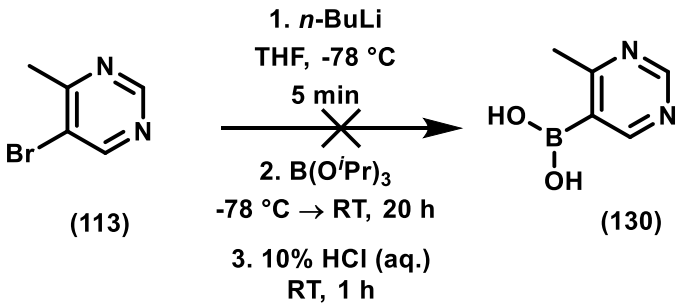


*Fig. 2-20: Alternate attempted synthetic route to (4-methylpyrimidin-5-yl)boronic acid **(130)***

After work-up, ^{1}H-NMR analysis showed that the majority component was the bromide cleavage product 4-methylpyrimidine **(134)**. Based on this result, it was decided not to pursue this line of research with the alternate Suzuki-Miyaura synthesis of **106** any further, and to concentrate on the synthesis of the phenyl pyrimidines **101, 104** and **106** *via* the Suzuki-Miyaura route that was originally proposed.

2.2.2 Synthesis of 5-Bromo-4-methylpyrimidine (113)

*2.2.2.1 Synthesis of 4-Hydroxy-6-methylpyrimidine **(135)***

When planning the convergent synthesis of the phenyl pyrimidine series as laid out in Figure 2-6, it was originally envisaged that the 4-hydroxy-6-methylpyrimidine **(135)** would be sourced commercially. This was done initially, however, it was only available in small quantities (< 1 g), which were quickly discovered to be unsuitable for starting a five-step synthetic route. Approximately 3 g of commercially sourced 4-hydroxy-6-methylpyrimidine **(135)** was used before a literature search produced a one-pot method of synthesising 4-hydroxy-6-methylpyrimdine **(135)** by forming sodium methoxide *in situ* and then adding formamidine acetate **(114)** and methyl acetoacetate **(115)** as detailed in Figure 2-21.[23]

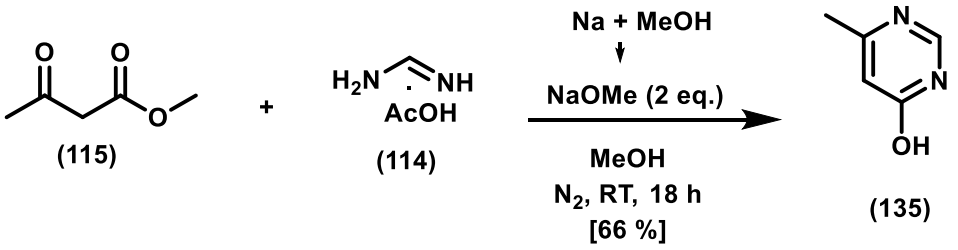
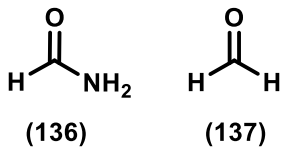


Fig. 2-21: Synthesis of 4-hydroxy-6-methylpyrimidine ***(135)***

The reaction was quenched by addition of glacial acetic acid until the mixture reached pH 7 (this quench later proved to be crucial to the success of a subsequent stage, as discussed in Section 2.2.2.3), and when ^{1}H-NMR analysis indicated the presence of potential product by distinctive pyrimidine signals in the 8 - 9 ppm region of the spectrum, an attempt was made at purification by flash column chromatography on silica gel, using 10 % methanol in dichloromethane (DCM) as an eluent system.

Streaking was observed on the column, with all fractions containing product but also organic impurities such as formamide **(136)** and formaldehyde **(137)**. Further research determined that a study by Mao *et al.* synthesising the same compound *via* an alternative route had a different approach to purification: they took the crude product and stirred it in acetone, precipitating out the product and rinsing it in acetone to recover it pure.[24]



When this was attempted for the crude product recovered from in-house synthesis of 4-hydroxy-6-methylpyrimidine **(135)**, a large quantity of white precipitate was recovered, however, when it was analysed by ^{1}H-NMR, it was noted to be mostly insoluble in the analytical solvent ($CDCl_3$) and produced a spectrum which had a noisy baseline and showed mostly solvent peaks.

Based on this evidence, it was surmised that the precipitate collected was an inorganic salt by-product of the reaction, and when the solvent was removed

from the filtrate *in vacuo* and the resultant thick yellow oil was analysed by ^{1}H-NMR, it was found to be mostly the desired product, with some minor impurities. When this material was purified by flash column chromatography (10 % methanol in DCM on silica gel), no streaking was observed and 4-hydroxy-6-methylpyrimidine **(135)** was recovered as a pale yellow solid in 66 % yield.

The pure product was fully characterised as summarised in Table 2-4:

Compound Number	Yield (%)	m.p. (°C) *[Lit m.p.]*	R_f (EtOAc:MeOH)	IR ν_{max} OH (cm^{-1})	HRMS (*m/z*)	
					Calc.	Found
135	66	145 - 147 (EtOAc) *[144^{23} (No recryst.)]*	0.16 (12:1)	3331	111.0558	111.0556

*Table 2-4: Yield, m.p., R_f, IR and HRMS data for 4-hydroxy-6-methylpyrimidine **(135)***

Full ^{1}H-NMR and ^{13}C-NMR analysis was also carried out, with characteristic pyrimidine signals observed at δ = 6.34 and 8.10 ppm in the ^{1}H-NMR and δ = 111.8, 147.6, 158.4 and 162.0 ppm in the ^{13}C-NMR. The methyl protons' signal was seen at δ = 2.34 ppm in the ^{1}H-NMR spectrum, a typical shift for this moiety, and the hydroxyl proton signal showed up as a broad bump at δ ~ 9.7 ppm. These signals are summarised in Figure 2-22.

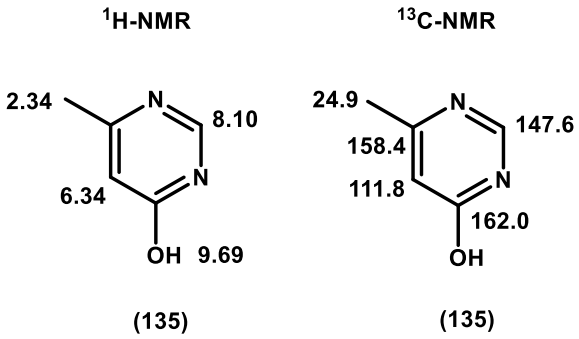


*Fig. 2-22: ^{1}H- and ^{13}C-NMR signals of 4-hydroxy-6-methylpyrimidine **(135)***

*2.2.2.2 Synthesis of 5-Bromo-4-hydroxy-6-methylpyrimidine **(138)***

Once the synthesis of 4-hydroxy-6-methylpyrimidine **(135)** was optimised, the synthesis of 5-bromo-4-hydroxy-6-methylpyrimidine **(138)** was attempted using a reaction described by Wang *et al.* as detailed in Figure 2-23.[23]

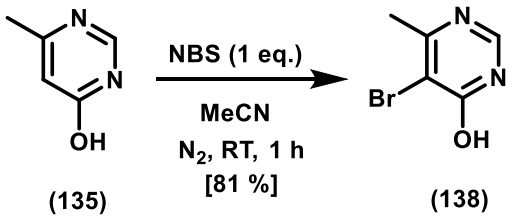


*Fig. 2-23: Synthesis of 5-bromo-4-hydroxy-6-methylpyrimidine **(138)***

Initially 5-bromo-4-hydroxy-6-methylpyrimidine **(138)** was recovered by removing the reaction solvent *in vacuo* and purifying by flash column chromatography to remove the succinimide by-product. However, in later runs the product was filtered pure as a white precipitate from the reaction mixture (an additional crop was collected by triturating the residue recovered *in vacuo* from the filtrate using ACN).

The pure product was fully characterised as detailed in Table 2-5.

Compound Number	**Yield (%)**	**m.p. (°C)** ***[Lit m.p.]***	**R_f (DCM:MeOH)**	**IR ν_{max} OH (cm^{-1})**	**HRMS (*m/z*)**	
					Calc.	**Found**
138	81	184 - 186 (No recryst.), *[184 - 185[23] (No recryst.)]*	0.06 (49:1)	3444	188.9663	188.9663

*Table 2-5: Yield, m.p., R_f, IR and HRMS data for 5-bromo-4-hydroxy-6-methylpyrimidine **(138)***

The ^{1}H-NMR spectrum of 5-bromo-4-hydroxy-6-methylpyrimidine **(138)** contained only two signals, a pyrimidine signal at δ = 8.11 ppm and the signal for the methyl protons at δ = 2.56 ppm (the hydroxyl signal did not appear).

The conversion from 4-hydroxy-6-methylpyrimidine **(135)** to 5-bromo-4-hydroxy-6-methylpyrimidine **(138)** was easily tracked by the disappearance of a pyrimidine signal at δ = 6.34 in the ^{1}H-NMR spectrum (as seen in Figure 2-24) and the corresponding change in the ^{13}C-NMR spectrum from δ = 111.8 ppm (**C**-H) for **135** to δ = 112.8 ppm (**C**-Br) for **138**.

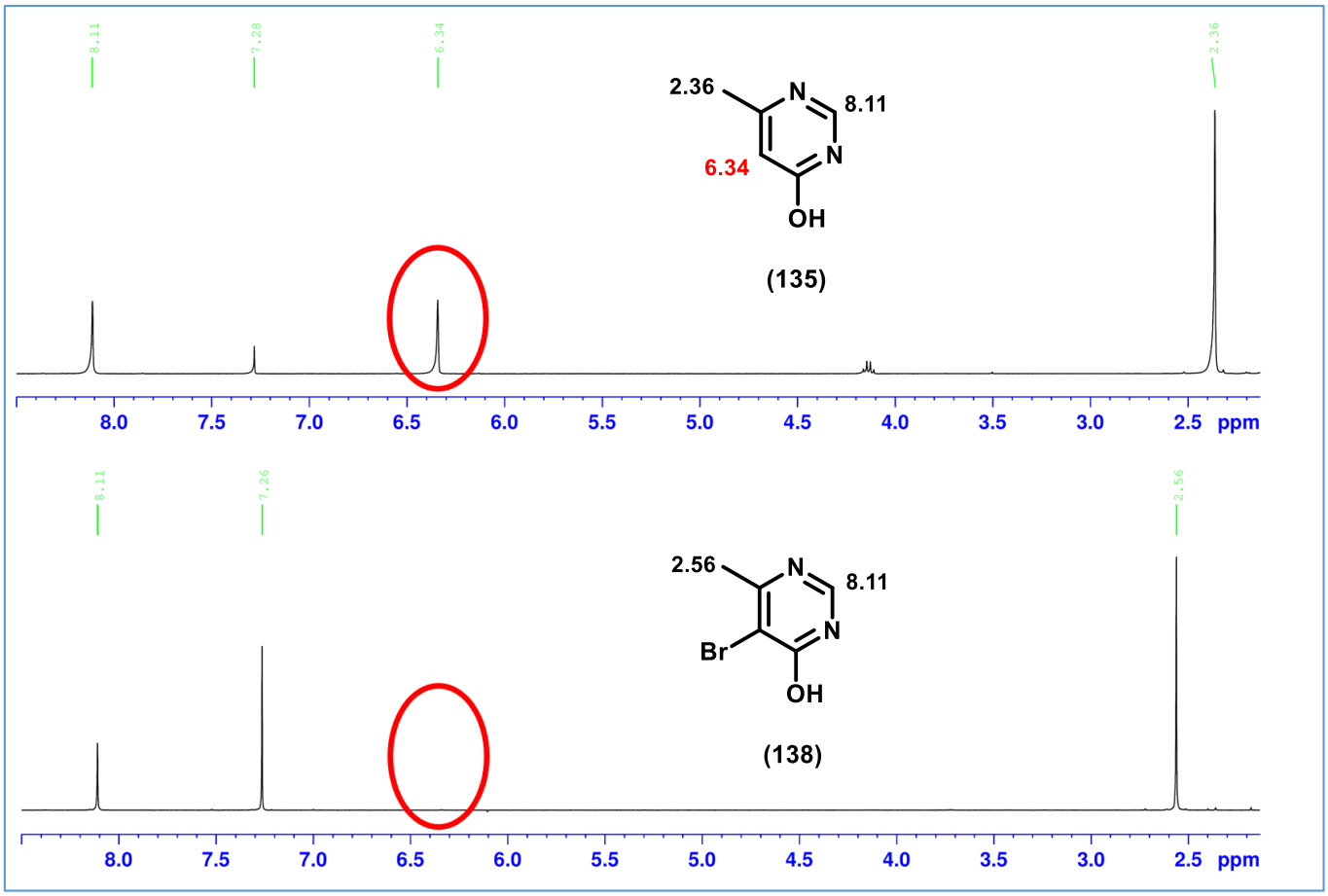


*Fig. 2-24: Differences in ^{1}H-NMR spectra between 4-hydroxy-6-methylpyrimidine **(135)** to 5-bromo-4-hydroxy-6-methylpyrimidine **(138)***

2.2.2.3 Synthesis of 5-Bromo-4-chloro-6-methylpyrimidine ***(139)***

Synthesis of 5-bromo-4-chloro-6-methylpyrimidine **(139)** was carried out according to a synthetic procedure proposed by Wang *et al.*, which involves refluxing 5-bromo-4-hydroxy-6-methylpyrimidine **(138)** in neat phosphorous oxychloride ($POCl_3$) as shown in Figure 2-25:[23]

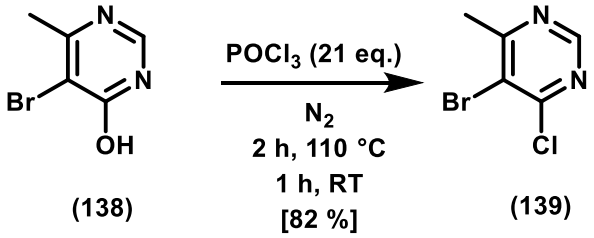


Fig. 2-25: Synthesis of 5-bromo-4-chloro-6-methylpyrimidine ***(139)***

The reaction was worked up by removal (*in vacuo*) and quenching $POCl_3$, followed by dissolution of the residue in ethyl acetate and a base wash of that solution to remove any traces of $POCl_3$. A plug column on silica gel using $CHCl_3$ as an eluent was then performed to isolate pure product.

This first attempt at the conversion of **138** to **139** (Figure 2-25) was done using 5-bromo-4-hydroxy-6-methylpyrimidine **(138)** that was synthesised using 4-hydroxy-6-methylpyrimidine **(135)** of commercial origin as a starting material (reaction described in Figure 2-23). The reaction to form 5-bromo-4-chloro-6-methylpyrimidine **(139)** proceeded without issue in good yield of 82 %.

However, a second attempt at the conversion of **138** to **139** using the same reaction conditions (Figure 2-25) was done using 5-bromo-4-hydroxy-6-methylpyrimidine **(138)** that was synthesised (as shown in Figure 2-23) using 4-hydroxy-6-methylpyrimidine **(135)** manufactured in the laboratory (Figure 2-21). This attempted conversion from **138** to **139** recorded an unexpected result: the desired product **139** was seen in analysis by ^{1}H-NMR, but it was a minor component, making up 14 % of the reaction mixture (this conversion was calculated using integration values from the ^{1}H-NMR spectrum).

The remaining 86 % was an unknown organic compound, which was identified as a probable pyrimidine based on a singlet at δ = 8.50 ppm in the ^{1}H-NMR spectrum (calibrated as integrating for one proton for the purpose of calculating % conversion), but which also clearly contained an ethyl fragment based on a 3H triplet at δ = 1.44 ppm and a 2H quartet at δ = 4.50 ppm, both with coupling constants of J = 8 Hz.

Based on starting materials used for this reaction (the conversion of **138** to **139** as shown in Figure 2-25) as well as the ^{1}H-NMR and ^{13}C-NMR analysis (as shown in Figure 2-27), the compound was provisionally identified as 5-bromo-4-ethoxy-6-methylpyrimidine **(140)** as detailed in Figure 2-26.

This proposed structure was confirmed by comparison to literature values for 5-bromo-4-ethoxy-6-methylpyrimidine **(140)** published in a study by Yamanaka *et al.* (1979), as seen in Figure 2-26.[25]

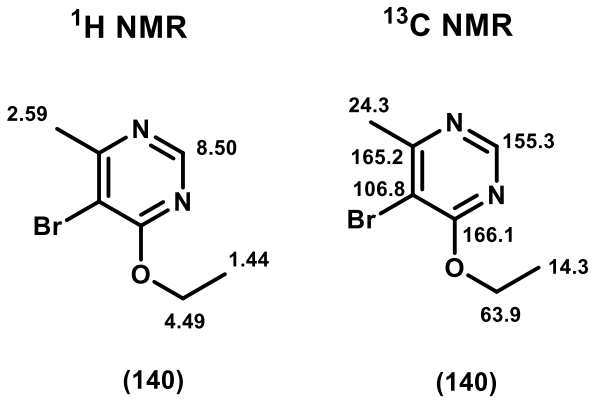


*Fig. 2-26: Assignments of ^{1}H- and ^{13}C-NMR signals to proposed structure 5-bromo-4-ethoxy-6-methylpyrimidine **(140)***

A review of the ^{1}H-NMR spectra of crude reaction mixtures and purified products **135** and **138** for previous steps showed trace amounts of acetic acid, assumed to be left over from the quench of the reaction to form 4-hydroxy-6-methylpyrimidine **(135)**, although the amounts present should not have been enough to convert over 80 % of the starting material **138** to 5-bromo-4-ethoxy-6-methylpyrimidine **(140)**.

A review of the reaction conditions noted that the reaction residue was dissolved in ethyl acetate after removal of the majority of $POCl_3$ *in vacuo*. $POCl_3$ decomposes in the presence of water to produce concentrated HCl and H_3PO_4. Ethyl acetate can contain up to 8.5 %w/w water, and thus if there was a significant amount of $POCl_3$ left in the residue when ethyl acetate was added, the $POCl_3$ could have been quenched to produce concentrated acid. This acid in turn could hydrolyse ethyl acetate to produce acetic acid and ethanol, as shown in Figure 2-27.

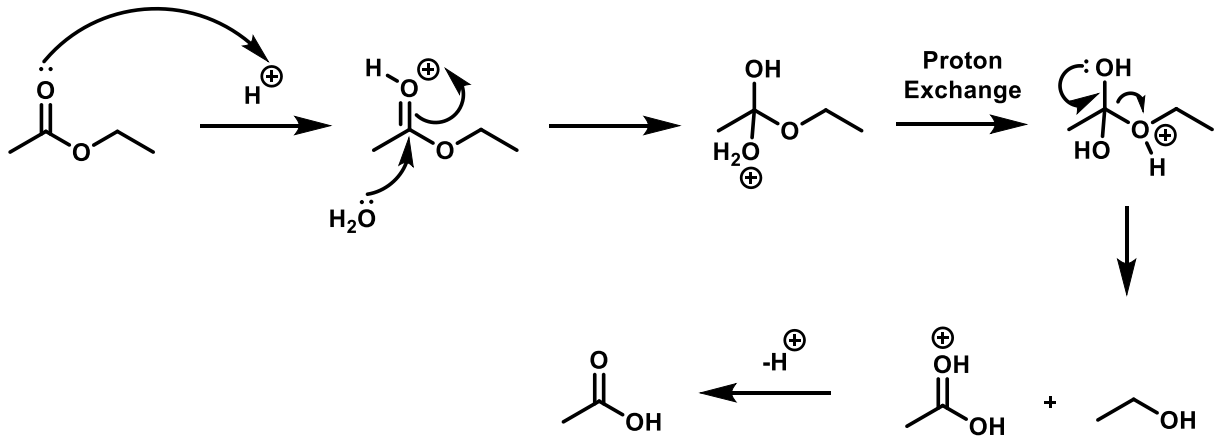


Fig. 2-27: Acid Hydrolysis of Ethyl Acetate

Based on the identity of the side-product, it was hypothesised that the product was contaminated with ethanol produced by the hydrolysis of ethyl acetate *in situ* during the work-up, which quickly led to the formation of **140** *via* nucleophilic aromatic substitution at C-6 in **139**, after the hydroxyl moiety was protonated by residual acetic acid. This proposed mechanism is detailed in Figure 2-28.

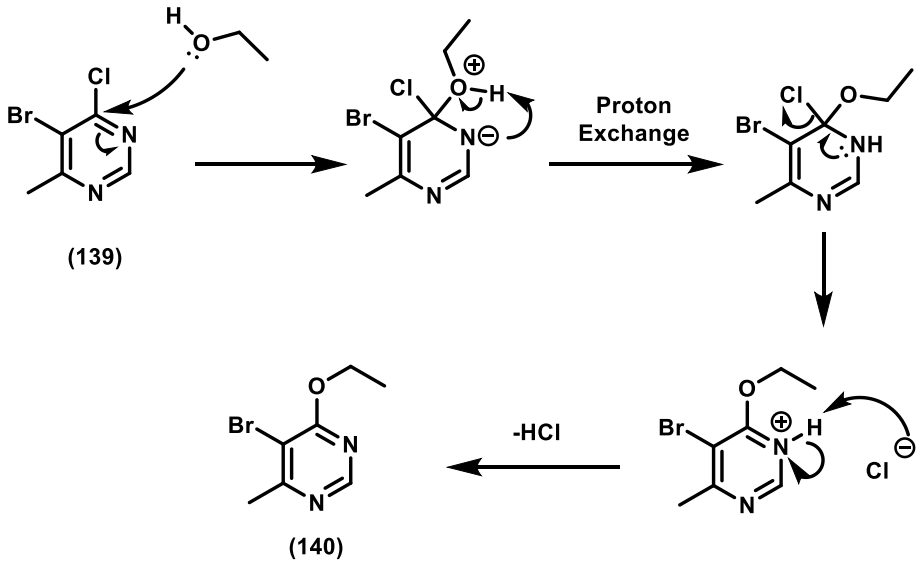


*Fig. 2-28: Proposed mechanism for the formation of **140***

In subsequent syntheses of 5-bromo-4-chloro-6-methylpyrimidine **(139)**, extra care was taken to ensure that as much $POCl_3$ as possible was removed *in vacuo* when working up the reaction to form **139** and the issue with formation of 5-bromo-4-ethoxy-6-methylpyrimidine **(140)** instead of 5-bromo-4-chloro-6-methylpyrimidine **(139)** did not recur.

An attempt was also made to reduce the amount of $POCl_3$ used in the synthesis of 5-bromo-4-chloro-6-methylpyrimidine **(139)**; $POCl_3$ reacts violently with water to produce concentrated phosphoric and hydrochloric acids and is therefore challenging to work with on larger scales (> 20 mL). It was decided to investigate the possibility of using a different solvent to conduct the reaction in and to use $POCl_3$ concurrently, but only as a reagent rather than as both solvent and reagent. As a solvent, $POCl_3$ is a polar aprotic, and dimethylformamide (DMF) was initially considered as an alternative solvent. However, this was dismissed due to the possibility of a competing Vilsmeier-Haack reaction (which uses $POCl_3$ in DMF), and ACN was chosen as an alternative polar aprotic solvent.

An initial reaction in ACN using 4 equivalents of $POCl_3$ and an extended reaction time at reflux of 22 h (instead of the standard 21 equivalents and 2 h reflux used when doing the reaction in neat $POCl_3$) led to a ~ 20 % yield

reduction of **139**, however a follow-up reaction with an extended reaction time of 48 h at reflux (82 °C) to try and increase the conversion led to the formation of a by-product (75 % conversion as measured by ^{1}H-NMR integration values). Unusual colour changes were observed during this reaction: clear yellow to clear orange to clear brown over the heating time, where the reaction usually remained clear yellow throughout. The by-product was later determined to be 5-bromo-4-methoxy-6-methylpyrimidine **(141)** based on its ^{1}H-NMR spectrum (which matched a literature synthesis by Wang *et al.*)[23] and a HRMS analysis that found the molecular ion with a mass accuracy of -1.0 ppm (within the standard of ±5 ppm), as shown in Figure 2-29.

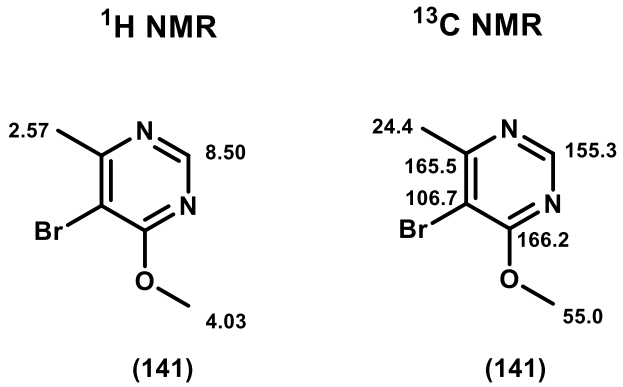


*Fig. 2-29: ^{1}H- and ^{13}C-NMR signals of proposed impurity 5-bromo-4-methoxy-6-methylpyrimidine **(141)***

It was unclear exactly how **141** was formed during the reaction: hydrolysis of acetonitrile by the strong acids produced by decomposition of $POCl_3$ at temperatures above 60 °C to give ammonium chloride and acetic acid is described in the literature by Achmatowicz *et al*. (see Figure 2-30).[57]

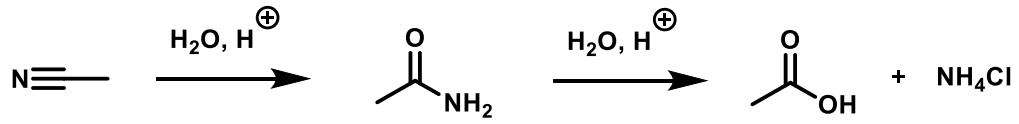


Fig. 2-30: Hydrolysis of acetonitrile in the presence of strong acid

However, while this decomposition was likely to occur during the reaction considering the reaction conditions (none of the reagents/solvents were dried and it was carried out at reflux), it does not present any obvious source of

methanol, which is the most likely reactant to produce **141** (analogous to the reaction of ethanol with **139** to produce **140** as shown in Figure 2-28).

Examination of the work-up procedure did not present an obvious source of methanol either, with ethyl acetate used as an extraction solvent. However, the analytical evidence for the presence of **141** was very strong (^{1}H- and ^{13}C-NMR data which reproduce literature values, and HRMS analysis which found the PMI), therefore while its origin within the reaction was undetermined, we were confident that **141** had been produced. Based on the initial yield reduction and subsequent synthesis of a side-product by an unknown side reaction, ACN was deemed to be an ineffective replacement for $POCl_3$ as a reaction solvent.

Following the unsuccessful trials using ACN, an attempt was made to synthesise **139** using dry tetrahydrofuran (THF) with 7.6 equivalents $POCl_3$, with a reflux reaction time of 48 h. On work up, a thick white semi-solid formed, which was insoluble in both aqueous and organic solvents. This was presumed to be a polymer formed from the reaction of THF with aqueous acid. While traces of product **139** were seen in the ^{1}H-NMR analysis of the crude reaction mixture, the polymer made the work-up extremely difficult to handle and eliminated THF as a viable solvent option for 5-bromo-4-chloro-6-methylpyrimidine **(139)** formation.

At this point, an attempt was made to eliminate $POCl_3$ from the synthesis of 5-bromo-4-chloro-6-methylpyrimidine **(139)** by using oxalyl chloride and catalytic DMF as detailed in Figure 2-31.

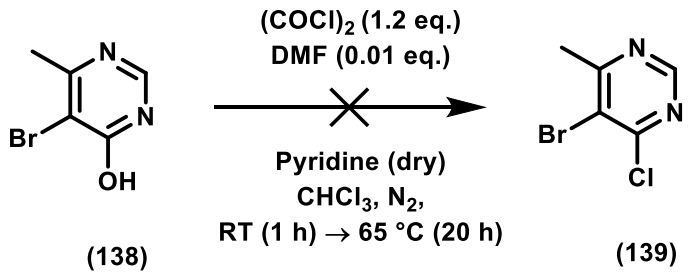


*Fig. 2-31: Attempted synthesis of 5-bromo-4-chloro-6-methylpyrimidine **(139)** using oxalyl chloride and catalytic DMF*

This method was ineffective, with only traces of product seen by ^{1}H-NMR analysis after work-up of the reaction.

After this attempt at using DMF and oxalyl chloride, it was decided to focus on reducing the equivalents of $POCl_3$ as a solvent to a more manageable volume instead of attempting to replace it. An initial run (based on the reaction conditions detailed in Figure 2-25) was done using 15 equivalents instead of 21, and this produced **139** in a comparable yield of 79 % in the same amount of time (2 h at reflux and 1 h at room temperature); all subsequent syntheses of 5-bromo-4-chloro-6-methylpyrimidine **(139)** were done with this reduced volume of $POCl_3$.

The pure 5-bromo-4-chloro-6-methylpyrimidine **(139)** was fully characterised as summarised in Table 2-6.

Compound Number	**Yield (%)**	**m.p. (°C)** ***[Lit m.p.]***	**R_f (Hex:EtOAc)**	**HRMS (*m/z*)**	
				Calc.	**Found**
139	82	56 - 57 (No recryst), *[59[23] (No recryst)]*	0.50 (4:1)	206.9325	206.9326

*Table 2-6: Yield, m.p., R_f, and HRMS data for 5-bromo-4-chloro-6-methylpyrimidine **(139)***

The ^{1}H and ^{13}C-NMR spectra of **139** were also measured, with only two signals in the ^{1}H-NMR spectrum: a pyrimidine signal at δ = 8.54 ppm and a 3H singlet at δ = 2.70 ppm representing the methyl group protons. The ^{13}C-NMR spectrum of **139** was similar to those seen previously for pyrimidines **135** and **138**, with only slight changes noted to the chemical shifts of the signals: the most notable of these was to the signal representing C-4 (**C**-Cl): in **135** and **138** (where C-4 is **C**-OH), this signal showed up at δ = 162.0 and 165.0 ppm respectively, while in **139**, it appeared at 160.6 ppm.

*2.2.2.4 Synthesis of 5-Bromo-4-methylpyrimidine **(113)***

The synthesis of 5-bromo-4-methylpyrimidine **(113)** from 5-bromo-4-chloro-6-methylpyrimidine **(139)** took place over two steps: formation of a novel tosyl hydrazone intermediate **142** followed by a Bamford-Stevens reaction as detailed in Figure 2-32.[28] The tosyl hydrazone intermediate **142** was isolated from the initial reaction as a pale yellow solid, and was stable for storage at ~4 °C for at least six months.

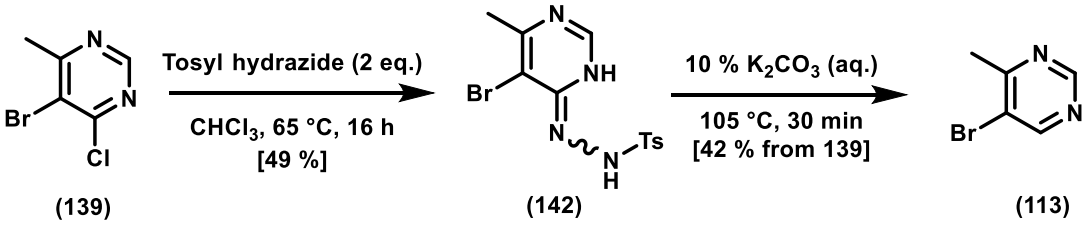


*Fig. 2-32: Synthesis of 5-bromo-4-methylpyrimidine **(113)***

The proposed mechanism (as detailed in Figure 2-33) for the overall transformation of 5-bromo-4-chloro-6-methylpyrimidine **(139)** to 5-bromo-4-methylpyrimidine **(113)** involves nucleophilic attack by the nitrogen lone pair of tosyl hydrazine followed by the Bamford-Stevens reaction: formation of a diazonium salt and loss of nitrogen gas to give the desired compound.

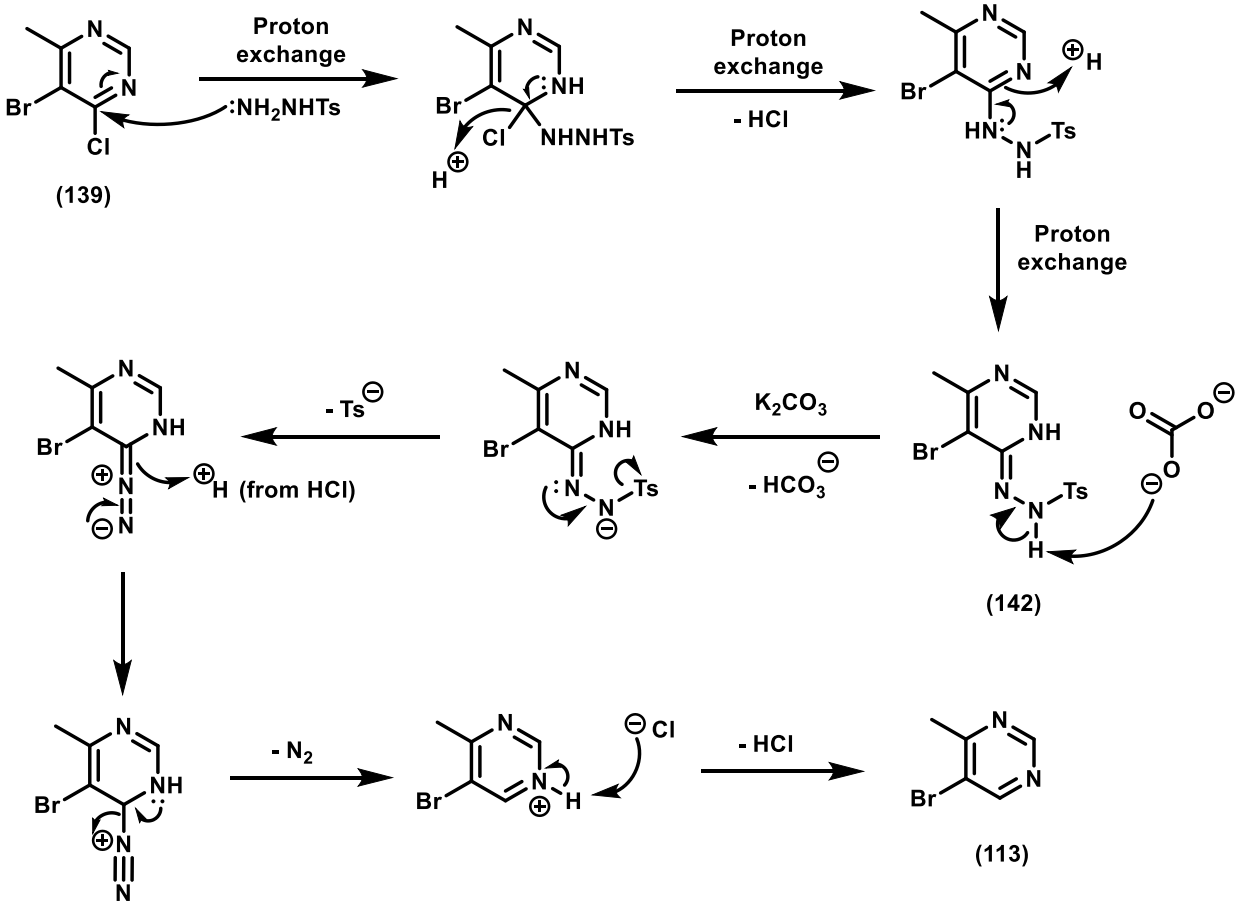


Fig. 2-33: Mechanism for the conversion of 5-bromo-4-chloro-6-methylpyrimidine ***(139)*** *to 5-bromo-4-methylpyrimidine* ***(113)***

The reaction proceeded as expected from literature precedent from Yamanaka *et al.*:[27] the only change that was made in this work from the literature procedure was a solvent switch from chloroform to DCM in the work-up. This was to facilitate isolation of the product, which had a boiling point of 90 °C and therefore had to be isolated by distillation at atmospheric pressure. Chloroform has a boiling point of 61 °C, while DCM has a boiling point of 40 °C and was therefore easier to remove by distillation without risking loss of product *in vacuo*.

5-Bromo-4-methylpyrimidine **(113)** and the novel substrate *N*'-(5-bromo-6-methylpyrimidin-4(3*H*)-ylidene)-4-methylbenzenesulfonohydrazide **(142)** were both isolated pure and fully characterised, as summarised in Table 2-7 (note that the yield of **113** is calculated from starting material **139**, not from intermediate **142**).

Compound Number	Yield (%)	m.p. (°C)	R_f (Hex:EtOAc)	HRMS (*m/z*)	
				Calc.	Found
113	42	Oil	0.16 (6:1)	172.9714	172.9711
142	49	209 - 210 (No recryst.)	0.16 (1:1)	357.0021	357.0021

*Table 2-7: Yield, m.p., R_f, and HRMS data for 5-bromo-4-methylpyrimidine **(113)** and azide intermediate **142***

The ^{1}H-NMR spectra of **113** and **142** are easily differentiated as the spectrum for **113** has only three signals (two 1H singlets at 8.72 and 8.92 ppm and a 3H singlet at 2.65 ppm), while **142** has one less signal in the pyrimidine region of the spectrum, along with a broad singlet at 6.06 ppm and another singlet at 10.40 ppm representing the two N-**H** moieties. There are also additional signals from the tosyl group in the ^{1}H-NMR of **142**, however, instead of the three extra signals which might be expected, there are six extra signals. This is due to the existence of two rotamers (*E* and *Z*) in **142**, as illustrated in Figure 2-34. These rotamers exist in an approximate ratio of major:minor = 5:1 under the conditions that the ^{1}H-NMR analysis was acquired (at room temperature in deuterated dimethylsulfoxide on a 400 MHz instrument).

It is hypothesised that the major rotamer is the *Z* rotamer, as there is a potential for hydrogen bonding to form a pseudo five-membered ring in this orientation (as illustrated in Figure 2-34), and there is less steric hindrance between the tosyl group and the large bromine atom. The only moiety which shows two sets of signals for the rotamers is the tosyl group: all other protons in the substrate appear as a single signal in the ^{1}H-NMR spectrum.

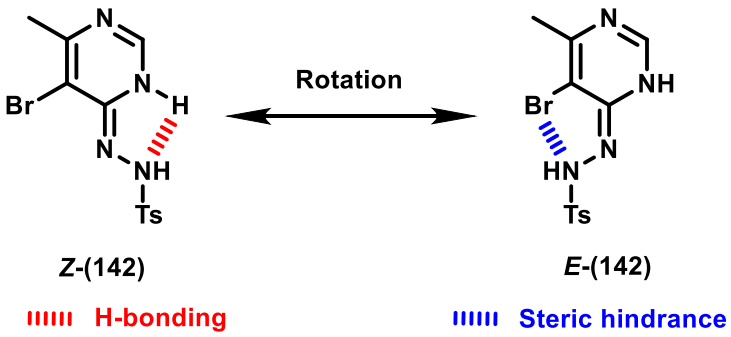


*Fig. 2-34: Rotamers of azide intermediate **142***

The only major difference between the ^{13}C-NMR spectra of **113** and its precursor **139** is the appearance of a **C**-H signal at 156.6 ppm in place of the quaternary carbon (**C**-Cl) signal at 160.6 ppm in **139**. The ^{13}C-NMR spectra of **113** and **142** can be easily distinguished by the appearance of two sets of signals for the *E*/*Z* tosyl groups in the spectrum of **142** (again, only the tosyl signals appear in duplicate). There is also a significant change in the shift of the signal representing **C**-Br between the two substrates, with that signal appearing at 121.6 ppm in **113**, but at 101.7 ppm in **142**, a shift of ~20 ppm.

An attempt was also made in this work to synthesise 5-bromo-4-methylpyrimidine **(113)** directly from 4-methylpyrimidine **(134)** using NBS, as detailed in Figure 2-35.

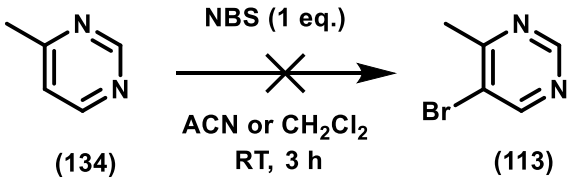


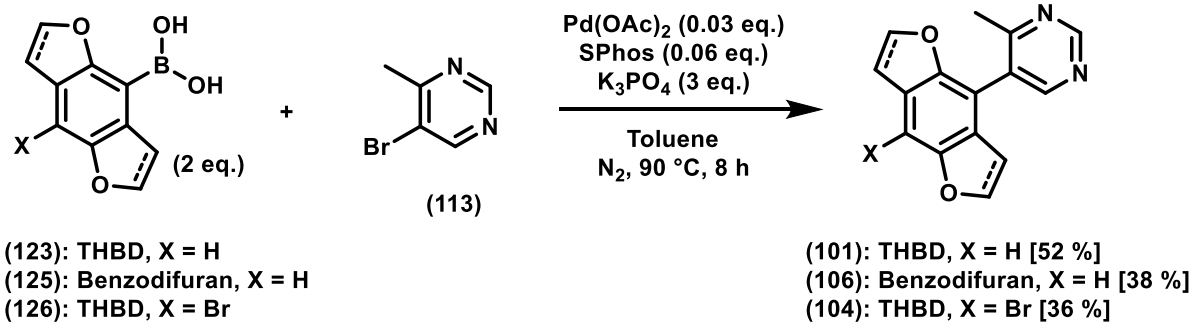
*Fig. 2-35: Synthesis of 5-bromo-4-methylpyrimidine **(113)** from 4-methylpyrimidine **(134)***

This was attempted in both ACN and DCM, but neither reaction produced any of the desired product and this route was deemed unviable.

2.2.3 Suzuki-Miyaura Reactions to Form Phenyl Pyrimidines

Once the boronic acids **123**, **125** and **126** were synthesised, along with a stock

of 5-bromo-4-methylpyrimidine **(113)**, three Suzuki-Miyaura reactions were performed according to the literature procedure from Blachut *et al.* to form the novel phenyl pyrimdines **101**, **104** and **106** in generally poor yields as seen in Figure 2-36.[7]



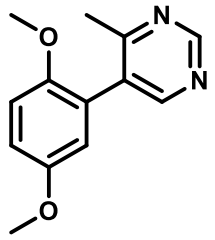
(123): THBD, X = H
(125): Benzodifuran, X = H
(126): THBD, X = Br

(101): THBD, X = H [52 %]
(106): Benzodifuran, X = H [38 %]
(104): THBD, X = Br [36 %]

*Fig. 2-36: Suzuki-Miyaura reactions to form novel phenyl pyrimidines **101**, **104** and **106***

The reactions themselves progressed without issue: the set up was not complex, nor was the work up, and the literature reaction conditions immediately produced the desired products, which were isolated by column chromatography on silica gel. The isolated yield of **101** was moderate although it was low compared to yields reported by Blachut *et al*.[7] in their work describing similar Suzuki-Miyaura reactions, which ranged from 75 - 92 %.

While Blachut *et al*. did not use substrates with THBD-type structures, they did use aryl substrates with multiple methoxy substituents (n = 1 - 3), with the 2,5-dimethoxy substituted aryl substrate **91** having the lowest yield of 75 %.

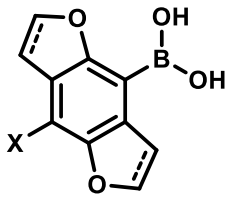


(91)

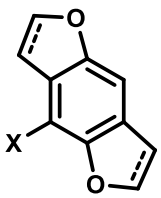
This led us to hypothesise that increased electron density in an aromatic system decreases the overall reactivity of the system towards borylation. This correlates to data previously gathered when synthesising boronic acid **125**

(see Section 2.2.1.4), and was also supported by the isolated yields of **104** and **106**, which were more disappointing at 36 % and 38 % respectively. Both **104** and **106** are more electron dense than **101** due to the bromine substituent (**104**) and the increased aromaticity of the system (**106**).

The main impurities seen in each of the crude reaction mixtures were the boronic acid starting material (**123**, **125** or **126**), and the related cleavage products (**42**, **43**, **116**) where the boronic acid moiety was replaced by a proton instead of coupling to 5-bromo-4-methylpyrimidine **(113)**.



(123): THBD, X=H
(125): Benzodifuran, X=H
(126): THBD, X=Br



(42): THBD, X=H
(43): Benzodifuran, X=H
(116): THBD, X=Br

THBD phenyl pyrimidine **101** was isolated by flash column chromatography, while brominated THBD phenyl pyrimidine **104** and benzodifuran phenyl pyrimidine **106** were isolated by preparative TLC as the reactions were performed on a scale that made column chromatography unsuitable. The pure novel products were fully characterised as summarised in Table 2-8.

Compound Number	Yield (%)	m.p. (°C)	R_f (Hex:EtOAc)	HRMS (*m/z*)	
				Calc.	Found
101	52	Semi-solid	0.08 (5:1)	255.1134	255.1134
104	36	Semi-solid	0.22 (1:1)	333.0239	333.0240
106	38	128 - 129 (No recryst)	0.32 (1:1)	251.0820	251.0821

*Table 2-8: Yield, m.p., R_f, and HRMS data for novel phenyl pyrimidines **101**, **104** and **106***

It was noted in the ^{1}H-NMR spectra of **101** and **104** that instead of the signals for H-3 and H-7 appearing as either two 2H triplets or a 4H multiplet at approximately 2.80 - 3.20 ppm – as seen for the analogous benzyl pyrimidines **100** and **103** (see Figure 2-83 and Figure 2-86 in Section 2.3) – a 2H triplet and two 1H multiplets were observed, as seen for **101** in Figure 2-37.

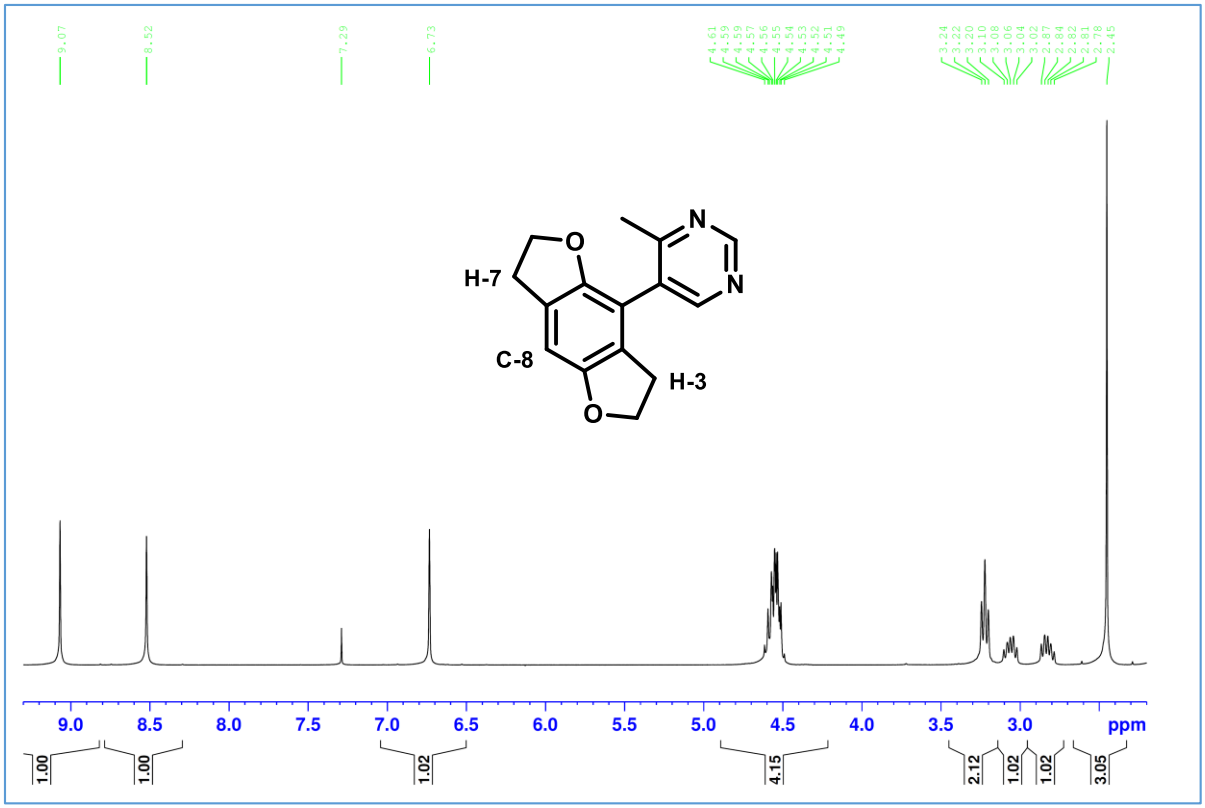
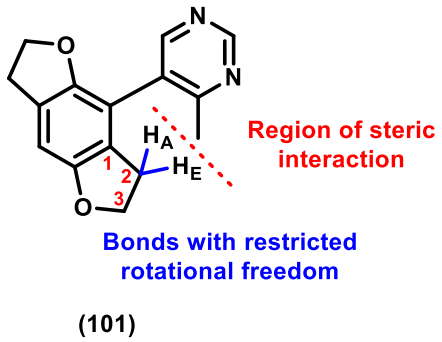


*Fig. 2-37: ^{1}H-NMR spectrum of **101***

Examination of the HMBC-NMR spectrum measured for **101** showed a correlation between the 2H triplet at 3.22 ppm and the ^{13}C-NMR signal at 106.6 ppm, a signal which represents the **C**-H of the aryl ring (C-8 in Figure 2-37). There was no correlation between either of the 1H multiplets at 2.83 and 3.06 ppm and the ^{13}C-NMR signal at 106.6 ppm. This confirms that the triplet at 3.22 ppm represents H-7 which are 3 bonds away from C-8, as opposed to H-3, which are 4 bonds away.

Initially it was hypothesised that this was caused by a phenomenon known as atropisomerism: this is a type of axial chirality where a compound exists as two rotamers due to rotational hindrance around a single bond, usually caused by steric strain within the molecule in question.[28] In this case it was envisaged

that the hydrogen atoms H_A and H_E in Figure 2-38 would be affected by steric strain from the nearby methyl group on the pyrimidine ring and are therefore forced into two distinct and energetically inequivalent positions, one axial (H_A) and one equatorial (H_E). Due to their difference in energetic properties, these protons would appear as distinct signals in the ^{1}H-NMR spectrum.



(101)

Fig. 2-38: Potential rotational hindrance in phenyl pyrimidine ***101***

However, there was also the possibility that the two 1H multiplets were caused by diastereotopic protons at H-3: this refers to two protons where if either proton were replaced by a substituent which was not a proton, it would result in the formation of diastereoisomers.[30] The easiest way to distinguish between these two possibilities was to perform variable temperature NMR (VT-NMR), an experiment in which NMR spectra are measured over a range of temperatures. If the 1H multiplets were caused by atropisomerism, recording the ^{1}H-NMR spectrum at a higher temperature should overcome the energy barrier to rotation and the two 1H multiplets should coalesce into one signal. However, if the multiplets are caused by diastereotopic protons, the phenomenon should be unaffected by the high temperature NMR experiment.

The VT-NMR experiment was carried out using **101** in deuterated DMSO (deuterated chloroform was used for previous NMR analysis, but due to the higher temperatures used during VT-NMR, the boiling point of chloroform – 61°C – rendered it unsuitable in this case). Three ^{1}H-NMR spectra were measured at 27, 47 and 67 °C, and the two 1H multiplets were observed at the same shifts in all three spectra, with no coalescence observed (see Figure 2-39: note that the singlet that moves from 3.33 to 3.20 to 3.11 ppm is the water signal).

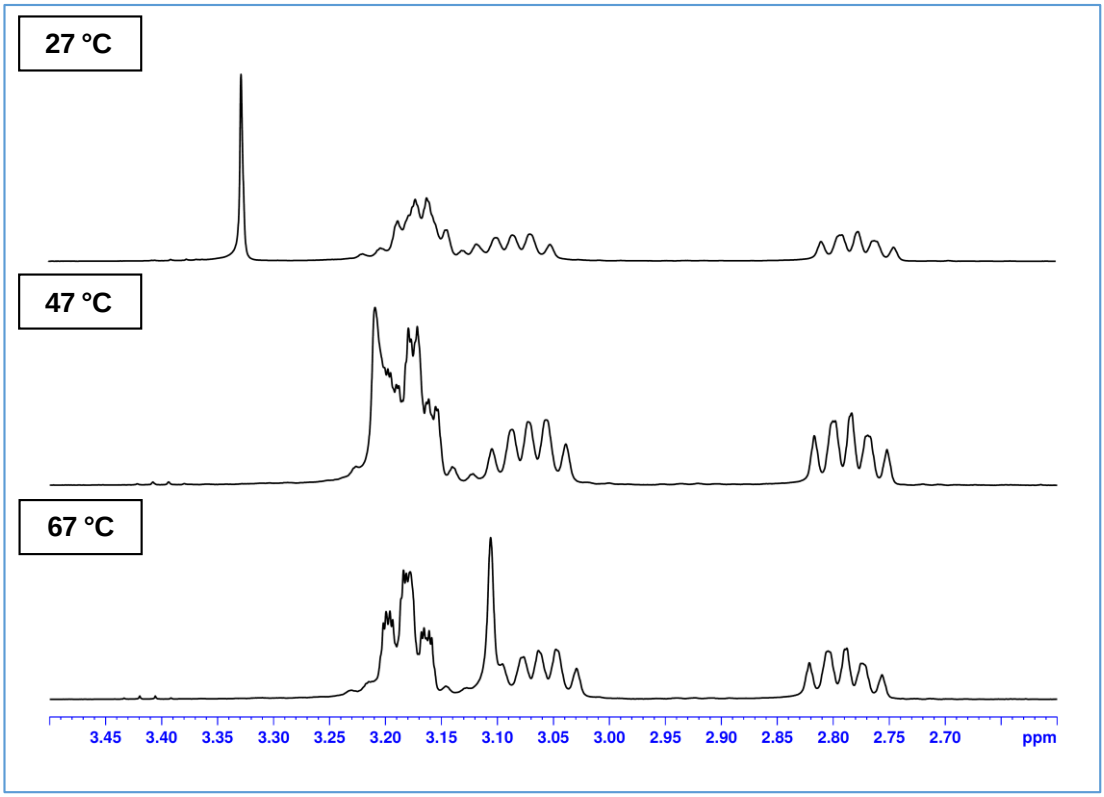
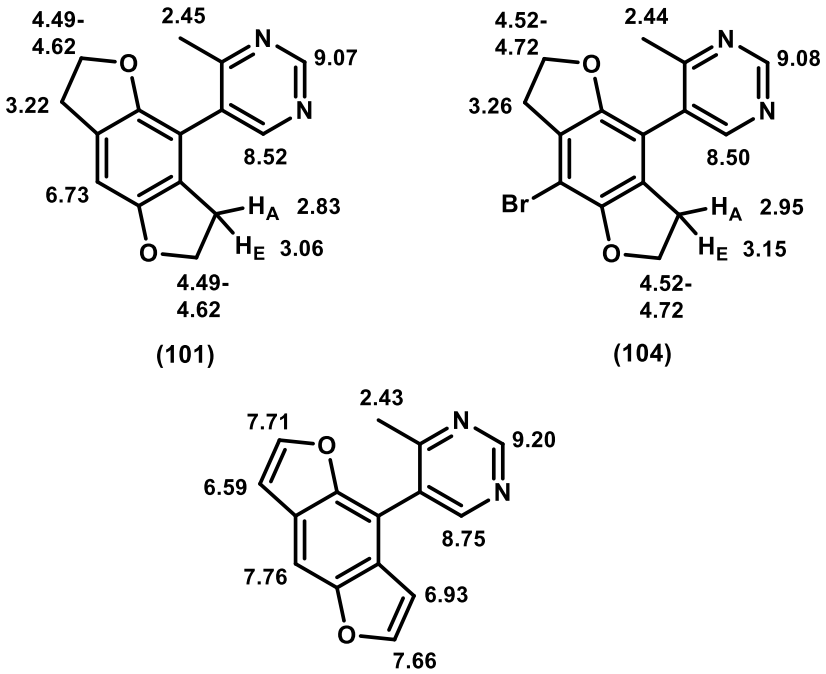


Fig. 2-39: VT-^{1}H-NMR experiment with phenyl pyrimidine ***101***

This indicates that the two 1H multiplets seen in the ^{1}H-NMR spectra of **101** and **104** are caused by the presence of diastereotopic protons at H-3, and not by atropisomerism. The diastereotopic protons couple to each other first in J_2 or geminal coupling, and then subsequently to the neighbouring two protons in more typical J_3 coupling. This should lead to a doublet of triplets for both protons, but in practice the 400 MHz NMR spectrometer used to acquire the spectrum shown in Figure 2-37 was unable to resolve this, and both proton signals are seen as two distinct multiplets between 2.6 - 3.2 ppm.

All the ^{1}H-NMR spectra for **101**, **104** and **106** have a distinctive signal between 2 - 2.5 ppm representing the protons of the methyl group on the pyrimidine ring. These signals can be used diagnostically, as the shift of the signal varies between pyrimidines. Signals characteristic of pyrimidine protons can also be seen in the ^{1}H-NMR spectra of compounds **101**, **104** and **106**, between 8 - 9 ppm. The ^{13}C-NMR spectra of the **101**, **104** and **106** were also acquired, with signals typical of pyrimidine carbon atoms seen in the 150 - 170 ppm region. The ^{1}H- and ^{13}C-NMR signals for **101**, **104** and **106** are shown in Figure 2-40.

^{1}H NMR



^{13}C NMR

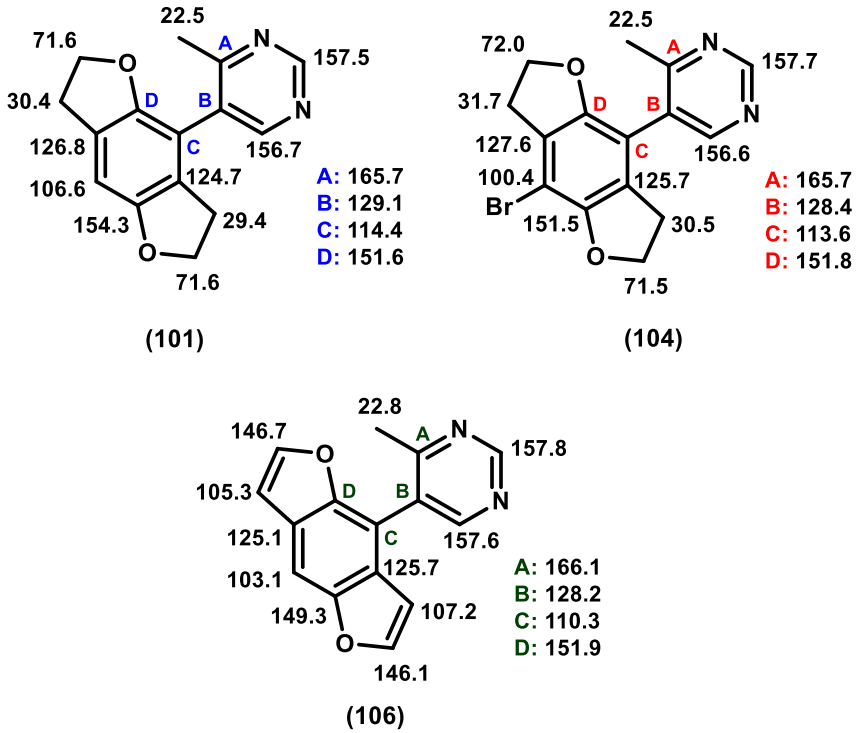


*Fig. 2-40: ^{1}H- and ^{13}C-NMR shift values of the phenyl pyrimidine series **101**, **104** and **106***

Two-dimensional NMR techniques (2D-NMR) including ^{1}H-^{1}H Correlated Spectroscopy NMR (COSY-NMR) and ^{1}H-^{13}C Heteronuclear Single Quantum Correlation NMR (HSQC-NMR) experiments were used to help assign signals in the ^{1}H- and ^{13}C-NMR spectra of the phenyl pyrimidines **101**, **104** and **106**. An example of the ^{1}H-^{1}H COSY-NMR spectrum measured for **101** can be seen in Figure 2-41.

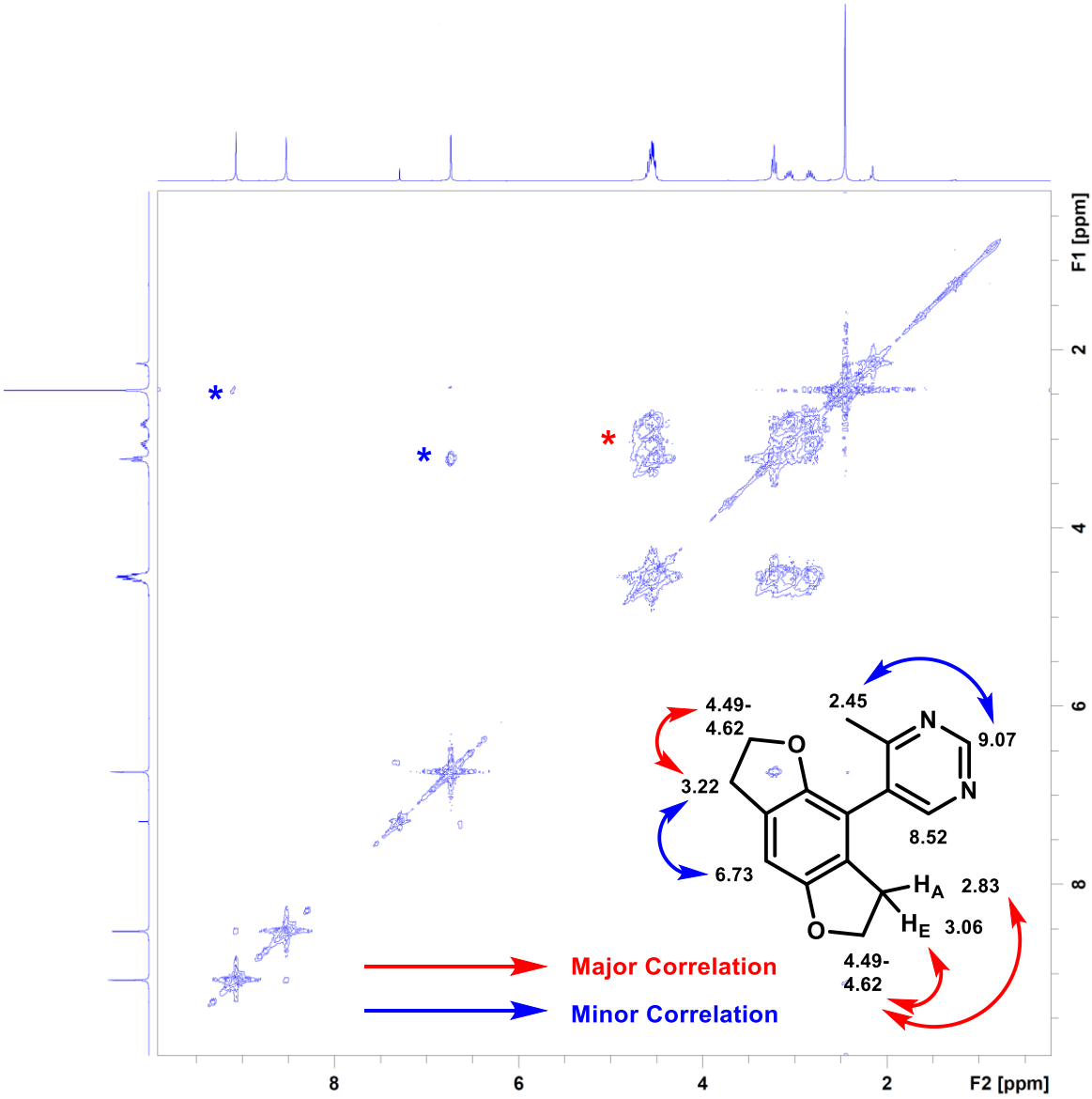


*Fig. 2-41: ^{1}H-^{1}H COSY-NMR spectrum of **101***

A summary of the major spin-spin coupling correlations in the ^{1}H-^{1}H COSY-NMR spectra measured for phenyl pyrimidines **104** and **106** can be seen in Figure 2-42.

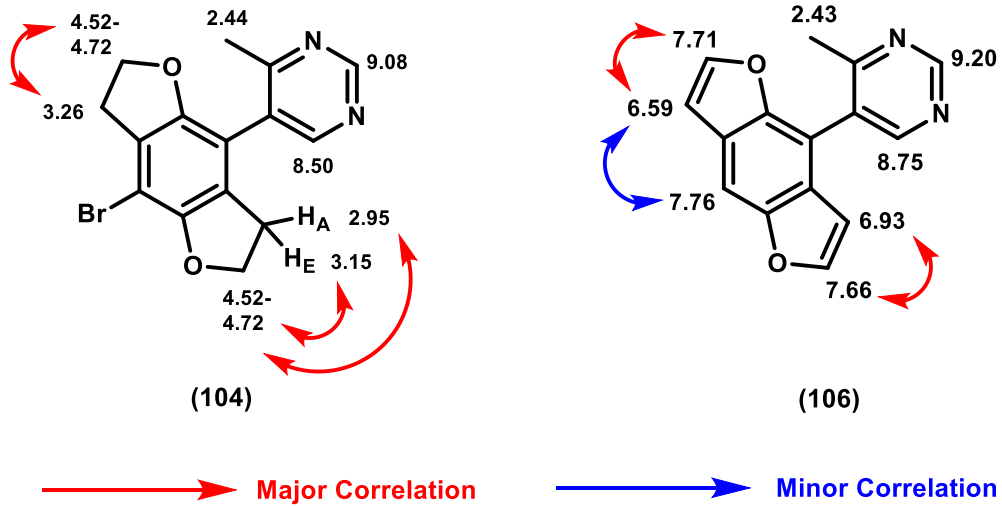


*Fig. 2-42: ^{1}H-^{1}H COSY-NMR correlations in phenyl pyrimidines **104** and **106***

The most significant of these correlations were:

- The correlation in the spectrum of **101** between the signals at 3.22 ppm and 6.73 ppm (see Figure 2-41); this correlation confirmed previous observations on which tetrahydrofuran ring the aliphatic protons were located.
- The correlation in the spectrum of **106** between the signals at 6.59 ppm and 7.76 ppm (see Figure 2-42); this correlation identified on which furan ring the proton with a signal at 6.59 ppm was located. The subsequent correlation between this signal and the signal at 7.71 ppm confirmed that the proton with a signal at 7.71 ppm was also on the northern furan ring. Process of elimination then directed that the protons with signals at 6.93 ppm and 7.66 ppm (which correlated to each other) represented the protons of the southern furan ring.

Unfortunately, in the ^{1}H-^{1}H COSY-NMR spectrum for **104**, overlap between signals representing the protons adjacent to the oxygen atoms in the dihydrofuran rings (represented by a multiplet from 4.52 - 4.72 ppm) meant that while correlations were seen between these protons and the adjacent

aliphatic protons at 2.95, 3.15 and 3.26 ppm, no conclusions could be drawn from the data. There was also a bromine atom at C-4 of the benzene ring (rather than the aromatic proton seen in **101** and **106**), meaning that no correlations were seen between this position and any other protons.

A summary of the major heteronuclear correlations in the ^{1}H-^{13}C HSQC-NMR spectra measured for the phenyl pyrimidine series can be seen in Figure 2-43, with the ^{13}C-NMR values in red (note that the THBD proton multiplets at ~4.5 ppm in **101** and **104** have been excluded as they are non-diagnostic).

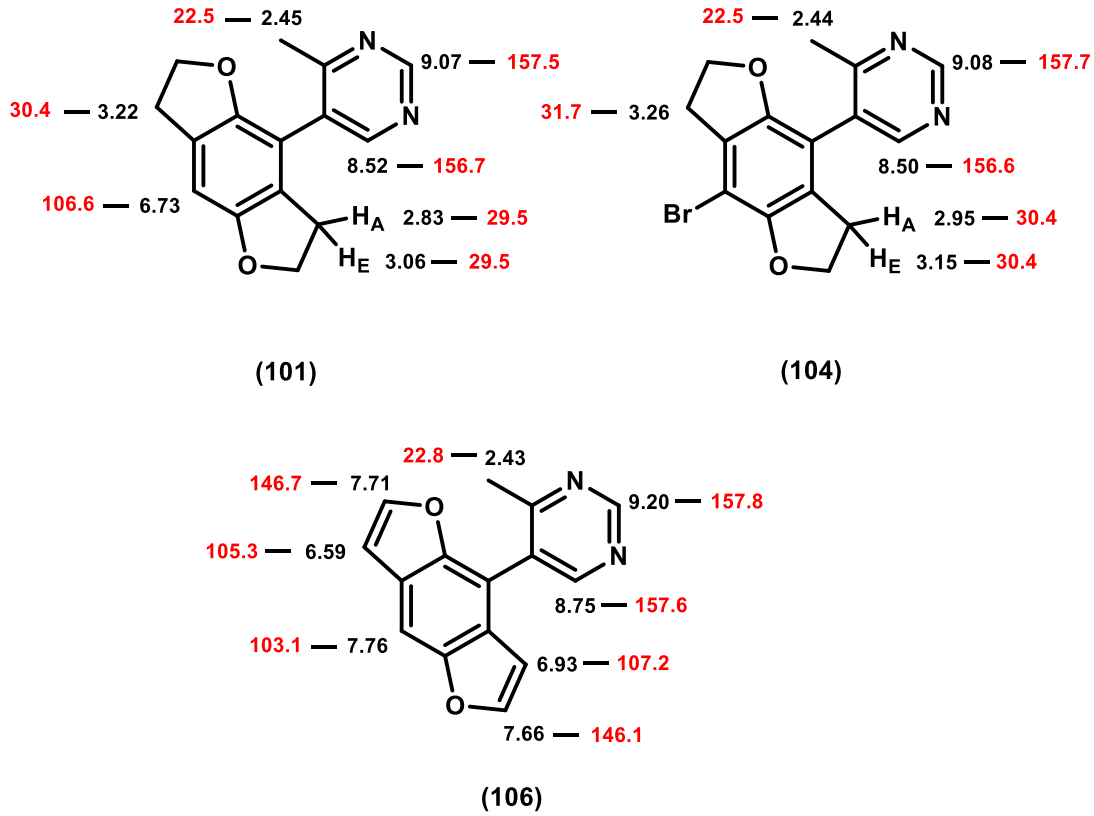


Fig. 2-43: ^{1}H-^{13}C HSQC-NMR correlations of the phenyl pyrimidine series

The ^{1}H-^{13}C HSQC-NMR correlations were particularly useful in this series of compounds for assigning ^{13}C-NMR signals to carbon atoms in the pyrimidine and (dihydro)furan rings, though in some cases there was too much overlap of signals in the ^{1}H-NMR spectra to make a definitive assignment.

2.2.4 Attempted Alternate Syntheses of 5-(8-bromo-2,3,6,7-tetrahydrobenzo[1,2-*b*:4,5-*b'*]difuran-4-yl)-4-methylpyrimidine (104)

*2.2.4.1 Attempted Synthesis from the Nonbrominated Analogue **101** Using NBS*

In Section 2.2.1.2 a procedure is described to brominate the phenyl ring of THBD **(42)** using NBS: it was hypothesised that the same procedure could be used to convert THBD phenyl pyrimidine **101** directly to its brominated analogue **104**, as seen in Figure 2-44.

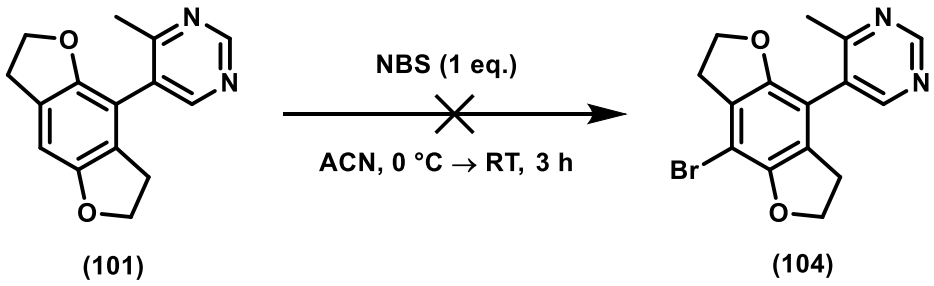


*Fig. 2-44: Attempted bromination of phenyl pyrimidine **101** using NBS*

The first attempt at this reaction produced an unexpected result: when purified by column chromatography, the only pyrimidine that was identified by ^{1}H-NMR analysis (that was not the starting material **101**) was not the brominated analogue **104**, but the fully aromatised benzodifuran analogue **106** (see Figure 2-45) with characteristic signals in the 6.5 - 9 ppm range. The only signal that appeared upfield of this area of the spectrum was the characteristic –C**H**$_3$ signal representing the protons of the methyl group on the pyrimidine ring, which appeared at δ = 2.43 ppm.

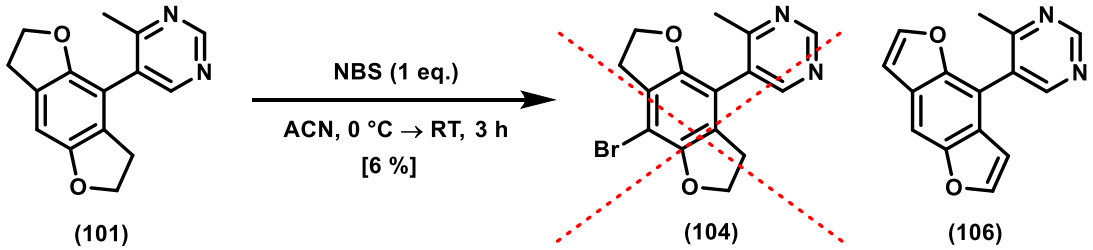


*Fig. 2-45: Synthesis of benzodifuran phenyl pyrimidine **106** using NBS*

While radical reactions involving NBS are known in the literature, for example the Wohl-Ziegler reaction[29] we have not previously observed them within our group when working with THBD-type compounds: when used stoichiometrically, NBS always participated in electrophilic aromatic substitution reactions, rather than radical reactions. There is no clear reason for the change in behaviour in this reaction, though it was hypothesised that the extended conjugated system with the phenyl ring bound directly to the pyrimidine may have made radical formation more stable and therefore more favoured. A potential mechanism for the conversion of **101** to **106** using NBS as a radical initiator is shown in Figure 2-46.

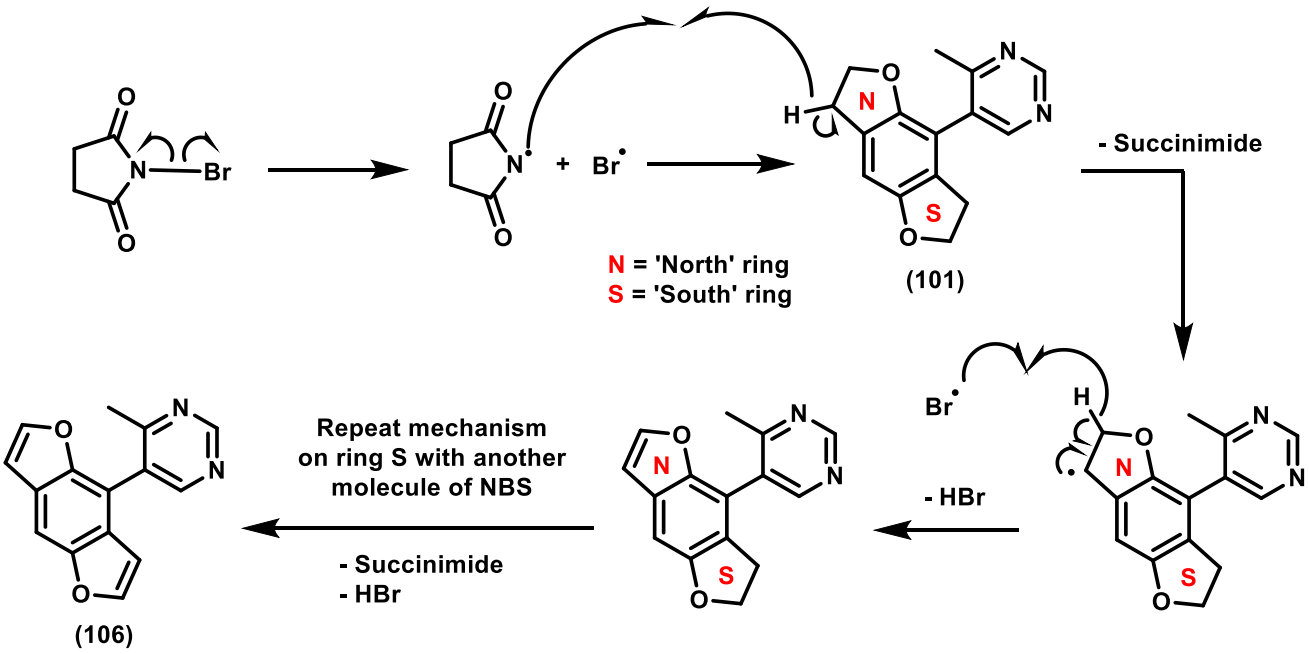


*Fig. 2-46: Proposed mechanism for the conversion of **101** to **106** using NBS as a radical initiator*

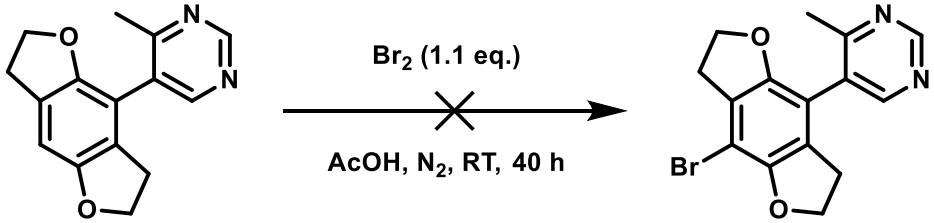
Initially, it was thought that the route described in Figure 2-45 to the benzodifuran phenyl pyrimidine **106** would be less complex than forming the benzodifuran boronic acid **125** for the Suzuki-Miyaura coupling reaction, however, subsequent attempts to repeat the outcome of the initial reaction (as per Figure 2-45) gave different results: while pyrimidine signals were observed in the crude ^{1}H-NMR, when the pyrimidine was isolated by preparative TLC, there was no signal at 2.45 ppm, indicating that the methyl group had been

substituted, likely by at least one bromine atom. This was supported by the appearance of a significantly deshielded 2H singlet in the ^{1}H-NMR spectrum at 6.58 ppm, which could represent a C**H$_2$**Br moiety. This lack of repeatability meant that an NBS-initiated radical mechanism to **106** could not be confirmed or disproved.

Due to the issues with repeatability, this route was discounted as a viable option for both the benzodifuran pyrimidine **106** and the brominated THBD pyrimidine **104**.

*2.2.4.2 Attempted Synthesis of **104** from Nonbrominated Analogue **101** using Elemental Bromine*

Following the unsuccessful attempt to brominate 4-methyl-5-(2,3,6,7-tetrahydrobenzo[1,2-*b*:4,5-*b'*]difuran-4-yl)pyrimidine **(101)** using NBS as a route to **104**, attention was turned to a different bromination procedure also used in our research group to brominate aromatic rings: the use of elemental bromine in glacial acetic acid.[31] While this method of bromination can lead to overbromination, it was hoped that this would not be an issue with **101**, as there is only one position unsubstituted on the phenyl ring. A procedure was adapted from Jonathan Quille (JQ), a former PhD student in our group, and was attempted as illustrated in Figure 2-47.[31]



(101) **(104)**

*Fig. 2-47: Attempted bromination of THBD pyrimidine **101** using bromine in acetic acid*

When water was added to the reaction mixture during the work-up procedure, a brown solid precipitated immediately out of solution, and was collected by vacuum filtration, while the rest of the reaction mixture was dissolved in DCM

and worked up using aqueous sodium bicarbonate washes to remove the glacial acetic acid.

The residue recovered from the DCM *in vacuo* was found to contain mostly starting material **101** when analysed by ^{1}H-NMR, however, when the precipitate was analysed by ^{1}H-NMR (see Figure 2-48), it was found to contain a mixture of products, none of which appeared to be the desired product **104**. The absence of a signal for methyl protons at *ca.* 2.5 ppm indicated that the methyl group on the pyrimidine ring of **101** had been brominated either in addition to or in place of the 4-position on the THBD phenyl ring.

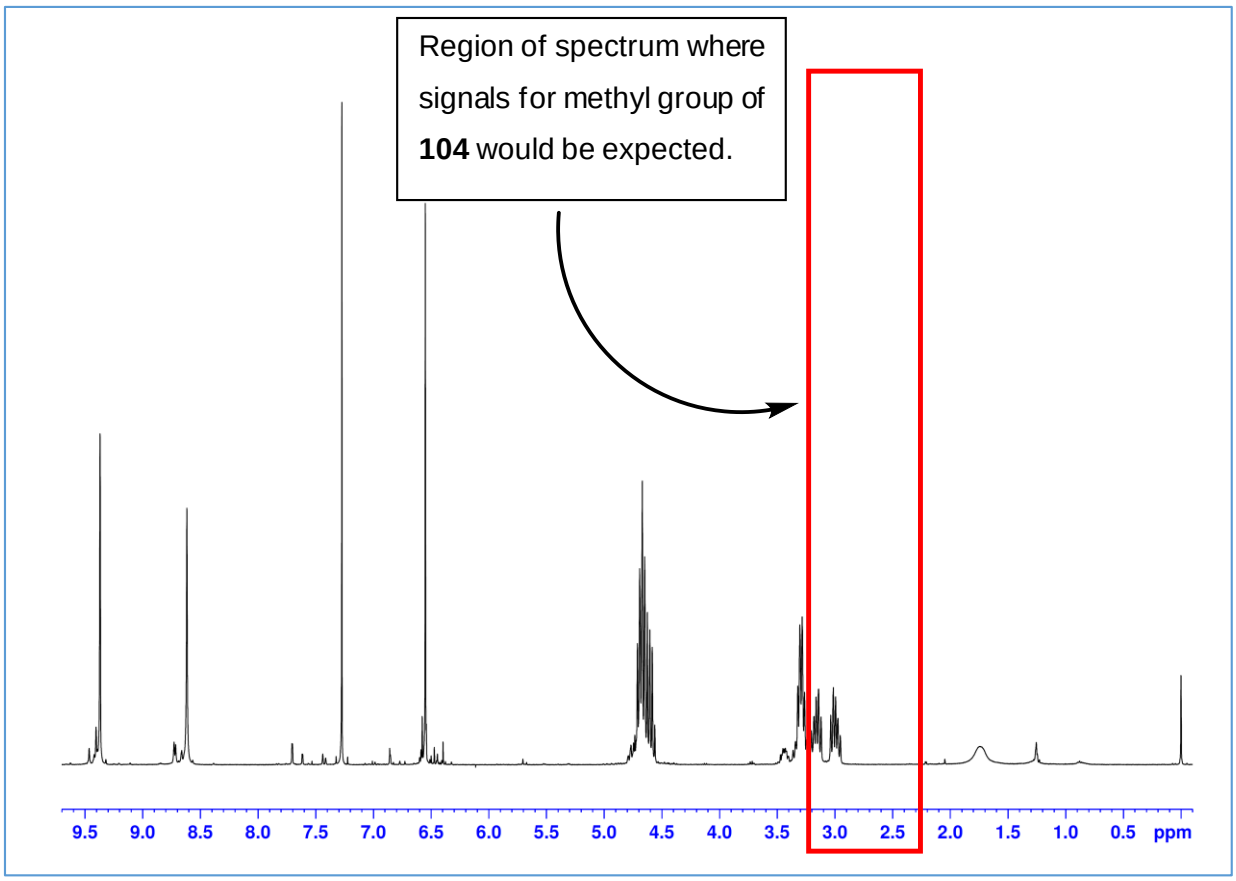


*Fig. 2-48: ^{1}H-NMR spectrum of precipitate isolated from reaction of **101** with bromine in acetic acid*

As seen in Figure 2-48, there appeared to be one major product in the reaction, with signals in the ^{1}H-NMR spectrum listed in Table 2-9 (m = multiplet, s = singlet).

δ (ppm)	2.94 - 3.05	3.10 - 3.20	3.25 - 3.32	4.55 - 4.70	6.55	8.61	9.37
Integration	1H	1H	2H	4H	1H	1H	1H
Multiplicity	m	m	m	m	s	s	s

*Table 2-9: ^{1}H-NMR signals of precipitate isolated from the reaction of **101** with bromine in acetic acid*

The integrations were calculated by assuming that the signal at 8.61 ppm represented a single proton on the pyrimidine ring and calibrating all the other signals accordingly. As seen in Figure 2-48, there were also other minor signals present in the same regions of the ^{1}H-NMR of the precipitate, indicating possible formation of other bromination products. Based on the sites available for bromination, a list of the most likely bromination products was compiled (summarised in Figure 2-49), all of which are novel products with no literature NMR spectra for comparative purposes.

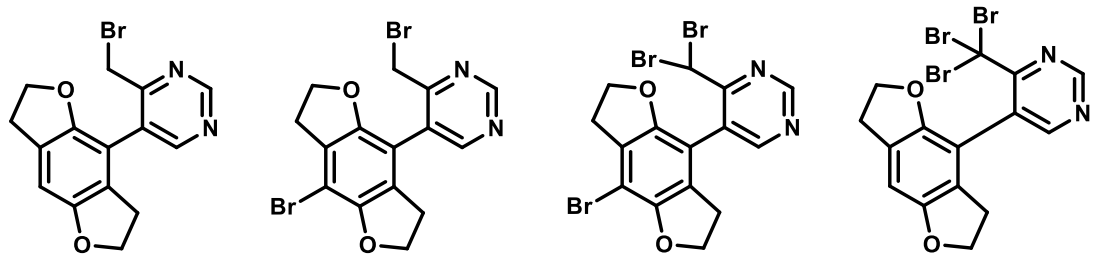


*Fig. 2-49: Potential bromination products from reaction of **101** with bromine in acetic acid*

Substrates **143** and **144** were dismissed as possibilities for the major product, as there were no –C**H$_2$** singlets in the ^{1}H-NMR spectrum, leaving **145** and **146** as the most likely options. ^{1}H-NMR is not sufficient to distinguish between these two substrates, as the aromatic proton on **146** and the -C**H**Br$_2$ proton on **145** would both be expected to appear at ~ 6.5 ppm.

At this point, HRMS analysis was carried out searching for the parent molecular ion (PMI) of a substrate with the molecular formula $C_{15}H_{11}Br_3N_2O_2$ as is the case for both **145** and **146** (these two substrates are isomers). The

calculated mass for this PMI (with the isotope ^{79}Br for all three bromine atoms) was *m/z* = 488.8425 and the PMI was found with *m/z* = 488.8449, a mass accuracy of -4.9 ppm. While this obviously does not differentiate between **145** and **146**, it does confirm that a substrate matching their accurate mass was present in the reaction.

To distinguish between **145** and **146**, the ^{13}C-NMR spectrum was acquired, along with DEPT-90, DEPT-135 and HSQC experiments. ^{13}C-NMR analysis (as seen in Figure 2-50) indicated that the most likely product of the experiment was **145**: this judgement was made based on the presence of a **C**H signal at 38.0 ppm, which also appeared in the DEPT-90 spectrum and the positive phase of the DEPT-135 spectrum and would correspond to C* in **145**. This is consistent with reports of -**C**HBr$_2$ chemical shifts in the literature, which appear between 35 - 45 ppm in ^{13}C-NMR spectra.[32,33] This signal would not appear in the ^{13}C-NMR of **146**, though the analysis did suggest that **146** might be present in small quantities: there was a **C**H signal at 105.9 ppm which would correspond to C* in **146**.

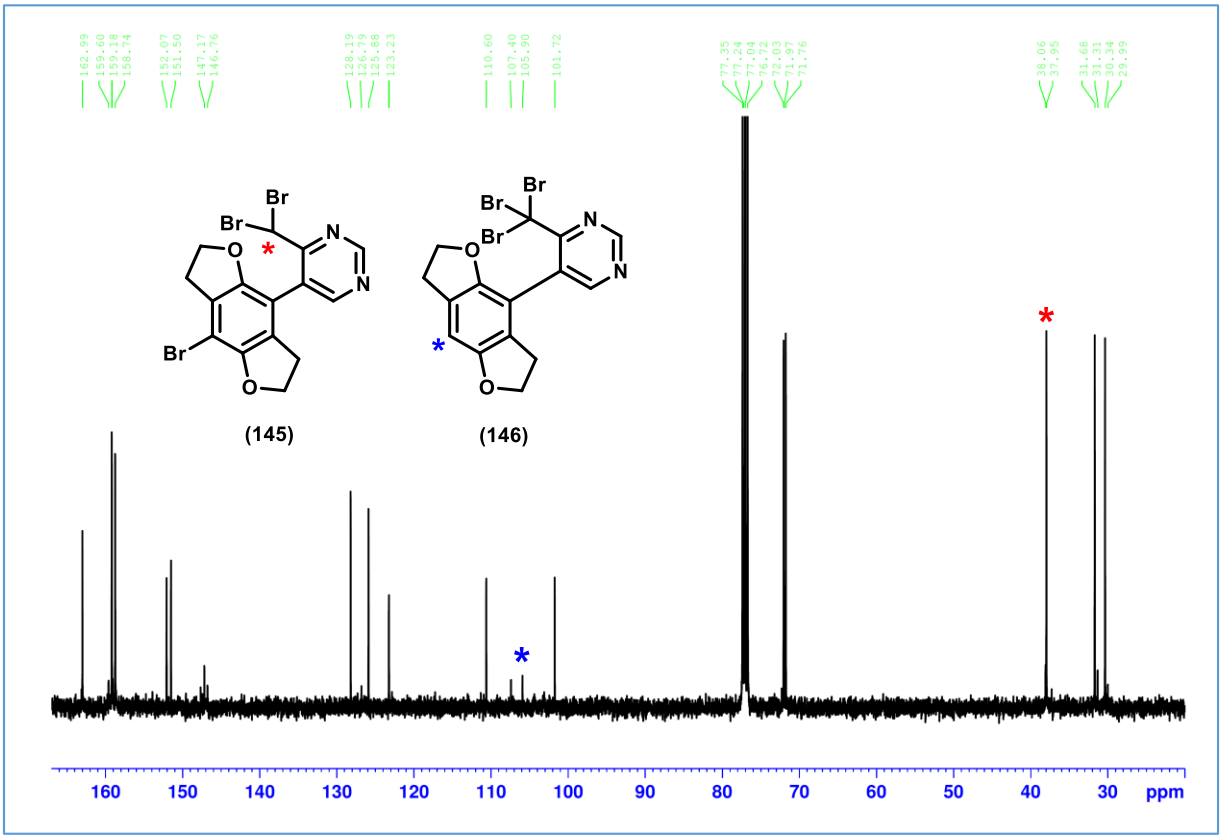


*Fig. 2-50: ^{13}C-NMR of precipitate isolated from reaction of **101** with bromine in acetic acid*

The ^{1}H-^{13}C HSQC experiment offered further confirmation for **145** as the major product of the reaction, with correlations between the ^{1}H-NMR signals and the ^{13}C-NMR signals aligning as expected (see Figure 2-51). The yield of the reaction was also as might have been expected for a substrate which was tribrominated with only 1.1 eq of Br_2 with respect to the starting material: the maximum theoretical yield of **145** under these circumstances is 37 %. For this reaction, that equates to a mass of 0.044 g, and the mass of the precipitate recovered from the reaction was 0.031 g, a yield of 26 % (which is approximately 70 % of the possible yield). The mass of the starting material recovered *in vacuo* was 0.035 g, which accounts for ~ 53 % of the starting weight. The remaining 21 % was likely lost during work up and purification.

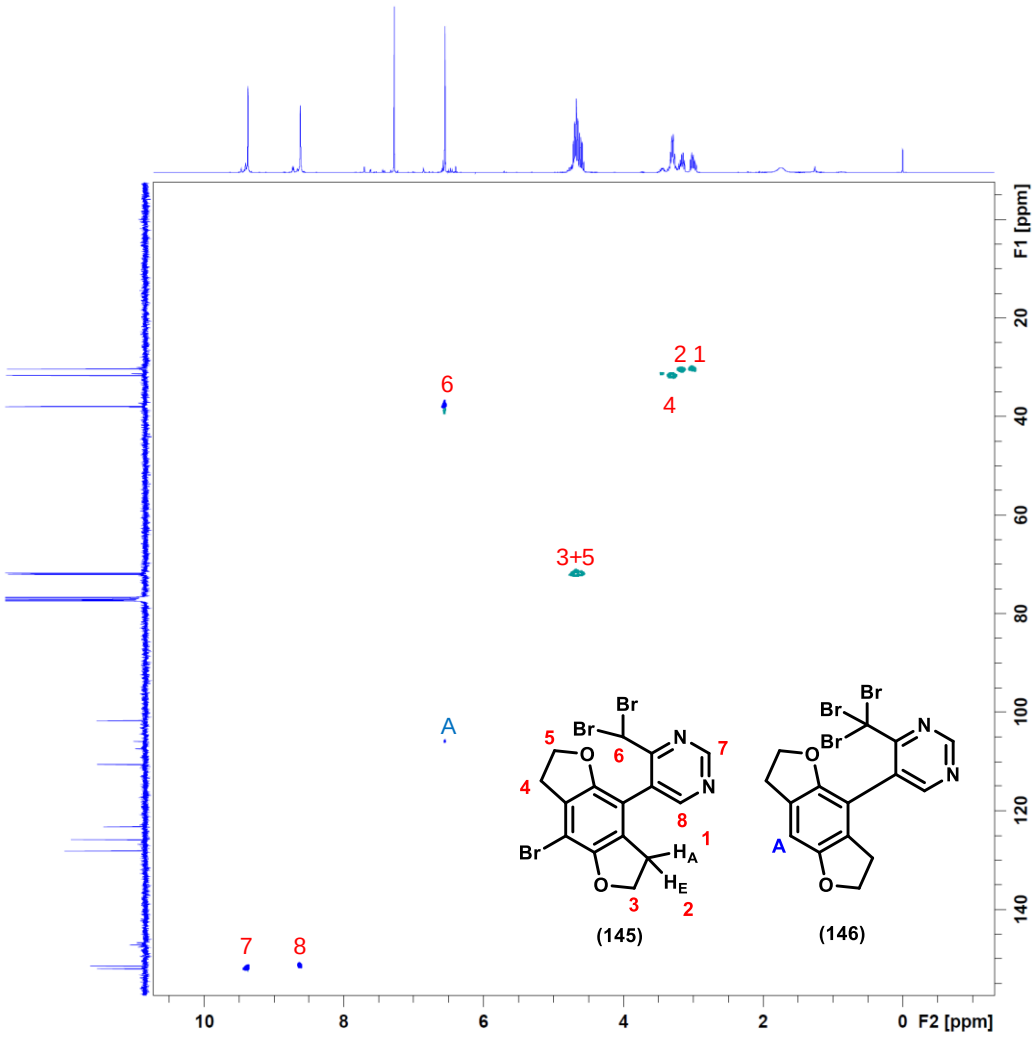


*Fig. 2-51: HSQC-NMR of precipitate isolated from reaction of **101** with bromine in acetic acid*

There was also further evidence for the existence of **146** as a minor product of the reaction, with a baseline signal at 6.58 ppm in the ^{1}H-NMR spectrum correlating with a weak signal in the ^{13}C-NMR at 105.9 ppm (A). These signals potentially represent C-4 of the THBD phenyl ring and the attached aromatic proton on **146**. While evidence for the presence of **146** is not as strong as that for **145**, it is significant nonetheless, because it implies that benzylic bromination of the methyl group on the pyrimidine occurs preferentially to bromination of the 4-position on the THBD phenyl ring. This in turn implies that the use of milder conditions would likely favour benzylic bromination over aromatic bromination, and so this line of research was discontinued (note: preparative TLC was employed in an effort to separate **145** from the potential **146** so that it could be characterised independently, but no separation was achieved).

*2.2.4.3 Attempted Synthesis of **104** using a Three-Component Coupling Reaction*

While experiencing difficulties in synthesising benzodifuran boronic acid **125** and brominated boronic acid **126** (detailed in Sections 2.2.1.4 and 2.2.1.5 respectively), and the inability to synthesise the brominated benzodifuran analogue **129**, alternate approaches that did not use Suzuki-Miyaura coupling strategies were investigated to access our target disubstituted pyrimidine. One such approach that was discovered in the literature involved the synthesis of pyrimidines using a three-component coupling reaction involving a phenone, triethyl orthoformate **(147)** and a nitrogen source, as illustrated in Figure 2-52.[34-37]

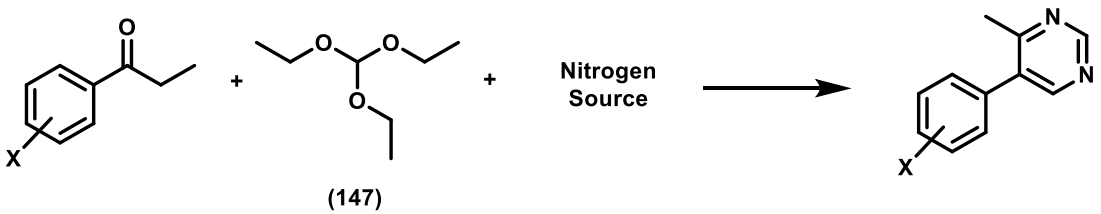
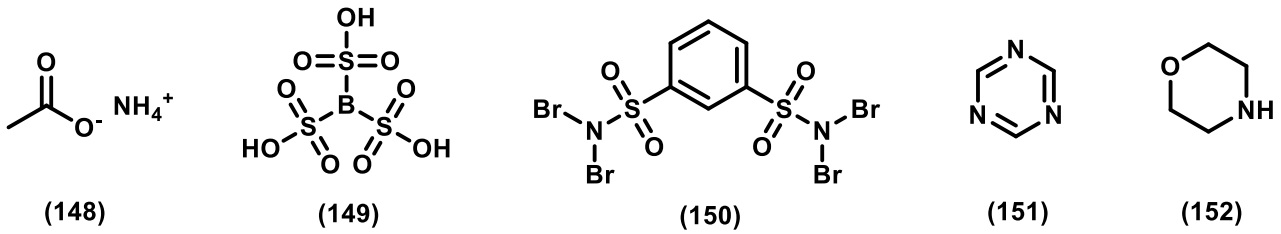


Fig. 2-52: Formation of pyrimidines using a three-component coupling reaction

Phenone and triethyl orthoformate **(147)** were consistently employed as substrates across most papers,[34-37] however, the reaction conditions and nitrogen sources vary depending on the literature source. Some of the reaction variations include (in all cases for the yield stated, X = H in Figure 2-53):

- Ammonium acetate **(148)** in boron sulfonic acid **(149)**, which is an ionic liquid [100 °C, 2 h, 80 % yield] (Soheilizad *et al.*)[34]
- Ammonium acetate **(148)** and zinc (II) chloride in toluene [100 °C, 72 h, 70 % yield] (Sasada *et al.*)[35]
- Ammonium acetate **(148)** and *N,N,N',N'*-Tetrabromobenzene-1,3-disulfonylamide **(150)**, another ionic liquid [100 - 110 °C, 2 h, 64 % yield] (Ghorbani-Vaghei *et al.*)[36]
- 1,3,5-Triazine **(151)** in methanol: this variant uses morpholine **(152)** in place of triethyl orthoformate **(147)** [90 °C, 72 h, 84 % yield] (Yang *et al.*)[38]



It was decided in this work to use the variant with ammonium acetate **(148)** and zinc (II) chloride in toluene from Sasada *et al.*[35] to attempt to access **104**, as it avoids the use of esoteric and expensive ionic liquids and also avoids 1,3,5-triazine **(151)**, which is difficult to source commercially. This reaction scheme is illustrated in Figure 2-53.

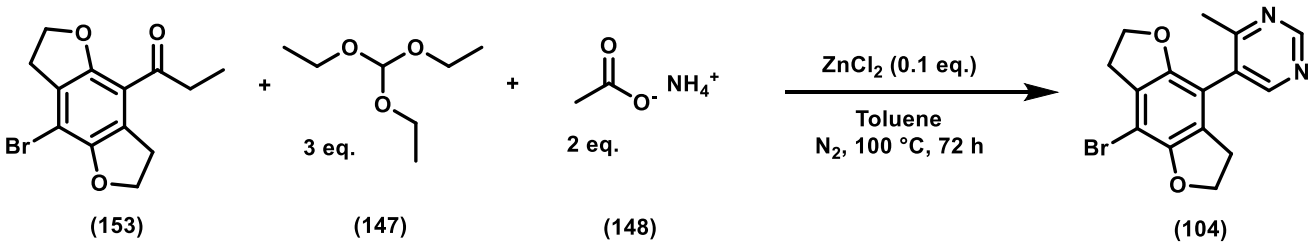


*Fig. 2-53: Synthesis of pyrimidine **104** using a three-component coupling reaction*

Sasada *et al.* included in their paper a reaction pathway for the preparation of 4-methyl-5-arylpyrmidines that they described as “plausible”, which is reproduced in Figure 2-54.[35] Starting from a phenone with an acidic α proton and a nitrogen source (in our work, ammonium acetate **(148)**) an enamine is generated. The enamine is then reacted sequentially with zinc chloride-activated triethyl orthoformate **(147)**, ammonia and another molecule of activated triethyl orthoformate **(147)**. The final step is elimination of ethanol to close the pyrimidine ring.[35]

While only two equivalents of triethyl orthoformate **(147)** are used in this mechanism, triethyl orthoformate **(147)** is also a water scavenger, so the third equivalent is likely used to consume the water by-product in the enamine formation reaction.

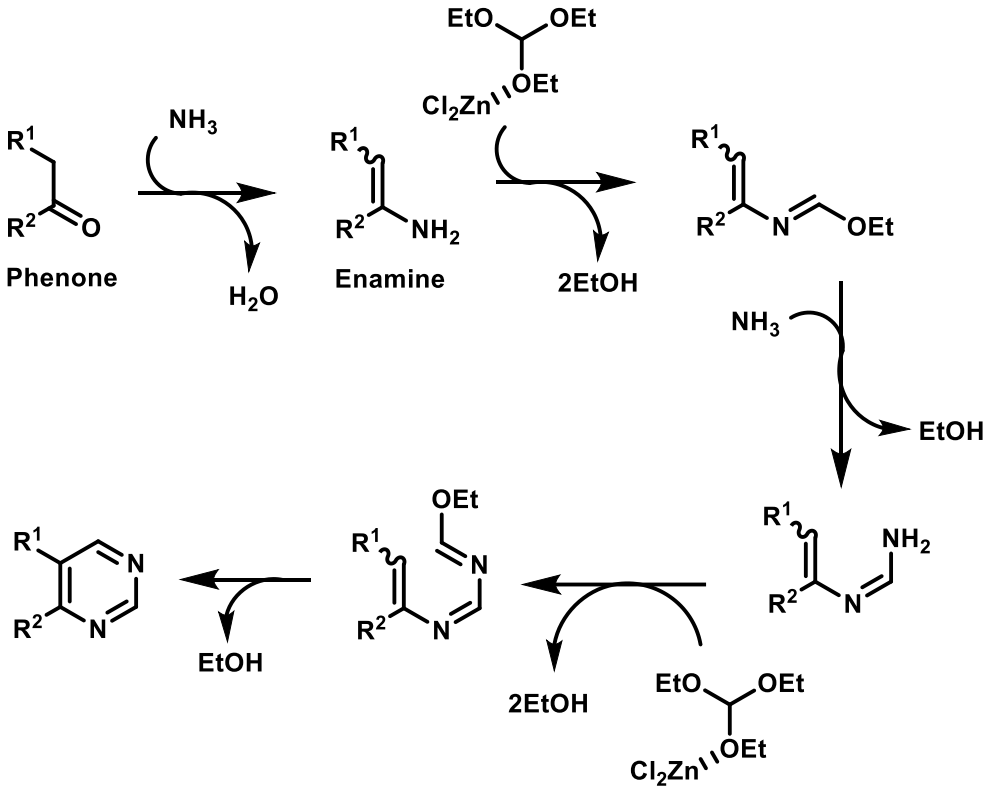


Fig. 2-54: Reaction pathway proposed by Sasada et al. for a three-component coupling reaction to form a pyrimidine[35]

All of the reagents for the three component coupling reaction were sourced commercially, with the exception of the propiophenone starting material **153**,

which is a novel substrate and had to be synthesised from brominated THBD **116** using a Friedel-Crafts acylation as shown in Figure 2-55.[38]

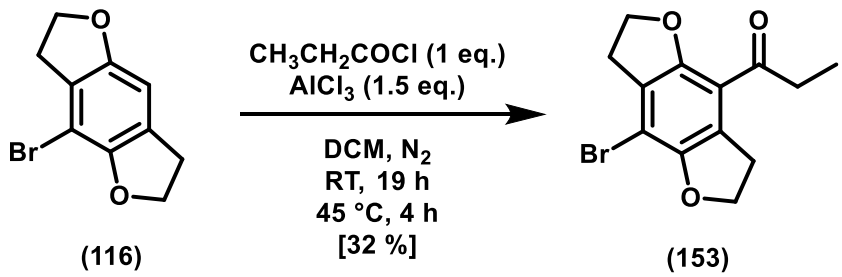


*Fig. 2-55: Preparation of ketone starting material **153** using a Friedel-Crafts acylation*

An initial attempt at this reaction was made using the reaction conditions described in Figure 2-55. After one hour, TLC analysis showed a majority of starting material **116**, but a faint, more polar spot was also evident. The reaction was left for a further 18 h, after which TLC analysis still showed some evidence of starting material **116**, though much fainter: at this point, the reaction was heated to 45 °C for four hours, worked up and the isolated crude product was analysed by ^{1}H-NMR spectroscopy.

The resultant ^{1}H-NMR spectrum (as seen in Figure 2-56) showed complete consumption of the starting material, but a mixture of THBD-type products was also seen, including a potential aldehyde or carboxylic acid with a singlet at δ = 12.91 ppm.

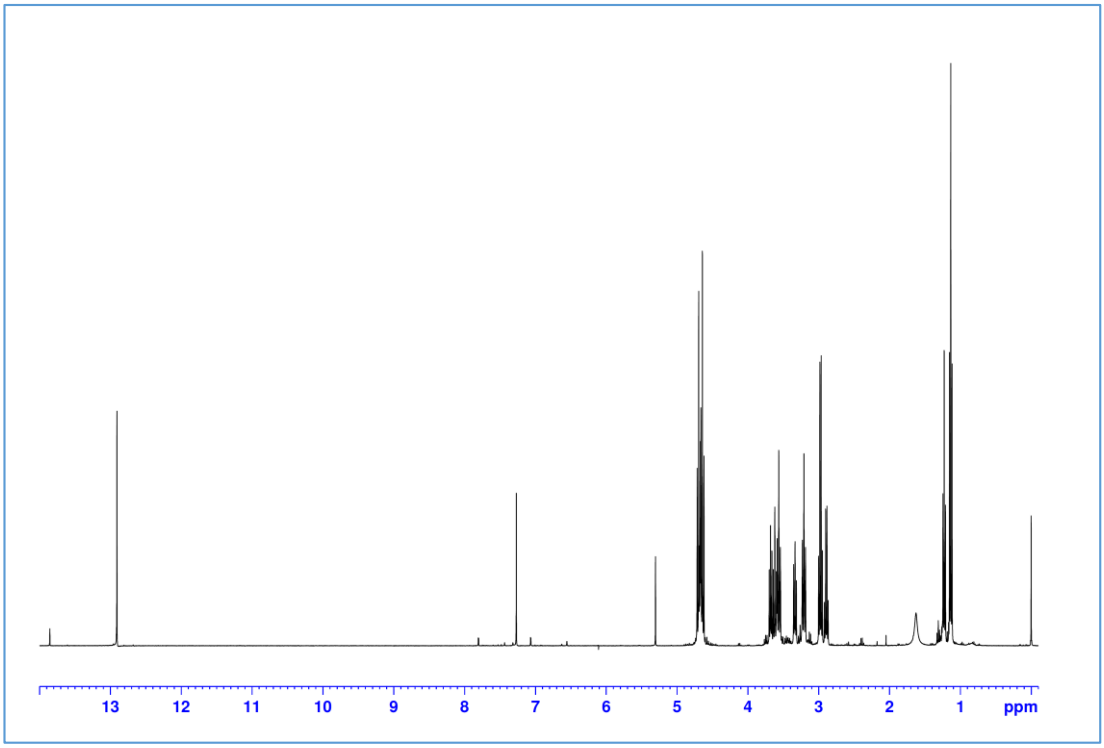


*Fig. 2-56: ^{1}H-NMR of Friedel-Crafts crude reaction mixture containing **153***

The crude reaction mixture was purified by flash column chromatography on silica gel to give the desired novel product **153** in 32 % yield, which was pure when analysed by ^{1}H- and ^{13}C-NMR. This sample was characterised fully, as summarised in Table 2-10.

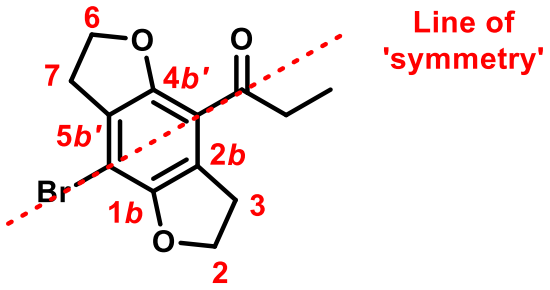
Compound Number	Yield (%)	m.p. (°C)	R_f (Hex:EtOAc)	IR ν_{max} C=O (cm^{-1})	HRMS (*m/z*)	
					Calc.	Found
153	32	167 - 169 ($CHCl_3$)	0.57 (5:1)	1665	297.0121	297.0125

*Table 2-10: Yield, m.p., R_f, IR and HRMS data for THBD ketone **153***

The ^{1}H-NMR spectrum of **153** was as expected: there were no signals in the aromatic region of the spectrum, but the signals typical of THBD-type compounds were seen between 3 and 5 ppm (the protons adjacent to the oxygen in the THBD ring were more deshielded). The propiophenone fragment of the substrate was clearly seen as a triplet at 1.13 ppm (3H, J = 7.2 Hz,

representing –$CH_2C\mathbf{H_3}$), and a quartet representing –$C\mathbf{H_2}CH_3$ at 2.97 ppm (2H, J = 7.2 Hz).

The ^{13}C-NMR spectrum of **153** was typical of THBD-type structures, with additional $\mathbf{C}H_2$ and $\mathbf{C}H_3$ signals from the ethyl ketone at 37.2 and 7.9 ppm respectively. The assignment of some signals in both the ^{1}H-NMR and ^{13}C-NMR spectra required additional 2D-NMR analysis to confirm: due to the near symmetry of the molecule (as illustrated in Figure 2-57), shifts for ^{1}H- and ^{13}C-NMR signals of the THBD protons were almost coincidental.



(153)

*Fig. 2-57: Pseudo-symmetry in the THBD-ketone **153***

Referring to the proton labelling system of **153** in Figure 2-57 (which is numbered in accordance with IUPAC naming for this compound), the signals for the protons H-2 and H-6 adjacent to the oxygen atoms in the tetrahydrofuran rings are represented in the ^{1}H-NMR spectrum by a multiplet at 4.62 - 4.71 ppm, which is made up of two overlapping triplets: these signals cannot be distinguished and are reported as a multiplet, however, the corresponding carbon atoms C-2 and C-6 produce distinguishable signals in the ^{13}C-NMR spectrum, with peaks at 71.8 and 72.5 ppm respectively.

Similarly, the signals for protons H-7 and H-3 in the ^{1}H-NMR spectrum appear as distinct triplets at 3.20 and 3.56 ppm respectively, with the corresponding carbon atom signals in the ^{13}C-NMR spectrum at 31.1 for C-7 and 32.7 ppm for C-3, and the signals for C-4*b'*/C-1*b* and C-2*b*/C-5*b'* exhibited at 127.6/128.8 ppm and 151.8/154.1 ppm respectively. However, these discrete signals are still close enough in shift that it is not possible to make definitive assignments

based on rationalisations of electron density distribution in the molecule. It is at this juncture that 2D-NMR techniques become particularly useful to unambiguously assign NMR signals.

The two forms of 2D-NMR which were employed in this case were ^{1}H-^{13}C HSQC-NMR (described previously) and ^{1}H-^{13}C Heteronuclear Multiple Bond Correlation NMR (HMBC-NMR).

The focal point for definitive assignment of ^{1}H- and ^{13}C-NMR signals was the unambiguous assignment of the signal for the aromatic carbon bound directly to bromine (**C**-Br). Previous examples in the literature and within our research group indicated that this signal usually appears in the 95 - 110 ppm range of the ^{13}C-NMR spectrum.[10,39] Only one such signal within this boundary was apparent in the ^{13}C-NMR of **153**: the signal at 104.9 ppm, and this was therefore assigned as the signal representing **C**-Br.

HSQC-NMR and HMBC-NMR spectra of **153** were then acquired. The HSQC-NMR spectrum is shown in Figure 2-58, with interactions recorded between signals at δ 1.13/7.9, 2.97/37.2, 3.20/31.1, 3.56/32.7 and [4.62 - 4.71]/[71.8 and 72.5] ppm (^{13}C-NMR signals shown in red).

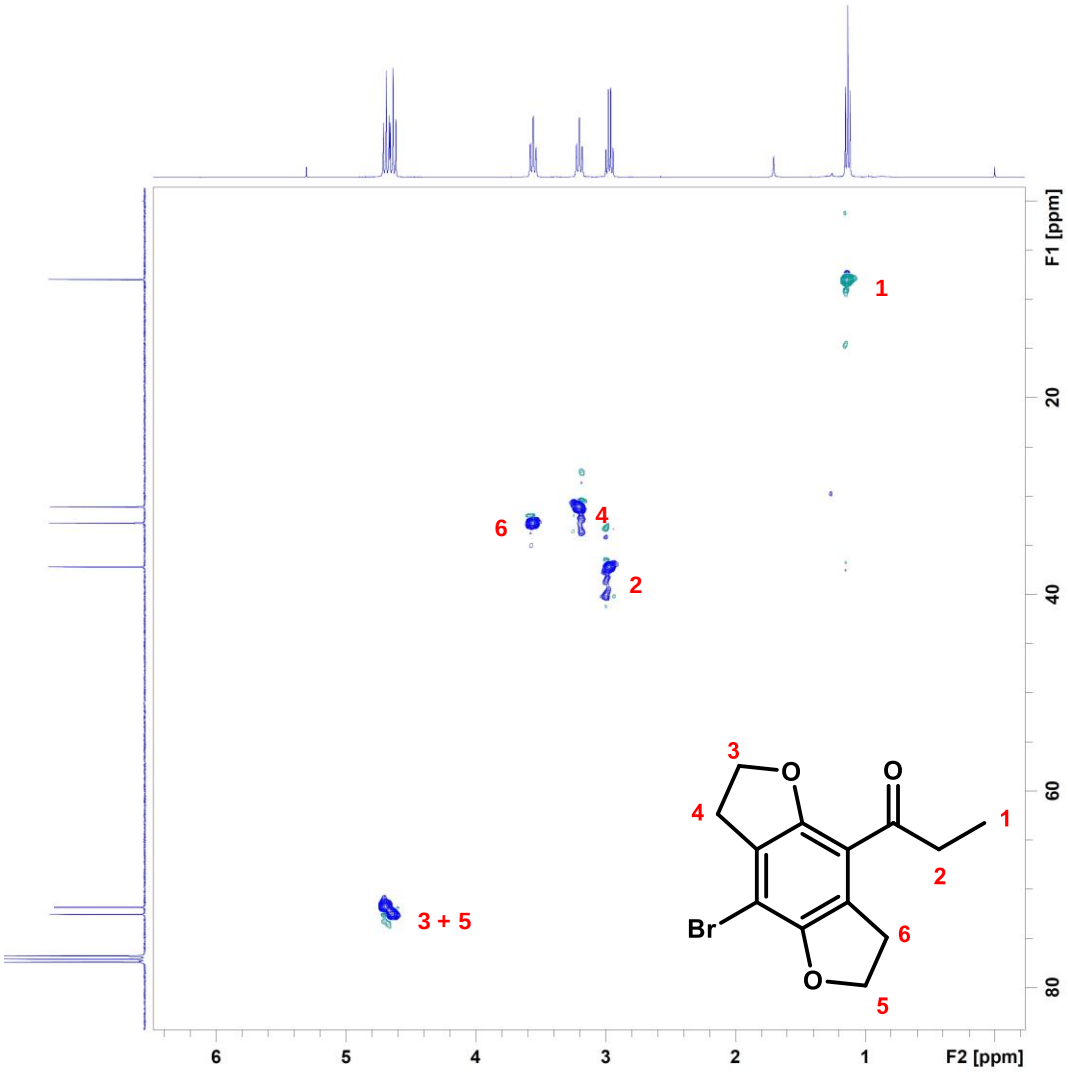


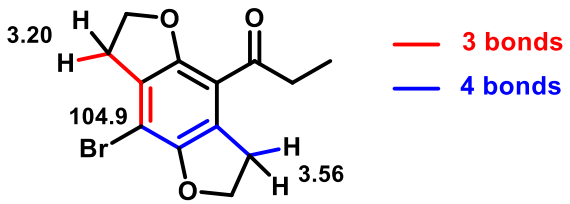
*Fig. 2-58: HSQC-NMR spectrum of **153***

While the information from the HSQC-NMR confirms which ^{1}H- and ^{13}C-NMR signals correspond to each other, it still does not definitely assign them within the substrate, a task for which HMBC-NMR data are required. These data were acquired and are summarised in Table 2-11 (note that data pertaining to the multiplet at 4.62 - 4.71 ppm have been excluded, as they are non-diagnostic).

^{1}H-NMR Signal [ppm]	Strong interactions (^{13}C-NMR signals) [ppm]	Weak interactions (^{13}C-NMR signals) [ppm]
1.13	37.2	200.7
2.97	7.9	200.7
3.20	71.8, **104.9**, 128.8,154.1	127.6, 151.8
3.56	72.5, 127.6, 151.8	**104.9**, 116.8, 128.8, 154.1

*Table 2-11: HMBC-NMR data measured for **153***

The key result to be considered in these data is the difference in strength of interaction between the ^{13}C-NMR signal at 104.9 ppm (representing **C**-Br) and the ^{1}H-NMR signals for the THBD protons at 3.20 and 3.56 ppm. The interaction between the signal at 104.9 ppm and the one at 3.20 ppm is stronger than that between the signal at 104.9 ppm and the one at 3.56 ppm. This indicates that the proton represented by the signal at 3.20 ppm is likely closer to **C**-Br than the proton for the signal at 3.56 ppm, as shown in Figure 2-59.



(153)

*Fig. 2-59: HMBC-NMR analysis of **153***

If the signal at 3.20 ppm represents the protons at H-7 and the signal at 3.56 ppm represents the protons at H-3, the correlations in the HSQC-NMR imply that the ^{13}C-NMR signals for C-7 and C-3 are 31.1 and 32.7 ppm respectively. From the strong interactions in the HMBC-NMR as listed in Table 2-11, the

assignments of ^{13}C-NMR signals to carbon atoms C-6, C-4*b'*, C-5*b'*, C-2*b*, C-1*b* and C-2 can be inferred, as summarised in Figure 2-60.

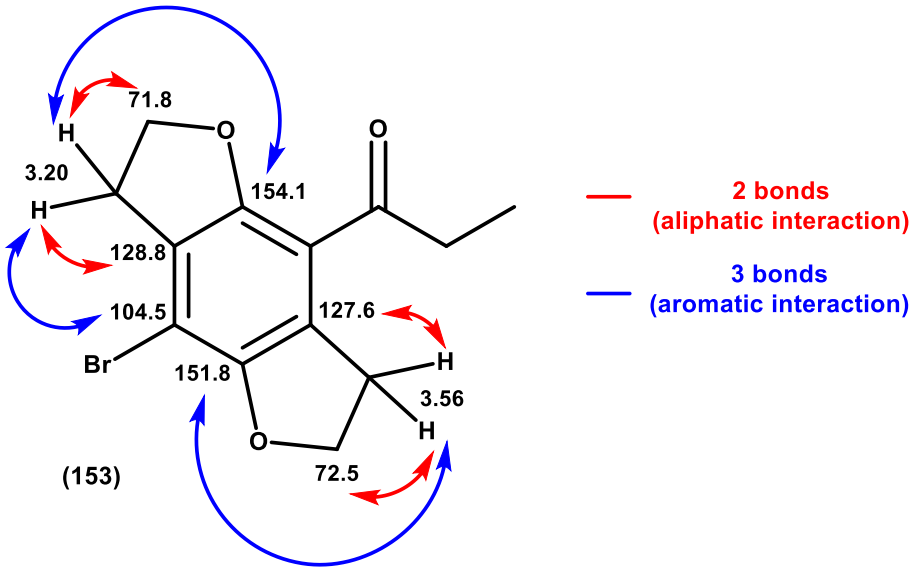


*Fig. 2-60: ^{13}C-NMR assignments of **153** as inferred from HMBC-NMR*

The difference between HSQC- and HMBC-NMR is neatly illustrated by the respective correlations seen for the signals in the ethyl moiety of **153**. In the HMBC-NMR spectrum, the ^{1}H-NMR signal at 1.13 ppm correlates to the ^{13}C-NMR signal at 7.9 ppm and the ^{1}H-NMR signal at 2.97 ppm correlates to the ^{13}C-NMR signal at 37.2 ppm. In the HMBC-NMR spectrum, the correlations invert, so the major interaction with the ^{1}H-NMR signal at 1.13 ppm is from the ^{13}C-NMR signal at 37.2 ppm, while the major interaction with the ^{1}H-NMR signal at 2.97 ppm is from the ^{13}C-NMR signal at 7.9 ppm.

The chemical shifts of all signals and the positions they correspond to within **153** are summarised in Figure 2-61.

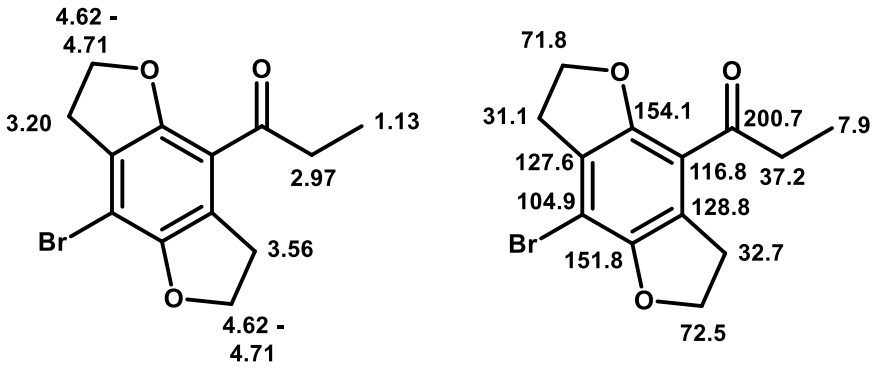


Fig. 2-61: [1]H- and [13]C-NMR signals of THBD propiophenone ***153***

After the first attempt at the Friedel-Crafts acylation, some optimisation work was carried out to try and increase the yield and purity of **153** recovered from the reaction. Initially it was hypothesised that the impurity with a signal seen at 12.91 ppm in the ^{1}H-NMR spectrum was most likely to be an aldehyde (rather than a carboxylic acid), as α-cleavage of benzylic ketones is a known phenomenon.[40,41] However, it was quickly realised that the phenone **153** was not a suitable substrate for this degradation reaction, as the carbonyl carbon atom is bonded directly to the aromatic ring, and not to the benzyl carbon atom as required by the Norrish reaction mechanism.

It was also noted a series of THBD and benzodifuran aldehyde substrates had been independently synthesised by O'Connor *et al.* within our research group: when the ^{1}H-NMR data of the compounds were consulted, it was seen that the aldehyde signal for those substrates appear at chemical shifts between 10.2 - 10.9 ppm in their respective ^{1}H-NMR spectra,[10] at least 2 ppm upfield of 12.91 ppm. It was speculated that the chemical shift of the signal at 12.91 ppm was more likely to represent a carboxylic acid than an aldehyde, as carboxylic acid protons tend to be more deshielded in ^{1}H-NMR spectra. Propionic acid (potentially formed from propionyl chloride and water from the hygroscopic $AlCl_3$) was considered, but it has a carboxylic acid proton which appears at ~11.9 ppm in ^{1}H-NMR spectra,[42] approximately 1 ppm upfield of the signal seen during the Friedel-Crafts acylation of **116**.

Further attempts were made to isolate and characterise the impurity by preparative TLC, however it was consistently recovered as part of an

inseparable mixture of unknown organic compounds, making it impossible to structurally characterise definitively. It was therefore decided to investigate the Friedel-Crafts' acylation conditions to see if a specific reaction variable led to the by-product formation.

The Friedel-Crafts acylation was therefore repeated with the same initial conditions as described in Figure 2-55, but with light excluded from the reaction (to prevent any UV-catalysed degradation). After one hour at room temperature, an aliquot was taken from the reaction, worked up and sent for ^{1}H-NMR analysis: this showed approximately 25 % product **153** and 75 % starting material **116** in the reaction mixture, with no sign of a signal at 12.91 ppm. An aliquot taken after a further five hours showed no change in distribution ratio, and so an extra equivalent of propionyl chloride was added and the reaction was left to stir overnight at room temperature (approximately eighteen hours total reaction time).

Fresh ^{1}H-NMR analysis after the extended stir at room temperature showed further conversion to product, with the product to starting material ratio at 53:47. In an attempt to drive the reaction to completion, it was heated at 45 °C for eighteen hours (thirty-six hours total reaction time), after which the reaction was worked up and sent for ^{1}H-NMR analysis. This analysis showed 40 % starting material, 51 % product and 9 % of the by-product with a signal at 12.91 ppm, suggesting that heating the reaction is at least a contributory cause to the degradant formation, as no trace of the signal at 12.91 ppm is seen in the ^{1}H-NMR spectra (Figure 2-62 (a) - (c)) until after the reaction was heated (Figure 2-62 (d)).

Note that in Figure 2-62, as the ^{1}H-NMR spectra represent reaction aliquots rather than a purified product, there is some contamination from common solvents. These are highlighted using coloured asterisks on the diagram, with the colours corresponding as follows: DCM, methanol, ethyl acetate and chloroform.

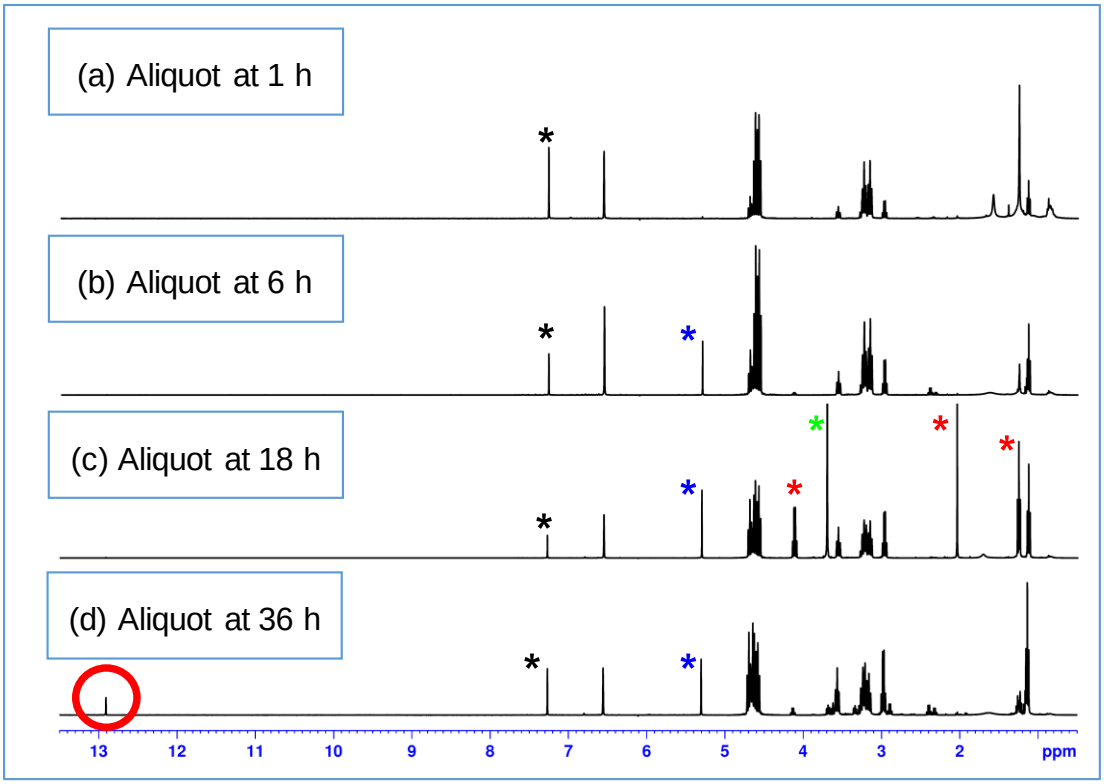


*Fig. 2-62: ^{1}H-NMR spectra of aliquots from the Friedel-Crafts formation of **153***

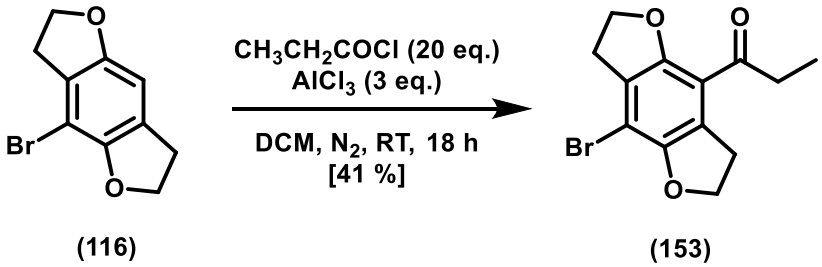
While the identity of the impurity was uncertain, we were confident that heating the Friedel-Crafts acylation reaction was contributing to its formation, and thus it was decided to avoid heating the reaction, but instead to look at other variables which could be adjusted to improve yield.

As addition of an extra equivalent of propionyl chloride appeared to double the conversion to product (from 25 % to 53 %), it was decided to run the reaction with an increased initial excess of propionyl chloride: ten equivalents instead of the previously used one equivalent. After two hours, an aliquot was taken, which revealed 49 % starting material and 51 % product present when analysed by ^{1}H-NMR. A further ten equivalents of propionyl chloride was added and the reaction was left to stir at room temperature overnight (18 h); when worked up, the ^{1}H-NMR spectrum of the reaction mixture showed 40 % starting material and 60 % product.

While the increase in equivalents of propionyl chloride clearly increased the initial conversion to product, the addition of further propionyl chloride did not

force the acylation to completion as hoped. At this point the potential issues of taking aliquots to monitor reaction progress were considered: they are not always representative of the reaction as a whole, but more importantly in this case, they can introduce air into what is otherwise an inert atmosphere. Both propionyl chloride and aluminium chloride are hygroscopic, with propionyl chloride the more sensitive of the two: as mentioned previously, it hydrolyses to the corresponding carboxylic acid in the presence of water vapour in air.

As the first attempt at the synthesis of **153** resulted in complete consumption of the starting material, it was decided to increase the equivalents of propionyl chloride to twenty (to be added in two ten-equivalent portions, one at the start and one four hours into the reaction) and to double the equivalents of aluminium trichloride, as shown in Figure 2-63.



(116) **(153)**

*Fig. 2-63: Optimised conversion of **116** to **153** using a Friedel-Crafts reaction*

This reaction was left to stir at room temperature for approximately 18 h without any aliquots taken, and when it was worked up, ^{1}H-NMR analysis revealed complete consumption of starting material with only trace impurities present. From this it was concluded that air introduced to the reaction by taking aliquots was the likely cause of previous issues with non-complete conversion to product.

The crude reaction mixture was purified by column chromatography, and **153** was recovered in 41 % yield, which was higher than previous results, but lower than expected as full consumption of starting material was seen in the ^{1}H-NMR. However, for the sake of expediency, it was decided to proceed to the next step of the reaction with the material that had been generated.

Once the reaction conditions for the synthesis of **153** had been adequately optimised and a stock of material synthesised, an initial attempt was made to synthesise brominated phenyl pyrimidine **104** using the three-component coupling reaction, as shown in Figure 2-64.

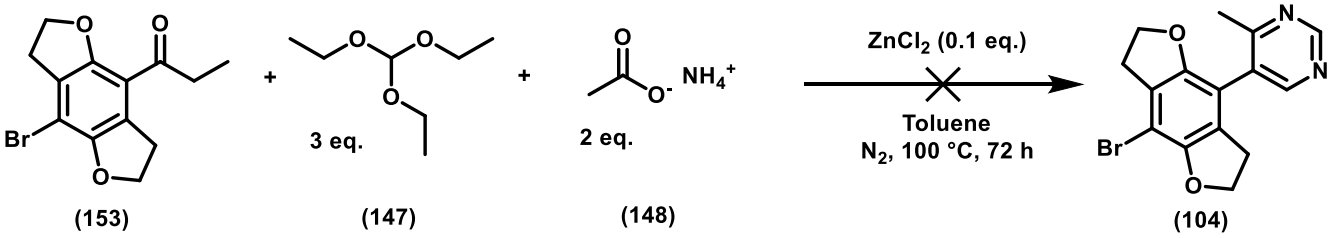


*Fig. 2-64: Attempted synthesis of brominated phenyl pyrimidine **104** using a three-component coupling reaction*

Once worked up, ^{1}H-NMR analysis of this initial attempt showed no conversion to product **104**, with only starting material **153** evident in the spectrum. It was decided to re-try the reaction again under inert conditions but within a sealed vessel as it was noticed that the volume of the reaction decreased in the round-bottomed flask as the procedure progressed. As previously discussed, other literature sources report this reaction as being carried out in ionic liquids or polar solvents,[34,36] and so it was decided to also attempt a variant of the reaction in DMF (Figure 2-65).

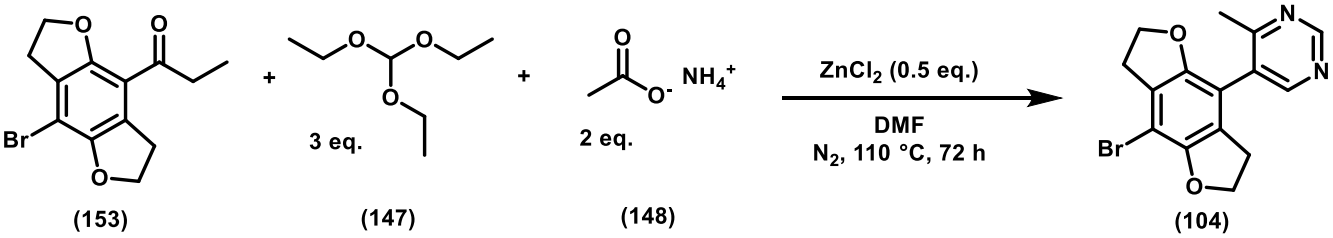


*Fig. 2-65: Modified synthesis of brominated phenyl pyrimidine **104** using a three-component coupling reaction*

When these reactions were worked up and sent for ^{1}H-NMR analysis, the spectra revealed a majority of starting material present, with possible traces of a pyrimidine moiety in both reactions: baseline signals were observed at 9.09, 8.63 and 2.25 ppm, which would be indicative of a pyrimidine derivative with a methyl group attached. The pyrimidine proton signals were more pronounced

in the toluene variant, however, there are literature reports of zinc chloride coordinating to DMF,[43] which would hinder the formation of the active form of the orthoformate ester, as described in the mechanism in Figure 2-54.

In light of this, the next attempt at the reaction used ACN as a solvent (a reaction temperature of 85 °C was employed to take into account the ACN boiling point) and a slight increase in the equivalents of zinc chloride (increased from 0.5 to 0.7 equivalents, as there were concerns that as a hygroscopic compound, some of the mass of weighed $ZnCl_2$ could be due to water), while keeping all other variables constant. Again, the ^{1}H-NMR spectrum of this reaction post work-up showed a majority of starting material **153** with traces of the desired pyrimidine **104** seen at baseline levels.

At this point, it was clear that the initial approach of using a more polar solvent was not having the desired effect of increasing conversion to product **104**, so it was decided to pursue two alternate lines of inquiry in an attempt to optimise the conditions:

1. Screen Lewis acids to determine the optimal catalyst
2. Dry all reaction apparatus and reagents to run a 'water free' attempt at the reaction (based on the sensitivity of the enamine formation reaction to water)

The first alternative Lewis acid catalyst trialled was aluminium chloride: the reaction was run in toluene as this had previously given the best results in terms of conversion to **104** and the equivalents of catalyst were increased (from 0.5 to 1.0 equivalents) as the aluminium chloride being used was not a freshly opened bottle; as a hygroscopic reagent, it was almost certainly not dry, which could reduce efficacy. When analysed by ^{1}H-NMR post work-up, the aluminium chloride attempt showed results similar to those garnered in previous runs using zinc chloride: mainly starting material **153** with baseline traces of pyrimidine **104** (see Table 2-12).

A further alternative Lewis acid catalyst was used in the form of tin tetrachloride: again, the reaction was run in toluene, this time with 0.5 equivalents of catalyst.

When analysed by ^{1}H-NMR post work-up, the majority component of the $SnCl_4$-mediated reaction was still starting material **153**, however, it was noted that the baseline pyrimidine signals appeared more pronounced (see Table 2-12), and so a comparison of the percentage conversions seen in reactions to that point was carried out. Integration values from ^{1}H-NMR spectra were used to determine the conversion. This was done by setting the signal at 9.09 ppm (a signal believed to represent a pyrimidine proton on **104**) to an integration value of 1.00 and comparing it to the integration of the signal at 2.97 ppm which represents the ethyl C**H$_2$** in the starting material **153**. The results are summarised in Table 2-12.

Lewis Acid Catalyst	Solvent	% Conversion to 104
$ZnCl_2$	DMF	0.9 %
$ZnCl_2$	ACN	2.3 %
$ZnCl_2$	Toluene	1.7 %
$AlCl_3$	Toluene	3.1 %
$SnCl_4$	Toluene	6.7 %

*Table 2-12: Percentage conversion to pyrimidine **104** in three-component coupling reaction*

From this, it is clear that tin tetrachloride is the best Lewis acid catalyst of those examined for the three-component coupling reaction, however, as all three of the Lewis acids tested are hygroscopic, it was decided to take the tin tetrachloride and zinc chloride variants and attempt the reactions under the driest conditions possible.

To this end, two reactions were performed under standard conditions as described in Figure 2-64 (using anhydrous toluene as a solvent), one with zinc

chloride and one with tin tetrachloride. The following preparation was done in order to ensure the reactions were as dry as possible:

- All reagents (except triethyl orthoformate **(147)**): reagents were dissolved in toluene and then concentrated to dryness using the rotary evaporator. Any water in the reagents should also have been removed by this azeotropic method.
- Solvent: toluene dried over 3Å molecular sieves for 24 h.
- All apparatus: dried in hot oven (150 °C) for 12 h, followed by immediate flushing with nitrogen gas.
- All transfers of reagents to reaction vessel were performed quickly and under a nitrogen gas funnel where possible.
- Reactions were performed in an inert atmosphere (N_2).

After the preparations, reactions were run and worked up as normal. The ^{1}H-NMR analysis of both reactions showed a majority of starting material **153**, with 0.4 % conversion to product **104** with zinc chloride, and 5.6 % conversion to product **104** with tin tetrachloride (these results were calculated from ^{1}H-NMR integration values as previously described for the data in Table 2-12). These results support those recorded earlier in suggesting that tin tetrachloride is the optimal Lewis acid catalyst of those tested for this reaction, however, the results also suggest that there is no advantage to ensuring an anhydrous reaction environment.

With tin tetrachloride established as the preferred Lewis acid catalyst, attention turned to other reagents in the attempt to increase the conversion to pyrimidine product **104**. A reaction was attempted as per Figure 2-64 but with increased equivalents of ammonium acetate **(148)** (2 → 5 equivalents) and triethyl orthoformate **(147)** (3 → 7.5 equivalents).

The rationale behind these increases was a re-consideration of the mechanism proposed by Sasada *et al.* (see Figure 2-54) in which the first step is the formation of an enamine from an α-acidic phenone and ammonium acetate **(148)**.[35] In their 2009 paper several reactions were reported beginning from phenones, and a number beginning from enamines which were prepared

and isolated before the three-component coupling reaction. The reaction times for the reactions starting from enamines ranged from 20 - 24 hours; however, when starting from ketones, the reaction times increased to 72 hours, suggesting that the enamine formation step is potentially rate limiting.

As enamine formation is an equilibrium, it was hoped in this work that adding more equivalents of starting materials **147** and **148** would follow Le Chatelier's Principle in helping drive the reaction to completion, and when the reaction was worked up and analysed by ^{1}H-NMR, it showed 10.7 % conversion to product **104**. While this was an improvement on previous runs, it is still very unsatisfactory, and it was decided to see if enamine **154** could be formed and isolated prior to the three-component coupling reaction.

While the enamine for the three-component coupling reaction is obviously formed *in situ* by Sasada *et al.*,[35] (see Figure 2-54) it is clearly a very slow reaction under those conditions. It was therefore decided to establish optimum conditions for enamine/imine formation. To this end, several variables were investigated using SciFinder® (refined to look only at enamine-forming reactions with > 60 % yield):

- Solvent: while some enamine formations were performed in toluene (as by Sasada *et al.*),[35] the majority of reactions favoured more polar solvents, e.g. ethanol, methanol and DMF.
- Ammonia source: ammonium acetate **(148)** was by far the most popular source of nitrogen nucleophile, though some reactions also reported the use of neat ammonia or methanolic ammonia. The most common procedure was to use an excess (at least three equivalents) of ammonium acetate **(148)**.[44]
- Reaction time: this varied, however, a reaction time of between 12 and 16 hours seemed typical.
- Reaction temperature: again, there were a variety of temperatures depending on the reagents used, but the most common procedure was to run the reaction at reflux.

- Reaction atmosphere: there were no references to an inert atmosphere in the literature – common practice was to run the reactions in air.

Based on these findings, an initial set of reaction conditions were decided upon (as shown in Figure 2-66): phenone **153** with three equivalents of ammonium acetate **(148)** in ethanol, refluxed for eighteen hours in a sealed vial.

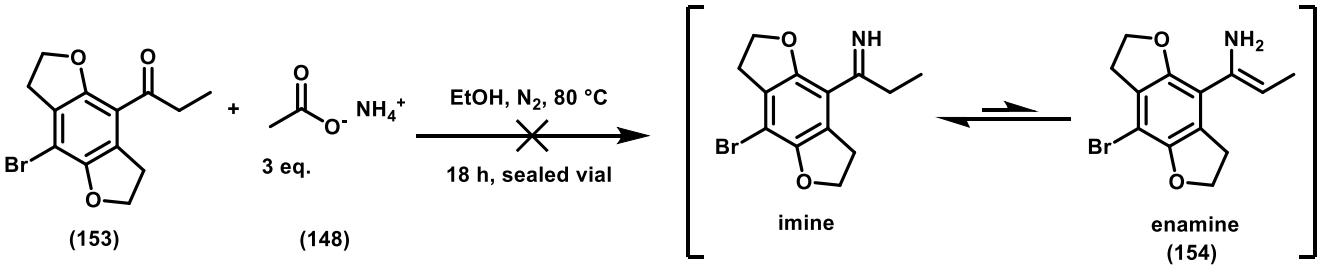


*Fig. 2-66: Formation of enamine **154** using ammonium acetate **(148)** in ethanol*

Unfortunately, analysis of the resultant crude reaction mixture after eighteen hours by ^{1}H-NMR (post work up) showed only starting material **153**, with no evidence of conversion to product seen.

Based on this result, it was decided to attempt the reaction in methanol with an increased excess of ammonium acetate **(148)** (3 → 12 equivalents) and a longer reaction time (18 → 40 hours). As water is a side-product of the enamine formation and is also known to hamper the reaction, it was decided to use distilled methanol and to add 3Å molecular sieves to the reaction to absorb any water side-product. However, as previously, on analysing the crude reaction mixture by ^{1}H-NMR after work-up, it became clear that there was no conversion to enamine **154**.

At this point, it was decided to change the nitrogen source from ammonium acetate **(148)** to methanolic ammonia to see if that would have any effect. This was done as described in Figure 2-67: the reaction time was extended further (40 → 60 hours), and the reaction was done in a sealed vessel to prevent methanol from boiling off.

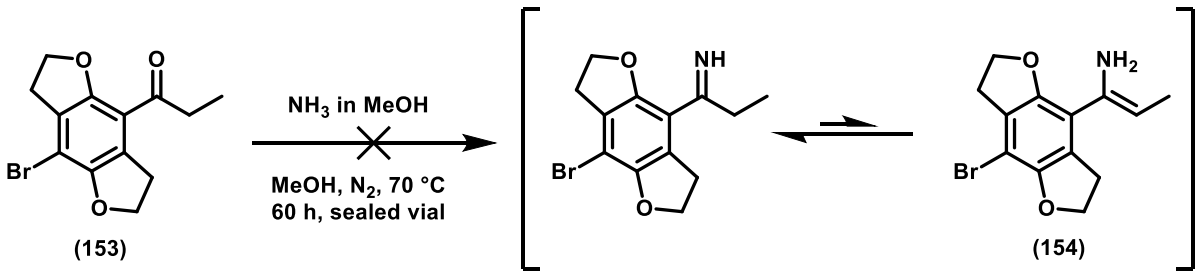


*Fig. 2-67: Modified formation of enamine **154** using methanolic ammonia*

At the beginning of the reaction, it was noted that the phenone **153** did not appear to be soluble in the reaction solvent even at reflux, an issue that was not noted in previous reactions. Once the reaction was finished and analysed by ^{1}H-NMR, again revealing no conversion to product, this insolubility was targeted as another possible issue with the enamine conversion.

In an attempt to solubilise **153** in the reaction, DCM was substituted for methanol and the reaction was refluxed under an inert atmosphere of N_2, using five equivalents of methanolic ammonia and 3Å molecular sieves.[45] The reaction time was also extended to 90 h and the reaction was undertaken in a sealed vessel.

When the DCM reaction variant was worked up and analysed by ^{1}H-NMR, it showed a majority of starting material, but there were trace amounts of what could be the enamine **154**, although the signal for what would be the alkene proton appeared further downfield than expected at 6.03 ppm (see Figure 2-68). It would have been expected to see the alkene signal closer to 5.00 ppm.

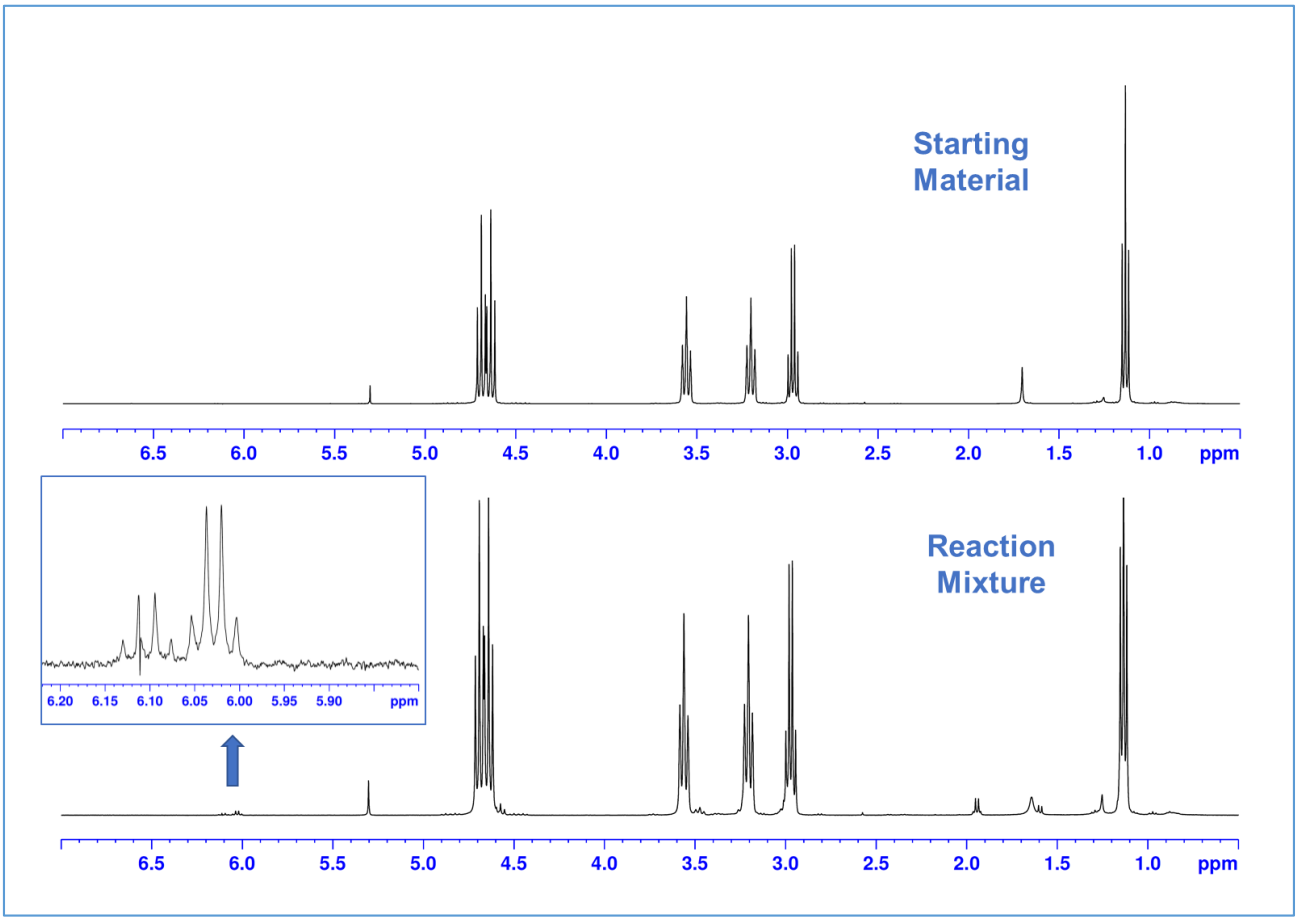


*Fig. 2-68: ^{1}H-NMR spectra of ketone **153** and potential enamine **154***

Based on the DCM variant result, it was hypothesised that tiny amounts of the enamine **154** are likely being formed in the three-component coupling reaction. However, in that reaction, the enamine is *in situ* converting to form pyrimidine **104**, with Le Chatelier's Principle meaning that more **154** is formed as it reacts and is 'removed' as the product of the enamine-forming reaction. This explains why even after extended reaction times, little to no enamine **154** is seen when trying to synthesise it independently, and why maximum conversions of 11 % are seen to **104** in the three-component coupling reaction.

This failure to pre-form enamine **154** also confirms that enamine formation is likely the rate-limiting step in the one-pot three-component coupling reaction. However, before stating that definitively, it was decided to run the enamine/imine forming reaction on a compound other than phenone **153** to prove that the transformation is feasible with other substrates.

The two substrates chosen for the imine formation test were 2,5-dimethoxybenzaldehyde **(155)** and benzaldehyde **(70)**. The reactions were run as detailed in Figure 2-69.

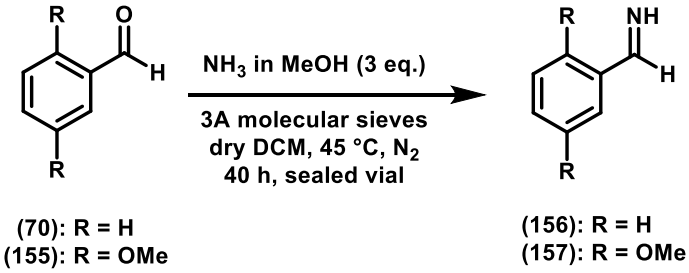


Fig. 2-69: Conversion of aldehydes to imines using methanolic ammonia

When both reactions were analysed by ^{1}H-NMR post work-up, they revealed partial conversion to imine product, 17 % in the case of 2,5-dimethoxybenzaldehyde **(155)** and 45 % in the case of benzaldehyde **(70)** (see Figure 2-70). This proves that the enamine/imine forming reaction is viable, but that the ketone **153** is not a suitable substrate.

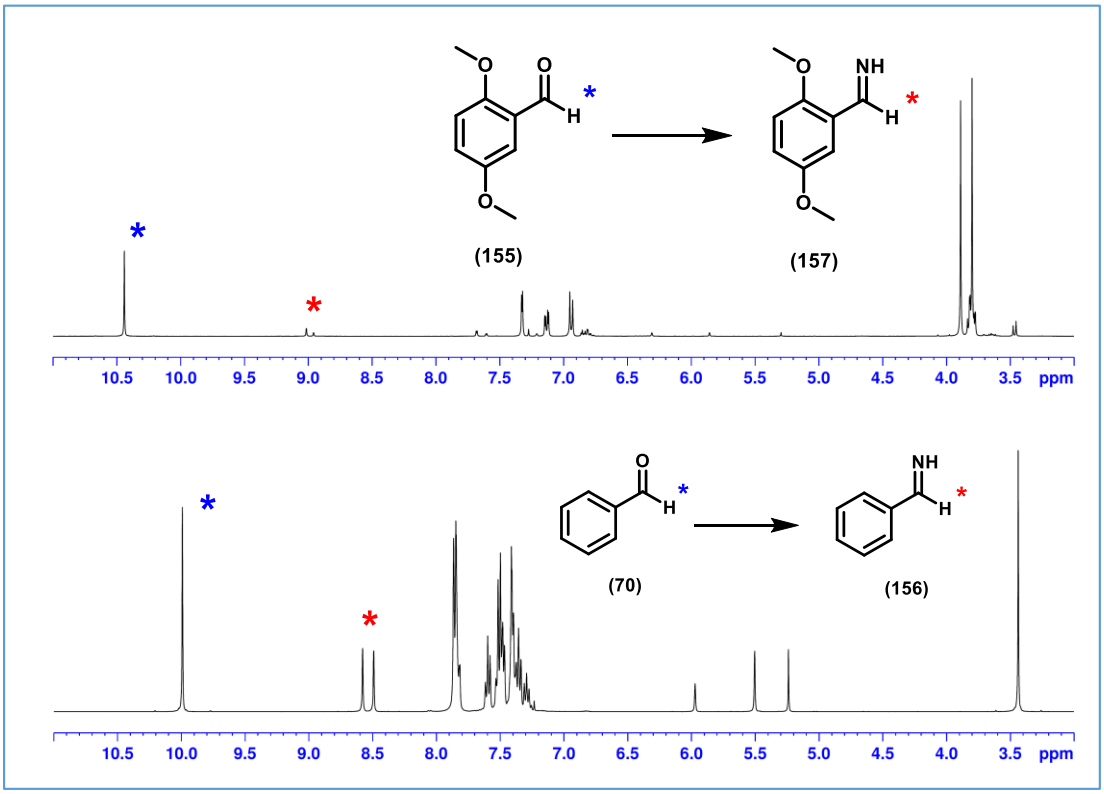
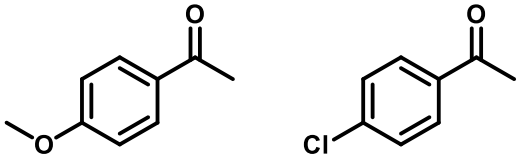


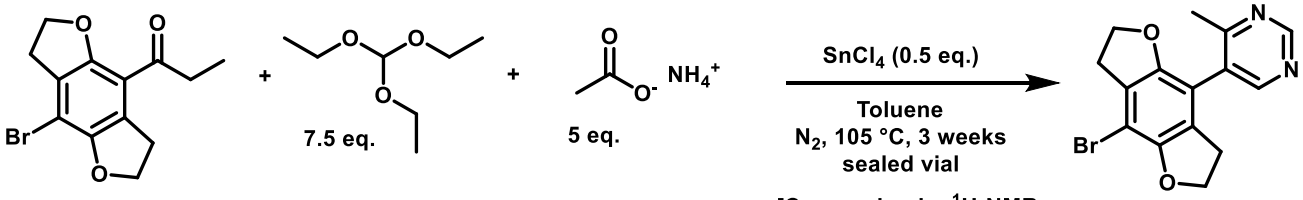
*Fig. 2-70: ^{1}H-NMR spectra of imines **156** and **157***

The results also suggest that having an electron rich aromatic ring has a likely negative impact on enamine/imine formation. This is in line with data from Sasada *et al.*, where the lowest yielding pyrimidines in their three-component coupling reactions utilised *p*-methoxy acetophenone **(158)** (40 % yield) and *p*-chloro acetophenone **(159)** (50 % yield) as substrates. The THBD moiety is very electron rich, with two resonance electron-donating alkoxy substituents and two inductively electron-donating alkyl substituents, and addition of bromine to the THBD system only increases the electron density further. It is therefore unsurprising that considerable difficulty was encountered in trying to form enamine **154** from ketone **153**.



(158) **(159)**

As a final attempt to increase the conversion of phenyl pyrimidine **104** using the three-component coupling reaction, it was decided to perform a reaction for an extended time period (three weeks) using previously optimised conditions (see Figure 2-71) to determine if the longer reaction time allowed for greater conversion to product **104**.



(153) **(147)** **(148)** **(104)**

*Fig. 2-71: Synthesis of brominated phenyl pyrimidine **104** using extended reaction time*

However, when the reaction was analysed after three weeks, the ^{1}H-NMR spectrum showed only 12.0 % conversion to product **104** post work-up (calculated by ^{1}H-NMR integration values as for Table 2-12). While this was

the best result recorded, it was not significantly better than the conversion seen in the three day reaction (10.7 %), which suggests a limiting factor other than enamine formation is at play. A paper by Bultman *et al.* employing trimethyl orthoformate as a water scavenger in a pyridine formation reaction stated that stability studies conducted on the trimethyl orthoformate indicated its degradation over time at temperatures higher than 35 °C.[46] While this thesis work employs triethyl orthoformate **(147)** rather than trimethyl orthoformate, it is not inconceivable that triethyl orthoformate **(147)** could face similar decomposition issues at higher temperatures for extended periods of time, possibly stalling the three week reaction. Unfortunately, after this result, the three-component coupling reaction was deemed unsuitable for substrate **153** and this line of research was not pursued further.

2.2.5 Attempted Alternate Syntheses of 5-(Benzo[1,2-*b*:4,5-*b'*]difuran-4-yl)-4-methylpyrimidine (106)

*2.2.5.1 Attempted Synthesis of **106** from Unaromatised Analogue **101** using NBS*

This body of work is described in detail in Section 2.2.4.2. In summary, an initial attempt to synthesise brominated THBD phenyl pyrimidine **104** from its nonbrominated analogue **101** resulted instead in the isolation of the benzodifuran phenyl pyrimidine **106**. All subsequent attempts to repeat this transformation frustratingly resulted in benzylic bromination of the methyl group of the THBD phenyl pyrimidine.

*2.2.5.2 Attempted Synthesis of **106** from Unaromatised Analogue **101** using DDQ*

In Section 2.2.1.2, a procedure is described for converting brominated THBD **116** to its benzodifuran analogue **117** using DDQ (Figure 2-8). The same aromatisation procedure was also attempted using THBD phenyl pyrimidine **101** as shown in Figure 2-72.

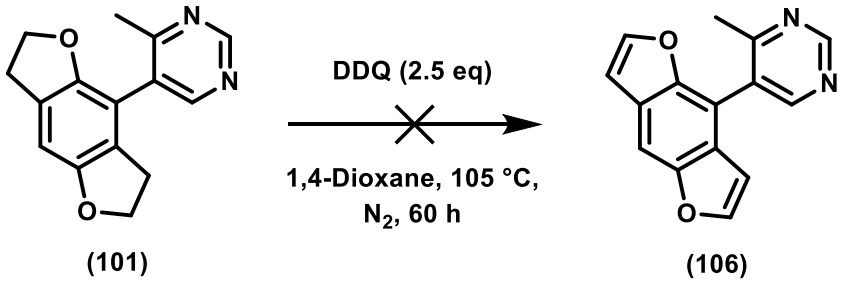


*Fig. 2-72: Attempted synthesis of benzodifuran pyrimidine **106** using DDQ*

The crude reaction residue showed a mixture of products when analysed by ^{1}H-NMR, and when purified by preparative TLC, the main component (that was not starting material **101**, which was also recovered) was a compound with signals both in the aromatic and aliphatic regions of the spectrum, indicating that the starting material was likely partially aromatised, but not fully converted to benzodifuran. While this problem could potentially be solved by increasing reaction time or equivalents of DDQ, it was also noted that the signal for the pyrimidinyl methyl group had unexpectedly vanished (no signal at 2.45 ppm, see Figure 2-74). Evidence of diastereotopic protons in the two multiplets at ~3.00 and 3.20 ppm was suggestive of aromatisation of the northern ring of **101**. This suggests that it is Ring N (see Figure 2-73) which has been aromatised.

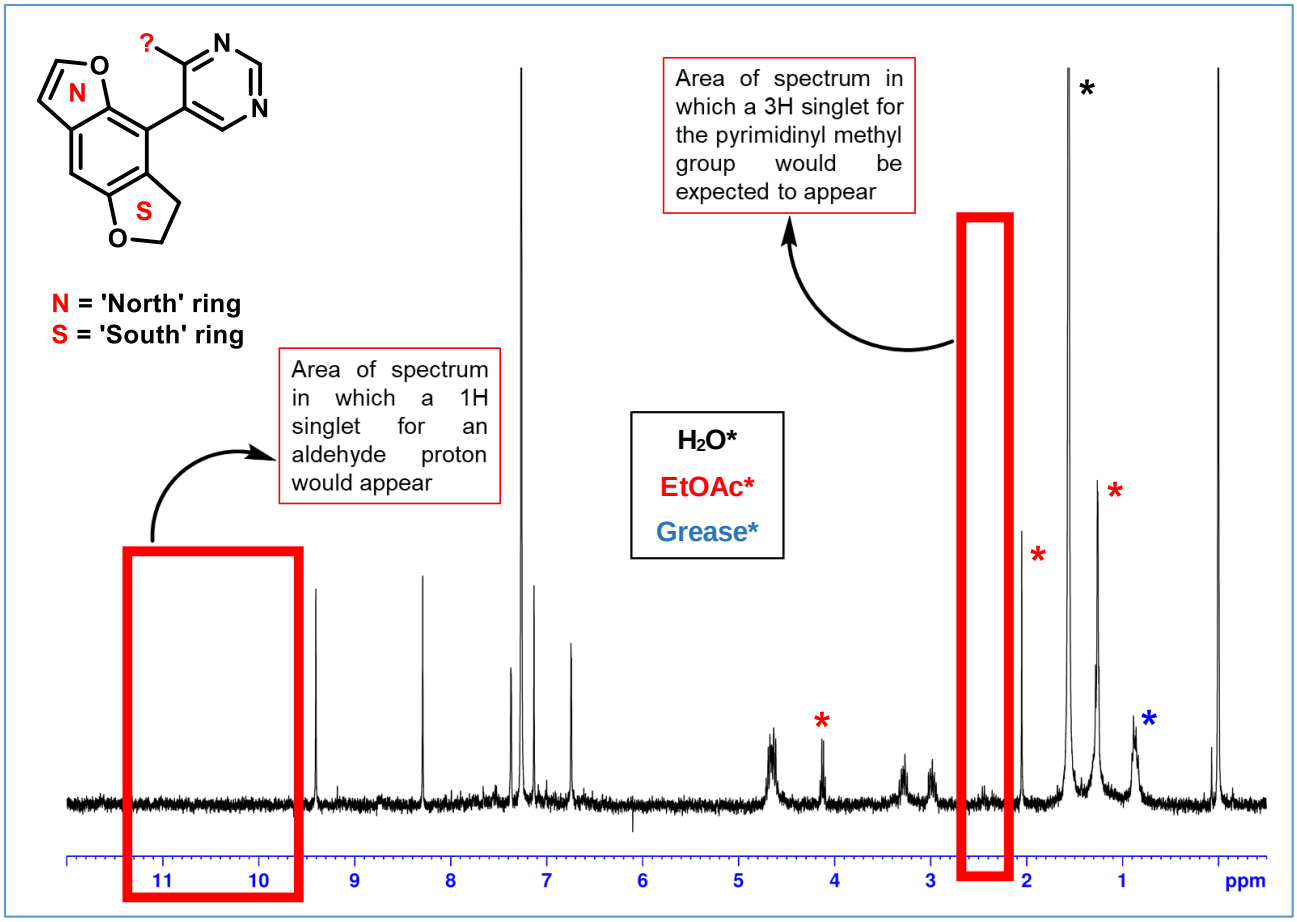
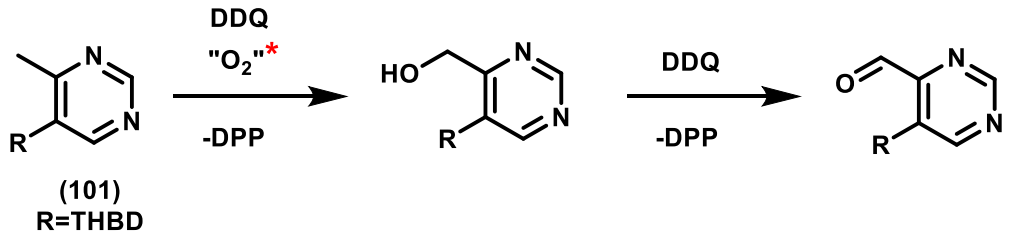


*Fig. 2-73: ^{1}H-NMR analysis of reaction product from attempted synthesis of **106** from unaromatised analogue **101** using DDQ*

The absence of a 3H singlet at ~ 2.50 ppm led us to believe that DDQ may potentially have facilitated a benzylic carbonylation, which is a known DDQ-mediated transformation,[47] although no evidence was seen of a signal for an aldehyde proton in the ^{1}H-NMR spectrum (see Figure 2-73). If DDQ-mediated benzylic carbonylation took place at the methyl group of the pyrimidine, an aldehyde moiety would be the expected result (as shown in Figure 2-74. Note that the hydroxyl intermediate shown would have a -CH_2- singlet in the ^{1}H-NMR spectrum at ~4.50 ppm: there is no evidence for this in Figure 2-73).



(101)
R=THBD

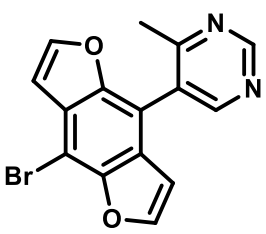
* This indicates a source of oxygen, such as water from undried solvents, oxygen from solvents that were not degassed, or air in reaction vessels that were not fully inerted

*Fig. 2-74: Proposed reaction scheme for DDQ-mediated benzylic carbonylation on the aryl methyl group of **101**.*

The reaction was repeated once to ensure that the results were reproducible, and the same ^{1}H-NMR spectrum was seen for the main component (that was not starting material **101**), confirming that the reaction was unsuitable for this substrate. Unfortunately, this compound was recovered in quantities too small (< 5 mg) to run ^{13}C-NMR analysis to check for the presence of a carbonyl signal.

2.2.6 Isolation of 5-(8-Bromobenzo[1,2-*b*:4,5-*b'*]difuran-4-yl)-4-methylpyrimidine (108)

After the synthesis (and attempted alternate syntheses) of phenyl pyrimidines **101**, **104** and **106** it was decided not to attempt the synthesis of the final brominated benzodifuran phenyl pyrimidine **108** due to the difficulties encountered in synthesising the brominated THBD and nonbrominated benzodifuran variants (**104** and **106** respectively). These included:



(108)

- Difficulty in synthesising dibrominated benzodifuran **119**, required for boronic acid synthesis: this reaction requires high excesses of DDQ and frequently results in a mixture of fully and partially aromatised products.
- Difficulty in synthesising boronic acids: synthesis of brominated boronic acids leads to problems in separating them from nonbrominated analogues, and the reaction to produce benzodifuran boronic acid **125** proved to be very poor yielding (13 %) after extended reaction times (Figure 2-13).
- Synthesis from nonbrominated analogue **106**: thus far no bromination procedure has been found which allows C-4 bromination of the benzodifuran ring without first brominating the pyrimidinyl methyl group.
- Synthesis from unaromatised analogue **104**: DDQ, currently the only viable procedure known within our group for aromatisation of a THBD moiety, leads to incomplete aromatisation and also potentially to benzylic carbonylation on the pyrimidinyl methyl group (Figure 2-74).
- Three-component coupling reaction: this failed using brominated THBD substrate **153** in part due to the high electron density aromatic ring: a brominated benzodifuran core (as would be needed to synthesise **108**) is even more electron dense and would almost certainly fail.

Despite the inability to independently synthesise the novel substrate 5-(8-bromobenzo[1,2-*b*:4,5-*b'*]difuran-4-yl)-4-methylpyrimidine **(108)**, it was later isolated by preparative TLC from the Leuckart reaction to form Bromo-DragonFLY **(15)** (described in Section 2.4.2.2) and fully characterised as summarised in Table 2-13. While this substrate lacks the verification of independent synthesis, the evidence for its identity is very strong, as it can be compared to other independently synthesised substrates which differ only by one atom or two degrees of unsaturation, and also given its origin within the Leuckart reaction.

Compound Number	Yield (%)	m.p. (°C)	R_f (Hex:EtOAc)	HRMS (*m/z*)	
				Calc.	Found
108	2.2	110 - 111 (No recryst.)	0.41 (1:1)	328.9920	328.9926

*Table 2-13: M.p., R_f, and HRMS data for brominated benzodifuran phenyl pyrimidine **108***

Full ^{1}H- and ^{13}C-NMR spectra were also measured and assigned by comparison to the corresponding spectra for 5-(benzo[1,2-*b*:4,5-*b'*]difuran-4-yl)-4-methylpyrimidine **106**, as seen in Figure 2-75 (full assignment of signals can be seen in Figure 2-112).

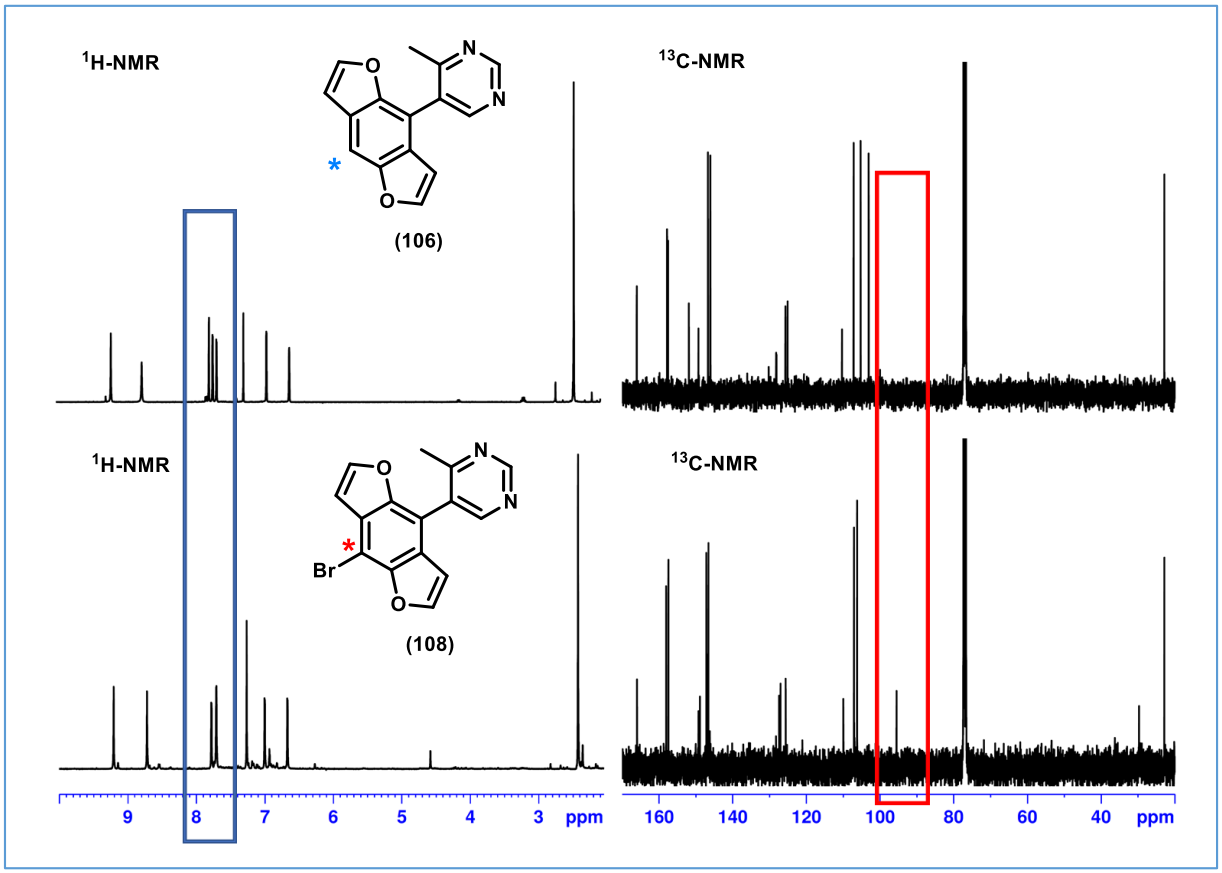


*Fig. 2-75: Comparison of ^{1}H- and ^{13}C-NMR spectra of **106** and **108***

The only minor difference between the spectra of **106** and **108** was the absence of an aromatic proton signal in the ^{1}H-NMR of **108** and an upfield shift

in the ^{13}C-NMR of the 107.2 ppm signal in **106** to 95.5 ppm in **108**, with the latter shift value being typical of a carbon bound to a bromine (**C**-Br).

2.3 Synthesis of Benzyl Pyrimidines Associated with the Leuckart Synthesis of Bromo-DragonFLY

The 2011 Blachut *et al.* paper containing the Suzuki-Miyaura synthetic procedure for accessing the phenyl pyrimidine series in this work also contains a procedure for the synthesis of benzyl pyrimidines, which was initially considered as a potential path to the synthesis of benzyl pyrimidines **100**, **103**, **105** and **107** in this work.[7] The Blachut route uses Negishi palladium coupling between 4-bromopyrimidine **(160)** and a benzyl zinc chloride, as shown in Figure 2-76.[7]

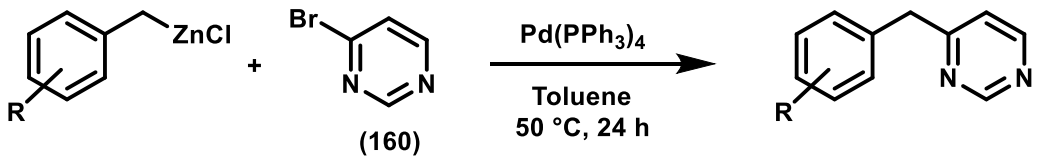


Fig. 2-76: Negishi palladium coupling reaction to produce a benzyl pyrimidine

With regards to the starting materials, 4-bromopyrimidine **(160)** is commercially available, but to access the THBD and benzodifuran zinc chlorides needed would have required several synthetic steps to be performed from THBD **(42)**, as described in Figure 2-77.

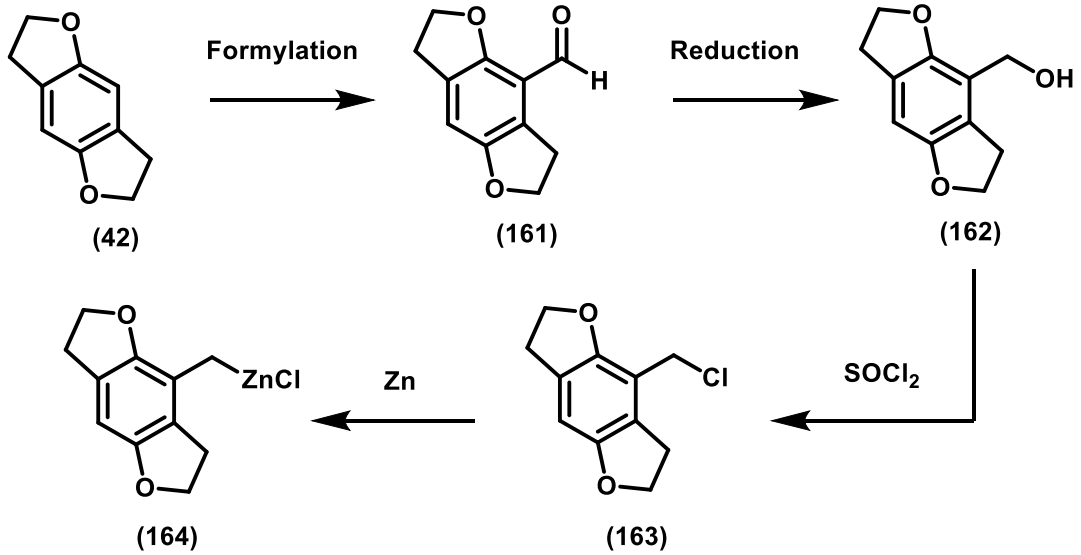


*Fig. 2-77: Proposed synthetic pathway from THBD **(42)** to the analogous benzyl zinc chloride **164***

These four steps would have to be extended to five or six steps (depending on required substrate) to accommodate bromination and/or aromatisation of the THBD moiety, which would have been a potentially long and challenging synthetic pathway. However, while reviewing the literature, an alternate synthetic route to access the desired benzyl pyrimidines was discovered. In 2010, Burton *et al.* described a palladium catalysed C-H activation coupling reaction between 4-methylpyrimidine **(134)** and an aryl bromide to form a benzyl pyrimidine in one step (see Figure 2-78).[48]

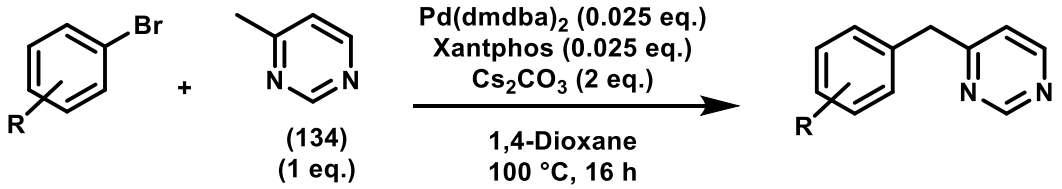


Fig. 2-78: C-H activation coupling reaction to form benzyl pyrimidines

Burton *et al.* described a range of diverse substrates on which they performed the reaction, and while the palladium catalyst ($Pd(dmdba)_2$, also known as Fairlamb's catalyst) shown in Figure 2-78 was described as the optimal catalyst, the paper also listed a large number of other palladium catalysts

which could be used, including palladium acetate ($Pd(OAc)_2$) and tris(dibenzylideneacetone)dipalladium(0) ($Pd_2(dba)_3$).[48]

Burton's benzyl pyrimidine route was more attractive in this work than the zinc chloride route for a number of reasons: the starting materials were all either commercially available, or accessible from THBD **(42)** in one or two synthetic steps depending on the level of aromatisation required, and thus it was decided to attempt this route initially and to only progress to the zinc chloride route if the C-H activation coupling failed.

2.3.1 Optimisation of C-H Activation Coupling Reaction

Brominated THBD **116** was synthesised as described in Section 2.2.1.2, and this was used in the initial attempt at the C-H activation coupling reaction with 4-methylpyrimidine **(134)** to form benzyl pyrimidine **100**. The catalyst used was $Pd(OAc)_2$ (2.5 mol%), with the conditions as described in Figure 2-79.

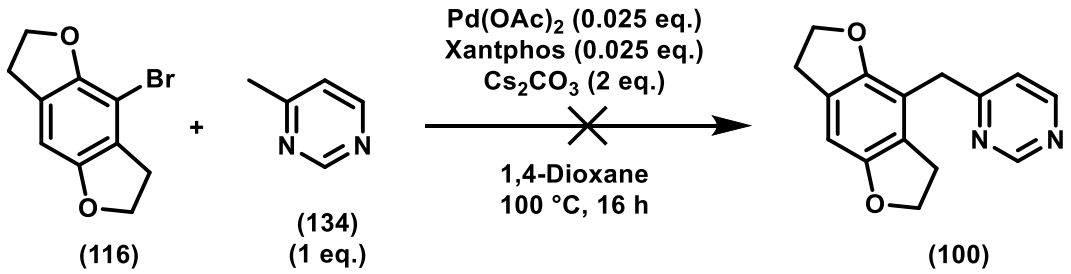


*Fig. 2-79: Attempted synthesis of THBD benzyl pyrimidine **100***

When the reaction was analysed by ^{1}H-NMR post work-up, there was no evidence present of the desired benzyl pyrimidine **100** (which should show a characteristic peak for the benzyl protons at approximately 4 ppm). Starting materials **116** and **134** were the only components evident in the ^{1}H-NMR spectrum. Replicating the reaction as described in Figure 2-79 afforded an identical result.

Based on this attempt, it was decided to test the reaction conditions using a substrate structurally similar to an example that had already been used by Burton; bromobenzene **(165)**, as shown in Figure 2-80. A similar reaction performed by Burton *et al.* used 2-bromotoluene **(166)** and 4-methylpyrimidine **(134)** and produced 4-(2-methylbenzyl)pyrimidine **(167)** in a yield of 81 %.[48]

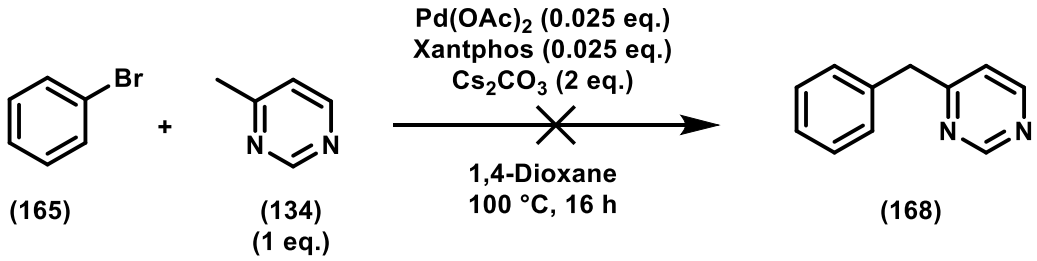
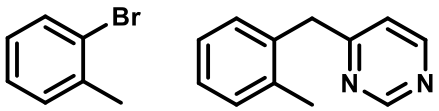


*Fig. 2-80: Attempted synthesis of 4-benzylpyrimidine **(168)***

The reaction to form **168** as seen in Figure 2-80 showed no evidence of product formation by ^{1}H-NMR analysis, but HRMS analysis did find a PMI which matched **168** (calculated *m/z*: 171.0922; found *m/z*: 171.0925; mass accuracy: 1.8 ppm), suggesting that trace amounts of the product were being formed, but were undetectable by ^{1}H-NMR analysis. A second attempt at the reaction extending the reaction time from 16 to 48 hours produced similar ^{1}H-NMR and HRMS results, but as Burton *et al.* reported yields of 81 % in their paper for an almost identical substrate **166**, the reaction was clearly not performing as it should in our hands.



(166) **(167)**

At this point, we contacted the authors of the original paper, who responded promptly to inform us that they had actually only ever used $Pd(OAc)_2$ for one substrate in their paper (not 2-bromotoluene **(166)**) and they advised us to switch catalyst to either $Pd_2(dba)_3$ or Fairlamb's catalyst, and increasing the catalyst and ligand loading if the catalyst change alone proved insufficient.[49]

Armed with this knowledge and Fairlamb's catalyst, a third attempt was made at the synthesis of THBD benzyl pyrimidine **100**, using reaction conditions as

in Figure 2-79, but with 2.5 mol% of Fairlamb's catalyst instead of $Pd(OAc)_2$. There were minor signals at ~ 3.8 and 4.0 ppm in the ^{1}H-NMR spectrum which could indicate conversion to product **100** (see signals circled in red in Figure 2-81) and HRMS did indicate that pyrimidine **100** had been formed (calculated *m/z*: 255.1134; found *m/z*: 255.1135; mass accuracy: 0.4 ppm), but there was clearly a majority of starting materials **116** and **134** in the crude mixture.

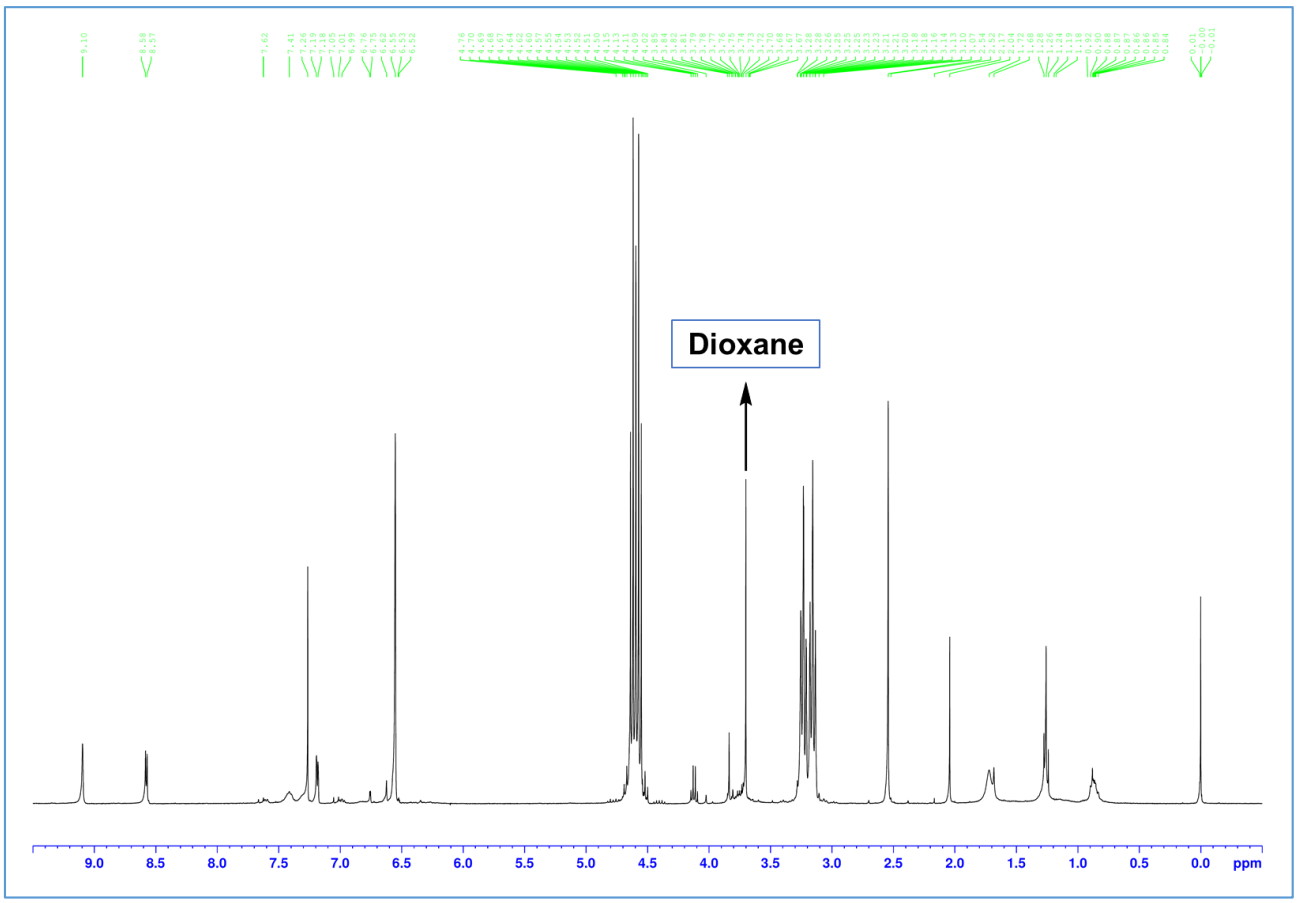


Fig. 2-81: ^{1}H-NMR spectra of crude reaction mixture from C-H activation coupling reaction using Fairlamb's catalyst

As the next step, it was decided to increase the catalyst and ligand loading in the reaction from 2.5 to 10 mol%, as shown in Figure 2-82.

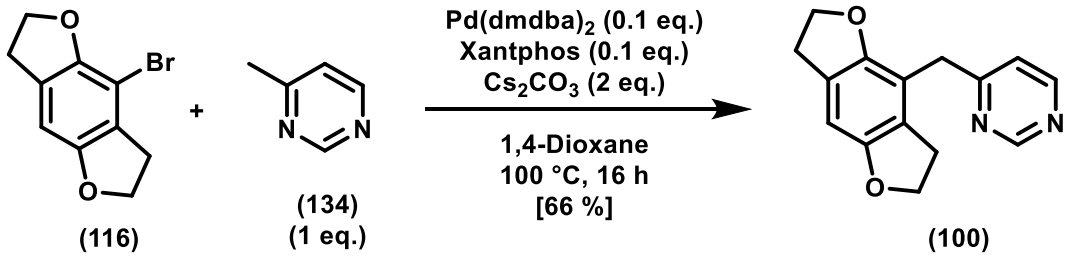


*Fig. 2-82: Modified synthesis of THBD benzyl pyrimidine **100***

The ^{1}H-NMR analysis of the crude reaction mixture post work-up showed strong evidence for the formation of the product, with a singlet at 4.03 ppm which could represent the two benzylic protons and overlapping multiplets at approximately 3.20 and 4.50 ppm that indicated the presence of more than one unsymmetrically substituted THBD core in the reaction mixture. The ^{13}C-NMR analysis offered further support, with the signal at 24.2 ppm for the methyl group in 4-methylpyrimidine **(134)** all but vanishing, and the appearance of a signal at 36.2 ppm (which appeared in the negative phase of the DEPT-135, indicating a **C**H$_2$ group).

The crude reaction mixture was purified by flash column chromatography, and the novel product **100** was gratifyingly isolated in moderate yield (66 %). The product was then fully characterised as summarised in Table 2-14.

Compound Number	Yield (%)	m.p. (°C)	R_f (Hex:EtOAc)	HRMS (*m/z*)	
				Calc.	Found
100	66	94 - 96 (Et_2O)	0.06 (5:1)	255.1134	255.1135

*Table 2-14: Yield, m.p., R_f, and HRMS data for THBD benzyl pyrimidine **100***

Pure samples were also analysed by ^{1}H- and ^{13}C-NMR, with the characteristic signal for the benzylic protons exhibited at 4.03 ppm in the ^{1}H-NMR spectrum (as shown in Figure 2-83), and the corresponding signal for the benzylic carbon appearing at 36.2 ppm in the ^{13}C-NMR spectrum.

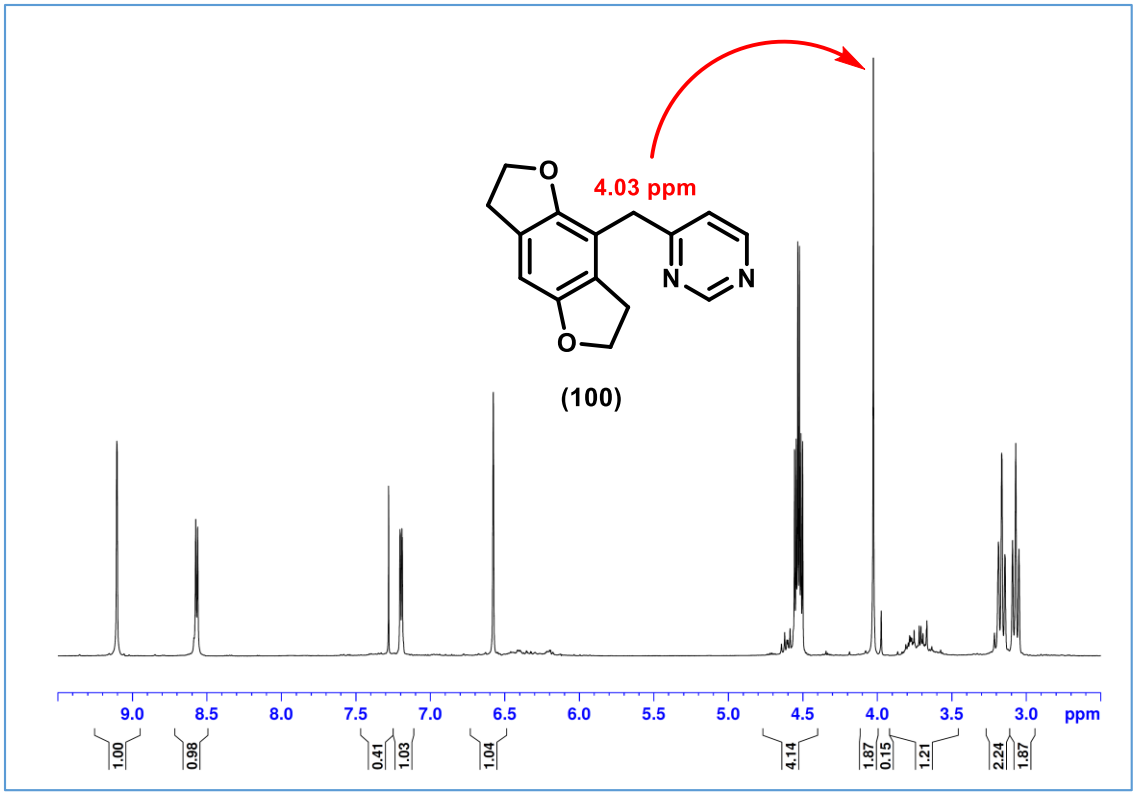


*Fig. 2-83: ^{1}H-NMR spectrum of **100***

All other signals in the ^{1}H-NMR appeared in the regions expected from previous work with both THBD-type substrates and pyrimidines, though there was of course an extra signal in the ^{1}H-NMR spectrum for the pyrimidine moiety due to the presence of three unsubstituted positions on the pyrimidine ring in the benzyl series of compounds, compared to only two unsubstituted positions in the phenyl pyrimidine series previously described. This extra signal appears in the ^{1}H-NMR spectrum of **100** at 7.19 ppm, and it also changes the multiplicity of the signal seen for the pyrimidine proton at ~ 8.50 ppm: in the phenyl pyrimidine series, the signal for this proton is a singlet. However, in the benzyl pyrimidine series, it is split into a doublet (with a coupling constant of J = 4.8 Hz) by the neighbouring proton at ~7.20 ppm. All the signals recorded during ^{1}H- and ^{13}C-NMR analysis are summarised in Figure 2-84.

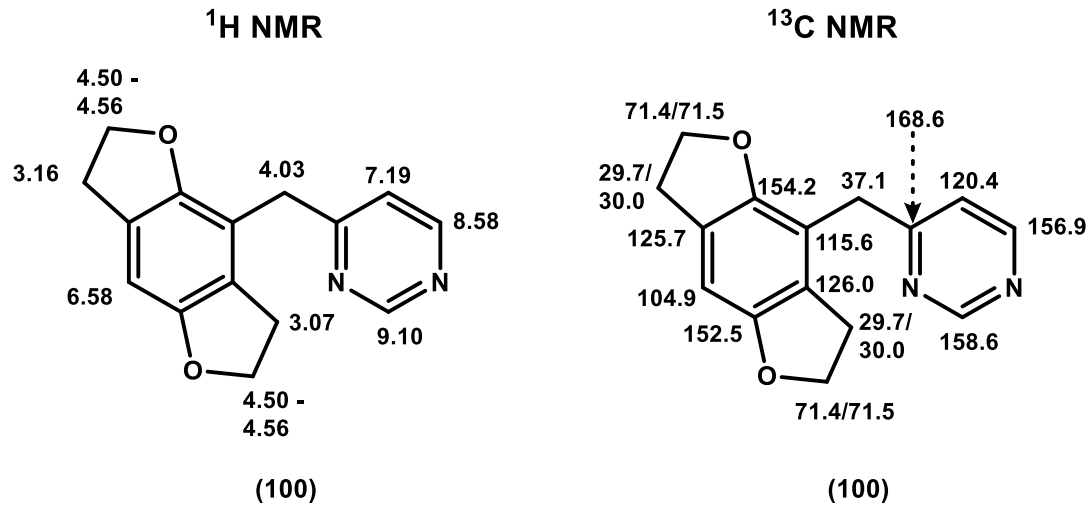
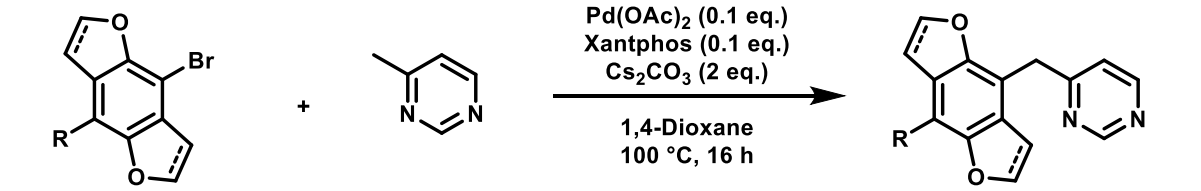


*Fig. 2-84: ^{1}H- and ^{13}C-NMR data for THBD benzyl pyrimidine **100***

2.3.2 Synthesis of Benzyl Pyrimidine Series using Optimised C-H Activation Coupling Reaction

Following the optimisation of the C-H activation coupling reaction using brominated THBD **116**, substrates **117** - **119** were synthesised as described in Section 2.2.1 and were subsequently employed as starting materials in the C-H activation coupling reaction to produce novel benzyl pyrimidines **103**, **105** and **107** (Figure 2-85).



(117): Benzodifuran, R = H
(118): THBD, R = Br
(119): Benzodifuran, R = Br

(134)
(1 eq.)

(105): Benzodifuran, R = H [7.3 %]
(103): THBD, R = Br [92 %]
(107): Benzodifuran, R = Br [8.2 %]

*Fig. 2-85: Synthesis of benzyl pyrimidines **103**, **105** and **107** via C-H activation coupling reaction*

While each of the three reactions was conducted under identical conditions, the yields were widely disparate, as summarised in Table 2-15.

Compound Number	R_1	Level of Oxidation	% Yield
100	H	THBD	66 %
105	H	Benzodifuran	7.3 %
103	Br	THBD	92 %
107	Br	Benzodifuran	8.2 %

Table 2-15: Yields of the benzyl pyrimidine series

These results indicate very clearly that the increased aromaticity of the benzodifuran system (compared to the THBD system) decreases the reactivity of **117** and **119** in the C-H activation coupling reaction. Despite attempts at further optimisation of the C-H activation coupling reaction (described in Section 2.3.3), no significant increases in yield were seen for **105** or **107**.

All the novel compounds were isolated by flash column chromatography on silica gel and were subsequently fully characterised as summarised in Table 2-16.

Compound Number	Yield (%)	m.p. (°C)	R_f (Hex:EtOAc)	HRMS (*m/z*)	
				Calc.	Found
103	92	118 - 120 (Et_2O)	0.06 (5:1)	333.0239	333.0241
105	7.3	88 - 90 (No recryst.)	0.06 (5:1)	251.0821	251.0812
107	8.2	105 - 106 (No recryst.)	0.15 (5:1)	328.9926	328.9930

*Table 2-16: Yield, m.p., R_f, and HRMS data for benzyl pyrimidines **103**, **105** and **107***

The compounds **103**, **105** and **107** were also fully characterised by ^{1}H- and ^{13}C-NMR analysis. The ^{1}H-NMR spectrum of **103** was similar to that of THBD

benzyl pyrimidine **100**, with the main difference being the absence of one aromatic signal (where the position on the THBD phenyl ring is now substituted by a bromine atom). There are also slight differences in chemical shifts between analogous signals. For example, the signal for the benzylic protons in **100** is seen at 4.03 ppm, whereas the signal for the analogous protons in **103** appears at 3.97 ppm.

In the case of benzodifuran benzyl pyrimidines **105** and **107**, all ^{1}H-NMR signals except for benzylic protons reside in the aromatic regions of respective ^{1}H-NMR spectra, within the range 6.5 - 9.5 ppm. Again, there is a subtraction of one signal in the aromatic region as a result of bromine substitution on the phenyl ring, but in all other respects, **105** and **107** spectra are very similar, with only slight chemical shift changes showing differences between both substrates.

It is also worth noting that there is a significant difference (~ 0.6 ppm) in chemical shift of the benzyl protons between the THBD and benzodifuran-type compounds. The THBD benzyl pyrimidine protons appear at ~ 4.0 ppm, while the analogous protons in the benzodifuran benzyl pyrimidines can be seen at ~ 4.6 ppm. A summary of the **103**, **105** and **107** ^{1}H-NMR analyses can be seen in Figure 2-86.

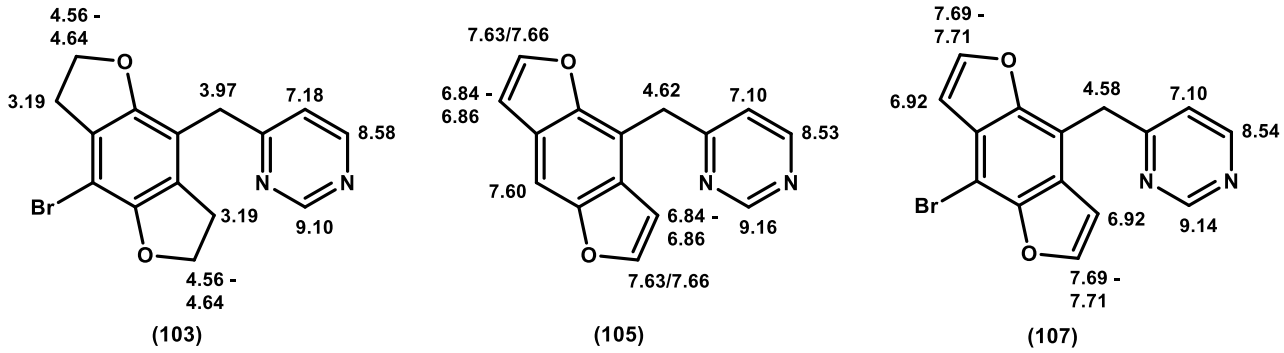


*Fig. 2-86: ^{1}H-NMR data for benzyl pyrimidines **103**, **105** and **107***

The ^{13}C-NMR spectra were also acquired, with the characteristic benzyl carbon signal for each compound appearing between 30 - 40 ppm. Other signals appeared as expected, with **105** and **107** having no signals in the aliphatic region of their spectra apart from the benzylic carbon. There was also

a clear difference between the brominated and nonbrominated analogues, with the brominated substrates **103** and **107** having **C**-Br signals at 98.4 ppm and 93.9 ppm respectively, while the **C**-H signals for the carbon atoms in the analogous position in **100** and **105** appeared further downfield at 104.9 and 101.4 ppm respectively. The significant change in chemical shift at the benzyl position between THBD and benzodifuran-type compounds which was noted in the ^{1}H-NMR analysis is not replicated in the ^{13}C-NMR analysis. A summary of the ^{13}C-NMR analysis of **103**, **105** and **107** can be seen in Figure 2-87.

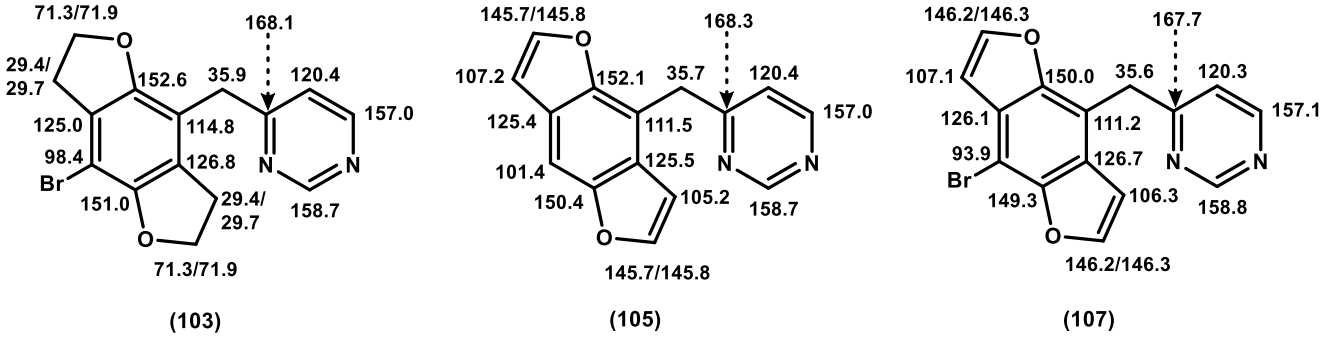


*Fig. 2-87: ^{13}C-NMR data for benzyl pyrimidines **103**, **105** and **107***

2.3.3 Attempted Optimisation of the C-H Activation Coupling Reaction for Benzodifuran Substrates

As seen in Section 2.3.2, there is a marked drop in yield when performing the C-H activation coupling reaction on substrates with benzodifuran cores (i.e. **105** and **107**). Described below are attempts which were made to optimise the reaction conditions for these substrates, focusing on two parameters: catalyst and reaction time.

2.3.3.1 Catalyst

When corresponding directly with Burton,[49] he suggested $Pd_2(dba)_3$ as a possible alternative catalyst to $Pd(OAc)_2$ for the C-H activation coupling. It was decided to trial this catalyst in our reaction conditions to prepare **105** (see Figure 2-88) in the hope that the addition of an extra palladium centre would facilitate a higher yielding reaction than its variant employing $Pd(dmdba)_2$.

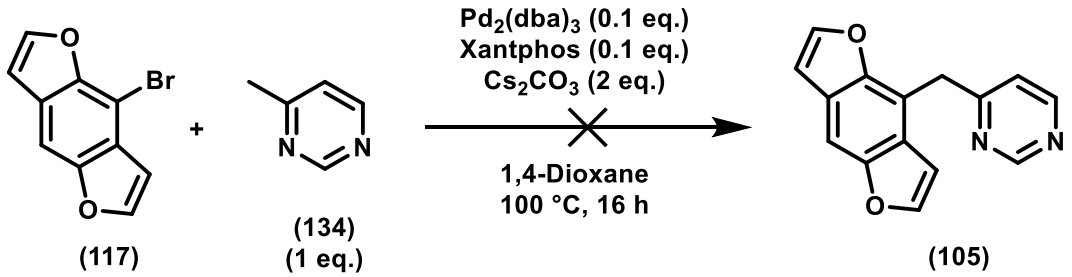


*Fig. 2-88: Use of $Pd_2(dba)_3$ as a catalyst in the attempted C-H activation coupling reaction of **117** and **134***

When a sample of the crude reaction mixture of **105** was sent for ^{1}H-NMR analysis there was some evidence of a pyrimidine structure due to the presence of signals in the region 8.0 - 9.5 ppm, but there was no clear evidence of a signal representing a benzylic C**H$_2$** group in the aliphatic region of the spectrum. When the crude reaction mixture was purified by preparative TLC, ^{1}H-NMR analysis of collected fractions confirmed these initial observations: none of the fractions showed any evidence of product formation, and the only pyrimidine signals seen were confirmed to be from starting material 4-methylpyrimidine **(134)**. It was therefore concluded that $Pd_2(dba)_3$ is not a suitable catalyst for the C-H activation coupling reaction.

2.3.3.2 Reaction Time

Another approach used in the attempt to increase the yield of the C-H activation coupling reaction when using benzodifuran-type starting materials was to extend the reaction time from 16 to 90 hours. This was done using **117** as a starting material to form the desired product **105**. The reaction was performed as described in Figure 2-85 (except for the extended reaction time).

When the crude reaction mixture was analysed by ^{1}H-NMR it seemed to indicate the presence of desired product **105**, but as a minor component, with the two starting materials **134** and **117** present as major components in the reaction mixture. This was confirmed after purification of the crude reaction mixture by flash column chromatography on silica gel, where the product **105** was isolated in 4.7 % yield. This represents no improvement over the reaction

run for 16 hours and suggests that increased reaction length has no impact on yield for the benzodifuran substrates in the C-H activation coupling reaction.

2.3.4 Attempted Alternate Syntheses of Benzodifuran Benzyl Pyrimidines 105 and 107

Due to the low-yielding nature of the C-H activation coupling reaction used to synthesise benzodifuran benzyl pyrimidine compounds **105** and **107**, several alternative routes were investigated, involving the oxidative synthesis of the benzodifuran benzyl pyrimidines from their THBD analogues. Three oxidising reagents were investigated and the results of each trial are detailed below.

2.3.4.1 DDQ

Oxidation of THBD moieties to their corresponding benzodifuran using DDQ is a well-known reaction in our research group (as described in Figure 2-8) and an attempt was made to oxidise both **100** and **103** to the corresponding benzodifuran benzyl pyrimidines **105** and **107** using the same method (see Figure 2-89).

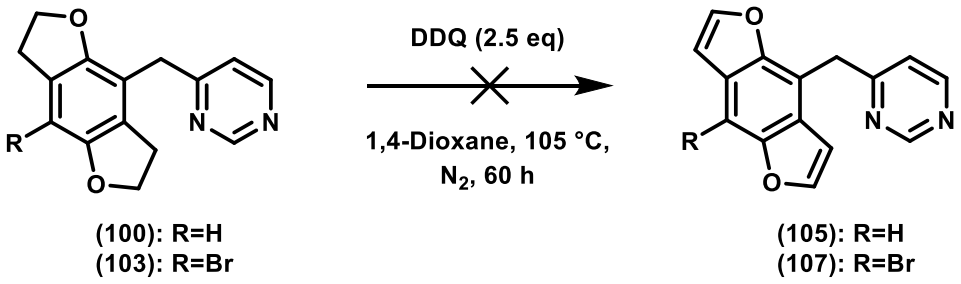
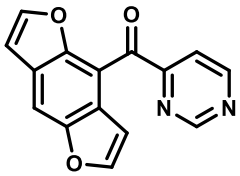


*Fig. 2-89: Attempted synthesis of benzodifuran benzyl pyrimidines **105** and **107** using DDQ*

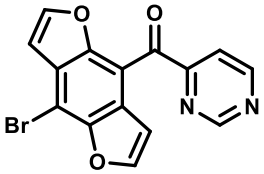
Both reactions were worked up and purified by flash column chromatography, with results as follows:

- Nonbrominated product **105**: a compound was isolated by flash column chromatography which had signals in the ^{1}H-NMR spectrum indicative of a benzodifuran core, with pyrimidine signals also evident. However,

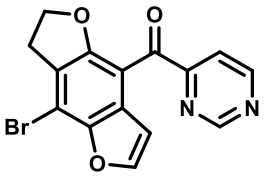
there were no signals in the aliphatic region of the spectrum (see Figure 2-90 (top)), suggesting that the benzylic C**H$_2$** position had been modified in some way. Subsequent analysis by ^{13}C-NMR revealed a signal at 191.4 ppm which is characteristic of a benzylic ketone, suggesting that the DDQ had fully aromatised the THBD core, but also performed a carbonylation reaction at the benzylic position to produce **169** in 25 % yield.



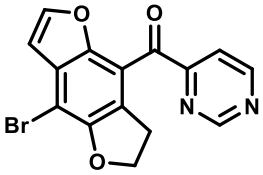
(169)



(170)



(171)



(172)

- Brominated product **107**: a fraction was isolated by flash column chromatography of this crude reaction mixture which contained ^{1}H-NMR signals indicative of a pyrimidine (see Figure 2-90 (bottom)). However, there were clearly too many signals present for one product. It was therefore hypothesised that the analysed fraction contained multiple pyrimidine derivatives, potentially a combination of fully **[170]** and partially **[171** and **172]** aromatised substrate. Again, there was no singlet in the aliphatic region which would usually indicate the presence of a benzylic C**H$_2$** moiety, leading to the conclusion that benzylic carbonylation had possibly occurred.

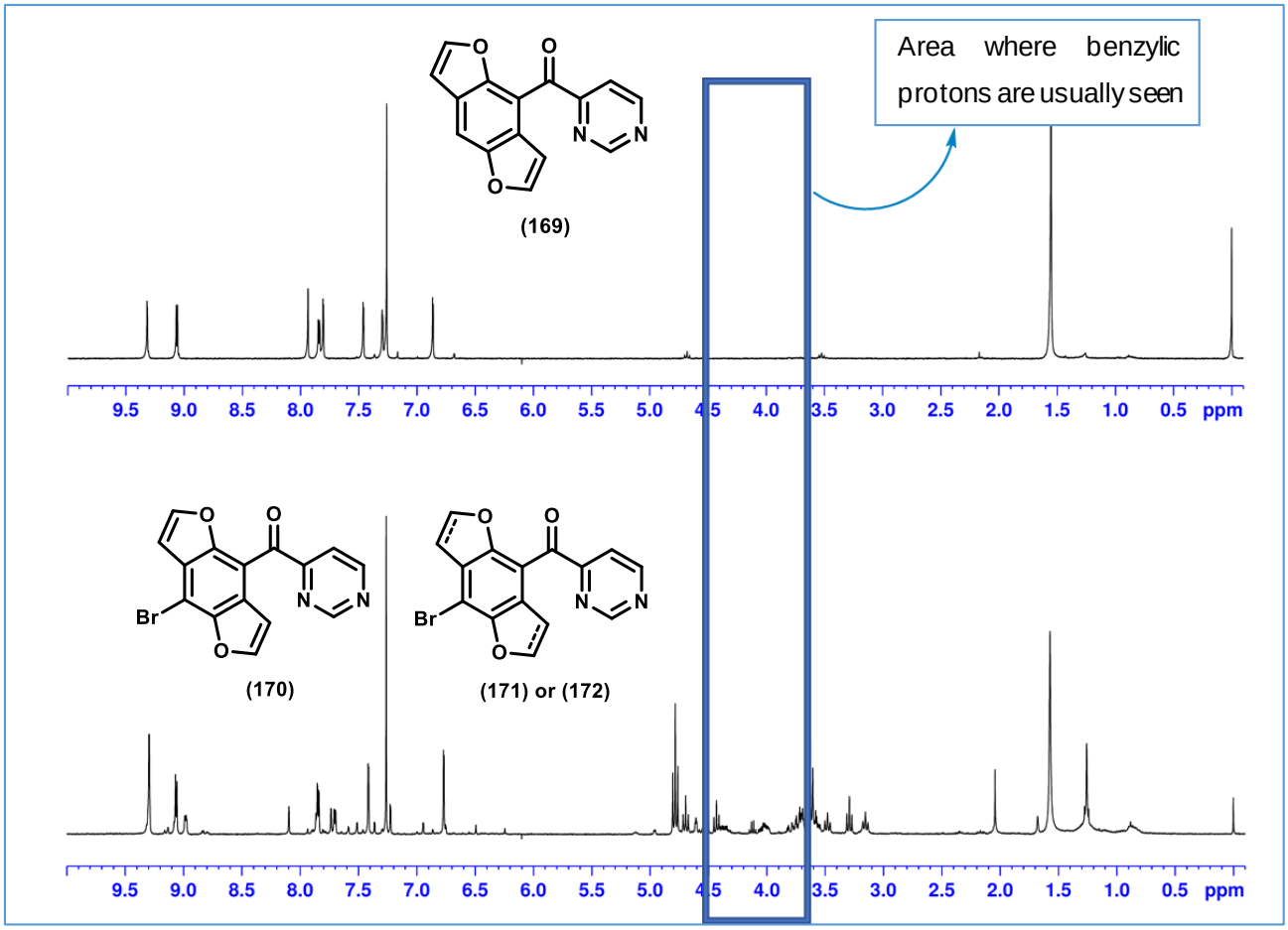


*Fig. 2-90: ^{1}H-NMR spectra of attempted DDQ oxidations of **100** (top) and **103** (bottom)*

The issue with benzylic carbonylation by DDQ has arisen previously in this work (see Section 2.2.5.2) and oxidative functionalisation of benzylic positions by DDQ is known in the literature.[47] Despite efforts to exclude oxygen from the reaction, this problem persisted when working with the benzyl pyrimidine series.

An attempt was made to further purify the product of the DDQ oxidation of **103**, (multiple products as seen in spectrum (b) in Figure 2-90) by preparative TLC, but these attempts failed. HRMS analysis was performed on the mixture, and the PMIs of both **170** (calculated *m/z*: 342.9720; found *m/z*: 342.9724; mass accuracy: 0.9 ppm) and **171/172** (calculated *m/z*: 344.9869; found *m/z*: 344.9860; mass accuracy: -1.0 ppm) were found.

Novel benzyl pyrimidine **169** was fully characterised without further purification as summarised in Table 2-17.

Compound Number	Yield (%)	m.p. (°C)	R_f (Hex:EtOAc)	IR ν_{max} C=O (cm^{-1})	HRMS (*m/z*)	
					Calc.	Found
169	25	148 - 150 (No recryst.)	0.17 (5:1)	1666	265.0608	265.0614

*Table 2-17: Yield, m.p., R_f, IR and HRMS data for benzyl pyrimidine **169***

Both ^{1}H- and ^{13}C-NMR spectra were also acquired for **169**. Both spectra were almost identical to those of its non-carbonylated benzyl pyrimidine analogue **105**, with only slight differences in chemical shift seen for most signals. The largest differences in chemical shift were seen in the pyrimidine ring protons. These protons in **169** appear at 9.32, 9.08 and 7.85 ppm, while the analogous protons in the **105** appear at 9.16, 8.53 and 7.10 ppm respectively. This shift downfield is hypothesised to be due to the addition of the inductively electron withdrawing carbonyl group to the benzyl position.

The most striking differences between the ^{1}H-NMR spectra of **169** and **105** are the differences seen in the signals for the benzyl position. In the ^{1}H-NMR spectra of **105**, the benzyl C**H$_2$** signal is seen at 4.62 ppm, however, there is no signal representing the analogous position in the ^{1}H-NMR spectrum of **169**. In the ^{13}C-NMR spectrum of **105**, the benzyl CH_2 carbon atom is represented by a signal at 35.7 ppm, however, in the ^{13}C-NMR spectrum of **169**, the benzyl carbon atom is now seen at 191.4 ppm. All other signals in the ^{13}C-NMR spectrum of **169** are within 3 ppm of the values recorded for the analogous signals in the ^{13}C-NMR spectrum of **105**. A full description of the ^{13}C-NMR signal assignments of **169** can be found in Section 4.2.2.

2.3.4.2 Chloranil

As an oxidising reagent, chloranil is milder than DDQ, and had been trialled before in this work in the conversion of brominated THBD **116** to its

benzodifuran analogue **117** (see Section 2.2.1.2) with minimal success. However, it was decided to attempt a trial oxidation of **100** using chloranil (Figure 2-91) to determine if it could be used to oxidise the substrate to **105** without the issue of benzylic carbonylation.

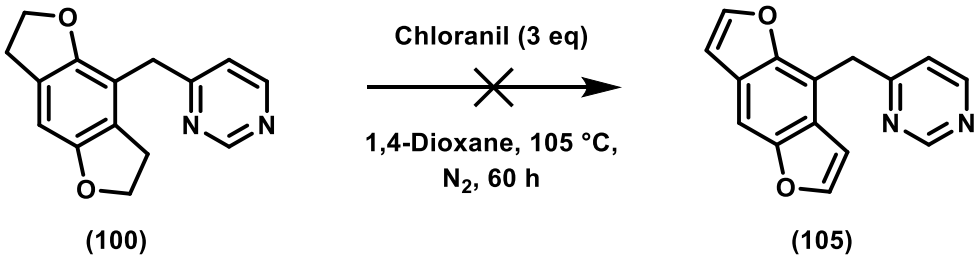


*Fig. 2-91: Oxidation of benzyl pyrimidine **100** using chloranil*

The crude reaction mixture was purified by flash column chromatography on silica gel, and the resultant fractions were analysed by ^{1}H-NMR spectroscopy. This revealed two fractions containing a mixture of pyrimidines, which were identified by the characteristic signals seen between 8.5 - 9.5 ppm. However, both the aromatic (from 6 - 8 ppm) and aliphatic regions (between 3 - 5 ppm where THBD signals are usually seen) of the spectra showed a complex mixture of indistinguishable signals. HRMS analysis did find evidence of the product **105** (calculated *m/z*: 251.0815; found *m/z*: 251.0810; mass accuracy: -1.9 ppm) but when attempts were made to further purify these fractions using preparative TLC, no separation was achieved. This reinforced the conclusion that chloranil is not an adequately strong oxidising reagent to efficiently convert THBD moieties to their corresponding benzodifurans, and this line of research was not further pursued.

2.3.4.3 NBS

In Section 2.2.4.2, an attempt was made to brominate THBD phenyl pyrimidine **101**, but instead, it was aromatised to its nonbrominated benzodifuran analogue **106**. Despite an inability to replicate this result, it was decided to attempt a similar reaction using the brominated THBD benzyl pyrimidine **103**, as shown in Figure 2-92. The brominated THBD benzyl pyrimdine was specifically chosen so that the usual position for NBS bromination on the

phenyl ring was not available: it was hoped that this would increase the chances of an aromatisation reaction.

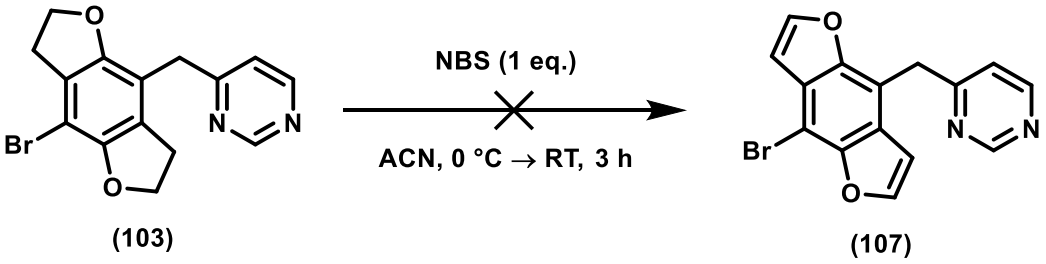


*Fig. 2-92: Attempted synthesis of benzodifuran benzyl pyrimidine **107** using NBS*

The crude reaction mixture was purified by preparative TLC, from which the majority product was the starting material **103** (70 % of the input mass of **103** was recovered). A second fraction from the preparative TLC produced a sample with a similar ^{1}H-NMR spectrum to the starting material **103**, indicating that no aromatisation had taken place, but the signal for the benzylic C**H$_2$** protons at 3.97 ppm (a 2H singlet) in **103** was not present, suggesting that a reaction had taken place at this position. A new 1H singlet was noted in what is usually thought of as the aromatic region of the spectrum, at 6.32 ppm (see Figure 2-93). However, as seen in the attempted bromination of **101** with bromine/acetic acid in Section 2.2.4.2, brominated benzyl group protons (i.e. Ar-C**H**Br) can be found in ^{1}H-NMR spectra between 6 - 7 ppm (see Figure 2-50 and Figure 2-51).

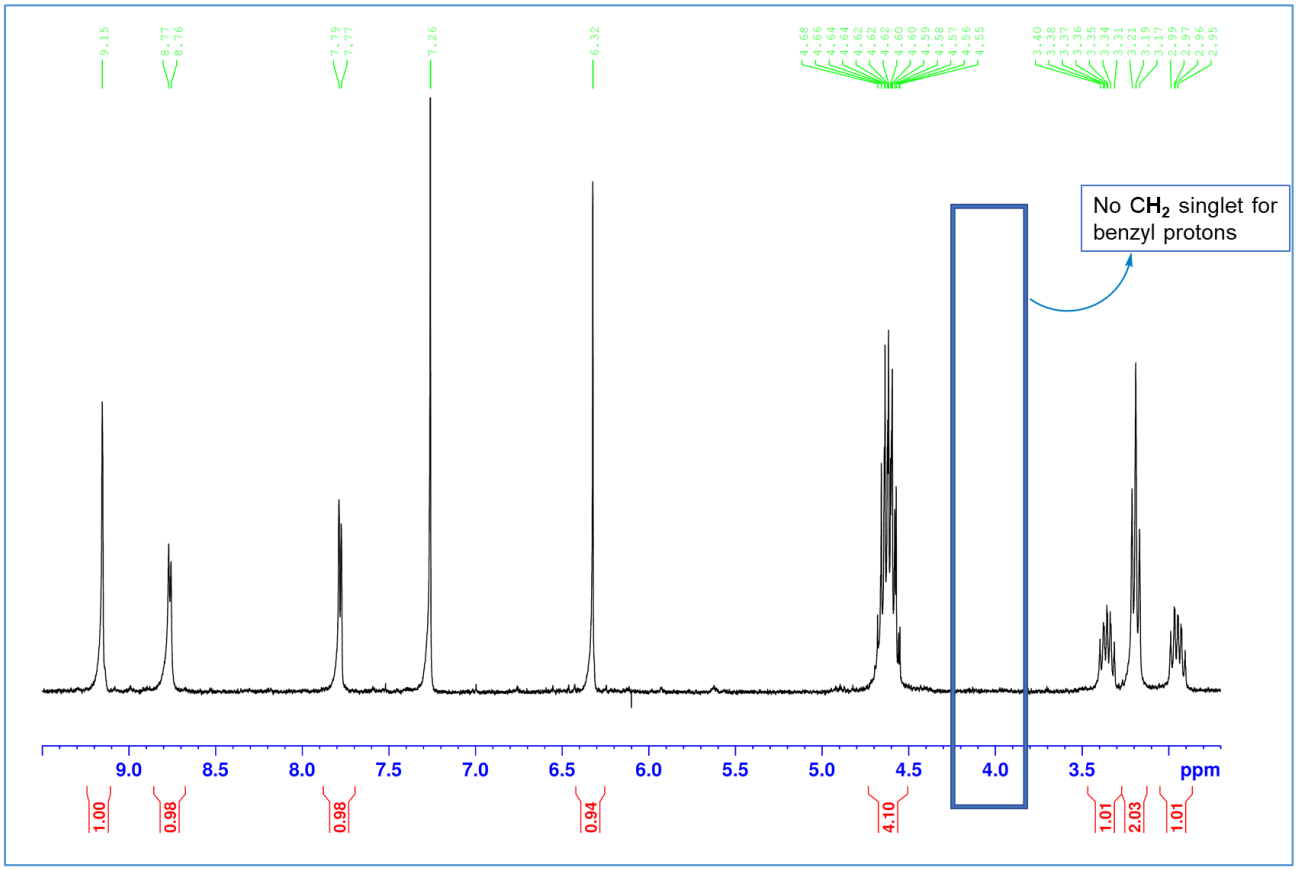
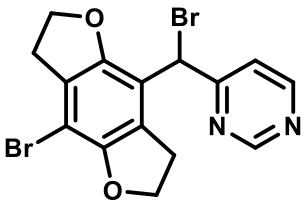


*Fig. 2-93: ^{1}H-NMR analysis of attempted oxidation of **103** using NBS*

It was also noted that the aliphatic signals for the THBD protons -C**H$_2$**-CH$_2$-O- had changed in both multiplicity and chemical shift. In the starting material **103**, these signals appear as a 4H multiplet from 3.17 - 3.21 ppm in the ^{1}H-NMR spectrum. However, in the spectrum for the isolated pyrimidine in Figure 2-93, this has changed to a 2H triplet at 3.17 ppm, and two 1H multiplets at 2.99 and 3.33 ppm. This is characteristic of diastereotopic protons (as seen for phenyl pyrimidines **101** and **104**, see Figure 2-37 and Figure 2-39). There was no evidence of an aromatisation of the THBD core.

When ^{13}C-NMR analysis of the substrate was conducted, it was noted that the signal for the benzylic **C**H$_2$ group had shifted from 35.9 ppm (in **103**) to 45.9 ppm (all other ^{13}C-NMR signals recorded were within 3 ppm of the chemical shifts recorded in the ^{13}C-NMR of **103**). Along with the disappearance of the benzylic proton signal from its position in the starting material **103** and the presence of diastereotopic protons in Figure 2-93, this led us to hypothesise

that benzylic bromination had taken place, giving the novel mono-brominated compound **173** in 7.2 % yield.



(173)

Further evidence of **173** was recorded when HRMS analysis successfully found the PMI (calculated *m/z*: 411.9179; found *m/z*: 411.9197; mass accuracy: 4.5 ppm). Benzylic bromination with NBS is a known reaction in the literature, and leads to the conclusion that NBS is not a suitable reagent for the desired transformation.[50]

2.4 Leuckart Reactions to Produce Bromo-DragonFLY and Structrual Analogues

Having successfully synthesised, isolated and characterised seven of the eight targeted pyrimidine impurities for use as analytical standards, attention was turned to the completion of the four Leuckart reactions which should produce those pyrimidines as by-products.

As described in Section 1.5, the Leuckart route to ATS from the analogous P2P-type starting materials takes place over two steps. The first step is the Leuckart reaction itself, which is the formation of an *N*-formyl product by refluxing the ketone starting material in formamide. The second step is the hydrolysis of this *N*-formyl substrate to the corresponding primary amine (i.e. the ATS) using aqueous HCl in methanol. These steps are shown in Figure 2-94, using P2P **(62)** and amphetamine **(1)** as an example.

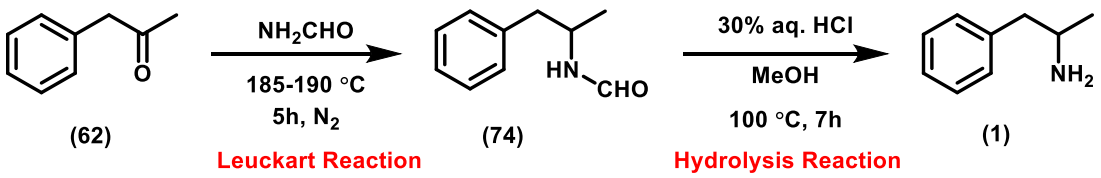


*Fig. 2-94: Leuckart route from P2P **(62)** to amphetamine **(1)***

As shown in Figure 2-1 at the beginning of this chapter, the pyrimidine impurities characteristic to the Leuckart route to ATS are formed in the Leuckart reaction, which is the first step of the route. This is why samples of crude reaction mixtures from the Leuckart reactions performed in this work were retained for HPLC analysis (as described further in this chapter), as purification would otherwise substantially remove the desired pyrimidines.

The analysis strategy in approaching these Leuckart reactions is visualised in the flowchart shown in Figure 2-95. The rationale behind splitting the crude Leuckart reaction mixture and only purifying one portion was that the crude *N*-formyl product would mimic the product of a clandestine process more closely, as it is unlikely that extensive purification would be carried out in a clandestine setting. This mimicry of clandestine conditions is also the rationale behind the use of crude *N*-formyl material being used in hydrolysis reactions to produce samples of crude ATS for HPLC analysis.

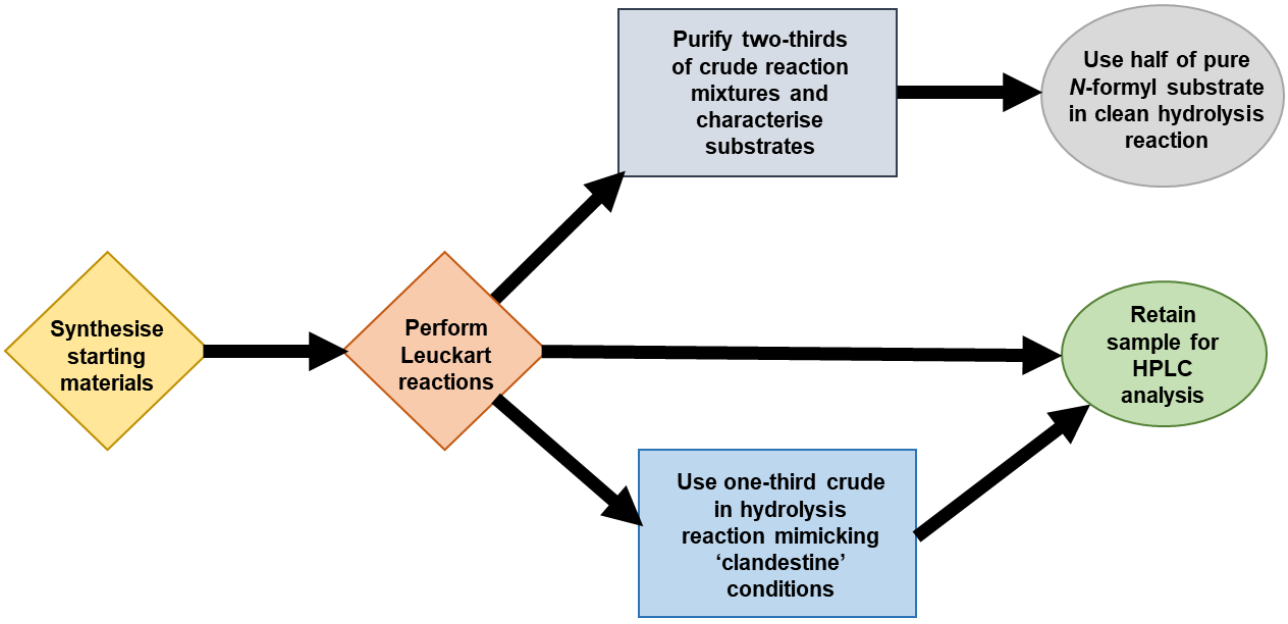
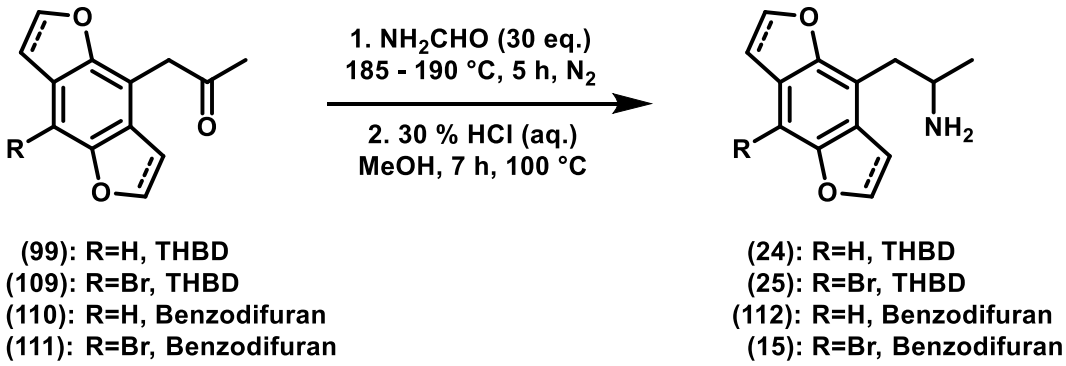


Fig. 2-95: Leuckart reaction analysis strategy

The general scheme for the 2 step synthesis of amphetamine products **15**, **24**, **25** and **112** from ketone starting materials **99**, **109** - **111** *via* the Leuckart reaction and subsequent hydrolysis of *N*-formyl intermediates is detailed in Figure 2-96.



(99): R=H, THBD
(109): R=Br, THBD
(110): R=H, Benzodifuran
(111): R=Br, Benzodifuran

(24): R=H, THBD
(25): R=Br, THBD
(112): R=H, Benzodifuran
(15): R=Br, Benzodifuran

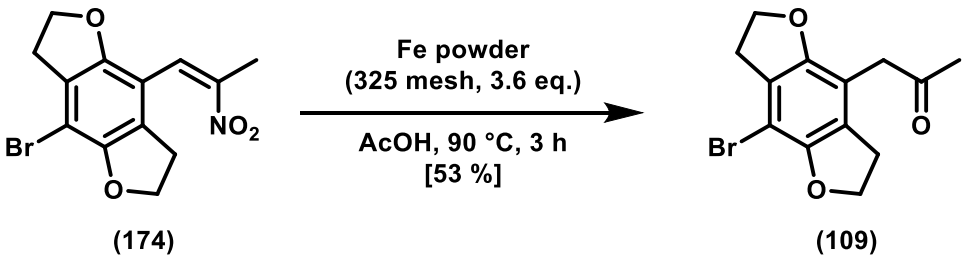
*Fig. 2-96: Leuckart synthesis of amphetamines **15**, **24**, **25** and **112***

2.4.1 Preparation of Ketone Starting Materials for Leuckart Reactions

All of the necessary ketone starting materials **99**, **109** - **111** were synthesised from intermediates provided by a previous member of our research group. The THBD ketone **99** available for this work[10] was > 97 % pure when analysed by ^{1}H-NMR. While the brominated THBD ketone **109** was not already synthesised, its precursor, the brominated THBD nitrostyrene **174**, was available in ample quantities,[10] and was also > 97 % pure when analysed by ^{1}H-NMR.

*2.4.1.1 Synthesis of 1-(8-Bromo-2,3,6,7-tetrahydrobenzo[1,2-b:4,5-b']difuran-4-yl)propan-2-one **(109)***

Using nitrostyrene **174** as a starting material,[10] brominated THBD ketone **(109)** was synthesised *via* an iron reduction reaction, a procedure which was already well established within our group.[31] This reduction uses elemental iron in acetic acid, and is performed as described in Figure 2-97.



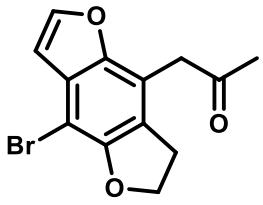
(174) (109)

*Fig. 2-97: Iron reduction reaction to convert nitrostyrene **174** to ketone **109***

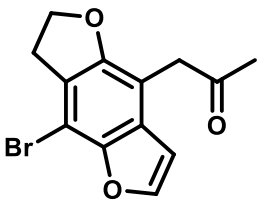
The iron was stirred in acetic acid heated at 90 °C, with nitrostyrene starting material **174** added portion-wise as a solution in acetic acid (also at 90 °C). When analysed by ^{1}H-NMR post work-up, the crude reaction mixture showed approximately 80 % conversion to product, however, after isolation *via* flash column chromatography on silica gel, this equated to a moderate yield of 53 %, much lower than had been previously seen for similar transformations in our research group.[31]

It was hypothesised that greater equivalents of iron powder might be needed to drive the reaction to completion. Although the iron was already present in excess, the reaction was stirred using a magnetic stirrer bar, to which the iron powder was attracted, thereby rendering it less available for reaction due to clumping about the magnetic stirrer bar. In a subsequent iteration, the equivalents of iron were increased to 4.6, and the reaction was run again as described in Figure 2-97 (with gradual addition of nitrostyrene **174** in solution to iron stirred in acetic acid).

This produced a crude reaction mixture which showed no trace of starting material when analysed by ^{1}H-NMR, but did contain some of a partially aromatised product, either **175** or **176** (it was not possible to distinguish between the two in the trace amounts present): the product **109** was isolated (again by flash column chromatography on silica gel), in 57 % yield.



(175)



(176)

This was a slight improvement on the initial attempt, but it was thought that further improvements could be made. Unexpectedly it was also noted that when the starting material **174** was heated in neat acetic acid (at 90°C for approximately 20 minutes), about 2 % conversion (when calculated using ^{1}H-NMR integration) to partially aromatised product **175**/**176** was seen pre-addition to the iron/acetic acid suspension: while not an issue for ketone which was due to be fully aromatised (to produce brominated benzodifuran ketone **111**, see Section 2.4.1.2), this was not desirable in the brominated THBD ketone **109**. Thus, it was decided to see if the yield of brominated THBD ketone **109** could be improved, while simultaneously reducing the amount of partially aromatised product **175**/**176** being formed.

To this end, several further variations on the scheme shown in Figure 2-97 were trialled (note that unless otherwise indicated, 4.6 eq. of iron powder was used in each reaction):

- Variation 1 (V1): After a literature search revealed similar iron reduction reactions being performed in ethanol,[51,52] the reaction solvent was changed to ethanol in this work and 5 equivalents of acetic acid were also added. The ^{1}H-NMR spectrum of the crude reaction mixture post work-up revealed almost no conversion to product **109** (baseline traces of potential **109**) leading us to believe more acetic acid was needed.

- Variation 2 (V2): Based on V1, another reaction was run in ethanol, but with 10 mL of acetic acid, a volume which equated to approximately 284 equivalents. The ^{1}H-NMR spectrum of the crude reaction mixture showed a mixture of product **109** and starting material **174** in a 1:1 ratio,

but there was no evidence of the partially aromatised product **175**/**176**.

- Variation 3 (V3): This variation contained no ethanol (returning to acetic acid as a reaction solvent) and had the nitrostyrene starting material **174** added as a solid (instead of in solution, to avoid the oxidation in acetic acid). The ^{1}H-NMR of the crude reaction mixture showed a mixture of product **109** and starting material **174** in approximately a 1:3 ratio.

- Variation 4 (V4): As V2 showed the best results, V4 was performed in a 3:1 ratio of acetic acid:ethanol (the nitrostyrene starting material **174** is more soluble in ethanol, so this was used for the addition, while the iron was stirred in acetic acid). The equivalents of iron in the reaction were also increased to 8. The ^{1}H-NMR spectrum of the crude reaction mixture showed 98.5 % **109**, with 1.5 % partially aromatised product **175**/**176** also present. Recrystallisation from diethyl ether gave pure product **109** in 85 % yield, which was the best % yield seen in this series of reactions.

The fourth variation on the process described in Figure 2-96 was adopted as the standard procedure for produce brominated THBD ketone **109** from its nitrostyrene precursor **174** and is shown in Figure 2-98.

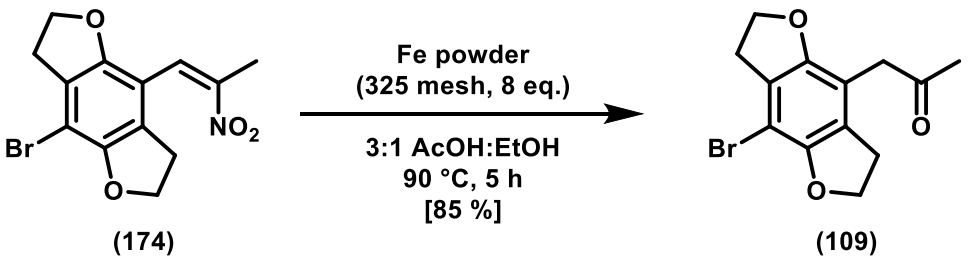


*Fig. 2-98: Optimised conversion of nitrostyrene **174** to ketone **109***

Brominated THBD ketone **109** was fully characterised: this is described in detail in Section 2.4.1.3.

*2.4.1.2 Synthesis of 1-(Benzo[1,2-b:4,5-b']difuran-4-yl)propan-2-one **(110)** and 1-(8-Bromobenzo[1,2-b:4,5-b']difuran-4-yl)propan-2-one **(111)***

Both 1-(benzo[1,2-*b*:4,5-*b'*]difuran-4-yl)propan-2-one **(110)** and 1-(8-bromobenzo[1,2-*b*:4,5-*b'*]difuran-4-yl)propan-2-one **(111)** were synthesised from their THBD analogues (**99** and **109** respectively) using DDQ, in a procedure described previously in Section 2.2.1.2. The nonbrominated THBD substrate **99** had been previously synthesised by a member of our research group and was used directly in this work,[10] while brominated THBD substrate **109** was synthesised as described in Section 2.4.1.1. The DDQ oxidation was performed as described in Figure 2-99.

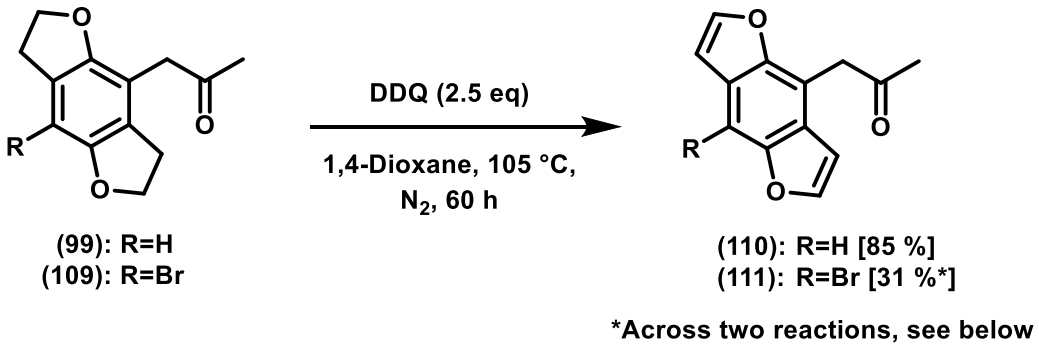
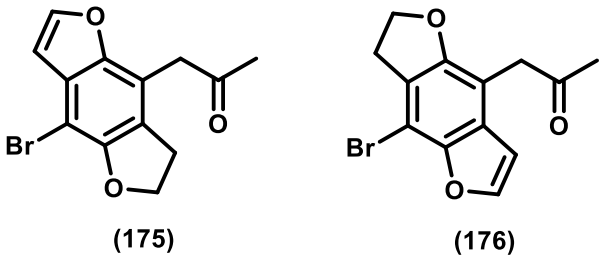


*Fig. 2-99: DDQ oxidation of THBD ketones **99** and **109***

Nonbrominated substrate **110** was synthesised in a good yield of 85 % after purification by a plug column on silica gel. However, when purification of the brominated analogue was attempted by plug column on silica gel, it was noted that while early fractions contained only pure product, later fractions contained a mixture of product **111** and partially-aromatised products **175** and **176**.



Those fractions containing partially-aromatised products were collected and oxidised with excess DDQ as described in Figure 2-99. Flash column

chromatography on silica gel returned pure product **111** without any traces of partially-aromatised products **175** and **176**, and the overall yield of the two reactions (based on the starting material **109** used in the initial reaction) was 31 %.

Both brominated and nonbrominated benzodifuran ketones **110** and **111** were fully characterised. This is described in detail in Section 2.4.1.3.

2.4.1.3 Characterisation of Ketone Precursors

Once isolated, ketones **109** - **111** were fully characterised as described in Table 2-18. The characterisation data included for THBD ketone **99** is listed as previously described by O'Connor *et al.*.[10] All of literature melting points are also from this work by O'Connor *et al.*, who synthesised this series of ketones in their 2010 paper on synthesis of ketone precursors to BDF **(15)**.[10]

Compound Number	Yield	m.p. (°C) *[Lit m.p.]*	R_f (Hex:EtOAc)	IR ν_{max} C=O (cm^{-1})	HRMS (*m/z*)	
					Calc.	Found
99	-	- *[81 - 83[10] ($CHCl_3$)]*	0.60 (1:1)	1715	219.1021	219.1029
109	85	119 - 121 (Et_2O), *[119 - 121[10] ($CHCl_3$)]*	0.23 (5:1)	1709	297.0216	297.0213
110	85	67 - 69 (Et_2O), *[67 - 69[10] (EtOAc)]*	0.41 (5:1)	1708	215.0708	215.0698
111	31	104 - 105 (Et_2O), *[107 - 109[10] (Et_2O)]*	0.24 (5:1)	1712	292.9813	292.9802

*Table 2-18: Yield, m.p., R_f, IR and HRMS data for ketones **99**, **109** - **111***

Full ^{1}H- and ^{13}C-NMR spectra were also acquired for all ketones. The pattern for the ^{1}H-NMR spectra closely mimicked that previously seen for THBD and benzodifuran compounds (see Section 2.2.1.2), with added benzyl proton signals at 3.5 - 4.2 ppm (2H singlet) and a signal for the terminal methyl group at ~2.2 ppm (3H singlet). There was also an extra signal in the aromatic region of the spectrum (between 6 - 7 ppm) in the nonbrominated substrates **109** and **111**. The ^{1}H-NMR signals of the ketone series **99**, **109** - **111** are summarised in Figure 2-100 (note that in the case of signals which appear within 1 ppm of each other, the signals were assigned using literature data from O'Connor *et al.*,[10] who unambiguously assigned these signals using 2D-NMR).

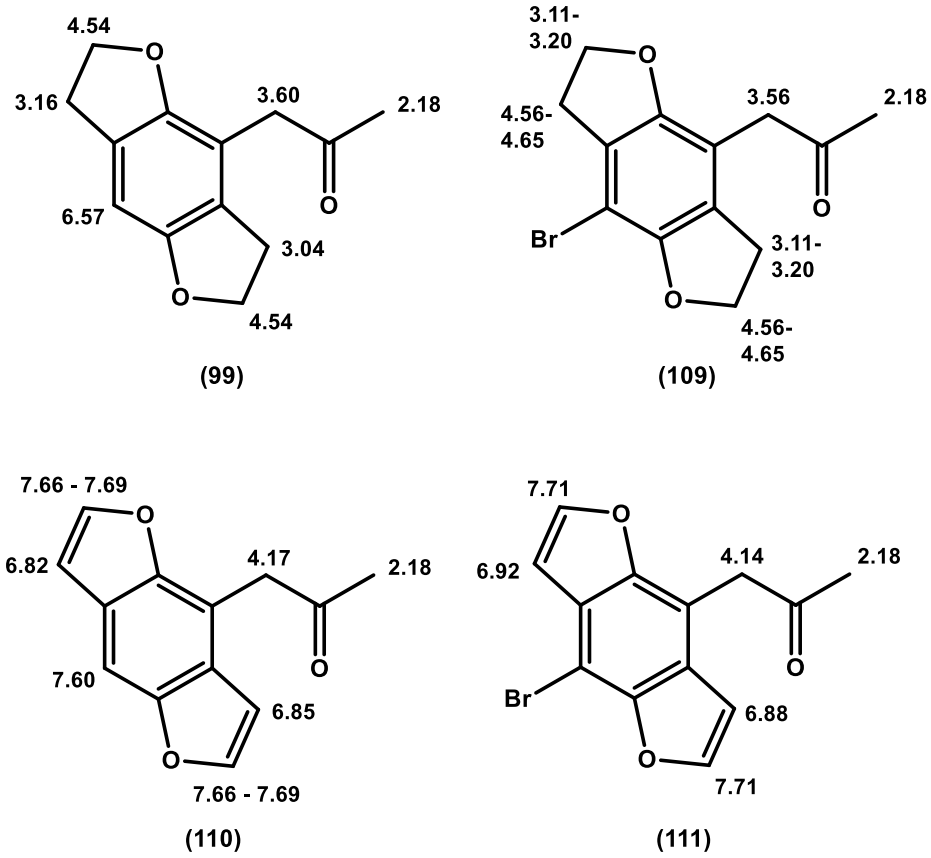


*Fig. 2-100: [1]H-NMR signal assignments in ketones **99**, **109** - **111***

The [13]C-NMR spectra for this series of compounds were also as expected from previous THBD and benzodifuran substrates: the major differences between the aryl bromides synthesised in Section 2.2.1.2 and the ketone series were the presence of extra signals for the benzyl carbon and the terminal methyl group at approximately 29 and 43 ppm respectively, and the presence of a distinctive carbonyl signal at approximately 205 ppm, which is characteristic of a benzyl ketone. The [13]C-NMR signals of the ketone series **99**, **109** - **111** are summarised in Figure 2-101 (note that in the case of signals which appear within 2 ppm of each other, the signals were assigned using literature data from O'Connor *et al.*,[10] who unambiguously assigned these signals using 2D-NMR).

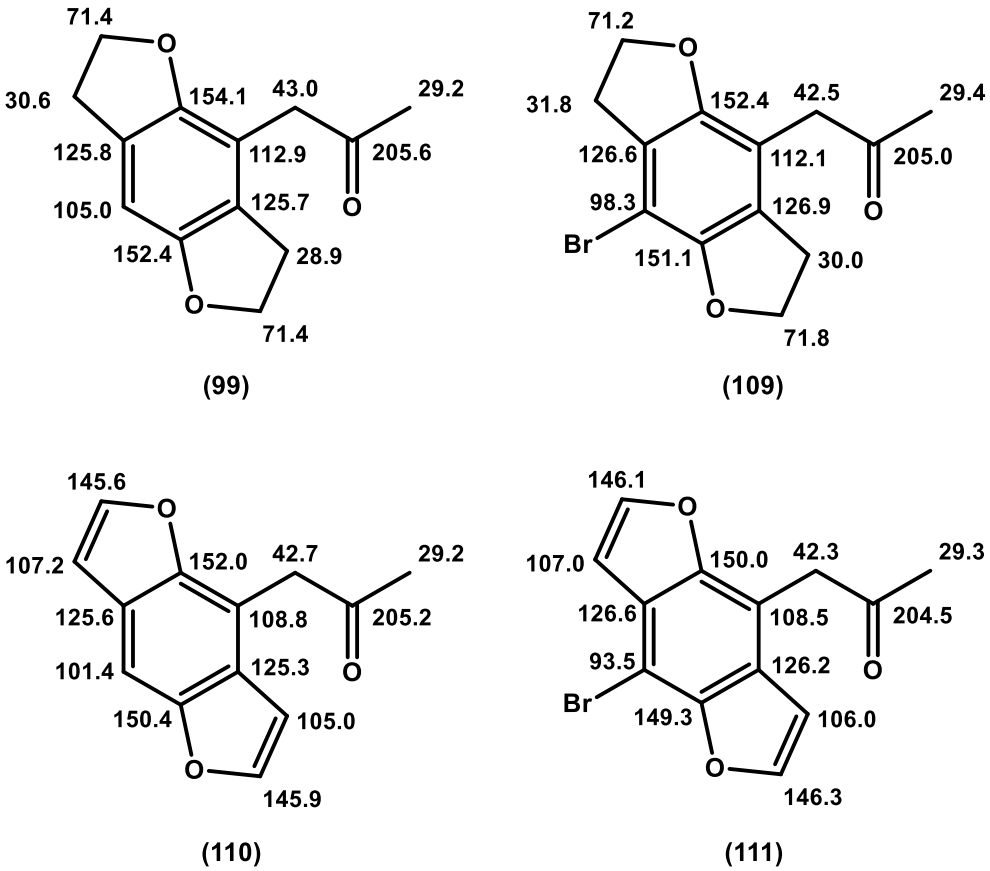
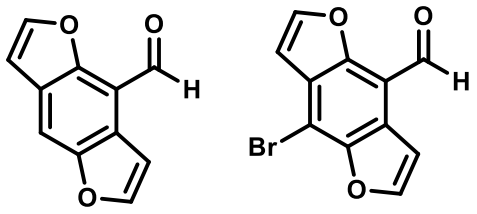


*Fig. 2-101: ^{13}C-NMR signal assignments in ketones **99**, **109** - **111***

2.4.1.4 Impurity Profiling of DDQ oxidations of Benzylic Ketones

In Section 2.4.1.2, the oxidation of two THBD ketones (**99** and **109**) to two benzodifuran ketones (**110** and **111**) is described. During purification of these benzodifuran ketones, two side-products were noted (one from each reaction) as major components in the first fractions from the column chromatography. Initial analysis by ^{1}H-NMR suggested that the substrates could be aldehydes, as both had signals at ~11 ppm. Based on the starting materials involved and the number of signals in the ^{1}H-NMR spectrum, it was hypothesised that the by-products could be benzaldehyde substrates **177** and **178** (see Figure 2-102 for ^{1}H-NMR analysis of **177**).



(177) (178)

These substrates were independently synthesised and characterised by O'Connor *et al.* in their previously referenced paper on synthesising ketone precursors to BDF **(15)**.[10] This gave us reference values with which to compare the recorded values that were acquired during analysis of the substrates synthesised as by-products in this work.

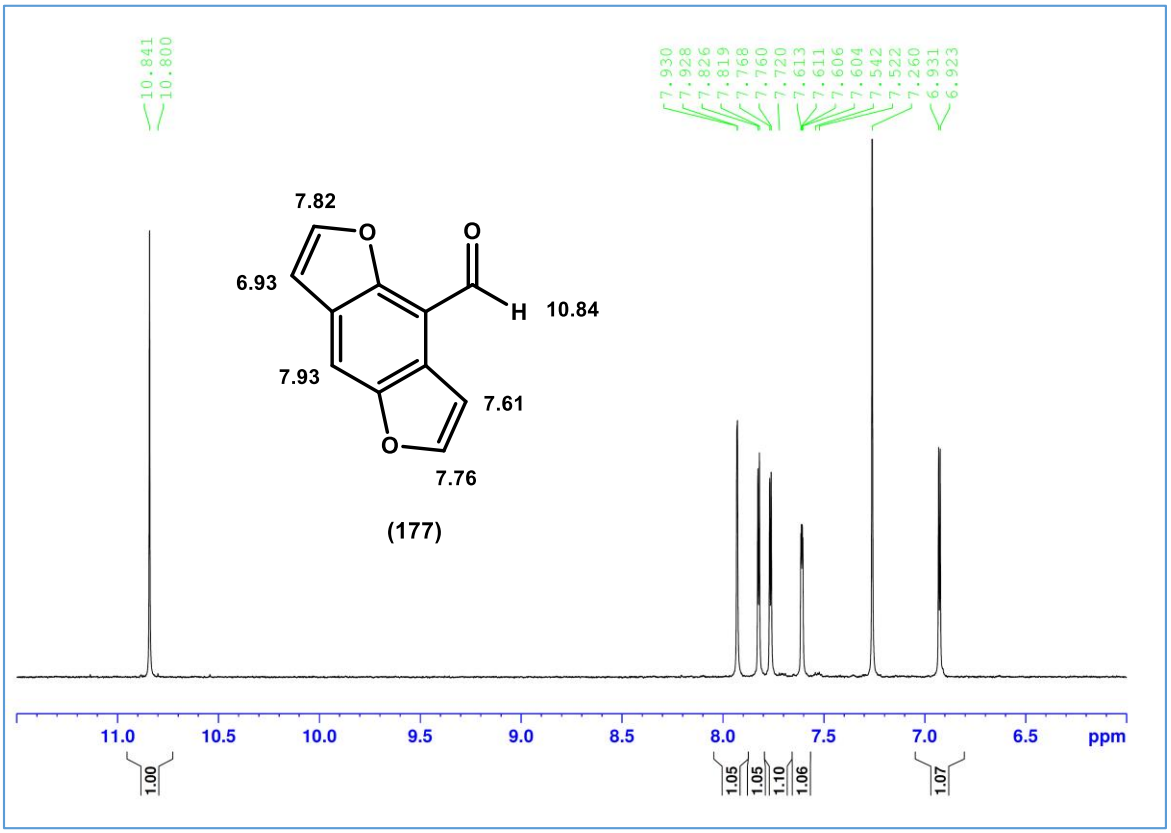


*Fig. 2-102: [1]H-NMR analysis of a potential aldehyde impurity **177** arising from DDQ oxidation of THBD ketone **99***

The values seen for the signals in the [1]H-NMR in Figure 2-102 almost exactly match the values listed by O'Connor *et al.* for the same substrate in their work

(δ = 6.92, 7.60, 7.76, 7.82, 7.92, 10.83 ppm),[10] providing strong evidence that the substrate isolated during DDQ oxidation of **99** is aldehyde **177**.

As no evidence was found for the formation of these aldehyde impurities in THBD analogues **99** and **109**, it stands to reason that their origin is in the DDQ oxidation reaction. Previous work in our research group by JQ described the decomposition of aryl ketone **179** to the corresponding benzaldehyde **180** *via* α-cleavage of the ketone and subsequent oxidation by atmospheric oxygen over a period of ~6 months, as described in Figure 2-103.[31]

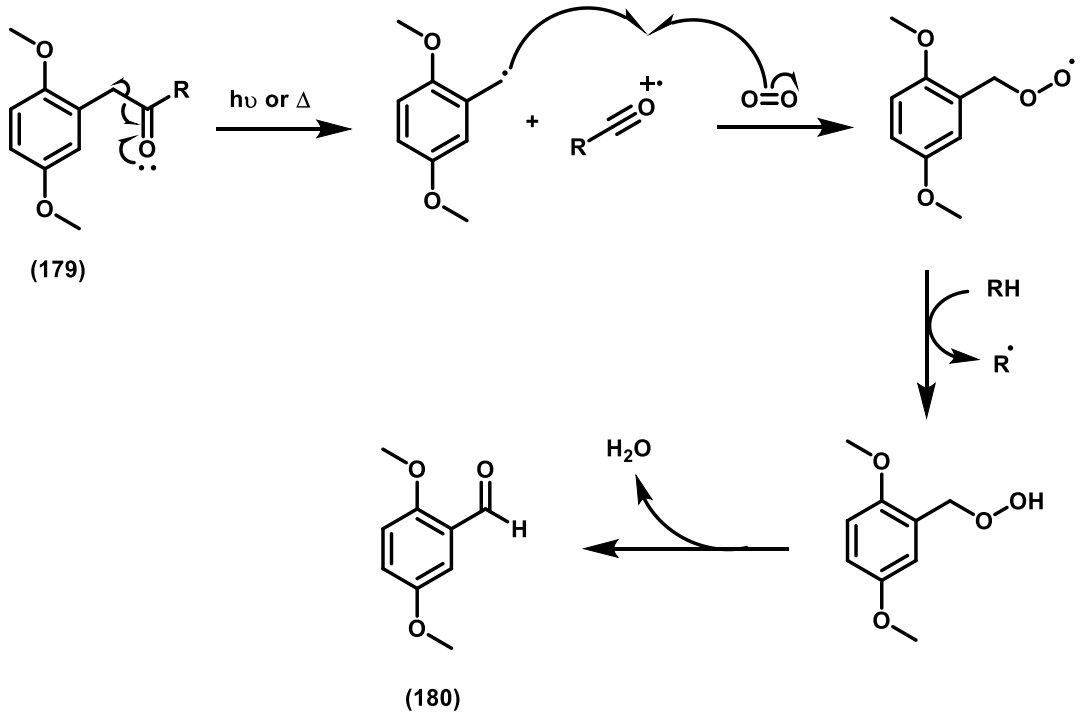


*Fig. 2-103: Decomposition of 2-propanone aryl ketone **179** to 2,5-dimethoxybenzaldehyde **(180)***

It was hypothesised that a similar mechanism was at play in this work, but accelerated due to the presence of DDQ as a radical initiator, and thus can be considered a likely route-specific impurity for the pathway that uses DDQ as an oxidant for THBD ketones.

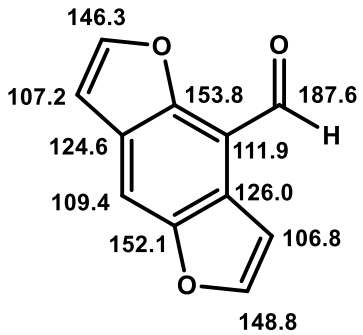
Further purification of **177** and **178** was attempted by means of preparative TLC, however while nonbrominated benzaldehyde **177** was isolated as a pure sample, it proved impossible to separate the brominated analogue **178** from

multiple unknown organic contaminants. Nonbrominated benzaldehyde **177** was fully characterised as described in Table 2-19.

Compound Number	Yield (%)	m.p. (°C) *[Lit m.p.]*	R_f (Hex:EtOAc)	IR ν_{max} C=O (cm^{-1})	HRMS (*m/z*)	
					Calc.	Found
177	1.9	104 - 106 (No recryst.), *[105 - 107[10] ($CHCl_3$)]*	0.63 (4:1)	1674	187.0935	187.0937

*Table 2-19: Yield, m.p., R_f, IR and HRMS data for aldehyde **177***

The IR value for the C=O stretch is lower than would typically be seen for an aldehyde, but this is likely due to the extended conjugation of the aldehyde with the aromatic system. The ^{1}H-NMR spectral analysis is detailed of **177** in Figure 2-102, and ^{13}C-NMR analysis was also acquired. The ^{13}C-NMR spectrum was very similar to that seen for benzodifuran bromide **117** (see Section 2.2.1.2), with the exception that instead of a C-Br signal at 94.3 ppm, there is an aldehyde C=O signal at 186.6 ppm. Full assignment of the ^{13}C-NMR signals can be seen in Figure 2-104.



(177)

*Fig. 2-104: ^{13}C-NMR signal assignments for aldehyde **177***

Despite the failure to fully isolate potential brominated aldehyde **178**, a comparison was made between the impure ^{1}H-NMR spectrum acquired, and the literature values for ^{1}H-NMR signals recorded by O'Connor *et al*.[10] The

literature values were δ = 6.99, 7.68, 7.81, 7.88 and 10.79 ppm. In Figure 2-105, the corresponding identical or almost identical signals are highlighted by peak-peaking in the impure ^{1}H-NMR spectrum. The integrations of the peak-picked signals are also shown, using the aldehyde signal at 10.80 ppm as a reference signal whose integration is calibrated to one proton. However, as can been seen in the enlarged sections of the spectrum highlighted in Figure 2-105, a complex mixture of organic compounds is present in the sample.

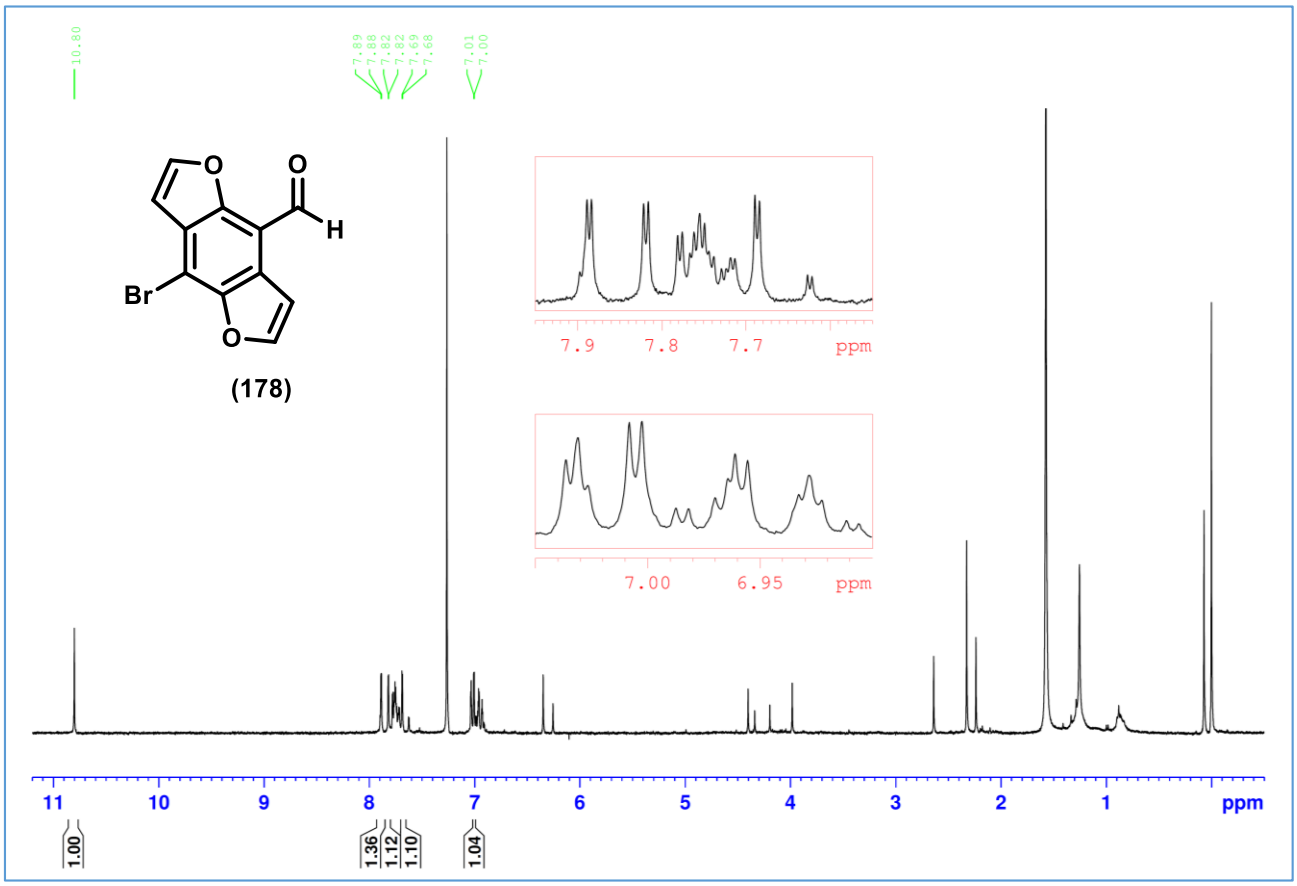
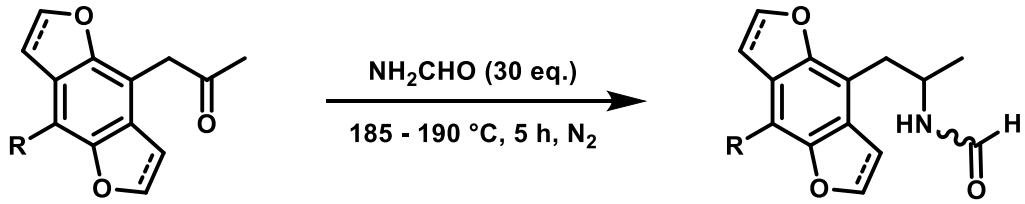


*Fig. 2-105: ^{1}H-NMR analysis of potential aldehyde **178***

HRMS analysis was also successfully acquired for **178** (calculated *m/z*: 264.9495; found *m/z*: 264.9503; mass accuracy: 3.2 ppm). This proof, combined with the confirmed presence of **177** in the oxidation of the analogous nonbrominated starting material **99**, provide strong evidence that aldehyde **178** is formed as an impurity during the DDQ-mediated oxidation of **109** to **111**.

2.4.2 Preparation of *N*-Formyl Intermediates from Precursor Ketones *via* the Leuckart Reaction

With access to the the four precursor ketones **99**, **109** - **111**, the next step in the synthetic route was the Leuckart reaction itself. This reaction is well known both in the literature and in our research group, and was carried out as described in Figure 2-106.[31]



(99): R=H, THBD
(109): R=Br, THBD
(110): R=H, Benzodifuran
(111): R=Br, Benzodifuran

(102): R=H, THBD [27 %]
(181): R=Br, THBD [27 %]
(182): R=H, Benzodifuran [13 %]
(183): R=Br, Benzodifuran [13 %]

*Fig. 2-106: Preparation of N-formyl intermediates **102**, **181** - **183** via the Leuckart reaction*

The four *N*-formyl intermediates **102, 181 - 183** were isolated in poor yields of 13 - 27 % (post purification) and ^{1}H-NMR analysis of the crude products post work-up revealed mixtures of the *N*-formyl products **102**, **181 - 183** with the expected pyrimidines also evident.

For the larger scale reactions (those done on a scale > 2 g), the crude reaction mixtures could be purified to access the pure *N*-formyl products by recrystallisation from a mixture of ethyl acetate and hexane. However, for reactions performed on a smaller scale, this recrystallisation was unworkable, and they were purified by flash column chromatography on silica gel and/or preparative TLC, using 20 % ethyl acetate in hexane as an eluent system in both cases. As mentioned in Section 2.4, it was decided to purify approximately two-thirds of each crude reaction mixture, and to retain one-third as crude material to run HPLC analysis and also to mimic 'clandestine' conditions in the final hydrolysis reaction.

*2.4.2.1 Characterisation of N-Formyl Intermediates **102, 181 - 183***

Once all four novel *N*-formyl substrates **102, 181 - 183** were synthesised and isolated, they were characterised as summarised in Table 2-20.

Compound Number	Yield (%)	m.p. (°C)	R_f (Hex:EtOAc)	IR ν_{max} C=O (cm^{-1})	HRMS (*m/z*)	
					Calc.	Found
102	27	104 - 106 (1:1 Hex:EtOAc)	0.09 (1:1)	1661	248.1281	248.1289
181	27	119 - 121 (1:1 Hex:EtOAc)	0.20 (1:1)	1661	326.0386	326.0391
182	13	115 - 116 (No recryst.)	0.32 (0:1)	1660	244.0968	244.0967
183	13	132 - 134 (No recryst.)	0.14 (1:1)	1679	322.0073	322.0075

*Table 2-20: Yield, m.p., R_f, IR and HRMS data **102**, **181** - **183***

Full ^{1}H- and ^{13}C-NMR analyses were also carried out on the *N*-formyl substrates **102, 181 - 183**. This analysis was complicated slightly by the fact that each of the *N*-formyl substrates **102, 181 - 183** exists as a pair of rotamers, due to the partial double bond nature of the C-N bond in the formyl group which results in restricted rotation about that bond, as illustrated in Figure 2-107. This leads to two sets of signals in the ^{1}H- and ^{13}C-NMR spectra, in a ratio of approximately 4:1 by ^{1}H-NMR integration (when measured on a 400 MHz instrument at 20 °C). The partial double bond nature of the C-N bond comes about due to the lone pair of electrons on the nitrogen atom being delocalised onto the oxygen atom of the *N*-formyl carbonyl group.

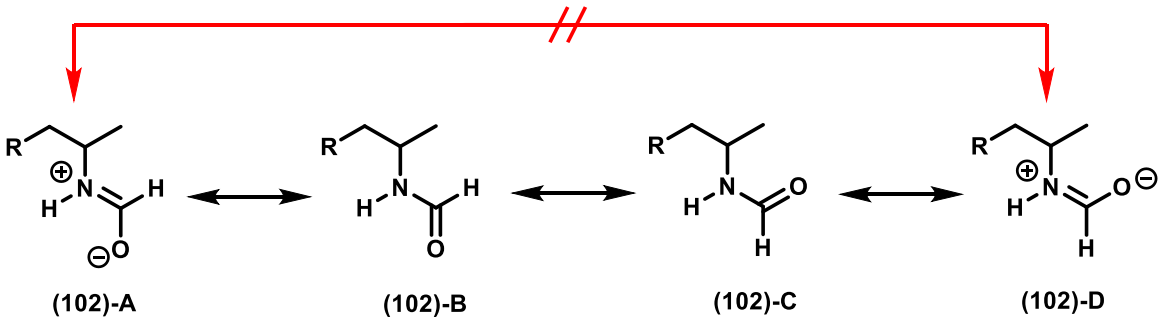


*Fig. 2-107: Rotamers of N-formyl substrate **102** (R = THBD)*

Zwitterions **102-A** and **102-D** do not have free rotation due to the geometry of the C=N double bond, and cannot interconvert between **A** and **D**. They are therefore described as rotamers, and are the basis for the observations of two sets of signals in the ^{1}H- and ^{13}C-NMR spectra of the *N*-formyl series of compounds. **102-A** and **102-D** can be assigned as *E* and *Z* respectively following the IUPAC rules of nomenclature. **102-B** is the non-delocalised form of **102-A**, and **102-C** is the non-delocalised form of **102-D**. **102-B** and **102-C** can freely interconvert as they do not have any restricted rotation around the C-N bond, however, the inability of their zwitterion analogues to interconvert leads to the double set of signals seen in ^{1}H- and ^{13}C-NMR spectra.

In general (for this series of compounds), it is possible to distinguish the signals for each rotamer from one spectrum as the unequal ratio of rotamers gives different intensities of signals. There are some cases in which the signals overlap and are indistinguishable: in these cases, the same chemical shift is reported in both rotamers in the experimental section (see Section 4.2.3).

The formyl proton on the minor rotamer exhibits splitting due to the N**H** proton (the signal is a 1H doublet at ~ 7.8 ppm with a coupling constant of approximately J = 12 Hz), while the formyl proton on the major rotamer is a 1H singlet at ~ 8.1 ppm. A study by Buchs *et al.* in 1982 investigating the properties of an *N*-formyl compound used crystallographic data to unambiguously assign *Z* and *E* rotamers (they defined *Z* as having (R)C-N *cis* to the C=O double bond of the *N*-formyl group, i.e. **102-C** in Figure 2-107), and then reported the ^{1}H-NMR data.[53] They determined that the *E*-rotamer formyl

proton appeared at ~7.4 ppm, upfield of the *Z*-rotamer formyl proton at ~ 7.9 ppm.

A later study by Deetz *et al.* in 2001 also reported that the ^{1}H-NMR signal for the formyl proton in the *E*-rotamer of their *N*-formyl compound appeared as a doublet at 8.11 ppm (J = 12 Hz), upfield of the formyl proton in the *Z*-rotamer which was seen at 8.43 ppm (doublet, J = 1.5 Hz).[54] The coupling constant of J = 12 Hz reported by Deetz *et al*. is identical to the formyl proton coupling constant seen for the minor rotamer in this work, and the much smaller coupling constant of J = 1.5 Hz seen for the *Z*-rotamer by Deetz *et al.* could be analogous to the singlet seen for the formyl proton of the major rotamer in this work. Based on this evidence, it was hypothesised that the major rotamer seen by ^{1}H-NMR analysis in this work is the *Z* rotamer.

An example of a ^{1}H-NMR spectrum of an *N*-formyl substrate (in this case the nonbrominated THBD *N*-formyl **102**) can be seen in Figure 2-108 on the next page, with signals for both sets of rotamers clearly evident. The hypothetical assignment of major/minor rotamers is indicated by the red and blue asterisks.

Aside from the presence of two rotamers in each spectrum, the ^{1}H- and ^{13}C-NMR spectra of the *N*-formyl substrates **102, 181 - 183** were very similar to the corresponding ketones described in Section 2.4.1.3. In their ^{1}H-NMR spectra, there were several additional signals: the N**H** formamide proton signal appeared as a broad singlet from 5.5 - 6.0 ppm, while the signal for the proton α to the formamide (C**H**NH) appeared as a multiplet 3.8 - 4.6 ppm. This multiplet was a result of having three discrete sets of neighbouring protons: it would require a very high frequency NMR instrument to resolve the signal into the quartet of triplets of doublets that might be expected.

The final additional signal in the ^{1}H-NMR spectrum was the signal for the formyl proton (C**H**O), which appeared at approximately 7.8 ppm (1H doublet, J = 12 Hz) in the minor rotamer, and at approximately 8.1 ppm (1H singlet) in the major rotamer. This is significantly more shielded than is normally seen for an aldehyde proton, due to electron density conferred by the resonance forms that are integral to amides, as seen in Figure 2-107. The full assignment of ^{1}H-

NMR signals to the *N*-formyl series **102, 181 - 183** can be found in Section 4.2.3.

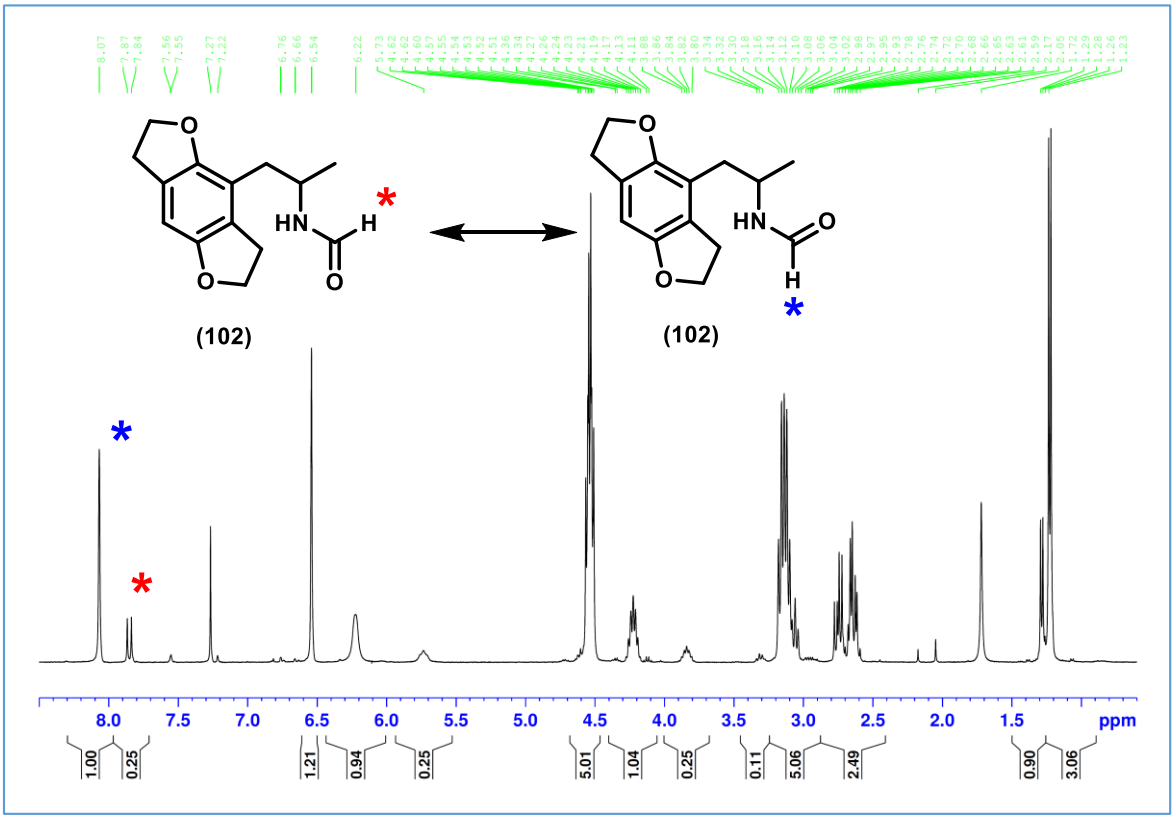


*Fig. 2-108: ^{1}H-NMR spectrum of N-formyl substrate **102***

The ^{13}C-NMR spectra of the *N*-formyl series **102, 181 - 183** contained one additional signal when compared to the ketone precursors **99, 109 - 111**: this represented the formyl carbon (**C**HO), which appeared in the range 160 - 165 ppm, with the formyl carbon in the minor rotamer generally appearing approximately 3 ppm downfield of the analogous signal in the major rotamer. Again, this is significantly shielded compared to what would be expected of an aldehyde carbon atom, more analogous to an amide carbonyl signal (usually seen in the range 160 - 170 ppm) than an aldehyde carbonyl, which typically appears at approximately 200 ppm.

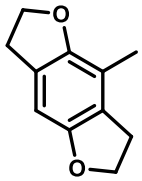
There are also variations in shift between signals for analogous carbon atoms in the *N*-formyl series **102, 181 - 183** and their ketone precursors **99, 109 - 111**, however, the only shift difference that is greater than 10 ppm is that which occurs at the carbon which is the quaternary carbonyl carbon in the ketones **99, 109 - 111**, appearing at > 200 ppm: in the corresponding *N*-formyl series

102, 181 - 183, this carbon is now a CH α to the amine (C**H**NH), and appears in the range 40 - 45 ppm. Full ^{13}C-NMR signal assignments of the *N*-formyl substrates **102, 181 - 183** can be found in Section 4.2.3.

2.4.2.2 Impurity Profiling of N-Formyl Intermediates

Although some of the product purification was carried out using recrystallisation, each of the four *N*-formyl substrates **102, 181 - 183** was also purified using chromatography to isolate any impurities which were also formed during the Leuckart step.

From the nonbrominated THBD *N*-formyl **102** crude reaction mixture, flash column chromatography on silica gel using 20 % ethyl acetate in hexane as an eluent produced pure product **102**, along with three distinct route-specific impurities: the phenyl and benzyl pyrimidines **100** and **101** (isolated in 4.1 % yield combined) and also an impurity **184** with a methylated THBD core (isolated in 0.57 % yield). This class of methylated impurity has been reported as a by-product of the Leuckart reaction previously by Keating, who suggested that it was formed by cleavage of the αC – βC bond.[55]



(184)

It also proved impossible to completely separate the phenyl and benzyl pyrimidines **100** and **101** from each other using column chromatography (the best separation achieved was a fraction containing both pyrimidines in a ratio of 1.15:1 **100:101**). This was expected, as this problem had been previously reported by O'Connor when he ran this Leuckart reaction.[6] However, as both pyrimidines had been independently synthesised at this point, it was possible to confirm their presence in the ^{1}H-NMR spectrum of what was hypothesised to be a mixture of pyrimidines **100** and **101** (see Figure 2-109).

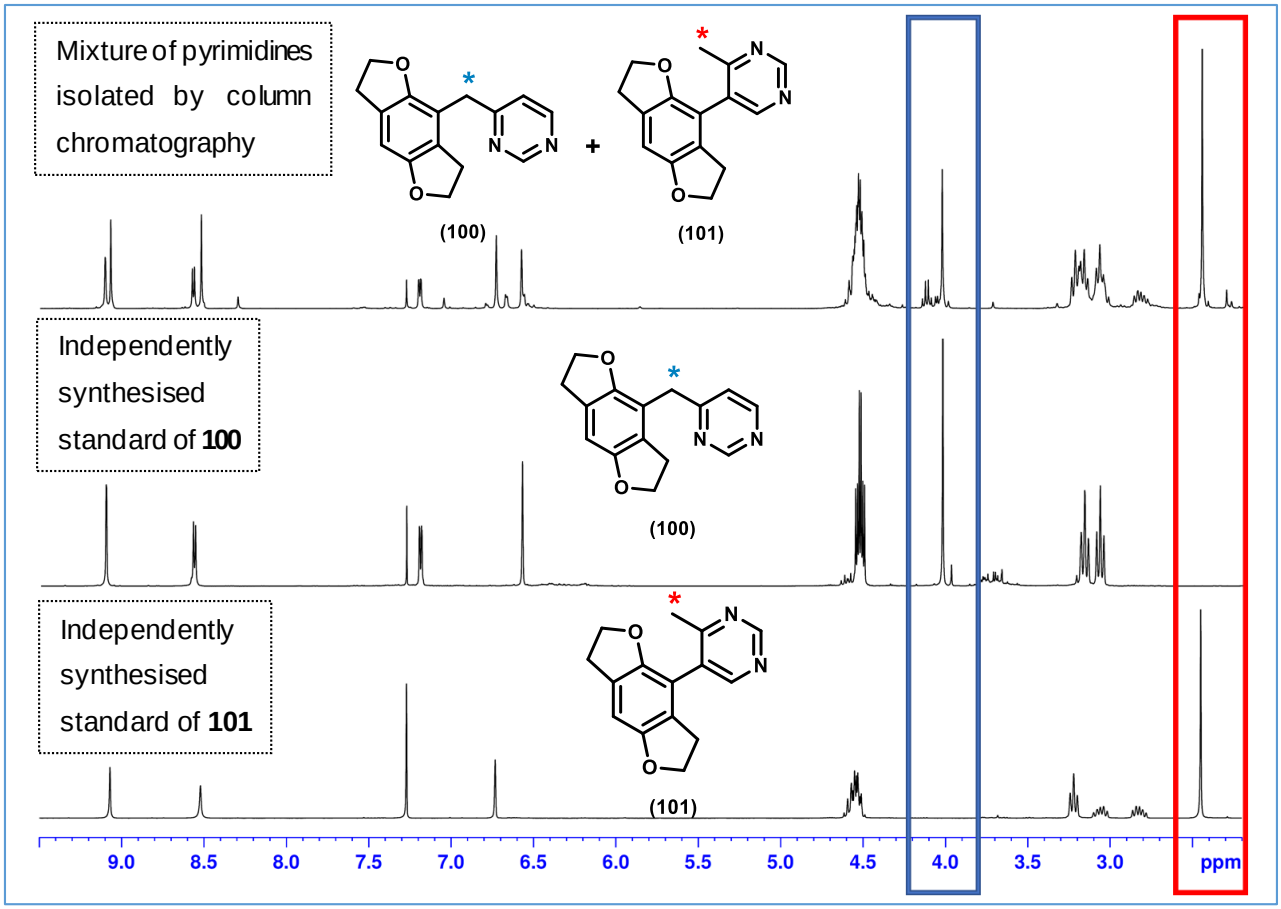
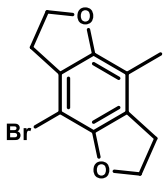


*Fig. 2-109: [1]H-NMR spectra of a mixture of benzyl and phenyl pyrimidines **100** and **101** and independently synthesised standards of **100** and **101***

The purification of brominated THBD *N*-formyl **181** crude reaction mixture by flash column chromatography returned similar results to that of its nonbrominated analogue. Both benzyl and phenyl pyrimidines **103** and **104** were observed by [1]H-NMR (isolated in 4.7 % yield combined) along with a methylated impurity **185** (isolated in 0.91 % yield) analogous to that seen for **102**.



(185)

As before, the pyrimidines **103** and **104** could not be completely segregated from each other (the best separation achieved was a fraction containing both

pyrimidines in a ratio of 2:1 **103:104**) but were identified by comparing the ^{1}H-NMR spectrum of a different fraction containing an approximately 1:1 ratio of **103** and **104** to the ^{1}H-NMR spectra of the independently synthesised substrates (see Figure 2-110).

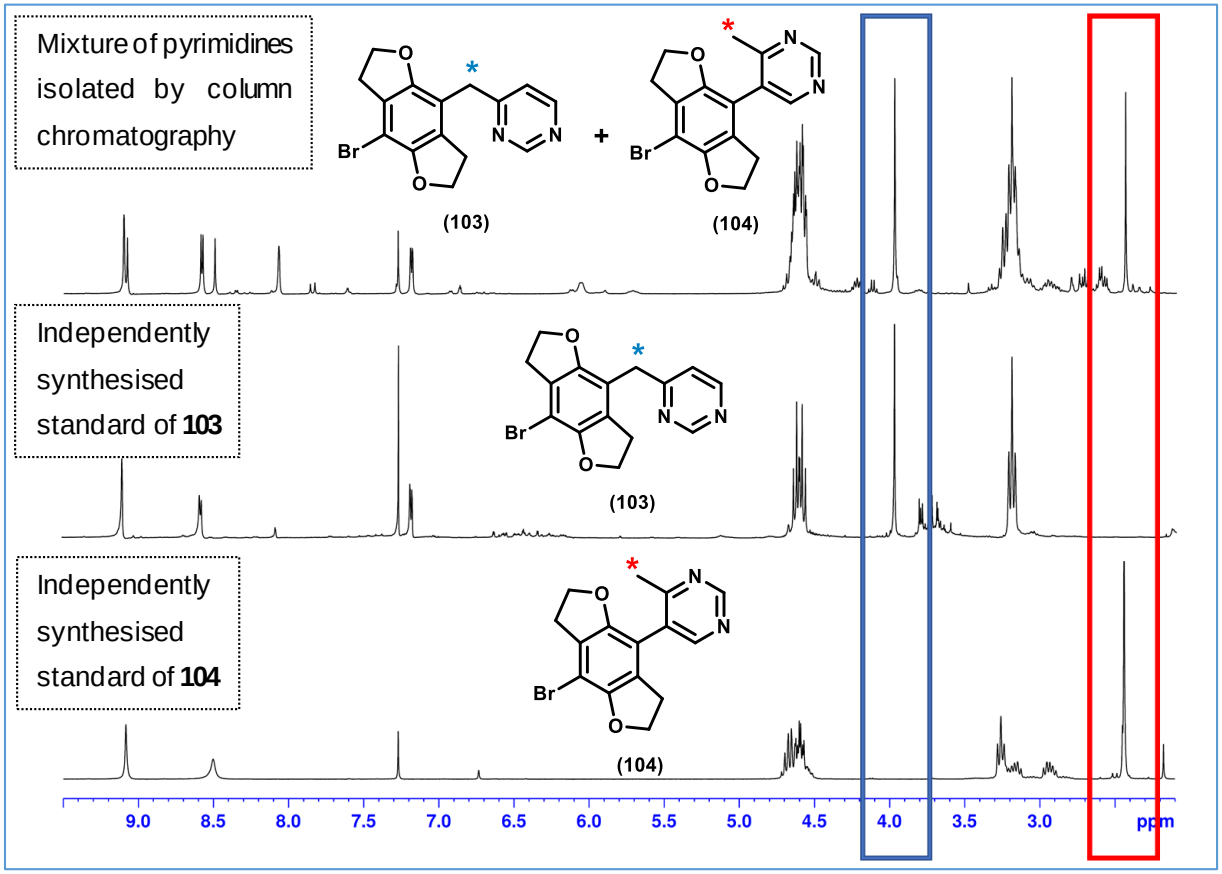
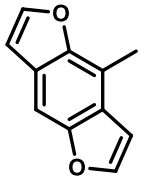


*Fig. 2-110: ^{1}H- NMR spectra of a mixture of benzyl and phenyl pyrimidines **103** and **104** and independently synthesised standards of **103** and **104***

The nonbrominated benzodifuran *N*-formyl **182** crude reaction mixture was purified by preparative TLC, using 20 % ethyl acetate in hexane as an eluent. Unlike the THBD *N*-formyl substrates **102** and **181**, no concrete evidence was seen in the ^{1}H-NMR for a methylated benzodifuran impurity **186**, which would be expected to have a structure as shown below.



(186)

Both benzyl and phenyl pyrimidines **105** and **106** were detected by ^{1}H-NMR (isolated in 3.9 % combined yield), though as for previous impurity profiling efforts, the two pyrimidines could not be completely separated from each other (the best separation achieved was a fraction containing both pyrimidines in a ratio of 2.8:1 **105:106**), but as previously, the presence of both pyrimidines was confirmed by comparison of the ^{1}H-NMR spectrum of a different fraction containing a ~1:2 mixture of **105** and **106** to the ^{1}H-NMR spectra of the independently synthesised substrates (see Figure 2-111).

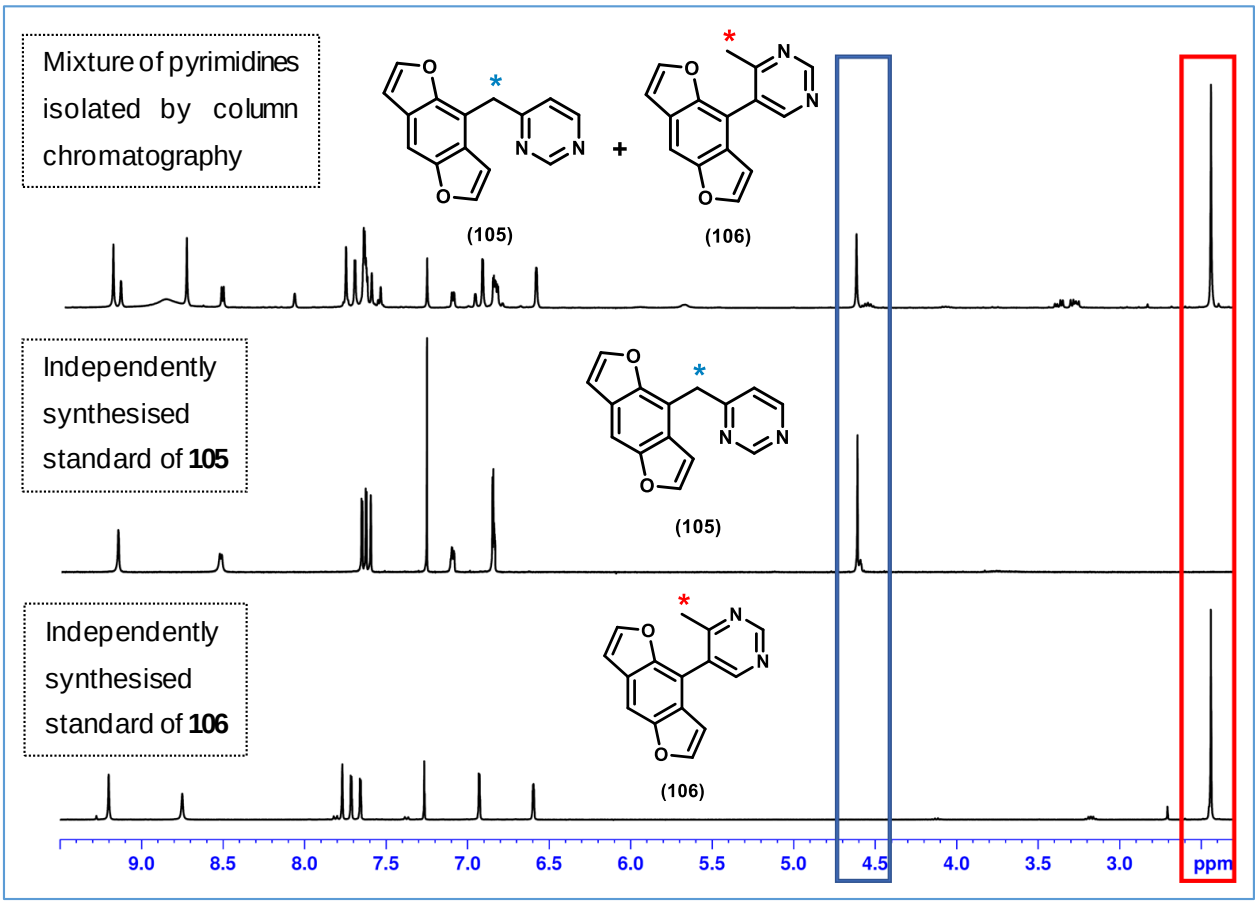
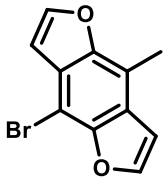


*Fig. 2-111: ^{1}H-NMR of a mixture of benzyl and phenyl pyrimidines **105** and **106***

The brominated benzodifuran *N*-formyl substrate **183** was also purified by preparative TLC using 20 % ethyl acetate in hexane as an eluent, and as for the nonbrominated analogue **182**, there was no evidence in the ^{1}H-NMR for the methylated impurity **187** seen for the THBD analogues **102** and **181**, which would be expected to have a structure shown below.



(187)

Both phenyl and benzyl pyrimidines **107** and **108** were detected in the ^{1}H-NMR. However, in this case, it was possible to separate phenyl pyrimidine **108** from the benzyl pyrimidine **107**, and they were isolated in yields of 2.2 % and 2.4 % respectively. This is not surprising if we examine the trend starting with the nonbrominated THBD Leuckart reaction and building to the brominated benzodifuran Leuckart reaction. As can be seen in Table 2-21, the brominated THBD pyrimidines **103** and **104** are more separable by column chromatography than their nonbrominated analogues **100** and **101**, and the nonbrominated benzodifuran pyrimidines **105** and **106** were more separable again. This makes it unsurprising that it was possible to fully separate the brominated benzodifuran pyrimidines **107** and **108** from each other.

Table 2-21 lists the best ratios (in terms of achieving a majority of one pyrimidine over another) of benzyl:phenyl pyrimidines recorded in fractions from column chromatography during the purification of each Leuckart reaction.

Leuckart Reaction	**Ratio of Benzyl:Phenyl Pyrimidine Isolated**
Nonbrominated THBD **102**	1.15:1
Brominated THBD **181**	2:1
Nonbrominated Benzodifuran **182**	2.8:1
Brominated Benzodifuran **183**	0:1

Table 2-21: Ratio of Benzyl:Phenyl Pyrimidines Isolated during Leuckart Reaction Impurity Profiling

Once phenyl pyrimidine **108** was isolated, it was fully characterised (see Table 2-13); this characterisation was not previously possible as **108** was not

synthesised independently. The two novel toluene-type impurities **184** and **185** isolated in < 1 % yield from their respective THBD *N*-formyl reactions were also characterised (Table 2-22).

Compound Number	Yield (%)	m.p. (°C)	R_f (Hex:EtOAc)	HRMS (*m/z*)	
				Calc.	Found
184	0.57	Semi-solid	0.84 (1:1)	177.0910	177.0913
185	0.91	133 - 135 (No recryst.)	0.88 (1:1)	252.9859	252.9868

*Table 2-22: Yield, m.p., R_f, and HRMS data for **184** and **185***

Both ^{1}H- and ^{13}C-NMR spectra were acquired for **108**, **184** and **185**. The brominated benzodifuran phenyl pyrimidine **108** was very similar to its nonbrominated analogue **106** from a ^{1}H- and ^{13}C-NMR spectral perspective, with only small changes in chemical shift seen in the majority of the proton and carbon signals. There was one less peak in the ^{1}H-NMR spectrum of **108** relative to **106**, with the aromatic signal seen at 7.76 ppm in **106** absent in the brominated analogue **108**. There was also one notable difference in the ^{13}C-NMR spectrum, with the signal for **C**-Br appearing at 95.5 ppm, significantly upfield of the signal for the corresponding **C**-H in the nonbrominated analogue **106**, which appears at 107.2 ppm. The ^{1}H- and ^{13}C-NMR assignments for phenyl pyrimidine **108** are summarised in Figure 2-112.

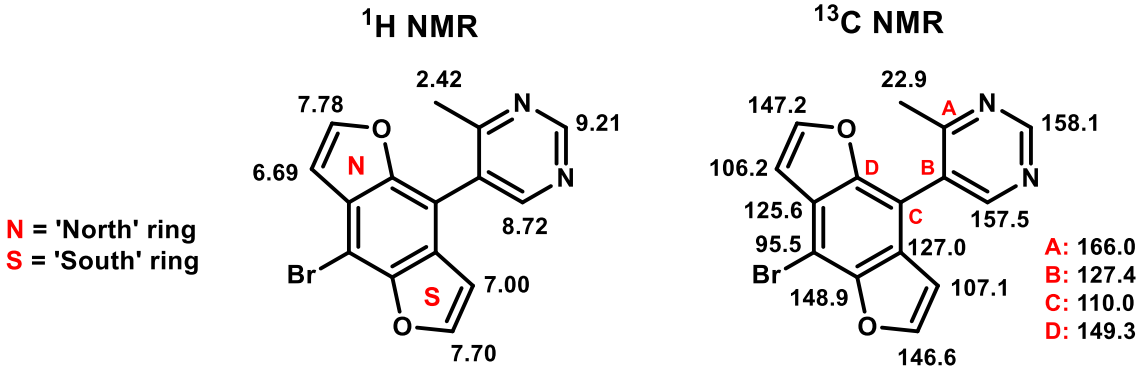


*Fig. 2-112: ^{1}H- and ^{13}C-NMR signal assignments for phenyl pyrimidine **108***

HSQC- and HMBC-NMR techniques were used to unambiguously assign several signals in the ^{1}H- and ^{13}C-NMR spectra of **108** which appeared within 1 ppm of each other. From the HSQC-NMR, it was noted that there were interactions between the following signals (^{13}C-NMR signals are in red): δ 6.69/106.2, 7.00/107.1, 7.70/146.6 and 7.78/147.2 ppm. Based on the integration values in the ^{1}H-NMR spectrum (all signals were 1H doublets), and the fact that all the corresponding ^{13}C-NMR signals appeared in the DEPT-90 spectrum (indicating that they were **C**H groups), it was concluded that these signals represented the four protons and the corresponding carbon atoms on the furan rings (N and S as labelled in Figure 2-112) of the benzodifuran moeity of **108**.

The HMBC-NMR spectrum was then analysed, and the diagnostic correlations which appeared are summarised in Table 2-23:

^{1}H-NMR Signal [ppm]	**Strong interactions (^{13}C-NMR signals) [ppm]**
2.42	127.4, 166.0
6.69	125.6, 149.3
7.00	127.0, 148.3
7.70	127.0, 148.3
7.78	125.6, 149.3
8.72	110.0, 127.4, 158.1, 166.0
9.21	127.4, 157.5, 166.0

*Table 2-23: HMBC-NMR interactions recorded for phenyl pyrimidine **108***

Unfortunately, no correlations were seen between any of the furan protons and the C-4 of the phenyl ring (**C**-Br) in the benzodifuran moiety, making it difficult to unambiguously assign the furan signals to either Ring N or Ring S (see Figure 2-112). It was hypothesised that the resonance electron donating properties of the bromine atom would cause the closest furan proton on Ring

N (C**H**=CH-O) to be shielded and thus upfield of the other furan proton signals in the ^{1}H-NMR spectrum. By this logic, the signal at 6.69 ppm was tentatively assigned as C**H**=CH-O on Ring N.

The ^{1}H-NMR signal at 6.69 ppm shows interactions in the HMBC-NMR with the ^{13}C-NMR signals at 125.6 and 149.3 ppm, as does the ^{1}H-NMR signal at 7.78 ppm, leading to the conclusion that the signal at 7.78 ppm represents CH=C**H**-O on Ring N. This led to the conclusion that the ^{1}H-NMR signals at 7.00 and 7.70 ppm represented C**H**=CH-O and CH=C**H**-O respectively on Ring S.

The HSCQ-NMR data was then used to assign the ^{13}C-NMR signals of the furan rings as shown in Figure 2-112, while the interactions between the pyrimidine proton signals (at 2.42, 8.72 and 9.21 ppm in the ^{1}H-NMR) and the ^{13}C-NMR signal at 127.4 ppm in the HMBC-NMR was used to assign that signal as **C**-Ph in the pyrimidine ring (C_B in Figure 2-112).

The ^{1}H- and ^{13}C-NMR spectra of methylated THBDs **184** and **185** were also as expected from previous THBD-type compounds (see Section 2.2.1.2), with the methyl group signals being the most significant difference between these and the bromide analogues **116** and **118**. The methyl signals appeared in the ^{1}H-NMR spectrum at 2.05 and 2.06 ppm for **184** and **185** respectively, each integrating for three protons, while the corresponding signals for the carbon atoms of the methyl groups were observed in their ^{13}C-NMR spectrum at 12.6 and 12.4 ppm for **184** and **185** respectively.

There were no aromatic signals in the ^{1}H-NMR of the brominated substrate **185**, rendering it instantly distinguishable from the nonbrominated substrate **184**, which has an aromatic signal at 6.42 ppm. The ^{1}H- and ^{13}C-NMR assignments for both methylated substrates **184** and **185** are summarised in Figure 2-113 (note that those ^{13}C-NMR signals which are marked with an asterisk (*) are tentative and not definitive assignments).

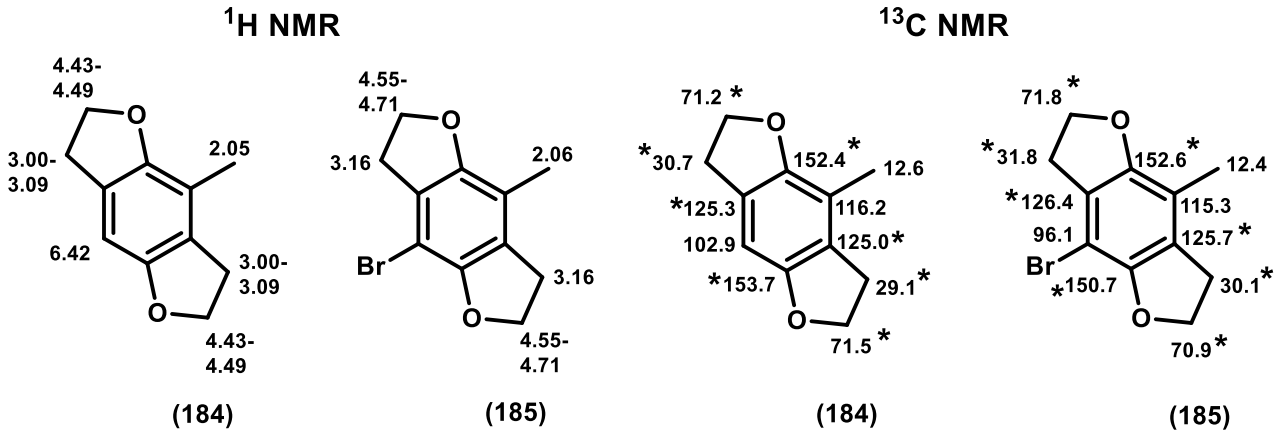
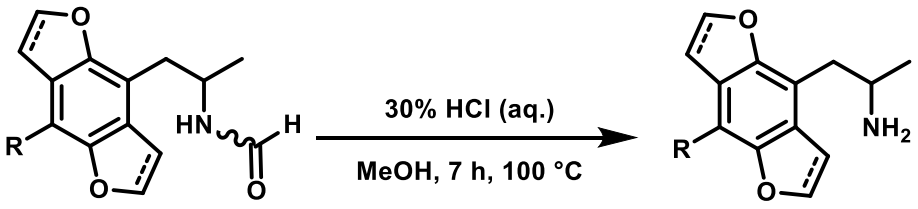


*Fig. 2-113: ^{1}H- and ^{13}C-NMR signal assignments for **184** and **185***

2.4.3 Hydrolysis of *N*-Formyl Intermediates to Amphetamines 15, 24, 25 and 112

As described in Section 2.4.2, when synthesising the *N*-formyl series **102, 181 - 183**, approximately two-thirds (by mass) of each *N*-formyl product was purified *via* chromatography, while the remainder was reserved in its crude state for HPLC analysis and 'clandestine' reactions. For this section, each hydrolysis was performed in duplicate using pure *N*-formyl input material and crude input material. All reactions were performed under identical conditions, as described in Figure 2-114. These reaction conditions are well known in the literature and have been used previously by members of our research group.[1,31]



(102): R=H, THBD
(181): R=Br, THBD
(182): R=H, Benzodifuran
(183): R=Br, Benzodifuran

(24): R=H, THBD [73 %]
(25): R=Br, THBD [68 %]
(112): R=H, Benzodifuran [59 %]
(15): R=Br, Benzodifuran [41 %]

*Fig. 2-114: Hydrolysis reaction conditions for conversion of N-formyl substrates **102**, **181** - **183** to analogous amphetamines **15**, **24**, **25** and **112***

The reactions were worked up by basifying to > pH 9 using 4 M aq. NaOH, and then extracted into DCM, followed by recovery of the crude product *in vacuo*. In all cases, the 'clean' reactions carried out using pure *N*-formyl input material produced pure amphetamine product post work-up (no need for further purification), while the 'clandestine' reactions carried out using crude *N*-formyl input material contained amphetamine product mixed with a number of impurities, including the expected pyrimidines seen originally in the Leuckart crude reaction mixtures.

The pure amphetamines recovered from the 'clean' reactions were fully characterised as summarised in Table 2-24. While **15**, **24**, and **25** are not novel amphetamines, all melting points found in the literature refer to salts of the amphetamine (i.e. $RNH_2.HCl$).[39,56] No literature melting points were found for the free base compounds, which are reported in this work. Nonbrominated benzodifuran amphetamine **112** is a novel structure which has not previously been reported in the literature.

Compound Number	Yield (%)	m.p. (°C)	R_f (EtOAc)	IR ν_{max} NH (cm^{-1})	HRMS (*m/z*)	
					Calc.	Found
15	41	124 - 126 (No recryst.)	0.09	3149	294.0124	294.0132
24	73	92 - 95 (EtOAc)	0.03	3353	220.1332	220.1339
25	68	115 - 116 (EtOAc)	0.05	3291	298.0437	298.0436
112	59	108 - 110 (No recryst.)	0.06	3114	216.1019	216.1028

*Table 2-24: Yield, m.p., R_f, IR and HRMS data for **15**, **24**, **25** and **112***

Full ^1H- and ^{13}C-NMR analysis of **15**, **24**, **25** and **112** was also carried out, with the spectra very similar to those previously described for THBD and

benzodifuran type compounds, especially the ketone and *N*-formyl precursors described in Sections 2.4.1.3 and 2.4.2.1 respectively.

In ^{1}H-NMR analysis, the main differences between spectra of amphetamines **15**, **24**, **25** and **112** and their *N*-formyl analogues **102, 181 – 183** (apart from slight differences in chemical shift and the absence of multiple rotamers in each spectrum) were the absence of the formyl proton at 7.5 - 8.0 ppm, and the increase in integration value of the N**H** proton from one to two protons (N**H** → N**H$_2$**). All THBD/benzodifuran protons appeared in ranges expected from previous spectral analysis of similar compounds. With the exception of **112**, the NMR spectral details of these amphetamines have been previously published in the literature: a full account of the ^{1}H-NMR signal assignments to the amphetamines **15**, **24**, **25** and **112** measured in this work can be found in Section 4.2.3.

The ^{13}C-NMR spectra of amphetamines **15**, **24**, **25** and **112** also showed signals in the ranges expected from previous analysis of similar THBD/benzodifuran substrates. There were slight differences in the chemical shifts of some signals, but the main difference between amphetamines **15**, **24**, **25** and **112** and the ^{13}C-NMR spectra of their ketone and *N*-formyl precursors was the absence of any carbonyl signals in the spectra, and the absence of any rotamers. A full account of the ^{13}C-NMR signal assignments to the amphetamines **15**, **24**, **25** and **112** can be found in Section 4.2.3.

2.5 Impurity Profiling of Amphetamine-Forming Reactions and Route-Specific Impurities by HPLC

Following the independent synthesis of seven route-specific impurities (pyrimidines **100**, **101**, **103** - **107**) as described previously in this chapter, attention turned to analysing these standards by HPLC. The analysis was run using an Agilent® 1260 Infinity® series instrument using a C-18 column (YMC®-Pack ODS-A, 5 µm, 120Å, 250 x 4.6 mm). Full experimental detail of the HPLC conditions employed can be found in Section 4.1.

2.5.1 HPLC Analysis of Individual Impurities

The retention times (t_R, measured in min) of each of the prepared impurities was measured first, with the retention times summarised below in Table 2-25 (note that the original chromatograms from which the retention times are taken can be seen in full in Appendix 1).

Compound Number	t_R (min) for individual standard	t_R Differential* (min)
100	4.22	0.13
101	4.35	
103	5.44	0.21
104	5.65	
105	4.98	0.42
106	5.40	
107	6.99	1.02
108	8.01**	

Table 2-25: Retention times of Leuckart route-specific impurities by HPLC

*This indicates the difference in t_R between pyrimidine isomers and is calculated by subtracting t_R(benzyl) from t_R(phenyl).

** This value was recorded from the HPLC chromatogram of the Leuckart Reaction of **111**, as **108** was isolated from a reaction mixture rather than prepared as an independent standard.

There are a number of general trends that can be observed when analysing this data:

- Increasing either the aromaticity of a substrate, or structurally adding a bromine increases retention time: this is to be expected as a C-18 column is what is referred to as 'reverse phase', meaning that non-polar

substrates take longer to elute. Both an increase in aromaticity and addition of a bromine atom increase the non-polar properties of a substrate, and it is no surprise that the longest retention times in the pyrimidines are seen for **107** and **108**, which have both benzodifuran and bromo moieties.

- When looking at pairs of pyrimidine isomers (i.e. one phenyl and one benzyl pyrimidine), the phenyl pyrimidine elutes later than its benzyl counterpart, e.g. t_r (**105**) = 4.98 min, while t_r (**106**) = 5.40 min. This may be due to extended conjugation in phenyl pyrimidines between the aryl systems of the THBD/benzodifuran and the pyrimidine, increasing the overall aromaticity and thus the non-polar characteristics of the phenyl pyrimidine substrates when compared to their benzyl analogues.
- The difference between t_R (benzyl) and t_R (phenyl) also increases with increase in aromaticity and/or bromination. For example, the difference in t_R between **107** and **108** is 1.02 min, which is over double the difference between their nonbrominated analogues **105** and **106** (0.42 min) and almost five times the difference between their unaromatised analogues **103** and **104** (0.21 min). This mirrors what is seen when attempting to separate pyrimidine isomers by normal phase chromatography, where the pyrimidines **107** and **108** are completely separable while other analogues are not.

2.5.2 HPLC Analysis of Pyrimidine Isomer Mixtures

Following the analysis of the individual analytical standards, a number of analyses were run using the same method, with mixtures of isomeric pyrimidines (**100** and **101**, **103** and **104**, **105** and **106**) with a view to investigating whether mixtures of the isomers could be separated by HPLC (these chromatograms can be seen in Figure 2-115). The mixtures were made by combining equal volumes of the 1 mg/mL standards prepared to create a new sample.

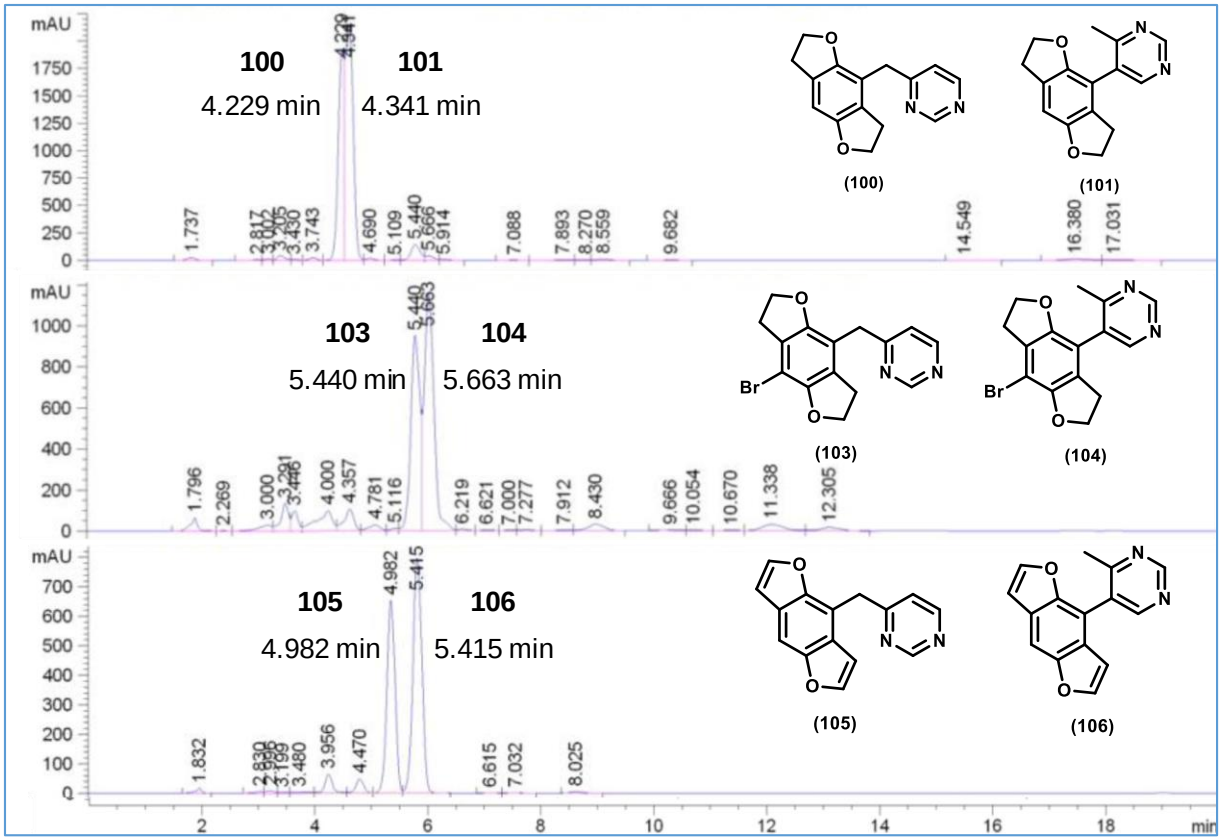


Fig. 2-115: HPLC chromatograms of isomeric pyrimidine mixtures

There was mixed success in this analysis. The nonbrominated THBD pyrimidines **100** and **101** almost completely co-eluted, with only the slightest difference in t_R recorded for their maxima (4.23 and 4.34 min respectively). While brominated THBD pyrimidines **103** and **104** also partially co-eluted, albeit less so than **100** and **101**, there was inadequate separation to see the baseline between the two peaks. The nonbrominated benzodifuran pyrimidine (**105** and **106**) isomer pair were separable to baseline.

2.5.3 HPLC Analysis of Crude Leuckart Reaction Mixtures

As described in Section 2.4.2, samples were kept of the crude reaction mixtures from each of the four Leuckart reactions to form *N*-formyl substrates **102, 181 - 183**. These were analysed by HPLC using the method as described in Section 4.1, and the resultant chromatograms were compared with the analytical standards run in Section 2.5.1.

The crude reaction mixture from the reaction to form the nonbrominated THBD *N*-formyl substrate **102** produced a chromatogram as seen in Figure 2-116.

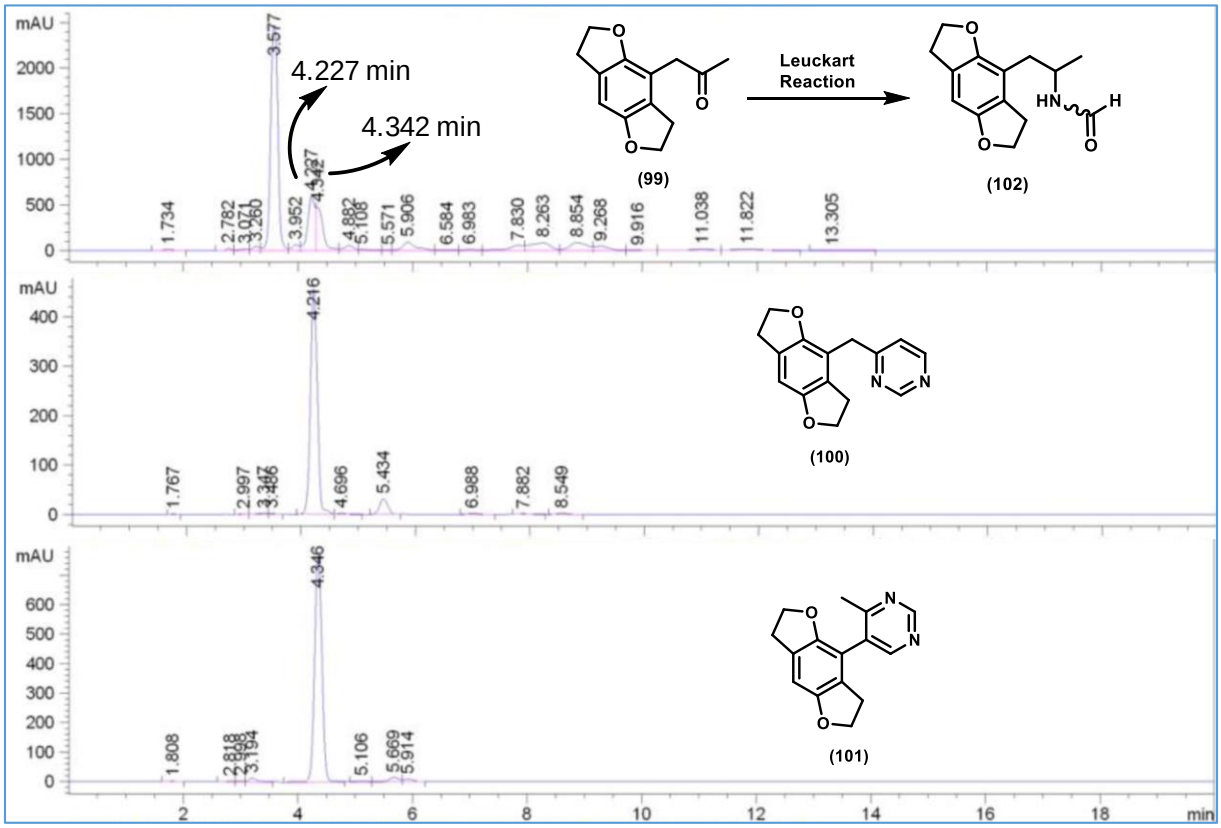


*Fig. 2-116: HPLC analysis of Leuckart reaction to produce nonbrominated THBD N-formyl substrate **102** (top) and comparison to analytical standards **100** (middle) and **101** (bottom)*

There was a clearly identifiable major peak at 3.58 min which is assumed to be the *N*-formyl substrate **102** (Figure 2-116 (top)) based on ^{1}H-NMR analysis of the sample prior to HPLC analysis. There were also two almost entirely overlapping peaks at 4.23 and 4.34 min, which correlate well with the retention times of the benzyl and phenyl pyrimidines (**100** and **101** respectively) analytical standards measured in Section 2.5.1.

The HPLC results for the crude brominated THBD *N*-formyl substrate **181** are similar to those seen for its nonbrominated analogue, with a clear major peak at 4.30 min assumed to be the *N*-formyl product **181**, and two overlapping peaks at 5.45 and 5.67 min which match well with the analytical standards of

the benzyl (**103**) and phenyl (**104**) pyrimidines as measured in Section 2.5.1 (see Figure 2-117).

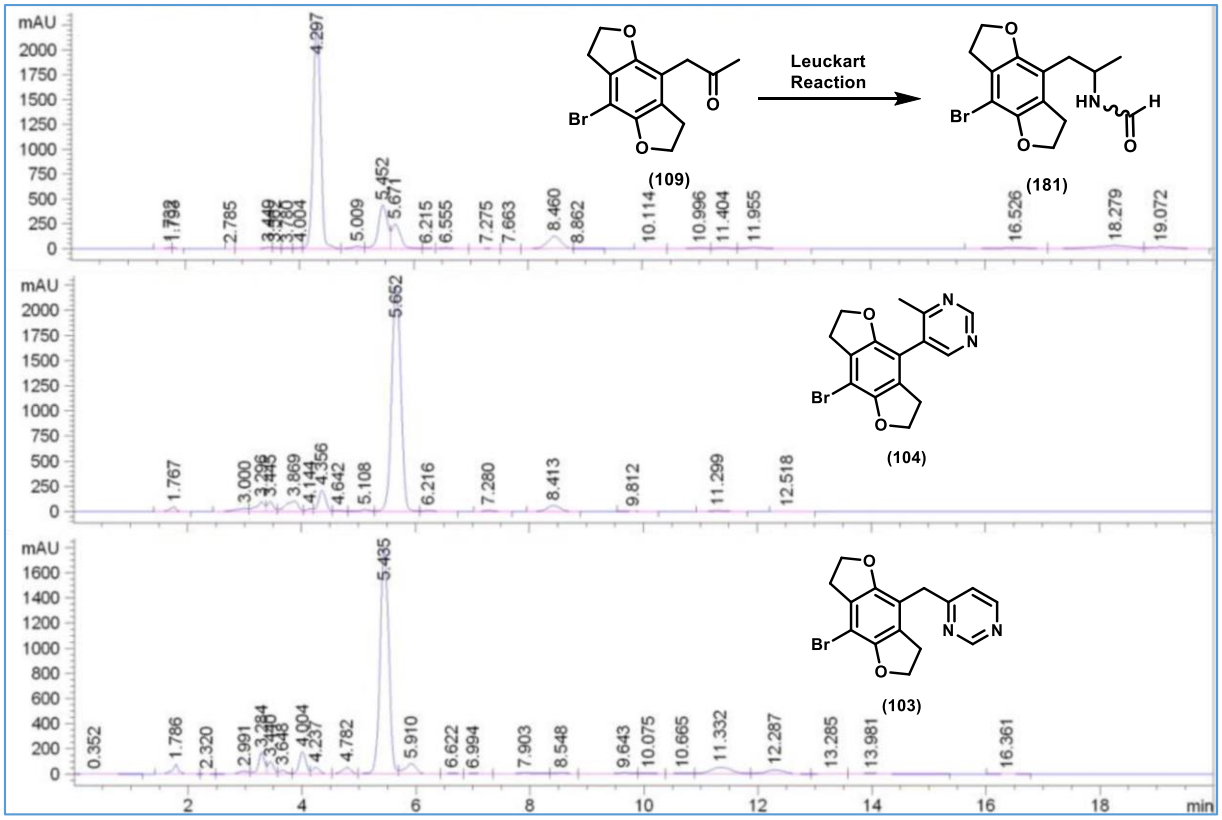


*Fig. 2-117: HPLC analysis of Leuckart reaction to produce brominated THBD N-formyl substrate **181** (top) and comparison to analytical standards **104** (middle) and **103** (bottom)*

The crude nonbrominated benzodifuran *N*-formyl substrate **182** HPLC followed the same pattern as previous analyses, with a major peak at 4.07 min assumed to be the *N*-formyl product **182** (again based on ^{1}H-NMR analysis of the sample prior to HPLC analysis) and the minor peaks at 4.98 and 5.42 min correlating well to the analytical standard markers measured for the benzyl (**105**) and phenyl (**106**) pyrimidines, as shown in Figure 2-118.

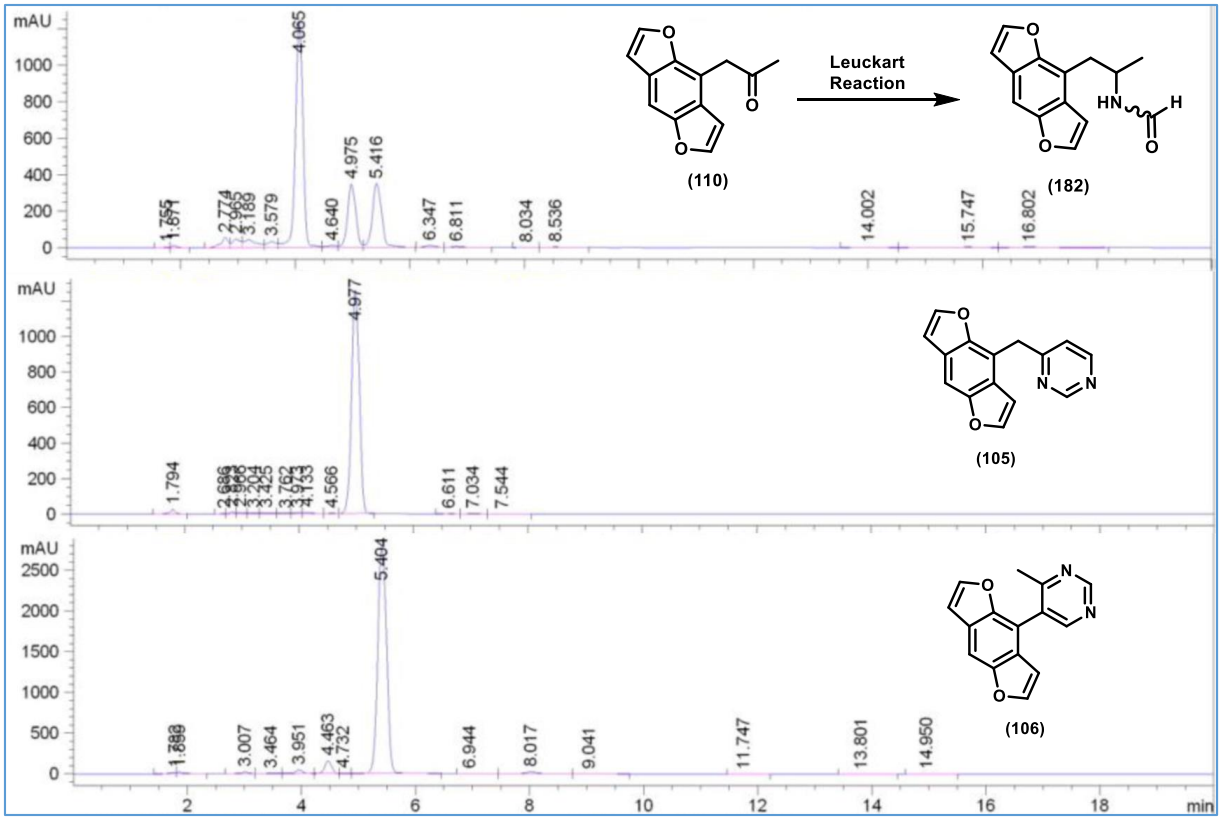


*Fig. 2-118: HPLC analysis of Leuckart reaction to produce nonbrominated benzodifuran N-formyl substrate **182** (top) and comparison to analytical standards **105** (middle) and **106** (bottom)*

Finally, the crude brominated benzodifuran *N*-formyl substrate **183** HPLC also followed the pattern seen in previous analyses, with a major peak assumed to be the *N*-formyl substrate **183** at 5.25 min, and the peak at 6.99 min corresponding well to the benzyl pyrimidine **107**. It was noted that there is a signal at approximately 8.01 min: based on the patterns observed in the HPLC analysis of Leuckart reactions and standards as described in Figures 2-116 to 2-118, where the benzyl pyrimidine isomer elutes first and is followed after by the phenyl pyrimidine isomer, it was inferred that the signal at 8.01 min is most likely to correspond to the phenyl pyrimidine **108** (this is the value listed in Table 2-25). No analytical standard chromatogram of **108** is available as it could not be independently synthesised in this work. There is also another significant peak at 4.71 min, but this does not correlate to any impurity markers known from this work for this reaction.

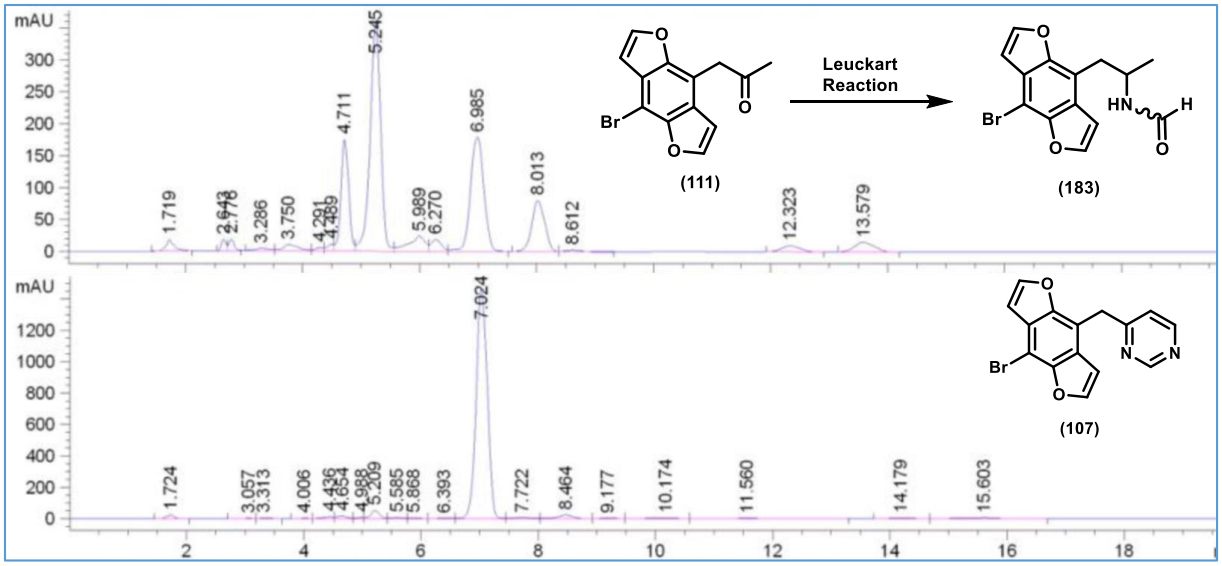


*Fig. 2-119: HPLC analysis of Leuckart reaction to produce brominated benzodifuran N-formyl substrate **183** (top) and comparison to analytical standard for **107** (bottom)*

2.5.4 HPLC Analysis of 'Clandestine' Amphetamine-Forming Hydrolysis Reactions

The crude products of all four of the 'clandestine' hydrolysis reactions described in Section 2.4.3 were analysed by HPLC and compared to the analytical standard markers which were analysed in Section 2.5.1. However, the results were more analogous to the isomeric pyrimidine mixtures seen in Section 2.5.2 than the HPLC analyses of crude Leuckart reaction mixtures in Section 2.5.3. The reason for this is that the crude reaction mixtures were run without derivatisation and as the amphetamine products are extremely polar amines, they eluted from the column with the solvent front and are not detected as peaks in the chromatograms.

The brominated and nonbrominated THBD hydrolysis reactions showed HPLC profiles almost identical to the mixtures of the relevant isomeric pyrimidines (**100**/**101** and **103**/**104** respectively), with the nonbrominated analogue's chromatogram showing two almost completely overlapped peaks at 4.24 and 4.34 min, and the brominated analogue's chromatogram showing two slightly less overlapped peaks at 5.47 and 5.67 min (see Figure 2-120).

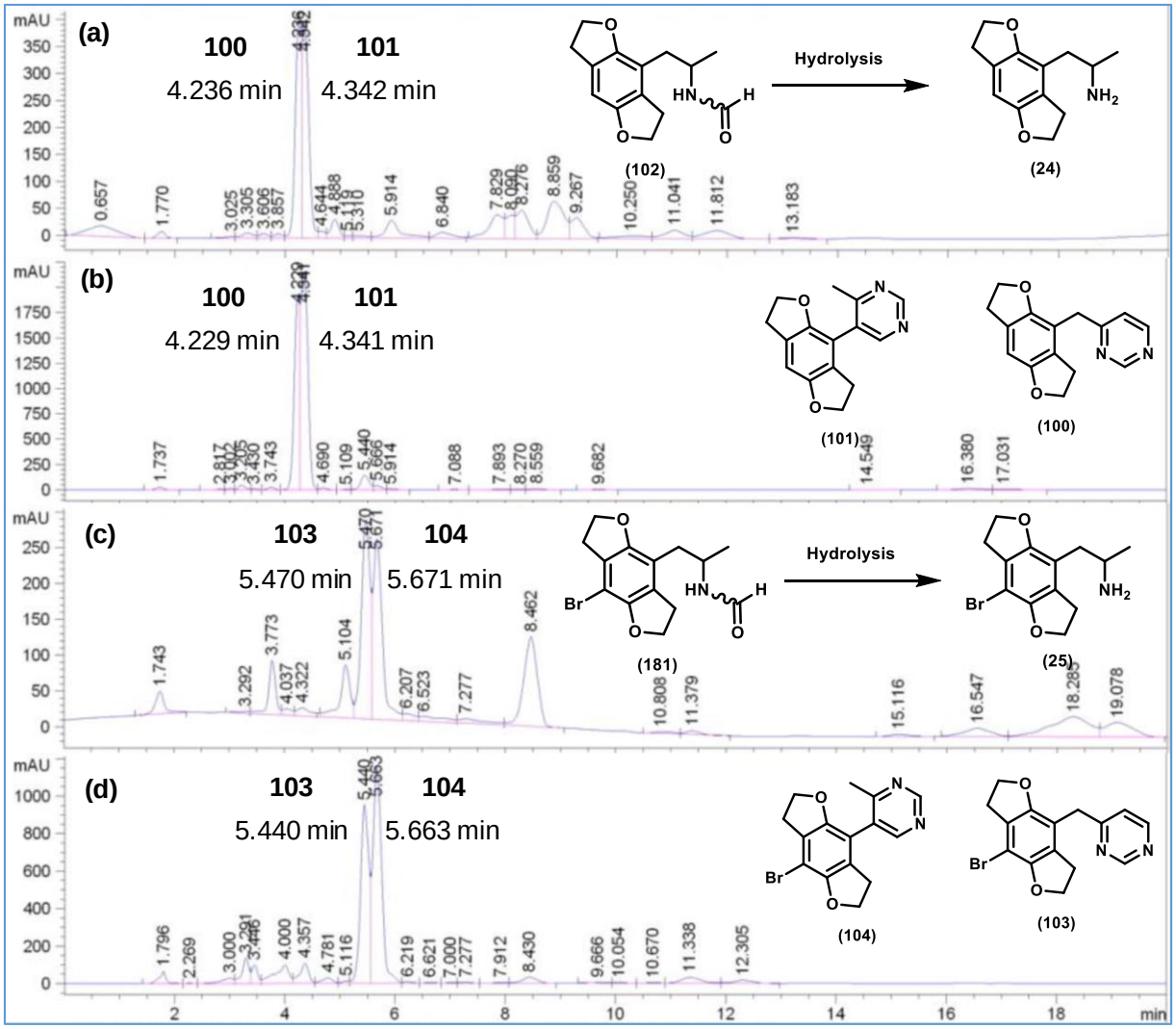


Fig. 2-120: HPLC analysis of nonbrominated (a) and brominated (c) THBD hydrolysis reactions compared with relevant isomeric pyrimidine mixtures (b) and (d) respectively

The nonbrominated benzodifuran hydrolysis reaction did not show an amphetamine peak for **112**, which was expected, but surprisingly, one of the pyrimidine peaks (benzyl pyrimidine **105**) was also missing, with the only major peak in the chromatogram corresponding to the phenyl pyrimidine **106** standard marker as seen in Figure 2-121.

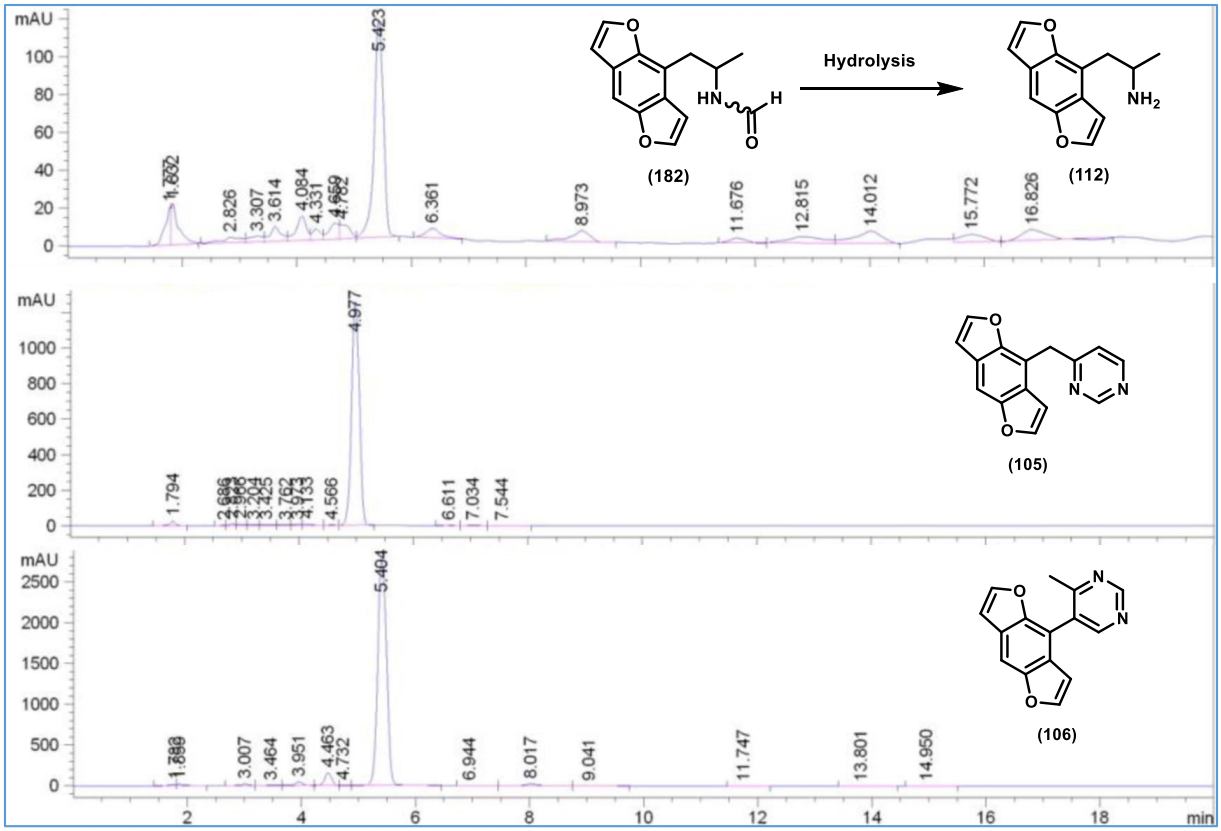


*Fig. 2-121: HPLC analysis of nonbrominated benzodifuran hydrolysis reaction (top) compared with benzyl pyrimidine **105** (middle) and phenyl pyrimidine **106** (bottom) standard markers*

The reason for this absence of pyrimidine **105** is unclear, however, the analysis was re-run with identical results.

The brominated benzodifuran hydrolysis (forming BDF **(15)**) reaction showed a signal for the benzyl pyrimidine **107** at 6.92 min as seen in comparison with the analytical standard marker as measured in Section 2.5.1, and the signal hypothesised to represent the phenyl pyrimidine **108** at 7.99 min. Again, no analytical standard chromatogram of **108** is available as it could not be independently synthesised in this work. The chromatogram also contained the previously observed unidentified peak at a retention time of 4.70 min (see Figure 2-122), in what appears to be a comparatively lower concentration, although this cannot be stated quantitatively. There were also two significant peaks at 12.29 and 13.55 min, but these do not correlate to any impurity markers for this reaction isolated in this work.

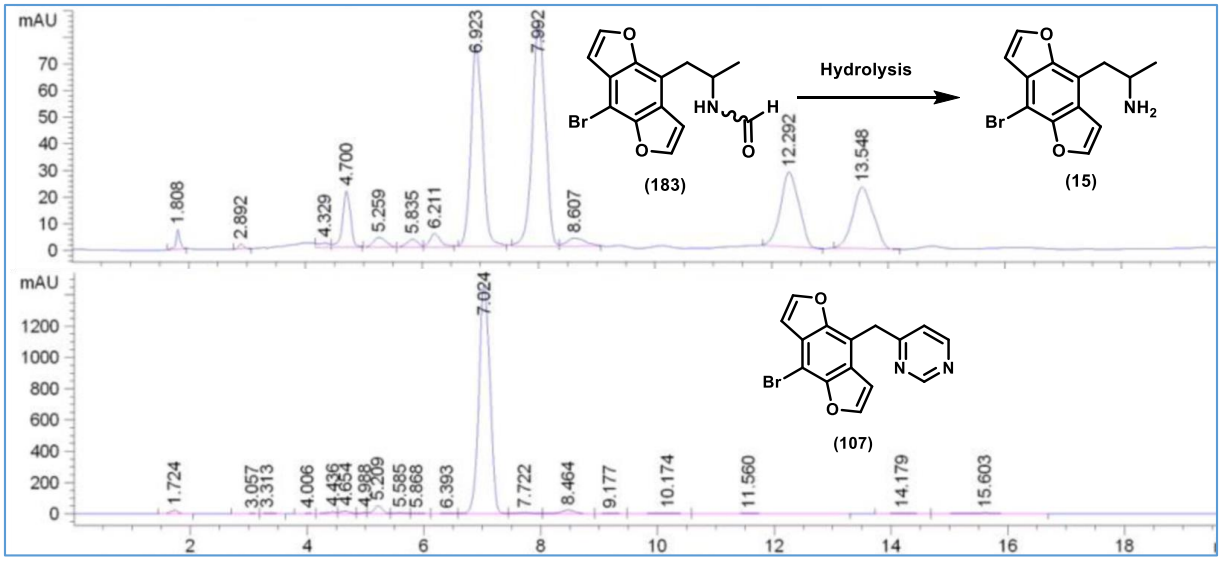


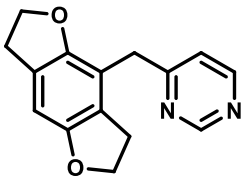
*Fig. 2-122: HPLC analysis of brominated benzodifuran hydrolysis reaction (top) compared with the analytical standard marker for **107** (bottom)*

In summary, it is clear from the HPLC analysis of both the Leuckart and hydrolysis reaction mixtures that the route-specific pyrimidine impurities prepared as analytical standards are suitable for use in identifying the Leuckart route as the reaction pathway for a crude sample of amphetamine product. The pyrimidines readily absorb in the UV region of the electromagnetic spectrum (making them easy to detect).

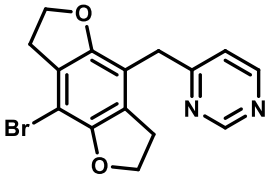
2.6 Summary of Results and Conclusions

The key results to note from this section of work are the independent synthesis of seven novel pyrimidine impurities (out of eight targeted), their use as analytical standards for HPLC analysis of Leuckart reactions related to the synthesis of BDF **(15)**, and some notable differences in reactivity between THBD and benzodifuran class compounds, which were uncovered in the course of the synthetic work.

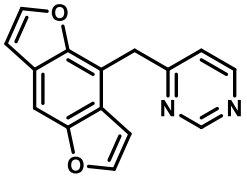
Four benzyl pyrimidine impurities **100**, **103**, **105** and **107** were successfully synthesised *via* a C-H activation palladium coupling reaction, in yields ranging from 7 - 92 %.



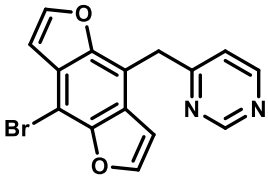
(100)
[66 %]



(103)
[92 %]



(105)
[7.3 %]



(107)
[8.4 %]

It was clear from the percentage yield distribution that the substrates containing fully aromatised benzodifuran moieties (**105** and **107**) were less active towards the palladium coupling reaction, and while several attempts were made to optimise the reaction conditions, including a catalyst screen, extended reaction times and increased reaction temperatures, no improvement in percentage yield was seen.

As an alternative to the C-H activation coupling for the benzodifuran substrates **105** and **107**, a number of oxidative routes from the THBD analogues **100** and **103** were explored. Use of NBS gave over-bromination instead of aromatisation. Employing DDQ resulted in oxidation to a benzodifuran moiety but also resulted in benzylic carbonylation. Finally, chloranil resulted in a mixture of partially aromatised products. It was therefore concluded that despite the low yield for some substrates, the C-H activation palladium coupling reaction was the optimal route to synthesising the targeted benzyl pyrimidine impurities.

Only three of the four phenyl pyrimidine impurities **101**, **104**, **106** and **108** were successfully synthesised independently. While it was subsequently isolated from the relevant Leuckart reaction, brominated benzodifuran phenyl pyrimidine **108** was not successfully independently synthesised in this work.

For accessing the phenyl pyrimidine series, the initial synthetic approach was a convergent synthesis culminating in a Suzuki-Miyaura coupling reaction, as summarised in Figure 2-123. The first strand of the route involved the

synthesis of 5-bromo-4-methylpyrimidine **(113)** from formamidine acetate **(114)** and ethyl acetoacetate **(115)**, a process which required some optimisation, but ultimately resulted in an overall yield of **113** of 18.5 % over 4 steps.

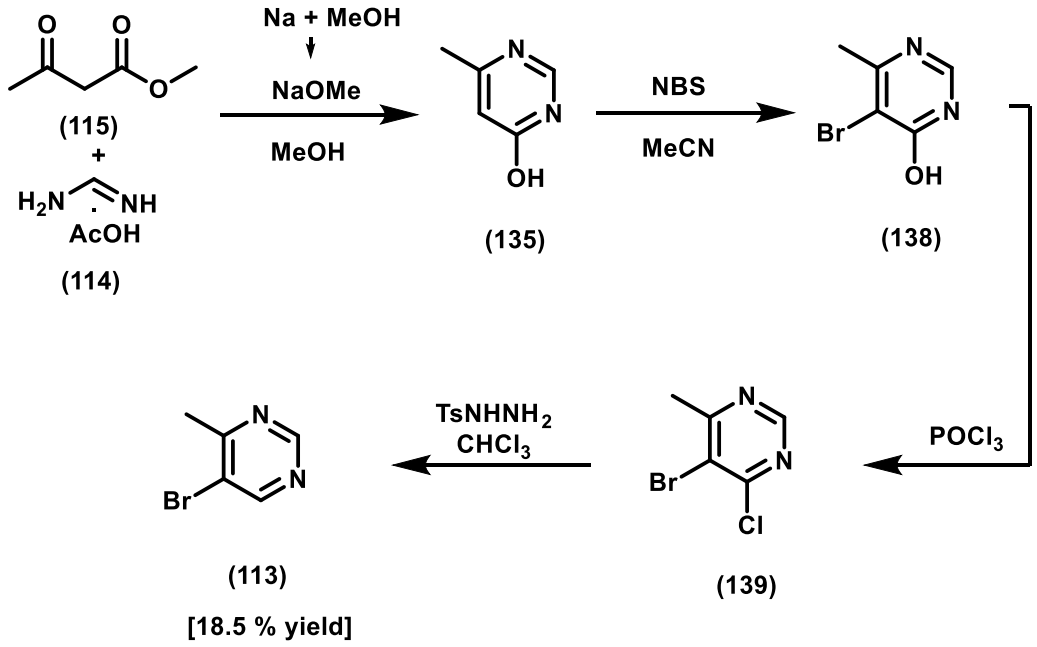
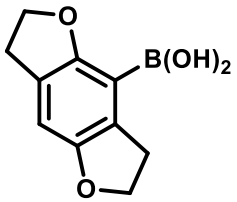


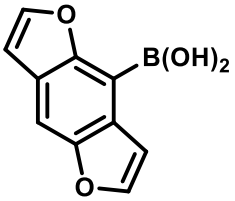
Fig. 2-123: First strand of phenyl pyrimidine synthetic plan

The second strand of the synthetic pathway required the synthesis of an aryl boronic acid, the structure of which determined the nature of the pyrimidine product (5-bromo-4-methylpyrimidine **(113)** was identical in all Suzuki-Miyaura couplings, so structural differences in products were conferred from the respective boronic acid starting materials). All the boronic acids synthesised in this work used THBD **(42)** as a starting point, and the overall yield of the boronic acid in question was dependent on how many structural modifications it had to undergo.

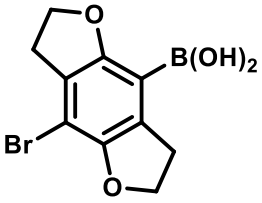
Ultimately the three novel boronic acids **123**, **125** and **126** were successfully synthesised and were isolated in yields ranging from 13 - 78 %. Some synthetic optimisation had to be carried out in the case of THBD brominated boronic acid **126** and it was again noted that the fully aromatised benzodifuran substrate **125** was significantly less active towards borylation than the THBD analogues, with a much lower yield.



(123)
[66 %]

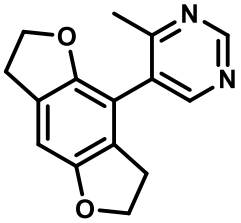


(125)
[13 %]

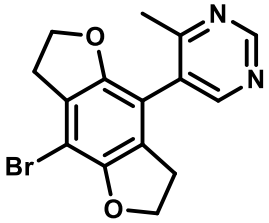


(126)
[78 %]

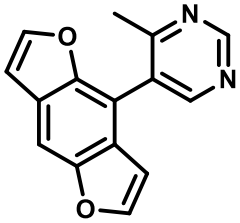
The final synthetic step for the phenyl pyrimidine series was a Suzuki-Miyaura coupling: this was performed using three discrete boronic acids **123**, **125** and **126** in conjunction with 5-bromo-4-methyl pyrimidine **(113)** to give three phenyl pyrimidines **101**, **104** and **106** in yields of 36 - 52 %.



(101)
[52 %]



(104)
[36 %]



(106)
[38 %]

Several other approaches were investigated in an attempt to reduce the number of synthetic steps used to reach target substrates, and also in an attempt to independently synthesise brominated benzodifuran phenyl pyrimidine **108**. The most notable of these included the following:

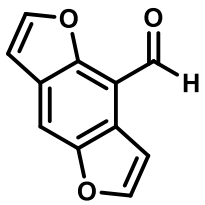
- DDQ to oxidise from THBD to benzodifuran pyrimidines: only partial aromatisation was observed, and there were issues with modification of the pyrimidine methyl group, potentially benzylic carbonylation.
- Brominating reagents to convert nonbrominated substrates to brominated analogues: these led either to overbromination (in the case of Br_2 in acetic acid) or oxidation instead of bromination (in the case of NBS), though the latter result could not be replicated.
- A three-component, zinc chloride-catalysed coupling reaction in which the pyrimidine ring is built onto a phenone: a rate limiting step (formation of an enamine intermediate) was found to be negatively impacted by

the high electron density of the aryl system used, and product yield was therefore limited to a maximum conversion of ~10 %.

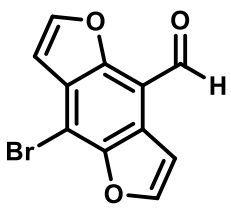
Thus it was concluded that despite the drawbacks associated with the route, the Suzuki-Miyaura synthesis was the optimal pathway for synthesis of the phenyl pyrimidine series **101**, **104** and **106**.

The seven novel pyrimidine impurities produced were isolated and fully characterised, and were used to develop a HPLC method which was capable of distinguishing between pairs of pyrimidines.

The starting material ketones for the four Leuckart reactions needed to produce the pyrimidine impurities *in situ* were synthesised from substrates previously produced within our research group, with characteristic aldehyde impurities **177** and **178** formed and isolated (fully and partially respectively) when using DDQ to aromatise THBD ketones.

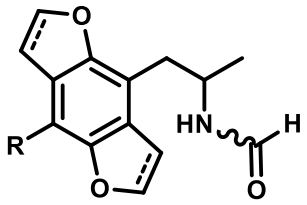


(177)



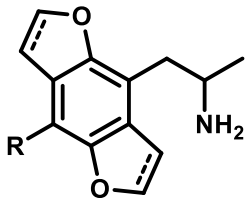
(178)

The four Leuckart reactions were carried out using ketone starting materials **99**, **109** - **111** with yields of the *N*-formyl products **102, 181** - **183** ranging from 13 - 27 %. When purified by flash column chromatography, the characteristic and expected pyrimidine impurities were noted in each reaction (analysed by ^{1}H-NMR), along with perplexing toluene-type impurities **184** and **185** in the case of the THBD-containing substrates **99** and **109** respectively. The reaction to produce the *N*-formyl precursor **183** to BDF **(15)** fortuitously led to the isolation and characterisation of the phenyl pyrimidine **108**, which was not prepared in an independent synthesis.



(102): R=H, THBD
(181): R=Br, THBD
(182): R=H, Benzodifuran
(183): R=Br, Benzodifuran

Two hydrolysis reactions were performed on each of the *N*-formyl substrates **102, 181 - 183** to form the analogous amphetamines **15**, **24**, **25** and **112**: one using purified *N*-formyl material, and one using unpurified material, intended to mimic a 'clandestine' reaction. The 'clean' reactions produced pure amphetamines with no need for further purification, while the 'clandestine' reactions produced amphetamines which were contaminated with characteristic pyrimidines and other impurities.



(24): R=H, THBD
(25): R=Br, THBD
(112): R=H, Benzodifuran
(15): R=Br, Benzodifuran

Using the HPLC method developed for the pyrimidine analytical standards, samples of the crude Leuckart reactions along with the 'clandestine' hydrolysis reactions were run and comparison to the analytical standards revealed that all pyrimidine impurities were present in the experimental runs and could be identified by comparison to their respective analytical standards: this is important, as it means that these analytical standards could be used to identify the Leuckart reaction as the synthetic route in a sample of BDF **(15)**. The differences in retention times between pairs of phenyl/benzyl pyrimidines also mean that this analysis can be used to tell the step in the synthetic pathway at which the Leuckart reaction was performed. Some recommendations for future HPLC work include:

- Performing HPLC analyses using an internal reference standard which can be used to cite relative retention times rather than absolute retention times, to ensure reproducibility.
- Derivatise amphetamines (i.e. with trifluoroacetic anhydride (TFAA)) so that they are visible in final HPLC chromatograms.
- Perform HPLC analyses on pure standard samples of *N*-formyl products and derivatised amphetamines.
- Spike impurity markers into reaction mixtures for HPLC analyses to see if there is a corresponding increase in percentage area of the impurity peak.

In summary, seven of the eight targeted novel pyrimidine compounds were successfully synthesised independently and fully characterised, with the eighth later isolated from a Leuckart reaction and characterised. Many of the reactions used required extensive optimisation, and alternative routes were also thoroughly investigated in the course of these syntheses. Finally, a HPLC method was developed which enabled the use of the independently synthesised pyrimidine markers to confirm the presence of route-specific pyrimidine impurities in crude reaction mixtures designed to mimic clandestine reaction conditions.

References (Chapter Two)

1. Griffin, D. Studies in the Synthesis and Impurity Profiling of 2,5-Dimethoxy Amphetamines. *Doctoral Thesis*; University College Cork, Cork, Ireland, **2009**.
2. van der Ark, A. M.; Verweij, A. M.; Sinnema, A., Weakly basic impurities in illicit amphetamine. *J Forensic Sci* **1978,** *23* (4), 693-700.
3. Sinnema, A.; Verweij, A. M. A., Impurities in illicit amphetamine: a review. *Laboratory and Scientific Section, United Nations Office on Drugs and Crime, Vienna* **1981**, 37-54.
4. Sanger, D. G.; Humphreys, I. J.; Patel, A. C.; Japp, M.; Osborne, R. G. L., The significance of gas chromatographic impurity patterns obtained from illicitly produced amphetamine. *Forensic Science International* **1985,** *28* (1), 7-17.
5. Lambrechts, M.; Klemetsrud, T.; Rasmussen, K. E.; Storesund, H. J., Analysis of Leuckart-specific impurities in amphetamine and methamphetamine. *Journal of Chromatography A* **1984,** *284*, 499-502.
6. O'Connor, R. E. Unpublished Doctoral Work. University College Cork, **2016**
7. Blachut, D.; Szawkalo, J.; Czarnocki, Z., Suzuki-Miyaura and Negishi Approaches to a Series of Forensically Relevant Pyridines and Pyrimidines. *Synthesis-Stuttgart* **2011,** (21), 3496-3506.
8. Redondo, M. C.; Veguillas, M.; Ribagorda, M.; Carreno, M. C., Control of the Regio- and Stereoselectivity in Diels-Alder Reactions with Quinone Boronic Acids. *Angewandte Chemie-International Edition* **2009,** *48* (2), 370-374.
9. Hyslop, A. G.; Therien, M. J., Synthesis of porphyrin-spacer-quinone compounds via metal-mediated cross-coupling: new systems for probing the relative magnitudes of axial and equatorial electronic coupling at the porphyrin macrocycle in thermal and photoactivated electron transfer reactions. *Inorganica Chimica Acta* **1998,** *276* (1-2), 427-434.
10. O'Connor, R. E.; Keating, J. J., Characterization of synthetic routes to 'Bromo-DragonFLY' and benzodifuranyl isopropylamine homologues utilizing ketone intermediates. Part 1: Synthesis of ketone precursors. *Drug Testing and Analysis* **2014,** *6* (7-8), 658-667.
11. O'Connor, R. E.; Bateman, L. M.; Eccles, K. S.; Slattery, C. N.; Lawrence, S. E., Structural Elucidation and Comparative Spectroscopic Analysis of Isomeric Benzodifurans. *Manuscript in Preparation* **2019**.
12. Morita, M.; Mihashi, S.; Itokawa, H.; Hara, S., Silver nitrate impregnation of preparative silica gel columns for liquid chromatography. *Analytical Chemistry* **1983,** *55* (2), 412-414.
13. Nakano, M.; Shinamura, S.; Sugimoto, R.; Osaka, I.; Miyazaki, E.; Takimiya, K., Borylation on Benzo[1,2-*b*:4,5-*b'*]- and Naphtho[1,2-*b*:5,6-*b'*]dichalcogenophenes: Different Chalcogene Atom Effects on Borylation Reaction Depending on Fused Ring Structure. *Organic Letters* **2012,** *14* (21), 5448-5451.
14. Yuen, A. K. L.; Lafon, O.; Charpentier, T.; Roy, M.; Brunet, F.; Berthault, P.; Sakellariou, D.; Robert, B.; Rimsky, S.; Pillon, F.; Cintrat, J.-C.; Rousseau, B., Measurement of Long-Range Interatomic Distances by Solid-State Tritium-

NMR Spectroscopy. *Journal of the American Chemical Society* **2010,** *132* (6), 1734-1735.
15. Imrie, C.; Loubser, C.; Engelbrecht, P.; W. McCleland, C., The use of a modified Suzuki reaction for the synthesis of monoarylferrocenes. *Journal of the Chemical Society, Perkin Transactions 1* **1999,** (17), 2513-2523.
16. Basarić, N.; Thomas, S. S.; Bregović, V. B.; Cindro, N.; Bohne, C., Phototautomerization in Pyrrolylphenylpyridine Terphenyl Systems. *The Journal of Organic Chemistry* **2015,** *80* (9), 4430-4442.
17. Kabalka, G. W.; Sastry, U.; Sastry, K. A. R.; Knapp Jr, F. F.; Srivastava, P. C., Synthesis of arylboronic acids via the reaction of borane with arylmagnesium halides. *Journal of Organometallic Chemistry* **1983,** *259* (3), 269-274.
18. Wang, L.; Dai, C.; Burroughs, S. K.; Wang, S. L.; Wang, B., Arylboronic Acid Chemistry under Electrospray Conditions. *Chemistry – A European Journal* **2013,** *19* (23), 7587-7594.
19. Bruns, S.; Sinnwell, V.; Voss, J., Increments for 1H and 13C NMR chemical shifts in areneboronic acids. *Magnetic Resonance in Chemistry* **2003,** *41* (4), 269-272.
20. Saygili, N.; Batsanov, A. S.; Bryce, M. R., 5-Pyrimidylboronic acid and 2-methoxy-5-pyrimidylboronic acid: new heteroarylpyrimidine derivatives via Suzuki cross-coupling reactions. *Organic & Biomolecular Chemistry* **2004,** *2* (6), 852-857.
21. Naseer, M. M.; Hameed, S., Double Suzuki cross-coupling reaction of pyrimidine boronic acid: synthesis of new versatile dielectrophile. *Applied Organometallic Chemistry* **2012,** *26* (7), 330-334.
22. Clapham, K. M.; Smith, A. E.; Batsanov, A. S.; McIntyre, L.; Pountney, A.; Bryce, M. R.; Tarbit, B., New Pyrimidylboronic Acids and Functionalized Heteroarylpyrimidines by Suzuki Cross-Coupling Reactions. *European Journal of Organic Chemistry* **2007,** *2007* (34), 5712-5716.
23. Wang, Z.; Chi, Y.; Harris, A. R.; Gray, D.; Davoren, J. E., Scalable Synthesis of 4-Substituted 5-Bromo-6-methylpyrimidines. *Synthesis-Stuttgart* **2011,** (10), 1529-1531.
24. Mao, Y.; Zhu, W.; Kong, X.; Wang, Z.; Xie, H.; Ding, J.; Terrett, N. K.; Shen, J.; Shen, J., Design, synthesis and biological evaluation of novel pyrimidine, 3-cyanopyridine and m-amino-N-phenylbenzamide based monocyclic EGFR tyrosine kinase inhibitors. *Bioorganic & Medicinal Chemistry* **2013,** *21* (11), 3090-3104.
25. Yamanaka, H.; Niitsuma, S.; Sakamoto, T.; Mizugaki, M., Studies on Pyrimidine Derivatives. XII. Reaction of 4, 6-Disubstituted Pyrimidine N-Oxides with Dimethyl Acetylenedicarboxylate. *Chemical & Pharmaceutical Bulletin* **1979,** *27* (10), 2291-2294.
26. McKinley, C., Dangerous properties of industrial materials. By N. Irving Sax. Van Nostrand Rein-hold, 5th Ed., **1979**, 1118 pages.
27. Yamanaka, H.; Sakamoto, T.; Nishimura, S.; Sagi, M., Studies on Pyrimidine Derivatives. XXXIX. Site-Selectivity in the Reaction of 5-Substituted and 4,5-Disubstituted Pyrimidine *N*-Oxides with Trimethylsilyl Cyanide. *Chemical & Pharmaceutical Bulletin* **1987,** *35* (8), 3119-3126.
28. Bringmann, G.; Price Mortimer, A. J.; Keller, P. A.; Gresser, M. J.; Garner, J.; Breuning, M., Atroposelective Synthesis of Axially Chiral Biaryl

Compounds. *Angewandte Chemie International Edition* **2005,** *44* (34), 5384-5427.
29. Incremona, J.H.; Martin, J.C., *N*-bromosuccinimide. Mechanisms of allylic bromination and related reactions. *Journal of the American Chemical Society* **1970,** *92* (3), 627-634.
30. Symmetry in NMR Spectra, https://www.chem.wisc.edu/areas/reich/nmr/05-hmr-08-symmetry.htm (accessed 08/02/20)
31. Quille, J. D. Impurity Profiling and Synthesis of Precursors to the Hallucinogenic Amphetamine DOB. *Doctoral Thesis*; University College Cork, Cork, Ireland, **2015**.
32. Yao, Q.; Li, C.-J., Development of an indicator for the direct visualization of radical intermediates in organic reactions. *Chemical Communications* **1970,** *53* (81), 11225-11228.
33. Hazrati, H.; Oestreich, M., Copper-Catalyzed Double C(sp3)-Si Coupling of Geminal Dibromides: Ionic-to-Radical Switch in the Reaction Mechanism. *Organic Letters* **2018,** *20* (17), 5367-5369.
34. Soheilizad, M.; Adib, M.; Sajjadifar, S., One-pot and three-component synthesis of substituted pyrimidines catalysed by boron sulfuric acid under solvent-free conditions. *Journal of Chemical Research* **2014,** *38* (9), 524-527.
35. Sasada, T.; Kobayashi, F.; Sakai, N.; Konakahara, T., An Unprecedented Approach to 4,5-Disubstituted Pyrimidine Derivatives by a ZnCl2-Catalyzed Three-Component Coupling Reaction. *Organic Letters* **2009,** *11* (10), 2161-2164.
36. Ghorbani-Vaghei, R.; Karimi-Nami, R.; Toghraei-Semiromi, Z.; Amiri, M.; Salimi, Z.; Ghavidel, M., One-pot synthesis of pyrimidines under solvent-free conditions. *Comptes Rendus Chimie* **2014,** *17* (4), 324-330.
37. Yang, G.; Jia, Q.; Chen, L.; Du, Z.; Wang, J., Direct access to pyrimidines through organocatalytic inverse-electron-demand Diels-Alder reaction of ketones with 1,3,5-triazine. *RSC Advances* **2015,** *5* (94), 76759-76763.
38. Ehrhardt, C.; Mcquire, L. W.; Rigollier, P.; Rogel, O.; Shultz, M.; Tommasi, R. A., Arylsulfonamide-based matrix metalloprotease inhibitors. Novartis, Ed. Google Patents: **2009**. WO2009118292A1
39. Monte, A. P.; Marona-Lewicka, D.; Parker, M. A.; Wainscott, D. B.; Nelson, D. L.; Nichols, D. E., Dihydrobenzofuran Analogues of Hallucinogens. 3. Models of 4-Substituted (2,5-Dimethoxyphenyl)alkylamine Derivatives with Rigidified Methoxy Groups. *Journal of Medicinal Chemistry* **1996,** *39* (15), 2953-2961.
40. Tada, N.; Hattori, K.; Nobuta, T.; Miura, T.; Itoh, A., Facile aerobic photooxidation of methyl group in the aromatic nucleus in the presence of an organocatalyst under VIS irradiation. *Green Chemistry* **2011,** *13* (7), 1669-1671.
41. Ruzicka, R.; Baráková, L.; Klán, P., Photodecarbonylation of Dibenzyl Ketones and Trapping of Radical Intermediates by Copper(II) Chloride in Frozen Aqueous Solutions. *The Journal of Physical Chemistry B* **2005,** *109* (19), 9346-9353.
42. Sigma-Aldrich FT-NMR of Propionic Acid, https://www.sigmaaldrich.com/spectra/fnmr/FNMR000254.PDF (accessed 25/07/19)

43. Dake;, S. A.; Tekale;, S. U.; Sarda;, S. R.; Jadhav;, W. N.; Bhusare;, S. R.; Pawar, R. P., Anhydrous zinc chloride: an efficient catalyst for one pot synthesis of 2,3,4,12-tetrahydrobenzothiazolo[2,3b]quinazolin-1-ones. *ARKIVOC* **2008,** (17), 241-247.
44. Roshchupkina, Galina I.; Gatilov, Yury V.; Rybalova, Tatyana V.; Reznikov, Vladimir A., Reactions of 1,3-Diaryl-2-chloropropane-1,3-diones with Nucleophiles − Cyanide-Induced Retro-Claisen−Claisen Condensation. *European Journal of Organic Chemistry* **2004,** *2004* (8), 1765-1773.
45. Blümel, M.; Chauhan, P.; Hahn, R.; Raabe, G.; Enders, D., Asymmetric Synthesis of Tetrahydropyridines via an Organocatalytic One-Pot Multicomponent Michael/Aza-Henry/Cyclization Triple Domino Reaction. *Organic Letters* **2014,** *16* (22), 6012-6015.
46. Bultman, M. S.; Fan, J.; Fanfair, D.; Soltani, M.; Simpson, J.; Murugesan, S.; Soumeillant, M.; Chen, K.; Risatti, C.; La Cruz, T. E.; Buono, F. G.; Hung, V.; Schild, R. L.; Ivy, S.; Sweeney, J. T.; Conlon, D. A.; Eastgate, M. D., Preparation of the HIV Attachment Inhibitor BMS-663068. Part 4. Synthesis of the 6-Azaindole Core. *Organic Process Research & Development* **2017,** *21* (8), 1131-1136.
47. Batista, V. S.; Crabtree, R. H.; Konezny, S. J.; Luca, O. R.; Praetorius, J. M., Oxidative functionalization of benzylic C–H bonds by DDQ. *New Journal of Chemistry* **2012,** *36* (5), 1141-1144.
48. Burton, P. M.; Morris, J. A., Palladium-Catalyzed Benzylic Arylation of 2-Methyl Azaarenes. *Organic Letters* **2010,** *12* (23), 5359-5361.
49. Burton, P. M., Private Communication. Jones, R., Ed. **2013**.
50. Shimizu, S.; Imamura, Y.; Ueki, T., Incompatibilities between N-Bromosuccinimide and Solvents. *Organic Process Research & Development* **2014,** *18* (2), 354-358.
51. Montanari, P.; Chiarini, A.; Budriesi, R.; Valenti, P., Xanthone analogues of milrinone. *Journal of Heterocyclic Chemistry* **1992,** *29* (1), 259-261.
52. Shakya, N.; Roy, K. K.; Saxena, A. K., Substituted 1,2,3,4-tetrahydroquinolin-6-yloxypropanes as β3-adrenergic receptor agonists: Design, synthesis, biological evaluation and pharmacophore modeling. *Bioorganic & Medicinal Chemistry* **2009,** *17* (2), 830-847.
53. Buchs, P.; Rice, K. C.; Brossi, A.; Silverton, J. V.; Potenzone, R., Spectroscopic, optical and crytallographic properties of *(S)-(+)-cis*-6′-bromo-N-formylnorreticuline *The Journal of Organic Chemistry* **1982**, *47* (21), 4134-4137
54. Deetz, M. J.; Fahey, J. E.; Smith, B. D., NMR studies of hydrogen bonding interactions with secondary amide and urea groups. *Journal of Physical Organic Chemistry* **2001**, *14* (7), 463-467
55. Keating, J. J. Studies in the synthesis and impurity profiling of Methylenedioxy and Alkylthioamphetamines. *Doctoral Thesis*; Trinity College Dublin, **2001**.
56. Parker, M.A.; Marona-Lewicka, D.; Lucaites, V.L.; Nelson, D.L.; Nichols, D.E., A Novel (Benzodifuranyl)aminoalkane with Extremely Potent Activity at the 5-HT2A Receptor. *Journal of Medicinal Chemistry* **1998**, *41* (26), 5148-5149.
57. Achmatowicz, M.M.; Thiel, O.R.; Coyler, J.T.; Hu, J.; Silva Elipe, M.V.; Tomaskevitch, J.; Tedrow, J.S.; Larsen, R.D., Hydrolysis of Phosphoryl

Trichloride ($POCl_3$): Characterization, *in Situ* Detection, and Safe Quenching of Energetic Metastable Intermediates. *Organic Process Research and Development* **2010**, *14* (6), 1490-1500.

Chapter Three: Targeted Synthesis of iTHBD

Table of Contents

Table of Contents **248**

List of Figures **250**

List of Tables **253**

3 Development of a Direct Synthetic Route to the Novel Pharmacophore 1,2,7,8-Tetrahydrobenzo[1,2-*b*:4,3-*b'*]difuran **254**

3.1 Introduction 254

3.2 Synthesis of 5,6-Dibromocyclohex-2-ene-1,4-dione **(193)** 256

3.2.1 Robustness of 5,6-Dibromocyclohex-2-ene-1,4-dione **(193)** Synthesis 261

3.2.2 Characterisation of **193**, **195** and **197** 263

3.3 Synthesis of 2,3-Dibromobenzene-1,4-diol **(194)** 264

3.3.1 Solvent Screen 268

3.3.2 Catalyst Screen 270

3.3.3 Reaction Conditions 272

3.3.4 Attempted Purification of 2,3-Dibromobenzene-1,4-diol **(194)** 275

3.3.5 Characterisation of 2,3-Dibromobenzene-1,4-diol **(194)** 275

3.4 Synthesis of 2,3-Dibromo-1,4-bis(2-chloroethoxy) benzene **(191)** 277

3.4.1 Optimisation of Alkylation to Synthesise 2,3-Dibromo-1,4-bis(2-chloroethoxy)benzene **(191)** 280

3.4.2 Alternate Route to 2,3-Dibromo-1,4-bis(2-chloroethoxy) benzene **(191)**…. 282

3.4.2.1 Synthesis of 2,2'-(1,4-Phenylenebis(oxy))diethanol **(188)** 284

3.4.2.2 Synthesis of 2,2'-((2,3-Dibromo-1,4-phenylene)bis(oxy))diethanol **(204)** 292

3.4.3 Characterisation of **190**, **191**, **204** and **206** 297

3.5 Synthesis of 1,2,7,8-Tetrahydrobenzo[1,2-*b*:4,3-*b'*] difuran **(90)**.... 300

3.5.1 Annulation of **191** Employing *n*-BuLi 300

3.5.2 Annulation of **191** Employing the Grignard Reaction 307

3.5.3 Characterisation of iTHBD **(90)** and Comparison to THBD **(42)** …….. 308

3.6 Summary of Results and Conclusions 310

References (Chapter Three) 314

List of Figures

Fig. 3-1: Formation of iTHBD **(90)** as a by-product in the synthesis of THBD **(42)**[2] 255
Fig. 3-2: Proposed synthetic route to iTHBD **(90)** 256
Fig. 3-3: Literature procedure for the synthesis of 5,6-dibromocyclohex-2-ene-1,4-dione **(193)**[4] 257
Fig. 3-4: Mechanism of formation of 5,6-dibromocyclohex-2-ene-1,4-dione **(193)** 257
Fig. 3-5: Comparison of ^{1}H-NMR spectra from syntheses of **193** with differing reaction times 258
Fig. 3-7: Synthesis of 2,3,5,6-tetrabromocyclohexane-1,4-dione **(197)** 261
Fig. 3-8: ^{1}H-NMR spectrum of 2,3,5,6-tetrabromocyclohexane-1,4-dione **(197)** 262
Fig. 3-9: ^{1}H- (red) and ^{13}C-NMR (black) signal assignments for **193**, **195** & **197** 264
Fig. 3-10: Synthesis of 2,3-dibromobenzene-1,4-diol **(194)**[9] 265
Fig. 3-11: ^{1}H-NMR spectrum of crude reaction mixture containing 2,3-dibromobenzene-1,4-diol **(194)** and an unidentified impurity…….265
Fig. 3-12: Proposed mechanism for the formation of 2,3-dibromobenzene-1,4-diol **(194)** and 2,5-dibromobenzene-1,4-diol **(195)** 266
Fig. 3-13: Solvent screen for the formation of of 2,3-dibromobenzene-1,4-diol **(194)** using conc. H_2SO_4 268
Fig. 3-14: Base-catalysed synthesis of 2,3-dibromobenzene-1,4-diol **(194)** 271
Fig. 3-15: Synthesis of **194** and **195** with extended reaction time 273
Fig. 3-16: Modified reaction conditions for the synthesis of **194** and **195** ... 274
Fig. 3-18: Comparison of ^{13}C-NMR spectra of 2,5-dibromobenzene-1,4-diol **(195)** (top) and a mixture of 2,3-dibromobenzene-1,4-diol **(194)** and 2,5-dibromobenzene-1,4-diol **(195)** (bottom) 277
Fig. 3-19: Alkylation of hydroquinone **(199)** as reported by Monte et al.[13] .. 278
Fig. 3-20: Alkylation of 2,3-dibromobenzene-1,4-diol **(194)** and its isomer 2,5-dibromobenzene-1,4-diol **(195)** 278

Fig. 3-22: Synthesis of 2,3-dibromo-1,4-bis(2-chloroethoxy)benzene **(191)** with increased equivalents of 1-choro-2-bromobutane **(198)** 281
Fig. 3-23: Synthesis of 2-phenoxyethanol **(201)** 283
Fig. 3-24: Updated proposed synthetic pathway to iTHBD **(90)** 284
Fig. 3-25: Ethoxylation of hydroquinone **(199)** using ethylene carbonate **(203)** and sodium hydride 285
Fig. 3-26: Ethoxylation of hydroquinone **(199)** using ethylene carbonate **(203)** and potassium carbonate 285
Fig. 3-27: ^{1}H-NMR spectrum of a crude mixture of **199**, **188** and **203** 286
Fig. 3-28: Ethoxylation of hydroquinone **(199)** using ethylene carbonate **(203)** as a solvent and a reagent 287
Fig. 3-29: Ethoxylation of hydroquinone **(199)** using ethylene carbonate **(202)** and sodium hydroxide 288
Fig. 3-30: Ethoxylation of hydroquinone **(199)** using ethylene carbonate **(202)** and potassium carbonate 289
Fig. 3-31: ^{1}H-NMR spectrum of crude reaction mixture containing **188** and **205** 290
Fig. 3-32: Further modification of the ethoxylation of hydroquinone **(199)** using ethylene carbonate **(203)** and potassium carbonate 291
Fig. 3-33: Synthesis of **204** and **206** using ethylene carbonate **(203)** and potassium carbonate 292
Fig. 3-34: ^{1}H-NMR spectra of **204** (top) and **206** (bottom) 294
Fig. 3-35: Modified synthesis of **204** and **206** using toluene as a solvent 294
Fig. 3-36: Base and solvent screen for the synthesis of 2,2'-((2,3-dibromo-1,4-phenylene)bis(oxy))diethanol **(204)** using ethylene carbonate **(203)** 295
Fig. 3-37: Synthesis of Alcohol Ethoxylate[21] 297
Fig. 3-38: ^{13}C-NMR signal assignments of **190**, **191**, **204** and **206** 299
Fig. 3-39: General mechanism for the synthesis of iTHBD **(90)** from 2,3-dibromo-1,4-bis(2-chloroethoxy)benzene **(191)** 300
Fig. 3-40: Attempted synthesis of iTHBD **(90)** using *n*-BuLi 301
Fig. 3-41: Modified synthesis of iTHBD **(90)** using *n*-BuLi 302
Fig. 3-43: ^{1}H-NMR spectrum of an aliquot taken from the synthesis of iTHBD **(90)** using *n*-BuLi 304

Fig. 3-44: ^{1}H-NMR spectra of pure iTHBD **(90)** (top) compared with crude Reaction 3 mixture containing iTHBD **(90)** (bottom) 306
Fig. 3-45: Synthesis of iTHBD **(90)** using a Grignard reaction approach 307
Fig. 3-46: Comparison of the ^{1}H-NMR spectra of iTHBD **(90)** (top) and THBD **(42)** (bottom) 309
Fig. 3-47: Comparison of the ^{13}C-NMR spectra of iTHBD **(90)** (top) and THBD **(42)** (bottom) 310
Fig. 3-48: Optimised synthetic route to iTHBD **(90)** 311

List of Tables

Table 3-1: Yield, m.p., R_f, and IR of **193**, **195** and **197** 263
Table 3-2: Monitoring of conversion of **193** to isomeric products **194** and **195** by ^{1}H-NMR analysis..... 267
Table 3-3: Solvent screen to optimise conversion to 2,3-dibromobenzene-1,4-diol **(194)** 269
Table 3-4: Reagent screen to optimise conversion to 2,3-dibromobenzene-1,4-diol **(194)** 271
Table 3-5: Summary of results of increased 1-bromo-2-chloroethane **(198)** trials 281
Table 3-6: Reagent screen for the synthesis of 2,2′-((2,3-dibromo-1,4-phenylene)bis(oxy))diethanol **(204)** 296
Table 3-7: Yield, m.p., R_f, IR and HRMS of **190**, **191**, **204** and **206** 298
Table 3-8: Reaction conditions for variations on *n*-BuLi reactions to form iTHBD **(90)** 305
Table 3-9: Yield, m.p., R_f, IR and HRMS of iTHBD **(90)** 308

3 Development of a Direct Synthetic Route to the Novel Pharmacophore 1,2,7,8-Tetrahydro benzo[1,2-*b*:4,3-*b*′]difuran

A pharmacophore is a discrete chemical moiety that can be recognised as a ligand by proteins and other biological macromolecules, and is defined by the International Union of Pure and Applied Chemistry (IUPAC) as "an ensemble of steric and electronic features that is necessary to ensure the optimal supramolecular interactions with a specific biological target and to trigger (or block) its biological response".[1] Due to this ability to trigger responses from biological molecules, pharmacophores are important in the field of *de novo* drug design, allowing research chemists to virtually assess the potential success of series of substrates before moving to physical preparation of the most likely candidates. As a result, the demand for new discrete chemical moieties is high to continue driving drug discovery. In this chapter, the development of a direct route to the novel pharmacophore 1,2,7,8-tetrahydrobenzo[1,2-*b*:4,3-*b*′]difuran (iTHBD) **(90)** is described in detail. This compound was first discovered in the Keating group as a by-product in the synthesis of Bromo-DragonFLY **(15)** and so the work described here is of interest both to researchers investigating the origin of impurities in BDF **(15)** and structurally-related ATS, and those specialising in drug development.

3.1 Introduction

The novel compound 1,2,7,8-tetrahydrobenzo[1,2-*b*:4,3-*b*′]difuran (iTHBD) **(90)** was first isolated by ROC within the Keating group while synthesising 2,3,6,7-tetrahydrobenzo[1,2-*b*:4,5-*b*′]difuran (THBD) **(42)** as an intermediate *en route* to the synthesis of BDF **(15)**, *via* the route illustrated in Figure 3-1.[2]

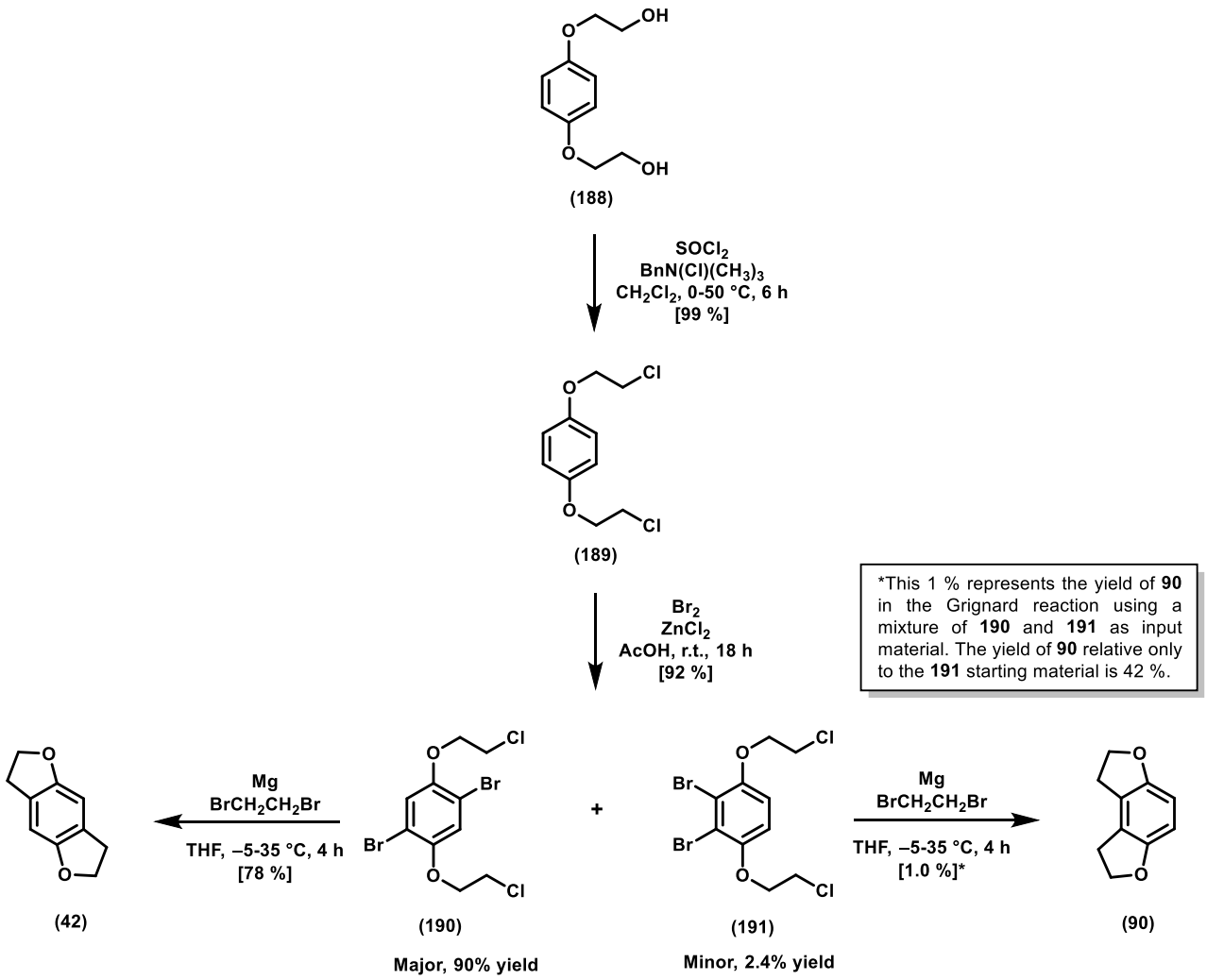


*Fig. 3-1: Formation of iTHBD **(90)** as a by-product in the synthesis of THBD **(42)**[2]*

In the bromination of chloroethoxy ether **189**, the predominant isomer formed was 2,5-dibromo isomer **190**. However, as a side-product of this reaction, 2,3-dibromo isomer **191** was also formed in approximately 2.4% yield. This preference for the 2,5-dibromo isomer is expected due to the steric strain caused by having two large bromine atoms substituted onto the same face of the aromatic ring in the 2,3-dibromo isomer. Dibromo *para* substitution creates the least possible steric strain and so is the favoured product.

When 2,3-dibromo side-product **191** was taken through the next step, a ring-closing Grignard reaction, an isomer of THBD **(42)** was formed. A search of the literature revealed that **90** had not previously been reported, either as an

impurity *en route* to BDF **(15)** or as a target compound in a different context. It was therefore decided to further investigate the direct synthesis of iTHBD **(90)**. As a novel and potentially versatile pharmacophore with the possibility of further functionalisation, **90** is a potentially interesting target for drug development and discovery, as well as being a novel impurity on the route to BDF **(15)**.

In light of this, a possible direct synthetic route to iTHBD **(90)** was proposed as shown in Figure 3-2.

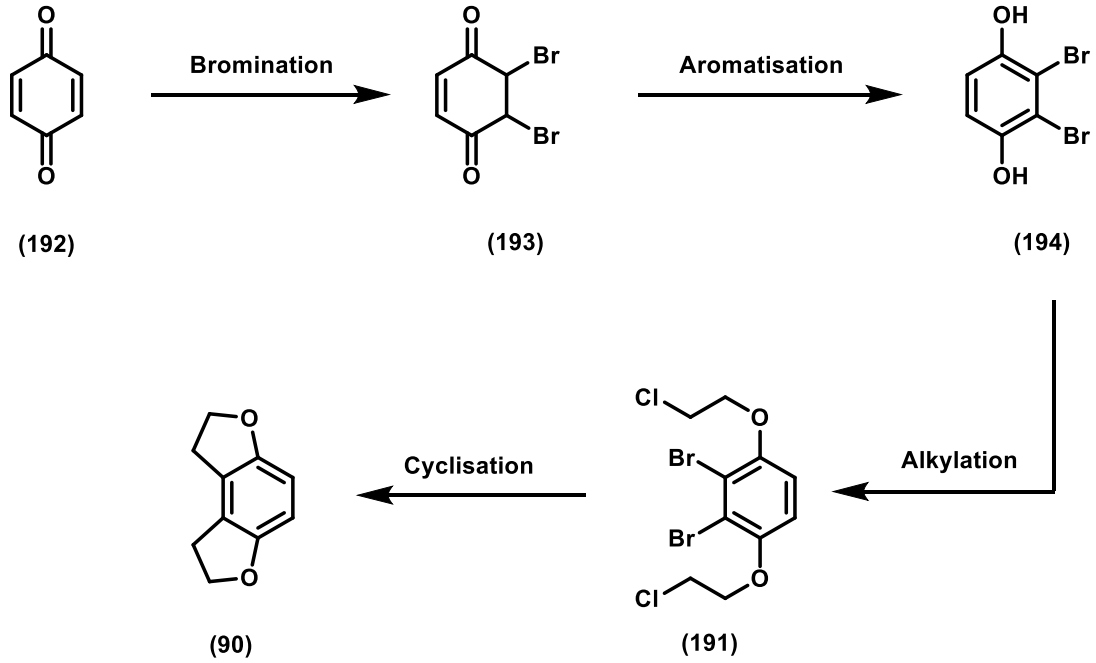


*Fig. 3-2: Proposed synthetic route to iTHBD **(90)***

In this chapter, each step of the route illustrated in Figure 3-2 is investigated and optimised, and the target compound iTHBD **(90)** is successfully synthesised.

3.2 Synthesis of 5,6-Dibromocyclohex-2-ene-1,4-dione (193)

A review of the literature revealed a procedure to synthesise **193** reported by D'Antona *et al.*[3] and Adelt *et al.*[4] involving the dibromination of 1,4-benzoquinone **(192)** with a yield of 98 %, as detailed in Figure 3-3.

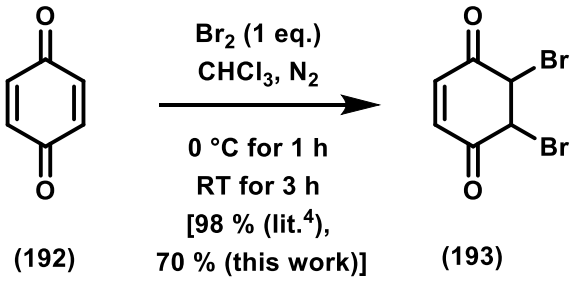


Fig. 3-3: Literature procedure for the synthesis of 5,6-dibromocyclohex-2-ene-1,4-dione ***(193)***[4]

When performed for this work, the procedure resulted in an isolated yield of 70 % on a 50 mmol scale. The crude product was analysed by ^{1}H-NMR and revealed **193** requiring no further purification. The proposed mechanism for the formation of 5,6-dibromocyclohex-2-ene-1,4-dione **(193)** is detailed in Figure 3-4.[5]

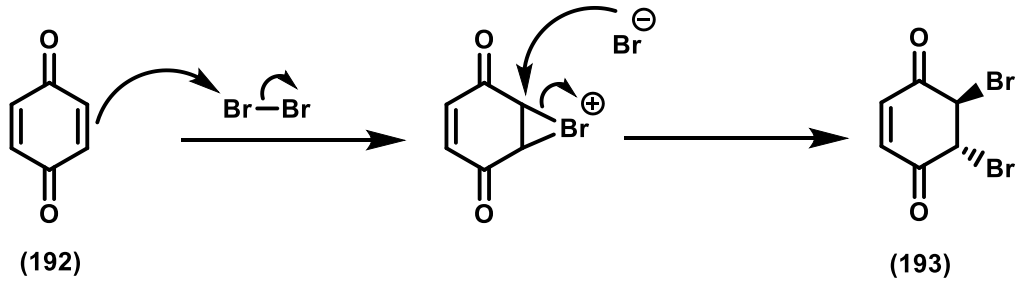


Fig. 3-4: Mechanism of formation of 5,6-dibromocyclohex-2-ene-1,4-dione ***(193)***[5]

In an attempt to increase the percentage yield to match the literature value of 98 %, a second reaction was performed as described in Figure 3-3, but with the reaction time at room temperature extended from 3 to 18 hours. It was noted that the crude product from the extended reaction was visually different from that of the shorter reaction: it was a light grey powder, while the crude product from the shorter reaction was a brown solid. When the crude product from the extended reaction was analysed by ^{1}H-NMR, it also showed a spectrum with only one major product evident. However, while the chemical shifts of the signals were within the range of what would be expected for the substrate **193**, they were significantly shifted downfield from those signals that

were seen in the ^{1}H-NMR spectrum of the crude product from the 3 h reaction. This difference is highlighted in Figure 3-5.

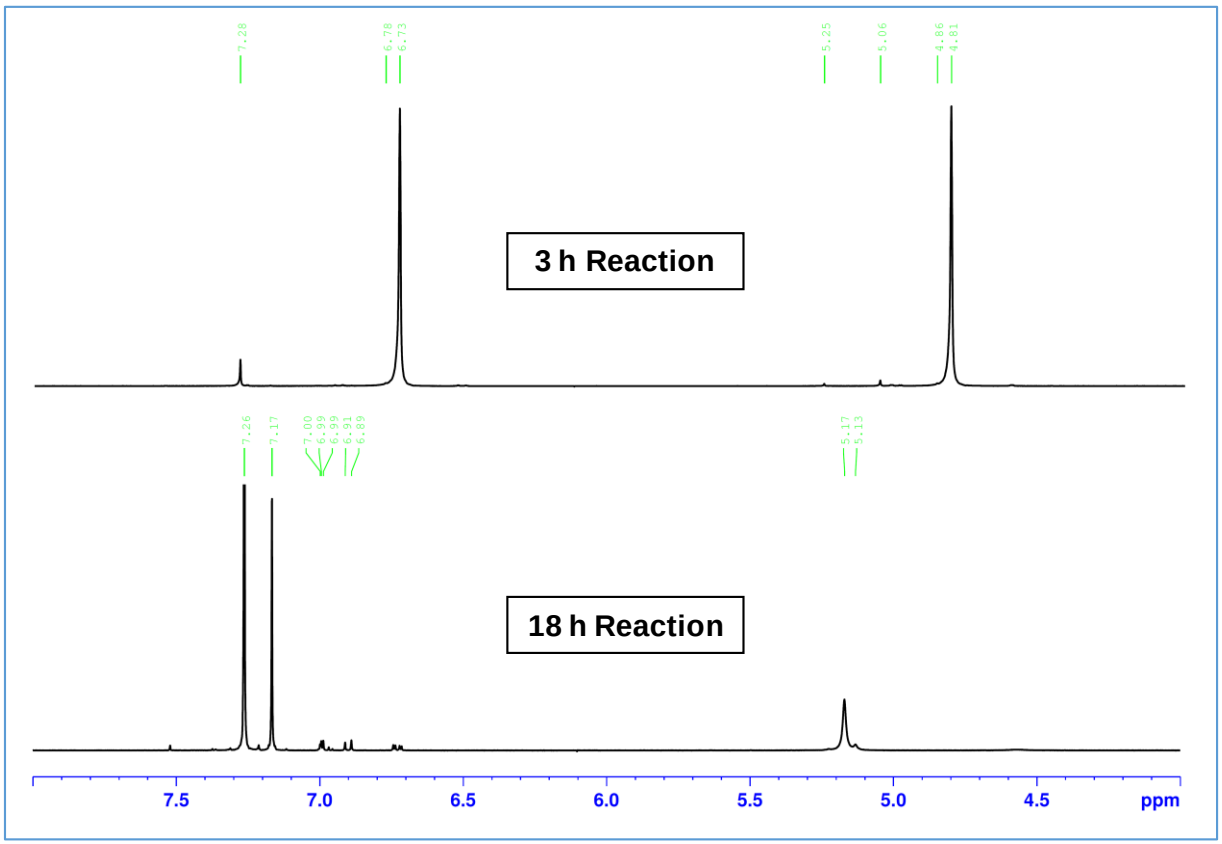


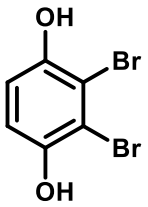
*Fig. 3-5: Comparison of ^{1}H-NMR spectra from syntheses of **193** with differing reaction times*

Initially, this caused some confusion as to which reaction had produced the desired product **193**, however, after comparing the ^{1}H-NMR spectra to literature sources for 5,6-dibromocyclohex-2-ene-1,4-dione **(193)**[4] it was determined that the product of the shorter 3 h reaction was in fact the desired product **193**.

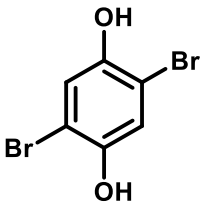
To verify the importance of reaction time to this reaction, two further reactions were performed simultaneously as described in Figure 3-3, one for 3 hours, and the other overnight for 18 hours to replicate the work described above. The crude products from both reactions were analysed by ^{1}H-NMR post work-up and produced the same results as before: the 3 h reaction produced clean

5,6-dibromocyclohex-2-ene-1,4-dione **193**, while the 18 h reaction produced a clean substrate, but with significantly downfield chemical shifts.

At first the identity of second substrate was unclear; however, in the second step of the synthesis of **90** (the conversion of 5,6-dibromocyclohex-2-ene-1,4-dione **(193)** to 2,3-dibromobenzen-1,4-diol **(194)** as detailed in Section 3.3), it was noted that two compounds were formed instead of the one desired product **194**. This undesired side-product was suspected to be the isomeric impurity 2,5-dibromobenzene-1,4-diol **(195)**, which was confirmed by comparison of the ^{1}H-NMR shifts to the literature values recorded by Bian *et al.*[6]



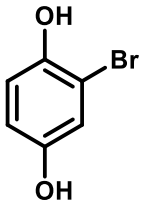
(194)



(195)

At this point, it was noted that the signals of the 2,5-dibromobenzene-1,4-diol **(195)** in the ^{1}H-NMR exactly matched the signals seen for the product of the 18 h reaction when attempting to synthesise 5,6-dibromocyclohex-2-ene-1,4-dione **(193)**. As there is no evidence of 2,5-dibromobenzene-1,4-diol **(195)** in the ^{1}H-NMR spectrum of the 3 h 5,6-dibromocyclohex-2-ene-1,4-dione **(193)** reaction mixture, it was concluded that they are not being formed simultaneously. 5,6-Dibromocyclohex-2-ene-1,4-dione **(193)** was formed initially, but was being converted to 2,5-dibromobenzene-1,4-diol **(195)** over time.

When the ^{1}H-NMR spectrum of 2,5-dibromobenzene-1,4-diol **(195)** from the 18 h reaction was re-examined, it was noted that there were trace signals from an aromatic compound which was identified as 2-bromobenzen-1,4-diol **(196)** by comparison to literature ^{1}H-NMR values as reported by Boruah *et al.*[7] The conversion to **196** in the 18 h sample was ~7.7 % by ^{1}H-NMR integration.



(196)

A paper from Atkinson *et al.* was found which discussed competing side reactions in the dihalogenation of 1,4-benzoquinone.[8] Atkinson *et al.* noted the tendency of C-Br bonds to be prone to elimination. In the presence of hydrogen bromide (of which there could be expected to be a catalytic amount in elemental bromine which was not stored in anhydrous conditions during this work), this tendency would be enhanced (as shown in Figure 3-6) which in practice means that the addition of bromine across the alkene double bond is partially reversible. This hydrogen bromide would then lead to the formation first of 2-bromobenzene-1,4-diol **(196)** (minor) and then 2,5-dibromobenzene-1,4-diol **(195)** (major) . Over time, all of the **193** could be converted to **195** and **196** as hypothesised in Figure 3-6.

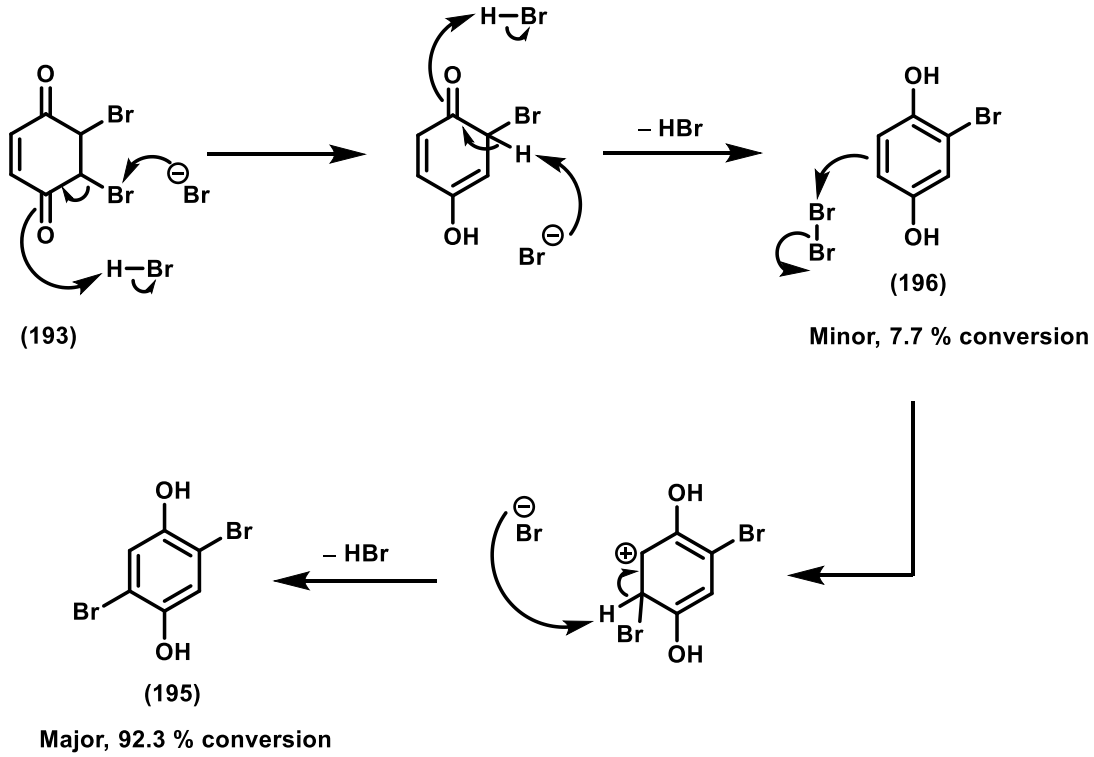


*Fig. 3-6: Proposed mechanism for conversion of dibromodione **193** to side products **196** and **195***

3.2.1 Robustness of 5,6-Dibromocyclohex-2-ene-1,4-dione (193) Synthesis

While it was quickly established that the reaction time was critical to the successful synthesis of 5,6-dibromocyclohex-2-ene-1,4-dione **(193)**, it was decided to investigate the effects of other variables, specifically the equivalents of bromine added and the addition time of the bromine to the starting material **192**.

The first factor investigated was the effect of additional bromine in the reaction on product distribution: a reaction was performed as described in Figure 3-7, with two equivalents of bromine. It was expected that this would result in the formation of 2,3,5,6-tetrabromocyclohexane-1,4-dione **(197)**, but it was not known initially if the reaction would go to completion.

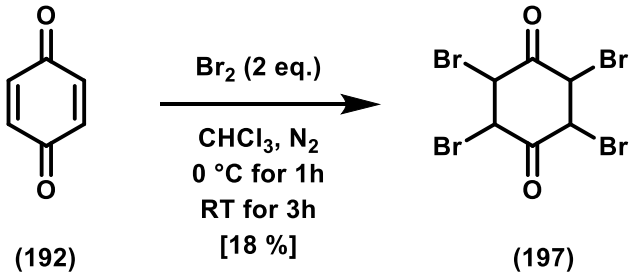


*Fig. 3-7: Synthesis of 2,3,5,6-tetrabromocyclohexane-1,4-dione **(197)***

The crude reaction mixture was analysed by ^{1}H-NMR after work-up and showed only one product, which had only one signal at 5.03 ppm, as would be expected for **197** (see Figure 3-8). The isolated yield after recrystallisation from toluene was 18 % (the crude yield pre-recrystallisation was 31 %), a low yield which suggests that the reaction did not fully go to completion despite the appearance of only **197** in the crude product.

The work-up for the reaction to synthesise both **193** and **197** involves the partial removal of reaction solvent *in vacuo*, causing the product to precipitate from solution. The precipitate is then collected by vacuum filtration. It is possible that the product **197** precipitated out of solution first, leaving any starting material **192** and dibrominated **193** in solution. This would account for

the low yield which was recorded for **197**, and implies that the reaction did not go to completion.

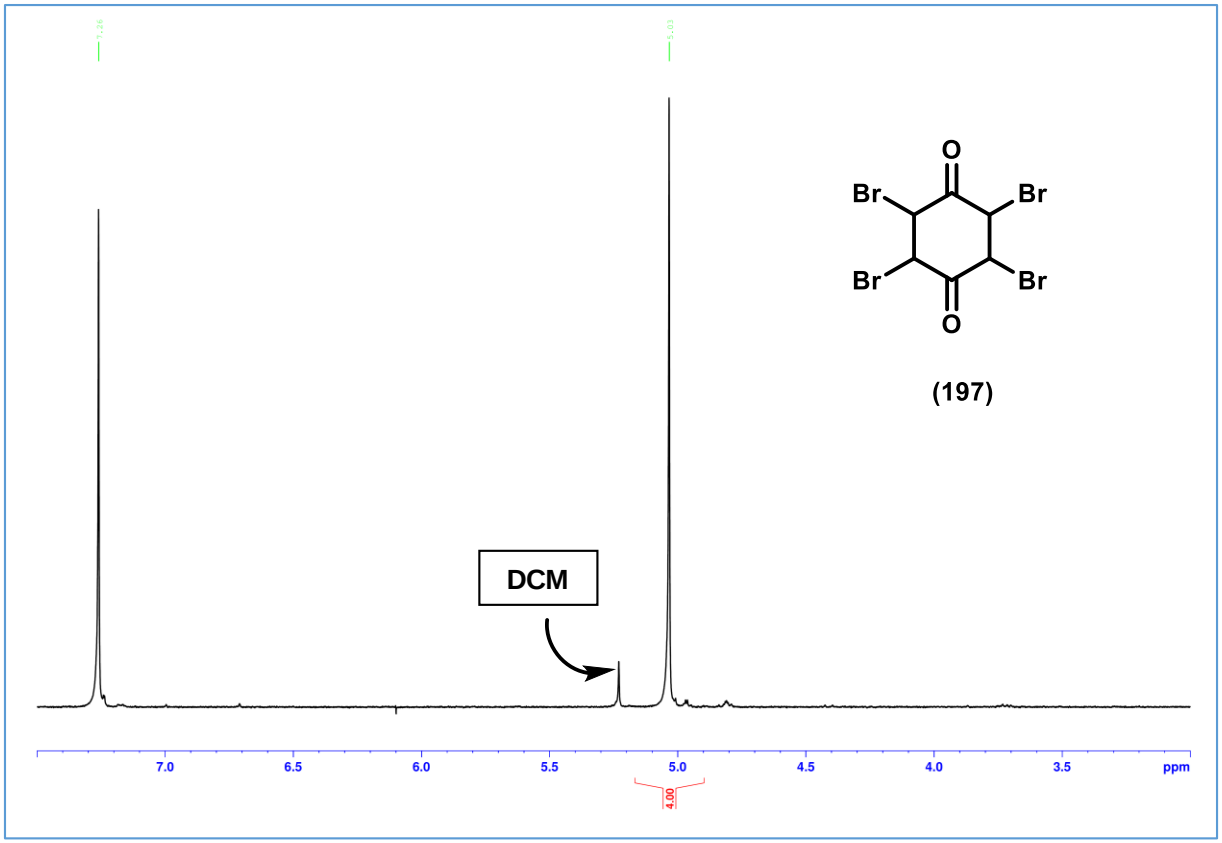


Fig. 3-8: ^{1}H-NMR spectrum of 2,3,5,6-tetrabromocyclohexane-1,4-dione ***(197)***

This low yield of 2,3,5,6-tetrabromocyclohexane-1,4-dione **(197)** under standard reaction conditions with an additional equivalent of bromine (see General Procedure P, Section 4.3.1.1) suggested that the reaction to form **193** (Figure 3-3) was robust with respect to excess bromine in the reaction. It also suggested that the addition of bromine to starting material **192** to form **193** could be done considerably quicker than the procedure adapted from Adelt *et al.*, which suggested a two hour addition at 0 °C for a reaction on a 1 mol scale.[4] This gradual addition at low temperature was not explained by Adelt *et al.*, but was assumed to have a two-fold purpose: the control of any exotherm, and prevention of over-reaction between excess bromine and **192** to form **197**.

This slow addition from Adelt *et al.* had been adapted to a 30 min addition at 0 °C on a 50 mmol scale in this work. However, based on the trial using two

equivalents of bromine, a much shorter addition time of five minutes at 0 °C was trialled followed by immediate warming to room temperature, with the rest of the reaction performed as in Figure 3-3. This resulted in a crude reaction mixture with 100 % conversion to product **193** when analysed by ^{1}H-NMR post work-up, and an isolated yield of 80 %. This is an increase of 10 % on the best recorded value for previous attempts with a longer addition time. This shorter addition time was adopted for all subsequent syntheses of **193** (when synthesising stocks of starting material for the synthetic pathway to **90**).

3.2.2 Characterisation of 193, 195 and 197

5,6-Dibromocyclohex-2-ene-1,4-dione **(193)** (see Figure 3-3, 3 h reaction), 2,5-dibromobenzene-1,4-diol **(195)** (see Figure 3-3, 18 h reaction) and 2,3,5,6-tetrabromocyclohexane-1,4-dione **(197)** (see Figure 3-7) were fully characterised as summarised in Table 3-1.

Compound Number	**Yield (%)**	**m.p. (°C)** ***[Lit m.p.]***	**R_f (Hex:EtOAc)**	**IR ν_{max} (cm^{-1})**
193	80	81 - 83 (Toluene) *[82 - 83[4] (No recryst.)]*	0.39 (9:1)	C=O: 1694
195	37	178 - 181 (Toluene) *[177 - 178[9] (Water)]*	0.65 (1:1)	O-H: 3272
197	18	140 - 143 (Toluene) *[N/A]*	0.54 (9:1)	C=O: 1738

*Table 3-1: Yield, m.p., R_f, and IR of **193**, **195** and **197***

We also repeatedly attempted to measure HRMS values for each of the three compounds, but they appeared incompatible with ESI mass spectrometry.

The ^{1}H-NMR spectra of each of the three compounds **193**, **195** and **197** were acquired: the low number of protons and high level of symmetry in each of the compounds led to simple spectra with only one to two signals observed. The ^{1}H-NMR spectrum of 5,6-dibromocyclohex-2-ene-1,4-dione **(193)** had two signals at 6.73 and 4.81 ppm, representing the alkene and bromine-adjacent protons respectively. The ^{1}H-NMR spectrum of 2,5-dibromobenzene-1,4-diol **(195)** also had two signals at 7.16 and 5.14 ppm, respectively representing the aromatic and hydroxyl protons. The ^{1}H-NMR spectrum of 2,3,5,6-tetrabromocyclohexane-1,4-dione **(197)** had only one signal at 5.03 ppm, representing all four protons. All these signals are shown in Figure 3-9, with ^{1}H-NMR signals in **red**.

The ^{13}C-NMR spectra of **193**, **195** and **197** were also acquired, again with only two to three signals observed in each spectrum. The ^{13}C-NMR results for all three substrates are summarised in Figure 3-9 (^{13}C-NMR signals in **black**), with the dashed lines indicating plane(s) of symmetry within the molecules, or one dot indicating the centre of symmetry in the case of **195**.

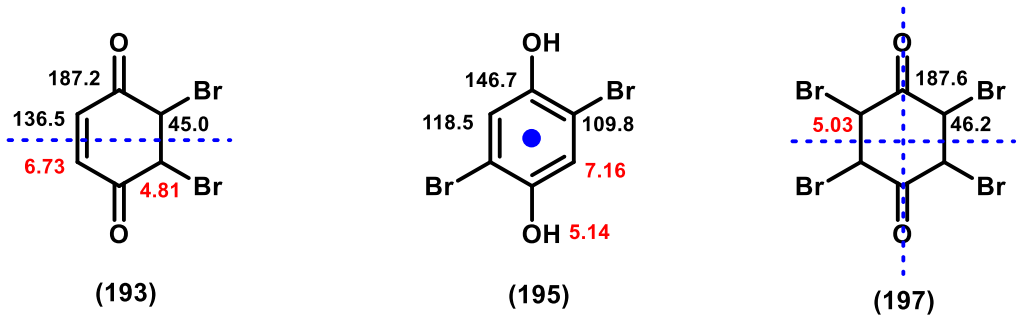


*Fig. 3-9: ^{1}H- (red) and ^{13}C-NMR (black) signal assignments for **193**, **195** & **197***

3.3 Synthesis of 2,3-Dibromobenzene-1,4-diol (194)

Once a stock of 5,6-dibromocyclohex-2-ene-1,4-dione **(193)** had been synthesised, attention was turned to the next step in the synthetic pathway: the conversion of the 1,4-benzoquinone **193** to its fully aromatised analogue 2,3-dibromobenzene-1,4-diol **(194)**. A literature procedure was found in a patent by Djaballah *et al.* detailing the synthesis of **194** from **193** as shown in Figure 3-10.[10]

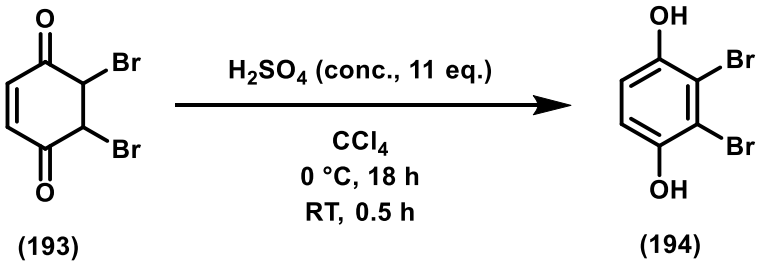


Fig. 3-10: Synthesis of 2,3-dibromobenzene-1,4-diol ***(194)***[10]

A reaction was attempted as described in Figure 3-10, with the exception that carbon tetrachloride was replaced with its less toxic analogue chloroform. However, when the crude reaction mixture was analysed by ^{1}H-NMR, it showed four signals instead of the expected two, as seen in Figure 3-11. The signals for 2,3-dibromobenzene-1,4-diol **(194)** were identified by comparison to the data provided by Djaballah *et al.*, however the other two signals did not match either the starting material **193** or the product **194**.

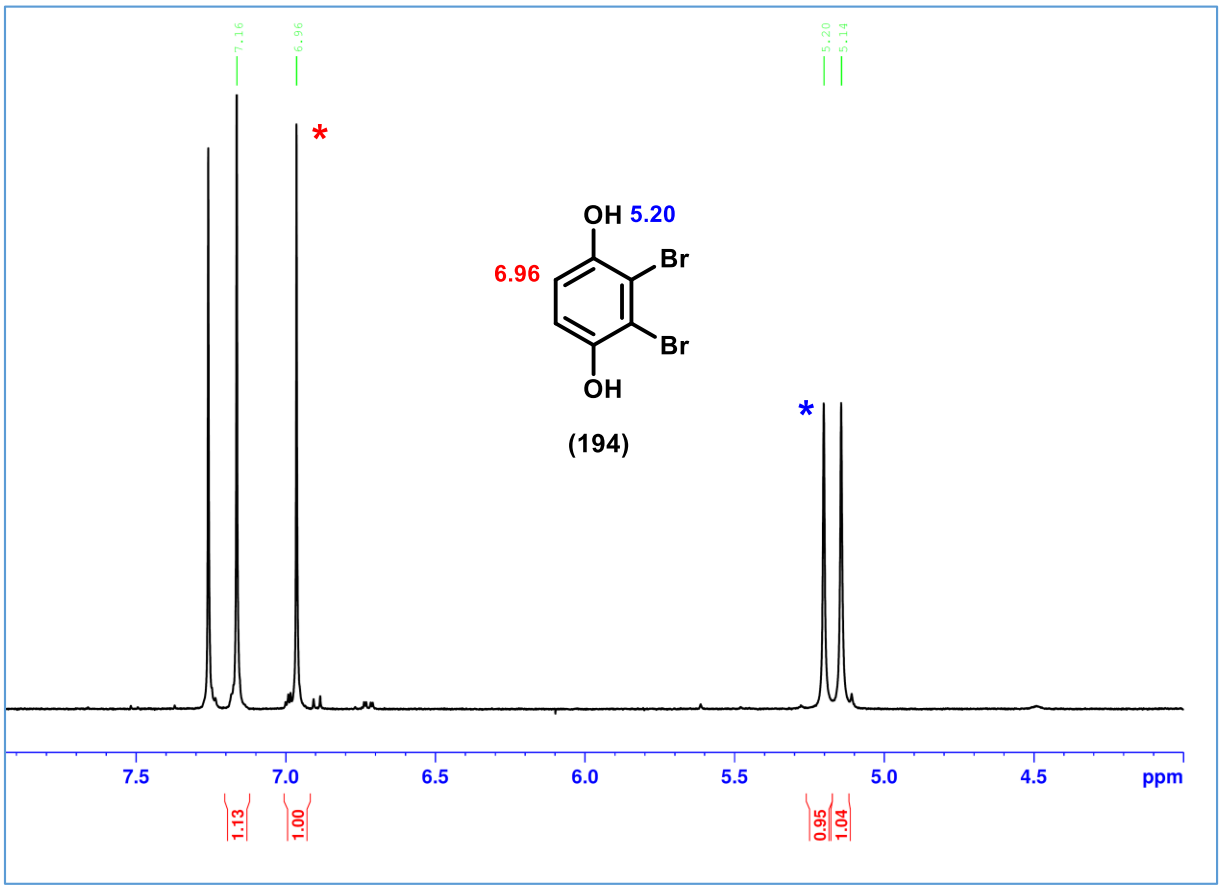


Fig. 3-11: ^{1}H-NMR spectrum of crude reaction mixture containing 2,3-dibromobenzene-1,4-diol ***(194)*** *and an unidentified impurity*

As Djaballah *et al.* had reported the synthesis of 2,3-dibromobenzene-1,4-diol **(194)** without any purification necessary, it had been assumed prior to performing the reaction that the mechanism proceeded *via* acid-catalysed keto-enol tautomerism. However, presented with a second product that appeared (based on ^{1}H-NMR analysis) to be present in approximately equal amounts to the desired product **194**, it was clear that keto-enol tautomerism alone was unlikely to be the mechanism. Instead, it was proposed that the reaction proceeded *via* an elimination (E_1 type)/re-addition reaction as shown in Figure 3-12, and that the second substrate detected in the ^{1}H-NMR of the crude reaction mixture was 2,5-dibromobenzene-1,4-diol **(195)**, an isomer of the desired product **194**.

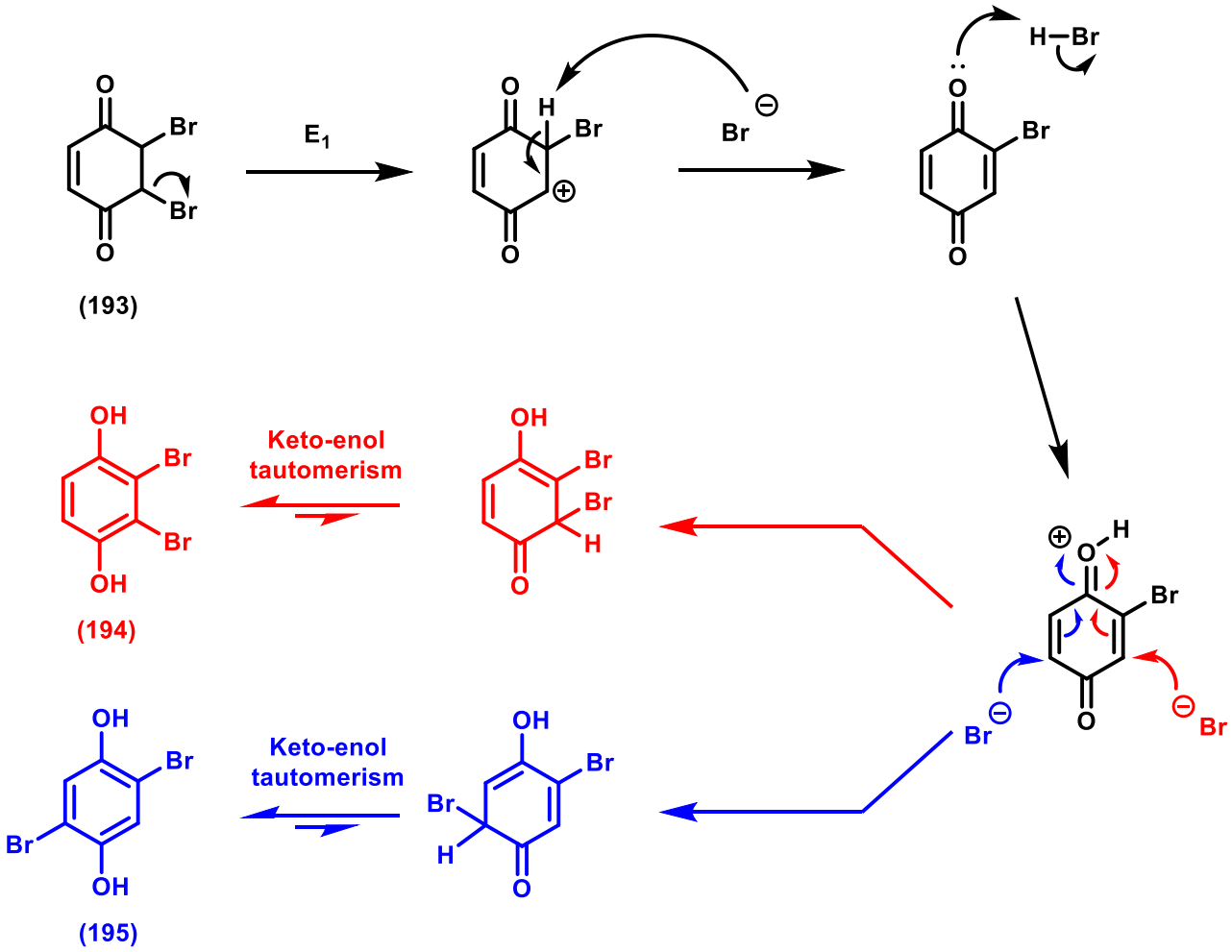


*Fig. 3-12: Proposed mechanism for the formation of 2,3-dibromobenzene-1,4-diol **(194)** and 2,5-dibromobenzene-1,4-diol **(195)***

Comparison of the ^{1}H-NMR signals of the impurity in the crude reaction mixture to the literature values of 2,5-dibromobenzene-1,4-diol **(195)** reported by Bian *et al.* confirmed that the impurity was 2,5-dibromobenzene-1,4-diol **(195)** and in so doing, confirmed elimination/re-addition as the most likely mechanistic pathway for its formation.[5]

This presented a problem with this reaction going forward: once HBr has been eliminated from the starting material 5,6-dibromocyclohex-2-ene-1,4-dione **(193)**, the regiospecificity of the substrate is lost, as the HBr can re-add across either of the two alkene bonds. A comparison of integrated areas in the ^{1}H-NMR spectrum of the crude reaction mixture indicated a slight preference for the unwanted isomer **195**, with a ratio of **194**:**195** of approximately 47:53. This is not unexpected, as 2,5-dibromobenzene-1,4-diol **(195)** has the bromine atoms *para* to each other and is therefore less sterically hindered than 2,3-dibromobenzene-1,4-diol **(194)**.

An investigatigation was undertaken to determine whether the isomers **194** and **195** formed simultaneously. This was determined by performing a reaction as described in Figure 3-10 (using chloroform as a solvent) and monitoring it by ^{1}H-NMR, the results of which are summarised in Table 3-2. The percentages were calculated using the integration of signals at 6.73 (for **193**), 6.96 (for **194**) and 7.16 (for **195**) ppm.

Time	193 % (S.M.)	194 % (product)	195 % (side product)
1 h	96	2.2	1.8
2 h	92	4.6	3.4
3 h	86	7.6	6.4
4 h	83	9.1	7.9

*Table 3-2: Monitoring of conversion of **193** to isomeric products **194** and **195** by ^{1}H-NMR analysis*

After four hours, it was clear that both isomers (**194** and **195**) form simultaneously, though the 2,3-dibromo isomer **194** forms at a faster rate initially, something which is interesting given that the final ratio of isomers in the crude reaction mixture marginally favours the 2,5-dibromo isomer **195**. It was therefore hypothesised that the 2,3-dibromo isomer **194** may be the kinetic product which forms first, and the 2,5-dibromo isomer **195** may be the more stable thermodynamic product. This suggested that any factor that speeds up the rate of reaction would favour the formation of the 2,3-dibromo isomer **194**. On this basis it was decided to perform a solvent and reagent screen, to see if the ratio of **194**:**195** could be shifted in the direction of the 2,3-dibromo isomer **194**.

3.3.1 Solvent Screen

The first factor that was investigated was the optimal solvent for the reaction: based on the literature use of CCl_4,[9] it was hypothesised that nonpolar solvents would be the most favourable, however, it was decided to also test polar protic and polar aprotic solvents. All trials were performed on a 1.12 mmol scale.

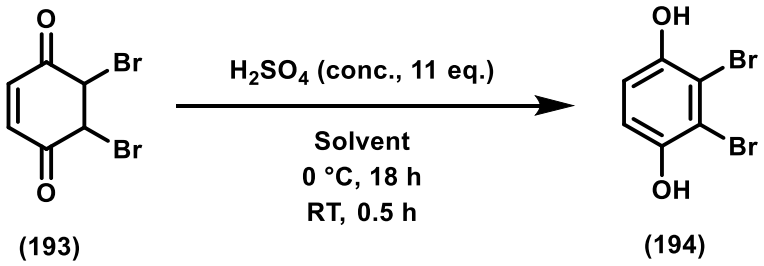


Fig. 3-13: Solvent screen for the formation of of 2,3-dibromobenzene-1,4-diol ***(194)*** *using conc. H_2SO_4*

The experiments were carried out as per Figure 3-13 using a different solvent each time, and the results are summarised in Table 3-3. As described previously, the conversions were calculated using the integration of diagnostic ^{1}H-NMR signals at 6.73 (for **193**), 6.96 (for **194**) and 7.16 (for **195**) ppm.

Solvent	Solvent Type	193 % (S.M.)	194 % (product)	195 % (side product)
Acetonitrile	Polar Aprotic	100	0	0
Dimethylformamide	Polar Aprotic	< 100	Trace	Trace
Diethyl Ether	Polar Aprotic	100	0	0
Methanol	Polar Protic	66	8.3	25
Ethanol	Polar Protic	< 100	Trace	Trace
Isopropyl Alcohol	Polar Protic	82	10	7.9
Chloroform (Original result)	Nonpolar	0	47	53
Dichloromethane	Nonpolar	0	45	55
Carbon Tetrachloride	Nonpolar	0	22	78
Toluene	Nonpolar	10	42	48

*Table 3-3: Solvent screen to optimise conversion to 2,3-dibromobenzene-1,4-diol **(194)***

As predicted, the nonpolar solvents produced the best results out of all those tested; the polar aprotic series of solvents produced little to no consumption of starting material **193**, while the polar protic series of solvents had varying levels of conversion, but none above 33 % combined conversion to product **194**/side product **195** (as seen for methanol).

Of the nonpolar series, the chlorinated solvents performed best, with dichloromethane, chloroform and carbon tetrachloride all resulting in full consumption of starting material **193**. Toluene gave approximately 90 % conversion to **194**/**195**, less than the chlorinated solvents, but a better result than any of the polar protic or polar aprotic solvents. It was noted during the reaction that starting material **193** was not fully soluble in toluene, which may have slowed down the reaction significantly.

Of the chlorinated solvents, dichloromethane and chloroform produced the best results, with isolated yields of 74 and 69 % respectively (combined **194** and **195**), and comparable ratios of **194**:**195** (45:55 for dichloromethane and 47:53 for chloroform). Despite being the literature solvent, carbon tetrachloride was not the optimal solvent in this work: the isolated yield of **194**/**195** was only 50 % and the ratio of **194**:**195** was 22:78, strongly favouring unwanted side product **195**. Some solubility issues were noted during the reaction with carbon tetrachloride, suggesting the reaction requires a 'sweet spot': a solvent adequately polar to dissolve the starting material, but sufficiently nonpolar to allow the reaction to progress.

Following the solvent screen experiments, it was decided to continue testing of other variables in the reaction using chloroform as a solvent, as it produced the best results with respect to conversion to the desired product 2,3-dibromobenzene-1,4-diol **(194)**.

3.3.2 Catalyst Screen

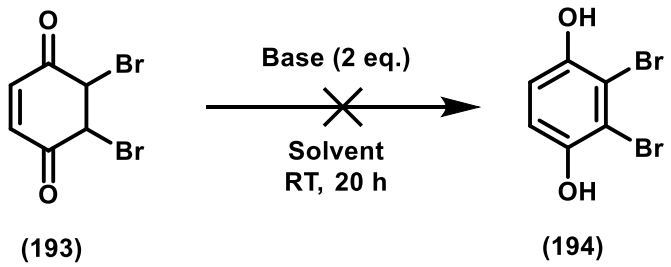
An investigation was undertaken to determine if there was a more suitable acid catalyst for the reaction, or alternatively, if the reaction could be base-catalysed. The results of this screen are summarised in Table 3-4, where the conversions are calculated from ^{1}H-NMR integration values as previously described in Section 3.3.1.

Catalyst	Eq. of Catalyst	Solvent	% 193 (S.M.)	% 194 (product)	% 195 (side product)
H_2SO_4 (conc.) (Original result)	11	$CHCl_3$	0	47	53
*p*TSA	11	$CHCl_3$	100	0	0
HCl (conc.)	11	$CHCl_3$	100	0	Trace
Acetic Acid	234	Acetic Acid	100	Trace	Trace
NEt_3	2	CH_2Cl_2	0	0	0
K_2CO_3	2	Acetone	0	0	0

Table 3-4: Reagent screen to optimise conversion to 2,3-dibromobenzene-1,4-diol ***(194)***

The *p*TSA and concentrated HCl reactions were carried out according to the procedure outlined in Figure 3-13, however, the acetic acid reaction was performed at room temperature, as it freezes at 16 °C.

The base-catalysed reactions were both carried out using the conditions described in Figure 3-14. These reaction conditions and the base/solvent combinations were taken from two separate papers: triethylamine in dichloromethane (Chou *et al.*,[11]) and potassium carbonate in acetone (Thomas *et al.*[12]). Reaction conditions were the same in both papers, with the exception of the base/solvent combinations used. Neither paper used these conditions for the exact substrate used in this work.



(193) (194)

Fig. 3-14: Base-catalysed synthesis of 2,3-dibromobenzene-1,4-diol ***(194)***

Several issues were discovered with the alternative acid catalysts which were trialled: *p*TSA proved to be insoluble in the reaction medium, and while it was hoped that any marginal solubility would drive the reaction to completion, the lack of conversion to product **194** or side-product **195** (when analysed by ^{1}H-NMR post work-up) proved this not to be the case.

The lack of success with concentrated HCl did not come as a surprise, as concentrated HCl is ~37 % w/v in water, and the solvent screen carried out in Section 3.3.1 indicated that polar protic solvents are not favourable for this reaction. When concentrated HCl was added to the reaction mixture, it was noted that a biphasic mixture was formed, and it was clear from the ^{1}H-NMR analysis of the crude reaction mixture post work-up that the reaction did not proceed. It was hoped that there might be some success with acetic acid despite its obvious polar protic qualities as a solvent, however, again ^{1}H-NMR analysis of the crude reaction mixture post work-up proved this not to be the case.

Only two reactions were done using basic catalysts, and both resulted in the complete loss of all starting material **193** without any conversion to product **194** evident by ^{1}H-NMR analysis post work-up. Instead, the crude products from the reactions using NEt_3 and K_2CO_3 were both found to be an inseparable mixture of unknown organic compounds. Both reactions were repeated to confirm initial findings, but at this point, it was assumed that the starting material was not base-stable and this line of investigation was stopped.

Based on this investigation, it was concluded that concentrated sulphuric acid remained the optimal acid for catalysis of the conversion of **193** to **194**, and no further attempts were made to source an alternative.

3.3.3 Reaction Conditions

Once it had been concluded that chloroform was the optimal solvent and that sulphuric acid was the optimal acid catalyst, it was decided to investigate if any reaction conditions could positively affect either the yield or the ratio of

products. The main variables studied were reaction temperature and the length of the reaction.

From the reaction monitoring experiment performed to see if **194** and **195** form simultaneously (as described in Section 3.3), it was evident that after five hours of reaction time, only 17 % conversion to product(s) was achieved. It can be inferred from this result that the 18 h reaction time described by Djaballah *et al.* is necessary for complete conversion from starting material **193**.[10]

Extending the reaction time was next explored to potentially increase the yield of **194/195**, and a reaction was performed as described in Figure 3-15, with the time at 0 °C extended from 18 to 40 h. Analysis of the crude reaction mixture using ^{1}H-NMR spectroscopy revealed complete conversion to product, with a ratio of **194**:**195** of 48:52, comparable to previous results.

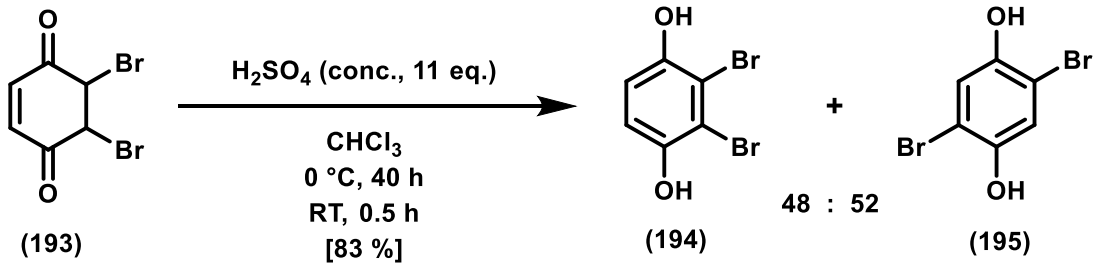


*Fig. 3-15: Synthesis of **194** and **195** with extended reaction time*

The combined yield of **194** and **195** from the 40 h reaction was 83 %, an improvement of almost 14 % on the previous best recorded value using a reaction time of 18 h in $CHCl_3$. This reaction was repeated using the same conditions, and a combined yield of **194/195** of 86 % was recorded, along with a ratio of **194**:**195** of 48:52, which closely matched expectations for product distribution, though it was not weighted as far towards the proposed thermodynamic product **195** as expected.

It was decided to see if a similar yield of **194/195** could be achieved by carrying out the reaction for 1 h at 0 °C followed by 18 h at ambient temperature: this reaction was performed according to Figure 3-16.

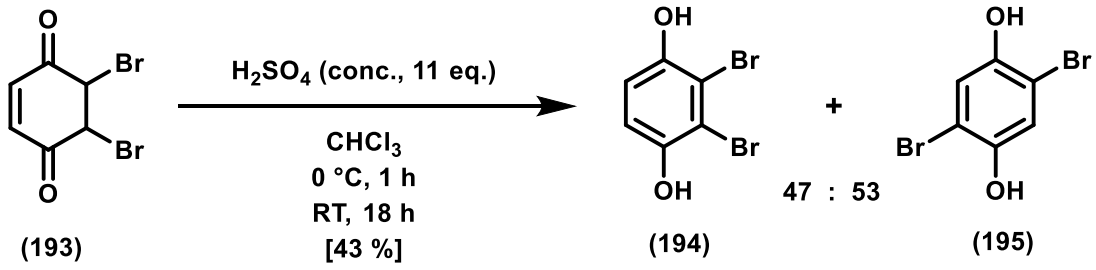


*Fig. 3-16: Modified reaction conditions for the synthesis of **194** and **195***

^{1}H-NMR analysis of the crude reaction mixture post work-up showed complete consumption of starting material **193** and a ratio of **194**:**195** of 47:53. This product distribution was comparable to attempts with a reaction time of 18 h at 0 °C, however, the isolated yield combined yield of **194/195** was only 43 %, half of what was recorded for the reactions with the longer reaction time of 40 h at 0 °C. As the yield was much lower than had previously been seen, but no evidence was seen of starting material **193** in the ^{1}H-NMR spectrum post work-up, it was concluded that either some starting material **193** or an unidentified intermediate must have been removed during the work-up to account for the low recovery.

An extended reaction time is clearly key to ensuring a good yield of **194** and **195**. Furthermore, it was also determined that raising the reaction temperature from 0 °C does not have a negative impact on the product distribution: this suggests that once formed, 2,3-dibromobenzene-1,4-diol **(194)** does not convert to its 2,5-isomer **195**, or does so at a very slow rate. When a mixture of **194** and **195** was analysed by ^{1}H-NMR approximately seven months after it had been synthesised, the ratio of **194**:**195** had decreased from 48:52 to 45:55, suggesting that **194** may convert to **195** over time. The slight preference seen for the 2,5-isomer **195** during the reaction may be due to its more sterically favourable arrangement of bromine atoms.

In conclusion, while the yield of the reaction was greatly improved (from 35 % to 86 %), no reagents or experimental conditions which distinctly favoured the 2,3-isomer **194** over the 2,5-isomer **195** were discovered despite extensive reaction optimisation.

3.3.4 Attempted Purification of 2,3-Dibromobenzene-1,4-diol (194)

Once it was determined that the desired product 2,3-dibromobenzene-1,4-diol **(194)** could not be synthesised without concurrently synthesising 2,5-dibromobenzene-1,4-diol **(195)**, attention was turned to the challenge of separating the two isomers.

Recrystallisation was attempted from toluene, dichloromethane and methanol, however, none of these recrystallisations changed the ratio of **194**:**195** in the isolated product, and so it was decided to attempt purification of 2,3-dibromobenzene-1,4-diol **(194)** by column chromatography.

When analysed by TLC, **194** and **195** were found to have R_f values of 0.51 and 0.65 respectively when measured in a 1:1 hexane:ethyl acetate eluent system. Despite this > 0.1 difference in R_f values, repeated attempts at column chromatography frustratingly showed streaking of **194** and **195** on the column, and 2,3-dibromobenzene-1,4-diol **(194)** proved inseparable from its 2,5-isomer **195**. The ratio in some collected chromatography fractions was variable, between 1:1 to a more favourable ~3:1 **194**:**195**. However, the columns were quite difficult to work with due to the streaking which necessitated that each fraction be isolated individually. It was therefore decided to simply telescope the mixture of products into the next step, where previous work by O'Connor *et al.* suggested that separation of products would be more facile.[2]

3.3.5 Characterisation of 2,3-Dibromobenzene-1,4-diol (194)

While the inability to separate 2,3-dibromobenzene-1,4-diol **(194)** from its 2,5-isomer **195** made it pointless to measure values such as melting point and IR data, it was still possible to assign ^{1}H- and ^{13}C-NMR spectra for **194** by comparison to the spectra of 2,5-dibromobenzene-1,4-diol **(195)** acquired in Section 3.2.2.

As for 2,5-dibromobenzene-1,4-diol **(195)**, the ^{1}H-NMR spectrum of 2,3-dibromobenzene-1,4-diol **(194)** is relatively simple, with two signals, one for

the equivalent aromatic protons at 6.96 ppm and one for the equivalent hydroxyl protons at 5.20 ppm. A comparison between the ^{1}H-NMR spectrum of isolated 2,5-dibromobenzene-1,4-diol **(195)** and the mixture of isomers **194** and **195** can be seen in Figure 3-17. This comparison allowed the signals for 2,5-dibromobenzene-1,4-diol **(195)** to be excluded from the assignment of the ^{1}H-NMR signals of the mixture.

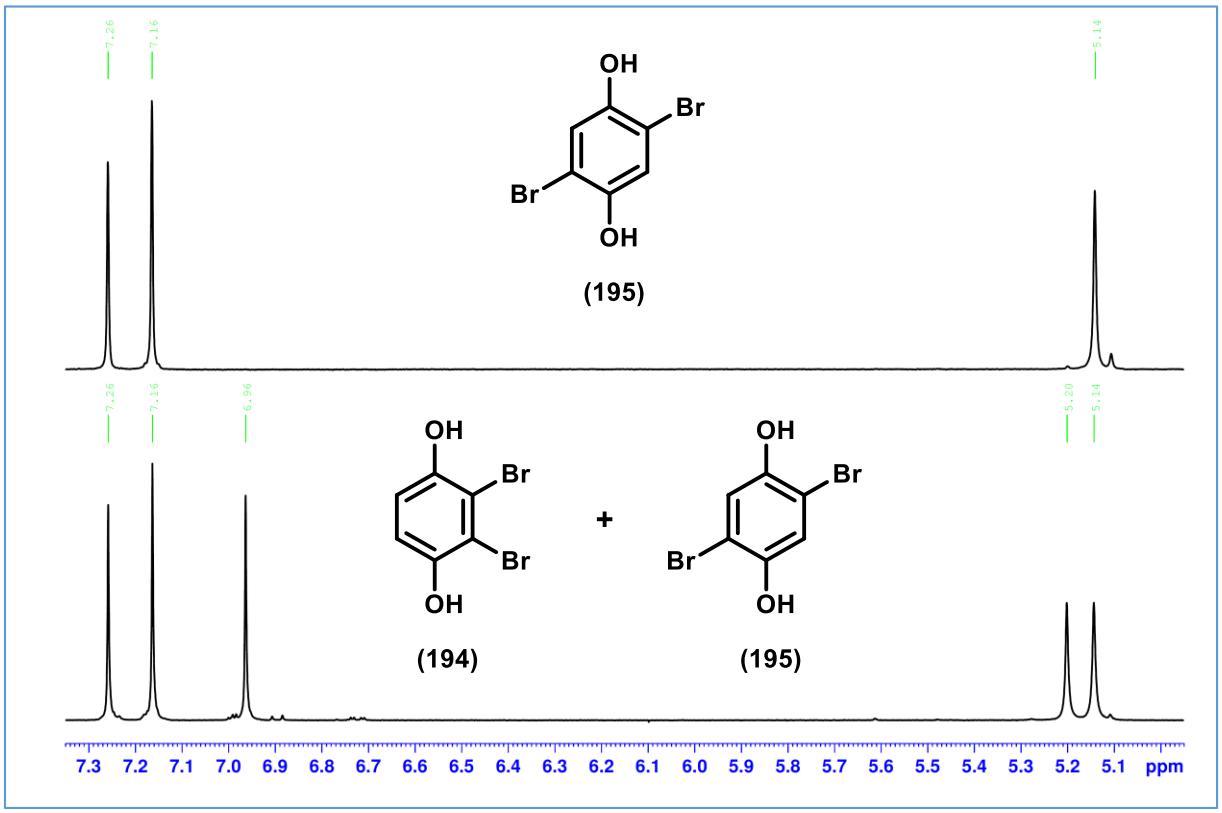


*Fig. 3-17: Comparison of ^{1}H-NMR spectra of 2,5-dibromobenzene-1,4-diol **(195)** (top) and a mixture of 2,3-dibromobenzene-1,4-diol **(194)** and 2,5-dibromobenzene-1,4-diol **(195)** (bottom)*

A similar comparison was performed with the ^{13}C-NMR spectra of the **194**/**195** mixture and the spectrum of 2,5-dibromobenzene-1,4-diol **(195)** to assign the ^{13}C-NMR signals for 2,3-dibromobenzene-1,4-diol **(194)** (see Figure 3-18). Again, the spectrum was simple, with only three signals representing all six carbon atoms in the symmetrical substrate **194**.

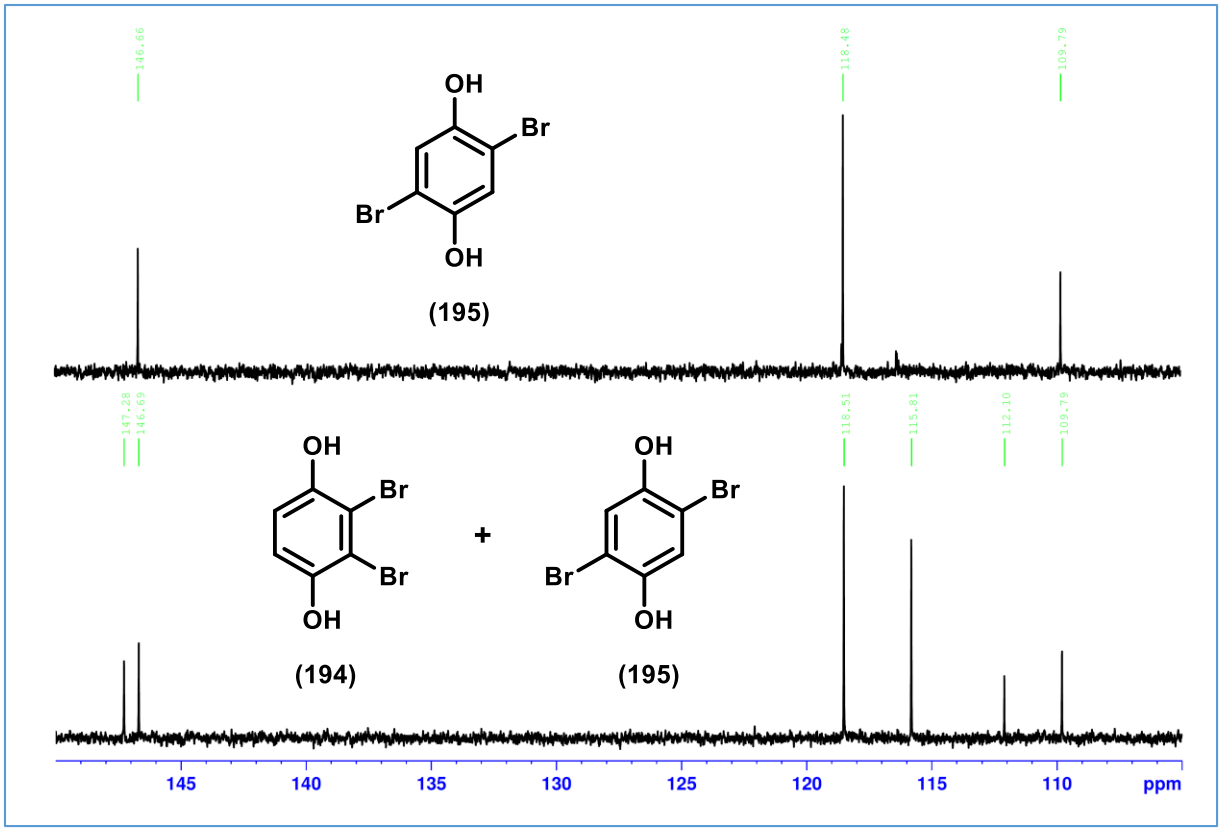


*Fig. 3-18: Comparison of ^{13}C-NMR spectra of 2,5-dibromobenzene-1,4-diol **(195)** (top) and a mixture of 2,3-dibromobenzene-1,4-diol **(194)** and 2,5-dibromobenzene-1,4-diol **(195)** (bottom)*

3.4 Synthesis of 2,3-Dibromo-1,4-bis(2-chloroethoxy) benzene (191)

Having established that it was not feasible to separate the precursor **194** from its 2,5-dibromo isomer **195**, it was decided to carry out step 3 in the reaction pathway to **90** using a mixture of both isomers. This step is the bis-alkylation to synthesise 2,3-dibromo-1,4-bis(2-chloroethoxy)benzene **(191)**. As the starting material **194** for the reaction was significantly contaminated with the 2,5-dibromo isomer **195**, it was expected that 2,5-dibromo-1,4-bis(2-chloroethoxy)benzene **(190)** would also be synthesised in at least 50 % yield, depending on the composition of the **194/195** mixture used as input material for the reaction.

A paper by Monte *et al.* suggested the use of potassium carbonate in acetone along with 1-bromo-2-chloroethane **(198)** as an alkylating reagent, a reaction which they reported gave a 32 % yield of **189** when performed on hydroquinone **(199)** as shown in Figure 3-19.[13]

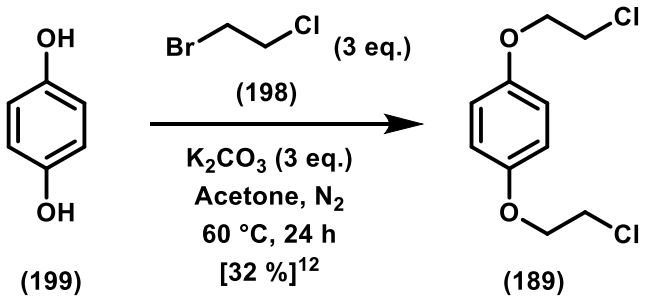


*Fig. 3-19: Alkylation of hydroquinone **(199)** as reported by Monte et al.[13]*

It was decided in this work to increase the reaction time using substrates **194/195** (in a ratio of **194**:**195** = 48:52) to determine if an increased yield could be recorded. A reaction was performed as shown in Figure 3-20, using the conditions set out by Monte *et al.*, but extending the reaction time from 24 to 48 h.[13]

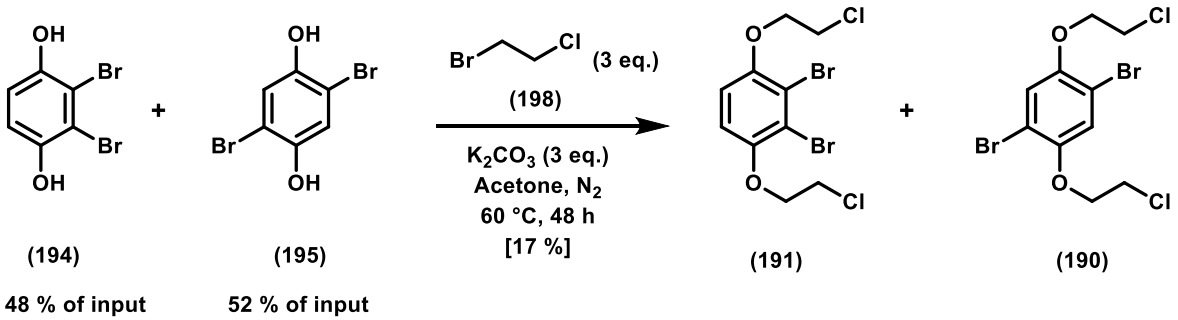


*Fig. 3-20: Alkylation of 2,3-dibromobenzene-1,4-diol **(194)** and its isomer 2,5-dibromobenzene-1,4-diol **(195)***

When the reaction was worked up and the crude mixture analysed by ^{1}H-NMR, it showed both the desired product **191** and its isomer **190**, however, the ratio of **191**:**190** based on integration values was 1:2.3, which was weighted towards the 2,5-dibromo isomer **190** more than expected, as the input material contained a ratio of **194**:**195** that was almost 1:1.

A sample of the 2,3-dibromo-1,4-bis(2-chloroethoxy)benzene **(191)** product was provided by ROC, as he had previously isolated it as a side product of a bromination reaction as detailed in Figure 3-1.[2] This was analysed by ^{1}H-NMR and was used to identify the signals for the product **191** in the ^{1}H-NMR spectrum of the crude reaction mixture from Figure 3-20, as shown in Figure 3-21.

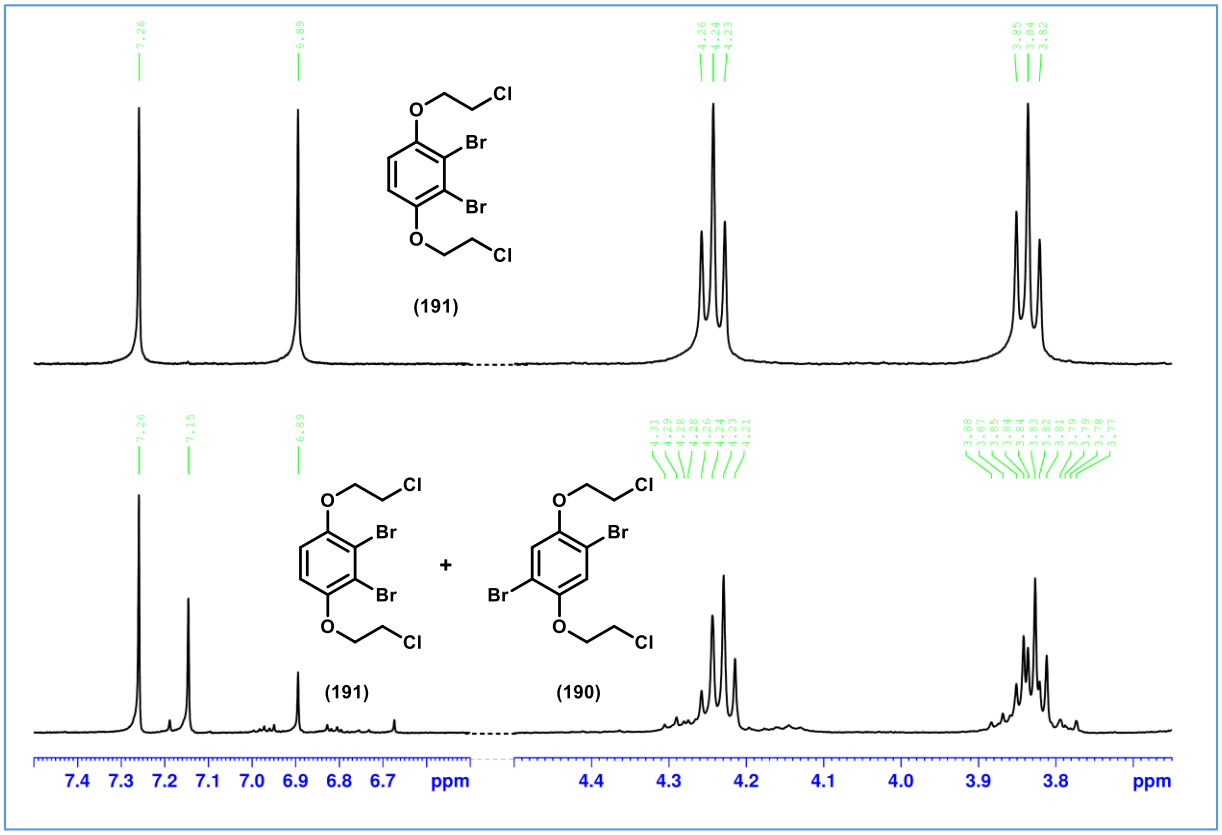


*Fig. 3-21: Comparison of ^{1}H-NMR spectra of pure 2,3-dibromo-1,4-bis(2-chloroethoxy)benzene **(191)** (top) and Figure 3-20 crude reaction mixture (bottom)*

This authentic sample of **191** was also used as a pure standard for TLC analysis, revealing that the product **191** had an R_f of 0.58 in a 2:1 hexane:ethyl acetate solvent system. The 2,5-dibromo isomer **190** had an R_f of 0.79, and it proved possible to separate the two isomers using preparative TLC. The isolated yields were very poor for both isomers, but did broadly reflect the product distribution seen in ^{1}H-NMR analysis of the crude reaction mixture: the isolated yield of 2,3-dibromo-1,4-bis(2-chloroethoxy)benzene **(191)** was 6.1 %

while the isolated yield of 2,5-dibromo-1,4-bis(2-chloroethoxy)benzene **(190)** was 11 %.

The aqueous layers from the work-up were combined, acidified to pH 1 and extracted with diethyl ether. When the crude residue was recovered *in vacuo* and analysed by ^{1}H-NMR spectroscopy, it revealed a complex mixture of unreacted starting materials **194/195** (which were the major components) and unknown organic impurities.

3.4.1 Optimisation of Alkylation to Synthesise 2,3-Dibromo-1,4-bis(2-chloroethoxy)benzene (191)

Given the disappointing yields and product distribution, it was decided to see if extending the reaction time further would improve either factor. A second procedure was carried out using the reaction conditions described in Figure 3-20, but the time was extended from 48 to 168 h. Unfortunately the work-up for this reaction encountered serious problems with emulsion formation (which was not seen during the work-up for the 48 h reaction), and only a very small amount of material could be isolated, which led to a very low and likely inaccurate yield of 11 % (combined **190** and **191**). Analysis of the crude reaction mixture by ^{1}H-NMR spectroscopy showed an even more unfavourable ratio of **191**:**190** of 1:4 relative to 1:2.3 ratio seen in the 48 h reaction (the ratio of starting materials **194**:**195** stayed the same at 48:52, or almost 1:1). Given the ratio of products and the difficulties with work-up, it was concluded that extension of the reaction time to 168 h was not beneficial to either yield or product distribution.

Next, the reaction time was adjusted to 70 h: still longer than the 48 h trialled initially (see Figure 3-20), in the hopes of increasing the yield, but shorter than the 168 h reaction which gave such problems with the work up. In addition, the equivalents of 1-bromo-2-chloroethane **(198)** were increased to determine if these parameter adjustments would favourably influence the yield (see Table 3-5). Procedures were performed as shown in Figure 3-22. All reactions had a starting material ratio of **194**:**195** = 48:52.

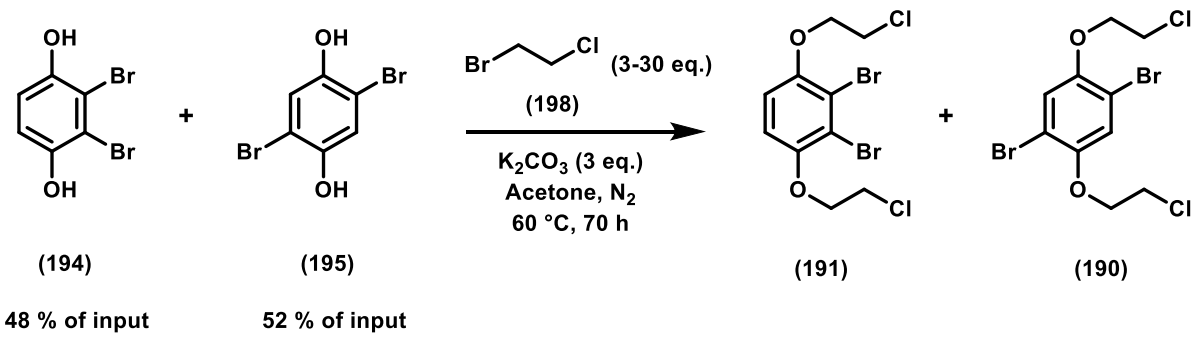


*Fig. 3-22: Synthesis of 2,3-dibromo-1,4-bis(2-chloroethoxy)benzene **(191)** with increased equivalents of 1-choro-2-bromobutane **(198)***

The results of these experiments, along with the results which were originally recorded for the 48 h reaction with three equivalents of 1-bromo-2-chloroethane **(198)**, are summarised in Table 3-5.

Equivalents of 198	Isolated yield of 191 [%]	Isolated yield of 190 [%]	Combined isolated yield [%]	191:190
3	6.1	11.2	17.3	1:1.8
6	7.0	17.4	24.4	1:2.5
12	12.8	23.2	36.0	1:1.8
30	14.0	23.2	37.2	1:1.7

*Table 3-5: Summary of results of increased 1-bromo-2-chloroethane **(198)** trials*

As can be seen in Table 3-5, the initial increase from 3 to 6 equivalents of 1-bromo-2-chloroethane **(198)** resulted in a ~ 7 % combined **190**/**191** yield increase but the product distribution ratio was worse at 1:2.5 **191**:**190**. The next increase from 6 to 12 equivalents of 1-bromo-2-chloroethane **(198)** also resulted in a combined yield increase, this time of over 11 % relative to the 6 eq. run, while the product distribution ratio changed from 1:2.5 to 1:1.8 **191**:**190**, back to the ratio previously observed for the 3 eq. reaction. This was a positive result, bringing the overall yield to slightly above that reported in the

literature while also increasing the proportion of the desired product in the reaction versus the 6 eq. reaction, however, as the ratio of isolated products is static in all other three trials, it is likely that the result of the 6 eq. reaction simply represents an unrelated decrease in successful isolation of **191**.[13]

The final increase from 12 to 30 equivalents of 1-bromo-2-chloroethane **(198)** did not result in a significant increase in combined yield (1.2 %), which is an increase that may well be attributed to slight differences in the efficacy of isolation between the two reactions rather than to greater conversion to product within the reaction. There was also a very slight increase in the ratio of **191**:**190**, changing from 1:1.8 to 1:1.7, however, again this is slight enough that it is more likely due to differences in isolation success than to increased conversion to the desired product **191**.

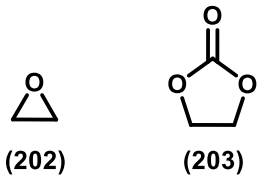
From this series of trials, it was concluded that increasing the equivalents of 1-bromo-2-chloroethane **(198)** from 3 to 12 led to the greatest increase in yield, but that increasing the equivalents beyond that leads only to negligible improvements. Product distribution appears static at ~ 1:2 **191**:**190**.

3.4.2 Alternate Route to 2,3-Dibromo-1,4-bis(2-chloroethoxy) benzene (191)

While the increase in yield described in Section 3.4.1 was positive, the product distribution ratio of the reaction ensured that the highest isolated yield of desired product **191** was only 14 %. It was therefore decided to investigate the possibility of an alternate, higher yielding route to 2,3-dibromo-1,4-bis(2-chloroethoxy)benzene **(191)**.

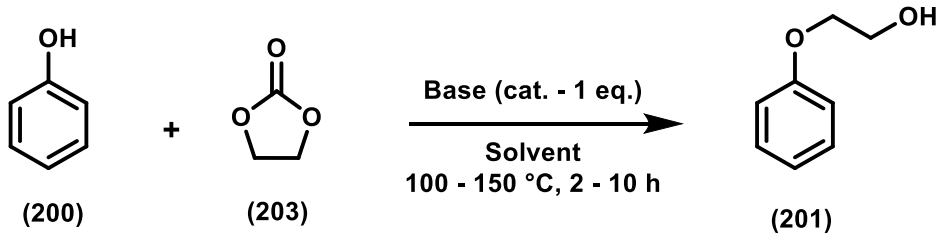
A literature search was performed, with a number of papers describing the conversion of phenol **(200)** to its alkylated analogue 2-phenoxyethanol **(201)**, bearing a terminal hydroxyl group instead of a chlorine atom.[14,15] This reaction is known as ethoxylation when performed using ethylene oxide **(202)** as a

reagent,[16] but the same result can be achieved using ethylene carbonate **(203)** as a reagent.



(202) **(203)**

For simplicity, ethoxylation in this thesis is taken to mean any reaction that results in the addition of an hydroxy ether chain (-CH_2CH_2OH) to a hydroxyl group. Yoshino *et al.* described a reaction in DMF using ethylene carbonate **(203)** as an alkylating agent and sodium hydride as a base,[14] while Carlson and Cretcher described a similar transformation in toluene, also using ethylene carbonate **(203)** as an alkylating reagent, but using either sodium hydroxide or potassium carbonate as base.[15] These approaches are summarised in Figure 3-23.



(200) **(203)** **(201)**

Fig. 3-23: Synthesis of 2-phenoxyethanol ***(201)***

It was envisioned for this work that if this approach could be used to synthesise the analogous compound 2,2'-((2,3-dibromo-1,4-phenylene)bis(oxy))diethanol **(204)**, this could then be converted to the chlorinated analogue **191** using thionyl chloride in a procedure already established in our group by ROC.[2] The new synthetic pathway to iTHBD **(90)** is outlined in Figure 3-24.

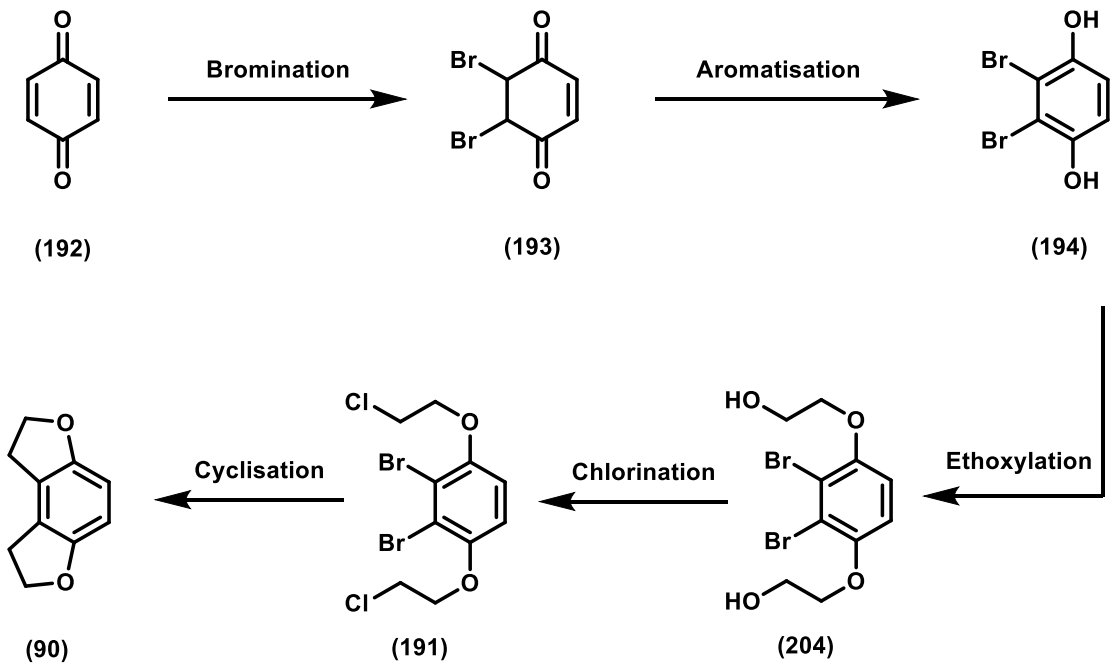


*Fig. 3-24: Updated proposed synthetic pathway to iTHBD **(90)***

While extending the number of steps in the synthetic pathway to increase overall yield may seem counterintuitive, both the reactions proposed (ethoxylation followed by chlorination) have literature yields of > 85 %, which would increase the overall yield compared to the 37 % recorded for the direct synthesis of **190** and **191** from their respective phenolic starting materials **195** and **194**. Yoshino *et al.* reported a yield of 89 % for their alkylation of phenol, while O'Connor reported a yield of 99 % for his conversion of a 2,2'-(1,4-phenylenebis(oxy))bis(ethan-1-ol) **(188)** to the chlorinated analogue 1,4-bis(2-chloroethoxy)benzene **(189)** using thionyl chloride.[2,14] This would give a potential overall yield of 88 % for the ethoxylation and chlorination steps.

*3.4.2.1 Synthesis of 2,2'-(1,4-Phenylenebis(oxy))diethanol **(188)***

It was decided to first investigate the synthesis of 2,2'-(1,4-phenylenebis(oxy)) diethanol **(188)** from hydroquinone **(199)**, which is available commercially, unlike its brominated analogue 2,3-dibromobenzene-1,4-diol **(194)**.

The first reaction attempted was an adaptation of that described by Yoshino *et al.*, using ethylene carbonate **(203)** and sodium hydride in DMF on a 4.5 mmol scale.[14] This can be seen in Figure 3-25.

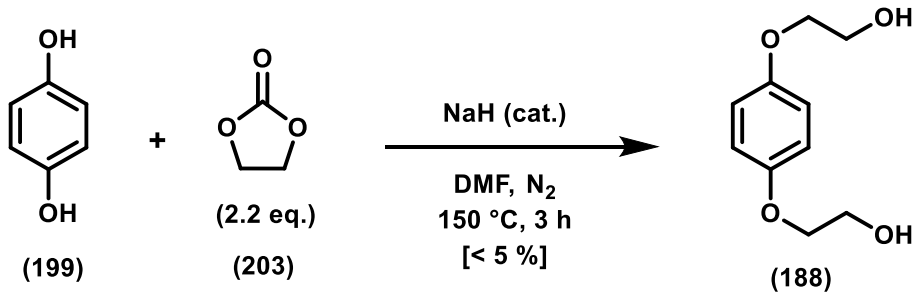


*Fig. 3-25: Ethoxylation of hydroquinone **(199)** using ethylene carbonate **(203)** and sodium hydride*

The work-up of this reaction proved challenging, as DMF was difficult to remove, requiring multiple washes and back-extractions. However, when crude product was isolated and analysed by ^{1}H-NMR, there were signals that potentially represented **188**. However, also present was clear evidence that indicated the presence of starting material **199**. The repeated washing during work-up had also resulted in a loss of crude product, and it was decided to attempt a conversion that excluded DMF in order to produce a workable yield (< 0.04 g **188** recovered, crude yield ~ 4.5 %).

With this in mind, the approach reported by Carlson and Cretcher was employed, using ethylene carbonate **(203)** as an ethoxylation agent, but using potassium carbonate as base and toluene as solvent.[14] This reaction is summarised in Figure 3-26.

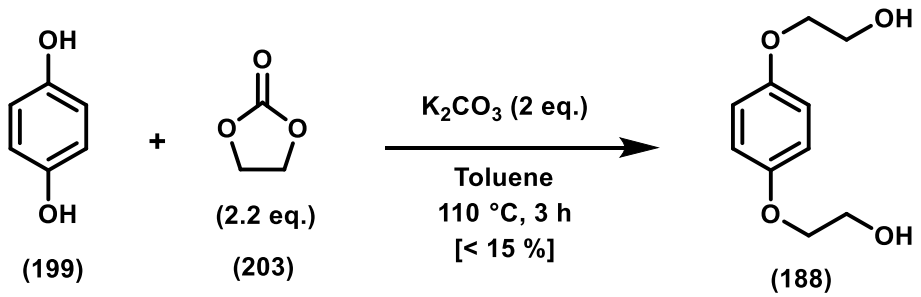


*Fig. 3-26: Ethoxylation of hydroquinone **(199)** using ethylene carbonate **(203)** and potassium carbonate*

The work-up for this reaction proceeded far more smoothly, however, when the crude product was isolated, the yield was disappointing. Based on the mass of product recovery and ^{1}H-NMR analysis, a total of ~14 % **188** was obtained in crude form, composed of a mixture of signals representing the starting material **199** and potential product **188**, as well as residual ethylene carbonate **(203)** (see Figure 3-27). Note that the hydroxyl proton signals for **199** and **188** did not appear.

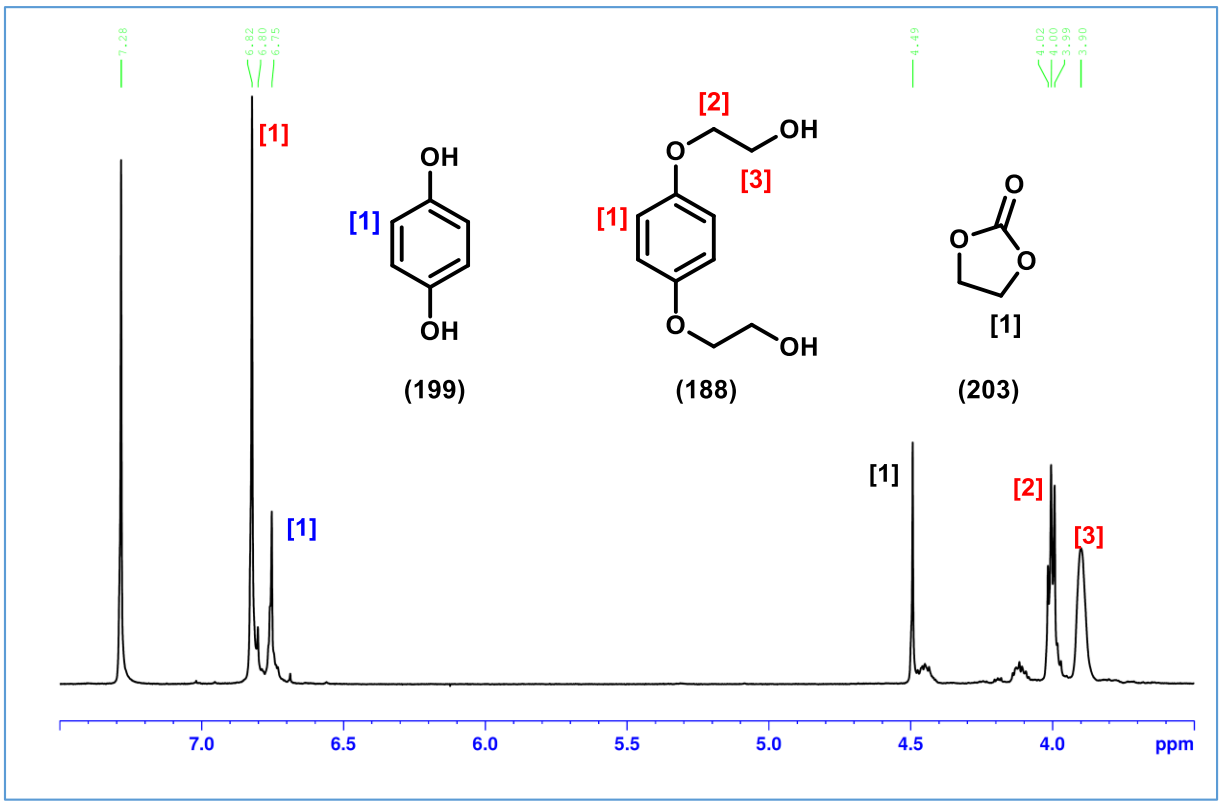


*Fig. 3-27: ^{1}H-NMR spectrum of a crude mixture of **199**, **188** and **203***

At this point, the equivalents of ethylene carbonate **(203)** being used in the reaction were examined. Yoshino *et al.*[14] and Carlson and Cretcher[15] used 1.1 and 2.5 equivalents respectively. In our work, the protocol of Yoshino *et al*. was followed, with 1.1 equivalents of ethylene carbonate **(203)** used per hydroxyl group.

It was also noted that ethylene carbonate **(203)** has a melting point of 34 - 37 °C, and has been used as a highly polar aprotic solvent (in the same class as DMF) for reactions.[17] Using ethylene carbonate **(203)** in higher

stoichiometric quantities as a combined solvent/reagent in this work (as seen in Figure 3-28), it was hoped that the increased equivalents would improve the yield of **188**, and that the work-up would be simplified.

A reaction was therefore performed as described in Figure 3-28, with ethylene carbonate **(203)** used as both reactant and solvent.

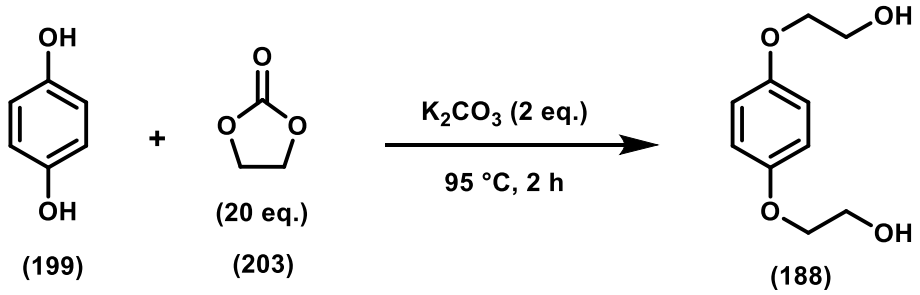


*Fig. 3-28: Ethoxylation of hydroquinone **(199)** using ethylene carbonate **(203)** as a solvent and a reagent*

The crude reaction mixture was worked up and analysed by ^{1}H-NMR, which showed an overwhelming majority of excess ethylene carbonate **(203)** and signals which potentially represented the product **188**. There was no evidence of any remaining starting material **199**. The mixture was purified by column chromatography on silica gel, which removed the majority of ethylene carbonate **(203)** and isolated partially pure product **188**, with traces of ethylene carbonate **(203)** (<5 % by ^{1}H-NMR integration). Small amounts of concentrated sulphuric acid were added to the partially pure product in attempt to destroy the ethylene carbonate **(203)**, as organic carbonates react with acids to form carbon dioxide, water and a salt.[18] However, this addition also degraded the product, and it was noted that in future, extra acid washes (dilute acid rather than concentrated) in the work-up procedure would be more appropriate for removing ethylene carbonate **(203)**.

Due to the degradation of product, it was not possible to calculate a yield for this first reaction (Figure 3-28), but as the results seemed positive, it was decided to repeat the reaction with fewer equivalents of ethylene carbonate **(203)**, in an attempt to eliminate complications with excess reagent. A second

reaction was performed as described in Figure 3-28, reducing the equivalents of ethylene carbonate **(203)** from 20 to 10.

When this reaction was worked up and analysed by ^{1}H-NMR, it thankfully showed that the crude reaction mixture contained a majority of the desired product **188**, along with some unknown organic impurities, but no starting material **199** or ethylene carbonate **(203)** were seen. The crude mixture was purified by column chromatography on silica gel, which returned pure product, however, the yield was poor at 28 %, falling far short of the 89 % reported by Yoshino *et al.*[14]

At this point, the work of Carlson and Cretcher was revisited; they had performed a variation on the reaction wherein they pre-formed the phenoxide anion by dissolving the starting material **200** in methanol and stirring with sodium hydroxide for one hour.[15] They then removed the methanol *in vacuo*, suspended the resultant salt in toluene and reacted the substrate with ethylene carbonate **(203)** to form **201** in 94 % yield. A variation of this reaction was attempted in this work as described in Figure 3-29, with the toluene omitted and the equivalents of ethylene carbonate **(203)** increased from 2.5 to 10, functioning as both reagent and solvent.

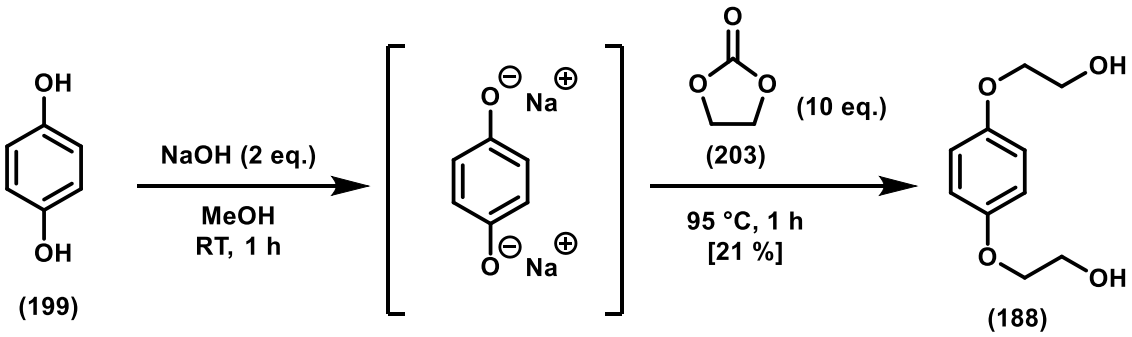


*Fig. 3-29: Ethoxylation of hydroquinone **(199)** using ethylene carbonate **(202)** and sodium hydroxide*

The reaction was difficult to handle physically: the disodium salt of **199** formed after removal of methanol *in vacuo* was cement-like in appearance and proved very difficult to remove from the walls of the reaction vessel in order to dissolve it in ethylene carbonate **(203)**. The work-up after the final step was also

challenging, with the formation of emulsions during acid washes. When the crude reaction mixture (**188** in Figure 3-29) was analysed by ^{1}H-NMR, it showed a majority of product **188**, with some unknown organic impurities, but no starting material **199** or ethylene carbonate **(203)**.

The crude reaction mixture was purified by preparative TLC, from which pure product was recovered, however, the yield was no better than the reaction with potassium carbonate (21 %). Given the difficulties with handling the reaction and the lack of increased yield, it was decided to return to the reaction as described in Figure 3-28, with a lengthened reaction time (increased from 2 to 24 h) and a change to 15 equivalents of ethylene carbonate **(203)**. These new reaction conditions are illustrated in Figure 3-30.

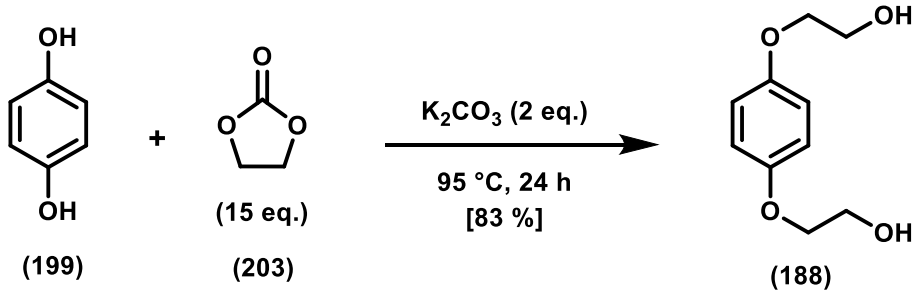


*Fig. 3-30: Ethoxylation of hydroquinone **(199)** using ethylene carbonate **(202)** and potassium carbonate*

Aside from the change in reaction conditions, there was also a modification to the work-up, which involved the acidification of the crude reaction to quench excess potassium carbonate remaining in solution. In previous reactions, the reaction mixture had been acidified to ~pH 6 using concentrated sulfuric acid, an adjustment which was monitored using universal indicator paper. However, for this reaction it was decided to acidify only to pH 7, and to do so accurately using a calibrated pH meter. This was due to concerns that over-acidification was leading to degradation of product, as was seen when concentrated sulfuric acid was added to a previous reaction to quench excess ethylene carbonate **(203)**.

When the reaction was worked up using the adjusted procedure after the extended reaction time, analysis by ^{1}H-NMR showed a mixture of product **188**

(89 %) and intermediate **205** (11 %), as seen in Figure 3-31. No signals representing starting materials **199** or **203** were evident. These percentages were calculated using the integration of aromatic signals in the ^{1}H-NMR spectrum, which could be definitively assigned to one of the substrates. The signals are indicated in Figure 3-31.

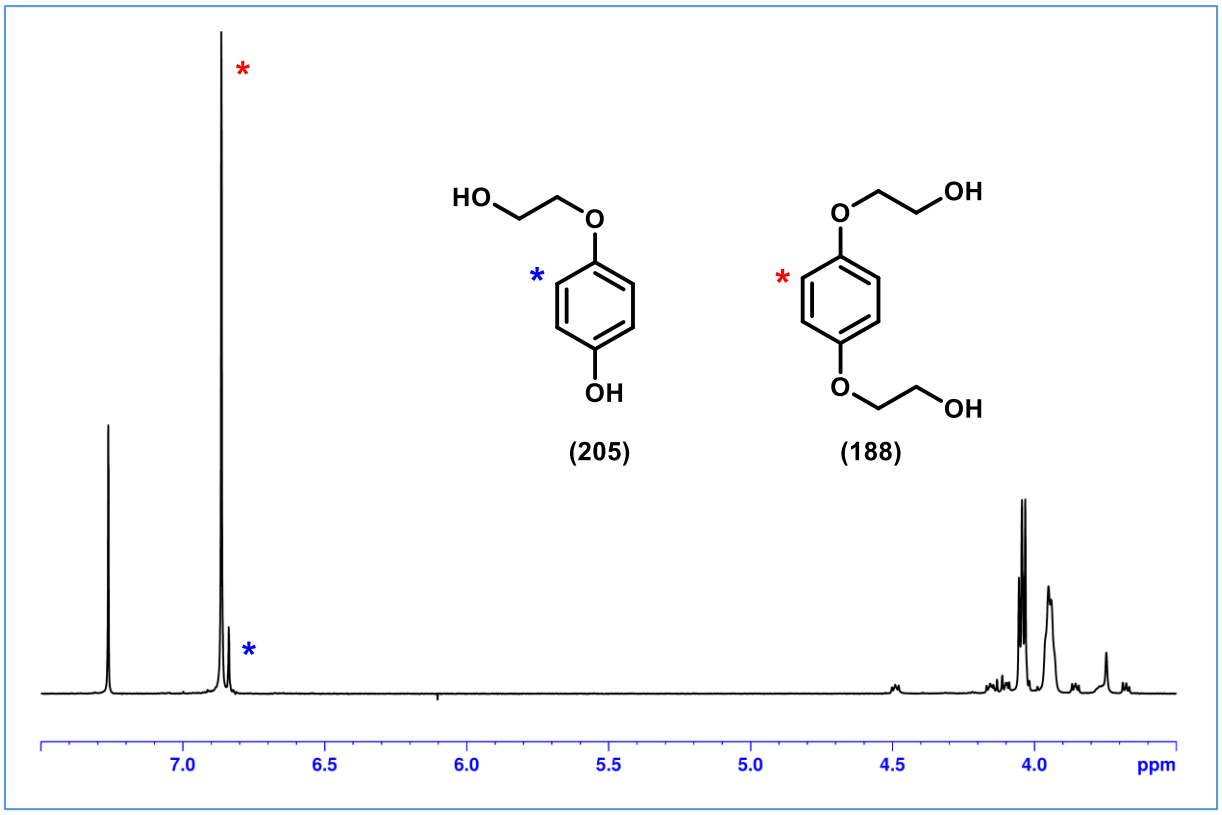


*Fig. 3-31: ^{1}H-NMR spectrum of crude reaction mixture containing **188** and **205***

The fact that this reaction showed the presence of intermediate **205** when a previous reaction with a shorter reaction time and fewer equivalents of ethylene carbonate **(203)** appeared to have no traces suggests that over-acidification during the work-up was likely leading to degradation of product **188** and intermediate **205**.

The crude material was a crystalline solid and it was decided to attempt recrystallisation as an alternative method of purification to column chromatography. Literature sources suggested the use of toluene, methanol and ethanol as recrystallisation solvents for analogous substrates,[14,19] and so each of these was trialled using a small amount of crude material.

The recrystallisations using methanol and ethanol both failed: the crude material dissolved in small amounts of both solvents when heated, but could not be induced to recrystallise. The recrystallisation from toluene was partially successful: when cooled to room temperature, crystallisation occurred without issue. However, when the recrystallised material was analysed by ^{1}H-NMR, it was found to be a mixture of product **188** (90 %) and mono-ethoxylated material **205** (10%). This is almost identical to their ratio in the crude before the recrystallisation, suggesting that they have similar solubilities and crystallisation characteristics in toluene.

Having failed to purify **188** by recrystallisation, it was decided to return to column chromatography on silica gel to purify the product. This was carried out successfully and the pure product **188** was recovered in 83 % yield, a significant improvement over previous attempts, and much closer to the literature value of 89 % reported by Yoshino *et al.*[14]

Based on the results of extending the reaction time and increasing the equivalents of ethylene carbonate **(203)**, a further modification (as shown in Figure 3-32) was enacted, increasing the equivalents of potassium carbonate from 2 to 3, and extending the reaction time further from 24 to 36 hours to see if complete conversion to product could be achieved.

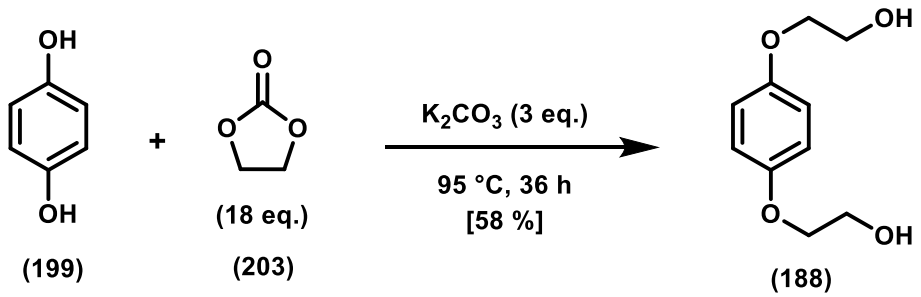


*Fig. 3-32: Further modification of the ethoxylation of hydroquinone **(199)** using ethylene carbonate **(203)** and potassium carbonate*

While it was originally intended to maintain the same equivalents of ethylene carbonate **(203)**, it was necessary to increase this figure from 15 to 18 as the addition of an extra equivalent of potassium carbonate made the reaction more

viscous and difficult to stir. The work-up with accurate acidification to pH 7 was maintained as per the previous reaction.

When the crude reaction mixture was analysed by ^{1}H-NMR, it showed a mixture of product **188** (95 %) and intermediate **205** (5 %). The ratio of product **188** to intermediate **205** was improved to 21:1 for this reaction compared to 9:1 for the reaction with 15 eq. of **203**. However, when the crude reaction mixture was purified by column chromatography on silica gel, the yield of **188** was only 58 %, a decrease of over 20 % with no obvious cause except the increased equivalents of potassium carbonate in the reaction. Based on this result, it was decided to keep the equivalents of potassium carbonate in any future reactions at a maximum of 2.2 equivalents, and to decrease the equivalents of ethylene carbonate **(203)** back to 15.

*3.4.2.2 Synthesis of 2,2'-((2,3-Dibromo-1,4-phenylene)bis(oxy))diethanol **(204)***

Having determined the optimal conditions for the ethoxylation of hydroquinone **(199)**, it was decided to apply these conditions to the conversion of 2,3-dibromobenzene-1,4-diol **(194)** and its 2,5-dibromo isomer **195** to 2,2′-((2,3-dibromo-1,4-phenylene)bis(oxy))diethanol **(204)** and 2,2′-((2,5-dibromo-1,4-phenylene)bis(oxy))diethanol **(206)** respectively. This reaction is described in Figure 3-33.

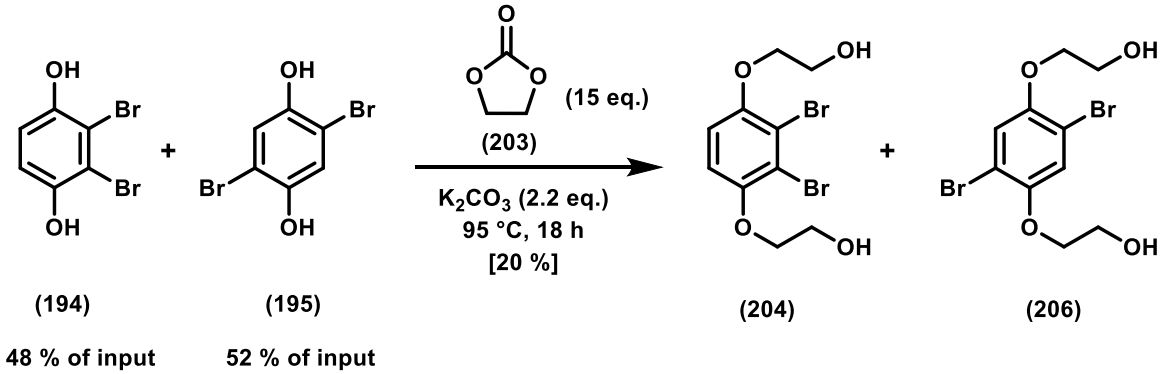


*Fig. 3-33: Synthesis of **204** and **206** using ethylene carbonate **(203)** and potassium carbonate*

The reaction was worked up and analysed by ^{1}H-NMR, which revealed a mixture of both expected products **204** and **206**, along with ethylene carbonate **(203)** and other unknown organic impurities. A sample of pure **206** was provided by ROC,[20] and this was used to definitively identify the signal for the aromatic proton at 7.16 ppm in the 2,5-dibromo isomer **206**.

The ratio of **204** to **206** was approximately 1:2 when calculated from integration of signals in the crude ^{1}H-NMR spectrum. The ratio of the 2,3 [**194**] to 2,5 [**195**] isomers in the starting material mixture was approximately 1:1, but the shift towards the 2,5-dibromo isomer **206** was not unexpected, as it had been seen previously when attempting to directly synthesise 2,3-dibromo-1,4-bis(2-chloroethoxy)benzene **(191)** from a 1:1 mixture of **194** and **195** (see Section 3.4.1).

The crude reaction mixture was purified by preparative TLC (^{1}H-NMR spectra of both products can be seen in Figure 2-34) and the resulting combined yield of **204** and **206** was ~20 % (7 % **204**, 13 % **206**, both isolated yields), which was very low compared to the 83 % yield of 2,2′-(1,4-phenylenebis(oxy))diethanol **(188)** in the optimised ethoxylation reaction. It was also lower than the 14 % yield seen in Section 3.4.1 for 2,3-dibromo-1,4-bis(2-chloroethoxy)benzene **(191)** synthesised directly from the hydroquinone starting material **194**.

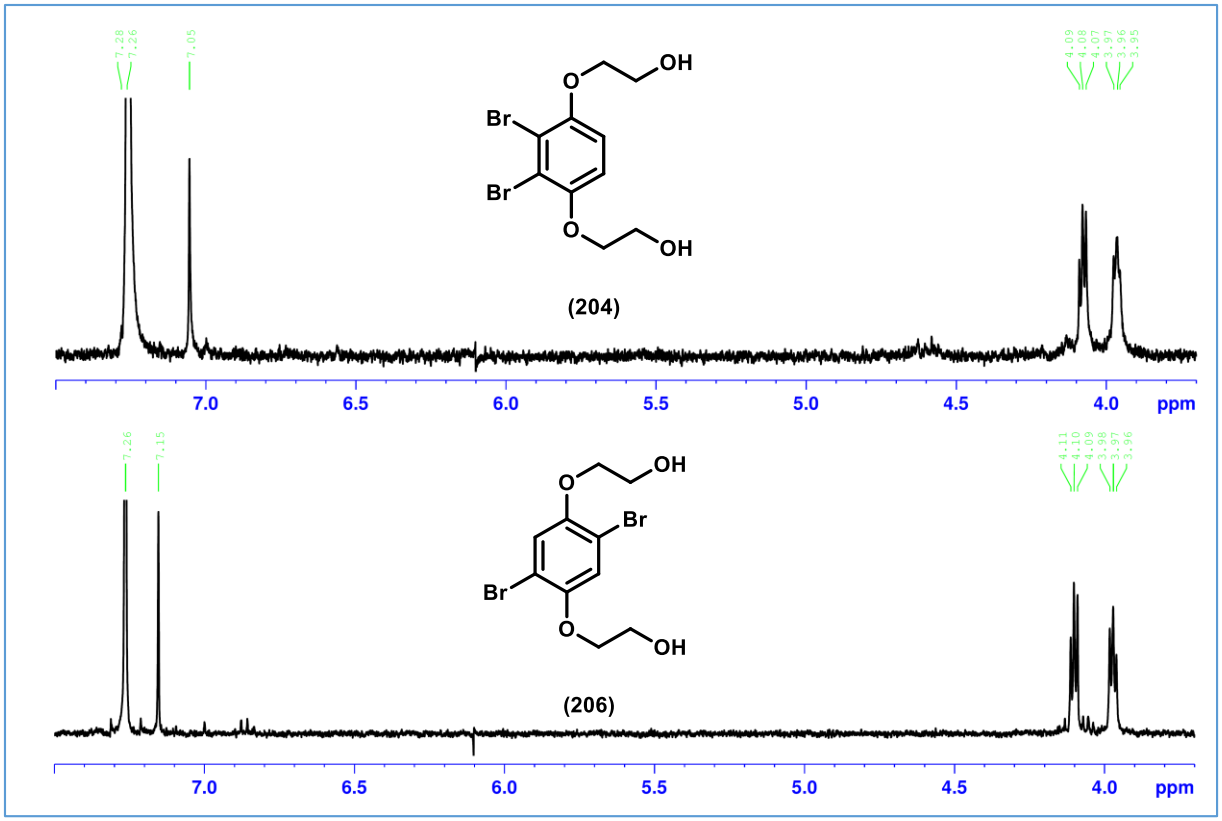


*Fig. 3-34: ^{1}H-NMR spectra of **204** (top) and **206** (bottom)*

Note that in this figure, the signal at 7.26 ppm represents chloroform.

From this result, it became obvious that the conditions which had been optimised for the ethoxylation of hydroquinone **(199)** were not optimal for the dibrominated analogue **194**. It was decided to see if doing the reaction in toluene as originally reported by Yoshino *et al.* would positively impact the product distribution ratio.[14] This reaction is described in Figure 3-35.

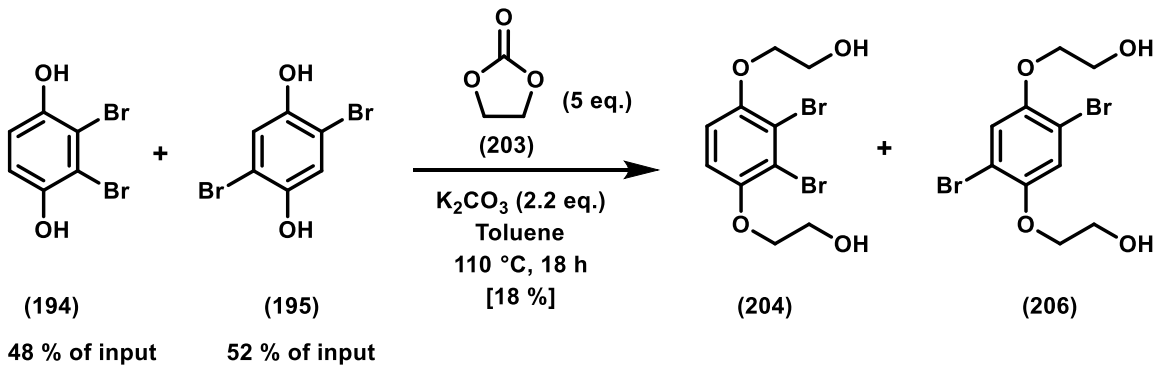


*Fig. 3-35: Modified synthesis of **204** and **206** using toluene as a solvent*

When this reaction was worked up and the crude product analysed by ^{1}H-NMR, the composition of the crude was broadly the same as the reaction depicted in Figure 3-33: unknown organic impurities, ethylene carbonate **(203)** and both products **204** and **206**. However, comparison of the integration values of signals in the ^{1}H-NMR spectrum revealed that the ratio of **204**:**206** had become even more unfavourable, changing from 1:2 to 1:5.

When the crude mixture was purified by preparative TLC, the combined **204**/**206** yield was slightly poorer (18 %) than the reaction from Figure 3-33, and the product distribution meant that the comparative yield of 2,2′-((2,3-dibromo-1,4-phenylene)bis(oxy))diethanol **(204)** was even less favourable (3 %). It was concluded that the approach of using ethylene carbonate **(203)** and potassium carbonate, which had worked well in the synthesis of 2,2′-(1,4-phenylenebis(oxy))diethanol **(188)**, was not applicable to the dibrominated analogue **204**.

At this stage a brief investigation of other base/solvent combinations as mentioned by Yoshino *et al.* and Pirrung *et al.* was conducted, to see if any of these would be favourable in terms of yield increase and/or product distribution ratio.[14,19] A general scheme for these reactions can be seen in Figure 3-36.

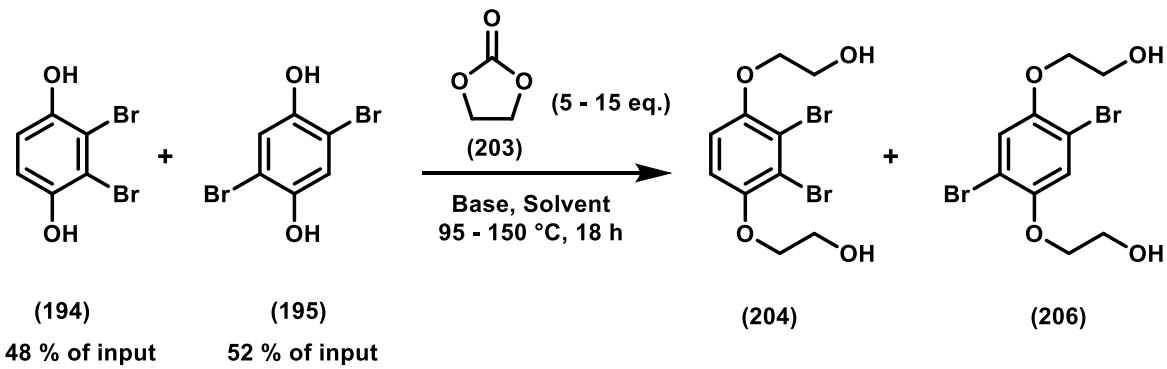


*Fig. 3-36: Base and solvent screen for the synthesis of 2,2′-((2,3-dibromo-1,4-phenylene)bis(oxy))diethanol **(204)** using ethylene carbonate **(203)***

The bases, solvents and results of this reagent screen can be seen in Table 3-6.

Base [Equivalents]	Solvent	Ratio of 204:206	Combined Yield (%)
Cs_2CO_3 [2.5 eq.]	DMF	1:5	5.8
NaH [2.5 eq.]	DMF	1:8	Not Purified
NaOH [0.85 eq]	Ethylene Carbonate	1:2.5	Not Purified

Table 3-6: Reagent screen for the synthesis of 2,2'-((2,3-dibromo-1,4-phenylene)bis(oxy))diethanol ***(204)***

As can be seen in Table 3-6, none of the altered conditions led to an improvement in product distribution. Reactions performed in DMF with caesium carbonate and sodium hydride lead to significant worsening of the product distribution ratio. The reactions carried out with sodium hydride and sodium hydroxide were not purified, as the crude mass recovery was so low that it was determined the yields in both cases would be < 5 %.

During all reactions using 2,3-dibromobenzene-1,4-diol **(194)** (and the inseparable 2,5-dibromo isomer **195**) as a starting material, the work-ups were significantly less straightforward than those done with hydroquinone **(199)** as a starting material. All aqueous washes of the crude reaction mixture dissolved in organic solvent resulted in the formation of emulsions, which required long settle times, and sometimes addition of brine or application of heat to facilitate separation. In all cases, even after these measures were taken, there was still an emulsified layer, the extent of which varied from reaction to reaction. These emulsions likely caused significant product loss to the aqueous layer.

In an effort to explain this increased emulsification during work up, a literature search for ethoxylation was performed, which quickly revealed that ethoxylation is commonly used in the production of non-ionic surfactants.[21,22] This is usually achieved by the reaction of a fatty alcohol with ethylene oxide, as shown in Figure 3-37.

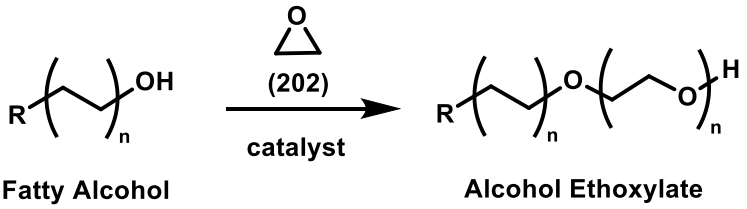


Fig. 3-37: Synthesis of Alcohol Ethoxylate[22]

Based on the emulsification seen during the work-up of 2,2′-((2,3-dibromo-1,4-phenylene)bis(oxy))diethanol **(204)** (and its 2,5-dibromo isomer **206**), the products were likely acting as surfactants, with the dibrominated aromatic core forming the lipophilic portion, and hydroxyl groups forming the hydrophilic portion. It is hypothesised that 2,2′-(1,4-phenylenebis(oxy))diethanol **(188)** is not as lipophilic at its core, and that the addition of two bromine atoms increased the lipophilic properties of **204** and **206**. This hypothesis is based on the fact that the surfactant effect was not seen when synthesising **188** using an otherwise identical procedure.

Given the slower conversion, unfavourable product distribution ratio, low yields and work-up problems which were intrinsic to the structure of 2,2′-((2,3-dibromo-1,4-phenylene)bis(oxy))diethanol **(204)**, this alternate synthetic pathway to 2,3-dibromo-1,4-bis(2-chloroethoxy)benzene **(191)** was not worth pursuing, and the line of research was discontinued without performing the chlorination step with $SOCl_2$.

3.4.3 Characterisation of 190, 191, 204 and 206

All substrates synthesised during optimisation of the alkylation and ethoxylation steps of the synthetic pathway to **90** were fully characterised, as shown in Table 3-7. This does not include 2,2′-(1,4-phenylenebis(oxy)) diethanol **(188)**, a compound which is both commercially available and well known in literature.[2,23]

Compound Number	Yield (%)	m.p. (°C) *[Lit. m.p.]*	R_f (Hex:EtOAc)	IR v_{max} (cm^{-1})	HRMS (*m/z*)	
					Calc.	Found
191	14	90 - 93 (MeOH) *[91 - 93[2] (MeOH)]*	0.58 (2:1)	N/A*	392.8474	392.8452
190	23	117 - 119 (EtOH) *[118 - 120[2] (EtOH)]*	0.79 (2:1)	N/A*	392.8474	Not Found
204	7	105 - 106 (Toluene) [Novel]	0.48 (1:1)	O-H: 3351	354.9175	Not Found
206	13	132 - 134 (Toluene) [N/A]	0.61 (1:1)	O-H: 3352	354.9175	354.9181

*Table 3-7: Yield, m.p., R_f, IR and HRMS of **190**, **191**, **204** and **206***

*While IR data were recorded for these compounds, none of the signals were so distinctive as to be diagnostic.

In addition, ^{1}H- and ^{13}C-NMR data were recorded for each compound. The ^{1}H-NMR spectra of **190** and **191** were very similar, with the only significant difference being the change in chemical shift of the aromatic protons (there are two magnetically equivalent aromatic protons on each substrate): the aromatic signal in **191** appeared at 6.89 ppm, while the equivalent aromatic signal in **190** was evident at 7.14 ppm. Both **190** and **191** had triplets representing the ethoxy protons at ~3.8 ppm (O-CH_2-C**H_2**-Cl) and ~4.2 ppm (O-C**H_2**-CH_2-Cl).

The ^{13}C-NMR spectra of **190** and **191** were also alike, with ethoxy carbon atom signals (O-**C**H_2-**C**H_2-Cl) coinciding and shifts of only 1 - 2 ppm seen in the signals representing aromatic carbon atoms. This was also true of non-

chlorinated analogues **204** and **206**. The only significant difference between the ^{13}C-NMR spectra of the chlorinated (**190** and **191**) and non-chlorinated (**204** and **206**) substrates was a change in signal shift of ~20 ppm from 41.5 ppm for **C**H$_2$-Cl in **190/191** to 61.3 ppm for **C**H$_2$-OH in **204/206**. Full assignment of the ^{13}C-NMR signals recorded are depicted in Figure 3-38.

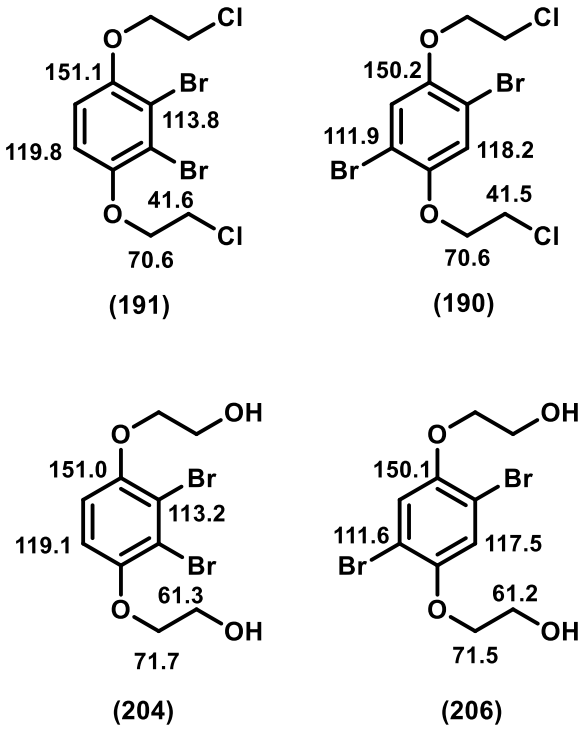


*Fig. 3-38: ^{13}C-NMR signal assignments of **190**, **191**, **204** and **206***

The ^{1}H-NMR spectra of non-chlorinated compounds **204** and **206** were also similar, with the only significant difference again being the variation in chemical shift between the analogous aromatic proton signals: the aromatic proton signal for the 2,5-dibromo isomer **206** was seen at 7.16 ppm, while the analogous aromatic proton signal for the 2,3-dibromo isomer **204** was observed at 7.06 ppm. The ethoxy protons for both substrates were located at ~4.0 ppm (O-CH$_2$-C**H$_2$**-OH) and ~4.1 ppm (O-C**H$_2$**-CH$_2$-OH).

3.5 Synthesis of 1,2,7,8-Tetrahydrobenzo[1,2-*b*:4,3-*b'*] difuran (90)

Having synthesised the precursor 2,3-dibromo-1,4-bis(2-chloroethoxy) benzene **(191)** albeit in low yields, attention was turned to the synthesis of our ultimate target, 1,2,7,8-tetrahydrobenzo[1,2-*b*:4,3-*b'*]difuran **(90)**, referred to as iTHBD throughout this thesis. A review of the literature for similar annulation reactions revealed generally two approaches adopted for reactions of this kind. The first employs *n*-BuLi to form a lithiated compound that acts like an aryl anion, followed by an intramolecular S_N2 cyclisation reaction, nucleophilically displacing chlorine in the chloroethoxy ether. The second approach employs a Grignard reaction. A general mechanism for the synthesis of iTHBD **(90)** from 2,3-dibromo-1,4-bis(2-chloroethoxy)benzene **(191)** is shown in Figure 3-39.

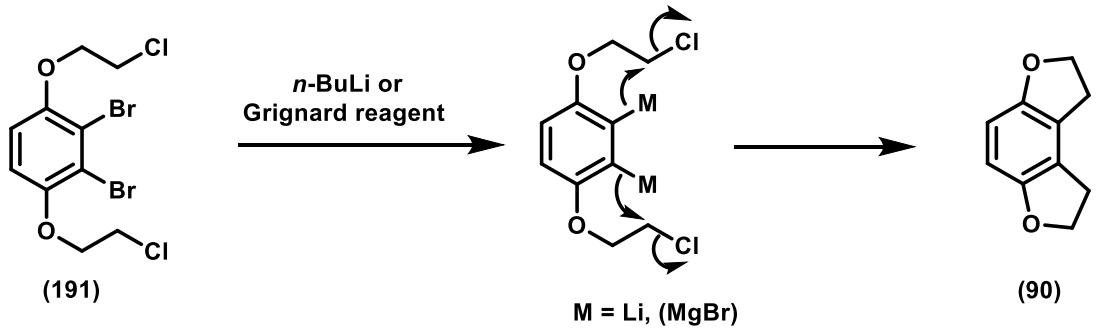


*Fig. 3-39: General mechanism for the synthesis of iTHBD **(90)** from 2,3-dibromo-1,4-bis(2-chloroethoxy)benzene **(191)***

3.5.1 Annulation of 191 Employing *n*-BuLi

The *n*-BuLi-facilitated transformation was investigated initially, with several literature sources reporting analogous reactions. Monte *et al.* synthesised THBD **(42)** on a 25 mmol scale using *n*-BuLi with 2,5-dibromo-1,4-bis(2-chloroethoxy)benzene **(190)** as a starting material.[13] This procedure was unusual in that the reaction was performed at 0 °C (the norm for *n*-BuLi reactions is – 78 °C, as described in Chapter 2), and had a reaction time of only 15 minutes. They also reported the *n*-BuLi addition rate was critical to

reaction yield: addition over 7 seconds gave a yield of **42** of 80 %, while an identical reaction with *n*-BuLi addition over 40 seconds led to a 25 % yield reduction.

Based on this information, a reaction was performed in this work using identical conditions on a 2.6 mmol scale with 2,3-dibromo-1,4-bis(2-chloroethoxy)benzene **(191)** as starting material. The *n*-BuLi addition was not timed, but was added as fast as possible, and is estimated to have been < 15 seconds. A summary of the reaction can be seen in Figure 3-40.

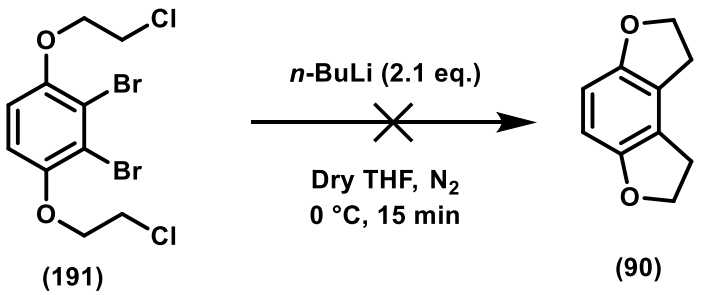


*Fig. 3-40: Attempted synthesis of iTHBD **(90)** using n-BuLi*

The reaction was worked up and analysed, showing a complex mixture of organic compounds both by TLC and ^{1}H-NMR analysis. An attempt was made at purifying the crude reaction mixture by column chromatography on silica gel (the eluent was a gradient from 5:1 → 3:1 hexane:ethyl acetate). However, when analysed by ^{1}H-NMR, all fractions were shown to contain an inseparable mixture of unidentifiable organic compounds. No definitive signs of the desired product **90** could be identified in any of the ^{1}H-NMR spectra. It was hypothesised that a more standard approach to the *n*-BuLi reaction (i.e. with a reaction temperature of – 78 °C and a reaction time > 24 h) might yield better results.

The paper by Monte *et al.*[13] cited another paper by Parham *et al.*[24] as the basis of their *n*-BuLi methodology. However, the synthesis detailed by Parham *et al.*[24] reported the addition of *n*-BuLi at – 100 °C, followed by a 1 h stir at that temperature before warming to room temperature and allowing to stir for 24 h. This experimental detail aligns more closely with *n*-BuLi reactions performed previously in this work, for example, the formation of boronic acids

using *n*-BuLi as described by Redondo *et al.* and referenced in Chapter 2.[25] The reaction performed in this work towards the synthesis of **90** from **191** based on the experimental described by Parham *et al.* can be seen in Figure 3-41 (note that this is referred to as Reaction 1 later in the chapter).[24]

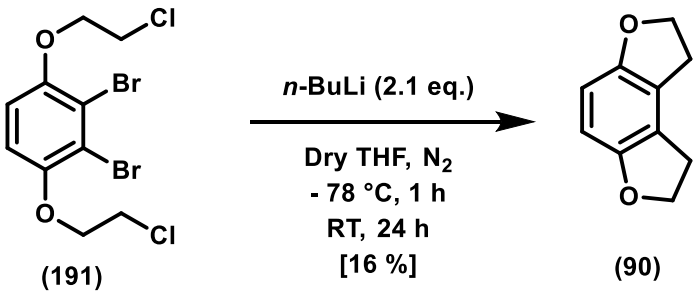


*Fig. 3-41: Modified synthesis of iTHBD **(90)** using n-BuLi*

Post work-up, ^{1}H-NMR analysis of the crude product revealed a mixture of starting material **191**, product **90** and a number of unknown organic compounds (signals assigned to **90** were determined by comparing the data to a sample of iTHBD **(90)** produced by ROC).[2] The crude reaction mixture was purified by preparative TLC, which produced several fractions containing only starting material **191** and product **90**. These fractions were triturated with hexane to give iTHBD **(90)** in 16 % isolated yield. The sample was pure when analysed by ^{1}H-NMR, as seen in Figure 3-42.

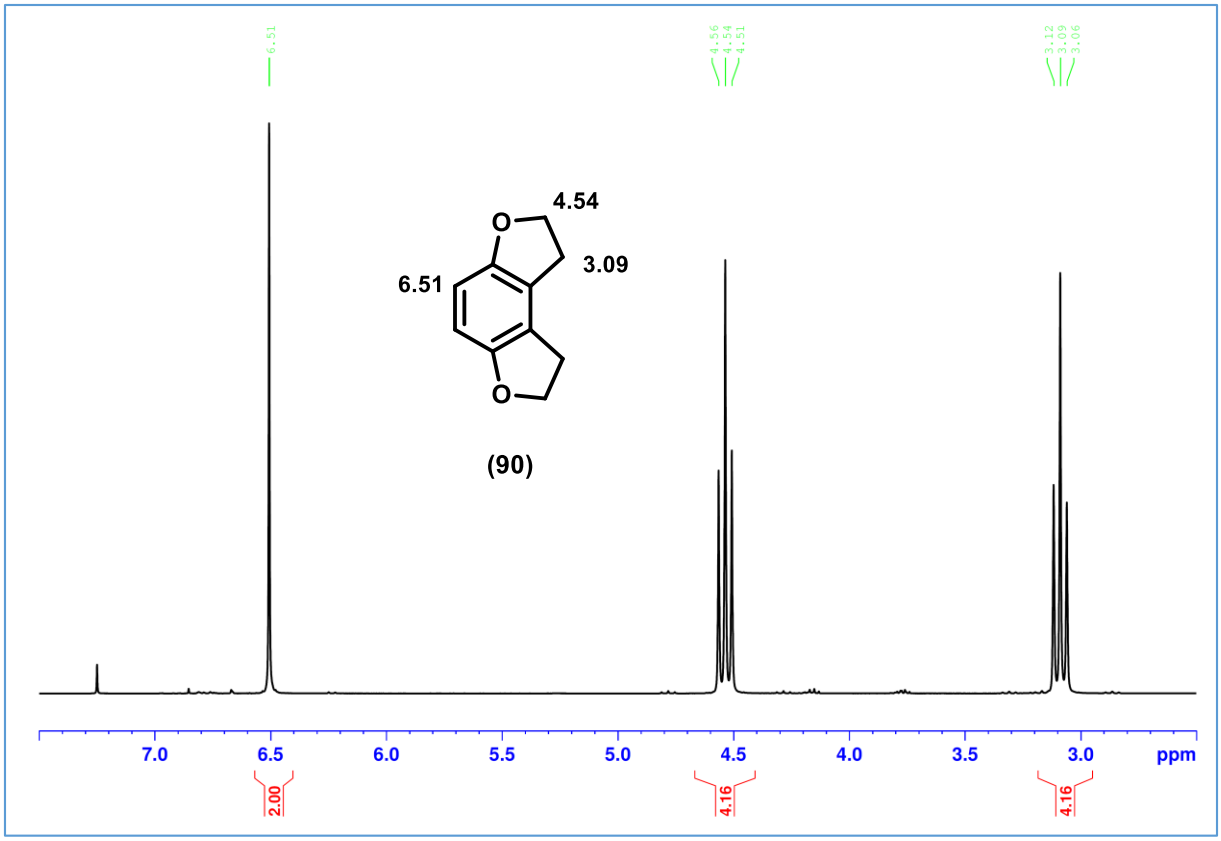


*Fig. 3-42: ^{1}H-NMR analysis of pure iTHBD **(90)***

While this reaction was more successful than the initial attempt using *n*-BuLi, it still had not gone to completion, with an integration ratio of starting material **191** to product **90** of 1:4 in the ^{1}H-NMR analysis of the crude reaction mixture. There was also a signal in the crude product ^{1}H-NMR spectrum at 6.68 ppm, possibly representing the aromatic protons of mono-annulated intermediate **209** (see Figure 3-43).

This mono-annulated compound **209** is a very likely intermediate of the reaction based on the mechanism described in Figure 3-39, as it is possible that the annulations happen in sequence rather than in parallel. However, the assignment of the signal at 6.68 ppm to **209** was purely speculation based on the likelihood of the intermediate appearing, as one signal is not sufficient to make a definitive assignment. HRMS analysis was attempted, but the PMI was unfortunately not found. Nonetheless, this result (with clear evidence of starting material **191** by ^{1}H-NMR) prompted us to repeat the annulation as per Figure 3-41, but to extend the time at room temperature from 24 to 60 h. Note that this is referred to as Reaction 2 later in this section.

At 60 h, an aliquot was taken from the reaction, worked up and sent for ^{1}H-NMR analysis. This revealed a mixture of product **90**, starting material **191** and another component that was hypothesised to be the mono-annulated intermediate **209**. Integration of the aromatic singlets in the ^{1}H-NMR spectrum showed that there was 53 % product **90**, 22 % starting material **191** and 25 % possible intermediate **209** (**90**:**191**:**209** = 2:1:1). If the signal tentatively assigned to **209** is discounted, the ratio of product **90** to starting material **191** is 2:1.

Based on this analysis, the decision was made to re-cool the reaction to – 78 °C, add another 1.1 equivalents of *n*-BuLi and, after holding at – 78 °C for 1 h, warm to room temperature and leave to stir for another 18 h. At this point another aliquot was taken, and analysis by ^{1}H-NMR showed the presence of product **90** and starting material **191** in a ratio of 5:1, as seen in Figure 3-43.

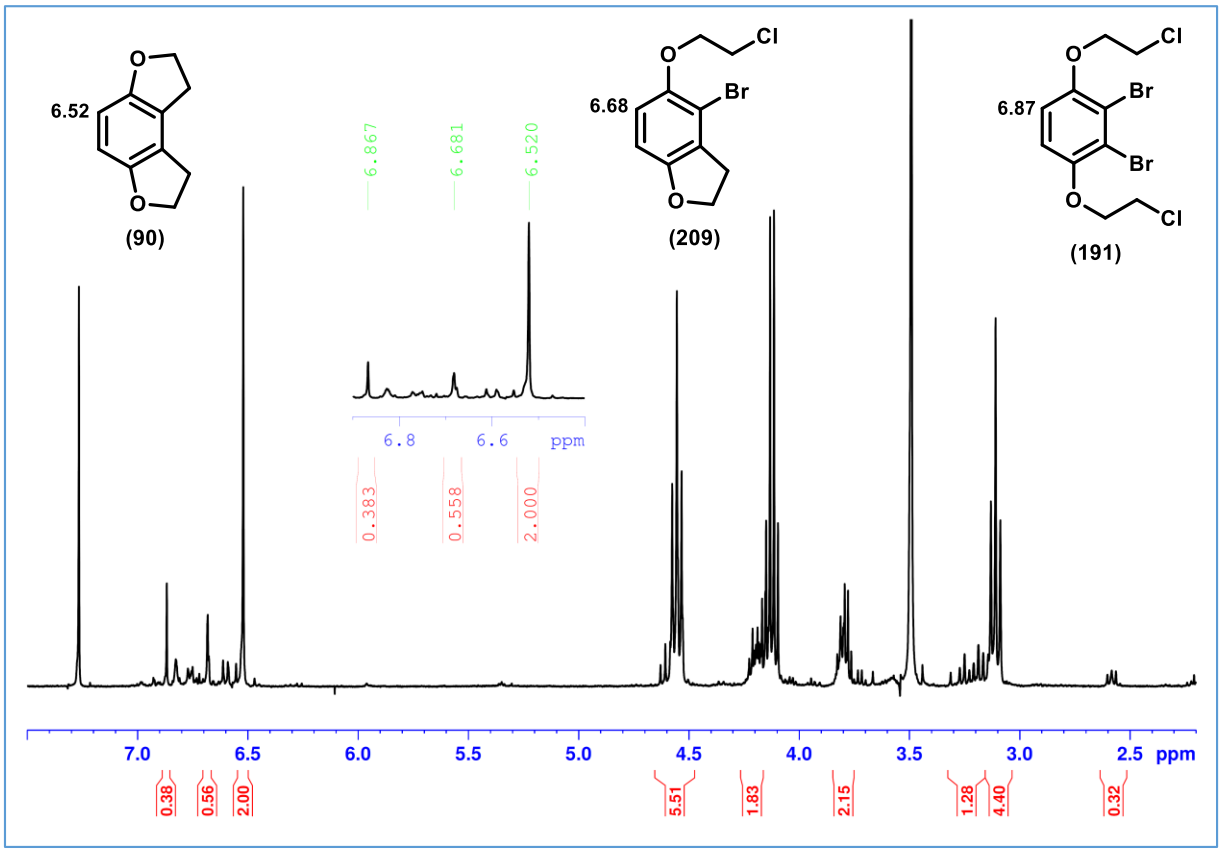


*Fig. 3-43: ^{1}H-NMR spectrum of an aliquot taken from the synthesis of iTHBD **(90)** using n-BuLi*

The reaction was cooled for a third time, another 1.1 equivalents of *n*-BuLi added, and after 1 h at – 78 °C, allowed to stir at room temperature for 18 h. ^{1}H-NMR analysis of an aliquot at this point showed product **90** and starting material **191** in a ratio of 22:1. At this point, the reaction was worked up in its entirety and purified by preparative TLC, affording pure iTHBD **(90)** in 47 % yield.

While this was a clear improvement from initial attempts to use *n*-BuLi as a reagent for synthesis of iTHBD **(90)**, the experimental process was long and involved, requiring one week, repeated re-cooling and addition of extra equivalents of *n*-BuLi.

Two further reactions were performed in an attempt to optimise process conditions, using the general reaction scheme as laid out in Figure 3-41, but with adjustments to reaction times and stoichiometry of reagents as explained in Table 3-8.

Reaction Number	*n*-BuLi	Reaction Time at – 78 °C	Reaction Time at Ambient Temp.	Isolated Yield of 90
3	6.6 eq	5 h	90 h	8.2 %
4	2.2 eq	20 h	48 h	9.6 %

*Table 3-8: Reaction conditions for variations on n-BuLi reactions to form iTHBD **(90)***

Reaction 3 focussed on increasing the initial equivalents of *n*-BuLi to the level of 6.6 eq. which was eventually reached during the Reaction 2 (which had incremental *n*-BuLi addition), to see if that would enable the reaction to go to completion without having to undertake several heat-cool cycles and further *n*-BuLi additions. Reaction times at both – 78 °C and ambient temperature were extended beyond what is described in Figure 3-41 to maximise the potential for complete conversion.

^{1}H-NMR analysis post work-up of Reaction 3 showed a clear major signal in the crude mixture at 6.51 ppm representing the aromatic protons in desired

product **90**. However, the crude spectrum was otherwise an indistinguishable mixture of signals and did not allow for quantification of conversion by ^{1}H-NMR integration (see Figure 3-44).

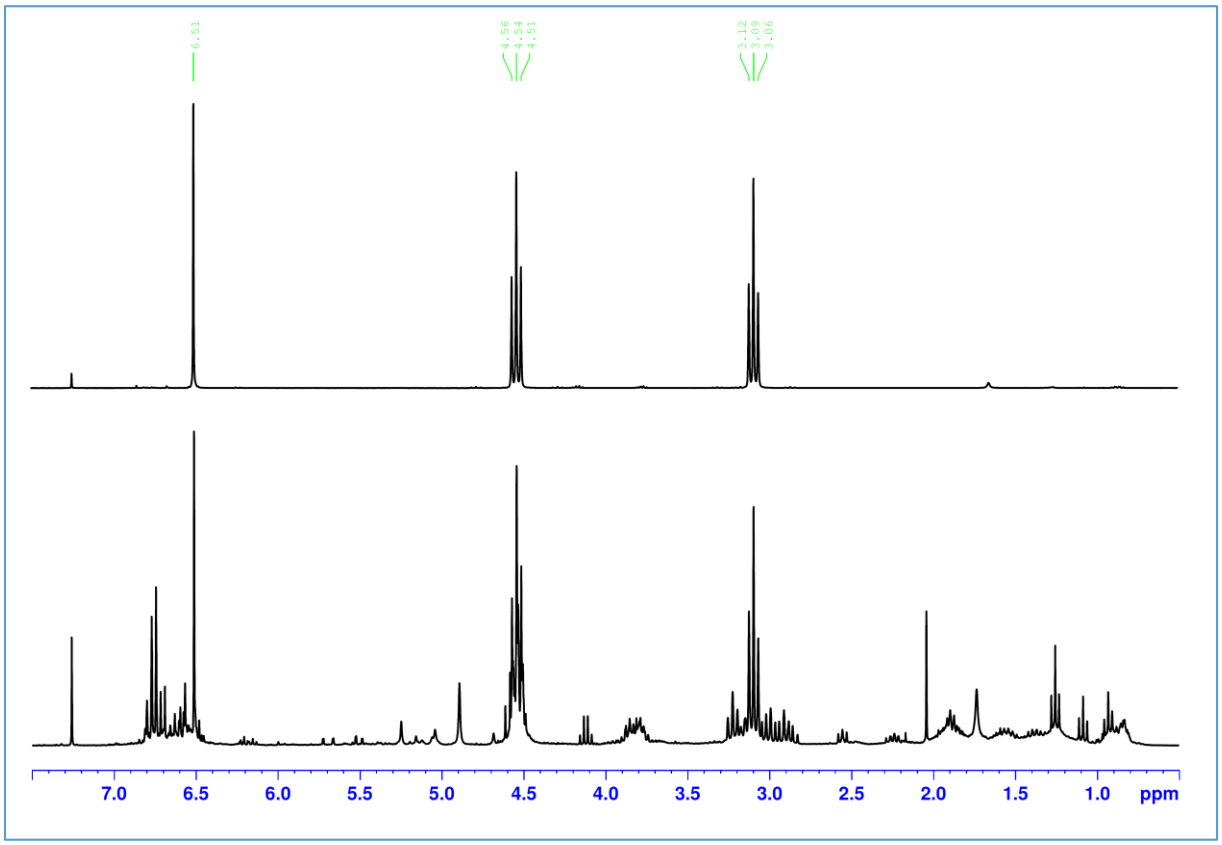


*Fig. 3-44: ^{1}H-NMR spectra of pure iTHBD **(90)** (top) compared with crude Reaction 3 mixture containing iTHBD **(90)** (bottom)*

This mixture required multiple attempts at column chromatography on silica gel to fully remove all impurities, finally affording **90** in a disappointingly low isolated yield of 8.2 %.

As excess *n*-BuLi appeared to cause degradation within the reaction (based on the complex mixture of products seen in the crude ^{1}H-NMR spectrum in Figure 3-44), Reaction 4 was executed returning to 2.2 equivalents of *n*-BuLi, but extending the reaction time at – 78 °C from 5 to 20 hours (Table 3-8). The crude Reaction 4 residue showed a mixture of product **90** and starting material **191** in a ratio of ~5:1, along with other unidentified organic compounds. Column chromatography on silica gel partially purified the product, and

subsequent preparative TLC and recrystallisation from hexane gave pure product **90**, but in a low yield of 9.6 %.

Based on the results from Reactions 1-4, it was determined that Reaction 2, with excess *n*-BuLi added incrementally over extended reaction times (with multiple cooling/warming cycles) is required to drive the reaction fully to completion, maximising the isolated yield.

3.5.2 Annulation of 191 Employing the Grignard Reaction

The second approach to the ring-closing reaction of **191** is the initial formation of its Grignard species. This approach has been used previously in our group by ROC in the synthesis of THBD **(42)**, as seen in Figure 3-1.[2] The procedure by ROC was based on a combination of the work of Chambers *et al.*[26] and Alabaster *et al.*[27] taking the work by Chambers *et al.* as a starting point, and making modifications based on the work by Alabaster *et al.* (lowering the reaction temperature from reflux to 35 °C and changing the magnesium form from powdered magnesium to freshly ground magnesium turnings).

This hybrid procedure was performed in this work as described in Figure 3-45, employing 2,3-dibromo-1,4-bis(2-chloroethoxy)benzene **(191)** as a starting material.

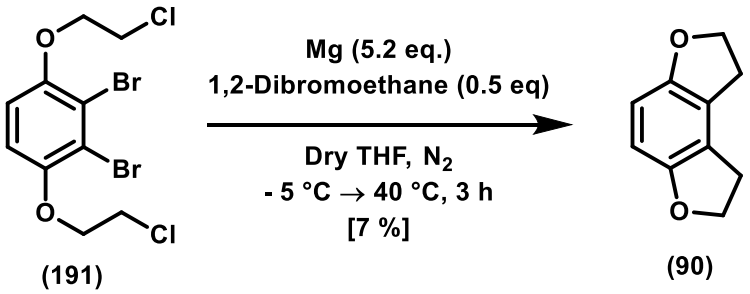


*Fig. 3-45: Synthesis of iTHBD **(90)** using a Grignard reaction approach*

The ^{1}H-NMR analysis of the crude reaction product revealed a mixture of product **90** and starting material **191** in a ratio of ~4:1 based on ^{1}H-NMR integration, along with other unknown organic contaminants. This was partially purified by column chromatography on silica gel, followed by preparative TLC

and finally recrystallisation from hexane to give pure iTHBD **(90)** in very low yield of 7 %.

The extensive purification required to recover pure **90** is likely to have impacted the yield significantly. However, the combination of involved set-up requirements for the Grignard reaction (preparing and activating magnesium turnings, flame-drying all glassware, drop-wise addition of starting material **191** in THF *via* canula to the magnesium) and low yields makes the *n*-BuLi approach more attractive than the Grignard process despite the longer reaction times.

3.5.3 Characterisation of iTHBD (90) and Comparison to THBD (42)

Following its successful synthesis, iTHBD **(90)** was fully characterised as summarised in Table 3-9.

Compound Number	Yield (%)	m.p. (°C) *[Lit m.p.]*	R_f (Hex:EtOAc)	HRMS (*m/z*)	
				Calc.	Found
90	47*	85 - 86 (Hexane) *[86 - 88[2] (Hexane)]*	0.57 (2:1)	163.0759	163.0757

*Table 3-9: Yield, m.p., R_f, IR and HRMS of iTHBD **(90)***

**Yield quoted based on Reaction 2 conditions*

The main differences in characterisation data between THBD **(42)** and iTHBD **(90)** are seen in their melting points and the R_f data. The R_f of THBD **(42)** in 2:1 hexane:ethyl acetate was 0.62, while that of iTHBD **(90)** in the same solvent was 0.57, making them distinguishable on a TLC plate. However, the most significant difference between the two substrates was seen in their melting points, with THBD **(42)** having a melting point of 153 - 154 °C, while iTHBD **(90)** measures 68 °C lower at 85 - 86 °C.

As well as the data recorded in Table 3-9, ^{1}H- and ^{13}C-NMR spectra were also acquired for iTHBD **(90)**. As iTHBD **(90)** is a symmetrical molecule (with an axis of symmetry as shown in Figure 3-46) there were three signals representing the ten protons of the substrate. The signal representing the aromatic protons appeared as a singlet at 6.51 ppm, while the aliphatic protons were represented by triplets at 3.09 ppm (C**H$_2$**-CH$_2$-O) and 4.54 ppm (CH$_2$-C**H$_2$**-O).

A comparative ^{1}H-NMR spectral analysis of iTHBD **(90)** and THBD **(42)** is displayed in Figure 3-46. The main spectral difference occurs in chemical shifts aromatic proton signals (6.51 ppm for iTHBD **(90)**, 6.62 ppm for THBD **(42)**). Chemical shifts of the aliphatic protons in both substrates are effectively coincidental.

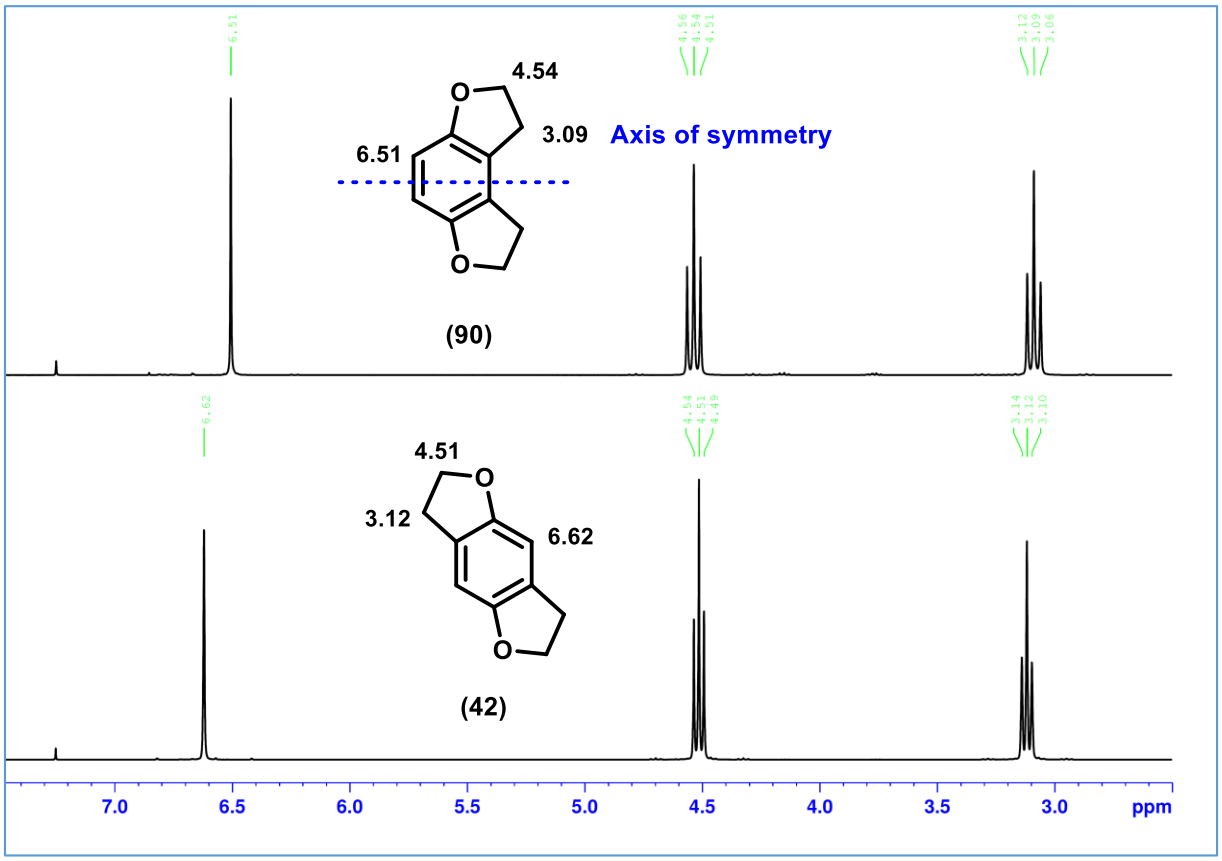


*Fig. 3-46: Comparison of the ^{1}H-NMR spectra of iTHBD **(90)** (top) and THBD **(42)** (bottom)*

The ^{13}C-NMR spectrum of iTHBD **(90)** was also reflective of the substrate's axis of symmetry, with five signals representing the substrate. The full assignment of these signals to iTHBD **(90)** can be seen in Figure 3-47. In comparison with THBD **(42)**, chemical shifts of analogous ^{13}C-NMR signals for the two substrates lie within 1 - 2 ppm of each other.

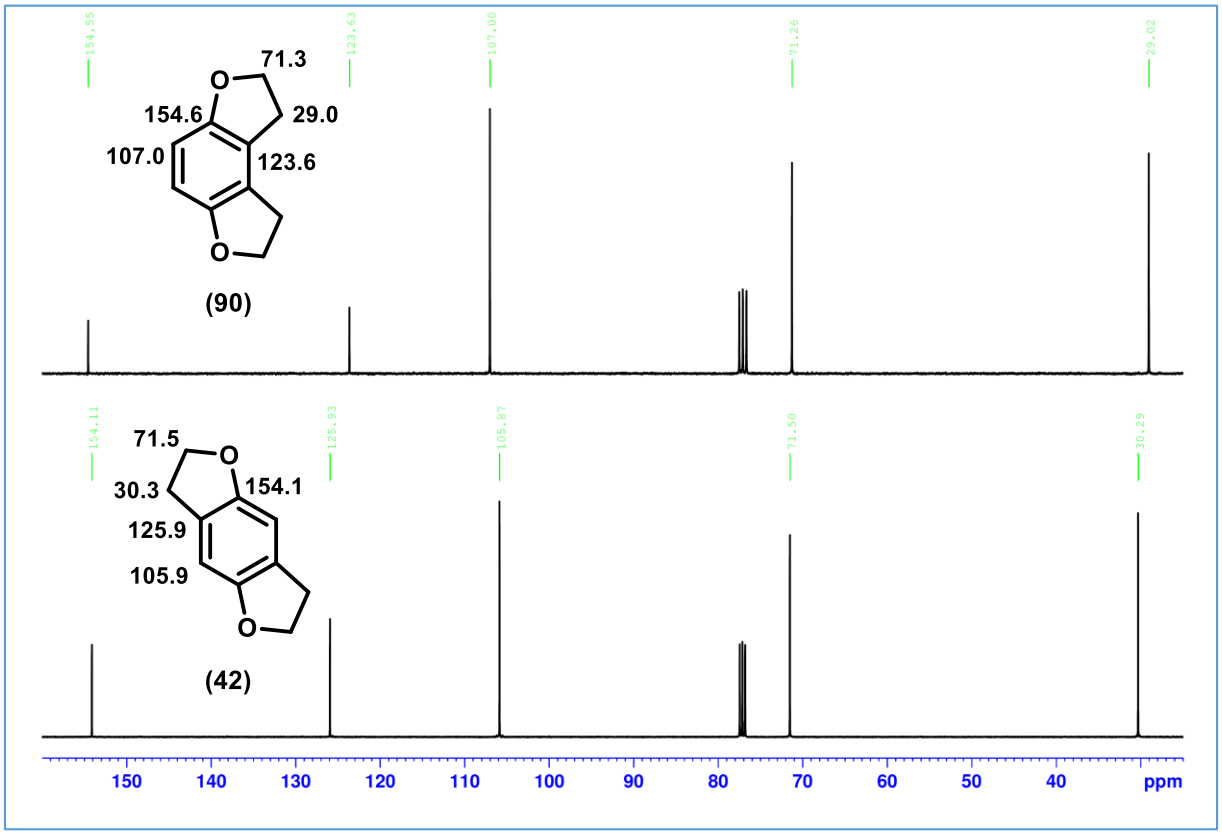


*Fig. 3-47: Comparison of the ^{13}C-NMR spectra of iTHBD **(90)** (top) and THBD **(42)** (bottom)*

From data discussed within this section, it is clear that when using NMR analysis, the easiest way to differentiate iTHBD **(90)** and THBD **(42)** is to scrutinise ^{1}H-NMR aromatic chemical shifts. However, the clearest diagnostic difference between iTHBD **(90)** and THBD **(42)** is their melting points, which have a difference of almost 70 °C.

3.6 Summary of Results and Conclusions

The key result to note from this section was that a selective route to the target

compound, iTHBD **(90)**, was successfully designed, implemented and optimised using the synthetic pathway set out Figure 3-2. This optimised synthetic route is depicted in Figure 3-48.

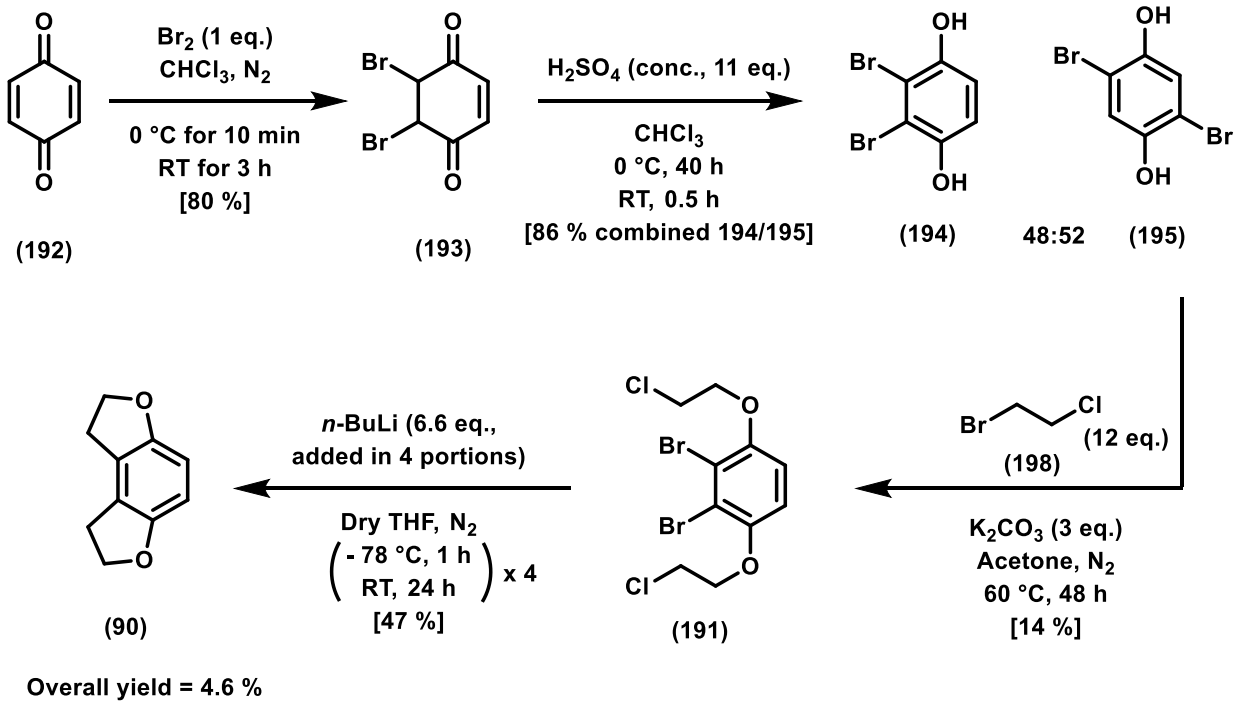


*Fig. 3-48: Optimised synthetic route to iTHBD **(90)***

The first step, bromination of 1,4-benzoquinone **(192)**, was carried out successfully with an optimised isolated yield of 80 % (see Figure 3-48). Reaction time was crucial to the reaction success; too long a reaction time (> 3 h) leads to conversion of 5,6-dibromocyclohex-2-ene-1,4-dione **(193)** to 2,5-dibromobenzene-1,4-diol **(195)**.

The second step (conversion of 5,6-dibromocyclohex-2-ene-1,4-dione **(193)** to its hydroquinone analogue 2,3-dibromobenzene-1,4-diol **(194)**) proved problematic, as the reaction mechanism involved sequential elimination/re-addition steps (as outlined in Figure 3-12). Elimination/re-addition of HBr resulted in a reaction residue composed of an almost 1:1 mixture of 2,3-dibromobenzene-1,4-diol **(194)** and its regioisomer 2,5-dibromobenzene-1,4-diol **(195)**.

This was a serious drawback as it limited the potential yield of desired product **194** to a maximum theoretical yield 48 % (see Figure 3-48, the other 52 % of starting material **193** was converted to undesired side-product **195**). An extensive solvent and reagent screen was conducted, resulting in a slight preference for the 2,5-dibromobenzene-1,4-diol **(195)** product even under the best conditions found (conc. H_2SO_4, $CHCl_3$, 40 h, 0 °C). Isomers **194** and **195** proved inseparable and so the crude reaction mixture was telescoped to the subsequent step.

Step 3 (Figure 3-48) concerned the alkylation of hydroquinones **194** and **195**, employing 1-bromo-2-chloroethane **(198)**. Several different conditions were screened for this step, the optimal being potassium carbonate (3 eq.) and 1-bromo-2-chloroethane **(198)** (12 eq.) in acetone at 60 °C for 90 h. Disappointingly, even the optimised reaction proved low yielding, favouring undesired 2,5-dibromo-1,4-bis(chloroethoxy)benzene **(190)** over the desired 2,3-dibromo-1,4-bis(chloroethoxy)benzene **(191)**. Longer reaction times (48 h → 90 h) and increased equivalents of 1-bromo-2-chloroethane **(198)** (3 eq. → 12 eq.) improved the overall combined yield from 24 to 37 %. However the 2,5-dibromo isomer **190** was still favoured over the 2,3-dibromo product **191**, with respective maximum isolated yields of 23 and 14 % respectively.

An alternative two step route to **191** from **194** was explored using ethylene carbonate as an ethoxylating agent, followed by chlorination using $SOCl_2$. While the ethoxylation reaction worked quite well and produced isolated yields of up to 83 % on the test substrate hydroquinone **(199)**, employing a mixture of 2,3-dibromobenzene-1,4-diol **(194)** and 2,5-dibromobenzene-1,4-diol **(195)** gave a lower yield (21 % combined yield of **204/206**), and the product distribution ratio still favoured the undesired 2,5-dibromo-1,4-bis(chloroethoxy)benzene **(204)** isomer (13 % isolated yield) over the desired 2,3-dibromo-1,4-bis(chloroethoxy)benzene **(206)** product (7% isolated yield). This was believed in part to be due to the surfactant nature of the products **204** and **206**, and although several attempts were made at optimisation, no improvement was recorded, and the line of research was discontinued.

The final step in the reaction sequence to **90** (see Figure 3-49) was the ring-closing reaction of 2,3-dibromo-1,4-bis(chloroethoxy)benzene **(191)**. This was performed using two different approaches, the first using *n*-BuLi, and the second using a Grignard reaction. The *n*-BuLi reaction had very long reaction times (one week), but ultimately resulted in a moderate isolated 47 % yield of **90**. The Grignard reaction was much shorter (4 h reaction time), but had a much lower isolated yield of 7 % after purification. It is probable that longer reaction times would lead to an improved yield in the Grignard approach, however, the complex set-up requirements led to the *n*-BuLi approach being adopted as the preferred methodology to synthesise iTHBD **(90)** (see Figure 3-48).

This route was carried out with an overall yield of 4.6 % from **192**, a result which was negatively impacted by the inability to form 2,3-dibromobenzene-1,4-diol **(194)** without also forming 2,5-dibromobenzene-1,4-diol **(195)**, and a subsequent inability to separate **194** and **195**. This halved the effective yield in the second step of the pathway and had a knock-on negative effect in the formation of 2,3-dibromo-1,4-bis(chloroethoxy)benzene **(191)**. However, all other bromination reactions found in the literature favoured the 2,5-dibromo isomer **190** almost exclusively, and so the route described in Figure 3-49 is believed to be the most effective way currently recorded of accessing iTHBD **(90)** directly.

References (Chapter Three)

1. Wermuth, C. G.; Ganellin, C. R.; Lindberg, P.; Mitscher, L. A., Glossary of terms used in medicinal chemistry (IUPAC Recommendations 1998). In *Pure and Applied Chemistry*, **1998**; Vol. 70, p 1129.
2. O'Connor, R. E.; Bateman, L. M.; Eccles, K. S.; Slattery, C. N.; Lawrence, S. E., Structural Elucidation and Comparative Spectroscopic Analysis of Isomeric Benzodifurans. *Manuscript in Preparation* **2019**.
3. D'Antona, N.; Nicolosi, G.; Morrone, R.; Kubáč, D.; Kaplan, O.; Martínková, L., Synthesis of novel cyano-cyclitols and their stereoselective biotransformation catalyzed by Rhodococcus erythropolis A4. *Tetrahedron: Asymmetry* **2010,** *21* (6), 695-702.
4. Adelt, S.; Plettenburg, O.; Stricker, R.; Reiser, G.; Altenbach, H.-J.; Vogel, G., Enzyme-Assisted Total Synthesis of the Optical Antipodes d-myo-Inositol 3,4,5-Trisphosphate and d-myo-Inositol 1,5,6-Trisphosphate: Aspects of Their Structure−Activity Relationship to Biologically Active Inositol Phosphates. *Journal of Medicinal Chemistry* **1999,** *42* (7), 1262-1273.
5. Roberts, I.; Kimball, G.E., The Halogenation of Ethylenes. *Journal of the American Chemical Society* **1937**, *59* (5), 947-948.
6. Bian, L.; Hai, J.; Zhu, E.; Yu, J.; Liu, Y.; Zhou, J.; Ge, G.; Tang, W., A versatile strategy to directly synthesize 4,8-functionalized benzo[1,2-*b*:4,5-*b'*]difurans for organic electronics. *Journal of Materials Chemistry A* **2015,** *3* (5), 1920-1924.
7. Boruah, J. J.; Das, S. P.; Borah, R.; Gogoi, S. R.; Islam, N. S., Polymer-anchored peroxo compounds of molybdenum and tungsten as efficient and versatile catalysts for mild oxidative bromination. *Polyhedron* **2013,** *52*, 246-254.
8. Atkinson, R. C.; de la Mare, P. B. D.; Larsen, D. S., The kinetics and mechanisms of additions to olefinic substances. Part 16. Addition of halogens to 1,4-benzoquinone and to 1,4-napthoquinone, and dehydrohalogenation of the resulting adducts. *Journal of the Chemical Society, Perkin Transactions 2* **1983,** (3), 271-279.
9. Feng, L.; Wang, Y.; Liang, F.; Xu, M.; Wang, X., Highly selective recognition of monosaccharide based on two-component system in aqueous solution. *Tetrahedron* **2011,** *67* (18), 3175-3180.
10. Djaballah, H. A., Christophe; Benzofuran-4,5-diones as Selective Peptide Deformylase Inhibitors. WO2010/129049, **2010**.
11. Chou, T.-C.; Hsu, C.-J.; Chen, J.-Y., Benzoannulation of Quinones by a Cycloaddition-Fragmentation Approach. A Simple Synthesis of Methoxycarbonyl-Substituted Polyacenoquinones. *Journal of the Chinese Chemical Society* **2004,** *51* (1), 167-174.
12. Thomas, A. D.; Miller, L. L., Repetitive Diels-Alder reactions for the growth of linear polyacenequinoid derivatives. *The Journal of Organic Chemistry* **1986,** *51* (22), 4160-4169.
13. Monte, A. P.; Marona-Lewicka, D.; Parker, M. A.; Wainscott, D. B.; Nelson, D. L.; Nichols, D. E., Dihydrobenzofuran Analogues of Hallucinogens. 3. Models of 4-Substituted (2,5-Dimethoxyphenyl)alkylamine Derivatives with Rigidified Methoxy Groups. *Journal of Medicinal Chemistry* **1996,** *39* (15), 2953-2961.

14. Yoshino, T.; Inaba, S.; Ishido, Y., Synthetic Studies by the Use of Carbonates. III. The Condensation Reactions of Ethylene Carbonate with a Variety of Phenols Catalyzed by Lithium Hydride or Tetraethylammonium Halides *Bulletin of the Chemical Society of Japan* **1973,** *46* (2), 553-556.
15. Carlson, W. W.; Cretcher, L. H., Hydroxyalkylation with Cyclic Alkylene Esters. I. Synthesis of Hydroxyethylapocupreine. *Journal of the American Chemical Society* **1947,** *69* (8), 1952-1956.
16. Gustin, J. L., "Safety of ethoxylation reactions", Hazards XV—The Process, its Safety and the Environment, (Symposium Series no. 147). *IChemE* **2000**, 251-263.
17. Schäffner, B.; Schäffner, F.; Verevkin, S. P.; Börner, A., Organic Carbonates as Solvents in Synthesis and Catalysis. *Chemical Reviews* **2010,** *110* (8), 4554-4581.
18. Shaikh, A.-A. G.; Sivaram, S., Organic Carbonates. *Chemical Reviews* **1996,** *96* (3), 951-976.
19. Pirrung, M. C.; Nunn, D. S., Photochemical rearrangements of quinone monoketals. *Tetrahedron* **1996,** *52* (16), 5707-5738.
20. O'Connor, R. E. Unpublished Doctoral Thesis. University College Cork, **2016**.
21. Kreutzer, U. R., Manufacture of fatty alcohols based on natural fats and oils. *Journal of the American Oil Chemists' Society* **1984,** *61* (2), 343-348.
22. What Is Alcohol Ethoxylate? (Accessed 29/06/19). https://http://www.oxiteno.us/what-is-alcohol-ethoxylate-uses/.
23. Hydroquinone bis(2-hydroxyethyl) ether (Accessed 01/07/19). https://http://www.sigmaaldrich.com/catalog/product/aldrich/237914?lang=en&region=IE.
24. Parham, W. E.; Jones, L. D.; Sayed, Y. A., Selective halogen-lithium exchange in bromophenylalkyl halides. *The Journal of Organic Chemistry* **1976,** *41* (7), 1184-1186.
25. Redondo, M. C.; Veguillas, M.; Ribagorda, M.; Carreno, M. C., Control of the Regio- and Stereoselectivity in Diels-Alder Reactions with Quinone Boronic Acids. *Angewandte Chemie-International Edition* **2009,** *48* (2), 370-374.
26. Chambers, J. J.; Kurrasch-Orbaugh, D. M.; Parker, M. A.; Nichols, D. E., Enantiospecific Synthesis and Pharmacological Evaluation of a Series of Super-Potent, Conformationally Restricted 5-HT2A/2C Receptor Agonists. *Journal of Medicinal Chemistry* **2001,** *44* (6), 1003-1010.
27. Alabaster, R. J.; Cottrell, I. F.; Marley, H.; Wright, S. H. B., The Synthesis of 5-Substituted 2,3-Dihydrobenzofurans. *Synthesis* **1988,** *1988* (12), 950-952.

Chapter Four: Experimental

Table of Contents

Table of Contents **317**

List of Figures **319**

4 Experimental **320**

4.1 General Procedures 320

4.2 Experimental Details Pertaining to Work Outlined in Chapter 2 323

4.2.1 Phenyl Pyrimidine Impurities 323

4.2.1.1 General Procedure A: Regioselective Aromatic Bromination Using *N*-bromosuccinimide (NBS) 323

4.2.1.2 General Procedure B: Aromatic Dibromination Using NBS 323

4.2.1.3 General Procedure C: Dehydrogenation of THBD Moiety to Benzodifuran Moiety Using 2,3-Dichloro-5,6-dicyano-1,4-benzoquinone (DDQ) 323

4.2.1.4 General Procedure D: Synthesis of Boronic Acids 324

4.2.1.5 General Procedure E: Synthesis of Hydroxy Pyrimidine **135** 325

4.2.1.6 General Procedure F: Bromination of Hydroxy Pyrimidine **135** Using NBS 325

4.2.1.7 General Procedure G: Chlorination of Hydroxyl Moeity of **138** Using $POCl_3$ 325

4.2.1.8 General Procedure H: Dechlorination of Pyrimidine **139** *via* the Bamford-Stevens Reaction 326

4.2.1.9 General Procedure I: Suzuki-Miyaura Coupling Reaction 326

4.2.1.10 General Procedure J: Bromination of Phenyl Pyrimidine Using Bromine in Acetic Acid 327

4.2.1.11 General Procedure K: Friedel-Crafts Acylation 327

4.2.2 Benzyl Pyrimidine Impurities 337

4.2.2.1 General Procedure L: Palladium-Catalysed C-H Activation Coupling Reaction 337

4.2.3 Leuckart Reactions and Subsequent Hydrolysis Reactions 341

4.2.3.1 General Procedure M: Iron-Catalysed Reduction of Nitrostyrene to Ketone 341

4.2.3.2 General Procedure N: Leuckart Reaction to Convert a P2P-type Ketone to an *N*-formyl Moeity 341

4.2.3.3 General Procedure O: Hydrolysis Reaction to Convert an *N*-formyl Substrate to the Corresponding Primary Amine 342

4.3 Experimental details pertaining to work outlined in Chapter 3 350

4.3.1.1 General Procedure P: Bromination of 1,4-Benzoquinone **(192)**…… 350

4.3.1.2 General Procedure Q: Conversion of Benzoquinones to Hydroquinones 351

4.3.1.3 General Procedure R: Alkylation of Hydroquinones 351

4.3.1.4 General Procedure S: Ethoxylation of Hydroquinones 352

4.3.1.5 General Procedure T: Preparation of iTHBD **(90)** Using *n*-BuLi……. 352

4.3.1.6 General Procedure U: Preparation of iTHBD **(90)** Using a Grignard Reaction 353

References (Chapter Four) 358

List of Figures

Fig. 4-1: Systematic numbering scheme used for THBD and benzodifuran derivatives 322

4 Experimental

4.1 General Procedures

Infrared (IR) spectra were recorded on a Perkin® Paragon 1000 FT-IR spectrometer or a PerkinElmer® UATR Two FT-IR spectrometer. Band positions are given in cm^{-1}. Solid samples were analysed as potassium bromide (KBr) discs; oils were analysed as neat films on sodium chloride (NaCl) plates.

R_f values are quoted for thin layer chromatography (TLC) on pre-coated silica gel plates (Merck® Silica Gel 60, PF254). Visualisation of the plates was by ultra violet (UV) light detection, either short wave (254 nm) or long wave (356 nm).

Column chromatography was carried out using Kieselgel 60 silica gel (particle size 0.040 - 0.063 mm). Unless stated otherwise, all solvents were bulk grade and were not pre-treated in any way before use.

Solvents that are preceded with 'dry' were distilled as follows: dichloromethane and ethyl acetate were distilled over phosphorous pentoxide. Ethanol and methanol were dried over a mixture of iodine and magnesium turnings. Tetrahydrofuran and diethyl ether were dried using a mixture of benzophenone and sodium. All commercial reagents were used without further purification.

^1H and ^{13}C nuclear magnetic resonance (NMR) were recorded at 20 °C on Bruker® Avance® 300, 400 or 600 spectrometers; ^1H (300.13 MHz, 400.13 MHz or 600.13 MHz); ^{13}C (75.47 MHz, 100.61 MHz or 150.9 MHz), in either $CDCl_3$ or DMSO-d_6 (internal standard was tetramethylsilane (TMS) in all cases). For $CDCl_3$, ^1H-NMR spectra were assigned relative to the TMS peak at 0.00 ppm δ; ^{13}C-NMR spectra were assigned relative to the middle shift of the $CHCl_3$ triplet at 77.00 ppm or for those ^{13}C-NMR spectra measured in DMSO-d_6, the shift of the DMSO septet at 39.5 ppm. For the ^1H-NMR assignments, chemical shifts are reported: shift value (δ) (number of protons, description of absorption, coupling constant(s) where applicable (in Hertz [Hz]), proton assignment). Splitting patterns in ^1H-NMR spectra are designated s (singlet), d (doublet), dd (doublet of doublets), t (triplet), q (quartet), m

(multiplet). For ^{13}C NMR assignments, shifts are reported in parts per million (ppm) followed by the carbon assignment in brackets.

For inseparable mixtures of isomers, rotamers or diastereoisomers, assignment of individual signals is attempted where feasible. Signals are either listed separately for each individual isomer/rotamer or listed together, with signals distinguished from one another through the use of a superscripted symbol after the assignment (e.g. ('signal')^{E} = denotes signal assigned to *E*-isomer). The symbol " * " is used to signify direct overlap of signals arising from two different isomers/rotamers.

Low-resolution mass spectra (LRMS) were acquired on a Waters/Micromass® LCT Premier Time of Flight spectrometer (ESI) and high-resolution mass spectra (HRMS) were acquired on a Waters/Micromass® Quattro Micro Triple Quadrupole spectrometer (ESI). All experimentally derived ("found") HRMS *m/z* values listed are within 5 ppm mass accuracy of the theoretical ("calc.") values.

The HPLC chromatograms featured in this body of work were acquired on the Agilent® 1260 Series HPLC, which is made up of the following hardware:

1. Binary Pump
2. Autosampler
3. Thermastated Column Compartment
4. Diode Array Detector

The conditions used to acquire these HPLC chromatograms were as follows:

- Mobile phases: All reagents used (CH_3CN, H_2O, etc) were of LC-MS grade. The solvent system used was an isocratic elution of 65:35 CH_3CN:H_2O at 30 °C at a flow rate of 1 mL/min.
- Sample preparation: All samples were made up in 65:35 CH_3CN:H_2O at a concentration of ~1 mg/mL and placed in an ultrasonic bath for ~5 min. Samples were then filtered into vials using a syringe filter.
- HPLC column: C-18 column [YMC-Pack®, ODS-A, S-5 µm, 120 Å, 250 x 4.6 mm]

- Detection: All samples were recorded at multiple wavelengths: 210, 230, 254 and 280 nm.

With regards to NMR analysis, to avoid any confusion as to which signals are being referred to, an illustration of the systematic numbering scheme used for THBD and benzodifuran derivatives is shown in Figure 4-1. This numbering scheme is aligned to the IUPAC numbering and naming system, with very minor differences for clarity.

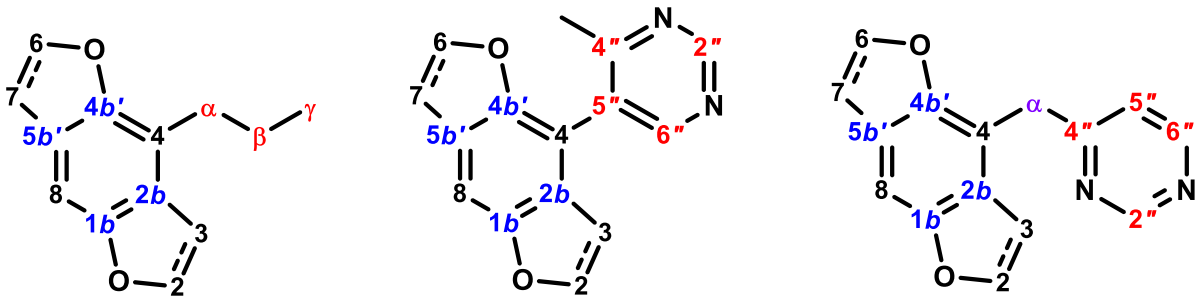


Fig. 4-1: Systematic numbering scheme used for THBD and benzodifuran derivatives

For all other compounds, the numbering also follows IUPAC rules in the same manner and in some cases is shown on the accompanying structure if thought to be unclear.

General reaction procedures are listed in the relevant experimental sections, each identified by a discrete letter. Each compound is then described as being synthesised by a general reaction procedure. If the scale of the reaction for a specific compound differs from that in the relevant general procedure, this will be noted in the experimental data. An example would read 'Compound **999** was synthesised according to General Procedure Z on a 1.0 mmol scale', where the scale quoted refers to the limiting reagent in the reaction and all other reactants are scaled accordingly.

4.2 Experimental Details Pertaining to Work Outlined in Chapter 2

4.2.1 Phenyl Pyrimidine Impurities

4.2.1.1 General Procedure A: Regioselective Aromatic Bromination Using N-bromosuccinimide (NBS)

To a stirred solution of THBD-type substrate (10.0 mmol) in acetonitrile (60 mL) at 0 °C, NBS (1.78 g, 10.0 mmol) was added in five portions over 30 min. The reaction was allowed to warm to room temperature and was stirred for a further 3 h. Deionised water (200 mL) was added to the solution resulting in the precipitation of the product. This was collected by vacuum filtration using a Büchner funnel and dissolved in DCM (60 mL), washed with deionised water (30 mL), dried over anhydrous $MgSO_4$, filtered and concentrated *in vacuo* to give pure product as a white to off-white solid. The sample was then recrystallised from methanol to give a white crystalline solid.

4.2.1.2 General Procedure B: Aromatic Dibromination Using NBS

To a stirred solution of 2,3,6,7-tetrahydrobenzo[1,2-*b*:4,5-*b'*]difuran **(42)** (1.62 g, 10.0 mmol) in acetonitrile (60 mL) at 0 °C, NBS (3.56 g, 20.0 mmol) was added in one portion. The reaction was allowed to warm to room temperature and was stirred for a further 3 h. Deionised water (200 mL) was added to the solution resulting in the precipitation of the product. This was collected by vacuum filtration using a Büchner funnel and dissolved in DCM (60 mL), washed with deionised water (30 mL), dried over anhydrous $MgSO_4$, filtered and concentrated *in vacuo* to give pure product as a white to off-white solid. The sample was then recrystallised from ethanol to give a white crystalline solid.

4.2.1.3 General Procedure C: Dehydrogenation of THBD Moiety to Benzodifuran Moiety Using 2,3-Dichloro-5,6-dicyano-1,4-benzoquinone (DDQ)

A solution of DDQ (1.14 g, 5.0 mmol) in 1,4-dioxane (20 mL) was slowly added

to a solution of the THBD-type substrate (2.0 mmol) in 1,4-dioxane (12 mL). The resulting solution was then heated at reflux for 60 h. The mixture was allowed to cool to room temperature and the 4,5-dichloro-3,6-dihydroxy-phthalonitrile (DDP) precipitate that formed was removed by filtering the crude product mixture through a short pad of silica gel in a sintered glass funnel under vacuum. The filter cake was then washed thoroughly with DCM and the combined filtrate transferred to a round bottom flask containing Celite® and evaporated to dryness *in vacuo*. The sample was subjected to flash column chromatography to remove any DDQ. The product was then recrystallised from a suitable solvent (see relevant experimental data).

4.2.1.4 General Procedure D: Synthesis of Boronic Acids

A solution of aryl bromide (2.0 mmol) was dissolved in dry THF (16 mL) and cooled to – 78 °C under a nitrogen atmosphere. To this was added *n*-BuLi (0.965 mL (2.5 M solution in hexane), 2.40 mmol) and the reaction was stirred for 5 min at – 78 °C before tri-isopropyl borate (1.167 mL, 5.0 mmol) was added. The reaction was allowed to stir for a further 5 min at – 78 °C before being allowed to warm to room temperature. Stirring was then continued at room temperature for a further 20 h (unless otherwise indicated in the experimental data). Aqueous HCl (10 %, 3.5 mL) was then charged to the reaction mixture, which was stirred for a further 1 h at room temperature. The reaction mixture was transferred to a separating funnel, diethyl ether (25 mL) was added and the phases were separated. The lower aqeous layer was extracted again with diethyl ether (25 mL) and the combined organic extracts were dried over anhydrous $MgSO_4$ and filtered. The filtrate was transferred to a round-bottomed flask (RBF), Celite® was added and the liqours were removed *in vacuo*. The remaining crude product was transferred to a column and purified by flash column chromatography on silica gel (6:1 hexane:ethyl acetate eluent). The recovered product was recrystallised from methanol or ethanol.

*4.2.1.5 General Procedure E: Synthesis of Hydroxy Pyrimidine **135***

Sodium methoxide was prepared by gradually adding sodium metal (0.92 g, 40 mmol) to dry methanol (50 mL) at 0 °C under a nitrogen atmopshere. When all the sodium had dissolved and the solution was clear and colourless, the reaction was allowed to warm to room temperature. Formamidine acetate **(114)** (3.39 g, 33 mmol) and methyl acetoacetate **(115)** (2.17 mL, 20 mmol) were then added to the reaction vessel. The mixture was then stirred under nitrogen at room temperature for 18 h. The pH of the reaction mixture was adjusted to pH 7 by the addition of glacial acetic acid (pH adjustment monitored by pH meter) and then concentrated *in vacuo*. The crude product was stirred in acetone (60 mL) and the resultant white precipitate (inorganic salts) was removed by vacuum filtration. The filtrate was concentrated *in vacuo* and the resultant crude residue purified by flash column chromatography on silica gel (12:1 ethyl acetate:methanol eluent).

*4.2.1.6 General Procedure F: Bromination of Hydroxy Pyrimidine **135** Using NBS*

NBS (8.1 g, 45.4 mmol) was added to a solution of 4-hydroxy-6-methylpyrimidine **(135)** (5.0 g, 45.5 mmol) in acetonitrile (150 mL) in a RBF (covered with aluminium foil to exlude light) at room temperature under a nitrogen atmosphere and the mixture was stirred for 1 h. The product precipitated out of solution as a white solid which was recovered by vacuum filtration and washed with cold acetonitrile (0 °C, 20 mL).

*4.2.1.7 General Procedure G: Chlorination of Hydroxyl Moeity of **138** Using $POCl_3$*

A solution of 5-bromo-4-hydroxy-6-methylpyrimidine **(138)** (2.0 g, 10.6 mmol) in phosphorous oxychloride (15 mL) was refluxed at 110 °C for 2 h, then allowed to cool to room temperature and stirred for a further 1 h. The reaction mixture was concentrated *in vacuo*, and the crude residue purified by plug column chromatography on ~ 10 cm of silica gel using chloroform as an eluent.

The pure product was recovered by removal of $CHCl_3$ *in vacuo* to leave a yellow solid.

Note: Phosphorous oxychloride was removed from the reaction mixture *in vacuo*. The distillate was collected and carefully quenched by adding slowly to a large excess of 1M NaOH (aq.), which was vigorously stirred in a beaker. The $POCl_3$ was added portionwise to control the exotherm of the reaction. It is imperative that this quench be carried out at room temperature and **NOT** on ice, as $POCl_3$ will not react at lower temperatures, which could lead to a runaway reaction once the quench mixture is allowed to warm to ambient temperature.

*4.2.1.8 General Procedure H: Dechlorination of Pyrimidine **139** via the Bamford-Stevens Reaction*

A mixture of 5-bromo-4-chloro-6-methylpyrimidine **(139)** (1.04 g, 5 mmol), and tosylhydrazine (1.87 g, 10 mmol) in chloroform (40 mL) was refluxed at 68 - 70 °C for 12 h, and then allowed to cool to room temperature. The resulting precipitate (a tosyl azide intermediate) was filtered off and added portionwise to aqueous K_2CO_3 (10 %, 40 mL) at 90 °C. The mixture was refluxed at 100 °C for 30 min and allowed to cool to room temperature. The reaction mixture was transferred to a separating funnel and extracted with dichloromethane (3 x 40 mL). The combined organic extracts were dried over anhydrous $MgSO_4$ and the solvent was removed by distillation at atmospheric pressure to give the product as a peach-coloured oil.

4.2.1.9 General Procedure I: Suzuki-Miyaura Coupling Reaction

A mixture of 5-bromo-4-methylpyrimidine **(113)** (0.35 g, 2.0 mmol), phenylboronic acid (4.0 mmol), $Pd(OAc)_2$ (13 mg, 3 mol%), SPhos (50 mg, 6 mol%), and K_3PO_4 (1.29 g, 6 mmol) in toluene (32 mL) was heated to 90 °C under a nitrogen atmosphere for 8 h. After cooling to room temperature, the reaction mixture was transferred to a separating funnel and washed with brine (30 mL). The organic layer was dried over anhydrous $MgSO_4$ and concentrated *in vacuo.* The residue was purified by column chromatography

on silica gel using hexane:ethyl acetate (10:1→ 5:1) followed by hexane:chloroform (3:1 → 1:1) solvent systems.

4.2.1.10 General Procedure J: Bromination of Phenyl Pyrimidine Using Bromine in Acetic Acid

To a stirred solution of 4-methyl-5-(2,3,6,7-tetrahydrobenzo[1,2-*b*:4,5-*b'*]difuran-4-yl)pyrimidine **(101)** (0.062 g, 0.24 mmol) in glacial acetic acid (3 mL), a solution of bromine (0.013 mL, 0.27 mmol) in glacial acetic acid (1 mL) was added dropwise. The reaction vessel was covered in aluminium foil to exclude light and allowed to stir at room temperature for 24 h. The reaction mixture was diluted with deionised water (7 mL), at which point a brown solid precipitated from solution and was collected by vacuum filtration.* This precipitate was dissolved in DCM (10 mL), washed with saturated aqueous sodium bicarbonate ($NaHCO_3$, 10 mL) and deionised water (10 mL) and the organic layer was then dried over anhydrous $MgSO_4$, filtered and a brown solid was recovered *in vacuo*.

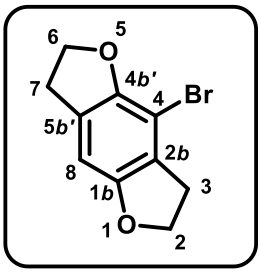
*A 5 % aqueous sodium thiosulfate ($Na_2S_2O_3$) solution was added dropwise to the filtrate until the solution's orange colour faded to cream. The solution was transferred to a separating funnel, DCM (10 mL) was added, and the phases were separated. The lower aqueous layer was extracted with DCM (2 x 15 mL). The combined organic extracts were then washed with $NaHCO_3$ (sat. aq., 3 x 15 mL) and deionised water (2 x 15 mL), before being dried over anhydrous $MgSO_4$, filtered and concentrated *in vacuo*.

4.2.1.11 General Procedure K: Friedel-Crafts Acylation

To a solution of 4-bromo-2,3,6,7-tetrahydrobenzo[1,2-*b*:4,5-*b'*]difuran **(116)** (1.0 g, 4.15 mmol) and $AlCl_3$ (0.83 g, 6.23 mmol) stirring in DCM (50 mL) under a nitrogen atmosphere was added propionyl chloride (7.3 mL, 83 mmol). The propionyl chloride was added in two portions; half at the start of the reaction, and half four hours into the reaction time. The reaction was left to stir at room temperature for 18 h, and was then poured onto 3 M aq. HCl/ice (50 mL) and

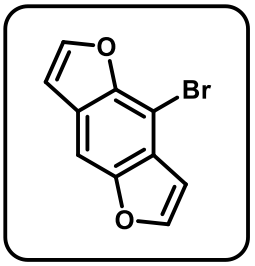
DCM (100 mL). The mixture was transferred to a separating funnel and the phases were separated. The upper aqueous layer was extracted with DCM (2 x 70 mL). The combined organic layers were then extracted with aq. NaOH (20 %, 3 x 50 mL) and brine (3 x 60 mL), before being dried over anhydrous $MgSO_4$, filtered and concentrated *in vacuo*. The crude residue was purified by column chromatography on silica gel (gradient elution from 7:1 hexane:DCM → 100 % DCM) and subsequently recrystallised from chloroform.

4-Bromo-2,3,6,7-tetrahydrobenzo[1,2-*b*:4,5-*b'*]difuran (116)



Prepared according to general procedure A using THBD **(42)** as a starting material, **116** was isolated as a white crystalline solid after recrystallisation from methanol in 72 % yield; R_f 0.60 (4:1 hexane:ethyl acetate); m.p. 80 - 82 °C (MeOH), (lit. m.p. 79 - 81 °C (MeOH))[1] ; IRν_{max} (KBr): 2968, 2913, 2894, 1594, 1474, 1452, 1302, 1233, 1172, 983, 868, 844, 752 cm^{-1}; ^{1}H-NMR δ (400 MHz, $CDCl_3$): 3.16 (2H, t, J = 8.7Hz, H-3), 3.24 (2H, t, J = 8.7 Hz, H-7), 4.58 (2H, t, J = 8.7 Hz, H-2), 4.63 (2H, t, J = 8.7 Hz, H-6), 6.56 (1H, s, H-8); ^{13}C-NMR δ (75.5 MHz, $CDCl_3$) 31.3 (C-7), 31.5 (C-3), 71.3 (C-2), 71.8 (C-6), 99.6 (C-4), 104.9 (C-8), 126.8, 126.9 (C-2*b*, C-5*b'*), 151.2, 154.3 (C-1*b*, C-4*b'*); HRMS calc. for $C_{10}H_9{}^{79}BrO_2$: ($M+H^+$) *m/z* 240.9864, found 240.9864.

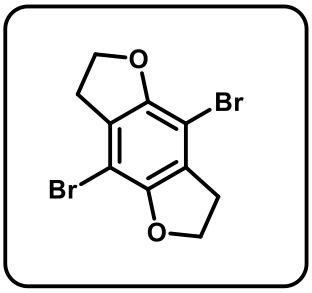
4-Bromobenzo[1,2-*b*:4,5-*b'*]difuran (117)



Prepared according to general procedure C on a 6 mmol scale, using **116** as a starting material, **117** was isolated as a white crystalline solid after recrystallisation from hexane in 73 % yield; R_f 0.77 (4:1 hexane:ethyl acetate); m.p. 107 - 109 °C (hexane), (lit. m.p. 107 - 109 °C (hexane))[1] ; IRν_{max} (KBr): 3125, 2921, 1581, 1430, 1415, 1298, 1178, 1028, 903, 847, 723, 650 cm^{-1}; ^{1}H-NMR δ (300 MHz, $CDCl_3$): 6.90 (2H, d, J = 3.0 Hz,

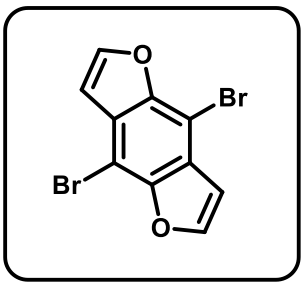
H-3 and H-7), 7.61 (1H, s, H-8), 7.71 (2H, d, J = 3.0 Hz, H-2 and H-6); ^{13}C-NMR δ (75.5 MHz, $CDCl_3$) 94.4 (C-4), 101.6 (C-8), 106.6, 107.7 (C-3, C-7), 126.1, 126.9 (C-2*b*, C-5*b'*), 145.8, 146.2 (C-2, C-6), 149.3, 151.6 (C-1*b*, C-4*b'*); HRMS calc. for $C_{10}H_5{}^{79}BrO_2$: ($M+H^+$) *m/z* 235.9473, PMI not found under standard conditions.

4,8-Dibromo-2,3,6,7-tetrahydrobenzo[1,2-*b*:4,5-*b'*]difuran (118)



Prepared according to general procedure B, **118** was isolated as a white crystalline solid after recrystallisation from ethanol in 71 % yield; R_f 0.69 (2:1 hexane:ethyl acetate); m.p. 207 - 209 °C (EtOH), (lit. m.p. 207 - 209 °C (EtOH))[2] ; IRν_{max} (KBr): 2970, 2909, 1466, 1422, 1306, 1228, 1169, 989, 969, 868, 804 cm^{-1}; ^{1}H-NMR δ (400 MHz, $CDCl_3$): 3.26 (4H, t, J = 8.8 Hz, H-3 and H-7), 4.67 (4H, t, J = 8.8 Hz, H-2 and H-6); ^{13}C-NMR δ (75.5 MHz, $CDCl_3$) 32.5 (C-3 and C-7), 71.6 (C-2 and C-6), 98.6 (C-4 and C-8), 127.6 (C-2*b* and C-5*b'*), 151.3 (C-1*b* and C-4*b'*); HRMS calc. for $C_{10}H_8{}^{79}Br_2O_2$: ($M+H^+$) *m/z* 318.8869, found 318.8873.

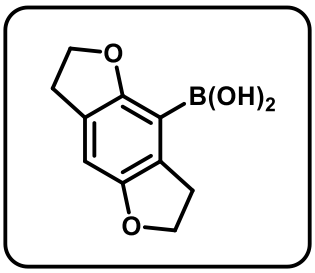
4,8-Dibromobenzo[1,2-*b*:4,5-*b'*]difuran (119)



Prepared according to general procedure C using **118** as a starting material, **119** was isolated as a white crystalline solid after recrystallisation from hexane in 40 % yield; R_f 0.77 (9:1 hexane:ethyl acetate); m.p. 233 - 235 °C (hexane), (lit. m.p. 235 - 237 °C (EtOH))[2]; IRν_{max} (KBr): 3146, 2922, 1721, 1622, 1544, 1490, 1348, 1299, 1262, 1136, 1026, 829, 754 cm^{-1}; ^{1}H-NMR δ (400 MHz, $CDCl_3$): 6.98 (2H, d, J = 2.4 Hz, H-3 and H-7), 7.76 (2H, d, J = 2.4 Hz, H-2 and H-6); ^{13}C-NMR δ (100.6 MHz, $CDCl_3$) 94.0 (C-4 and C-8), 107.5 (C-3 and C-7),

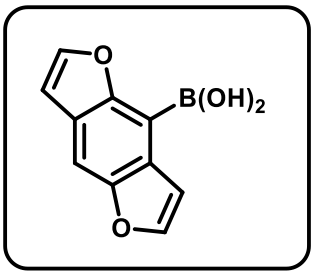
127.2 (C-2*b* and C-5*b'*), 146.6 (C-2 and C-6), 149.0 (C-1*b* and C-4*b'*); HRMS calc. for $C_{10}H_4{}^{79}Br_2O_2$: ($M+H^+$) *m/z* 314.8656, found 314.8659.

(2,3,6,7-Tetrahydrobenzo[1,2-*b*:4,5-*b'*]difuran-4-yl)boronic acid (123)



Prepared according to general procedure D using **116** as a starting material, novel boronic acid **123** was isolated as a beige solid after recrystallisation from MeOH in 66 % yield; R_f 0.06 (6:1 hexane:ethyl acetate); m.p. 160 - 162 °C (MeOH); IRν_{max} (KBr): 3375, 3062, 2982, 1617, 1466, 1438, 1335, 1080, 987, 958, 730 cm^{-1}; ^{1}H-NMR δ (400 MHz, $CDCl_3$): 3.14 (2H, t, J = 8.4 Hz, H-7), 3.35 (2H, t, J = 8.4 Hz, H-3), 4.51 - 4.62 (4H, m, H-2 and H-6), 5.62 (2H, s, O**H**), 6.74 (1H, s, H-8); ^{13}C-NMR δ (100.6 MHz, $CDCl_3$) 29.7, 31.9 (C-3, C-7), 72.0 (C-2 and C-6), 109.0 (C-8), 124.6 (C-5*b'*), 132.4 (C-2*b*), 154.3 (C-1*b*), 159.6 (C-4*b'*), C-4 signal absent; HRMS calc. for $C_{10}H_{11}{}^{11}BO_4$: ($M+H^+$) *m/z* 206.0751, PMI not found under standard conditions.

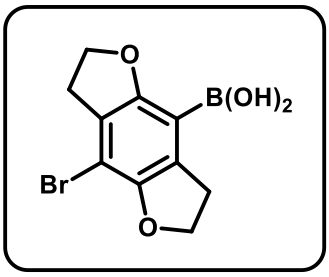
Benzo[1,2-*b*:4,5-*b'*]difuran-4-ylboronic acid (125)



Prepared according to general procedure D on a 4.2 mmol scale using **117** as a starting material (with a reaction time at room temperature of 140 h), novel boronic acid **125** was isolated as a beige solid after recrystallisation from MeOH in 13 % yield; R_f 0.12 (6:1 hexane:ethyl acetate); m.p. 174 - 175 °C (MeOH); IRν_{max} (KBr): 3401, 3152, 2924, 1611, 1548, 1415, 1382, 1286, 1125, 1027, 855, 762 cm^{-1}; ^{1}H-NMR δ (400 MHz, $CDCl_3$): 5.59 (2H, s, O**H**), 6.88 (1H, d, J = 2.0 Hz, H-7), 7.38 (1H, d, J = 2.0 Hz, H-3), 7.69 (1H, d, J = 2.0 Hz, H-2 or H-6), 7.71 (1H, d, J = 2.0 Hz, H-2 or H-6), 7.77 (1H, s, H-8); ^{13}C-NMR δ (100.6 MHz, $CDCl_3$) 105.7 (C- 8) 107.1, 108.8 (C-3, C-7), 124.0 (C-5*b'*), 131.3 (C-2*b*), 144.8, 146.5 (C-2, C-6), 151.9 (C-1*b*), 157.5 (C-4*b'*), C-4 signal absent; HRMS

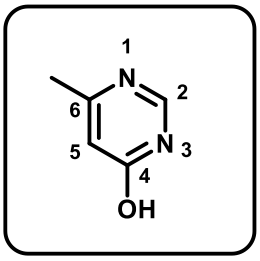
calc. for $C_{10}H_7{}^{11}BO_4$: $(M+H^+)$ *m/z* 202.0438, PMI not found under standard conditions.

(8-Bromo-2,3,6,7-tetrahydrobenzo[1,2-*b*:4,5-*b'*]difuran-4-yl)boronic acid (126)



Prepared according to general procedure D on a 6 mmol scale using **118** as a starting material (the product precipitated out of solution after stirring with aqueous HCl and was isolated by vacuum filtration, therefore the work-up and column were not performed), novel boronic acid **126** was isolated as a white solid after recrystallisation from EtOH in 78 % yield; R_f 0.09 (6:1 hexane:ethyl acetate); m.p. 232 - 235 °C (EtOH); IRν_{max} (KBr): 3374, 2917, 2850, 1602, 1479, 1424, 1360, 1084, 990, 970, 776, 674 cm^{-1}; ^{1}H-NMR δ (300 MHz, $CDCl_3$) 3.18 (2H, t, J = 9.0 Hz, H-7), 3.45 (2H, t, J = 9.0 Hz, H-3), 4.58 - 4.69 (4H, m, H-2 and H-6), 5.46 (2H, s, O**H**); ^{13}C-NMR δ (75.5 MHz, DMSO-d_6): 31.0, 32.3 (C-3 and C-7), 71.3, 71.8 (C-2 and C-6), 101.2 (C-8), 125.8 (C-5*b'*), 132.4 (C-2*b*), 150.7 (C-1*b*), 158.3 (C-4*b'*), C-4 signal absent; HRMS calc. for $C_{10}H_{10}{}^{11}B^{79}BrO_4$: $(M+H^+)$ *m/z* 283.9856, PMI not found under standard conditions.

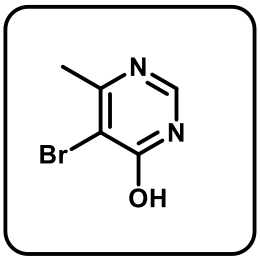
4-Hydroxy-6-methylpyrimidine (135)



Prepared according to general procedure E, **135** was isolated in 66 % yield as a pale yellow solid after recrystallisation from ethyl acetate; R_f 0.16 (12:1 ethyl acetate:methanol); m.p. 145 - 147 °C (ethyl acetate), (lit. m.p. 143.6 - 144.3 °C (no recryst.))[3] ; IRν_{max} (KBr): 3331, 2966, 2917, 1682, 1423, 1313, 984 cm^{-1}; ^{1}H-NMR δ (400 MHz, $CDCl_3$): 2.34 (3H, s, C**H$_3$**), 6.34 (1H, s, H-5), 8.10 (1H, s, H-2), 9.69 (1H, bs, O**H**); ^{13}C-NMR

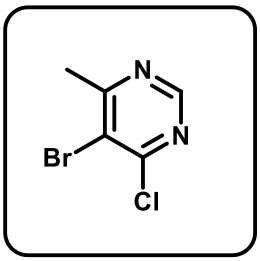
δ (100.6 MHz, $CDCl_3$) 24.9 (**C**H_3), 111.8 (C-5), 147.6 (C-2), 158.4 (C-6), 162.0 (C-4); HRMS calc. for $C_5H_6N_2O$: $(M+H^+)$ *m/z* 111.0558, found 111.0556.

5-Bromo-4-hydroxy-6-methylpyrimidine (138)



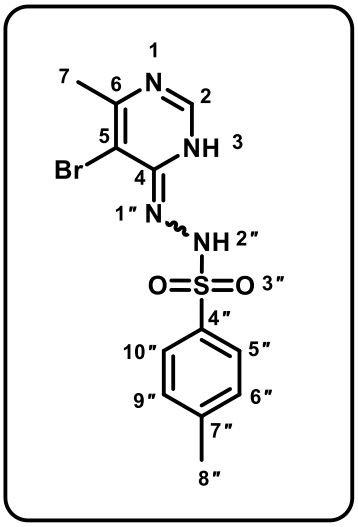
Prepared according to general procedure F, **138** was isolated in 81 % yield as a white solid; R_f 0.06 (49:1 dichloromethane: methanol); m.p. 184 - 186 °C (no recryst.), (lit. m.p. 184.1 - 185.2 °C (no recryst.))[3] ; IRν_{max} (KBr): 3444, 3125, 2930, 2831, 1652, 1603, 1400, 1310, 1207, 1061, 1016, 924, 824, 769, 607, 554 cm^{-1}; ^{1}H-NMR δ (400 MHz, $CDCl_3$): 2.56 (3H, s, C**H$_3$**), 8.11 (1H, s, H-2); ^{13}C-NMR δ (75.5 MHz, $CDCl_3$) 29.6 (**C**H_3), 112.8 (C-5), 145.7 (C-2), 160.2 (C-6), 165.0 (C-4); HRMS calc. for $C_5H_5{}^{79}BrN_2O$: $(M+H^+)$ *m/z* 188.9663, found 188.9663.

5-Bromo-4-chloro-6-methylpyrimidine (139)



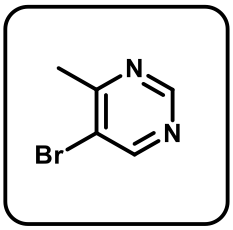
Prepared according to general procedure G, **139** was isolated in 82 % yield as a yellow crystalline solid; R_f 0.50 (4:1 hexane: ethyl acetate); m.p. 56 - 57 °C (no recryst.), (lit. m.p. 58.8 - 59.4 °C (no recryst.))[3] ; IRν_{max} (KBr): 2924, 1541, 1508, 1424, 1377, 1329, 1270, 1197, 1041, 881, 782 cm^{-1}; ^{1}H-NMR δ (400 MHz, $CDCl_3$): 2.70 (3H, s, C**H$_3$**), 8.54 (1H, s, H-2); ^{13}C-NMR δ (75.5 MHz, $CDCl_3$) 25.8 (**C**H_3), 121.0 (C-5), 155.6 (C-2), 160.6 (C-4), 168.8 (C-6); HRMS calc. for $C_5H_4{}^{79}Br{}^{35}ClN_2$: $(M+H^+)$ *m/z* 206.9325, found 206.9326.

_N′_-(5-Bromo-6-methylpyrimidin-4(3_H_)-ylidene)-4-methylbenzenesulfono hydrazide (142)



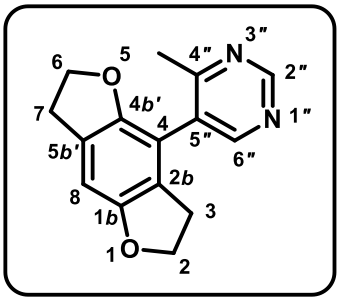
Novel azide **142** was isolated as an intermediate as noted in general procedure H, in 49 % yield as a pale yellow solid. The compound was isolated as a mixture of *E*/*Z* rotamers in a ratio of major:minor = 5:1; R_f 0.16 (1:1 hexane:ethyl acetate); m.p. 209 - 210 °C (no recryst.); IRν_{max} (KBr): 2919, 2850, 1582, 1331, 1162, 1033, 813, 551 cm^{-1}; ^{1}H-NMR δ (300 MHz, DMSO-d_6): 2.36 (s, (H-8″)^Z) 2.41 (s, (H-8)^E) 2.50 (s, H-7), 6.06 (bs, H-3), 7.34 (d, J = 6.0 Hz, (H-6″ and H-9″)^Z), 7.46 (d, J = 6.0 Hz, (H-6″ and H-9″)^E), 7.66 (d, J = 6.0 Hz, (H-5″ and H-10″)^Z), 7.80 (d, J = 6.0 Hz, (H-6″ and H-9″)^E), 8.46 (s, H-2), 10.40 (s, (H-2″)*); ^{13}C-NMR δ (75.5 MHz, DMSO-d_6) 21.3 (C-8″)^Z, 21.5 (C-8″)^E, 21.6 (C-7), 101.7 (C-5), 128.1 (C-5″ and C-10″)^Z, 128.4 (C-5″ and C-10″)^E, 129.8 (C-6″ and C-9″)^Z, 130.3 (C-6″ and C-9″)^E, 134.8 (C-7″)^E, 136.6 (C-7″)^Z, 144.1 (C-4″)^Z, 144.8 (C-4″)^E, 151.24 (C-6), 158.6 (C-4), 160.4 (C-2); HRMS calc. for $C_{12}H_{13}{}^{79}BrN_4O_2{}^{32}S$: ($M+H^+$) *m/z* 357.0021, found 357.0021.

5-Bromo-4-methylpyrimidine (113)



Prepared according to general procedure H, **113** was isolated in 42 % yield (from **139**) as a pale peach oil; R_f 0.16 (6:1 hexane: ethyl acetate); IRν_{max} (NaCl): 2892, 2832, 1640, 1604, 1400, 1310, 1208, 1189, 1061, 1015, 948, 824, 769, 607, 555 cm^{-1}; ^{1}H-NMR δ (400 MHz, $CDCl_3$): 2.65 (3H, s, C**H$_3$**) 8.72 (1H, s, H-6), 8.98 (1H, s, H-2) ; ^{13}C-NMR δ (75.5 MHz, $CDCl_3$) 24.4 (**C**H_3), 121.6 (C-5), 156.6 (C-2), 158.0 (C-6), 166.0 (C-4); HRMS calc. for $C_5H_5{}^{79}BrN_2$: ($M+H^+$) *m/z* 172.9714, found 172.9711.

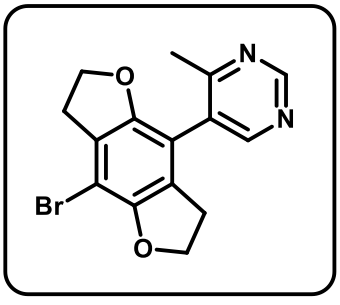
4-Methyl-5-(2,3,6,7-tetrahydrobenzo[1,2-*b*:4,5-*b*′]difuran-4-yl)pyrimidine (101)



Prepared according to general procedure I using **123** as a starting material, novel pyrimidine **101** was isolated as a yellow semi-solid in 52 % yield after column chromatography; R_f 0.08 (5:1 hexane:ethyl acetate); IRν_{max} (NaCl): 2921, 2853, 1722, 1572, 1478, 1422, 1448, 1219, 1166, 985, 958, 736 cm^{-1}; ^{1}H-NMR δ (400 MHz, $CDCl_3$): 2.45 (3H, s, C**H$_3$**), 2.79 - 2.87 (1H, m, H-3$_A$), 3.02 - 3.11 (1H, m, H-3$_B$), 3.22 (2H, t, J = 8.4 Hz, H-7), 4.49 - 4.62 (4H, m, H-2 and H-6), 6.73 (1H, s, H-8), 8.52 (1H, s, H-6″), 9.07 (1H, s, H-2″); ^{13}C-NMR δ (75.5 MHz, $CDCl_3$) 22.5 (**C**H$_3$), 29.4 (C-3), 30.4 (C-7), 71.6 (C-2, C-6), 106.6 (C-8), 114.4 (C-4), 124.7 (C-2*b*), 126.8 (C-5*b*′), 129.1 (C-5″), 151.6 (C-4*b*′), 154.3 (C-1*b*), 156.7 (C-6″), 157.5 (C-2″), 165.7 (C-4″); HRMS calc. for $C_{15}H_{14}N_2O_2$: (M+H$^+$) *m/z* 255.1134, found 255.1134; HPLC λ_{max} t_R at 211 nm: 4.35 min.

Note: H_A and H_B in the ^{1}H-NMR spectrum assignment for **101** refer to magnetically non-equivalent H-3 hydrogen atoms. This is due to diastereotopic protons in the compound, which is discussed in detail in Chapter Two (Section 2.2.3). This phenomenon also appears in the ^{1}H-NMR spectra of **104** and **173**.

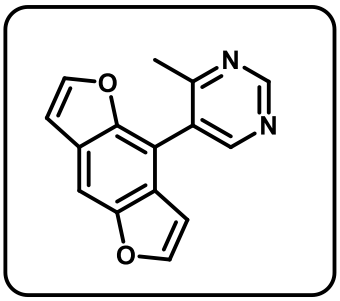
5-(8-Bromo-2,3,6,7-tetrahydrobenzo[1,2-*b*:4,5-*b*′]difuran-4-yl)-4-methylpyrimidine (104)



Prepared according to general procedure I on a 1.5 mmol scale using **126** as a starting material, novel pyrimidine **104** was isolated as a yellow semi-solid in 36 % yield after column chromatography; R_f 0.22 (1:1 hexane:ethyl acetate); IRν_{max} (NaCl): 2964, 2903, 1573, 1546, 1445, 1404, 1307, 1219, 992, 798, 785 cm^{-1}; ^{1}H-NMR δ (400 MHz, $CDCl_3$): 2.44 (3H, s, C**H$_3$**), 2.89 -

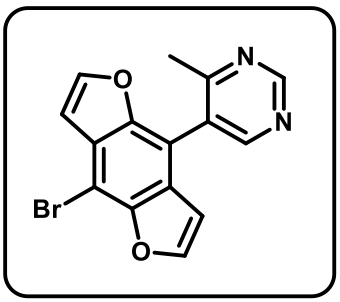
2.97 (1H, m, H-3$_A$), 3.10 - 3.19 (1H, m, H-3$_B$), 3.26 (2H, t, J = 8.4 Hz, H-7), 4.52 - 4.72 (4H, m, H-2 and H-6), 8.50 (1H, s, H-6″), 9.08 (1H, s, H-2″); ^{13}C-NMR δ (100.6 MHz, $CDCl_3$) 22.5 (**C**H$_3$), 30.5 (C-3), 31.7 (C-7), 71.5 (C-2), 72.0 (C-6), 100.4 (C-8), 113.6 (C-4), 125.7 (C-2*b*), 127.6 (C-5*b*′), 128.4 (C-5″), 151.5 (C-1*b*), 151.8 (C-4*b*′), 156.6 (C-6″), 157.7 (C-2″), 165.7 (C-4″); HRMS calc. for $C_{15}H_{13}{}^{79}BrN_2O_2$: (M+H$^+$) *m/z* 333.0239, found 333.0240; HPLC λ_{max} t_R at 211 nm: 5.65 min.

5-(Benzo[1,2-*b*:4,5-*b*′]difuran-4-yl)-4-methylpyrimidine (106)



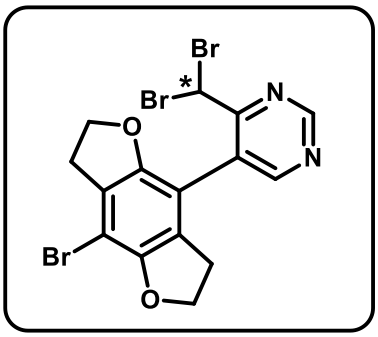
Prepared according to general procedure I on a 0.35 mmol scale using **125** as a starting material, novel pyrimidine **106** was isolated as a brown solid in 38 % yield after purification by preparative TLC (eluent 3:1 hexane:chloroform); pyrimidine **106** was also synthesised in 6 % yield using general procedure A with **101** as a starting material, however this result could not be repeated; R_f 0.32 (1:1 hexane:ethyl acetate); m.p. 128 - 129 °C (no recryst.); IRν_{max} (NaCl): 2922, 1678, 1573, 1547, 1448, 1398, 1157, 1128, 1028, 854, 760, 750 cm^{-1}; ^{1}H-NMR δ (400 MHz, $CDCl_3$): 2.43 (3H, s, C**H$_3$**), 6.59 (1H, d, J = 1.6 Hz, H-7), 6.93 (1H, d, J = 2.4 Hz, H-3), 7.66 (1H, d, J = 2.4 Hz, H-2), 7.71 (1H, d, J = 1.6 Hz, H-6), 7.76 (1H, s, H-8), 8.75 (1H, s, H-6″), 9.20 (1H, s, H-2″); ^{13}C-NMR δ (100.6 MHz, $CDCl_3$) 22.8 (**C**H$_3$), 103.1 (C-8), 105.3 (C-7), 107.2 (C-3) 110.3 (C-4), 125.1 (C-5*b*′), 125.7 (C-2*b*), 128.2 (C-5″), 146.1 (C-2), 146.7 (C-6), 149.3 (C-1*b*), 151.9 (C-4*b*′), 157.6 (C-6″), 157.8 (C-2″), 166.1 (C-4″); HRMS calc. for $C_{15}H_{10}N_2O_2$: (M+H$^+$) *m/z* 251.0820, found 251.0821; HPLC λ_{max} t_R at 211 nm: 5.40 min.

5-(8-Bromobenzo[1,2-*b*:4,5-*b′*]difuran-4-yl)-4-methylpyrimidine (108)



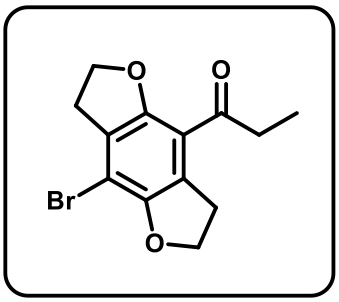
Prepared according to general procedure N, novel pyrimidine **108** was isolated as an impurity by preparative TLC (eluent 3:1 hexane:ethyl acetate) as a brown solid in 2.2 % yield; R_f 0.41 (1:1 hexane:ethyl acetate); m.p. 110 - 111 °C (no recryst.); IRν_{max} (KBr): 3020, 2921, 1547, 1386, 1265, 905, 755, 726, 669, 650 cm^{-1}; ^{1}H-NMR δ (400 MHz, $CDCl_3$): 2.42 (3H, s, C**H$_3$**), 6.69 (1H, d, J = 2.4 Hz, H-7), 7.00 (1H, d, J = 2.4 Hz, H-3), 7.70 (1H, d, J = 2.4 Hz, H-2), 7.78 (1H, d, J = 2.4 Hz, H-6), 8.72 (1H, s, H-6′), 9.21 (1H, s, H-2′); ^{13}C-NMR δ (100.6 MHz, $CDCl_3$) 22.9 (**C**H$_3$), 95.5 (C-8), 106.2 (C-7), 107.1 (C-3) 110.0 (C-4), 125.6 (C-5*b′*), 127.0 (C-2*b*), 127.4 (C-5′), 146.6 (C-2), 147.2 (C-6), 148.9 (C-1*b*), 149.3 (C-4*b′*), 157.5 (C-6′), 158.1 (C-2′), 166.0 (C-4′); HRMS calc. for $C_{15}H_9{}^{79}BrN_2O_2$: (M+H$^+$) *m/z* 328.9926, found 328.9920.

5-(8-Bromo-2,3,6,7-tetrahydrobenzo[1,2-*b*:4,5-*b′*]difuran-4-yl)-4-(dibromomethyl)pyrimidine (145)



Prepared according to general procedure J (originally intended to synthesise **104**), novel pyrimidine **145** was isolated as a precipitate from the crude reaction mixture as a brown solid in 25 % yield after purification by preparative TLC (eluent 1:1 hexane: ethyl acetate); R_f 0.41 (1:1 hexane:ethyl acetate); m.p. 103 - 105 °C (no recryst.); IRν_{max} (KBr): 2921, 1569, 1542, 1410, 1223, 1142, 992, 734, 669, 606; ^{1}H-NMR δ (300 MHz, $CDCl_3$): 2.94 - 3.05 (1H, m, H-3$_A$), 3.10 - 3.20 (1H, m, H-3$_E$), 3.25 - 3.32 (2H, m, H-7), 4.55 - 4.70 (4H, m, H-2 and H-6), 6.55 (1H, s, H*****), 8.61 (1H, s, H-6′), 9.37 (1H, s, H-2′); ^{13}C-NMR δ (100.6 MHz, $CDCl_3$) 30.0, 30.3 (C-3, C-7), 38.0 (C*), 71.8, 72.0 (C-2, C-6), 101.7 (C-8), 110.6 (C-4), 123.2 (C-5′), 125.9, 128.2 (C-2*b*, C-5*b′*), 151.5, 152.0 (C-1*b*, C-4*b′*) 158.7 (C-6′), 159.2 (C-2′), 163.0 (C-4′); HRMS calc. for $C_{15}H_{11}{}^{79}Br_3N_2O_2$: (M+H$^+$) *m/z* 488.8425, found 488.8449.

1-(8-Bromo-2,3,6,7-tetrahydrobenzo[1,2-*b*:4,5-*b'*]difuran-4-yl)propan-1-one (153)



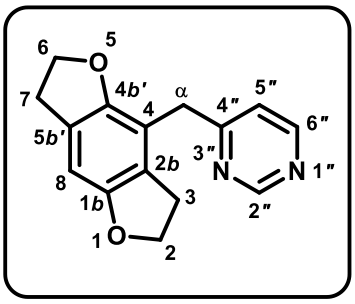
Prepared according to general procedure K, novel compound **153** was isolated as a yellow solid in 41 % yield; R_f 0.57 (5:1 hexane:ethyl acetate); m.p. 167 - 169 °C ($CHCl_3$); IRν_{max} (KBr): 2974, 2912, 1665, 1587, 1417, 1293, 1222, 1112, 1052, 995, 977, 823 cm^{-1}; ^{1}H-NMR δ (400 MHz, $CDCl_3$): 1.13 (3H, t, J = 7.2 Hz, H-γ), 2.97 (2H, q, J = 7.2 Hz, H-β), 3.20 (2H, t, J = 8.8 Hz, H-7), 3.56 (2H, t, J = 8.9 Hz, H-3), 4.62 - 4.71 (4H, m, H-2 and H-6); ^{13}C-NMR δ (100.6 MHz, $CDCl_3$) 7.9 (C-γ), 31.1 (C-7), 32.7 (C-3), 37.2 (C-β), 71.8 (C-6), 72.5 (C-2), 104.9 (C-8), 116.8 (C-4), 127.6 (C-5*b'*), 128.8 (C-2*b*), 151.8 (C-1*b*) 154.1 (C-4*b'*), 200.7 (C-α); HRMS calc. for $C_{15}H_{13}{}^{79}BrN_2O_2$: ($M+H^+$) *m/z* 297.0121, found 297.0125.

4.2.2 Benzyl Pyrimidine Impurities

4.2.2.1 General Procedure L: Palladium-Catalysed C-H Activation Coupling Reaction

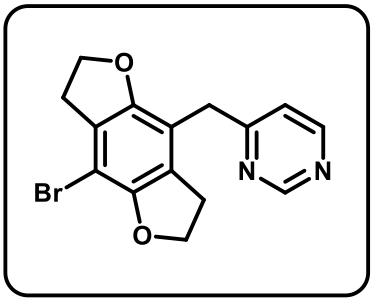
A 250 mL RBF was charged with 4-methylpyrimidine **(134)** (0.091 mL, 1.0 mmol), caesium carbonate (0.65 g, 2.0 mmol), $Pd(dmdba)_2$ (85 mg, 0.1 mmol), and Xantphos (56 mg, 0.1 mmol). 1,4-Dioxane (8 mL) was then added, followed by the aryl bromide (1.0 mmol), and a stirrer bar. A reflux condenser was fitted and the atmosphere was purged with nitrogen. The reaction was then heated to 100 °C (reflux) and stirred overnight. After 16 h, the reaction was allowed to cool and then filtered through a pad of Celite® to remove catalyst, washing through with ethyl acetate (30 mL). The filtrate was then concentrated *in vacuo* onto Celite®, and purified by column chromatography on silica gel (eluent system: 98:2 → 3:7 hexane:ethyl acetate).

4-((2,3,6,7-Tetrahydrobenzo[1,2-*b*:4,5-*b*′]difuran-4-yl)methyl)pyrimidine (100)



Prepared according to general procedure L using **116** as a starting material, novel pyrimidine **100** was isolated as a yellow solid in 66 % yield after recrystallisation from diethyl ether; R_f 0.06 (5:1 hexane:ethyl acetate); m.p. 94 - 96 °C (diethyl ether); IRν_{max} (KBr): 2960, 2891, 1581, 1547, 1436, 1385, 1206, 1157, 996, 981 cm^{-1}; ^{1}H-NMR δ (400 MHz, $CDCl_3$): 3.07 (2H, t, J = 8.4 Hz, H-3), 3.16 (2H, t, J = 8.4 Hz, H-7), 4.03 (2H, s, H-α), 4.50 - 4.56 (4H, m, H-2 and H-6), 6.58 (1H, s, H-8), 7.19 (1H, d, J = 4.8 Hz, H-5″) 8.58 (1H, d, J = 4.8 Hz, H-6″), 9.10 (1H, s, H-2″); ^{13}C-NMR δ (100.6 MHz, $CDCl_3$) 29.7, 30.0 (C-3, C-7), 37.1 (C-α), 71.4, 71.5 (C-2, C-6), 104.9 (C-8), 115.6 (C-4), 120.4 (C-5″), 125.7, 126.0 (C-2*b*, C-5*b*′), 152.5 (C-1*b*), 154.2 (C-4*b*′), 156.9 (C-6″), 158.6 (C-2″), 168.6 (C-4″); HRMS calc. for $C_{15}H_{14}N_2O_2$: ($M+H^+$) *m/z* 255.1134, found 255.1135; HPLC λ_{max} t_R at 211 nm: 4.22 min.

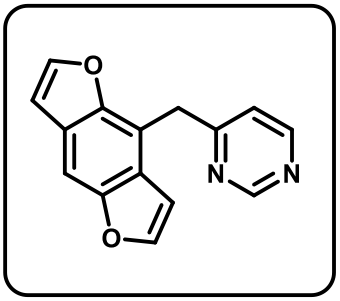
4-((8-Bromo-2,3,6,7-tetrahydrobenzo[1,2-*b*:4,5-*b*′]difuran-4-yl)methyl)pyrimidine (103)



Prepared according to general procedure L using **118** as a starting material, novel pyrimidine **103** was isolated as an orange solid in 92 % yield after recrystallisation from diethyl ether; R_f 0.06 (5:1 hexane:ethyl acetate); m.p. 118 - 120 °C (diethyl ether); IRν_{max} (KBr): 2960, 2918, 1579, 1422, 1386, 1206, 1156, 992, 848 cm^{-1}; ^{1}H-NMR δ (400 MHz, $CDCl_3$): 3.19 (4H, t, J = 8.4 Hz, H-3 and H-7), 3.97 (2H, s, H-α), 4.56 - 4.64 (4H, m, H-2 and H-6), 7.19 (1H, d, J = 5.2 Hz, H-5″) 8.58 (1H, d, J = 5.2 Hz, H-6″), 9.10 (1H, s, H-2″); ^{13}C-NMR δ (100.6 MHz, $CDCl_3$) 29.4, 29.7 (C-3, C-7), 35.9 (C-α), 71.3, 71.9 (C-2, C-6), 98.4 (C-8), 114.8 (C-4), 120.4 (C-5″), 125.0, 126.8 (C-2*b*, C-5*b*′), 150.4 (C-1*b*), 152.6 (C-4*b*′), 157.0 (C-6″), 158.7 (C-2″), 168.1 (C-4″); HRMS

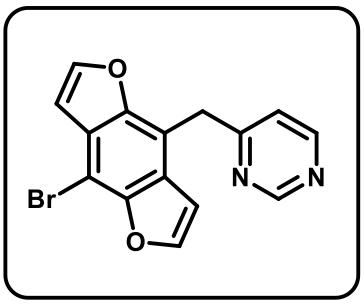
calc. for $C_{15}H_{13}{}^{79}BrN_2O_2$: (M+H$^+$) *m/z* 333.0239, found 333.0241; HPLC λ_{max} t_R at 211 nm: 5.44 min.

4-(Benzo[1,2-*b*:4,5-*b′*]difuran-4-ylmethyl)pyrimidine (105)



Prepared according to general procedure L on a 0.6 mmol scale using **117** as a starting material, novel pyrimidine **105** was isolated as a yellow solid in 7.3 % yield; R_f 0.06 (5:1 hexane:ethyl acetate); m.p. 88 - 90 °C (no recryst.); IRν_{max} (KBr): 2919, 2850, 1580, 1551, 1417, 1385, 1176, 1156, 1050, 1018, 760 cm^{-1}; ^{1}H-NMR δ (400 MHz, $CDCl_3$) 4.62 (2H, s, H-α), 6.84 - 6.86 (2H, m, H-3 and H-7), 7.10 (1H, d, J = 5.2 Hz, H-5″), 7.60 (1H, s, H-8), 7.63 (1H, d, J = 2.0 Hz, H-2 or H-6), 7.66 (1H, d, J = 2.0 Hz, H-2 or H-6), 8.53 (1H, d, J = 5.2 Hz, H-6″), 9.16 (1H, s, H-2″); ^{13}C-NMR δ (100.6 MHz, $CDCl_3$) 35.7 (C-α), 101.4 (C-8), 105.2, 107.2 (C-3, C-7), 111.5 (C-4), 120.4 (C-5″), 125.4, 125.5 (C-2*b*, C-5*b′*), 145.7, 145.8 (C-2, C-6), 150.4 (C-1*b*), 152.1 (C-4*b′*), 157.0 (C-6″), 158.7 (C-2″), 168.3 (C-4″); HRMS calc. for $C_{15}H_{10}N_2O_2$: (M+H$^+$) *m/z* 251.0820, found 251.0812; HPLC λ_{max} t_R at 211 nm: 4.98 min.

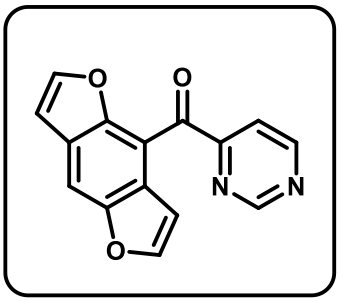
4-((8-Bromobenzo[1,2-*b*:4,5-*b′*]difuran-4-yl)methyl)pyrimidine (107)



Prepared according to general procedure L on a 0.5 mmol scale using **119** as a starting material, novel pyrimidine **107** was isolated as an orange solid in 8.2 % yield; R_f 0.15 (5:1 hexane:ethyl acetate); m.p. 105 - 106 °C (no recryst.); IRν_{max} (KBr): 3115, 2922, 1580, 1549, 1387, 1312, 1207, 1141, 1024, 843, 761, 696 cm^{-1}; ^{1}H-NMR δ (400 MHz, $CDCl_3$): 4.58 (2H, s, H-α), 6.92 (2H, d, J = 2.0 Hz, H-3 and H-7), 7.10 (1H, d, J = 5.2 Hz, H-5″), 7.69 - 7.71 (2H, m, H-2 and H-6), 8.54 (1H, d, J = 5.2 Hz, H-6″), 9.14 (1H, s, H-2″); ^{13}C-NMR δ (100.6 MHz, $CDCl_3$) 35.6 (C-α), 93.9 (C-8), 106.3, 107.1 (C-3, C-7), 111.2 (C-4), 120.3 (C-5″), 126.1, 126.7 (C-2*b*, C-5*b′*), 146.2, 146.3 (C-2, C-

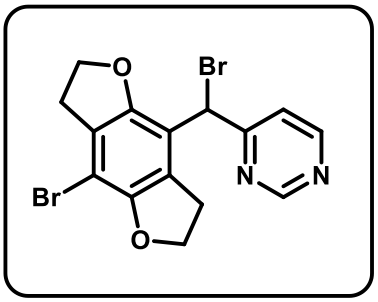
6), 149.3, 150.0 (C-1*b*, C-4*b*′), 157.1 (C-6″), 158.8 (C-2″), 167.7 (C-4″); HRMS calc. for $C_{15}H_9{}^{79}BrN_2O_2$: (M+H$^+$) *m/z* 328.9926, found 328.9930; HPLC HPLC λ_{max} t_R at 211 nm: 7.00 min.

Benzo[1,2-*b*:4,5-*b*′]difuran-4-yl(pyrimidin-4-yl)methanone (169)



Prepared according to general procedure C on a 0.4 mmol scale using **100** as a starting material (originally intended to synthesise **105**), novel pyrimidine **169** was isolated as a yellow solid in 25 % yield; R_f 0.17 (5:1 hexane:ethyl acetate); m.p. 148 - 150 °C (no recryst.); IRν_{max} (KBr): 3124, 2925, 1666, 1575, 1546, 1380, 1281, 1127, 1023, 866, 704, 654 cm^{-1}; ^{1}H-NMR δ (400 MHz, $CDCl_3$): 6.86 (1H, d, J = 2.2 Hz, H-7), 7.30 (1H, d, J = 2.2 Hz, H-3), 7.46 (1H, d, J = 2.2 Hz, H-6), 7.80 (1H, d, J = 2.2 Hz, H-2), 7.84 (1H, dd, J = 1.3, 5.0 Hz, H-5″), 7.94 (1H, s, H-8), 9.06 (1H, d, J = 5.0 Hz, H-6″), 9.32 (1H, d, J = 1.3 Hz, H-2″); ^{13}C-NMR δ (100.6 MHz, $CDCl_3$): 106.7, 107.4 (C-3, C-7), 108.8 (C-8), 111.4 (C-4), 119.0 (C-5″), 126.1, 126.9 (C-2*b*, C-5*b*′), 146.0, 148.3 (C-2, C-6) 151.2, 152.1 (C-1*b*, C-4*b*′), 158.5 (C-6″), 158.7 (C-2″), 162.8 (C-4″), 191.4 (C-α); HRMS calc. for $C_{15}H_8N_2O_3$: (M+H$^+$) *m/z* 265.0608, found 265.0614.

4-(Bromo(8-bromo-2,3,6,7-tetrahydrobenzo[1,2-*b*:4,5-*b*′]difuran-4-yl)methyl)pyrimidine (173)



Prepared according to general procedure A on a 0.5 mmol scale using **103** as a starting material (originally intended to synthesise **107**), novel pyrimidine **173** was isolated as a yellow solid in 7.2 % yield after preparative TLC (1:1 hexane:ethyl acetate eluent); R_f 0.54 (1:1 hexane:ethyl acetate); m.p. 204 - 207 °C (no recryst); IRν_{max} (KBr): 2963, 2911, 1464, 1420, 1305, 1224, 1169, 988, 866, 803 cm^{-1}; ^{1}H-NMR δ (400 MHz,

$CDCl_3$): 2.90 - 2.99 (1H, m, H-3$_A$), 3.19 (2H, t, J = 8.4 Hz, H-7), 3.31 - 3.40 (1H, m, H-3$_B$), 4.55 - 4.68 (4H, m, H-2 and H-6), 6.32 (1H, s, H-α), 7.78 (1H, d, J = 5.1 Hz, H-5″), 8.76 (1H, d, J = 5.1 Hz, H-6″), 9.15 (1H, s, H-2″); ^{13}C-NMR δ (100.6 MHz, $CDCl_3$) 30.6, 31.7 (C-3, C-7), 45.9 (C-α), 71.7, 71.9 (C-2, C-6), 101.3 (C-8), 116.4 (C-4), 120.4 (C-5″), 125.9, 127.9 (C-2*b*, C-5*b*′), 151.7, 152.0 (C-1*b*, C-4*b*′), 157.7 (C-6″), 158.3 (C-2″), 166.0 (C-4″); HRMS calc. for $C_{15}H_{12}{}^{79}Br_2N_2O_2$: ($M+H^+$) *m/z* 411.9179, found 411.9197.

4.2.3 Leuckart Reactions and Subsequent Hydrolysis Reactions

4.2.3.1 General Procedure M: Iron-Catalysed Reduction of Nitrostyrene to Ketone

A suspension of iron powder (325 mesh, 1.37 g, 24.6 mmol) in acetic acid (50 mL) was heated to 90 °C for 20 min. Simultaneously, 4-bromo-8-(2-nitroprop-1-en-1-yl)-2,3,6,7-tetrahydrobenzo[1,2-*b*:4,5-*b*′]difuran **(174)** (1.00 g, 3.1 mmol) in absolute ethanol (17 mL) was heated in a conical flask to 75 °C for 20 min. The solution of **174** was added portionwise to the iron suspension over 20 min using a glass pipette. The reaction mixture was stirred at 90 °C for 5 h followed by cooling to room temperature. After cooling, the reaction mixture was poured onto ice/water (50 mL), filtered through Celite® in a sintered glass funnel and washed through with dichloromethane (60 mL). The mixture was transferred to a separating funnel and allowed to settle before the phases were separated. The upper aqueous phase was extracted further with dichloromethane (3 x 40 mL). The combined organic phases were then washed with aq. NaOH (15 %, 3 x 40 mL) and deionised water (3 x 40 mL), dried over anhydrous $MgSO_4$, filtered and concentrated *in vacuo* and recrystallised from diethyl ether to give pure product.

4.2.3.2 General Procedure N: Leuckart Reaction to Convert a P2P-type Ketone to an N-formyl Moeity

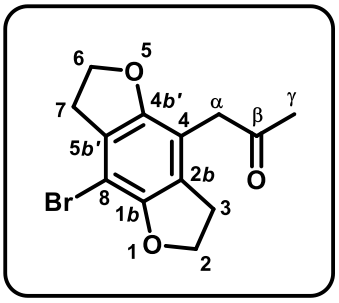
A mixture of the P2P ketone analogue (6 mmol) and formamide **(136)** (7.2 mL,

181.6 mmol) were heated to reflux (190 °C) for 5 h using a DrySyn® heating block or a sand bath. After cooling to room temperature, deionised water (30 mL) and ethyl acetate (40 mL) were added and the mixture was transferred to a separating funnel and allowed to settle. The phases were separated and the lower aqueous phase was extracted with ethyl acetate (4 x 20 mL). The ethyl acetate washes were combined with the original organic phase and washed with deionised water (3 x 20 mL). The organic phase was then dried over anhydrous $MgSO_4$, filtered and concentrated *in vacuo* to give the crude product, which was purified by chromatography and/or recrystallisation (see relevant experimental data for details).

4.2.3.3 General Procedure O: Hydrolysis Reaction to Convert an N-formyl Substrate to the Corresponding Primary Amine

To a stirred solution of *N*-formyl substrate (0.4 mmol) in MeOH (0.75 mL) in a glass pressure tube was added aq. HCl (30 %, 2.5 mL). The tube was then sealed and heated to reflux (100 °C) for 7 h, before being cooled to room temperature. Deionised water (10 mL) was added and the mixture was transferred to a beaker. Aqueous NaOH (4 M) was added gradually until the solution reached pH 12, and the mixture was transferred to a separating funnel. DCM (10 mL) was added and the phases were separated. The upper aqueous phase was extracted further with DCM (2 x 10 mL). The combined organic phases were then washed with deionised water (10 mL) dried over anhydrous $MgSO_4$, filtered and concentrated *in vacuo* to give the product.

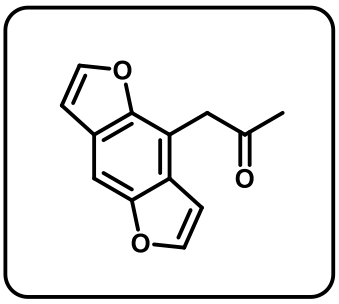
1-(8-Bromo-2,3,6,7-tetrahydrobenzo[1,2-*b*:4,5-*b*′]difuran-4-yl)propan-2-one (109)



Prepared according to general procedure M, **109** was isolated as a yellow solid in 85 % yield after recrystallisation from diethyl ether; R_f 0.23 (5:1 hexane:ethyl acetate); m.p. 119 - 121 °C (diethyl ether), (lit. m.p. 119 - 121 °C (chloroform))[1] ; IRν_{max} (KBr): 2970, 2905, 1709, 1480, 1423, 1315, 1215,

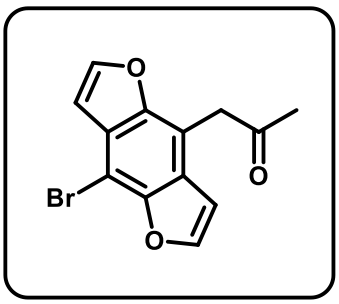
1162, 1042, 984, 961, 844, 560 cm^{-1}; ^{1}H-NMR δ (400 MHz, $CDCl_3$): 2.18 (3H, s, H-γ), 3.11 - 3.20 (4H, m, H3 and H7), 3.56 (2H, s, H-α), 4.56 - 4.65 (4H, m, H-2 and H-6); ^{13}C-NMR δ (100.6 MHz, $CDCl_3$) 29.4 (C-γ), 30.0 (C-3), 31.8 (C-7), 42.5 (C-α), 71.2 (C-6), 71.8 (C-2), 98.3 (C-8), 112.1 (C-4), 126.6 (C-5*b'*), 126.9 (C-2*b*), 151.1 (C-1*b*), 152.5 (C-4*b'*), 205.0 (C-β); HRMS calc. for $C_{13}H_{14}{}^{79}BrO_3$: ($M+H^+$) *m/z* 297.0216, found 297.0213.

1-(Benzo[1,2-*b*:4,5-*b'*]difuran-4-yl)propan-2-one (110)



Prepared according to general procedure C on a 1.7 mmol scale using **99** as a starting material, **110** was isolated as a white solid in 85 % yield after recrystallisation from diethyl ether; R_f 0.41 (5:1 hexane:ethyl acetate); m.p. 67 - 69 °C (diethyl ether), (lit. m.p. 67 - 69 °C (ethyl acetate))[1] ; IRν_{max} (KBr): 3116, 2919, 1708, 1552, 1416, 1356, 1160, 1126, 1018, 842, 758, 701, 551 cm^{-1}; ^{1}H-NMR δ (400 MHz, $CDCl_3$): 2.18 (3H, s, H-γ), 4.17 (2H, s, H-α), 6.82 (1H, d, J = 2.4 Hz, H-7), 6.85 (1H, d, J = 2.4 Hz, H-3), 7.60 (1H, s, H-8), 7.66 - 7.69 (2H, m, H-2 and H-6); ^{13}C-NMR δ (100.6 MHz, $CDCl_3$) 29.2 (C-γ), 42.7 (C-α), 101.4 (C-8), 105.0, 107.2 (C-3, C-7), 108.8 (C-4), 125.3, 125.6 (C-2*b*, C-5*b'*), 145.6, 145.9 (C-2, C-6), 150.4, 152.0 (C-1*b*, C-4*b'*), 205.2 (C-β); HRMS calc. for $C_{13}H_{11}O_3$: ($M+H^+$) *m/z* 215.0708, found 215.0698.

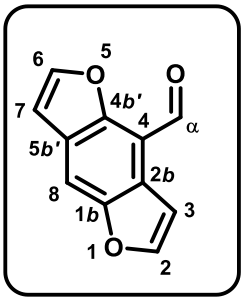
1-(8-Bromobenzo[1,2-*b*:4,5-*b'*]difuran-4-yl)propan-2-one (111)



Prepared according to general procedure C on a 1.0 mmol scale using **109** as a starting material, **111** was isolated as a white solid in 31 % yield after recrystallisation from diethyl ether; R_f 0.41 (5:1 hexane:ethyl acetate); m.p. 104 - 105 °C (diethyl ether), (lit. m.p. 107 - 109 °C (ethyl acetate))[1] ; IRν_{max} (KBr): 3149, 2922, 1712, 1496, 1362, 1327, 1206, 1140, 1024, 843, 760, 696 cm^{-1}; ^{1}H-NMR δ (300 MHz, $CDCl_3$): 2.18 (3H, s, H-γ), 4.14 (2H, s, H-

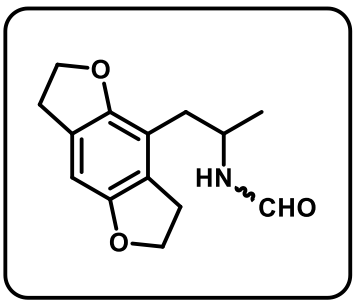
α), 6.88 (1H, d, J = 2.3 Hz, H-3), 6.92 (1H, d, J = 2.3 Hz, H-7), 7.70 - 7.72 (2H, m, H-2 and H-6); ^{13}C-NMR δ (75.5 MHz, $CDCl_3$) 29.3 (C-γ), 42.3 (C-α), 93.5 (C-8), 106.0 (C-3), 107.0 (C-7), 108.5 (C-4), 126.2 (C-2*b*), 126.6 (C-5*b'*), 146.1, 146.3 (C-2, C-6), 149.3 (C-1*b*), 150.0 (C-4*b'*), 204.5 (C-β); HRMS calc. for $C_{13}H_{10}{}^{79}BrO_3$: ($M+H^+$) *m/z* 292.9813, found 292.9802.

Benzo[1,2-*b*:4,5-*b'*]difuran-4-carbaldehyde (177)



When preparing **110** according to general procedure C using **99** as a starting material, **177** was isolated as an impurity by column chromatography in 1.9 % yield; R_f 0.63 (4:1 hexane:ethyl acetate); m.p. 104 - 106 °C (no recryst.), (lit. m.p. 106 - 107 °C ($CHCl_3$))[1] ; IRν$_{max}$ (KBr): 3125, 2920, 2850, 1674, 1586, 1546, 1377, 1224, 1126, 1010, 766, 627 cm^{-1}; ^{1}H-NMR δ (300 MHz, $CDCl_3$): 6.93 (1H, d, J = 2.2 Hz, H-7), 7.61 (1H, dd, J = 0.8, 2.2 Hz, H-3), 7.76 (1H, d, J = 2.2 Hz, H-2), 7.82 (1H, d, J = 2.2 Hz, H-6), 7.93 (1H, d, J = 0.8 Hz, H-8), 10.84 (1H, s, H-α); ^{13}C-NMR δ (150.9 MHz, $CDCl_3$): 106.8 (C-3), 107.2 (C-7), 109.4 (C-8), 111.9 (C-4), 124.6, 126.0 (C-2*b*, C-5*b'*), 146.3 (C-2), 148.8 (C-6), 152.1, 153.8 (C-1*b*, C-4*b'*), 187.6 (C-α); HRMS calc. for $C_{11}H_7O_3$: ($M+H^+$) *m/z* 187.0935, found 187.0937.

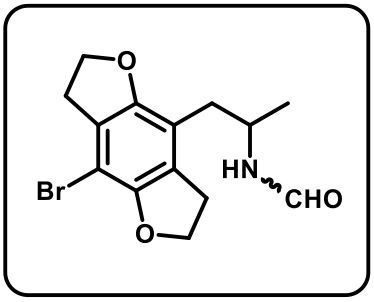
***N*-(1-(2,3,6,7-Tetrahydrobenzo[1,2-*b*:4,5-*b'*]difuran-4-yl)propan-2-yl)formamide (102)**



Prepared according to general procedure N using **99** as a starting material, novel compound **102** was isolated as a yellow solid in 27 % yield after purification by column chromatography (4:1 hexane:ethyl acetate on silica gel) and subsequent recrystallisation from 1:1 hexane:ethyl acetate. The compound was isolated as a mixture of *E*/*Z* rotamers in a ratio of *E*:*Z* = 1:4; R_f 0.09 (1:1 hexane:ethyl acetate); m.p. 104 - 106 °C (1:1 hexane:ethyl acetate); IRν$_{max}$ (KBr): 3283, 2970, 2889, 1661, 1449, 1435, 1216, 1165, 981,

956, 732 cm^{-1}; ^{1}H-NMR δ (400 MHz, $CDCl_3$): 1.22 (d, J = 6.4 Hz, (H-γ)^Z), 1.28 (d, J = 6.8 Hz, (H-γ)^E), 2.59 - 2.78 (m, (H-α)*), 3.04 - 3.14 (m, (H-3 and H-7)*), 3.80 - 3.88 (m, (H-β)^E), 4.19 - 4.24 (m, (H-β)^Z), 4.51 - 4.60 (m, (H-2 and H-6)*), 5.73 (bs, (N**H**)^E), 6.22 (bs, (N**H**)^Z), 6.54 (s, (H-8)*), 7.85 (d, J = 12.0 Hz, (C**H**O)^E), 8.07 (s, (C**H**O)^Z); ^{13}C-NMR δ (100.6 MHz, $CDCl_3$) 20.7 (C-γ)^Z, 22.5 (C-γ)^E, 29.1, 30.6 (C-3, C-7)^Z, 29.2, 30.5 (C-3, C-7)^E, 34.2 (C-α)^Z, 36.6 (C-α)^E, 45.4 (C-β)^Z, 48.2 (C-β)^E, 71.4, 71.5 (C-2, C-6)*, 104.4 (C-8)^Z, 104.7 (C-8)^E, 116.1 (C-4)^E, 116.7 (C-4)^Z, 125.2, 126.0 (C-2*b*, C-5*b'*)^E, 125.5, 125.7 (C-2*b*, C-5*b'*)^Z, 152.2, 154.3 (C-1*b*, C-4*b'*)^Z, 152.4, 154.1 (C-1*b*, C-4*b'*)^E, 160.8 (**C**HO)^Z, 163.6 (**C**HO)^E; HRMS calc. for $C_{14}H_{17}NO_3$: ($M+H^+$) *m/z* 248.1281, found 248.1289.

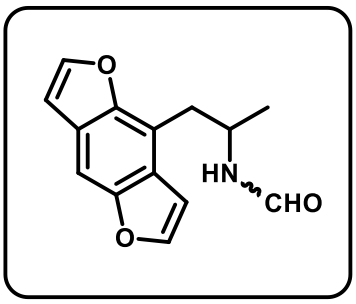
N-(1-(8-Bromo-2,3,6,7-tetrahydrobenzo[1,2-*b*:4,5-*b'*]difuran-4-yl)propan-2-yl)formamide (181)



Prepared according to general procedure N using **109** as a starting material, novel compound **181** was isolated as a pale yellow solid in 27 % yield after purification by column chromatography (4:1 hexane:ethyl acetate on silica gel) and subsequent recrystallisation from 1:1 hexane:ethyl acetate. The compound was isolated as a mixture of *E*/*Z* rotamers in a ratio of *E*:*Z* = 1:4; R_f 0.20 (1:1 hexane:ethyl acetate); m.p. 119 - 121 °C (1:1 hexane:ethyl acetate); IRν_{max} (KBr): 3278, 2970, 2908, 1661, 1480, 1420, 1208, 988, 966, 842, 735 cm^{-1}; ^{1}H-NMR δ (400 MHz, $CDCl_3$): 1.21 (d, J = 6.5 Hz, (H-γ)^Z), 1.28 (d, J = 6.5 Hz, (H-γ)^E), 2.54 - 2.74 (m, (H-α)*), 3.14 - 3.25 (m, (H-3 and H-7)*), 3.80 - 3.85 (m, (H-β)^E), 4.19 - 4.26 (m, (H-β)^Z), 4.56 - 4.66 (m, (H-2 and H-6)*), 5.56 (bs, (N**H**)^E), 5.99 (bs, (N**H**)^Z), 7.85 (d, J = 12.0 Hz, (C**H**O)^E), 8.07 (s, (C**H**O)^Z); ^{13}C-NMR δ (100.6 MHz, $CDCl_3$) 20.6 (C-γ)^Z, 22.3 (C-γ)^E, 30.1, 31.8 (C-3, C-7)^Z, 30.3, 31.7 (C-3, C-7)^E, 34.1 (C-α)^Z, 36.5 (C-α)^E, 45.0 (C-β)^Z, 48.0 (C-β)^E, 71.1, 71.8 (C-2, C-6)^Z, 71.3, 71.7 (C-2, C-6)^E, 97.8 (C-8)^Z, 98.1 (C-8)^E, 115.3 (C-4)^E, 115.9 (C-4)^Z, 126.3, 126.5 (C-2*b*, C-5*b'*)^E, 126.3, 126.7 (C-2*b*, C-5*b'*)^Z, 151.2, 152.6 (C-1*b*, C-4*b'*)^E, 151.4, 152.5

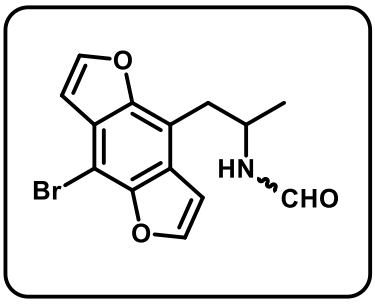
(C-1*b*, C-4*b'*)^{Z}, 160.7 (**C**HO)^{Z}, 163.5 (**C**HO)^{E}; HRMS calc. for $C_{14}H_{16}{}^{79}BrNO_3$: (M+H$^+$) *m/z* 326.0386, found 326.0386.

N-(1-(Benzo[1,2-*b*:4,5-*b'*]difuran-4-yl)propan-2-yl)formamide (182)



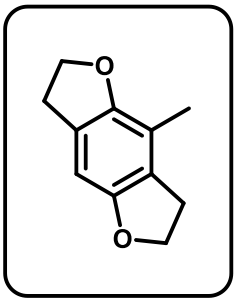
Prepared according to general procedure N on a 0.7 mmol scale using **110** as a starting material, novel compound **182** was isolated as a pale yellow solid after preparative TLC (3:1 hexane:ethyl acetate eluent system) in 13 % yield. The compound was isolated as a mixture of *E*/*Z* rotamers in a ratio of *E*:*Z* = 1:4; R_f 0.32 (ethyl acetate); m.p. 115 - 116 °C (no recryst.); IRν_{max} (KBr): 3267, 2861, 1660, 1551, 1415, 1381, 1176, 1130, 1018, 759, 702 cm^{-1}; ^{1}H-NMR δ (400 MHz, $CDCl_3$): 1.20 (d, J = 6.7 Hz, (H-γ)^{Z}), 1.33 (d, J = 6.6 Hz, (H-γ)^{E}), 3.25 - 3.40 (m, (H-α)*), 4.05 - 4.12 (m, (H-β)^{E}), 4.50 - 4.60 (m, (H-β)^{Z}), 5.61 (bs, (N**H**)*), 6.80 (dd, J = 0.9, 2.4 Hz, (H-3)^{E}), 6.84 (d, J = 2.2 Hz, (H-7)^{Z}), 6.86 (d, J = 2.4 Hz, (H-7)^{E}), 6.98 (dd, J = 0.8, 2.2 Hz, (H-3)^{Z}), 7.65 (d, J = 2.2 Hz, (H-2 and H-6)^{Z}), 7.66 (d, J = 2.4 Hz, (H-2 and H-6)^{E}), 7.81 (d, J = 12.0 Hz, (C**H**O)^{E}), 8.07 (s, (C**H**O)^{Z}); ^{13}C-NMR δ (100.6 MHz, $CDCl_3$) 20.3 (C-γ)^{Z}, 22.3 (C-γ)^{E}, 33.8 (C-α)^{Z}, 36.2 (C-α)^{E}, 45.2 (C-β)^{Z}, 48.7 (C-β)^{E}, 104.8, 107.2 (C-3, C-7)^{E}, 105.5, 107.2 (C-3, C-7)^{Z}, 100.8 (C-8)^{Z}, 101.2 (C-8)^{E}, 112.0 (C-4)^{E}, 112.5 (C-4)^{Z}, 125.1, 125.3 (C-2*b*, C-5*b'*)^{E}, 125.3, 125.8 (C-2*b*, C-5*b'*)^{Z}, 145.4, 145.6 (C-2, C-6)^{Z}, 145.6, 145.9 (C-2, C-6)^{E}, 149.9, 152.1 (C-1*b*, C-4*b'*)^{E}, 150.8, 152.0 (C-1*b*, C-4*b'*)^{Z}, 160.6 (**C**HO)^{Z}, 163.3 (**C**HO)^{E}; HRMS calc. for $C_{14}H_{13}NO_3$: (M+H$^+$) *m/z* 244.0968, found 244.0967.

_N_-(1-(8-Bromobenzo[1,2-_b_:4,5-_b'_]difuran-4-yl)propan-2-yl)formamide (183)



Prepared according to general procedure N on a 0.5 mmol scale using **111** as a starting material, novel compound **183** was isolated after preparative TLC (3:1 hexane:ethyl acetate eluent system) as a pale yellow solid in 13 % yield. The compound was isolated as a mixture of *E*/*Z* rotamers in a ratio of *E*:*Z* = 1:4; R_f 0.14 (1:1 hexane:ethyl acetate); m.p. 132 - 134 °C (1:1 hexane:ethyl acetate); IRν_{max} (KBr): 3148, 2965, 1679, 1547, 1495, 1362, 1312, 1207, 1141, 1025, 842, 759, 736, 696 cm^{-1}; ^{1}H-NMR δ (400 MHz, $CDCl_3$): 1.18 (d, J = 6.4 Hz, (H-γ)^Z), 1.32 (d, J = 6.4 Hz, (H-γ)^E), 3.21-3.38 (m, (H-α)*), 4.01 - 4.09 (m, (H-β)^E), 4.46 - 4.55 (m, (H-β)^Z), 5.60 (bs, (N**H**)^Z), 5.71 (bs, (N**H**)^E), 6.80 (dd, J = 0.9, 2.4 Hz, (H-3)^E), 6.84 (d, J = 2.2 Hz, (H-7)^Z), 6.88 - 6.93 (m, (H-3 and H-7)^E, (H-7)^Z), 7.08 (d, J = 2.0 Hz, (H-3)^Z), 7.69 - 7.72 (m, (H-2 and H-6)*), 7.80 (d, J = 12.0 Hz, (C**H**O)^E), 8.09 (s, (C**H**O)^Z); ^{13}C-NMR δ (100.6 MHz, $CDCl_3$) 20.1 (C-γ)^Z, 22.2 (C-γ)^E, 33.7 (C-α)^Z, 36.1 (C-α)^E, 45.0 (C-β)^Z, 48.6 (C-β)^E, 92.7 (C-8)^Z, 93.0 (C-8)^E, 105.8, 107.0 (C-3, C-7)^E, 106.5, 106.9 (C-3, C-7)^Z, 111.6 (C-4)^E, 112.3 (C-4)^Z, 126.1, 126.6 (C-2*b*, C-5*b'*)^E, 126.4, 126.5 (C-2*b*, C-5*b'*)^E, 146.0, 146.1 (C-2, C-6)^Z, 146.1, 146.4 (C-2, C-6)^E, 149.2, 150.2 (C-1*b*, C-4*b'*)^E, 149.2, 150.4 (C-1*b*, C-4*b'*)^Z, 160.7 (**C**HO)^Z, 163.2 (**C**HO)^E; HRMS calc. for $C_{14}H_{12}{}^{79}BrNO_3$: (M+H$^+$) *m/z* 322.0073, found 322.0075.

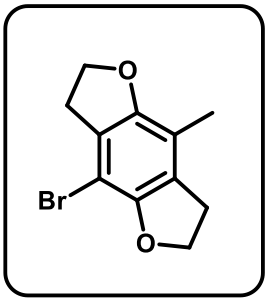
4-Methyl-2,3,6,7-tetrahydrobenzo[1,2-_b_:4,5-_b'_]difuran (184)



When **102** was synthesised according to general procedure N, novel compound **184** was isolated as an off-white semi-solid after column chromatography (4:1 hexane:ethyl acetate on silica gel) in 0.57 % yield; R_f 0.84 (1:1 hexane:ethyl acetate); IRν_{max} (KBr): 2920, 2853, 1479, 1451, 1432, 1260, 1211, 1038, 1021, 979, 945, 798 cm^{-1}; ^{1}H-NMR δ (400 MHz, $CDCl_3$): 2.05 (3H, s, H-α), 3.00 - 3.09 (4H, m, H-3 and

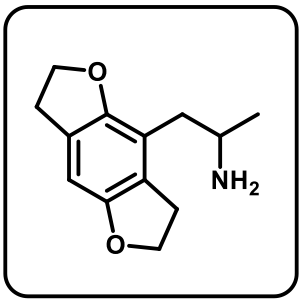
H-7), 4.43 - 4.49 (4H, m, H-2 and H-6), 6.42 (1H, s, H-8); ^{13}C-NMR δ (100.6 MHz, $CDCl_3$) 12.6 (C-α), 29.1, 30.7 (C-3, C-7), 71.2, 71.5 (C-2, C-6), 102.9 (C-8), 116.2 (C-4), 125.0, 125.3 (C-2*b*, C-5*b'*), 152.4, 153.7 (C-1*b*, C-4*b'*); HRMS calc. for $C_{11}H_{12}O_2$: ($M+H^+$) *m/z* 177.0910, found 177.0913.

8-Bromo-4-methyl-2,3,6,7-tetrahydrobenzo[1,2-*b*:4,5-*b'*]difuran (185)



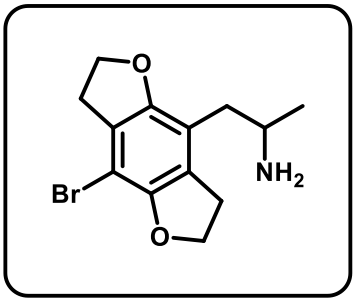
When **181** was synthesised according to general procedure N, novel compound **185** was isolated as a pale yellow solid after column chromatography (4:1 hexane:ethyl acetate on silica gel) in 0.91 % yield; R_f 0.88 (1:1 hexane:ethyl acetate); m.p. 133 - 135 °C (no recryst.); IRν_{max} (KBr): 2918, 2852, 1480, 1417, 1311, 1210, 981, 953, 839 cm^{-1}; ^{1}H-NMR δ (400 MHz, $CDCl_3$): 2.06 (3H, s, H-α), 3.16 (4H, t, J = 8.8 Hz, H-3 and H-7), 4.55 - 4.71 (4H, m, H-2 and H-6); ^{13}C-NMR δ (100.6 MHz, $CDCl_3$) 12.4 (C-α), 30.1, 31.8 (C-3, C-7), 70.9, 71.8 (C-2, C-6), 96.1 (C-8), 115.3 (C-4), 125.7, 126.4 (C-2*b*, C-5*b'*), 150.7, 152.6 (C-1*b*, C-4*b'*); HRMS calc. for $C_{11}H_{11}{}^{79}BrO_2$: ($M+H^+$) *m/z* 252.9859, found 252.9868.

1-(2,3,6,7-Tetrahydrobenzo[1,2-*b*:4,5-*b'*]difuran-4-yl)propan-2-amine (24)



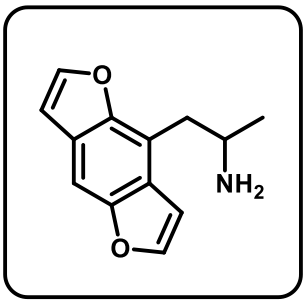
Prepared according to general procedure O using **102** as a starting material, **24** was isolated as a yellow solid in 73 % yield after recrystallisation from ethyl acetate; R_f 0.03 (ethyl acetate); m.p. 92 - 95 °C (ethyl acetate), (no lit. m.p. available for free base); IRν_{max} (KBr): 3353, 2961, 2890, 1579, 1449, 1436, 1317, 1210, 1189, 983, 957 cm^{-1}; ^{1}H-NMR δ (400 MHz, $CDCl_3$): 1.12 (3H, d, J = 6.4 Hz, H-γ), 2.45 - 2.60 (2H, m, H-α), 3.09 - 3.15 (4H, m, H-3 and H-7), 3.21 - 3.29 (1H, m, H-β), 4.48 - 4.55 (4H, m, H-2 and H-6), 6.53 (1H, s, H-8); ^{13}C-NMR δ (100.6 MHz, $CDCl_3$) 23.7 (C-γ), 29.4, 30.6 (C-3, C-7), 38.9 (C-α), 46.9 (C-β), 71.1, 71.3 (C-2, C-6), 103.8 (C-8), 118.4 (C-4), 125.5, 125.6 (C-2*b*, C-5*b'*), 152.6, 153.9 (C-1*b*, C-4*b'*); HRMS calc. for $C_{13}H_{17}NO_2$: ($M+H^+$) *m/z* 220.1332, found 220.1339.

1-(8-Bromo-2,3,6,7-tetrahydrobenzo[1,2-*b*:4,5-*b'*]difuran-4-yl)propan-2-amine (25)



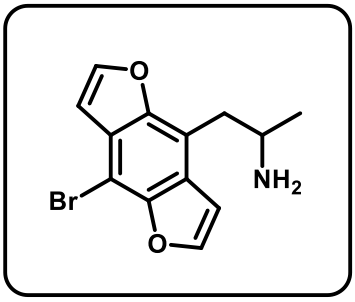
Prepared according to general procedure O using **181** as a starting material, **25** was isolated as a yellow solid in 68 % yield after recrystallisation from ethyl acetate; R_f 0.05 (ethyl acetate); m.p. 115 - 116 °C (ethyl acetate), (no lit. m.p. available for free base); IRν_{max} (KBr): 3358, 2960, 2915, 1480, 1419, 1311, 1207, 988, 965, 841 cm^{-1}; ^{1}H-NMR δ (400 MHz, $CDCl_3$): 1.10 (3H, d, J = 6.4 Hz, H-γ), 2.40 - 2.55 (2H, m, H-α), 3.09 - 3.15 (4H, m, H-3 and H-7), 3.15 - 3.24 (1H, m, H-β), 4.56 (2H, t, J = 8.4 Hz, H-2 or H-6), 4.63 (2H, t, J = 8.4 Hz, H-2 or H-6); ^{13}C-NMR δ (100.6 MHz, $CDCl_3$) 23.7 (C-γ), 30.5, 31.7 (C-3, C-7), 38.6 (C-α), 46.8 (C-β), 71.0, 71.8 (C-2, C-6), 97.2 (C-8), 117.6 (C-4), 126.3, 126.6 (C-2*b*, C-5*b'*), 150.9, 152.9 (C-1*b*, C-4*b'*); HRMS calc. for $C_{13}H_{16}{}^{79}BrNO_2$: ($M+H^+$) *m/z* 298.0437, found 298.0437.

1-(Benzo[1,2-*b*:4,5-*b'*]difuran-4-yl)propan-2-amine (112)



Prepared according to general procedure O on a 0.05 mmol scale using **182** as a starting material, novel compound **112** was isolated as a tan solid in 59 % yield; R_f 0.06 (ethyl acetate); m.p. 108 - 110 °C (no recryst.); IRν_{max} (KBr): 3114, 2922, 2851, 1551, 1414, 1380, 1211, 1175, 1142, 1030, 845, 760, 701 cm^{-1}; ^{1}H-NMR δ (400 MHz, $CDCl_3$): 1.19 (3H, d, J = 6.4 Hz, H-γ), 3.07 - 3.21 (2H, m, H-α), 3.46 - 3.51 (1H, m, H-β), 6.82 (1H, d, J = 2.0 Hz, H-3 or H-7), 6.89 (1H, d, J = 2.0 Hz, H-3 or H-7), 7.54 (1H, s, H-8), 7.63 - 7.65 (2H, m, H-2 and H-6); ^{13}C-NMR δ (100.6 MHz, $CDCl_3$) 23.8 (C-γ), 38.2 (C-α), 47.7 (C-β), 100.3 (C-8), 105.5, 107.0 (C-3, C-7), 114.5 (C-4), 125.2, 125.6 (C-2*b*, C-5*b'*), 145.3, 145.5 (C-2, C-6), 150.7, 152.0 (C-1*b*, C-4*b'*); HRMS calc. for $C_{13}H_{13}NO_2$: ($M+H^+$) *m/z* 216.1019, found 216.1028.

1-(8-Bromobenzo[1,2-*b*:4,5-*b'*]difuran-4-yl)propan-2-amine (15)



Prepared according to general procedure O on a 0.03 mmol scale using **183** as a starting material, **15** was isolated as a tan solid in 41 % yield; R_f 0.09 (ethyl acetate); m.p. 124 - 126 °C (no recryst.), (no lit. m.p. available for free base); IRν_{max} (KBr): 3149, 2959, 2964, 1548, 1495, 1363, 1324, 1208, 1144, 1026, 842, 760, 696 cm^{-1}; ^{1}H-NMR δ (400 MHz, $CDCl_3$): 1.18 (3H, d, J = 6.4 Hz, H-γ), 3.05 - 3.17 (2H, m, H-α), 3.42 - 3.49 (1H, m, H-β), 6.89 (1H, d, J = 2.0 Hz, H-3 or H-7), 6.97 (1H, d, J = 2.0 Hz, H-3 or H-7), 7.69 - 7.70 (2H, m, H-2 and H-6); ^{13}C-NMR δ (100.6 MHz, $CDCl_3$) 23.9 (C-γ), 38.0 (C-α), 47.6 (C-β), 92.1 (C-8), 106.4, 106.8 (C-3, C-7), 114.3 (C-4), 126.2, 126.4 (C-2*b*, C-5*b'*), 145.8, 146.0 (C-2, C-6), 149.2, 150.4 (C-1*b*, C-4*b'*); HRMS calc. for $C_{13}H_{12}{}^{79}BrNO_2$: ($M+H^+$) *m/z* 294.0124, found 294.0132.

4.3 Experimental details pertaining to work outlined in Chapter 3

*4.3.1.1 General Procedure P: Bromination of 1,4-Benzoquinone **(192)***

A RBF containing a solution of 1,4-benzoquinone **(192)** (5.41 g, 50 mmol) in chloroform (150 mL) was covered in aluminium foil to exclude light and cooled to 0 °C. Bromine (1 - 2 eq., see relevant experimental data) was added over ~ 10 min, and the reaction was allowed to warm to room temperature and was stirred for 3 h (unless otherwise stated in relevant experimental data). The reaction mixture was transferred to a separating funnel and washed with aq. $Na_2S_2O_3$ (5 %, 4 x 50 mL). The organic phase was dried over anhydrous $MgSO_4$, filtered and the solvent was removed *in vacuo* until a yellow solid precipitated out of solution. Hexane (50 mL) was added to the RBF, and the mixture was sonicated at room temperature for ~ 20 min. The precipitate was collected by vacuum filtration and washed with hexane (2 x 20 mL), and was subsequently recrystallised from toluene.

4.3.1.2 General Procedure Q: Conversion of Benzoquinones to Hydroquinones

Concentrated sulphuric acid (H_2SO_4, 21 mL) was added to a reaction vessel containing 5,6-dibromocyclohex-2-ene-1,4-dione **(193)** (9.6 g, 35.8 mmol) in chloroform (300 mL) at 0 °C under a nitrogen atmosphere. The reaction was stirred at 0 °C for 40 h using a cryocooler, then allowed to warm to room temperature and stirred for a further 30 min. The reaction mixture was poured onto a mixture of ice water (300 mL) and diethyl ether (300 mL). This mixture was transferred to a separating funnel and allowed to settle before the phases were separated. The upper aqueous layer was extracted with diethyl ether (150 mL). The combined organic phases were then dried over anhydrous $MgSO_4$, filtered and concentrated to dryness *in vacuo*.

4.3.1.3 General Procedure R: Alkylation of Hydroquinones

A mixture of hydroquinones 2,3-dibromobenzane-1,4-diol **(194)** and 2,5-dibromobenzene-1,4-diol **(195)** (0.30 g, 1.12 mmol), potassium carbonate (0.46 g, 3.36 mmol), 1-bromo-2-chloroethane (1.12 mL, 13.44 mmol) and acetone (7.5 mL) were charged to a glass pressure tube (which was purged with nitrogen prior to use) which was then sealed and heated to 60 °C for 90 h. The reaction was allowed to cool to room temperature, transferred to a RBF, and the solvent was removed *in vacuo*. The crude residue was partitioned between deionised water (100 mL) and diethyl ether (50 mL). The lower aqueous layer was extracted with diethyl ether (50 mL). The combined organic layers were washed with aq. NaOH (4 M, 2 x 40 mL) and brine (40 mL) before being dried over anhydrous $MgSO_4$, filtered and concentrated to dryness *in vacuo*.

The combined aqueous layers were acidified to pH 1 with conc. HCl and extracted with diethyl ether (3 x 80 mL). These combined organic layers were dried over anhydrous $MgSO_4$, filtered and concentrated to dryness *in vacuo*. All crude residue recovered was purified by preparative TLC (2:1 hexane:ethyl acetate eluent system).

4.3.1.4 General Procedure S: Ethoxylation of Hydroquinones

Ethylene carbonate **(203)** (1.48 g, 16.8 mmol) was charged to a round bottomed flask equipped with a magnetic stirrer bar and the vessel was heated to 95 °C. A mixture of hydroquinones 2,3-dibromobenzane-1,4-diol **(194)** and 2,5-dibromobenzene-1,4-diol **(195)** (0.30 g, 1.12 mmol) and potassium carbonate (0.34 g, 2.46 mmol) were charged to the vessel, and the reaction mixture was stirred at 95 °C for 18 h. The reaction was cooled to ~ 35 °C (to prevent **203** from solidifying) and was quenched with cold aq. 1 M NaOH. The mixture was transferred to a separating funnel and extracted with chloroform (3 x 30 mL). The combined organic phases were dried over anhydrous $MgSO_4$, filtered and concentrated to dryness *in vacuo*.

The aqueous phase was acidified to pH 7 using conc. HCl and was extracted with chloroform (2 x 30 mL) followed by ethyl acetate (2 x 30 mL). The combined organic phases were dried over anhydrous $MgSO_4$, filtered and concentrated to dryness *in vacuo*. All crude residues were purified by preparative TLC (1:1 hexane:ethyl acetate used as eluent).

*4.3.1.5 General Procedure T: Preparation of iTHBD **(90)** Using n-BuLi*

A solution of 2,3-dibromo-1,4-bis(2-chloroethoxy)benzene **(191)** (0.25 g, 0.64 mmol) in dry THF (10 mL) was cooled to – 78 °C under a nitrogen atmosphere, and *n*-BuLi (2.5 M in hexane, 0.56 mL, 1.40 mmol) was added. The reaction was stirred for 1 h at – 78 °C, then allowed to warm to room temperature and stirred for 24 h. The reaction was re-cooled to – 78 °C and *n*-BuLi (2.5 M in hexane, 0.28 mL, 0.70 mmol) was added. The reaction was stirred for 1 h at – 78 °C, then allowed to warm to room temperature and stirred for 24 h. This process was repeated twice more, giving a total reaction time of 100 h. The reaction was then partitioned over ethyl acetate (15 mL) and deionised water (10 mL), transferred to a separating funnel and allowed to settle. The phases were separated and the upper organic layer was washed with deionised water (10 mL). The combined aqueous phases were then washed with ethyl acetate (2 x 15 mL) and the combined organic phases were dried over anhydrous

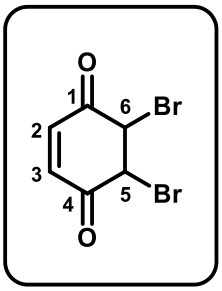
$MgSO_4$, filtered and concentrated to dryness *in vacuo*. The crude residue recovered was purified by preparative TLC (5:1 hexane:ethyl acetate eluent system) and subsequent recrystallisation from hexane.

*4.3.1.6 General Procedure U: Preparation of iTHBD **(90)** Using a Grignard Reaction*

Magnesium turnings (0.16 g, 6.63 mmol) were freshly ground using a mortar and pestle. The turnings were collected using a Büchner funnel and were washed with hexane (5 mL) and diethyl ether (5 mL). The turnings were then transferred to an oven dried two-neck RBF fitted with a stirrer bar and condenser. The flask was sealed using a rubber septum and purged with nitrogen. The set-up was then flame-dried using a Bunsen burner and allowed to cool to room temperature. Dry THF (5 mL) was added, stirring was started and the vessel was cooled to – 5 °C. Ethylene dibromide (0.05 mL, 0.58 mmol) was added dropwise to the Mg suspension.

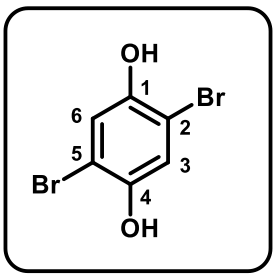
In a separate vessel, a solution of 2,3-dibromo-1,4-bis(2-chloroethoxy)benzene **(191)** (0.50 g, 1.27 mmol) in dry THF (10 mL) was prepared and held under a nitrogen atmosphere at 0 °C. The solution of **191** was added dropwise to the Mg suspension *via* a canula over ~ 15 min. When the addition was completed, the reaction was allowed to warm to room temperature, and was subsequently heated to 35 - 40 °C for 3 h. The reaction was then cooled to room temperature and quenched by slow addition of cold aq. HCl (1 M, 40 mL). The mixture was then transferred to a separating funnel and extracted with diethyl ether (3 x 30 mL). The combined organic phases were then washed with aq. NaOH (1 M, 4 x 20 mL) and brine (20 mL), dried over anhydrous MgSO4, filtered and concentrated *in vacuo*. The crude residue was purified by preparative TLC (9:11 hexane:ethyl acetate) and subsequent recrystallisation from hexane.

5,6-Dibromocyclohex-2-ene-1,4-dione (193)



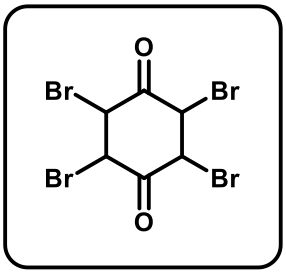
Prepared according to general procedure P (1 eq. Br_2) **193** was isolated in 80 % yield as a yellow solid after recrystallisation from toluene; R_f 0.39 (9:1 hexane:ethyl acetate); m.p. 81 - 83 °C (toluene), (lit. m.p. 82 - 83 °C (no recryst.))[4] ; IRν_{max} (KBr): 2997, 1694, 1371, 1286, 1218, 1109, 1014, 854, 645 cm^{-1}; ^{1}H-NMR δ (400 MHz, $CDCl_3$) 4.81 (2H, s, H-5 and H-6), 6.73 (2H, s, H-2 and H-3); ^{13}C-NMR δ (75.5 MHz, $CDCl_3$) 45.0 (C-5 and C-6), 136.5 (C-2 and C-3), 187.2 (C-1 and C-4); HRMS calc. for $C_6H_4{}^{79}Br_2O_2$: (M+H$^+$) *m/z* 265.8578, PMI not found under standard conditions.

2,5-Dibromobenzene-1,4-diol (195)



Prepared according to general procedure P (1 eq. Br_2, 18 h reaction time) **195** was isolated in 37 % yield as a grey solid after recrystallisation from toluene; R_f 0.65 (1:1 hexane:ethyl acetate); m.p. 178 - 181 °C (toluene), (lit. m.p. 177 - 178 °C (water))[5] ; IRν_{max} (KBr): 3272, 2780, 1640, 1412, 1190, 1057, 857, 794 cm^{-1}; ^{1}H-NMR δ (400 MHz, $CDCl_3$) 5.14 (2H, s, 2 x O**H**), 7.16 (2H, s, H-3 and H-6); ^{13}C-NMR δ (100.6 MHz, $CDCl_3$) 109.8 (C-2 and C-5), 118.5 (C-3 and C-6), 146.7 (C-1 and C-4); HRMS calc. for $C_6H_4{}^{79}Br_2O_2$: (M+H$^+$) *m/z* 265.8578, PMI not found under standard conditions.

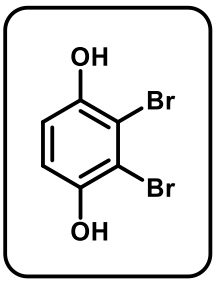
2,3,5,6-Tetrabromocyclohexane-1,4-dione (197)



Prepared according to general procedure P on a 3.0 mmol scale (2 eq. Br_2), **197** was isolated in 18 % yield as an orange solid after recrystallisation from toluene; R_f 0.54 (1:1 hexane:ethyl acetate); m.p. 140 - 143 °C (toluene); IRν_{max} (KBr): 2921, 1738, 1692, 1418,

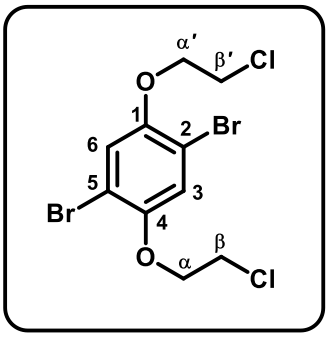
1292, 1190, 1051, 936, 803, 575 cm^{-1}; ^{1}H-NMR δ (400 MHz, $CDCl_3$) 5.03 (4H, s, H-2, H-3, H-5 and H-6), ^{13}C-NMR δ (75.5 MHz, $CDCl_3$) 46.2 (C-2, C-3, C-5 and C-6), 187.6 (C-1 and C-4); HRMS calc. for $C_6H_4{}^{79}Br_4O_2$: ($M+H^+$) *m/z* 423.6945, PMI not found under standard conditions.

2,3-Dibromobenzene-1,4-diol (194)



Prepared according to general procedure Q, compound **194** could not be isolated from isomer **195** which was formed in the same reaction. However, by comparison to ^{1}H- and ^{13}C-NMR data recorded for **195** (which was independently synthesised by general procedure P), it was possible to assign ^{1}H- and ^{13}C-NMR signals for **194** from the analysis of the mixture of **194/195**; R_f 0.51 (1:1 hexane:ethyl acetate); ^{1}H-NMR δ (400 MHz, $CDCl_3$): 5.20 (2H, s, 2 x O**H**), 6.96 (2H, s, H-5 and H-6); ^{13}C-NMR δ (100.6 MHz, $CDCl_3$) 112.1 (C-2 and C-3), 115.8 (C-5 and C-6), 147.3 (C-1 and C-4); HRMS calc. for $C_6H_4{}^{79}Br_2O_2$: ($M+H^+$) *m/z* 265.8578, PMI not found under standard conditions.

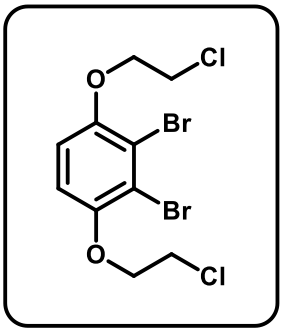
2,5-Dibromo-1,4-bis(2-chloroethoxy)benzene (190)



Prepared according to general procedure R, **190** was isolated in 23 % yield as a brown solid after recrystallisation from ethanol; R_f 0.79 (2:1 hexane:ethyl acetate); m.p. 117 - 119 °C (ethanol), (lit. m.p. 118 - 120 °C (ethanol))[2] ; IRν_{max} (KBr) (Note: the IR spectroscopic data listed here was not measured during this work, but was recorded by O′Connor *et al.*[2]): 2928, 1736, 1496, 1454, 1428, 1363, 1303, 1212, 1080, 1035 cm^{-1}; ^{1}H-NMR δ (300 MHz, $CDCl_3$); 3.85 (4H, t, J = 6.0 Hz, H-α and H-α′), 4.23 (4H, t, J = 8.0 Hz, H-β and H-β′), 7.14 (2H, s, H-3 and H-6); ^{13}C-NMR δ (75.5 MHz, $CDCl_3$): 41.5 (C-α and C-α′), 70.6 (C-β and C-β′), 111.9 (C-2 and C-5), 118.2 (C-3 and C-6), 150.2 (C-1 and C-4); HRMS calc. for

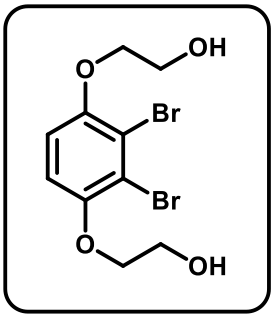
$C_{10}H_{10}{}^{79}Br_2{}^{35}Cl_2O_2$: $(M+H^+)$ *m/z* 389.8474, PMI not found under standard conditions.

2,3-Dibromo-1,4-bis(2-chloroethoxy)benzene (191)



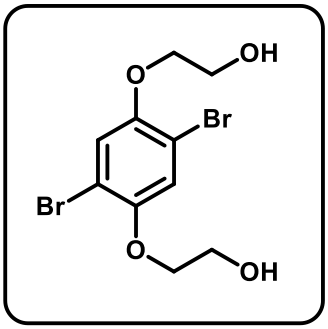
Prepared according to general procedure R, **191** was isolated in 14 % yield as a brown solid after recrystallisation from ethanol; R_f 0.79 (2:1 hexane:ethyl acetate); m.p. 90 - 93 °C (ethanol), (lit. m.p. 91 - 93 °C (ethanol))[2] ; IRν_{max} (KBr): 2967, 2925, 1466, 1451, 1427, 1386, 1265, 1100, 1076, 1034, 865, 790, 669 cm^{-1}; ^{1}H-NMR δ (300 MHz, $CDCl_3$): 3.84 (4H, t, J = 6.0 Hz, H-α and H-α′), 4.24 (4H, t, J = 6.0 Hz, H-β and H-β′), 6.89 (2H, s, H-5 and H-6); ^{13}C-NMR δ (75.5 MHz, $CDCl_3$): 41.6 (C-α and C-α′), 70.6 (C-β and C-β′), 113.8 (C-2 and C-3), 119.8 (C-5 and C-6), 151.1 (C-1 and C-4); HRMS calc. for $C_{10}H_{10}{}^{79}Br_2{}^{35}Cl_2O_2$: $(M+H^+)$ *m/z* 389.8474, found 389.8452.

2,2′-((2,3-Dibromo-1,4-phenylene)bis(oxy))diethanol (204)



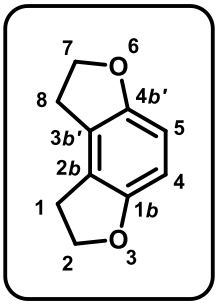
Prepared according to general procedure S, novel compound **204** was isolated in 7 % yield as a white solid after recrystallisation from toluene; R_f 0.48 (1:1 hexane:ethyl acetate); m.p. 105 - 106 °C (toluene); IRν_{max} (KBr): 3351, 2926, 2875, 1478, 1448, 1261, 1199, 1035, 921, 789, 733 cm^{-1}; ^{1}H-NMR δ (400 MHz, $CDCl_3$); 3.96 (4H, t, J = 4.8 Hz, H-α and H-α′), 4.08 (4H, t, J = 4.8 Hz, H-β and H-β′), 7.06 (2H, s, H-5 and H-6); ^{13}C-NMR δ (100.6 MHz, $CDCl_3$); 61.3 (C-α and C-α′), 71.7 (C-β and C-β′), 113.2 (C-2 and C-3), 119.1 (C-5 and C-6), 151.0 (C-1 and C-4); HRMS calc. for $C_{10}H_{12}{}^{79}Br_2O_4$: $(M+H^+)$ *m/z* 354.9175, PMI not found under standard conditions.

2,2′-((2,5-Dibromo-1,4-phenylene)bis(oxy))diethanol (206)



Prepared according to general procedure S, **206** was isolated in 13 % yield as a white solid after recrystallisation from toluene; R_f 0.61 (1:1 hexane:ethyl acetate); m.p. 132 - 134 °C (toluene), (no lit. m.p. available); IRν_{max} (KBr): 3352, 2925, 2874, 1471, 1448, 1261, 1199, 1063, 895, 789, 733 cm^{-1}; ^{1}H-NMR δ (400 MHz, $CDCl_3$); 3.97 (4H, t, J = 4.4 Hz, H-α and H-α′), 4.10 (4H, t, J = 4.8 Hz, H-β and H-β′), 7.16 (2H, s, H-3 and H-6); ^{13}C-NMR δ (100.6 MHz, $CDCl_3$); 61.2 (C-α and C-α′), 71.5 (C-β and C-β′), 111.6 (C-2 and C-5), 117.5 (C-3 and C-6), 150.1 (C-1 and C-4); HRMS calc. for $C_{10}H_{12}{}^{79}Br_2O_4$: (M+H$^+$) *m/z* 354.9175, found 354.9181.

1,2,7,8-Tetrahydrobenzo[1,2-*b*:4,3-*b*′]difuran (90)



Prepared according to general procedure T, **90** was isolated in 47 % yield as a white solid after recrystallisation from hexane; **90** was also prepared according to general procedure U in 7 % yield; R_f 0.57 (2:1 hexane:ethyl acetate); m.p. 85 - 86 °C (hexane), (lit. m.p. 86 - 88 °C (hexane))[2] ; IRν_{max} (KBr): 2965, 2899, 1478, 1458, 1435, 1217, 1187, 1122, 976, 957, 815, 768, 737 cm^{-1}; ^{1}H-NMR δ (400 MHz, $CDCl_3$): 3.09 (4H, t, J = 12.0 Hz, H-1 and H-8), 4.54 (4H, t, J = 12.0 Hz, H-2 and H-7), 6.51 (2H, s, H-4 and H-5); ^{13}C-NMR δ (100.6 MHz, $CDCl_3$): 29.0 (C-1 and C-8), 71.3 (C-2 and C-7), 107.0 (C-4 and C-5), 123.6 (C-2*b* and C-3*b*′), 154.6 (C-1*b* and C-4*b*′); HRMS calc. for $C_{10}H_{12}{}^{79}Br_2O_4$: (M+H$^+$) *m/z* 163.0759, found 163.0757.

References (Chapter Four)

1. O′Connor, R. E.; Keating, J. J., Characterization of synthetic routes to ′Bromo-DragonFLY′ and benzodifuranyl isopropylamine homologues utilizing ketone intermediates. Part 1: Synthesis of ketone precursors. *Drug Testing and Analysis* **2014,** *6* (7-8), 658-667.
2. O′Connor, R. E.; Bateman, L. M.; Eccles, K. S.; Slattery, C. N.; Lawrence, S. E.; Keating, J. J., Structural Elucidation and Comparative Spectroscopic Analysis of Isomeric Benzodifurans. *Manuscript in Preparation* **2019**.
3. Wang, Z.; Chi, Y.; Harris, A. R.; Gray, D.; Davoren, J. E., Scalable Synthesis of 4-Substituted 5-Bromo-6-methylpyrimidines. *Synthesis-Stuttgart* **2011,** (10), 1529-1531.
4. Adelt, S.; Plettenburg, O.; Stricker, R.; Reiser, G.; Altenbach, H.-J.; Vogel, G., Enzyme-Assisted Total Synthesis of the Optical Antipodes d-myo-Inositol 3,4,5-Trisphosphate and d-myo-Inositol 1,5,6-Trisphosphate: Aspects of Their Structure−Activity Relationship to Biologically Active Inositol Phosphates. *Journal of Medicinal Chemistry* **1999,** *42* (7), 1262-1273.
5. Feng, L.; Wang, Y.; Liang, F.; Xu, M.; Wang, X., Highly selective recognition of monosaccharide based on two-component system in aqueous solution. *Tetrahedron* **2011,** *67* (18), 3175-3180.

Overall Summary and Future Work

In Chapter Two, pyrimidine impurities arising from the Leuckart synthesis of BDF **(15)** and structurally related ATS were investigated. The Leuckart reaction is one of the most common reactions used to synthesise ATS in a clandestine setting, and BDF **(15)** is a potent hallucinogenic ATS that has been known in the literature for twenty years and has been responsible for several cases of hospitalisation and, in rare cases, death following overdose. Eight target pyrimidines **(100, 101, 103-108)** were identified based on examination of the synthetic steps required to convert a phenone precursor to the corresponding ATS. The aim was to synthesise each pyrimidine independently, characterise them and use them as analytical standards to detect the pyrimidines in crude Leuckart reaction mixtures.

As described in Chapter Two, seven of the eight targeted pyrimidines were successfully synthesised, isolated and characterised, and the eighth **(108)** was subsequently isolated from a Leuckart reaction and characterised. The series of phenyl pyrimidines **(101, 104, 106)** were synthesised using a Suzuki-Miyaura coupling reaction and the series of benzyl pyrimidines **(100, 103, 105, 107)** were synthesised using a palladium-catalysed C-H activation coupling reaction.

During the synthesis of the pyrimidines, a number of alternate routes to the target compounds were trialled, including oxidation using DDQ, bromination using NBS or Br_2 and a three-component coupling reaction using $SnCl_4$ as a catalyst. While none of these approaches provided an alternate route to the desired pyrimidines, a number of interesting novel compounds were isolated, including the tribrominated phenyl pyrimidine **145**, a benzyl pyrimidine **169** with a carbonyl group in the benzyl position and a benzyl pyrimidine **173** with a bromine substituent in the benzyl position. It was also determined during the course of the research that the three-component coupling reaction using $SnCl_4$ is unsuited to electron dense aromatic systems, as the rate-limiting step (enamine formation) becomes very slow.

While many alternate synthetic routes were explored, it was still not possible to independently synthesise phenyl pyrimidine **108**, and any future work in this area could concentrate either on further alternate methods of synthesis.

Alternatively, focus could be turned to scaling up the synthesis of aryl bromide precursor **119** and optimising the synthesis of boronic acid **129** in order to produce pyrimidine **108** *via* the Suzuki-Miyaura coupling reaction (as for the rest of the phenyl pyrimidine series).

Also in Chapter Two, four Leuckart reactions were carried out to synthesise BDF **(15)** and structurally related ATS, and crude samples were retained for HPLC analysis. A HPLC method was developed to analyse the pyrimidine analytical standards and the crude Leuckart reactions. Good correlation in retention times was seen between the standards and the major impurity peaks in the analysis of the crude Leuckart reactions. This was an important result as it proved that producing analytical standards of pyrimidine impurities can be used to identify the Leuckart route in the synthesis of ATS.

However, despite this success, there are a number of ways in which future impurity profiling of pyrimidine impurities (or other route-specific impurities) by HPLC could be improved. These include:

- Further method development to optimise resolution between signals: this could be done by investigating longer run times in combination with different elution gradients, as well as investigating the effects of flow rate and column temperature on peak separation.
- Using an internal reference standard to cite relative retention times rather than absolute retention times (to ensure reproducibility).
- Derivatising ATS (i.e. with TFAA) to ensure that they do not elute with the solvent front on a reverse phase HPLC column (note that this is not necessary for the *N*-formyl products of Leuckart reactions).
- Ensure that HPLC analysis of pure ATS (derivatised) and *N*-formyl compounds is available to confirm the identity of the major peak in crude reaction analysis.
- Once sufficient resolution has been achieved in method development, spike crude samples with pure analytical marker to see if there is a corresponding increase in percentage area of the impurity peak. This will

identify any response factor, and if calibration curves are separately produced, it would allow for quantitative analysis of the impurities.

It would also be very useful to transfer the fully developed HPLC method to an LC-MS instrument: this would allow for unambiguous determination of the identity of each of the signals, and would rule out the possibility of coincidental co-elution. Previous attempts within our research group to source clandestinely synthesised samples of ATS have been unsuccessful, but it is possible in the future that this will become feasible. If clandestine samples can be acquired, testing these against the analytical standards would provide invaluable information about the applicability of these techniques in a forensic setting.

Chapter Three focused on the optimisation of a synthetic route to an isomeric side-product iTHBD **(90)**, which was isolated by a previous member of our research group (ROC) as part of the synthesis of THBD **(42)**, a key precursor in the synthesis of BDF **(15)**. In terms of impurity profiling, this marker could be used in the future to shed light on the early stages of clandestine BDF **(15)** synthesis, an area that has not been studied in detail. iTHBD **(90)** is also a novel compound, and could potentially be a useful pharmacophore in the field of drug discovery.

As described in Chapter Three, iTHBD **(90)** was successfully synthesised from 1,4-benzoquinone **(192)** over four steps in an overall yield of ~5 %, but a persistent side-product (**195**) was the cause of significant yield loss throughout the synthetic route. Extensive reaction optimisation was carried out to try and maximise the yield of the route, with an alternative reaction pathway also investigated (this alternative was unsuccessful due to the formation of unworkable emulsions).

However, there are many options for further optimisation of the route if this work were to be revisited in the future. For example, if a direct route to **194** could be devised without the simultaneous synthesis of **195**, this would improve the overall yield of the process significantly. This might require changing the initial steps of the synthetic pathway, for example, if a starting

material such as 2,3-dibromo-1,4-dimethoxy benzene was used, hydrolysis of the methoxy groups to give **194** could be the first step of the synthetic process, potentially avoiding the possibility for formation of **195**.

Another area of interest for future study would be the further functionalisation of iTHBD **(90)** to ultimately convert it to an isomeric analogue of BDF **(15)**. This marker would be useful for potential testing of clandestine material to determine if a dibromination reaction using Br_2 was used in the early stages of BDF **(15)** synthesis.

The library of impurity compounds related to BDF **(15)** identified throughout this thesis (both those linked to the Leuckart reaction and those relevant to early stages of precursor synthesis), along with their spectroscopic and analytical data, may be valuable to synthetic and analytical chemists engaged in impurity profiling in the future. They may provide data on the synthetic route used during manufacture, as well as the origin of secondary/tertiary by-products.

They may also provide valuable pharmacological and toxicological data: little is known at the time of writing about the potential toxicity of these impurities and side-products, and in a street sample of a drug, it is possible that the toxicity of the impurities may outstrip the toxicity of the ATS itself. A clear overview of potential impurities, along with specific methods for their synthesis, would help those working through toxicological assessments to identify and carry out specific toxicity assessments of potentially harmful compounds much more quickly.

Appendix

Table of Contents

Table of Contents **365**

5 Appendix: Pyrimidine Markers HPLC Data **366**

5.1 Phenyl Pyrimidine Markers 367

5.1.1 4-Methyl-5-(2,3,6,7-tetrahydrobenzo[1,2-*b*:4,5-*b'*]difuran-4-yl) pyrimidine **(101)** 367

5.1.2 5-(8-Bromo-2,3,6,7-tetrahydrobenzo[1,2-*b*:4,5-*b'*]difuran-4-yl)-4-methylpyrimidine **(104)** 370

5.1.3 5-(Benzo[1,2-*b*:4,5-*b'*]difuran-4-yl)-4-methylpyrimidine **(106)** 374

5.2 Benzyl Pyrimidine Markers 377

5.2.1 4-((2,3,6,7-Tetrahydrobenzo[1,2-*b*:4,5-*b'*]difuran-4-yl)methyl) pyrimidine **(100)**.. 377

5.2.2 4-((8-Bromo-2,3,6,7-tetrahydrobenzo[1,2-*b*:4,5-*b'*]difuran-4-yl) methyl)pyrimidine **(103)** 380

5.2.3 4-(Benzo[1,2-*b*:4,5-*b'*]difuran-4-ylmethyl)pyrimidine **(105)**.. 384

5.2.4 4-((8-Bromobenzo[1,2-*b*:4,5-*b'*]difuran-4-yl)methyl)pyrimidine **(107)**..... 388

5 Appendix: Pyrimidine Markers HPLC Data

This appendix shows the full raw data captured during the HPLC analysis of the independently synthesised analytical markers of the Leuckart synthesis of BDF **(15)** described in Chapter Two: benzyl pyrimidines **100**, **103**, **105** and **107**, and phenyl pyrimidines **101**, **104** and **106**.

The full HPLC method used to capture this raw data is described in Chapter Four: Experimental. Data were recorded on an Agilent® 1260 Series HPLC, a system which employs a variant wavelength diode array detector. In essence, this means that it can analyse a single sample at multiple wavelengths, giving rise to the four chromatograms seen for each sample in this Appendix. Each of these chromatograms represents the same sample seen at a discrete wavelength. The four wavelengths used for detection in this work were 210, 230, 254 and 280 nm.

In some cases, the sample being analysed does not absorb at 280 nm: in these cases, the chromatogram may appear 'messy' or impure when compared to the other chromatograms for that sample, and there is no clear major peak. However, closer inspection will reveal that the absorbance of these samples does not rise above 5 mAU, while chromatograms with clear majority signals will absorb in a range of ~ 500 - 3000 mAU.

The tables under the chromatograms for each sample list the peak data represented graphically in those chromatograms.

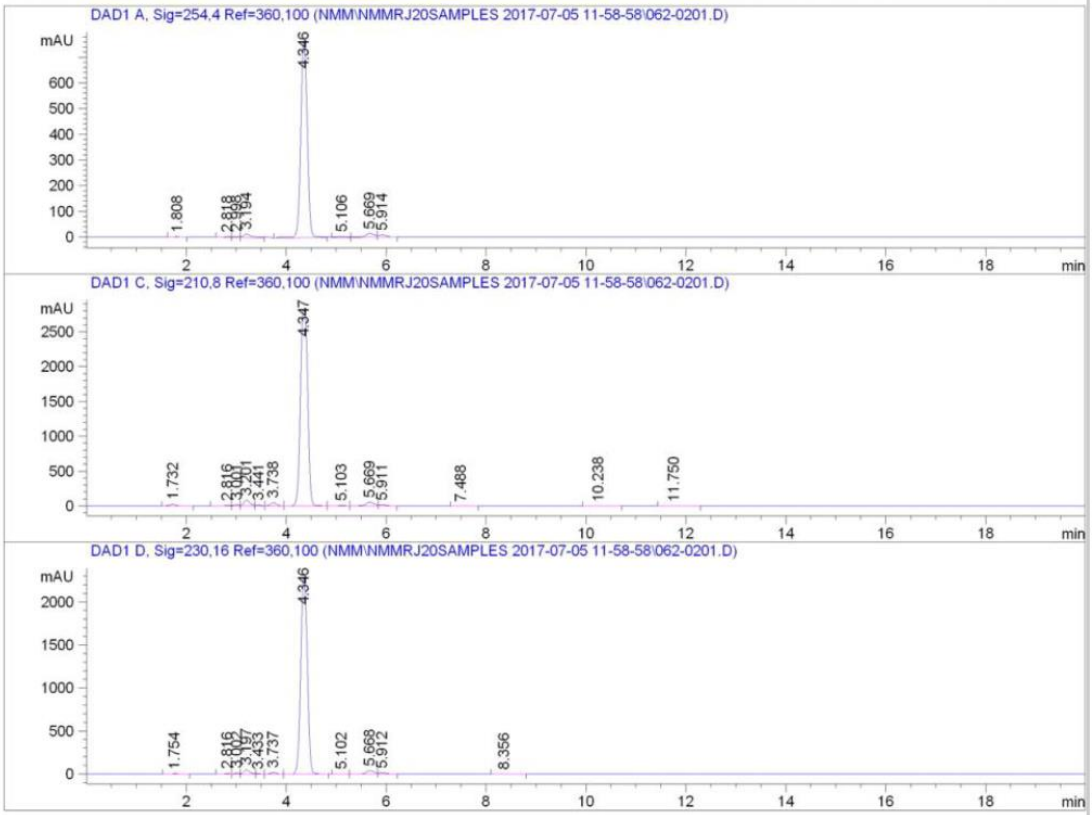
5.1 Phenyl Pyrimidine Markers

5.1.1 4-Methyl-5-(2,3,6,7-tetrahydrobenzo[1,2-*b*:4,5-*b'*]difuran-4-yl)pyrimidine (101)

```
Data File C:\CHEM32\1\DATA\NMM\NMMRJ20SAMPLES 2017-07-05 11-58-58\062-0201.D
Sample Name: 010

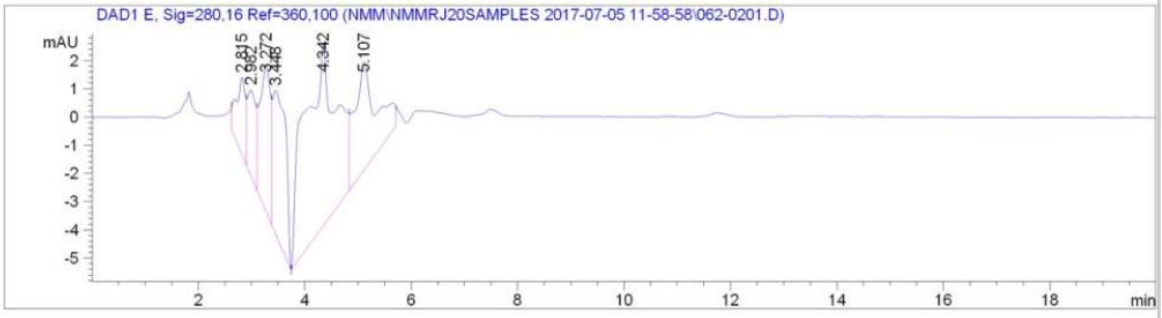
    ======================================================================
    Acq. Operator   : Nuala Maguire                  Seq. Line :   2
    Acq. Instrument : 1260 LC                        Location : Vial 62
    Injection Date  : 05/07/2017 12:20:40                 Inj :   1
                                                   Inj Volume : 10 µl
    Acq. Method     : C:\Chem32\1\DATA\NMM\NMMRJ20SAMPLES 2017-07-05 11-58-58\NUALA35RJ.M
    Last changed    : 04/07/2017 05:40:25  by Nuala Maguire
    Analysis Method : C:\CHEM32\1\DATA\NMM\NMMRJ20SAMPLES 2017-07-05 11-58-58\062-0201.D\DA.M (
                      NUALA35RJ.M)
    Last changed    : 04/07/2017 05:40:25  by Nuala Maguire
    Method Info     : Water:Acetonitrile, 35:65 RJ

    Sample Info     : First sample RJ - 010?
```




```
1260 LC 06/07/2017 10:49:37  Denis Lynch                    Page   1 of 3
```

Data File C:\CHEM32\1\DATA\NMM\NMMRJ20SAMPLES 2017-07-05 11-58-58\062-0201.D
Sample Name: 010



==========

Area Percent Report

==========

Sorted By : Signal
Multiplier : 1.0000
Dilution : 1.0000
Use Multiplier & Dilution Factor with ISTDs

Signal 1: DAD1 A, Sig=254,4 Ref=360,100

Peak #	RetTime [min]	Type	Width [min]	Area [mAU*s]	Height [mAU]	Area %
1	1.808	BB	0.1176	17.29866	1.98614	0.2270
2	2.818	BV	0.1594	36.67265	3.15983	0.4813
3	2.998	VV	0.1245	39.36948	4.57056	0.5167
4	3.194	VB	0.1807	189.98364	14.51549	2.4932
5	4.346	BB	0.1440	6948.65381	764.89594	91.1900
6	5.106	BV	0.2212	73.53264	4.84061	0.9650
7	5.669	VV	0.2055	208.44252	15.24336	2.7355
8	5.914	VB	0.1809	106.02420	9.17152	1.3914
Totals :				7619.97760	818.38344	

Signal 2: DAD1 C, Sig=210,8 Ref=360,100

Peak #	RetTime [min]	Type	Width [min]	Area [mAU*s]	Height [mAU]	Area %
1	1.732	BB	0.1359	304.26886	31.72512	0.9711
2	2.816	BV	0.1223	120.14919	14.25311	0.3835
3	3.001	VV	0.1112	151.09416	20.68995	0.4822
4	3.201	VV	0.1313	749.47321	86.33020	2.3919
5	3.441	VV	0.1208	134.91452	17.34189	0.4306
6	3.738	VV	0.1411	445.44012	48.51311	1.4216
7	4.347	VV	0.1610	2.82805e4	2820.87061	90.2558
8	5.103	VV	0.2035	119.85582	8.65632	0.3825
9	5.669	VV	0.1963	722.49109	56.83690	2.3058
10	5.911	VB	0.1676	206.72752	19.51636	0.6598
11	7.488	BB	0.2128	19.19202	1.34253	0.0613

Data File C:\CHEM32\1\DATA\NMM\NMMRJ20SAMPLES 2017-07-05 11-58-58\062-0201.D
Sample Name: 010

Peak #	RetTime [min]	Type	Width [min]	Area [mAU*s]	Height [mAU]	Area %
12	10.238	BB	0.2737	35.09674	1.95267	0.1120
13	11.750	BB	0.3115	44.50434	2.06460	0.1420
Totals :				3.13337e4	3130.09335	

Signal 3: DAD1 D, Sig=230,16 Ref=360,100

Peak #	RetTime [min]	Type	Width [min]	Area [mAU*s]	Height [mAU]	Area %
1	1.754	BB	0.1615	69.30849	5.55709	0.3089
2	2.816	BV	0.1148	62.30845	8.00527	0.2777
3	3.002	VV	0.1092	96.46608	13.52046	0.4299
4	3.197	VV	0.1279	425.11243	50.66777	1.8947
5	3.433	VV	0.1106	40.17956	5.53895	0.1791
6	3.737	VV	0.1439	186.74339	19.81687	0.8323
7	4.346	VB	0.1463	2.08309e4	2285.81714	92.8400
8	5.102	BV	0.1843	39.15728	3.21140	0.1745
9	5.668	VV	0.1909	485.19748	39.60027	2.1624
10	5.912	VB	0.1725	180.03688	16.60295	0.8024
11	8.356	BB	0.2647	22.00559	1.29213	0.0981
Totals :				2.24374e4	2449.63030	

Signal 4: DAD1 E, Sig=280,16 Ref=360,100

Peak #	RetTime [min]	Type	Width [min]	Area [mAU*s]	Height [mAU]	Area %
1	2.815	BV	0.1624	32.16866	2.71094	5.3225
2	2.982	VV	0.1606	34.74462	3.01065	5.7487
3	3.272	VV	0.1911	70.40279	5.16394	11.6485
4	3.448	VV	0.2346	89.74183	5.06784	14.8483
5	4.342	VV	0.5122	270.21899	6.45730	44.7092
6	5.107	VB	0.3669	107.11561	3.87031	17.7229
Totals :				604.39250	26.28099	

==========

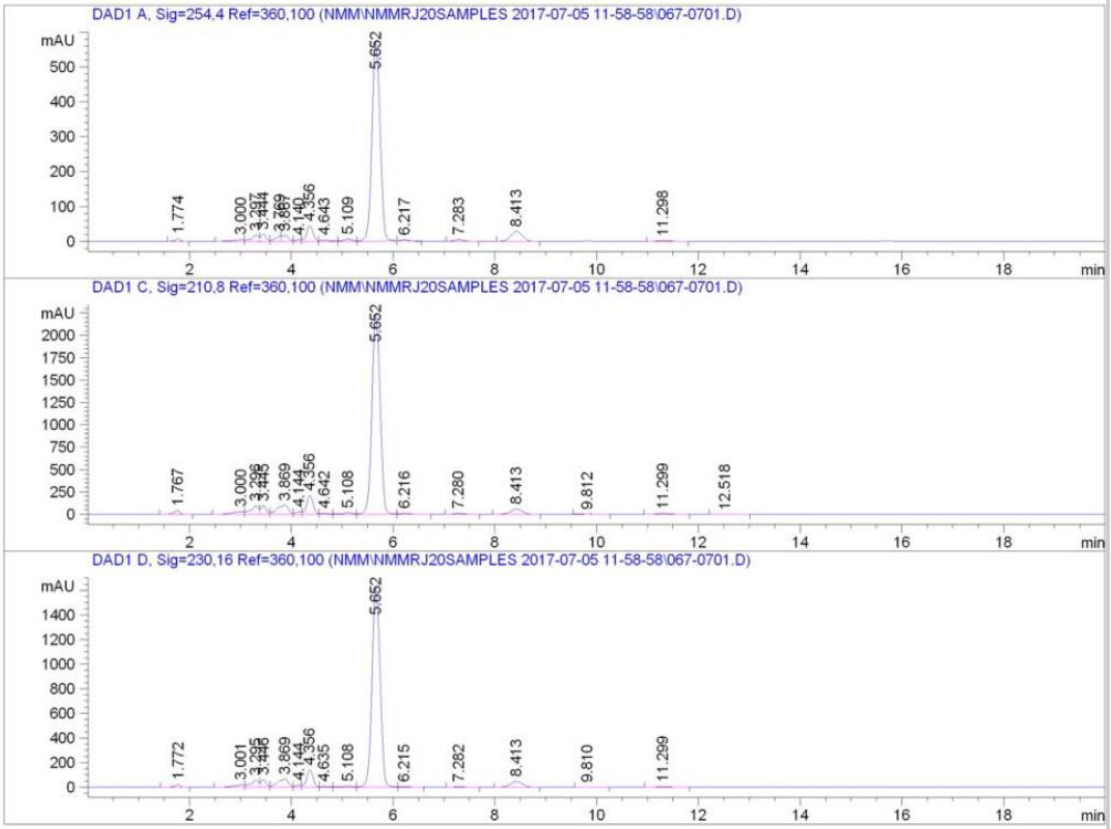
*** End of Report ***

5.1.2 5-(8-Bromo-2,3,6,7-tetrahydrobenzo[1,2-*b*:4,5-*b*']difuran-4-yl)-4-methylpyrimidine (104)

```
Data File C:\CHEM32\1\DATA\NMM\NMMRJ20SAMPLES 2017-07-05 11-58-58\067-0701.D
Sample Name: 3

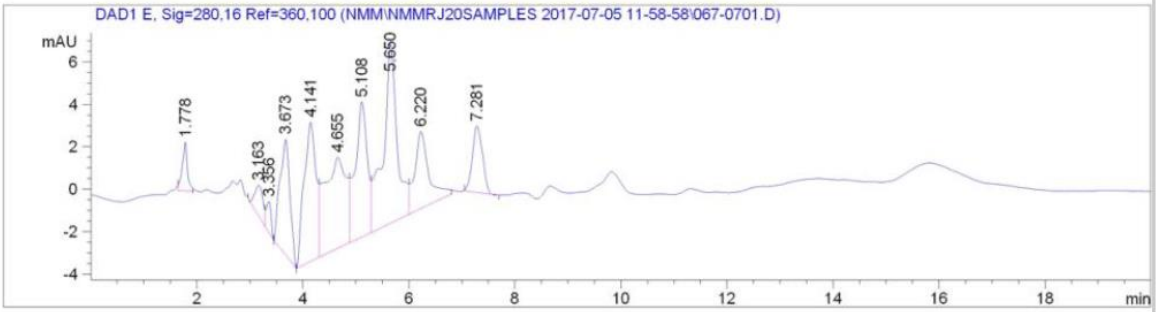
    ======================================================================
    Acq. Operator   : Nuala Maguire                  Seq. Line :   7
    Acq. Instrument : 1260 LC                       Location : Vial 67
    Injection Date  : 05/07/2017 02:07:43               Inj :   1
                                                   Inj Volume : 10 µl
    Acq. Method     : C:\Chem32\1\DATA\NMM\NMMRJ20SAMPLES 2017-07-05 11-58-58\NUALA35RJ.M
    Last changed    : 04/07/2017 05:40:25  by Nuala Maguire
    Analysis Method : C:\CHEM32\1\DATA\NMM\NMMRJ20SAMPLES 2017-07-05 11-58-58\067-0701.D\DA.M (
                      NUALA35RJ.M)
    Last changed    : 04/07/2017 05:40:25  by Nuala Maguire
    Method Info     : Water:Acetonitrile, 35:65 RJ

    Sample Info     : Sample 3 - 041
```




```
1260 LC 06/07/2017 11:10:47  Denis Lynch                    Page   1 of 4
```

Data File C:\CHEM32\1\DATA\NMM\NMMRJ20SAMPLES 2017-07-05 11-58-58\067-0701.D
Sample Name: 3



Area Percent Report

Sorted By : Signal
Multiplier : 1.0000
Dilution : 1.0000
Use Multiplier & Dilution Factor with ISTDs

Signal 1: DAD1 A, Sig=254,4 Ref=360,100

Peak #	RetTime [min]	Type	Width [min]	Area [mAU*s]	Height [mAU]	Area %
1	1.774	BB	0.0912	65.84434	9.94566	0.7801
2	3.000	BV	0.2071	91.88631	5.79167	1.0886
3	3.297	VV	0.1463	184.40298	17.88136	2.1847
4	3.444	VV	0.1178	155.53316	20.20784	1.8427
5	3.769	VV	0.1162	126.19757	15.31088	1.4951
6	3.867	VV	0.1406	160.15790	16.89074	1.8975
7	4.140	VV	0.1166	43.62693	5.37876	0.5169
8	4.356	VV	0.1434	408.14487	45.16589	4.8355
9	4.643	VB	0.1861	56.42472	4.44618	0.6685
10	5.109	BV	0.1768	88.70907	7.68040	1.0510
11	5.652	VV	0.1782	6394.15771	572.91052	75.7545
12	6.217	VB	0.1944	64.93812	5.24822	0.7694
13	7.283	BB	0.2155	74.68898	5.53104	0.8849
14	8.413	BB	0.2605	479.57513	29.37531	5.6817
15	11.298	BB	0.2854	46.33842	2.35657	0.5490
Totals :				8440.62621	764.12105	

Signal 2: DAD1 C, Sig=210,8 Ref=360,100

Peak #	RetTime [min]	Type	Width [min]	Area [mAU*s]	Height [mAU]	Area %
1	1.767	BB	0.1147	398.21597	46.15578	1.1779
2	3.000	BV	0.2005	537.58502	35.13444	1.5901
3	3.296	VV	0.1502	1021.89911	96.00999	3.0226
4	3.445	VV	0.1160	753.01685	97.58823	2.2273

Data File C:\CHEM32\1\DATA\NMM\NMMRJ20SAMPLES 2017-07-05 11-58-58\067-0701.D
Sample Name: 3

Peak #	RetTime [min]	Type	Width [min]	Area [mAU*s]	Height [mAU]	Area %
5	3.869	VV	0.2081	1598.33044	104.69432	4.7277
6	4.144	VV	0.1179	238.51315	29.64869	0.7055
7	4.356	VV	0.1418	1863.41675	209.54021	5.5117
8	4.642	VV	0.1713	155.61882	13.41603	0.4603
9	5.108	VV	0.2040	275.38672	20.07736	0.8146
10	5.652	VV	0.1821	2.53109e4	2235.01221	74.8664
11	6.216	VB	0.2119	188.58650	13.58995	0.5578
12	7.280	BB	0.2172	161.57536	12.14606	0.4779
13	8.413	BB	0.2643	1000.53851	60.08664	2.9595
14	9.812	BB	0.2675	60.67607	3.34648	0.1795
15	11.299	BB	0.3137	214.48923	10.10282	0.6344
16	12.518	BB	0.2997	29.34532	1.41667	0.0868
Totals :				3.38081e4	2987.96587	

Signal 3: DAD1 D, Sig=230,16 Ref=360,100

Peak #	RetTime [min]	Type	Width [min]	Area [mAU*s]	Height [mAU]	Area %
1	1.772	BB	0.0976	180.07722	25.13508	0.7710
2	3.001	BV	0.1902	292.91629	20.32004	1.2541
3	3.295	VV	0.1457	606.28833	59.07367	2.5958
4	3.446	VV	0.1159	467.78305	62.10441	2.0028
5	3.869	VV	0.2072	1011.97656	66.62672	4.3328
6	4.144	VV	0.1121	126.55570	16.38471	0.5418
7	4.356	VV	0.1419	1246.88159	140.00699	5.3385
8	4.635	VV	0.1704	80.61675	6.89764	0.3452
9	5.108	VV	0.2253	134.89154	8.67793	0.5775
10	5.652	VV	0.1779	1.81061e4	1625.53333	77.5211
11	6.215	VB	0.2071	80.85476	6.00502	0.3462
12	7.282	BB	0.2166	71.09749	5.36571	0.3044
13	8.413	BB	0.2626	798.05963	48.33000	3.4169
14	9.810	BB	0.2595	32.16171	1.82602	0.1377
15	11.299	BB	0.3059	120.07418	5.74334	0.5141
Totals :				2.33563e4	2098.03061	

Signal 4: DAD1 E, Sig=280,16 Ref=360,100

Peak #	RetTime [min]	Type	Width [min]	Area [mAU*s]	Height [mAU]	Area %
1	1.778	BB	0.0931	15.68850	2.31442	2.2202
2	3.163	BV	0.1619	15.64322	1.45003	2.2138
3	3.356	VV	0.0944	8.83410	1.46351	1.2502
4	3.673	VV	0.1794	70.99660	5.47077	10.0472
5	4.141	VV	0.2181	104.04483	6.59335	14.7241
6	4.655	VV	0.3714	123.44313	4.31973	17.4692
7	5.108	VV	0.2271	101.35574	6.38789	14.3435

Data File C:\CHEM32\1\DATA\NMM\NMMRJ20SAMPLES 2017-07-05 11-58-58\067-0701.D
Sample Name: 3

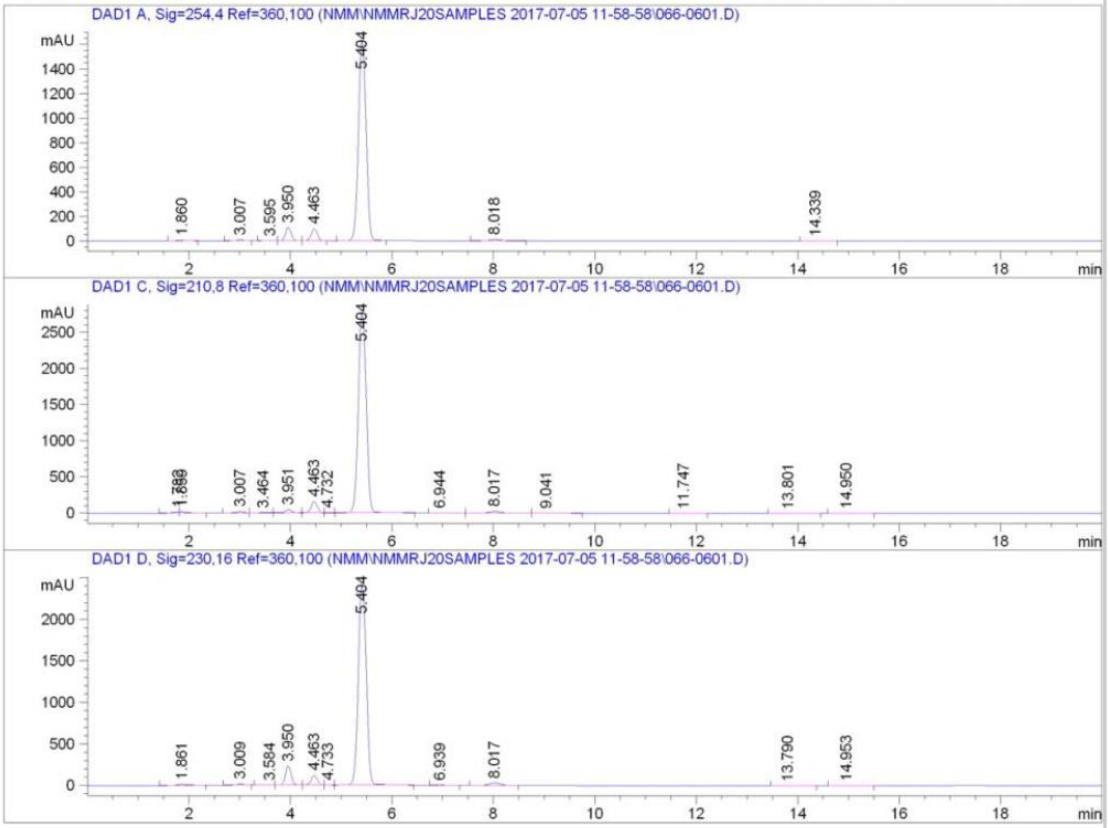
Peak #	RetTime [min]	Type	Width [min]	Area [mAU*s]	Height [mAU]	Area %
8	5.650	VV	0.2599	156.91774	8.47941	22.2064
9	6.220	VB	0.2691	68.21362	3.66555	9.6533
10	7.281	BB	0.2164	41.49435	3.13552	5.8721
Totals :				706.63183	43.28018	

*** End of Report ***

5.1.3 5-(Benzo[1,2-*b*:4,5-*b*']difuran-4-yl)-4-methylpyrimidine (106)

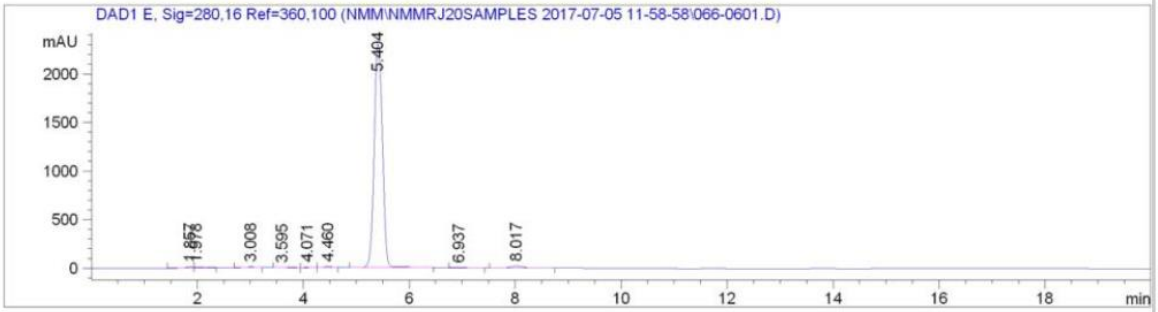
Data File C:\CHEM32\1\DATA\NMM\NMMRJ20SAMPLES 2017-07-05 11-58-58\066-0601.D
Sample Name: 2

Acq. Operator	: Nuala Maguire	Seq. Line	: 6
Acq. Instrument	: 1260 LC	Location	: Vial 66
Injection Date	: 05/07/2017 01:46:19	Inj	: 1
		Inj Volume	: 10 µl
Acq. Method	: C:\Chem32\1\DATA\NMM\NMMRJ20SAMPLES 2017-07-05 11-58-58\NUALA35RJ.M		
Last changed	: 04/07/2017 05:40:25 by Nuala Maguire		
Analysis Method	: C:\CHEM32\1\DATA\NMM\NMMRJ20SAMPLES 2017-07-05 11-58-58\066-0601.D\DA.M (NUALA35RJ.M)		
Last changed	: 04/07/2017 05:40:25 by Nuala Maguire		
Method Info	: Water:Acetonitrile, 35:65 RJ		
Sample Info	: Sample 1 - 028		



1260 LC 06/07/2017 11:08:24 Denis Lynch Page 1 of 3

Data File C:\CHEM32\1\DATA\NMM\NMMRJ20SAMPLES 2017-07-05 11-58-58\066-0601.D
Sample Name: 2



==========

Area Percent Report

==========

Sorted By : Signal
Multiplier : 1.0000
Dilution : 1.0000
Use Multiplier & Dilution Factor with ISTDs

Signal 1: DAD1 A, Sig=254,4 Ref=360,100

Peak #	RetTime [min]	Type	Width [min]	Area [mAU*s]	Height [mAU]	Area %
1	1.860	BB	0.1276	78.06503	7.88184	0.4068
2	3.007	BB	0.1293	84.73924	9.75696	0.4416
3	3.595	BV	0.1612	15.05708	1.33842	0.0785
4	3.950	VV	0.1260	856.97632	108.61763	4.4658
5	4.463	VB	0.1388	833.52191	96.50034	4.3436
6	5.404	BB	0.1689	1.70801e4	1621.23865	89.0068
7	8.018	BB	0.2610	212.90086	13.00412	1.1095
8	14.339	BB	0.2830	28.29380	1.46711	0.1474
Totals :				1.91896e4	1859.80507	

Signal 2: DAD1 C, Sig=210,8 Ref=360,100

Peak #	RetTime [min]	Type	Width [min]	Area [mAU*s]	Height [mAU]	Area %
1	1.782	BV	0.1571	176.60216	17.89671	0.5279
2	1.859	VB	0.1112	214.63828	25.25559	0.6416
3	3.007	BV	0.1437	219.88139	22.17360	0.6573
4	3.464	VV	0.2899	99.12440	4.44927	0.2963
5	3.951	VV	0.1536	467.62604	45.60830	1.3979
6	4.463	VV	0.1410	1381.16785	156.43965	4.1287
7	4.732	VV	0.1437	26.88864	2.86041	0.0804
8	5.404	VB	0.1763	3.02330e4	2749.80786	90.3757
9	6.944	BV	0.2660	34.16425	1.88054	0.1021
10	8.017	VB	0.2622	416.39752	25.27517	1.2447
11	9.041	BB	0.4047	51.44106	1.83686	0.1538

Data File C:\CHEM32\1\DATA\NMM\NMMRJ20SAMPLES 2017-07-05 11-58-58\066-0601.D
Sample Name: 2

Peak #	RetTime [min]	Type	Width [min]	Area [mAU*s]	Height [mAU]	Area %
12	11.747	BB	0.2920	29.20876	1.42010	0.0873
13	13.801	BB	0.3675	55.10874	2.13225	0.1647
14	14.950	BB	0.3200	47.34975	2.10881	0.1415
Totals :				3.34526e4	3059.14512	

Signal 3: DAD1 D, Sig=230,16 Ref=360,100

Peak #	RetTime [min]	Type	Width [min]	Area [mAU*s]	Height [mAU]	Area %
1	1.861	BB	0.1674	234.07190	17.57422	0.7687
2	3.009	BB	0.1395	163.36978	17.09617	0.5365
3	3.584	BV	0.2549	71.15639	3.69185	0.2337
4	3.950	VV	0.1278	1870.01501	232.62067	6.1408
5	4.463	VV	0.1417	1032.40845	116.18855	3.3903
6	4.733	VV	0.1447	23.50223	2.47629	0.0772
7	5.404	VB	0.1770	2.64771e4	2394.05615	86.9465
8	6.939	BB	0.1977	35.10033	2.93222	0.1153
9	8.017	BB	0.2575	456.81830	28.42278	1.5001
10	13.790	BB	0.3456	42.81986	1.79981	0.1406
11	14.953	BB	0.3275	45.82411	2.09207	0.1505
Totals :				3.04522e4	2818.95077	

Signal 4: DAD1 E, Sig=280,16 Ref=360,100

Peak #	RetTime [min]	Type	Width [min]	Area [mAU*s]	Height [mAU]	Area %
1	1.857	BV	0.1094	112.56303	13.77017	0.4327
2	1.978	VB	0.1846	85.89857	6.74174	0.3302
3	3.008	BB	0.1233	76.25505	9.33522	0.2932
4	3.595	BV	0.2941	56.24675	2.54262	0.2162
5	4.071	VV	0.1783	71.68456	5.87782	0.2756
6	4.460	VV	0.1786	158.07129	13.11779	0.6077
7	5.404	BB	0.1750	2.50998e4	2305.81470	96.4958
8	6.937	BB	0.1810	22.70400	2.18989	0.0873
9	8.017	BB	0.2581	328.06470	20.34799	1.2612
Totals :				2.60113e4	2379.73794	

==========

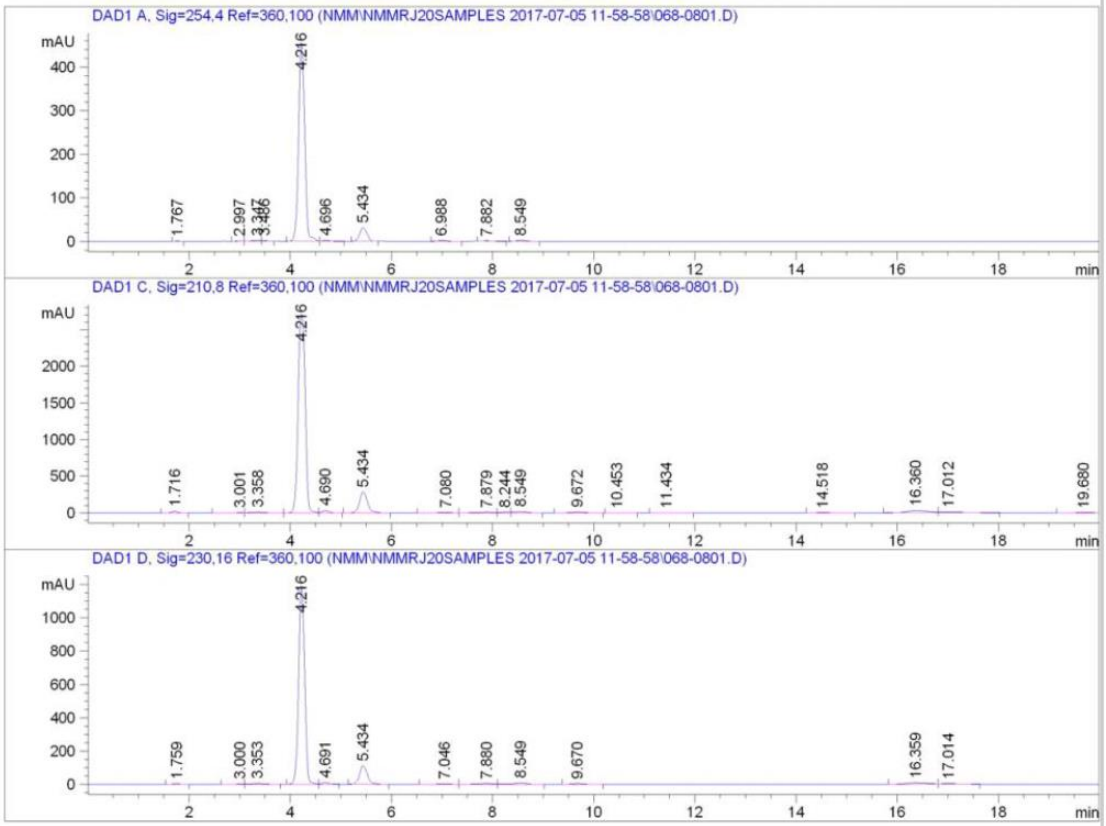
*** End of Report ***

5.2 Benzyl Pyrimidine Markers

5.2.1 4-((2,3,6,7-Tetrahydrobenzo[1,2-*b*:4,5-*b'*]difuran-4-yl)methyl)pyrimidine (100)

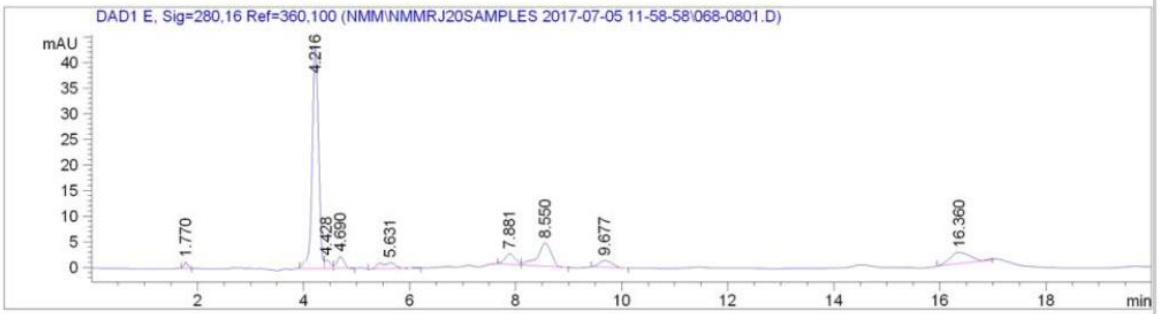
Data File C:\CHEM32\1\DATA\NMM\NMMRJ20SAMPLES 2017-07-05 11-58-58\068-0801.D
Sample Name: 4

Acq. Operator	: Nuala Maguire	Seq. Line	: 8
Acq. Instrument	: 1260 LC	Location	: Vial 68
Injection Date	: 05/07/2017 02:29:08	Inj	: 1
		Inj Volume	: 10 µl
Acq. Method	: C:\Chem32\1\DATA\NMM\NMMRJ20SAMPLES 2017-07-05 11-58-58\NUALA35RJ.M		
Last changed	: 04/07/2017 05:40:25 by Nuala Maguire		
Analysis Method	: C:\CHEM32\1\DATA\NMM\NMMRJ20SAMPLES 2017-07-05 11-58-58\068-0801.D\DA.M (NUALA35RJ.M)		
Last changed	: 04/07/2017 05:40:25 by Nuala Maguire		
Method Info	: Water:Acetonitrile, 35:65 RJ		
Sample Info	: Sample 4- 015		



1260 LC 06/07/2017 11:12:16 Denis Lynch Page 1 of 3

Data File C:\CHEM32\1\DATA\NMM\NMMRJ20SAMPLES 2017-07-05 11-58-58\068-0801.D
Sample Name: 4



==========

Area Percent Report

==========

Sorted By : Signal
Multiplier : 1.0000
Dilution : 1.0000
Use Multiplier & Dilution Factor with ISTDs

Signal 1: DAD1 A, Sig=254,4 Ref=360,100

Peak #	RetTime [min]	Type	Width [min]	Area [mAU*s]	Height [mAU]	Area %
1	1.767	BB	0.0792	12.57578	2.25151	0.2883
2	2.997	BV	0.1355	14.38809	1.53252	0.3298
3	3.347	VV	0.1990	37.23571	2.51169	0.8535
4	3.486	VB	0.1256	17.43294	2.08381	0.3996
5	4.216	BV	0.1322	3833.97021	455.53647	87.8845
6	4.696	VB	0.1573	24.82390	2.51169	0.5690
7	5.434	BB	0.1671	331.67282	31.94994	7.6028
8	6.988	BB	0.2107	30.15899	2.33521	0.6913
9	7.882	BB	0.2111	18.78769	1.43154	0.4307
10	8.549	BB	0.2276	41.46605	2.81877	0.9505
Totals :				4362.51218	504.96316	

Signal 2: DAD1 C, Sig=210,8 Ref=360,100

Peak #	RetTime [min]	Type	Width [min]	Area [mAU*s]	Height [mAU]	Area %
1	1.716	BB	0.1121	249.31287	29.64263	0.7430
2	3.001	BV	0.1589	106.74821	9.23369	0.3181
3	3.358	VV	0.2549	286.16534	14.58663	0.8528
4	4.216	VV	0.1565	2.61518e4	2711.25903	77.9339
5	4.690	VB	0.1606	346.69614	33.55010	1.0332
6	5.434	BB	0.1744	3243.89868	290.33719	9.6670
7	7.080	BV	0.2947	171.69089	7.74310	0.5116
8	7.879	VV	0.3177	297.01880	12.47829	0.8851
9	8.244	VV	0.1951	161.78354	11.86019	0.4821

Data File C:\CHEM32\1\DATA\NMM\NMMRJ20SAMPLES 2017-07-05 11-58-58\068-0801.D
Sample Name: 4

Peak #	RetTime [min]	Type	Width [min]	Area [mAU*s]	Height [mAU]	Area %
10	8.549	VB	0.2539	363.49060	22.33486	1.0832
11	9.672	BB	0.3016	268.82089	13.89871	0.8011
12	10.453	BB	0.2214	16.95900	1.12817	0.0505
13	11.434	BB	0.3188	40.47047	1.92838	0.1206
14	14.518	BB	0.3940	116.16292	4.13231	0.3462
15	16.360	BV	0.4776	1058.15247	31.85047	3.1534
16	17.012	VB	0.4763	535.10492	15.51790	1.5946
17	19.680	BBA	0.4311	142.10405	4.64319	0.4235
Totals :				3.35564e4	3216.12484	

Signal 3: DAD1 D, Sig=230,16 Ref=360,100

Peak #	RetTime [min]	Type	Width [min]	Area [mAU*s]	Height [mAU]	Area %
1	1.759	BB	0.1254	61.39594	6.42997	0.4940
2	3.000	BV	0.1735	45.45753	3.59510	0.3658
3	3.353	VB	0.2823	135.84470	6.18470	1.0931
4	4.216	BV	0.1306	9891.92676	1195.11682	79.5960
5	4.691	VB	0.1497	102.23035	10.87201	0.8226
6	5.434	BB	0.1713	1224.07898	112.15413	9.8496
7	7.046	BV	0.3369	86.92514	3.77156	0.6994
8	7.880	VV	0.3105	129.60469	5.67345	1.0429
9	8.549	VB	0.3110	214.78032	10.14377	1.7282
10	9.670	BB	0.2862	86.56000	4.80340	0.6965
11	16.359	BV	0.4686	314.60364	9.69574	2.5315
12	17.014	VB	0.4163	134.26320	4.54958	1.0804
Totals :				1.24277e4	1372.99023	

Signal 4: DAD1 E, Sig=280,16 Ref=360,100

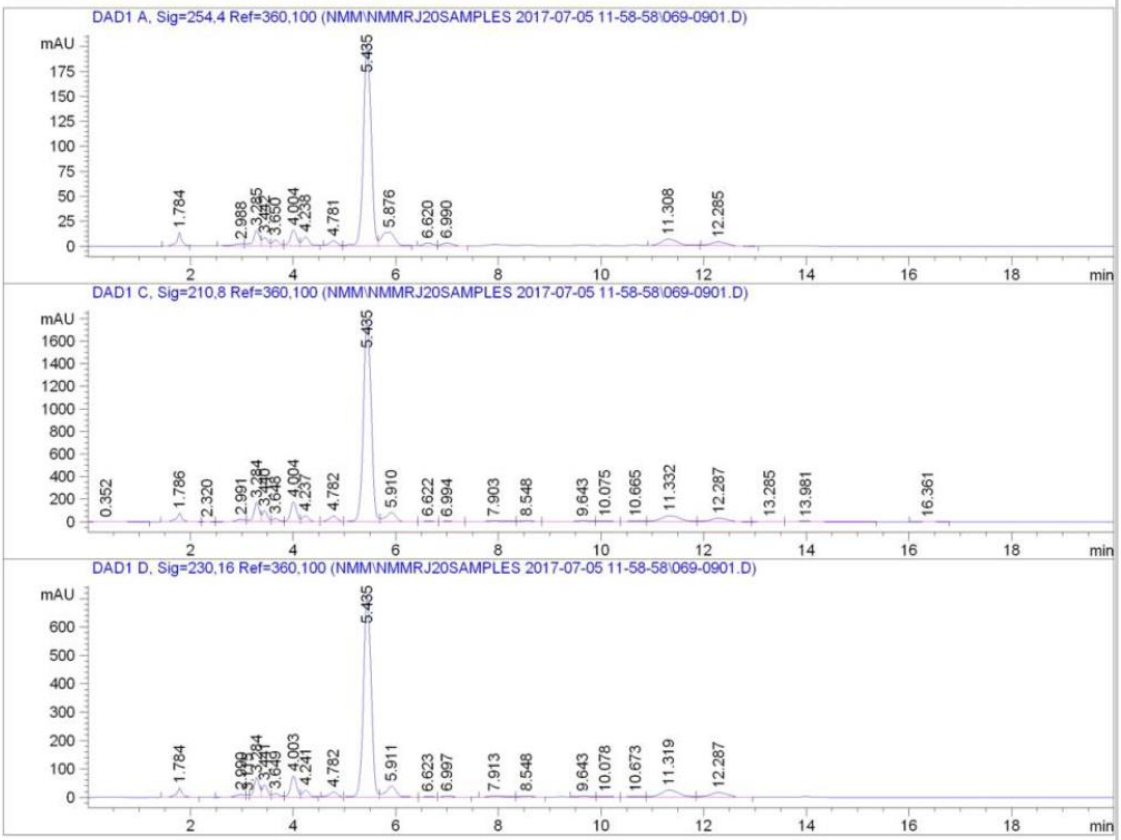
Peak #	RetTime [min]	Type	Width [min]	Area [mAU*s]	Height [mAU]	Area %
1	1.770	BB	0.0765	7.00892	1.26788	1.1292
2	4.216	BV	0.1319	365.01038	43.50998	58.8072
3	4.428	VV	0.1194	12.35704	1.61201	1.9909
4	4.690	VB	0.1468	20.70539	2.26276	3.3359
5	5.631	BB	0.2940	25.42754	1.18686	4.0967
6	7.881	BV	0.2114	28.82513	2.05792	4.6440
7	8.550	VB	0.2716	80.69365	4.53467	13.0006
8	9.677	BB	0.2584	22.50196	1.36417	3.6253
9	16.360	BB	0.3744	58.15958	2.20031	9.3702
Totals :				620.68958	59.99656	

==========

5.2.2 4-((8-Bromo-2,3,6,7-tetrahydrobenzo[1,2-*b*:4,5-*b*']difuran-4-yl)methyl)pyrimidine (103)

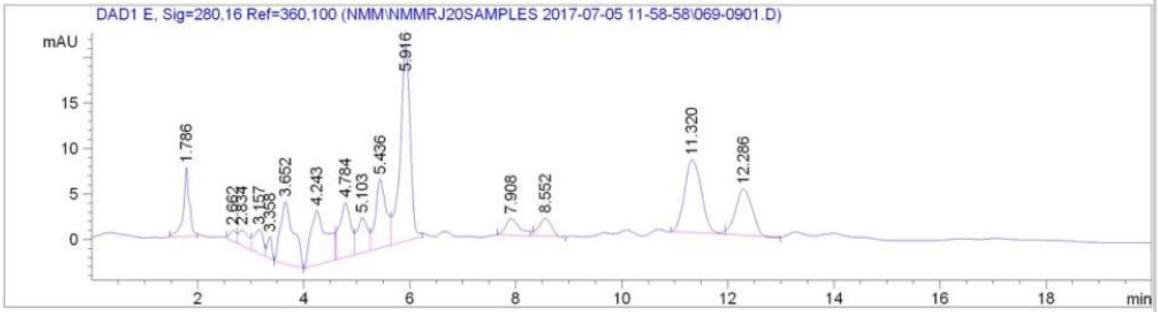
Data File C:\CHEM32\1\DATA\NMM\NMMRJ20SAMPLES 2017-07-05 11-58-58\069-0901.D
Sample Name: 5

Acq. Operator	: Nuala Maguire	Seq. Line	: 9
Acq. Instrument	: 1260 LC	Location	: Vial 69
Injection Date	: 05/07/2017 02:50:37	Inj	: 1
		Inj Volume	: 10 µl
Acq. Method	: C:\Chem32\1\DATA\NMM\NMMRJ20SAMPLES 2017-07-05 11-58-58\NUALA35RJ.M		
Last changed	: 04/07/2017 05:40:25 by Nuala Maguire		
Analysis Method	: C:\CHEM32\1\DATA\NMM\NMMRJ20SAMPLES 2017-07-05 11-58-58\069-0901.D\DA.M (NUALA35RJ.M)		
Last changed	: 04/07/2017 05:40:25 by Nuala Maguire		
Method Info	: Water:Acetonitrile, 35:65 RJ		
Sample Info	: Sample 5 - 023		



1260 LC 06/07/2017 11:13:13 Denis Lynch Page 1 of 4

Data File C:\CHEM32\1\DATA\NMM\NMMRJ20SAMPLES 2017-07-05 11-58-58\069-0901.D
Sample Name: 5



==========

Area Percent Report

==========

Sorted By : Signal
Multiplier : 1.0000
Dilution : 1.0000
Use Multiplier & Dilution Factor with ISTDs

Signal 1: DAD1 A, Sig=254,4 Ref=360,100

Peak #	RetTime [min]	Type	Width [min]	Area [mAU*s]	Height [mAU]	Area %
1	1.784	BB	0.0939	91.64589	13.38168	2.7249
2	2.988	BV	0.2023	36.11060	2.31070	1.0737
3	3.285	VV	0.1268	137.37401	15.89899	4.0845
4	3.442	VV	0.1183	64.87193	8.38278	1.9288
5	3.650	VV	0.1329	53.95741	5.99981	1.6043
6	4.004	VV	0.1366	143.59048	16.00864	4.2694
7	4.238	VB	0.1520	90.76278	8.97464	2.6986
8	4.781	BV	0.1681	56.35373	5.13420	1.6756
9	5.435	VV	0.1687	2119.38184	201.48990	63.0153
10	5.876	VB	0.2365	245.95251	13.89228	7.3129
11	6.620	BV	0.2043	37.81607	3.01533	1.1244
12	6.990	VB	0.2151	41.46459	3.11856	1.2329
13	11.308	BB	0.3610	154.27625	6.69134	4.5871
14	12.285	BB	0.3200	89.72245	4.15449	2.6677
Totals :				3363.28054	308.45332	

Signal 2: DAD1 C, Sig=210,8 Ref=360,100

Peak #	RetTime [min]	Type	Width [min]	Area [mAU*s]	Height [mAU]	Area %
1	0.352	BB	0.4132	77.13081	2.81915	0.2531
2	1.786	BB	0.1079	620.47217	77.09028	2.0358
3	2.320	BV	0.1318	14.19307	1.62661	0.0466
4	2.991	VV	0.1793	308.64362	23.49074	1.0127
5	3.284	VV	0.1159	1321.73059	171.53708	4.3367

Data File C:\CHEM32\1\DATA\NMM\NMMRJ20SAMPLES 2017-07-05 11-58-58\069-0901.D
Sample Name: 5

Peak #	RetTime [min]	Type	Width [min]	Area [mAU*s]	Height [mAU]	Area %
6	3.440	VV	0.1112	703.76428	98.72971	2.3091
7	3.648	VV	0.1353	271.82065	29.56501	0.8919
8	4.004	VV	0.1307	1497.10535	177.04068	4.9121
9	4.237	VV	0.1442	500.01672	52.91845	1.6406
10	4.782	VV	0.1734	611.32721	53.47035	2.0058
11	5.435	VV	0.1696	1.89094e4	1785.27808	62.0426
12	5.910	VV	0.2209	1246.75073	83.15688	4.0906
13	6.622	VV	0.2367	134.31396	8.76854	0.4407
14	6.994	VV	0.2665	134.07759	7.50133	0.4399
15	7.903	VV	0.4344	369.55713	11.33473	1.2125
16	8.548	VV	0.2780	220.33537	11.68514	0.7229
17	9.643	VV	0.4233	359.32767	11.17143	1.1790
18	10.075	VV	0.3091	200.15599	9.68498	0.6567
19	10.665	VV	0.3459	198.96391	8.79432	0.6528
20	11.332	VV	0.4163	1518.80383	55.66247	4.9833
21	12.287	VV	0.3886	852.02435	34.20667	2.7955
22	13.285	VV	0.3710	131.51682	4.93359	0.4315
23	13.981	VB	0.4729	234.71666	6.73011	0.7701
24	16.361	BV	0.3559	41.95824	1.66540	0.1377
Totals :				3.04781e4	2728.86172	

Signal 3: DAD1 D, Sig=230,16 Ref=360,100

Peak #	RetTime [min]	Type	Width [min]	Area [mAU*s]	Height [mAU]	Area %
1	1.784	BB	0.1053	260.32391	33.28326	2.2009
2	2.990	VV	0.2031	130.24065	9.67048	1.1011
3	3.115	VV	0.0624	32.78252	7.58219	0.2772
4	3.284	VV	0.1120	513.65723	69.69453	4.3426
5	3.441	VV	0.1118	306.56589	42.70155	2.5918
6	3.649	VV	0.1363	125.09605	13.48075	1.0576
7	4.003	VV	0.1328	629.48346	74.32582	5.3218
8	4.241	VB	0.1425	224.79323	24.62822	1.9005
9	4.782	BV	0.1715	208.37987	18.48313	1.7617
10	5.435	VV	0.1679	7415.44971	709.92719	62.6925
11	5.911	VB	0.2113	550.62750	38.86963	4.6552
12	6.623	BV	0.2065	31.65096	2.45302	0.2676
13	6.997	VB	0.2127	49.47021	3.73147	0.4182
14	7.913	BV	0.3394	96.83162	3.93137	0.8186
15	8.548	VB	0.2360	66.03329	4.23256	0.5583
16	9.643	BV	0.2761	66.88121	3.45063	0.5654
17	10.078	VV	0.2757	44.33487	2.51437	0.3748
18	10.673	VV	0.3091	54.28486	2.74000	0.4589
19	11.319	VV	0.3910	619.73975	24.50759	5.2395
20	12.287	VB	0.3743	401.66034	17.08456	3.3958
Totals :				1.18283e4	1107.29233	

Data File C:\CHEM32\1\DATA\NMM\NMMRJ20SAMPLES 2017-07-05 11-58-58\069-0901.D
Sample Name: 5

Signal 4: DAD1 E, Sig=280,16 Ref=360,100

Peak #	RetTime [min]	Type	Width [min]	Area [mAU*s]	Height [mAU]	Area %
1	1.786	BB	0.1044	60.12972	7.58850	4.7428
2	2.662	BV	0.1242	10.84742	1.23874	0.8556
3	2.834	VB	0.1773	22.78218	1.71147	1.7970
4	3.157	BV	0.1814	31.40339	2.62856	2.4770
5	3.358	VV	0.0902	13.69057	2.41097	1.0799
6	3.652	VV	0.2314	118.20301	6.84582	9.3235
7	4.243	VB	0.2786	126.22944	6.02101	9.9566
8	4.784	BV	0.2088	88.53373	6.04636	6.9833
9	5.103	VV	0.2014	53.26292	3.89869	4.2012
10	5.436	VV	0.2054	108.02304	7.61903	8.5205
11	5.916	VB	0.1998	282.83746	21.73326	22.3094
12	7.908	BB	0.2689	32.83941	1.79932	2.5903
13	8.552	BB	0.2408	30.89481	1.97124	2.4369
14	11.320	BB	0.3551	179.48164	8.01925	14.1570
15	12.286	BB	0.3173	108.63879	5.12515	8.5691
Totals :				1267.79753	84.65737	

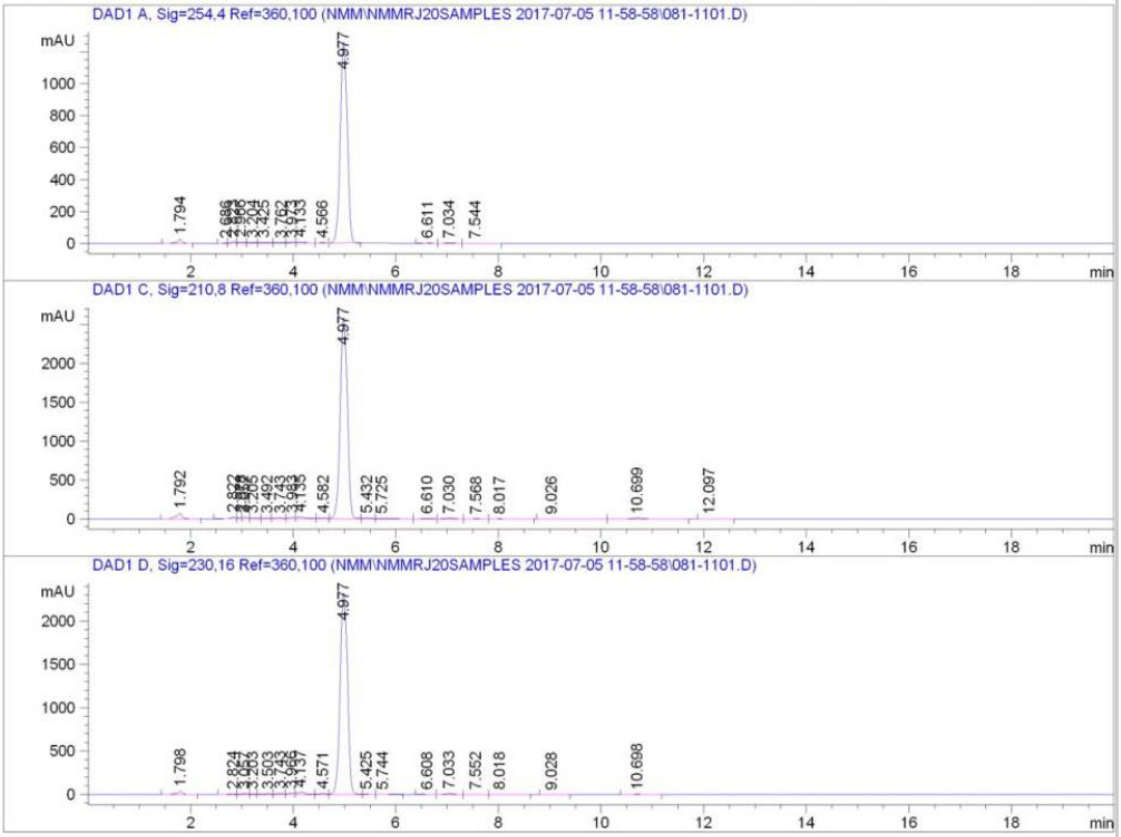
==========

*** End of Report ***

5.2.3 4-(Benzo[1,2-*b*:4,5-*b*']difuran-4-ylmethyl)pyrimidine (105)

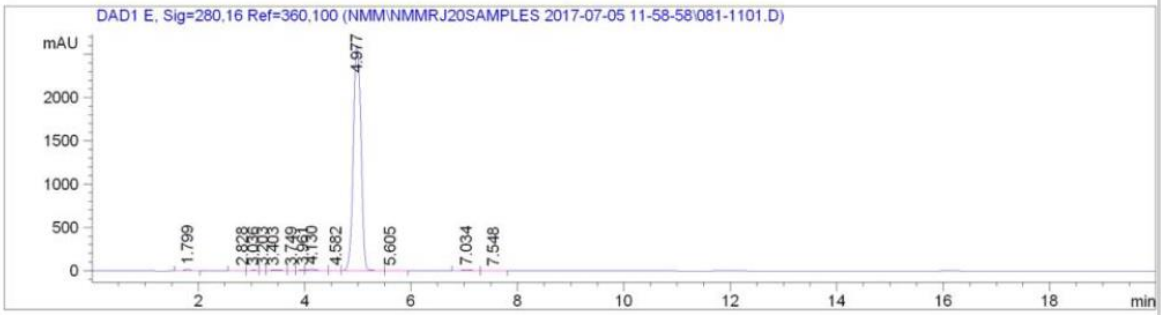
Data File C:\CHEM32\1\DATA\NMM\NMMRJ20SAMPLES 2017-07-05 11-58-58\081-1101.D
Sample Name: 7

Acq. Operator	: Nuala Maguire	Seq. Line	: 11
Acq. Instrument	: 1260 LC	Location	: Vial 81
Injection Date	: 05/07/2017 03:33:32	Inj	: 1
		Inj Volume	: 10 µl
Acq. Method	: C:\Chem32\1\DATA\NMM\NMMRJ20SAMPLES 2017-07-05 11-58-58\NUALA35RJ.M		
Last changed	: 04/07/2017 05:40:25 by Nuala Maguire		
Analysis Method	: C:\CHEM32\1\DATA\NMM\NMMRJ20SAMPLES 2017-07-05 11-58-58\081-1101.D\DA.M (NUALA35RJ.M)		
Last changed	: 04/07/2017 05:40:25 by Nuala Maguire		
Method Info	: Water:Acetonitrile, 35:65 RJ		
Sample Info	: Sample 7 - 025		



1260 LC 06/07/2017 11:16:34 Denis Lynch Page 1 of 4

Data File C:\CHEM32\1\DATA\NMM\NMMRJ20SAMPLES 2017-07-05 11-58-58\081-1101.D
Sample Name: 7



==========

Area Percent Report

==========

Sorted By : Signal
Multiplier : 1.0000
Dilution : 1.0000
Use Multiplier & Dilution Factor with ISTDs

Signal 1: DAD1 A, Sig=254,4 Ref=360,100

Peak #	RetTime [min]	Type	Width [min]	Area [mAU*s]	Height [mAU]	Area %
1	1.794	BB	0.0982	203.80722	28.24485	1.5895
2	2.686	BV	0.0878	20.77122	3.57160	0.1620
3	2.823	VV	0.1090	82.80116	11.37088	0.6458
4	2.966	VV	0.1236	72.43296	8.65655	0.5649
5	3.204	VV	0.1679	68.16691	5.93891	0.5316
6	3.425	VV	0.2382	93.43624	5.85313	0.7287
7	3.762	VV	0.1860	60.55771	4.30825	0.4723
8	3.973	VV	0.1433	69.39994	7.14758	0.5412
9	4.133	VV	0.1795	95.49748	7.65821	0.7448
10	4.566	VV	0.1630	33.99005	3.17312	0.2651
11	4.977	VB	0.1522	1.19137e4	1261.09912	92.9147
12	6.611	BV	0.1943	36.24921	3.01357	0.2827
13	7.034	VV	0.2027	54.01517	4.29462	0.4213
14	7.544	VB	0.2350	17.37048	1.06084	0.1355
Totals :				1.28222e4	1355.39122	

Signal 2: DAD1 C, Sig=210,8 Ref=360,100

Peak #	RetTime [min]	Type	Width [min]	Area [mAU*s]	Height [mAU]	Area %
1	1.792	BB	0.1203	686.09442	75.28967	2.3530
2	2.822	BV	0.1257	220.88188	25.33070	0.7575
3	2.978	VV	0.0778	102.47190	19.99606	0.3514
4	3.057	VV	0.1154	182.06175	22.25664	0.6244
5	3.205	VV	0.1650	178.91078	15.24024	0.6136

Data File C:\CHEM32\1\DATA\NMM\NMMRJ20SAMPLES 2017-07-05 11-58-58\081-1101.D
Sample Name: 7

Peak #	RetTime [min]	Type	Width [min]	Area [mAU*s]	Height [mAU]	Area %
6	3.492	VV	0.1552	165.26585	15.16352	0.5668
7	3.743	VV	0.2080	254.63925	16.32215	0.8733
8	3.983	VV	0.1441	217.27797	21.84144	0.7452
9	4.135	VV	0.2268	410.26874	25.08193	1.4070
10	4.582	VV	0.1879	204.01277	15.88221	0.6997
11	4.977	VV	0.1555	2.52552e4	2595.19019	86.6125
12	5.432	VV	0.1965	210.91783	15.92220	0.7233
13	5.725	VV	0.3382	217.23886	8.85465	0.7450
14	6.610	VV	0.2363	137.70969	8.71767	0.4723
15	7.030	VV	0.2389	194.19186	12.52567	0.6660
16	7.568	VV	0.2853	80.16846	4.11565	0.2749
17	8.017	VB	0.3501	99.04142	4.06742	0.3397
18	9.026	BV	0.4038	93.27352	3.07589	0.3199
19	10.699	VB	0.3112	222.68958	11.43673	0.7637
20	12.097	BB	0.2743	26.50964	1.42985	0.0909
Totals :				2.91588e4	2917.74047	

Signal 3: DAD1 D, Sig=230,16 Ref=360,100

Peak #	RetTime [min]	Type	Width [min]	Area [mAU*s]	Height [mAU]	Area %
1	1.798	BB	0.1097	323.51074	39.44804	1.2834
2	2.824	BV	0.1431	91.13475	8.92704	0.3615
3	3.057	VV	0.1603	130.20474	11.14477	0.5165
4	3.203	VV	0.1153	58.04376	7.26191	0.2303
5	3.503	VV	0.2272	152.58940	8.93723	0.6053
6	3.743	VV	0.1660	139.47023	11.96507	0.5533
7	3.966	VV	0.1338	143.34547	15.80189	0.5687
8	4.137	VV	0.1736	312.18658	26.09459	1.2384
9	4.571	VV	0.1842	125.52476	10.01694	0.4980
10	4.977	VV	0.1605	2.32434e4	2327.01611	92.2069
11	5.425	VV	0.1855	86.60793	6.94508	0.3436
12	5.744	VB	0.2414	66.24366	3.99626	0.2628
13	6.608	BV	0.1832	31.56072	2.60760	0.1252
14	7.033	VV	0.2099	153.64206	11.79876	0.6095
15	7.552	VV	0.2150	34.45795	2.49749	0.1367
16	8.018	VB	0.2113	18.12564	1.41672	0.0719
17	9.028	BB	0.2148	14.25323	1.00878	0.0565
18	10.698	BB	0.2795	83.57686	4.52397	0.3316
Totals :				2.52079e4	2501.40826	

Signal 4: DAD1 E, Sig=280,16 Ref=360,100

Data File C:\CHEM32\1\DATA\NMM\NMMRJ20SAMPLES 2017-07-05 11-58-58\081-1101.D
Sample Name: 7

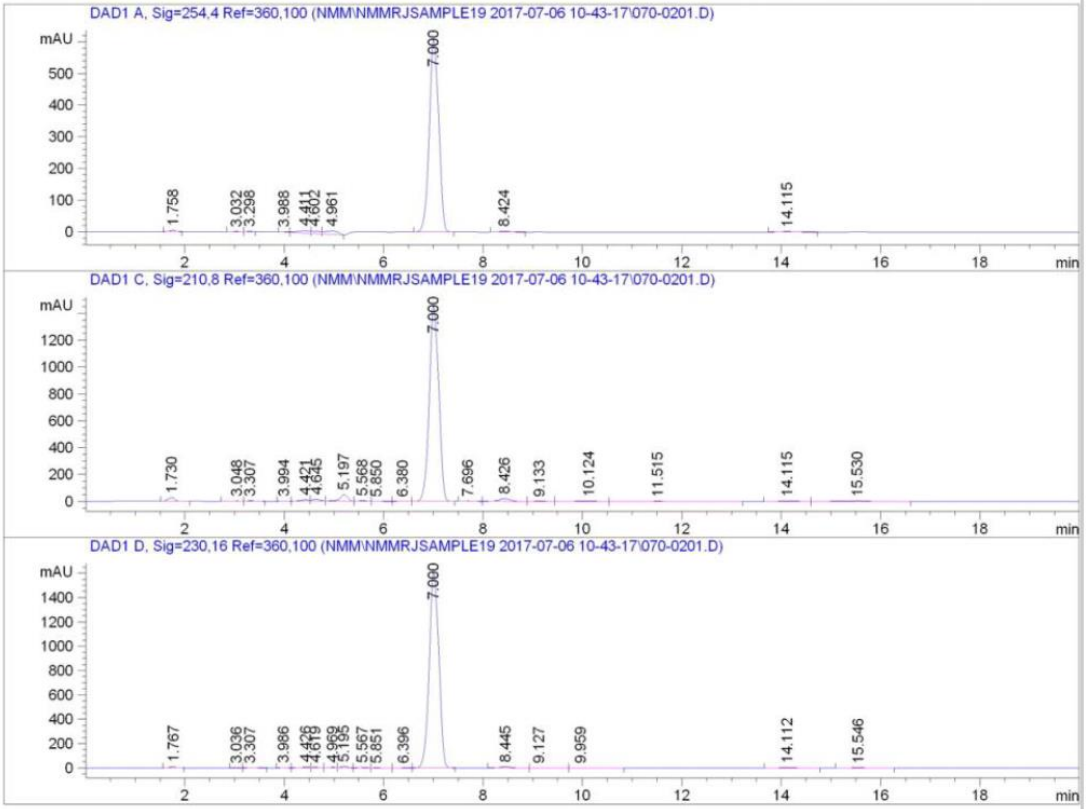
Peak #	RetTime [min]	Type	Width [min]	Area [mAU*s]	Height [mAU]	Area %
1	1.799	BB	0.0971	141.97491	19.93510	0.5218
2	2.828	BV	0.1473	33.77567	3.19555	0.1241
3	3.036	VV	0.1428	63.68369	6.36370	0.2340
4	3.203	VV	0.1090	24.69476	3.31287	0.0908
5	3.403	VV	0.2420	119.22433	6.38007	0.4382
6	3.749	VV	0.1296	39.70067	4.38693	0.1459
7	3.961	VV	0.1153	65.53610	8.37163	0.2409
8	4.130	VB	0.1863	212.50801	16.49173	0.7810
9	4.582	BV	0.1776	42.79880	3.52580	0.1573
10	4.977	VV	0.1635	2.62617e4	2606.93604	96.5153
11	5.605	VB	0.2046	33.76672	2.25639	0.1241
12	7.034	VV	0.2083	138.22281	10.72703	0.5080
13	7.548	VV	0.2184	32.28608	2.34863	0.1187
Totals :				2.72098e4	2694.23146	

*** End of Report ***

5.2.4 4-((8-Bromobenzo[1,2-*b*:4,5-*b'*]difuran-4-yl)methyl)pyrimidine (107)

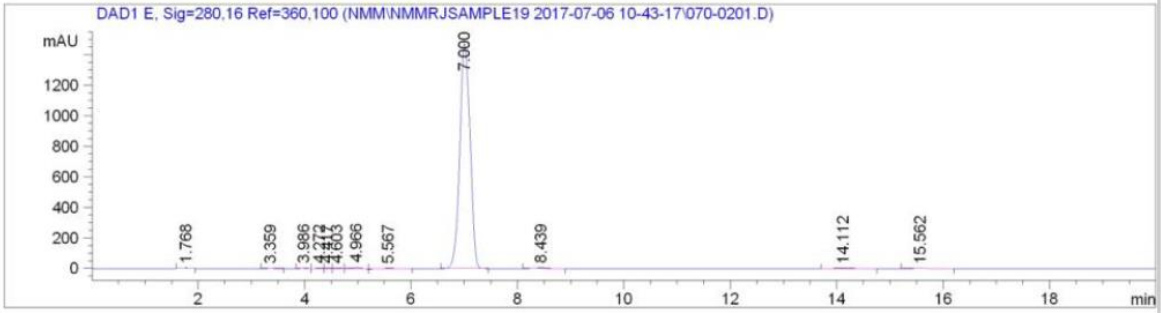
Data File C:\CHEM32\1\DATA\NMM\NMMRJSAMPLE19 2017-07-06 10-43-17\070-0201.D
Sample Name: Sample 6

Acq. Operator	: Nuala Maguire	Seq. Line	: 2
Acq. Instrument	: 1260 LC	Location	: Vial 70
Injection Date	: 06/07/2017 11:05:01	Inj	: 1
		Inj Volume	: 10 µl
Acq. Method	: C:\Chem32\1\DATA\NMM\NMMRJSAMPLE19 2017-07-06 10-43-17\NUALA35RJ.M		
Last changed	: 04/07/2017 05:40:25 by Nuala Maguire		
Analysis Method	: C:\CHEM32\1\DATA\NMM\NMMRJSAMPLE19 2017-07-06 10-43-17\070-0201.D\DA.M (NUALA35RJ.M)		
Last changed	: 04/07/2017 05:40:25 by Nuala Maguire		
Method Info	: Water:Acetonitrile, 35:65 RJ		
Sample Info	: Sample 6 - 024		



1260 LC 06/07/2017 11:58:04 Denis Lynch Page 1 of 4

Data File C:\CHEM32\1\DATA\NMM\NMMRJSAMPLE19 2017-07-06 10-43-17\070-0201.D
Sample Name: Sample 6



==========

Area Percent Report

==========

Sorted By : Signal
Multiplier : 1.0000
Dilution : 1.0000
Use Multiplier & Dilution Factor with ISTDs

Signal 1: DAD1 A, Sig=254,4 Ref=360,100

Peak #	RetTime [min]	Type	Width [min]	Area [mAU*s]	Height [mAU]	Area %
1	1.758	BB	0.1056	39.33508	5.24107	0.4525
2	3.032	BV	0.1347	12.88977	1.35880	0.1483
3	3.298	VV	0.1275	13.97268	1.63753	0.1607
4	3.988	BV	0.1765	22.58235	1.79790	0.2598
5	4.411	VV	0.2459	143.54152	7.90477	1.6513
6	4.602	VV	0.1857	97.61454	7.70810	1.1230
7	4.961	VV	0.2902	215.56819	11.32017	2.4799
8	7.000	BB	0.2149	8046.43213	606.01990	92.5672
9	8.424	BB	0.2511	44.66290	2.78523	0.5138
10	14.115	BB	0.3628	55.93538	2.30794	0.6435
Totals :				8692.53453	648.08141	

Signal 2: DAD1 C, Sig=210,8 Ref=360,100

Peak #	RetTime [min]	Type	Width [min]	Area [mAU*s]	Height [mAU]	Area %
1	1.730	BB	0.1717	278.99057	27.18353	1.2674
2	3.048	BV	0.1575	40.82265	3.73560	0.1854
3	3.307	VB	0.1807	65.26616	5.18886	0.2965
4	3.994	BV	0.1346	23.89455	2.82774	0.1085
5	4.421	VV	0.1755	155.13445	12.26783	0.7047
6	4.645	VV	0.1880	189.55214	15.15068	0.8611
7	5.197	VV	0.1782	586.19177	50.95320	2.6629
8	5.568	VV	0.1838	77.71194	6.67838	0.3530
9	5.850	VB	0.1740	26.94210	2.49424	0.1224

Data File C:\CHEM32\1\DATA\NMM\NMMRJSAMPLE19 2017-07-06 10-43-17\070-0201.D
Sample Name: Sample 6

Peak #	RetTime [min]	Type	Width [min]	Area [mAU*s]	Height [mAU]	Area %
10	6.380	BV	0.2163	35.31092	2.50671	0.1604
11	7.000	VB	0.2156	1.93737e4	1452.30591	88.0105
12	7.696	BV	0.2474	83.44897	4.73998	0.3791
13	8.426	VB	0.2737	380.39188	21.57157	1.7280
14	9.133	BV	0.2784	49.46832	2.85125	0.2247
15	10.124	VV	0.3772	115.95177	4.10975	0.5267
16	11.515	VB	0.6221	116.46085	2.55345	0.5291
17	14.115	BV	0.3834	143.08096	5.32654	0.6500
18	15.530	VB	0.5813	270.62912	6.19881	1.2294
Totals :				2.20130e4	1628.64402	

Signal 3: DAD1 D, Sig=230,16 Ref=360,100

Peak #	RetTime [min]	Type	Width [min]	Area [mAU*s]	Height [mAU]	Area %
1	1.767	BB	0.1108	88.64381	10.68402	0.3901
2	3.036	BV	0.1331	9.06267	1.00555	0.0399
3	3.307	VB	0.2070	31.39585	2.11724	0.1382
4	3.986	BV	0.1267	39.02473	4.91340	0.1717
5	4.426	VV	0.1936	109.81911	8.02785	0.4833
6	4.619	VV	0.1718	69.90195	6.09438	0.3076
7	4.969	VV	0.1638	75.29293	6.37678	0.3313
8	5.195	VV	0.1603	146.85159	14.72849	0.6462
9	5.567	VV	0.1777	64.00463	5.67168	0.2817
10	5.851	VB	0.1747	31.04231	2.85947	0.1366
11	6.396	BV	0.1831	15.25215	1.29792	0.0671
12	7.000	VB	0.2171	2.15873e4	1602.93433	94.9964
13	8.445	BB	0.2577	185.39330	11.28456	0.8158
14	9.127	BB	0.1994	14.89274	1.21148	0.0655
15	9.959	BB	0.3068	29.02674	1.28842	0.1277
16	14.112	BB	0.3598	133.10019	5.35768	0.5857
17	15.546	BB	0.3959	94.32768	3.43976	0.4151
Totals :				2.27244e4	1689.29299	

Signal 4: DAD1 E, Sig=280,16 Ref=360,100

Peak #	RetTime [min]	Type	Width [min]	Area [mAU*s]	Height [mAU]	Area %
1	1.768	BB	0.0984	28.09436	3.97875	0.1376
2	3.359	BB	0.1257	9.09070	1.06336	0.0445
3	3.986	BV	0.1374	30.36341	3.42562	0.1487
4	4.272	VV	0.1512	37.77134	3.63729	0.1850
5	4.417	VV	0.1343	31.42023	3.44867	0.1539
6	4.603	VV	0.1793	45.57984	3.81847	0.2232
7	4.966	VV	0.2120	130.06534	9.13851	0.6369
8	5.567	VB	0.3243	89.46240	3.77703	0.4381

Data File C:\CHEM32\1\DATA\NMM\NMMRJSAMPLE19 2017-07-06 10-43-17\070-0201.D
Sample Name: Sample 6

Peak #	RetTime [min]	Type	Width [min]	Area [mAU*s]	Height [mAU]	Area %
9	7.000	BB	0.2165	1.97960e4	1476.17725	96.9405
10	8.439	BB	0.2579	92.00924	5.53711	0.4506
11	14.112	BB	0.3581	78.82524	3.19222	0.3860
12	15.562	BB	0.3619	52.08275	2.05366	0.2550
Totals :				2.04207e4	1519.24792	

*** End of Report ***